DIRECT DESIGN OF

REINFORCED CONCRETE TRANSFER GIRDERS

By

GHOUS BUX KHASKHELI

B.Eng(*Mehran*), M.Eng(*Sheffield*)

A thesis submitted for the degree of

Doctor of Philosophy

Department of Civil Engineering

University of Glasgow

ProQuest LLC.
789 East Eisenhower Parkway
P.O. Box 1346
Ann Arbor, MI 48106 – 1346

TO MY ELDER BROTHER

BUKHASHAN KHAN KHASKHELI

Who sacrificed his education to give me a chance

Acknowledgements

The work described in this thesis was carried out in the Department of Civil Engineering at the University of Glasgow under the general direction of Professor A. Coull whose encouragement is gratefully acknowledged. The author would like to express his appreciation to Dr. D.R Green, the head of the department for providing all the required facilities of the department.

The Author is indebted to his supervisors, Dr. D.R. Green and Dr. D.V. Phillips for their valuable supervision, active interest, advice and constant encouragement throughout the work.

The author is grateful to Dr. P. Bhatt for his valuable proposals and advice, especially in the beginning of this research.

Mr. R.W. Watson, for useful discussion on steel structure matters involved in the designing of the test rig.

Dr. M. S. Mohmad previously a research fellow student at the University of Glasgow for his valu-able advice and help on the finite element analysis.

The staff members of Civil Engineering Department and Computing Services at the University of Glasgow, in particular, Miss A. MacKinnon, Miss E. McArthur, Miss J. Sutherland and Mr. G. Irving for their help on computer programming and plotting matters etc.

The staff of the concrete laboratory, in particular, Mr. A.A. Burnett, Mr R. McCaskie, Mr. A.I. Todd, Mr. A. Yuill, Mr. J. Thomson, Mr. B. Thomson and R. Thornton, Mr. R. Hawthorn for all tedious work involved in the preparation of the

specimens and assisting in experimental work.

The Government of Pakistan for financial support during the period of stay.

I am grateful to my wife Asma for her patience and understanding throughout this work, and my daughter Leena for keeping me cheerful in the final stages of this work.

Last, but not least my thanks are reserved for my parents and parents– in– law for their continuous encourgements, moral support throughout this work and financial support at the end of my scholarship.

SUMMARY

This thesis reports experimental and theoretical investigations into the in-plane behaviour of reinforced concrete transfer girders designed by the direct design method. The girders tested were either continuous over two spans or single span. The direct design technique investigated used an elastic stress field obtained from a linear-elastic finite element analysis using the uncracked properties of concrete in conjunction with Nielson's yield criterion given by:-

$$(\sigma x^* - \sigma x)\ (\sigma y^* - \sigma y) - \tau xy^2 = 0$$

where σx, σy and τxy are the applied stresses at the ultimate load, and σx^* and σy^* are the ultimate capacities of the section. An averaging procedure was used to smear out reinforcement requirements and select final bar sizes. This proved more satisfactory than selecting bars based on maximum stresses.

A finite element procedure for obtaining an elasto-plastic stress field was developed in order to design the reinforcement. This approach may be better in producing more economical distributions for design the reinforcement. However, this was not adequately evaluated in this research.

The experimental study consisted of testing eleven large scale girders. The major parameters studied for the two span continuous girders were; span to depth (L/D) ratio, the influence of the web reinforcement, the effect of using skew reinforcement and the main reinforcement distributions according to either CIRIA Guide 2 or the direct design technique. For the single span girders, the main purpose was to examine the direct design technique for girders with web openings which interrupt the load path. Also, to find the best location of the opening in the girder. One solid single span girder was tested with the aim of justifying the theoretical

calculated amount of steel at each point, so that structure must yield simultaneously. Also, to justify the maximum and averaging envelope procedures.

The theoretical study consisted of using a nonlinear plane stress finite element analysis. The material properites of reinforced concrete were represented by fixed crack smeared cracking model in conjunction with steel yielding behaviour etc. The experimental measured behaviour and the behaviour predicted by finite element model showed good agreement and allowed a greater insight into the behaviour of the girders.

The test results indicate that the direct design approach is satisfactory in both ultimate strength and serviceability behaviour as given by 0.3mm crack width.

CONTENTS

CHAPTER 3 – FINITE ELEMENT MODELLING

CHAPTER 4 – NONLINEAR MODELLING OF REINFORCED CONCRETE

NOTATIONS

Major symbols used in the text are listed below, others are defined as they first appear. Some symbols have different meanings in different contexts, these are clearly defined.

General Sumbols

$\{\ \}$, $\{\ \}^T$	Curly brackets denote column and rows vectors
$[\ ]$, $[\ ]^T$	Square brackets denote rectangular matrices
	In both cases T over the brackets denotes the transpose;
	-1 over square matrices denotes the inverse
$\|\ \|$	Straight brackets denote the determinant of square matrices
det $\|\ \|$	Denotes the determinant of a square matrix

Subscripts and Superscripts

e	Pertains to element
i	Pertains to nodes
q	Pertains to integrating points
s	Pertains to steel
T	Pertains to tangential values
l	Pertains to transformed directions
*	Pertains to crack direction
o	Pertains to initial values

Scalers

A	Area of individual bars crossing the diagonal crack joining the support and loading point, including main and shear reinforcement bars (Kong et al)
Ac	Area of concrete (BSCP8110)
Ah	Area of horizontal web steel bars (ACI Code)
As	Area of main reinforcement bars
Asc	Area of compressive reinforcement

Av	Area of vertical web steel bars (ACI Code)
Ax,Ay	Reinforcement areas per unit thickness in the x and y directions.
a	Shear span
a_u	Shear span below the opening
a_L	Shear span above the opening
β	Shear retention factor
β'	Coefficient of shear strength (Ramakrishnan et al)
b	Breadth (thickness) of the beam
C	Compressive force of concrete
C1	Empirical coefficient in Kong et al's equation for normal weight concrete C1= 1.4 for light weight concrete C1= 1.35
C2	Empirical coefficient in Kong et al's equation for normal weight concrete C2= 300N/mm^2 for light weight concrete C2= 130N/mm^2
c	Cohesive force of concrete (Varghese et al)
D	Overall depth of beam
dA	elementary area
dv	elementary volume
d	Effective depth of beam
Ec,E,Eo,E_T	Young's modulii
Es	Young's modulus of steel
Ew	Strain hardening modulus of steel
fc'	Characteristic compressive strength of concrete
fcb	Equal biaxial strength of concrete
fcu	Characteristic cube strength of concrete
F_{DT}	Normal force on inclined crack in deep beams
fs,fs'	Specified yield strength of tension and compression reinforcement respectively
ft'	Characteristic tensile strength of concrete

fy	Characteristic yield strength of steel
fx,fy	reinforcement stresses in direction x and y respectively
G,Go,G_T	Shear modulii
H	Horizontal force induced around a web opening in the model
H_F	Value of H corresponding to rotational failure of the model
H_S	Value of H corresponding to shear failure in the region between the beam end and the web opening
ha	Effective height of the beam
h_L	Depth of the beam web below an opening (Fig. 2.14– a)
h_o	Depth of the beam web above an opening (Fig. 2.14– b)
h_u	Depth of the beam web above an opening (Fig. 2.14– c)
h_1	Depth of an opening
h_2	Coefficient defining the position of an opening
I_1,I_2,I_3	1st, 2nd and 3rd invariants
J_2	Secant deviatoric stress invariant
k	Splitting coefficient (Ramakrishnan et al
k1,k2	Coefficient defining the position of an opening (Kong et al)
K,Ko,K_T	Bulk modulii
L'	Overall length of beam span
L	Simple span of the beam, generally refer to a distance between centre lines of supports.
lc	Characteristic length of a crack
ln	Clear span measured from face to face of the support (Crist)
M	Design moment at ultimate limit state
M_{FL}	Flexural capacity of a beam (Rangan)
M_{CR}	Shear strength of a deep beam (Rangan)
M_u	Ultimate moment at the section (ACI Code)
M_1,M_2,M_3,M_4	Hinge moments (Kong and Kubik)
Nx,Ny,Nxy	Applied inplane forces
n	Number of bars (Kong et al)
η	$(Q_B)_S/(Q_B)_F$

Pc	Calculated ultimate load
P1	Predicted ultimate load (by Ramakrishnan et al's equation)
P2	Predicted ultimate load (by de Paiva and Siess's formula)
P3	Predicted ultimate load (by ACI Code's formulae)
P4	Predicted ultimate load (by Kong et al method)
P5	Predicted ultimate load (by CIRIA Guide 2 method)
Ps	Serviceability load (kN) based on 0.3mm crack width
Pu,Pum	Measured ultimate load (kN)
ρ,ρt	(As/b.d)
ρx,ρy	Reinforcement ratios in directions of x and y.
Puc	Calculated load (Ramakrishnan et al)
Q	Shear force
Q_B	Shear transmitted below a web opening
$(Q_B)F$	Value of Q_B corresponding to rotational failure of the load path below the opening
$(Q_B)_S$	Value of Q_B corresponding to shear failure of the load path below the web opening
Q_T	Shear transmitted above a web opening
$(Q_T)F$	Value of Q_T corresponding to rotational failure of the load path above the opening
$(Q_T)_S$	Value of Q_T corresponding to shear failure of the load path above the web opening
$(Q_T)_{S1}$	Value of Q_T corresponding to shear failure of the beam in the region above the web opening
$(Q_T)_{S2}$	Value of Q_T corresponding to shear failure of the beam in the region between the beam end and the web opening
Q_{ult}	Ultimate shear strength in kN
Ri^*	Norm of applied load
S	Shear fractional force along inclined crack (ACI Code)
S'	Spacing of the web reinforcement Figure (2.6)
Sh	Spacing of horozontal web reinforcement (ACI Code)

Sv	Spacing of vertical web reinforcement (ACI Code)
T	Total tensile force resisted by As
t'	Distance between web opening and beam end (Kubik)
μ	Ratio of shear strength to flexural strength of the load path over the to of the opening $(Q_T)_S/(Q_T)_F$
Vc	Shear capacity of concrete (ACI Code)
Vs	Shear capacity of web reinforcement (ACI Code)
V	Design shear force at a critical section
vc	Shear stress carried by concrete
vn	Nominal shear stress carried by concrete (ACI Code)
vu	Limiting concrete shear stress (ACI Code)
W	Design load (kN)
ω	Reduction factor (ω= 0.85, ACI Code)
X	Clear shear span
X_L	Clear shear span below a web opening
X_o	Length of a web opening (Kubik)
X_u	Clear shear span above a web opening
X_1	Length of web opening (Kubik)
X_2	Coefficient defining the position of an opening
y	The depth at which a typical bar intersects the potential critical diagonal crack in a deep beam which is approximately the line joining the loading and reaction points.
y_L, y_u, y_t	These are used in Kubik's equation (2.22) to (2.24) and are given in Figure (2.14)
z	Lever arm
α	Acute angle between a typical bar and critical diagonal crack described in definition of y.
$\alpha 1, \alpha_L, \alpha_t, \alpha_u$	These symbols are used in equation (2.22) to (2.24) in conjunction with Figure (2.14)
αc	Direction of crack
γm	Partial safety factor for material

$\epsilon x, \epsilon y, \gamma xy, \epsilon z$	Strain components in global direction
$\epsilon t^*, \epsilon n^*, \gamma^*$	Strain in cracked direction
ϵcr	Cracking strain
$\sigma_1, \sigma_2, \sigma_3$	Principal concrete stresses
$\sigma x, \sigma y, \tau xy$	In– plane direct and shear stresses
$\sigma x^*, \sigma y^*$	Steel forces in x and y directions respectively
$\sigma x, \sigma y, \tau xy, \sigma z$	Stress components in global direction
$\sigma t^*, \sigma n^*, \tau^*$	Stress in cracked direction
$\triangle\sigma x, \triangle\sigma y, \triangle\tau xy, \triangle\sigma z$	Incremental stress components in global directions
$\triangle\sigma x, \triangle\sigma y, \triangle\gamma xy, \triangle\sigma z$	Incremental strain components in global directions
σoct τoct	Octahedral stresses
σm	Mean stress
γoct	Octahedral strain
$\nu, \nu o, \nu T$	Poisson's ratio
θ	Orientation of major principal concrete stress to y– axis

Vectors and Matrices

$[B]$	Strain matrix
$[D][D_T][D_T]^*$	Elasticity matrix
$\{F\}^e$	Nodal forces at nodes of an element
$\{F\}^e{}_{\epsilon o}$	Nodal forces vector due to initial strains
$\{F\}^e{}_{\sigma o}$	Nodal forces vector due to initial stresses
$\{F\}_p$	Nodal forces vector due to distributed load per unit volume
$\{F\}$	Nodal force vector due to external load
$[J]$	Jacobian matrix
$[j], [j']$	Distortion matrix
$[K], [K_T], [K]_o$	Overall stiffness matrix
$[K]^e$	Element stiffness matrix
$[M]$	Modular matrix
$[N]$	Matrix of shape functions
$\{R\}$	Vector of total imposed loads

$[T]$	Transformation matrix
$\{\delta\},\{\delta\}_o$	Nodal displacements
$\{\delta\}^e$	Nodal displacements associated with element e
$\{\psi\}$	Vector of residual nodal forces
$\{\sigma\}$	Total stress vector
$\{\sigma\}_o$	Initial stress vector
$\{\sigma\}_p$	Principal stress vector
$\triangle\{\sigma\}$	Incremental stress vector
$\{\sigma\}^*$	Stress vector in crack direction
$\{\sigma_e\}$	Elastic stresses stress vector
$\{\epsilon\}$	Total strain vector
$\{\epsilon\}_o$	Initial strain vector
$\{\epsilon\}_p$	Principal strain vector
$\triangle\{\epsilon\}$	Incremental strain vector
$\{\epsilon\}^*$	Strain tensor

CHAPTER ONE

INTRODUCTION

1.1 Preamble

This thesis is primarily concerned with the application of the direct design approach to in-plane structures, focusing on deep beams in general and on continuous transfer girders in particular. The research had three phases. Firstly the direct design approach was developed for the design of deep beams and continuous transfer girders. Secondly, the behaviour of designed beams was studied by testing them experimentally to destruction. Thirdly, designed beams were analysed by nonlinear finite element methods, in order to compare experimental and theoretical results, and to provide further in-depth information about behaviour. This strategy would enable conclusions to be drawn regarding the efficiency and rationality of the direct design approach for transfer girder design.

Deep beams have a common practical importance, they are characterized as being relatively short and deep, having thicknesses that are small relative to their span or depth, and are loaded in the plane of the member. They are "two dimensional" members in a state of biaxial plane stress, in which shear is a dominant feature. The internal stresses cannot be determined by simple bending theory, and shallow beam theory is not applicable for determining strength. Deep beams appear frequently in complex structures in the form of transfer girders, brackets, pilecaps, foundation walls, tanks, bins, folded plate roof structures, shearwalls and retaining walls. Figure. (1.1) shows a typical situation where deep beams are used as load bearing walls, whereas Figure (1.2) illustrates a situation where a deep beam spreads column loads into a continuous foundation.

In modern construction, high-rise buildings are fashionable and have been constructed on a large scale. It is fairly common practice to use heavy column construction to take the entire load of the building. In such buildings it is often an

architectural requirement that the ground floor should be free of columns as much as possible to accommodate departmental stores, hotel foyers, car parks, etc. This can be made possible by using deep beams in the form of transfer girders to provide large spans across the column free spaces, and to carry the rest of the building above it as shown in Figure (1.3).

Another typical example, encountered in practice is a framing plan for tall buildings which uses interior walls as story high structural members spanning the width of the structure. The wall members are staggered on alternative floors. This framing system provides large column free spaces as shown in Fig. (1.4). Hence, the slabs carry the floor loads to the walls and act as beam flanges, while the wall acts as a beam web.

Access from one part of a building to another frequently entails the provision of openings in the webs of deep reinforced concrete beams. A wall separating two rooms and designed as a deep beam may require openings for the passage of ventilating ducts, heating pipes or other essential services. Openings are often required to provide a central doorway between compartments. If the structure is to be designed safely and efficiently it is important to understand the effect of web openings on the behaviour of deep beams under service and ultimate loads.

It has been reported by various researchers that the type of loading and the shear span to depth ratios are important parameters which effect deep beam behaviour, i.e. when a beam is subjected to a direct point load acting on the top edge, the shear capacity of the beam increases as it becomes deeper and deeper, and arching behaviour becomes significant. In such beams diagonal tension cracks can appear suddenly along a line joining the support and the loading point, when the tensile stresses perpendicular to the compressive concrete strut joining the loading point and support exceeds the tensile strength of concrete. Hence, shear or diagonal splitting is

a likely cause of failure in such beams. For uniformly distributed loads, the tied–arch behaviour would be different and the strength would change. Furthermore, in the vicinity of point loads, irregular and often severe stress distributions occur which do not exist with uniformly distributed loads. Deep beams, either in continuous foundations or as shearwalls, often carry columns which provide direct point loads acting on the top edge, and it is this type of loading which was investigated in this study. Figure (1.5) illustrates this loading schematically.

In the last 30 years, many experimental and analytical studies have been conducted on deep beams. However, most of these studies are markedly different from one another in geometry, reinforcement ratios, reinforcement distributions, loading conditions, as well as the methods of analysis. Authors have typically developed and validated empirical formulae for their own test results, irrespective of its applicability to other situations. In addition, there has been far less attention devoted to their design. Consequently design of deep continuous girders is one of the most undefined in codes of practice. It appears that most of current practical design procedures use elastic stress fields. There are no design procedures which takes into account other stress field such as elasto–plastic stress fields. Designs based on current design methods give a very high difference between the design load and the measured ultimate load which implies there is wastage of material.

Neither the British Code of Practice CP110 (1972)[1], nor its updated version BSCP8110 (1985)[2], contain recommendations for deep reinforced concrete beams. The CEB–FIP (1970)[3] model code did include some design recommendations for simple and continuous deep beams based on Leonhardt and Walther's[4] findings in Germany. This Code does not provide precisely for shear reinforcement design and there is no provision for deep beams with web openings. The design criteria for multi–span deep beams have been developed from semi–empirical formulae based on limited data of simply supported deep beam studies. Continuous deep beam

behaviour and analysis is more complex in comparison to a simply supported deep beam due to the effects of the extra supports.

The ACI Code (1971)[5] and its new updated version ACI Code (1983)[6] included recommendations only for the shear design of deep beams and was based on Crist's findings at New Mexico(7). These provisions evolved from simply supported deep beam studies and are not directly applicable to continuous deep beams. As a result, the ACI Code equations "blow up" for continuous deep beams, when the critical section for shear is near or at the point of contra-flexure, which happens frequently, since the design equation requires division by zero. Secondly the ACI Code equation for ultimate capacity includes a negligible contribution from the steel, which means that the estimated total load is provided only by the concrete which may not be true. The Code recommends that the Portland Cement Association (PCA) Pamphlet (1946)[8] should be consulted if flexural reinforcement is required. This was an extension of earlier work by Dischinger (1932)[9] who considered reinforced concrete as an isotropic, homogeneous and elastic material, which is not very realistic, once concrete has cracked.

The Construction Industry Research Information Association (CIRIA) Guide 2 (1977)[10] is a comprehensive guide for deep beam design and has a similar procedure to the CEB-FIP (1970)[3] model code. However, its recommendations seem to be conservative for both main and shear reinforcement. It does not provide specific criteria for shear reinforcement calculation, only an ad hoc procedure. The CIRIA Guide does cover web opening design, but only if the openings are placed in a dead zone area, which is called, in its own terminology, an "admissible" opening. In practice, openings often interrupt load paths, and can cause a serious problem. Thus the CIRIA Guide lacks information for "inadmissible" web opening design. Also the CIRIA Guide provisions for web openings are based on elastic theory.

During the last two decades study of plasticity in reinforced concrete has grown extensively. Limit analysis techniques have been used to predict both upper and lower bound capacities of slabs, panels and beams under bending, shear, torsion and combined actions. These techniques are based on the basic theorems of plasticity, which demand that at collapse two of three conditions, i.e. the equilibrium condition, the yield criterion and the mechanism condition, are satisfied. Also the material must possess sufficient ductility so that areas which yield before collapse, can deform plastically without loss of strength until ultimate conditions are reached.

In lower bound methods for reinforced concrete, the applied loads are less or equal to the combined internal resistance offered by the concrete and steel. In upper bound systems, sufficient hinges or yield zones are formed in the structure which transform it into a mechanism. Upper bound methods are unsafe if the wrong mechanism is assumed, whereas lower bound methods are safe although they may be uneconomical.

In recent years various proposals have been made for the design of reinforcement for both bending and in-plane forces, based on the lower bound limit state approach, in which a stress field in equilibrium with the design ultimate load is used in conjunction with an appropriate yield criterion. This approach is termed the direct design method in this thesis. Such a stress field can be obtained by any suitable procedure such as a linear elastic finite element analysis or by an elasto-plastic finite element analysis. Reinforcement is then provided so that the combined resistance of steel and concrete at each point is equal to or greater than the applied stresses.

An elastic stress field will produce steel reinforcement ratios which may vary continuously throughout the continuum, and is likely to give ultimate loads which are higher than the design loads. Also, when taken in conjunction with the objective of

simultaneous yielding throughout the continuum, excessive deformations and cracking are unlikely at working loads and therefore they should not result in poor serviceability behaviour. On the other hand, an elasto–plastic stress field might provide more uniform and efficient flow of forces producing uniform reinforcement fields which would be more convenient for selecting bar sizes and spacing. However, such fields are likely to produce less satisfactory serviceability behaviour.

In theory, by satisfying equilibrium and the yield criterion at every point simultaneously, the entire structure will become a mechanism at ultimate load. Practical considerations, such as the provision of reinforcement as discrete bars, make it impossible to achieve this idealised behaviour. Nevertheless, in general, direct design has been proved satisfactory in ultimate and serviceability behaviour, although the theory gives no guarantee that serviceability behaviour will be satisfactory.

Recent research has demonstrated that the direct design approach using an elastic stress field is satisfactory for both bending and in–plane actions[11,12,13,14] for certain classes of structures at serviceability and ultimate conditions. In these studies the yield criterion and associated design equations given by Wood and Armer[15,16] were used to design reinforcement for bending actions, whilst for in–plane actions, Nielsen's[17] yield criterion was used with the design equations proposed by Clark[18].

The studies by Lin [13] on solid deep beams and by Memon[14] on perforated deep beams were on relatively small scale models so that practical bar sizes were difficult to select. Also, because continuously varying reinforcement fields were produced throughout the continuum, difficulties were encountered in choosing practical distribution of reinforcement. These factors indicate that there is a need to test large–scale models which could simulate practical situations more closely.

These studies have also indicated that measured ultimate loads were always higher than the designed ultimate loads. This can be explained by the following points:

(a) The reinforcement provided was always higher than the calculated amount of reinforcement.

(b) Strain-hardening in the steel is ignored in the design equations. This could play an important role, particularly for high tensile strength steel.

(c) The effect of dowel action and shear transfer across cracks is ignored in the design process. These can have an important influence in deep beam behaviour.

(d) The tensile strength of concrete is assumed zero in the design process.

There are still several other aspects of the direct design method which requires further investigation and development. These include the following.

(i) As implemented currently the direct design technique is semi-automatic. However, it has the potential to be fully automated from the initial design conception to the final working drawings. Automatic procedures have been produced for calculating the elastic stress field, the steel ratios and the steel areas required, which can then be plotted by computer directly to assist in the subsequent design stages. Discrete bars are then selected manually, based either on maximum or average value procedures in conjunction with the rules for spacing and concrete cover as specified in codes of practice and other design guides. Once these rules for bar selection have been established experimentally and theoretically, it also could be made automatic.

(ii) Multi load cases have not yet been studied experimentally or theoretically. It is often the case that deep beams or other structures are subjected to such loading. Clearly it is impossible to produce a single practical reinforcement arrangement which will simultaneously satisfy the idealised basic conditions for two or more independent load cases. It is still necessary to work out practical procedures for detailing in this situation

(iii) The use of skew reinforcement is not covered by any code of practice. However, Leonhardt and Walther[4] and Lin[13] have studied skew reinforcement as main reinforcement in deep beams and have concluded that it is better than orthogonal reinforcement in increasing ultimate capacities of beams, reducing deflections and giving a better control on crack widths. Skew reinforcement is conveniently handled by the direct design equations and thus it would be useful to further investigate the efficiency of this type of reinforcement using the direct design approach.

(iv) The direct design of deep beams in which web openings interrupt the load path, has not yet been studied. This is an important practical situation which needs further investigation, especially as no code of practice or design procedure includes this situation.

Since deep beams can develop arch action, attempts have been made to develop Plastic Truss Models[19,20,21,22] for analysis and design. However, these do not strictly duplicate the true behaviour of deep beams, they are not straightforward to use and they only · predict ultimate loads. An iterative process is required which rebuilds the geometry, changes support dimensions, and adjusts the material properties. The reliability of solutions appears to be dependent on the choice of an approximate effective concrete strength, fc*, using a so– called concrete effectiveness factor, v.

The plastic truss model also assumes that any horizontal web reinforcement is ineffective, which might not be the case in reality; also since shear failure in deep beams is dominant, the top and bottom cords of steel, in the plastic truss model may not reach its ultimate capacity as is assumed. To the author's knowledge, the plastic truss model does not appear to have been used, to actually design either

simple or continuous deep beams, which have then been tested experimentally to confirm its applicability. For example, two series of deep beams tested by Rogowsky and MacGregor[19], and Ricketts and MacGregor[20] were analysed, but not designed, by the plastic truss model. Although good agreement was obtained, it was only possible by making adjustments to material properties, such as the characteristic cylindrical compressive strength of concrete.

As indicated earlier, current codes of practice and design methods rely heavily on empirical or semi–empirical formulae derived from large amounts of experimental data. This is mainly because of the complexities associated with the development of rational analytical approaches. Neveretheless, it is difficult and expensive to conduct exhaustive experimental studies on each topic, in order to develop empirical methods. In such situations, numerical techniques offer alternative approximate solutions if material behaviour is properly modelled.

Nowadays a number of such techniques are available for analysing a given structure, all based on the basic principles of continuum mechanics, that is equilibrium, compatibility and the constitutive relationships of the material. They transform a body of an infinite number of variables into one with a finite number of variables, governed by a set of simultaneous equations, the solution of which provides an approximation to the real situation. The most powerful general technique is the Finite Element Method (FEM). It is an engineering tool of wide applicability for the solution of partial differential equation systems, subject to known boundary and loading conditions, and has been described[23,24,25] very widely. Its development is still continuing, particularly in nonlinear analysis, and it is being applied in the development of rational approaches for structural design in computer aided design (CAD) techniques.

In the finite element analysis of reinforced concrete structures, many nonlinearties

can be approximately modelled, these include the cracking of concrete, tension stiffening, shear transfer across cracks, nonlinear multiaxial material behaviour, and complex steel–concrete interface behaviour. Thus, in principle, the FEM can estimate the most important aspects of behaviour throughout the entire loading range.

However, understanding of concrete behaviour is still incomplete despite the significant advances made in the last two decades. Disparities in experimental results are commonplace due to the difficulties in obtaining consistent test procedures and test specimens, as well as in the natural variability of concrete itself. This makes it difficult to model concrete behaviour exactly, therefore approximate theories have to suffice. The behaviour of steel is more straightforward and can be modelled more easily, particularly as reinforcement provides a predominantly axial force.

However, composite action of concrete and steel as reinforced concrete, especially when the concrete is cracked, is much more complex. Factors such as bond–slip phenomenon between steel and concrete, dowel action of reinforcement under shear deformation, etc. can significantly influence reinforced concrete behaviour. These phenomena are still under investigation in order to provide better understanding and information, which are essential for theoretical modelling.

In testing the reliability of a FEM model, it is important to understand the numerical and material parameters which influence a solution and ensure that predicted behaviour is compared with quantities which have practical engineering significance. However, once the integrity of a finite element analysis for a particular problem is confirmed against experimental evidence, then a numerical parametric study can be employed to investigate various factors in that field more economically than by experimental means. Also, a wider range of parameters can be studied when a FE model is used in conjunction with carefully selected laboratory models. Such

an approach may be better for developing rational design approaches for codes of practice.

Nonlinear finite element models have been applied by various researchers, for example[26,27,28,29], on single span solid and perforated deep beams. Also, the ASCE State–of–the–Art Report[30] reviews the various finite element models developed by researchers for the analysis of reinforced concrete. Reasonable comparisons between predicted behaviour and experimental behaviour have been reported. However, no finite element studies appear to have been conducted on continuous deep girders, although in principle there should be little extra difficulty.

1.2 Scope and purpose of this study

The main objectives and scopes of this study were:

1:– To test the applicability of the direct design approach as a rational design procedure for in–plane structures, in particular deep beams and continuous transfer girders. Such beams would contain a range of features such as perforations and skew reinforcement. This was achieved by:–

(i) Developing a linear–elastic finite element model which incorporated the direct design equations for both orthogonal and skew reinforcement design.

(ii) Carrying out experimental tests on large–scale and full–scale models to destruction.

(iii) Carrying out nonlinear finite element analysis.

2:– To test the validity of the nonlinear FEM model by comparing strains, displacements, crack patterns, ultimate loads and failure mechanisms with experimental evidence.

3:– To compare the direct design technique at serviceability and ultimate conditions with other design methods recommended by various codes of practice, and also with

the plastic truss models.

4:— To draw some general conclusions regarding the design recommendations of the British Code of Practice for deep beams and transfer girders.

1.3 General Layout of the thesis

Chapter Two reviews and critically assesses the historical background of experimental and theoretical work carried out on reinforced concrete deep beams relevant to this study. It also reviews four main design methods and the direct design method, in order to compare these methods.

Chapter Three is concerned with a brief review of the finite element method and its use in the design program for obtaining an elastic stress field. This program also contains the equations for reinforcement design and gives three dimensional views of stress behaviour in the continuum.

Chapter Four presents a review of the nonlinear finite element method. The mathematical material models describing the behaviour of concrete and steel are discussed. These include cracking and post—cracking behaviour of concrete, two dimensional strain—stress laws and crushing of concrete, and steel stress—strain behaviour. Also elasto—plastic analysis is described in relation to obtaining other stress fields for use in the direct design procedure. An assessment of the models is made with respect to boundary conditions, mesh convergence, nonlinear numerical parameters etc.

Chapter Five describes in detail the direct design methodology with its limitations and applications to continuous girders. The complete step by step design of several beams is included. These use the linear elastic model for obtaining elastic stress fields and Nielsen's[17] yield criterion in conjunction with Clark's[18] design equations

to design the reinforcement.

Chapter Six describes the test–rig which was designed to carry out the experimental investigation on large and full scale models of transfer girders, and describes the experimental procedures and instrumentation.

Chapter Seven presents the experimental results. General experimental behaviour is reported and results are discussed.

Chapter Eight presents the nonlinear finite element assessment of the tested girders, and examines the various material and numerical parameters which have an influence on general behaviour of the transfer girders and offers practical guidance in its use. In addition, comparisons of experimental behaviour with the predicted behaviour of the FE model are presented. It also describes in detail a comparison of other methods of designing and analysing for deep beams. The discussion leads to an attempt to suggest improvements in codes of practice such as CEB–FIP, ACI Code and CIRIA Guide 2, and suggests that the British code of practice might also include these recommendations.

Finally, Chapter Nine offers general comments and conclusions regarding the applicability of the direct design approach for the design of transfer girders and makes suggestions for further research in this area.

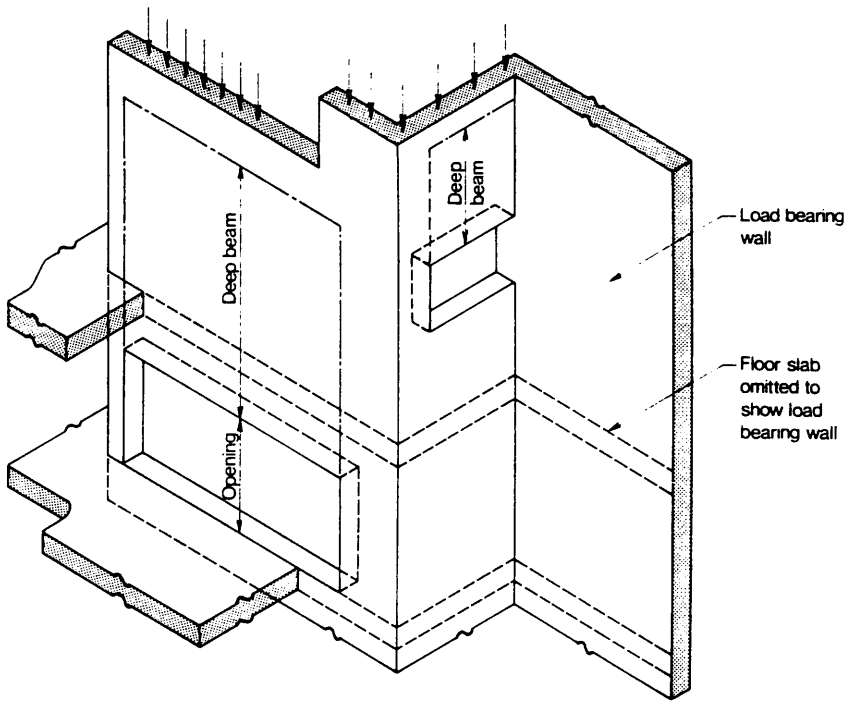

Fig. (1.1) Deep beams used as load bearing walls.

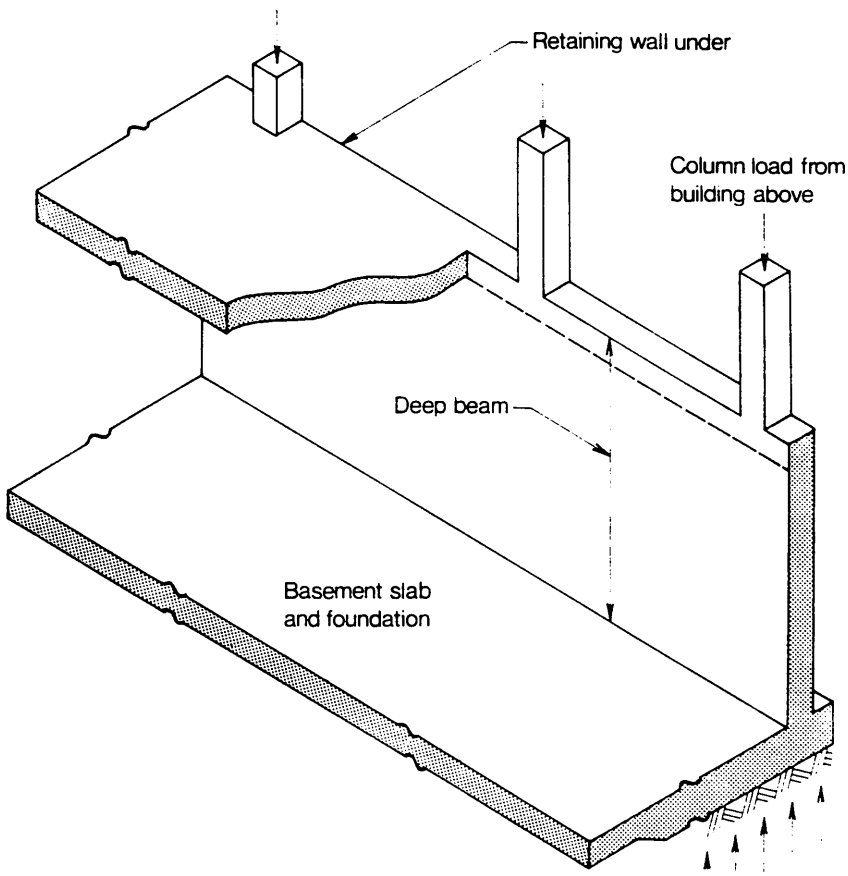

Fig. (1.2) Typical deep beam use to spread column loads to a continuous foundation

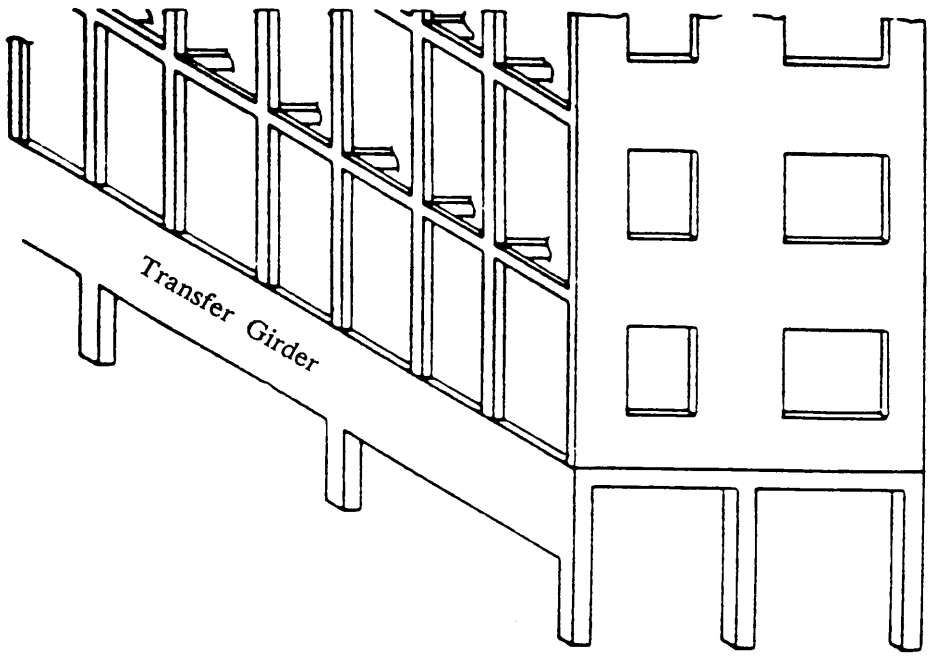

Fig. (1.3) The use of transfer girder and frame supported shearwalls in high– rise buildings

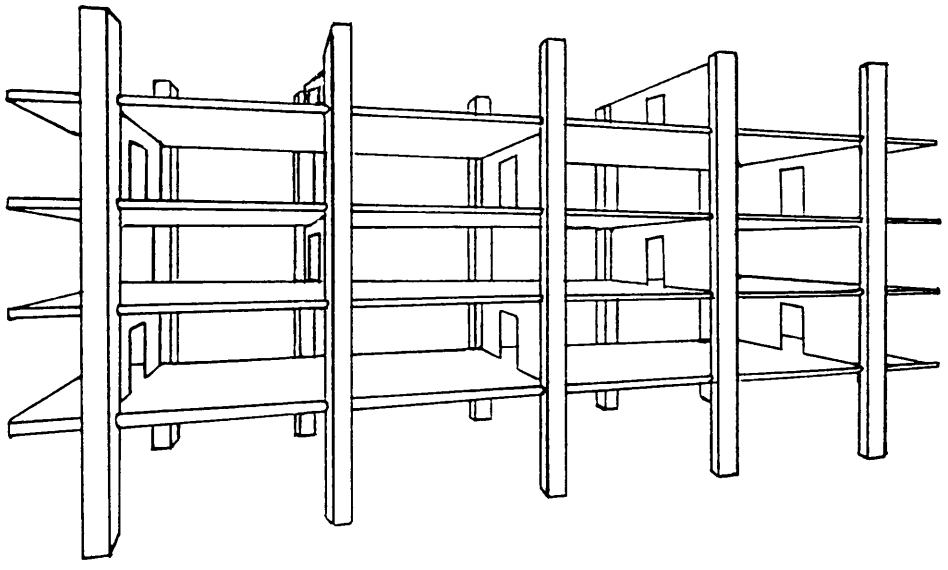

Fig. (1.4) The staggered wall beam framing system.

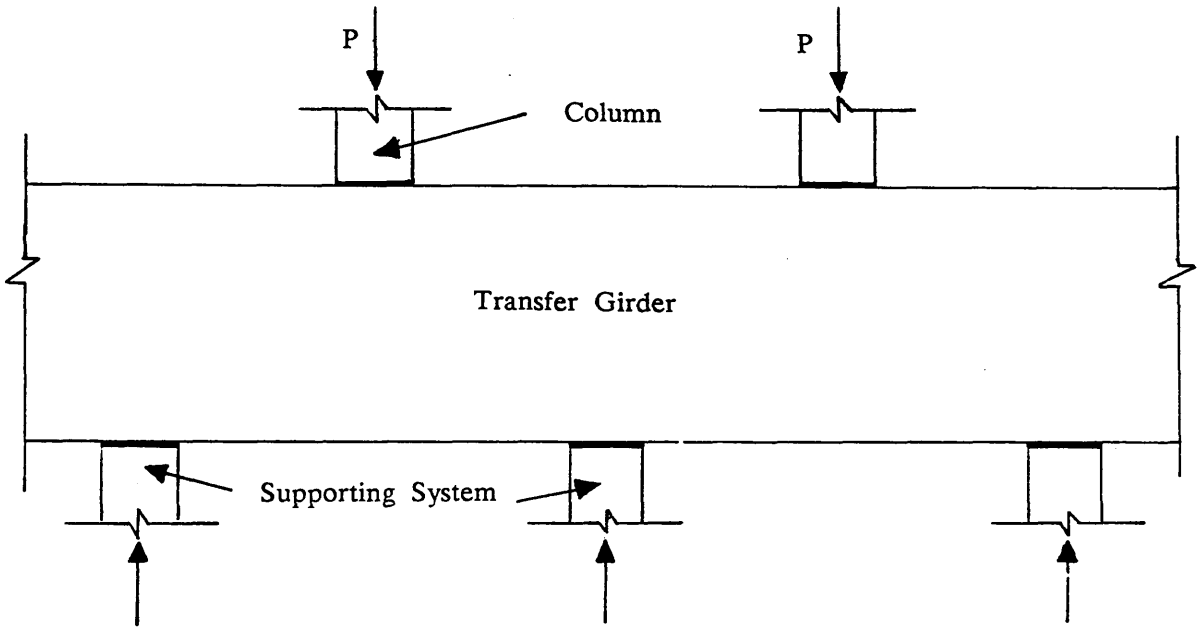

Fig. (1.5) Typical schematic illustration of loading system used in this study.

References

1. The council for codes of practice, Biritish standards institution, "The structural use of concrete" Code of practice 110, 1972.

2. The council for codes of practice, British standards institution, " The structural use of concrete" Code of practice 8110, 1985.

3. Comite europeen du beton– federation internationale de la precontrainte (CEB–FIP), International recommendations for the design and construction of concrete structures, Appendix 3, "Deep beams", 1970.

4. LEONHARDT, F. and WALTHER, R., "Wandartige trager, deutscher ausschuss fur stahlbton, Vol. 178, Wilhelm ernst und sohn, Berlin, West Germany, 1966.

5. ACI committee 318, "Building code requirements for reinforced concrete (ACI–318–71), American concrete institute, Detroit, Michigan, 1971.

6. ACI committee 318, "Building code requirements for reinforced concrete (ACI–318–71), American concrete institute, Detroit, Michigan, 1971.

7. CRIST, R.A., "Static and dynamic shear behaviour of uniformly loaded reinforced concrete deep beams, Ph.D. Thesis, University of New Mexico, Albuguerque, New Mexico, 1971.

8. "Design of deep girders" Concrete information No. ST66, Portland cement association, Structural bureau, Chicago, 1946.

9. DISCHINGER, F., "Beitrag zur therrie der halbscheibe und des wandartigen balkens", International association for bridge and structural engineering publication, Zurich, Volume 1, 1932, (pp 69–93).

10. CIRIA, "The design of deep beams in reinforced concrete" Guide 2, Construction industry research and information association, London, 1977.

11. HAGO, A.W., "Direct design of reinforced concrete slabs", Ph.D. Thesis, University of Glasgow, 1982.

12. ABDUL–HAFEZ, L.M., "Direct design of reinforced concrete skew slabs", Ph.D. Thesis, University of Glasgow, 1986.

13. LIN, C.K., "Ultimate strength design of deep beams", M.Sc. Thesis, University of Glasgow, 1979.

14. MEMON, G.H., "Ultimate strength of perforated deep beams", M.Sc. Thesis, University of Glasgow, 1982.

15. WOOD, R.H., "The reinforcement of slab in accordance with a pre-determined field of moments", Concrete, Feb. 1968, (PP. 69-76).

16. ARMER, G.S.T., Correspondance on "The reinforcement of slab in accordance with a pre-determined field of moments", Concrete, Aug. 1968, (PP. 319-320).

17. NIELSEN, M.P., "Yield conditions for reinforced concrete shells in the membrance state" Non-classical shell problems, IASS symposium, Warsaw, 1963, (PP. 1030-1038).

18. CLARK, L.A., "The provision of tension and compression reinforcement to resist in-plane forces", Mag. Conc. Res., Vol. 28, No. 94, 1976, (PP. 3-12).

19. ROGOWSKY, D.M. and Macgregor, J.G., "Shear strength of deep reinforced continuous beams", Structural engineering report No.110, Department of civil engineering, University of Alberta, Canada, 1983.

20. RICKETTS, D.R. and MACGREGOR, J.G., "Ultimate behaviour of continuous deep reinforced concrete beams", Structural engineering report No.126, Department of civil engineering, University of Alberta, Canada, 1985.

21. MARTI, P., "Basic tools of reinforced concrete design", ACI Journal, Proceedings, Vol. 82, No. 1, Jan.-Feb. 1985, (PP. 46-56).

22. COLLINS, M.P., and MITCHELL, D., "A rational approach to shear design - The 1984 Canadian code provisions", ACI Journal, Nov.-Dec. 1986, (PP. 925-933).

23. ZIENKIEWICZ, O.C. "The einite element method in engineering science" Mcgrave Hill, New York, 1971.

24. OWEN, D.R. and HINTON, E., "Finite elements in plasticity, Theory and practice" Pineridge press limited Swansea, U.K. 1980.

25. HINTON, E. and OWEN, D.R., "Finite element programming" Acadmic press inc., London, 1983.

26. PHILLIPS, D.V., "Nonlinear analysis of structural concrete by finite element methods", Ph.D. Thesis, University of Swansea, 1973.

27. AL-MAHAIDI, R.S.H., "Nonlinear finite element analysis of reinforced concrete deep members", Report No. 79-1, Cornell University, Itheca, New York, 1979.

28. AL-MANASEER, A.A., "A nonlinear finite element study of reinforced concrete beams", Ph.D. Thesis, University of Glasgow, 1983.

29. MOHAMD, M.S., "A finite element and experimental study of reinforced concrete in torsion", Ph.D. Thesis, University of Glasgow, 1986.

30. ASCE, "Finite element analysis of reinforced concrete", State-of-the-art Report 1982.

CHAPTER TWO

LITERATURE REVIEW OF STUDIES ON TRANSFER GIRDERS

2.1 Introduction.

Transfer girders are found in the form of simply supported or continuous deep beams of various types. A detailed description with the form of loadings they take, and where they appear in practical applications, was given in Chapter One. A fair amount of experimental and theoretical work has been reported on simply supported solid and perforated deep beams, but the amount of work is small compared to that made on shallow reinforced concrete beams. Little experimental work has been reported on continuous deep beams.

Analysis of continuous deep beams is more complex in comparison to simply supported ones because of the increased number of boundary conditions to be satisfied. Although much of the literature on simply supported deep beam studies has little direct relevance to this study, such information gives an approximate guide to the behaviour of transfer girders and continuous deep beams. Hence a review of single span deep beams has been undertaken to provide a basic foundation.

The aim of this chapter is to select a representative sample of the most recent investigations in order to give a brief summary of general deep beam behaviour. Also the different experimental and analytical approaches which are directly or indirectly related to the present investigation are reviewed. The publication list is too long to give here but an early comprehensive review was given by Albritton[1] which has been followed by more recent reviews[2–5]. Finally, some of the current design methods specified by various codes of practice and guides are reviewed.

2.2 Basic behaviour and definition of deep beams.

In simply supported beams with span to depth (L/D) ratios greater than approximately 2.0, and in continuous beams with ratios greater than about 2.5, the stress and strain distributions can be satisfactorily predicted by simple bending theory. This implies that

the basic assumption of Navier Bernoulli's hypothesis (plane sections remain plane before and after loading) is approximately valid. It then follows that the flexural stress and strain distribution is linear and that the shear stress distribution is parabolic across a vertical section. However, the stress distributions over a cross-section deviates increasingly from these as the span to depth (L/D) ratio decreases as shown in Figure (2.1).

In the case of small (L/D) ratios, stresses based on a straight line distribution may be seriously in error. The simple theory of flexure takes no account of normal pressures on the top and bottom edges of the beams, caused by the load and reaction points. The effect of these normal pressures is such that the distribution of bending stresses on a vertical section is not linear, and consequently a section which is plane before bending does not remain even approximately plane after bending. The neutral axis will not necessarily lie at the mid-depth of the beam, and its position may vary along the span. There may even be more than one neutral axis.

As the beam becomes deeper and deeper, the lever arm increases. This increase produces flexural stress which is less significant in deep beams than in shallow beams, and the shear stresses become significant. The vertical and shear strains in deep beams are of the same magnitude as the bending strains and therefore make a more significant contribution to the total deformations than in shallow beams.

The applied loads on the top surface give rise to vertical compressive stresses and a concrete strut forms along a line joining the support and the loading point. This is the plane where a diagonal shear crack may appear and the beam transforms immediately into a tied-arch. Therefore, the concepts of lever arm in shallow beams and strut action in deep beams are introduced to give a simplified representation of the internal stress flow and deformations within the beam.

2.3 Deep beam studies based on linear elastic behaviour.

2.3.1 Theoretical investigations.

The era of deep beam research was started by Franz Dischinger[6]. He presented a Fourier series solution for beams of decreasing span to depth ratios, resting on a series of supports. He assumed reinforced concrete was elastic, homogeneous and isotropic. He showed that plane sections do not remain plane after loading. He emphasized that a knowledge of the lever arm in deep beams is of great importance. Although his work was concerned with continuous deep beams, he suggested that the lever arm for simply supported girders could be twice as great as that of continuous girders.

Later, the Portland Cement Association (PCA)[7] published the pamphlet "Design of deep girders" based on Dischinger's findings. This pamphlet covered all possible cases of loadings, although it lacked a design procedure for continuous girders with concentrated loads on the top surface at the centre of the spans. The ACI Code[8] still refers to this pamphlet for the design of flexural reinforcement. This is explained in detail in section (2.6) on the review of design methods.

Other approximate linear elastic methods of analysis have been given Conway, Chow and Morgan[9], Chow, Conway and Winter[10] and Uhlmann[11] using finite difference techniques. Archer and Kitchen[12] have presented a solution for stresses in deep beams using strain energy methods. Some linear finite element analysis has also been applied in earlier studies, for example CIRIA Guide 2 has incorporated elastic stress distributions for deep beams and has indicated that the distribution is not linear as in shallow beams.

All these methods only apply to elastic homogeneous materials, whereas the behaviour of reinforced concrete beams involves cracking and nonhomogeneous nonlinear material behaviour. Nevertheless, these studies have revealed that the behaviour of deep beams is quite different than that of shallow beams and have laid the foundations for

recommendations for the design of reinforced concrete deep beams. However such recommendations have not been supported by experimental tests, therefore there is some doubt about their validity.

2.3.2 Experimental investigations.

Although Kaar[13]'s work was not on reinforced concrete deep beams, it appears that he might be the first researcher who experimentally investigated stresses in deep beams. Kaar carried out his tests on homogeneous, isotropic and elastic materials, one series of six aluminium beams and another series of six steel beams. He discovered that when the span to depth (L/D) ratio was less than 1.5 the use of flexural formula for measuring the stresses was seriously in error.

Archer and Kitchen[14] studied stress distributions on three deep steel plates using eight different loading conditions in order to verify their proposed strain energy method. Experiment and analysis were in agreement for the case where the span to depth (L/D) ratio was 1. At all points along the lower edge of the beam the stresses were markedly different from those given by simple theory. For the cases where the (L/D) ratio was 1.5 and 2.0 the experimental values were approximately midway between values obtained by strain energy method and those given by simple theory.

The experimental work described above reveals that stress analysis based on elastic theory gives reasonable predictions when specimens were made from materials which closely obey Hooke's law. Nevertheless, this experimental research indicated that the simple bending theory was not applicable to deep beams. Thus there was a need to test reinforced concrete deep beams themselves in order to develop appropriate design methods.

2.4 Reinforced concrete deep beam studies.

Various theoretical studies have been carried out which are based on experimental behaviour, resulting in semi-empirical formulae. A selected sample of representative

theoretical studies proposed over last three decades is presented in this section.

2.4.1 Theoretical investigations.

Varghese and Krishnamoorthy.

Varghese and Krishnamoorthy[15] developed a theory for ultimate load of deep beams based on published experimental data, including their own. Their theory was based on the shear type failure under various types of loading. They believed that only shear failure occurs due to diagonal cracking along the line joining the support to the nearest loading point, as shown in Figure (2.2). A formula was derived based on the equilibrium of the segment of the beam, and by assuming that failure occurs by shear along the line joining the loading point and support, and by yielding of the steel. Their formula is applicable for single span deep beams subjected to a centrally concentrated load on the top edge, loads at third points and uniformly distributed loads. They applied this formula to a small number of tests and achieved reasonable agreement with experimental values.

The ultimate load of the beam is then calculated by

$$Pu = \frac{2.c.b.D}{\sin\alpha.\cos\alpha(\tan\alpha+\tan\varphi)} + \frac{2.Fs(\tan\alpha.\tan\varphi-1)}{(\tan\alpha+\tan\varphi)} \qquad 2.1$$

where α is the angle of the diagonal crack, Fs is the force in the longitudinal steel as illustrated in Figure (2.3– a) based on the yield stress fy of steel, b is the breadth of the beam and D is the overall depth of the beam. The term φ and c are obtained from the compressive and tensile strength of the material by using Mohr's theory, illustrated in Figure (2.3– b). Thus $\varphi = (fcu - fc')/2\sqrt{(fc'.ft)}$ and $c = (\sqrt{fc'.ft})/2$.

Moreover, they proposed a design procedure for main reinforcement based on the assumption of a shear failure mode. The amount of reinforcement is calculated by assuming that the depth of the compression zone is 0.1D. The proposed formula is then

$$As = M/fy(d - (0.1D/2)) \qquad 2.2$$

where M is the design bending moment and d is the effective depth.

Ragan

Ragan[16] described a theoretical approach for predicting the ultimate strength of reinforced concrete deep beams which was similar to that applied by Sundara Raja Iyengar and Rangan[17] for shallow beams. He derived two formulae, one for beams failing in flexure and one for beams failing in shear:

Flexure failure:— This assumes a nonlinear stress block for concrete in the compression zone at failure, a triangular distribution for the tensile zone of concrete, and that the main steel yields at failure.

The formula for beams failing in flexure then follows as:

$$M_{FL}/bd^2 = [\ (\rho t fy/fc').j + 0.15\ \lambda\ ] \qquad 2.3$$

where j and λ are empirical constants defined as:

$$j = [1 - 0.48\ k]$$

$$\lambda = [(1 - 1.4\ k)\ (2.0 - 0.3\ k)] / 6.0$$

and $k = [(\rho fy/fc') + 0.075\ ]$,

where $\rho t = As/bd$

Shear failure:— This assumes that the contribution of shear carried by the longitudinal tension steel and the shear resisted by the concrete in the tension zone is negligible. A rectangular distribution was assumed for the shear stress in the compression zone of concrete and a nonlinear stress block was considered for the compressive stresses in the concrete.

The formula for beams failing in shear then follows as:

$$M_{CR} = (2k_1.k_3.bc.fc'.jd)/(1+\sqrt{1+(2jk_1.k_3)/\alpha_1})^2 \qquad 2.4$$

where $k_1.k_3=0.8$ and $k_2=0.42$ were used to estimate ultimate shear

and $\alpha_1 = M_{CR}/Vd$

$$c = d/k_2(1-d)$$

where M_{CR} is the shear failure capacity and V is the shear force at the critical section. Ragan presented two graphs of equations (2.3) and (2.4) from which the ultimate strength can be estimated. Comparing formulae with published data, the flexural strength was predicted in the range 0.75 to 1.28 and shear strength in the

range 0.75 to 1.45 of measured ultimate strengths.

Shaikh, de Paiva and Neville[18] described an iterative method for estimating the flexure–shear strength of reinforced concrete deep beams similar to one they derived for ordinary beams[19]. The flexure–shear strength calculations were derived mainly from the properties of the compression zone of the beam, and the deformation and equilibrium conditions. An iteration process was used to find the correct stress block.

The method was compared with experimental results published in the literature. The average of predicted to observed ultimate strengths was 1.06. It was proposed that the strain hardening of steel is important in permitting deep beams to attain their high strengths and this characteristic must be available in order to use this method effectively. This resulted in inevitable restrictions on the use of the available published data, which rarely includes information regarding the strain hardening behaviour of steel in tested deep beams.

Kumar

Kumar[20] presented a rigorous truss model for estimating the collapse load of deep beams. This was based on the assumption that deep beam behaviour is like an arch or truss, and so it was thought that a truss model could predict ultimate strength more accurately. The analysis carried out by Kumar on published data indicated that estimated values were not close to measured values, the average ratio of measured to estimated values being 1.3. However, its use was still recommended.

Marti

Marti[21] also developed a truss analogy based on the lower bound principles of the theory of plasticity. This method is intended for design of reinforced concrete members such as shearwalls and deep beams. Admissible stress fields are obtained by defining a truss composed of concrete struts and reinforcement ties which meet at nodal zones. Nodal zones are the biaxially or triaxially stressed regions of concrete

which mainly exist in regions close to load or support points. Nodal zones are assumed to be pin connections in the analogous truss. The geometry is revised and rebuilt iteratively in order to come close to measured ultimate loads. However, these methods do not appear to have been used for deep beam design, so that its validity is not assured.

Collins and Mitchel

Collins and Mitchell[22] have also developed a truss model for deep beam design called" A rational approach to shear design—The 1984 Canadian concrete code provisions". Their proposal is based on the flow of forces in the beam and locations of nodal zones. The nodal zones must be chosen large enough to ensure that the nodal zone stresses are less than the limiting stresses given by the Canadian Code. The limiting stress for upper and lower nodal zones are given $0.85.\varphi c.fc'$ and $0.75.\varphi c.fc'$ respectively, where φc is the the resistance factor for concrete ($\varphi c = 0.6$) The geometry of the truss is determined by locating the nodes of the truss at the points of intersection of the forces meeting at the nodal zones (Figure 2.4).

From these, the forces in the strut and ties of the truss can be determined by statics. Once the forces are determined, the required area of tension tie reinforcement is chosen. The tensile reinforcement must be effectively anchored to transfer the required tension to the nodal zone of the truss and reinforcement should be distributed over the lower nodal zone depth. A formula was also proposed to check the crushing of the strut.

For the design of shear reinforcement, the minimum criteria of the Canadian Code is recommended. According to this, the transverse and longitudinal reinforcement must be provided with a minimum volumetric ratio of 0.002 in each direction to control crack widths and to ensure ductility.

The authors did not analyse any deep beam, but they outlined the design procedure

by designing a deep beam. The also re-designed this beam using the empirical equations of ACI Code to examine the capability of their method.

Kotsovos

Recently Kotsovos[23] proposed a design method for both simply supported and continuous deep beams based on modelling behaviour by a "tied frame with inclined legs". He concluded that the load carrying capacity of reinforced concrete deep beams is associated with the strength of concrete in the region of the path along which the compressive forces are transmitted to the supports. He believed that experimental evidence indicated that the force in the tension reinforcement within the length of the horizontal projection of the inclined portion of the path was constant, so that the compressive force acting along the inclined portion of the path was also constant. Referring to Figure (2.5), moment equilibrium is given by:

$$Cz=Pa \qquad 2.5$$

where $z=(d-x/2)$ is a reasonably assumed value. This will yield the depth of the compression zone x, from which the compressive force, C, can be obtained. Since from equilibrium $C=T$, the required amount of steel can be calculated as:

$$As=T/fy \qquad 2.6$$

This method was applied to published experimental data and it appears that it only predicted reasonable values for simply supported beams with two point loads. For single span centrally loaded and continuous deep beams the results were less accurate. Thus the method is not yet sufficiently developed for use in design. However, this method will be compared with the direct design technique in Chapter Eight.

2.4.2 Experimental investigations.

Some of the most extensive investigations on reinforced concrete deep beams to date have been conducted at the University of Illinois, Stuttgart University, Coimbatore College India, New Mexico, Nottingham University, University of Cambridge, University of Glasgow, University of Alberta, and the University of Dundee.

de Paiva and Siess

de Pavia and Siess[24] tested a series of 19 moderately deep beams with L/D ratios varying from 2 to 4.0. The aim was to study beam behaviour in the transition between shallow and deep beams. The main variables were the percentage of reinforcement, concrete strength, the amount of web reinforcement, the span to depth (L/D) ratios and two types of web reinforcements (i.e vertical and bent–up bars). All beams were loaded at the third points. Anchorage was obtained by welding tension reinforcement at each end of the beam to 1/2 inch steel end bearing plates.

Behaviour was observed as follows:

1:– Three different modes of failure were observed from the tests as explained in Appendix A. Nine beams failed in flexure, five failed in flexure–shear and five failed in shear failure. Shear failures were attributed either to diagonal tension failure or to diagonal compression failure.

2:– The increase in concrete strength had little effect on beams failing in flexure, but increased the strength of those beams failing in shear. The increase of shear strength with increase of concrete strength was more noticeable with lower span to depth (L/D) ratios beams

3:– The addition of 1.42% of shear reinforcement had no effect on the inclined cracks, but seemed to produce a slight increase in the ultimate strength. There was also decrease in the ultimate mid–span deflection. Whereas vertical stirrups did not increase the ultimate load at all.

4:– The effectiveness of bent–up bars increased as inclination increased up to a value of $\alpha_1 = 62.7°$.

The ultimate flexural strengths for moderately deep beams were reasonably predicted using ultimate strength theory for shallow beams. In addition there was an increased value of the uniaxial compressive concrete strain at failure to 0.008in/in which confirmed the findings of earlier work carried out at the University of Illinois[25–28].

The inclined cracking load was reasonably predicted by Diaz de Cossio's[29] equation

$$V/b.d = 2.14\sqrt{fc'} + 4600.\rho.V.d/M \qquad 2.7$$

(It should be noted that this equation is intended for use with U.S. customary units i.e lbf).

For beams failing in shear, the ultimate strength was reasonably predicted using a formula derived by Laupa et al[30] for moderately deep beams and T− beams, when a correction factor was included to take into account the clear shear span to depth (X/D) ratio. Both these results and those of Laupa et al[30] indicated that a transition occurs at X/D equal to 1.0 (i.e at the transition from deep to shallow beams). Thus, the shear capacity of beams for X/D ratios less or equal 1 was given by:

$$Qult = 0.8(1-0.6(X/D)).(200+0.188fc'+21300\rho t).bD \qquad 2.8$$

where the quantity $\rho t = As(1+\sin\alpha)/bD$ is the total steel area crossing a vertical section between the loading point and the support, and α is the angle of inclination of bent up bars to the horizontal axis of the beam.

Ramakrishnan and Ananthanarayana et al

Ramakrishnan, Ananthanarayana and Obli[31] tested 12 single span deep reinforced concrete beams at P.S.G. College Coimbatore, India, under two point loading acting on the top edge. The aim was to study the modes of failure, the strengths and the load deformation behaviour and to compare the results with shallow beams. The major parameters were span to depth (L/D) ratio, percentage of tension reinforcement and the presence of a nominal amount of web reinforcement.

A linear relationship was developed between the ratio of measured ultimate load (Pu) to calculated ultimate load according to Whitney's theory (Pcu) and the depth to span (D/L) ratio for values between 0.94 and 2.0 i.e.

$$Pu = Puc\ (1+(1/L/D)) \qquad 2.9$$

This study concluded that design procedures were not adequate for predicting the

ultimate strength of deep reinforced concrete beams, and although Whitney's theory, with some modification, could serve immediate design needs, there was a need to explore a rational method for analysis and design which could fully explain the strength of deep beams.

Ramakrishnan and Ananthanarayana[32] extended this work by testing another 26 simply supported deep beams. The major variables studied were (L/D) ratio varying from 0.55 to 1.11 and different types of loading (i.e central point load, two point loads and uniformly distributed load). The beams were reinforced longitudinally with plain mild steel bars, and had little or no web reinforcement.

The major observations from these test results are summarized as follows:

1:– The majority of the beams failed in diagonal tension failure whereas 5 beams failed in flexure, 4 beams failed in flexure–shear and 3 beams failed in diagonal–compression failure. The various failure modes are summarized in Appendix A.

2:– The stiffnesses of the beams increased as the (L/D) ratio decreased, and concentrated loads produced relatively more deflection than the uniformly distributed loads.

3:– As the depth of a beam increased, the load was transmitted more directly to the support with a consequent reduction in bending stresses, thus forcing the beam to behave essentially as a tied arch.

4:– After the formation of inclined cracks, the beams still carried a considerable load. Hence the load corresponding to the ultimate stage was taken as the collapse load due to the splitting failure in the concrete struts formed by the diagonal tension crack.

From their test results, the following general formula for estimating the ultimate shear strength was developed i.e.

$$Pu = \beta' . k . ft' . b . D \qquad 2.10$$

where β' is a shear span coefficient ($\beta' = 2$ for a single span deep beam with two symetrical third point loads, single point or uniform loadings) and an empirical constant k is the splitting coefficient.

Leohardt and Walther's tests

Leonhardt and Walther[33] have carried out considerable research at the University of Stuttgart on the shear strength of simply supported and continuous deep beams and indirectly supported and loaded deep beams. Most of their work was reported in German and had not been translated into other languages, so up to 1970 it had not found its way into design codes. These tests covered deep beams having span to depth (L/D) ratios equal to 1 different arrangements of reinforcement including bent-up bars and inclined shear reinforcement, and bottom loadings. These results were included in the compilation of the CEB-FIP model in 1970 which proposed design recommendations for deep beams.

In some beams, the main reinforcement was concentrated over the bottom portion in the region of positive bending moment. Steel resulting from negative bending moment was divided into two halves, one was distributed over 0.2D to 0.8D from the bottom with bars being curtailed at 0.4L from the centre of intermediate support in both directions, the remaining reinforcement was distributed over a depth of 0.2D from top extending from the one end of the beam to the other. They concluded that the tension steel resulting from negative or positive bending moment should be calculated on the basis of the following lever arms:

$$Z = 0.6D \text{ for } L/D \geq 1$$

$$Z = 0.6L \text{ for } L/D \leq 1 \qquad 2.11$$

Leonhardt and Walther found that elastic solutions provide a good description of behaviour before cracking, but stresses measured after cracking differed significantly from the elastic stresses predicted by classical theory. In particular, actual stresses in the reinforcement of the bottom tensile chord were much smaller at the centre than

those predicted by elastic theory. Also the stresses in the tension reinforcement were approximately constant from one end of the beam to the other. Hence it was recommended that the main flexural reinforcement must be carried to the end supports without cutoff, and adequately anchored there. They suggested that this could be best accomplished with 180 degree hooks lying in the horizontal plane because vertical hooks appeared to cause some premature failure problems.

Crist's tests

Crist[34] tested 9 beams with span to depth (L/D) ratios varying from 1.6 to 3.8 under uniformly distributed loads. The common observed mode of failure was shear failure. Equations were derived based on his results and results of other researchers. These equations, slightly modified, then became the basis for the ACI Code[8] recommendations for estimating the shear capacity of deep beams.

He stated that the ultimate shear capacity of a deep beam was the sum of contributions from the concrete and steel, as follows

$$Pu = Vc + Vs \qquad 2.12$$

where Vc is the shear capacity of the concrete and Vs is the shear capacity of the web reinforcement.

The shear capacity of concrete was empirically derived as

$$(Vc/b.d) = [3.5-4/3(M/V)_c.(Ln/d)][1.9\sqrt{fc'}+2500(V/M)_c\rho.d] \qquad 2.13$$

(It should be noted that this equation is intended for use with U.S. customary units i.e lbf).

The second term in this equation represents the inclined cracking load. The critical section Xc is assumed to occur midway between the support and loading point for a concentrated load. For a uniformly distributed load, it is assumed to occur at:

$$Xc = 0.2L \quad \text{when } L/D \leqslant 5 \qquad 2.14$$

The shear capacity of the web reinforcement was developed considering shear friction along the inclined crack as illustrated in Figure (2.6). The shear analogy gives:

$$Vs=fy.d.\varphi'[(Av/sv).1/12(1+(Ln/d))]+[(Ah/sh).1/12(11-(Ln/d)] \quad 2.15$$

where Ln is the clear span of the beam, Av is the area of the vertical web bars, Ah is the area of horizontal web bars, sv is the spacing of vertical web bars and sh is the spacing of horizontal web bars.

This equation was used by Cristl[28] to calculate the shear carried by web reinforcement using the coefficient of friction $\varphi'=1.5$.

Kong et al tests.

Extensive research on solid and perforated deep beams made of normal and lightweight concrete has been carried out by Kong et al at Nottingham University[35– 40].

They tested 146 solid beams whose (L/D) ratios varied from 1 to 3 and whose clear shear span to depth (X/D) ratio varied from 0.23 to 0.7. One hundred beams were made from normal weight concrete and the remainder from lightweight concrete. The other main parameters were the influence and effectiveness of the type and amount of web reinforcement on ultimate strength. The ultimate aim of this exhaustive study was to develop an ultimate shear strength formula for deep beams. Kong and Robins[35,36] reviewed existing literature, and concluded that existing methods had shortcomings in that the influence and effectiveness of shear reinforcement had not been properly investigated, and that ultimate shear strength formulae were based on concrete properties irrespective of L/D or X/D ratios.

Their major observations for solid deep beams were as follows:

1:– The effectiveness of vertical and horizontal web reinforcement was dependent on the L/D and X/D ratios. For very deep beams vertical web reinforcement had no major influence on the strength, but horizontal web reinforcement, if closely spaced near the beam soffit, did effect the ultimate strength. For moderately deep beams

with the L/D ratios greater than 1.5, vertical web reinforcement was found to be more effective than horizontal reinforcement.

2:— In all the beams, inclined web reinforcement increased the ultimate strength and improved serviceability behaviour. The deflection in such beams was also smaller than for other types of web reinforced beams.

3:— The deflections of beams with no web reinforcement was higher than for beams with web reinforcement.

4:— The diagonal cracking loads and the ultimate shear strengths of lightweight concrete beams were lower than those for normal weight concrete beams of comparable concrete strengths. Therefore a formula for normal weight concrete cannot be applied to lightweight concrete deep beams.

5:— It was observed that the clear shear span to depth (X/D) ratio was a more important parameter than span to depth (L/D) ratio for all beams.

They put forward several formulae as their research progressed. The final form of their formula for simply supported deep beams, and calibrated on all their test results, is made up of a contribution from the concrete and steel as follows:

$$Qult = [C1\ (1 - 0.35(X/D)).ft'.b.D + C2 \sum^{n} A(y/D)\sin^2\alpha]10^{-3} \quad 2.16$$

where

Qult = is the ultimate shear strength of the beam in kN.

C1 = is an empirical coefficient;

= 1.4 for normal weight concrete

= 1.0 for lightweight concrete

C2 = is an empirical coefficient;

= 130N/mm^2 for normal weight concrete

= 300N/mm^2 for lightweight concrete

b = breadth or thickness of beam in mm.

D = overall depth of beam in mm

A = area of the individual web bars;for the purpose of this

equation main longitudinal bars are also considered as web bars (mm^2).

y = is the depth measured from the top of the beam to the point of intersection of an individual web bar and the line joining the inside edge of the bearing block at the support to the outside edge of the loading point (mm).

α = is the angle between the web bar being considered and the line described above, as shown in Figure(2.7) within the range $\pi/2 \geqslant \alpha \geqslant 0$

n = total number of bars, including the main longitudinal bars that cross the line described in definition of y. The quantity $A(y/D)\sin^2\alpha$ is summed for all n bars.

Manual et al

Manual et al[41,42] tested 24 reinforced concrete deep beams. The major objectives were to isolate the more influential parameters of span to depth (L/D) ratio, clear span to depth (X/D) ratio and the effectiveness of the web reinforcement in controlling the inclined crack. From this study, it was concluded that the ultimate strength of deep beams was controlled by the X/D ratio and the diagonal crack width was controlled by placing vertical or inclined stirrups midway between the loading and support point. In addition Manual proposed a method for simply supported deep beam analysis based on the truss analogy[43].

Lin's tests

Lin[2] tested 11 simply supported reinforced concrete deep beams under central concentrated top loads, with L/D ratios of 1.8 and 0.9. Other variables were the concrete strength and the orientation of the main reinforcement. The main object of this study was to test the applicability of the direct design technique for deep beam design.

The observed behaviour was as follows:

1:— The strain distribution was found to be approximately linear when the L/D ratio was 1.8, and not linear when L/D was 0.9.

2:— Ultimate strength was found to be dependent on the concrete strength. An increase of $16N/mm^2$ in the concrete strength caused a 37% increase in ultimate strength for beams whose L/D ratio was 1.8. An increase of $31N/mm^2$ in the concrete strength increased the ultimate strength of beams whose L/D was 0.9 by 37% also.

3:— Skew reinforcement was found to be more effective than orthogonal reinforcement in controlling the crack width, reducing deflections and increasing the serviceability and ultimate strengths.

4:— Four of the beams failed by splitting of the concrete near the support and seven failed in shear. The main cause of such splitting failure was probably the high compression force in the support region and the lack of confinement of concrete beyond the region where the reinforcement was terminated.

Smith et al

52 single span reinfored concrete deep beams under two point loads were tested by Smith et al and Smith and Vantsiotis[44]. The major objectives were to study the effect of vertical and horizontal web reinforcement, shear span to depth (X/D) ratio on inclined cracks, ultimate shear strengths etc. The results indicated that web reinforcement produced no effect on the formation of inclined cracks and that vertical web reinforcement moderately improved the ultimate shear strength, but the addition of horizontal web reinforcement had no influence. They concluded that web reinforcement would not increase the ultimate shear strength by more than 30%.

MacGregor et al

MacGregor et al[45—47] tested altogether 28 beams, 6 of them were simple and 22 were two span continuous deep beams. Four different span to depth (L/D) ratios were studied, i.e. 2.1, 3.5, 4.2 and 5.25. Other main parameters studied were a/d ratio,

web reinforcement arrangements, continuity conditions and the effect of the concrete strength on the ultimate strength.

Each shear span was reinforced with a different arrangement of web reinforcement, four different arrangements were studied for two span continuous beams. The lengths of the beam were kept constant and depth and size of the loading column was varied to meet the desired shear span to depth (a/d) ratios.

When the first failure of any shear span of the beam occurred, the beams were then retested until the other shear span failed. In this process of retesting, beams were externally reinforced by steel stirrups consisting of a yoke above and below the beam with 12 tie rods of 3/4 in. diameter acting as stirrups, running from one yoke to the other.

The major observations for all the beams were as follows:

1:— The influence of vertical web reinforcement was significant in increasing the ultimate strength and improving the ductility. The beams which were reinforced with heavy vertical stirrups exhibited ductile failure behaviour, whereas all the other beams which were reinforced with other types of web reinforcement failed in a brittle manner.

2:— In very deep beams the steel strains in the bottom flexural reinforcement were approximately uniform throughout the entire length of the beam. The top steel was always in tension except when a/d was equal to 2.5 (i.e L/D was equal to 5.25).

Since flexural cracks over the intermediate support did not appear first, it would appear that positive bending moments were always higher than the negative bending moments.

3:– The beams which were reinforced with horizontal web reinforcement showed earlier cracking and wider cracks in comparison to beams having vertical stirrups of similar shear span to depth (a/d) ratios.

4:– The final failure was in a shear mode. After the formation of inclined cracks, the beams behaved as a "truss" and "tied arch", and took considerably higher loads before failure. This is due to the reserve strength of steel and the contribution of dowel action and aggregate interlocking in transfering shear.

5:– Simple spans were stronger than continuous beams for lower a/d ratios, whereas the reverse was true for high a/d ratios.

6:– The strength of the beam having a/d equal to 1.83 (i.e L/D equal to 4.2) dropped close to $0.17\sqrt{fc'}$ suggesting that the transition from shallow beam to deep beam behaviour occurs at or near a/d equal to 1.83.

The primary aim of these bench mark tests on continuous deep beams was to develop a physical model which could be used for deep beam analysis and design. In order to do so a plastic truss model was developed which was based on Thurliman[48], Marti[21], Jenson[49], and Nielson[50]'s work on the plasticity of concrete. This model was used to analyse the tested beams. However, the success of the model depended on the concrete effectiveness factor, ν', which was left to the analyst to choose so that the experimental and theoretical results were more closely matched. How this was achieved was not fully explained.

Nevertheless, compared with the ultimate shear strengths predicted by the ACI Code (using the upper bound equation), the plastic truss model was in closer agreement to experimental values.

Subedi et al

Subedi et al[51] tested 19 single span deep beams with span to depth (L/D) ratios varying from 1 to 3. He concluded from these test results that the CIRIA Guide 2 ought to cover deep beams whose L/D ratios are greater than 2.0. Subedi [52] also proposed a method for the analysis of deep beams which is based on equilibrium and compatibility considerations. However, factors such as shear transfer across diagonal cracks and dowel action in the reinforcing bars were omitted from the main equation, which could explain why it did not adequately predict his own or other experimental results.

2.5 Reinforced concrete perforated deep beam studies.

Openings in the beams are generally provided for utilities such as ducts and pipes as well as other essential requirements. A knowledge of the behaviour of beams with web openings is therefore essential for design. However deep beams with web openings is not yet covered by major codes of practice, such as the ACI Code[8], CEB– FIP Model Code[53], or the British Code of practice BSCP8110[54]. Although the CIRIA Guide 2 made provisions for openings, these must not interrupt the load path.

2.5.1 Theoretical investigations.

Uhlmann[11] used an elastic finite difference method to study the state of stress around a rectangular opening. Refering to Figure (2.8), if ox and oy are the average directions of the maximum and minimum principal stresses respectively in the region of the opening when the member is regarded as unperforated, Uhlmann showed that the effect of an opening on the unperforated stress distribution is as follows:

(i) The intercepted load path deviates around the opening on each side, but produces a stress rise along those edges of the opening which are approximately tangential to the unperforated lines of stress (near corners A and A').

(ii) A force of the opposite sign is induced along the edge of the opening approximately perpendicular to the unperforated lines of stress (near corners B and B').

Uhlmann was then able to determine the design tensile force from which the required amount of the reinforcement could be calculated. This was achieved by considering the values of increased force parallel to the original stress direction, and the induced force perpendicular to the original stress direction, in terms of total force intercepted by the opening. He suggested that reinforcement should be proportioned according to the predicted tensile force but gave no limit to the size of the opening and imposed no restriction on its location[4,11].

The provision made in the CIRIA Guide[5] for openings is also based on elastic analysis and is a similar to the one proposed by Uhlmann. However the effect of the size and location of the opening on the stress distribution is considered. The design rules only allow admissible openings, i.e openings which to a large extent do not interrupt the load path. The dimensions of the opening must not be greater than 0.2 times the width of the band in which stress is locally concentrated.

If the opening satisfies the criterion of admissibility, then reinforcement calculations are made by considering the opening to be surrounded by four simply supported deep beams subjected to the resolved forces set up within the primary deep beam. An appendix is given in CIRIA Guide 2 containing principal stress diagrams from which loads can be calculated.

No guidance appears to exist for design of openings which severely interrupt the load path.

2.5.2 Experimental investigations.

Kong and Sharp et al tests

Kong and Sharp[55–59] tested 73 simply supported beams with openings, 56 were lightweight concrete beams and 17 normal weight beams. The beams had spans of 1500mm, 1125mm and 750mm, an overall depth of 750mm and a thickness of 100mm. A wide range of sizes and locations of openings were studied with several

arrangements of web reinforcement. The L/D ratios were 1.0, 1.5 and 2.0, and the X/D ratios were 0.20, 0.25, 0.3 and 0.4.

The major observations were as follows:

1:— Beam behaviour was found to depend on the extent to which the opening interrupted the load path. Strength reduction was dependent on the size of the opening and its location in the beam, the greater the interception of the load path, the greater the reduction in shear strength.

2:— Three different modes of failure were observed and these were also related to the extent to which the web opening interrupted the load path as illustrated in Figure (2.9).

(a) When the web opening was clear of the load path, failure mode 1 occurred and the strength of the beam was similar to that in solid deep beams.

(b) When the opening interrupted the load path between the loading and the supporting points, either failure mode 2 or 3 occurred, as illustrated in Figure (2.9).

3:— The order of the crack development was found to depend on the size and location of the opening. Crack widths increased the more the web opening intercepted the load path.

4:— Web reinforcement was found to be significant in controlling crack widths and in protecting both the diagonal regions above and below the opening. Inclined web reinforcement had significantly more influence than vertical and horizontal web reinforcement, and was particularly effective for crack width control and increasing ultimate strength.

A structural idealization using a truss model was proposed based on the observed behaviour as shown in Figure (2.10). According to this idealization, the load is mainly transmitted along ABC and partly along an upper path AEC. In the absence of the web opening the upper and lower paths become one, being the natural path joining the loading and reaction points. A formula developed by Kong et al for solid deep

beams was extended to estimate the ultimate shear strength of deep beams with web openings as:

$$Qult = C1\left[1-0.35(k_1X/k_2D)\right]f't.b.k_2.D + \sum^{n}\lambda.C2.A.(y/D).\sin^2\alpha \quad 2.17$$

where

k_1, k_2 = coefficients defining the position of an opening.

λ = is the empirical coefficient equal to 1.5 for web bars and 1.0 for main bars.

y = is the depth at which a typical bar intersects a typical diagonal crack - either AE of the upper path or BC of the lower path.

α = is the angle of intersection between the reinforcing bar and the strut AE or BC.

All other symbols are the same as in equation (2.16).

Kubik's tests

Kubik[59,60] tested 8 large scale simply supported deep beams at the University of Cambridge. The aim was to support the previous tests of Kong and Sharp[55–56] by testing more practically sized beams in order to develop a model for predicting the ultimate strengths of deep beams with web openings. The beams were 4000*1800*250mm with a clear span of 3500mm. The specimens were therefore approximately $2^1/_2$ times the size of beams tested by Kong and Sharp. The volume of the reinforcement was approximately scaled up from the small scale specimens. Four 20mm deformed bars were used as flexural reinforcement, and were anchored at the ends by 90° bends. In the small specimens one 20mm diameter deformed bar was used as main longitudinal steel and was anchored to external blocks at the ends. A single size of web opening in two different locations in the shear span was studied.

The major observations were as follows:

1:— The cracks and modes of failure were fairly similar to those reported by Kong and Sharp and depended on the location of the web opening. New crack types g, h and k which formed within the web of the beam as shown in Figure (2.11) had important influence on the failure of the beam. These crack types were not indentified by Kong and Sharp. These cracks were widest at points close to their mid length, reducing to zero at both ends and were referred to as splitting cracks.

2:— Inclined web reinforcement was found to be more effective than orthogonal reinforcement mesh of horizontal and vertical bars. Using inclined reinforcement in the web of the beam the splitting cracks above and below the opening were more effectively restrained. This observation agrees reasonably well with Kong and Sharp's conclusion regarding the contribution of web reinforcement in the region above and below the opening.

3:— Different failure modes observed in the tests are shown in Figure (2.9) and (2.12). Figure (2.9) shows that for openings outside the load path failure occurred by separation along the planes above and below the opening (failure mode 1) which is similar to shearing failure of a deep beam without an opening. The other failure modes shown in Figure (2.9) were observed when the opening intercepted the load path. Another special type of failure occurred as shown in Figure (2.12— a), made up from a crack from the top inside corner of the opening to the loading point, a crack from the top outside corner to the beam end and either a crack running from the beam soffit towards the inside bottom corner of the opening, or a crack running between the inside face of the support and inside bottom corner of the opening (Figure (2.12— b)).

Kubik proposed an idealised deformation model at failure, based on the same ideas as Kong and Sharp[55— 58], which is only applicable to deep beams in which openings intercept the load path. The proposed model was based on the rotation of three distinct blocks A, B, C with a fourth block D moving downwards as illustrated in Figure (2.13). The force interaction between the blocks was replaced by one moment and two forces at each of the hinges 1 to 4. From equilibrium requirements the

horizontal force H is same at all hinges; the sum of the vertical forces Q_T and Q_B acting at the hinges are equal to the applied load Q. In essence, Q_T represents the portion of the applied load carried by the beam above the opening and load path, whereas Q_B represents the load carried below the opening. Q_T and Q_B were then derived in terms of the hinge moments M_1, M_2, M_3 and M_4, and the geometrical properties of the beam, by:

$$Q_T = \frac{M_1(h_o + h_L) + M_2 h + M_3 h_u}{a_u(h_o + h_L) - h_u(a_L - x_o)} \qquad 2.18$$

$$Q_B = \frac{M_3 + M_4}{a_L} - \frac{h_L . M_1(a_L - x_o) + M_2 . a + M_3 . a_u}{a_L a_u(h_o + h_L) - h_u(a_L - x_o)} \qquad 2.19$$

$$H = \frac{M_1(a_L - x_o) + M_2 . a + M_3 . a_u}{a_u(h_o + h_L) - h_u(a_L - x_o)} \qquad 2.20$$

The hinge moments are determined by considering the regions around the opening as shown in Figure (2.14). The ultimate moment of the hinge is assumed to occur when the strain perpendicular to the hinge at the far end of the region from the hinge reaches the yield strain of the reinforcement. The total hinge moment is assumed to be equal to the sum of the moments exerted by all reinforcing bars in that block, i.e.

$$M = \sum^{n} \frac{A . fy . y^2 . \sin^2\alpha}{h \sin\theta} \qquad 2.21$$

The ultimate strength can therefore be found once the hinge moments have been determined at incipient collapse.

If the hinge areas are under-reinforced in flexure, then the moments $M_1 - M_4$ will reach their ultimate values at failure, and the above equations will produce the ultimate strength of the beam.

However, it is possible that premature shearing failure may occur in any of the regions shown in Figure (2.14) before the ultimate moments at the hinges have been reached. Kubik proposed the following formulae to check for premature shear failures.

Above the opening it was assumed that failure occurred along the plane shown in

Figure (2.14– a) when Q_T exceeds $(Q_T)_{S1}$, given by

$$(Q_T)_{S1}=C1[\,1-0.35(x_u/h_u)\,]ft.b.h_u+C2.\sum_n A(y_u/h_u).\sin^2\alpha_u \qquad 2.22$$

In the region between the end of the beam and the web opening failure occurs along the plane shown in Figure (2.14– b) when the horizontal force H exceeds the shear strength H_S, given by

$$H_S=C1[\,1-0.35(h_o/t)\,]ft.b.t+C2\sum_n A(y_t/t).\sin^2\alpha_t \qquad 2.23$$

Failure below the opening was assumed to occur along the plane shown in Figure (2.14– c) when the load Q_B exceeds $(Q_B)_S$

$$(Q_B)_{S2}=C1[\,1-0.35(x_L/h_L)\,]ft.b.h_L+C2\sum_n A(y_L/h_L).\sin^2\alpha_L \qquad 2.24$$

Kubik then described a procedure for checking the cause of the failure due to either flexural or premature shearing failure by comparing the predicted strengths from equations (2.18) to (2.20) with (2.22) to (2.24).

Comparisons made with other published data and Kubik's own data indicated that his model produced results which were fairly conservative. Also a clear design procedure was not presented and it would appear that reinforcement was provided in a fairly arbitrary way in order to study the reslting behaviour.

Memon's tests

Memon[4] tested seven deep beams, six of them perforated and one solid. The beams were designed by the direct design technique. The main variables were X/D ratios of 0.47, 0.35 and 0.32, concrete strength, and size and location of openings.

The major observed behaviour were as follows:

1:– When the shear span to depth (X/D) ratio was 0.2 to 0.32 the influence of horizontal reinforcement was more noticeable than for vertical reinforcement.

2:– Ultimate strength increased with increasing concrete strength.

3:— Openings nearer the beam soffit had less influence on the ultimate strength because they less interrupted the load path, the strength of such beams being similar to solid beams. Hence, he recommended the best location for openings was near the beam soffit.

4:— High steel strains were observed in the bottom main reinforcement within the regions of the shear spans. High compressive forces in the region of supports probab-ly resulted in an increased horizontal tension due to the Poisson's effect thus causing these higher strains.

5:— Four beams failed due to shear failure, two due to bearing failure, and one due to splitting and spalling failure. Those beams which failed in bearing was probably due the fact that high forces developed in the compression strut causing severe cracking and crushing at the support points, suggesting that direct design procedure adopted by Memon had led to an over provision of reinforcement elsewhere in the beam.

2.6 Design guides for deep beams.

2.6.1 Portland cement association (PCA) method.

This method for deep girder design is based on the elastic analysis of Franz Dischinger[6] and it is applicable for a height to length ratio of 2/5 or more for continuous girders and 4/5 or more for single span girders. It contains detailed recommendations for most loadings. Design is carried out using a number of charts. The design method is briefly explained as follows:

Step 1 : Calculation of Characteristic ratios ϵR *and* βR

$$\epsilon R=(C/L)$$

$$\beta R=(D/L) \qquad 2.25$$

where ϵR and βR are the characteristic ratio of support to the span of the beam and overall depth to the span of the beam respectively.

For single span girder, with a concentrated load at the centre of span ratios

$$\epsilon R=(C/2L)$$

$$\beta R=(D/2L) \qquad 2.26$$

Step 2 : Calculation of mid-span longitudinal reinforcement

Knowing ϵR and βR, a tension coefficient is obtained from an appropriate design curve (reported in Figure 2.15) so that the tensile force to be resisted by longitudinal reinforcement can be calclated. Thus

T=Coefficient x Load at centre of span

$$As = T/fs \qquad 2.27$$

where fs is the allowable stress of steel

The PCA pamphlet states that vertical stirrups have no function and that therefore do not need to be provided.

Step 3 : Calculation of reinforcement over the centre of interior support.

Before calculating the tension reinforcement over the intermediate support the tensile stresses are to checked from Figure (2.16), if the outcome is higher than the tensile strength than reinforcement is required. In a similar way reinforcement is calculated from the appropriate curves of Figure (2.15).

Step 4: Check of shear force with beam width condition

It is recommended that the shear force is checked to ensure that the cross section has an adequate width. The shear in flexural members is calculated by conventional procedures using a unit stress defined as:

The unit stress is computed as

$$8.V/7.b.D \geqslant (v(1+5\beta R)/3 \qquad 2.28$$

where v is the allowable shear stress for the shallow beams. When βR is greater than 2/5 then the value of v, allowable shear stress, must be adjusted to 2v for $\beta R = 1$ accordingly.

2.6.2 CEB– FIP design recommendations.

CEB– FIP[53] put forward design procedures for both simple and continuous deep beams in 1970. According to this, a beam is categorized as a deep beam when its span to depth (L/D) ratio is less than 2 if simply supported and 2.5 if continuous. For simplicity only the multi– span deep beam design procedure is given here.

Step 1 Calculation of principal longitudinal reinforcement

This method also uses the lever arm criterion for principal longitudinal reinforcement

calculations similar to Leonhardt and Walther as follows:

$$z = 0.2(L+1.5D) \quad \text{for } 1 < L/D < 2.5$$

$$z = 0.5L \quad \text{for } L/D<1 \qquad 2.29$$

where L is the effective length and D is the total depth of the beam

It is clear from these equations that when the height is greater than the length, then the lever arm is dependent on the length of the beam. Alternatively, when the span to depth (L/D) ratio is between 1 and 2.5, the lever arm is dependent on the depth and length of the beam. CEB– FIP indicates that the moment over the interior support is always smaller than that in a comparable beam of normal dimensions.

The principal longitudinal reinforcement for positive and negative bending moment is then determined by the equation:

$$As=(M.\gamma m)/(fy.Z) \qquad 2.30$$

where γm is the material partial safety factor (i.e $\gamma m= 1.15$ for steel)

Step 2: Positioning of the principal longitudinal reinforcement

Principal tension reinforcement should not be curtailed and must be anchored at end supports. The positive principal tension reinforcement should be uniformly distributed over a depth equal to 0.25D– 0.05L, measured from the beam soffit (in this expression the maximum value of D is limited to L). One half of the principal tension reinforcement resulting from the negative bending moment over the interior support should be extended over the full length of the spans and uniformly distributed over a depth of 0.2D from the beam top. The other half may be stopped at either 0.4D or 0.4L and is uniformly distributed over a depth of 0.6D in between 0.2D from the bottom to 0.2D to top. It also recommends the use of smaller diameter bars which give better cracking control.

Step 3: Check on shear

CEB– FIP does not give any direct method for calculating shear reinforcement, but it states that the shear due to permanent and imposed loads should be determined as for normal beams. In addition the design shear force should not exceed:

$$V=0.10.b.D.fc' \qquad 2.31$$

When the height is greater than the span length, then L replaces D.

Step 4: Shear reinforcement calculations

For top loaded beams it is recommended that an orthogonal reinforcement mesh be provided as web reinforcement. The amount is expressed in terms of the percentages of cross sectional area, 0.25% in each direction for mild steel and 0.20% for high yield strength steel. It is also suggested that horizontal shear reinforcement in the orthogonal mesh be at a smaller spacing near the supports.

2.6.3 ACI Code design recommendations.

In 1971 the ACI Code[8] for the first time provided special provisions for the shear design of deep beams. It recommended that the Portland Cement Association's pamphlet be consulted if flexural design was required. The ACI procedure emphasises that the shear capacity provided by both the concrete and web reinforcement can resist the shear force. The provisions apply to deep beams whose span to depth ratios are less than 5, and which are loaded on the top or compression face. The calculations are based on critical sections, which are defined differently for concentrated and uniformly distributed loaded beams. For concentrated loads, the critical sections are taken mid-way between the load and support face, whereas for uniformly distributed loaded beams they are assumed to be at 0.15Ln from the support, where Ln is the clear span distance to the face of the support.

The nominal shear stress vn is determined from the design shear force V by

$$vn = (V/\omega.b.d) \qquad 2.32$$

where ω is the capacity reduction factor and is taken as 0.85, b is the width of the beam and d is the effective depth of the beam. To ensure that the beam dimensions are satisfactory, the following checks are made:

$$vn \geq 8\sqrt{fc'} \qquad \text{for } Ln/d < 2$$

$$vn \geq 2/3(10+(Ln/d)).\sqrt{fc'}.b.d \qquad \text{for } 2 \leq Ln/d \leq 5 \qquad 2.33$$

where fc' is the characteristic concrete cylindrical compressive strength.

The nominal shear stress vc carried by concrete is given by

$$vc=[3.5-2.5(M/V)1/d)][1.9\sqrt{fc'}+2500\rho(V.d/M)]$$

$$\}2.5[1.9\sqrt{fc'}+2500(V.d/M)] \quad 2.34$$

where M is the design bending moment at the critical section, ρ is the ratio of the main steel area As to the area of concrete (b.d).

The use of shear reinforcement is obligatory irrespective of the values of vn and vc as calculated above. It recommends an area of vertical reinforcement Av which must not be less than 0.0015b.Sv, where Sv$\geq$ d/5, nor 18in. The area of horizontal web reinforcement Ah must not be less than 0.0025b.Sh, where Sh $\geq$ d/3 nor 18in. Alternatively if vn exceeds vc then web reinforcement must be provided to satisfy the following equation:

$$[Av/Sv][(1(Lw/d))/12]+[Ah/Sh][(11-(Lw/d)/12]=((vn-vc).b)/fc' \quad 2.35$$

2.6.4 CIRIA Guide 2 design recommendations.

These recommendations owe much to the work of Leonhardt and Walther[33] and Kong et al[35–40,55–60]. Its design procedure is similar to CEB–FIP as explained earlier.

Step 1: Calculation of Longitudinal Reinforcement

Longitudinal reinforcement is calculated from

$$As=(M/0.87.fy.Z) \quad 2.36$$

where M is the design moment and Z is the lever arm which is equal to 0.2L+ 0.3D for continuous deep beams. D is the effective height of the beam.

Step 2: Distribution of Longitudinal Reinforcement (Sagging Moment)

It is recommended that the reinforcement be extended from end to end of a beam and be distributed over one fifth of the beam depth from the beam soffit. The bars must be anchored beyond the face of the support to develop 80% of the maximum ultimate force beyond the face of the support and at or beyond a point 0.20L from the face of the support to develop 20% of the maximum force.

Step 3 Distribution of Longitudinal reinforcement (Hogging Moment)

Half of the reinforcement calculated from the hogging moment should be extended over the full length of the adjacent spans and may be counted as part of the

minimum web reinforcement. This is distributed over a depth of 0.20D from the beam top. The remaining reinforcement must be curtailed at a distance 0.4L from the face of the support. The distribution is given in Figure (2.18).

Step 4: Shear Reinforcement Calculations

The CIRIA Guide does not given any criteria for shear reinforcement, but refers to Clauses 3.11 and 5.5 of BSCP8110[54]. The amount of web reinforcement should not exceed the recommendations of the British Code.

2.6.5 General conclusion.

In the light of this review of design methods, the following general conclusions may be drawn:

1:– It appears that the majority of design methods are based on elastic analysis using a factor of safety on the material's performance, which leads to the measured ultimate loads being higher than the design ultimate loads. This is because the reserve strength of steel, and the contributions of dowel action of main reinforcing bars and aggregate interlocking in shear transfer are ignored.

2:– Design procedures for continuous deep beams are extrapolated from simply supported deep beam studies and earlier elastic design methods. Tests have shown that in a continuous deep beam the bottom and top chord always take tensile forces but the force in the top chord is less than the bottom one. Therefore, the proportions of reinforcement based on elastic methods is not quite accurate for continuous deep beam design.

3:– In deep beams, a neutral axis appears more than once. Hence there is no clear idea of a moment arm with which to calculate the principal tension reinforcement.

4:– Shear reinforcement is mostly provided on ad hoc basis and there is no formulae to calculate its value except by the direct design method.

5:– The design of deep beams with web openings has not yet been covered by the majority of codes. CIRIA Guide 2 does cover the design of deep beams with web openings, but when an opening interrupts the load path the CIRIA Guide is not valid.

6:— Recent applications of plastic truss models suggest that they are better design tools, although shear reinforcement is still provided on an ad hoc basis. Moreover, it is not yet known whether these techniques have actually been used to design any deep beams. Thus, there is no clear idea how well these methods would behave in practice at serviceability or ultimate limit state.

2.7 Direct design technique.

In recent years the direct design technique has been examined for the design of a large variety of structures i.e slab column connection, beams under torsion and bending, deep beams and reinforced concrete slabs etc. The technique has a sound theoretical framework based on the theory of plasticity and so far has proved satisfactory in both serviceability and ultimate stages. The application of the direct design technique to deep beams has been undertaken by Lin[3] and Memon[4] who have demonstrated its potential as a useful design tool because of this potential, it is being further examined in this thesis will be fully explained and reviewed in Chapter Five. However, some of its other advantages learned from the previous studies are listed as follows:

a: It designs both web and main reinforcement automatically, It includes a procedure for skew reinforcement. It distributes reinforcement in a natural way according to the flow of applied stresses existing in structure, rather than on arbitrary basis.

b: It has good cracking control in addition to satisfactory behaviour at serviceability and ultimate limit states.

c: Any geometrical shape can be handled easily, for example beams with web openings, providing extra reinforcement is used in zones of high stress concentration.

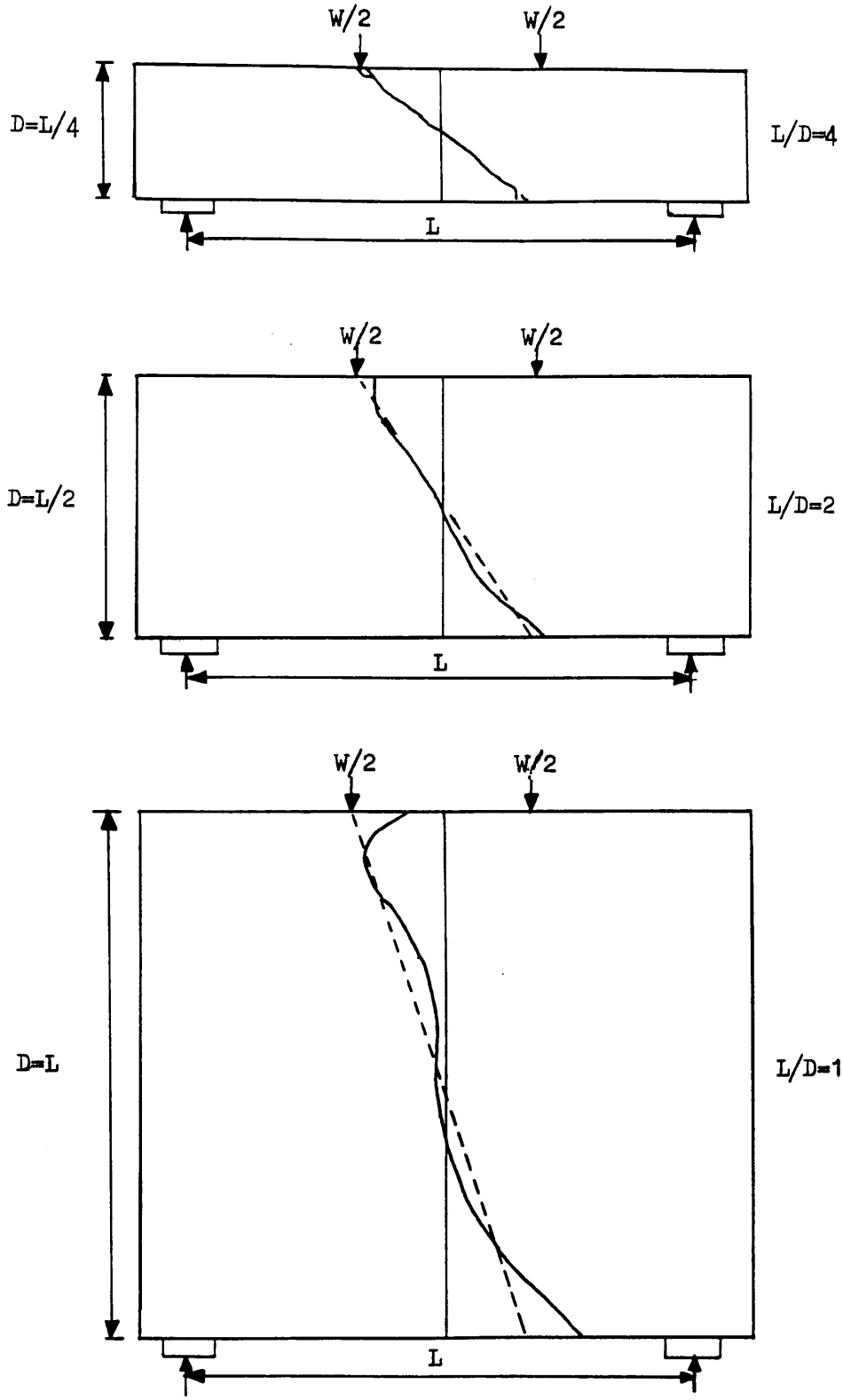

Figure(2.1) Theoretical stress distribution for varying L/D ratios.

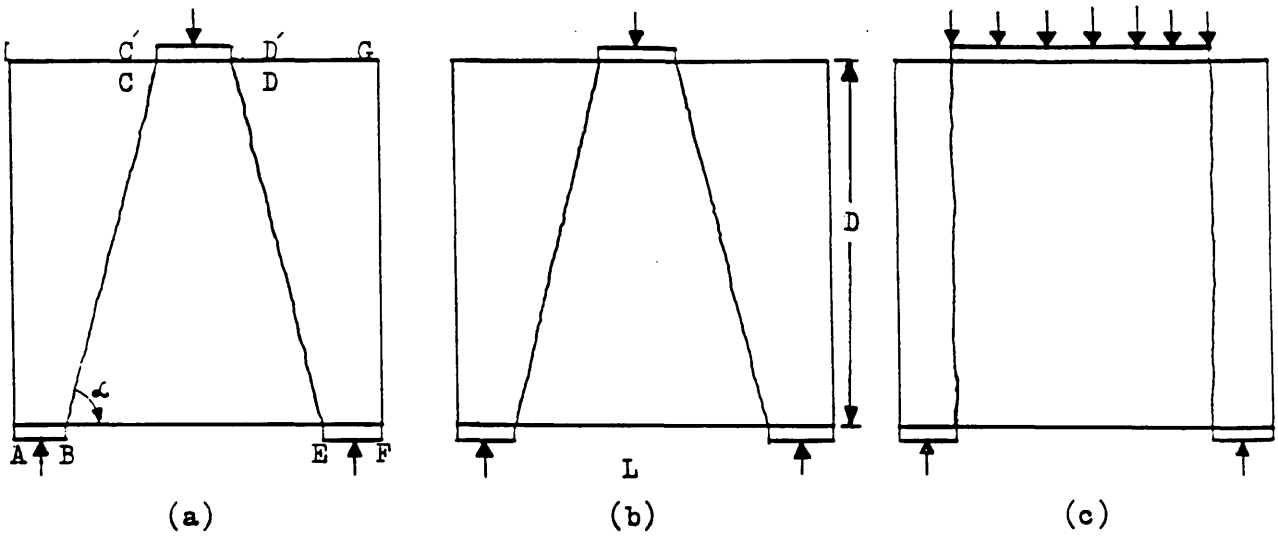

Figure(2.2) Typical crack pattern in deep reinforced concrete beams.

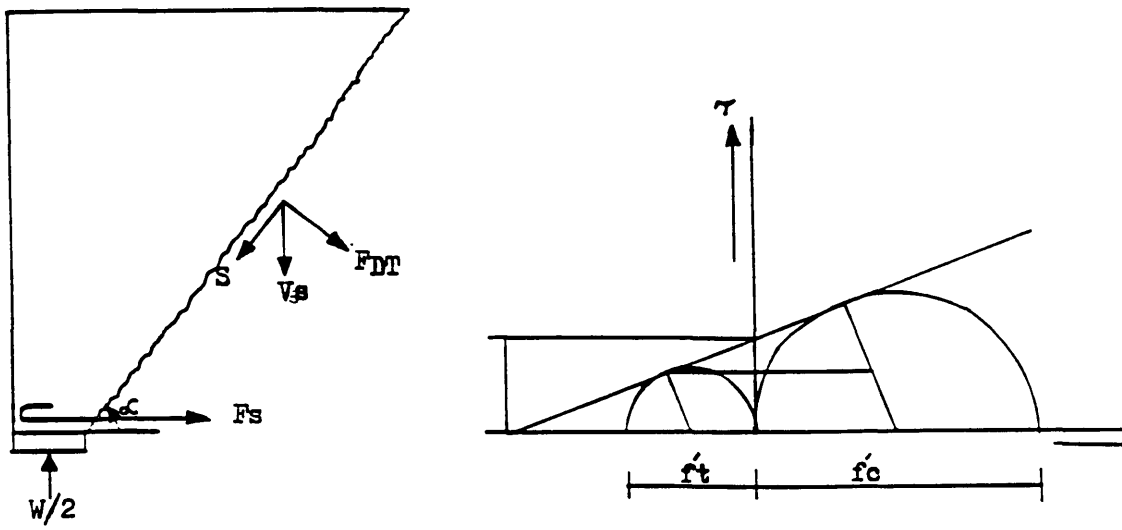

Figure(2.3) Derivation of Varghese and Krishnanmoorthy's ultimate load equation.

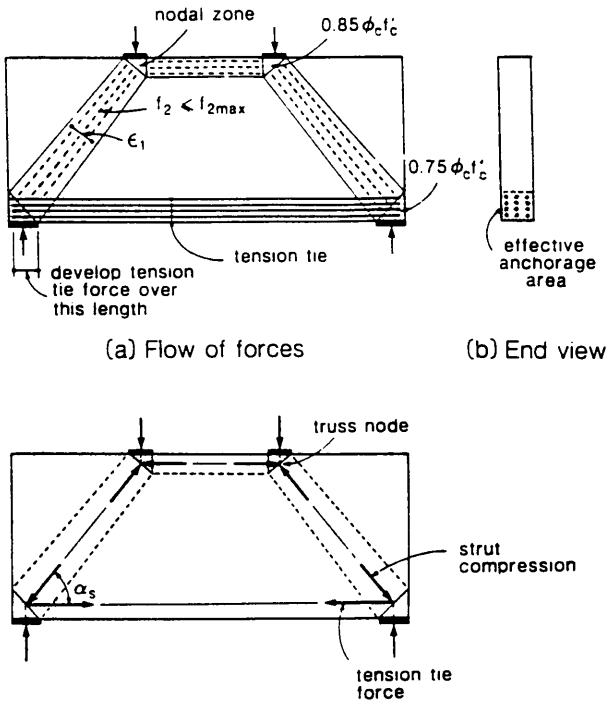

Figure(2.4) Strut and tie truss model for a deep beam.

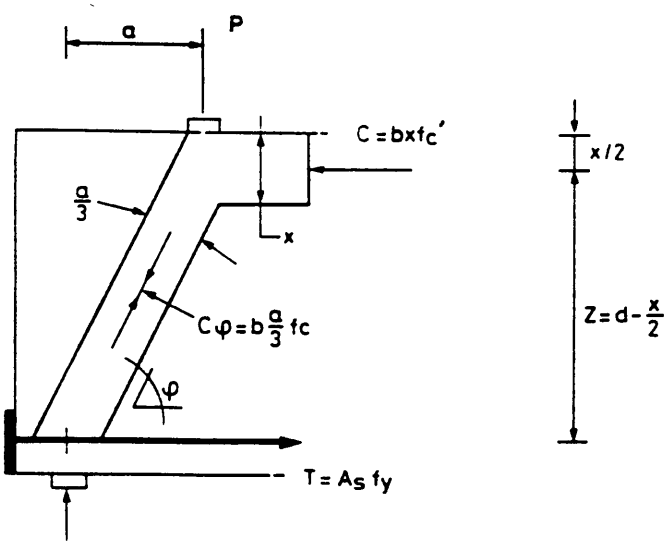

Figure(2.5) Proposed method for designing the RC deep beams.

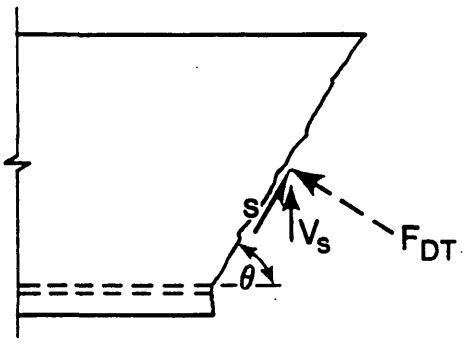

(a) Forces on Inclined Crack Plane

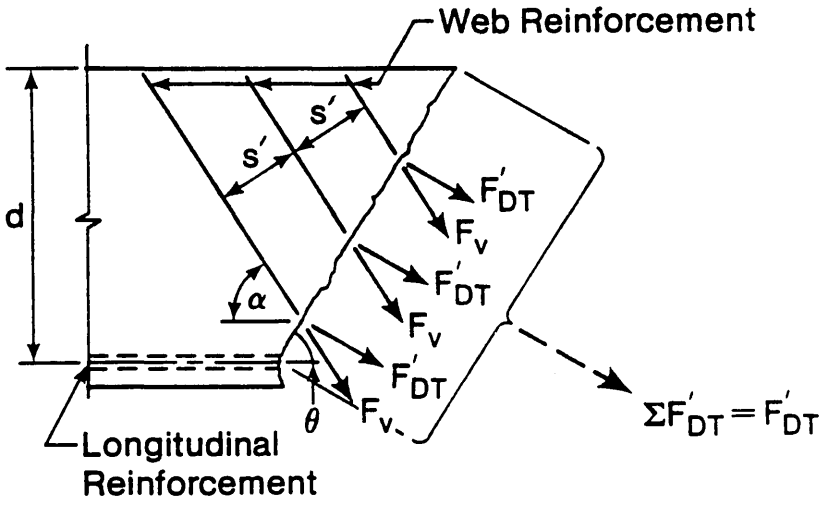

(b) Forces in Stirrups Along Inclined Crack Plane

Figure(2.6) Derivation of equations for web reinforcement in deep beams.

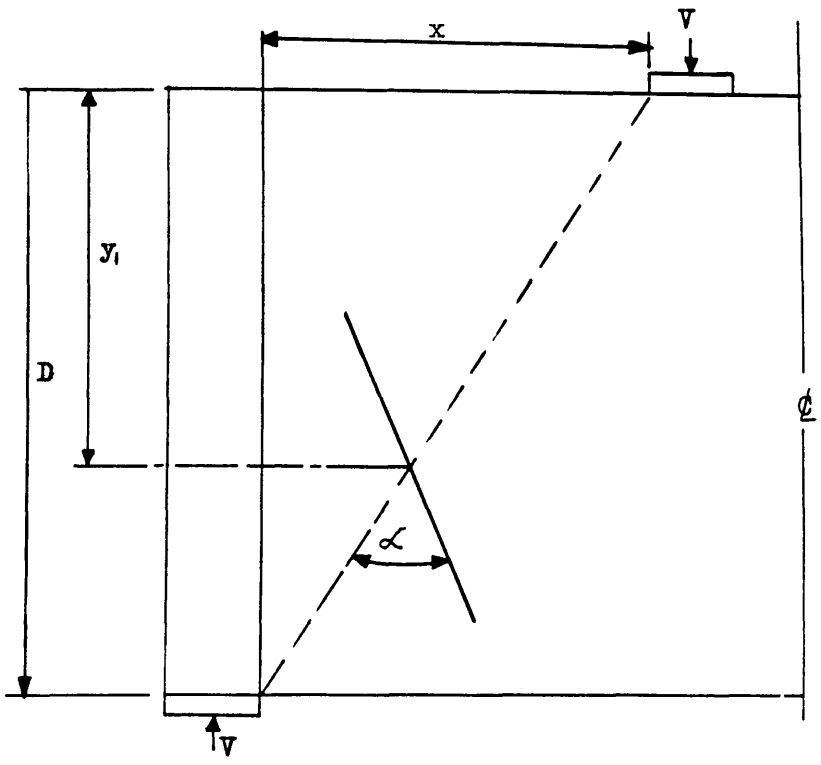

Figure(2.7) Symbols definitions (Kong et al)

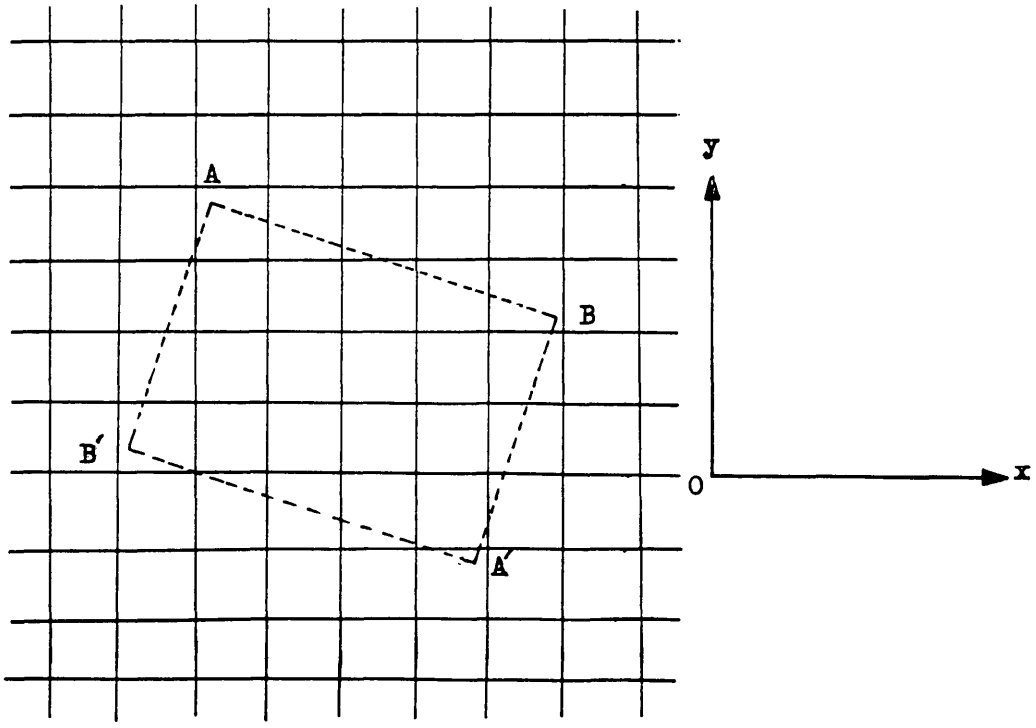

Figure(2.8) Location of opening in an unperforated stress field.

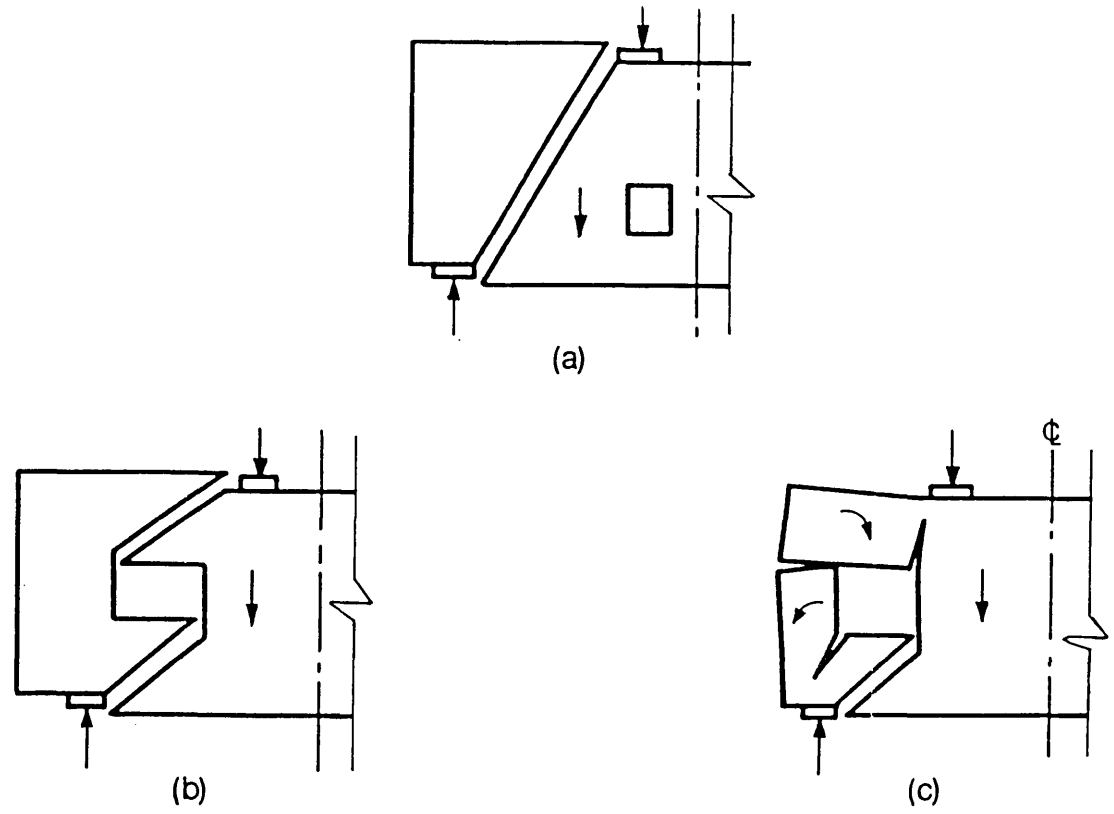

Figure(2.9) Different failure modes observed by Sharp.

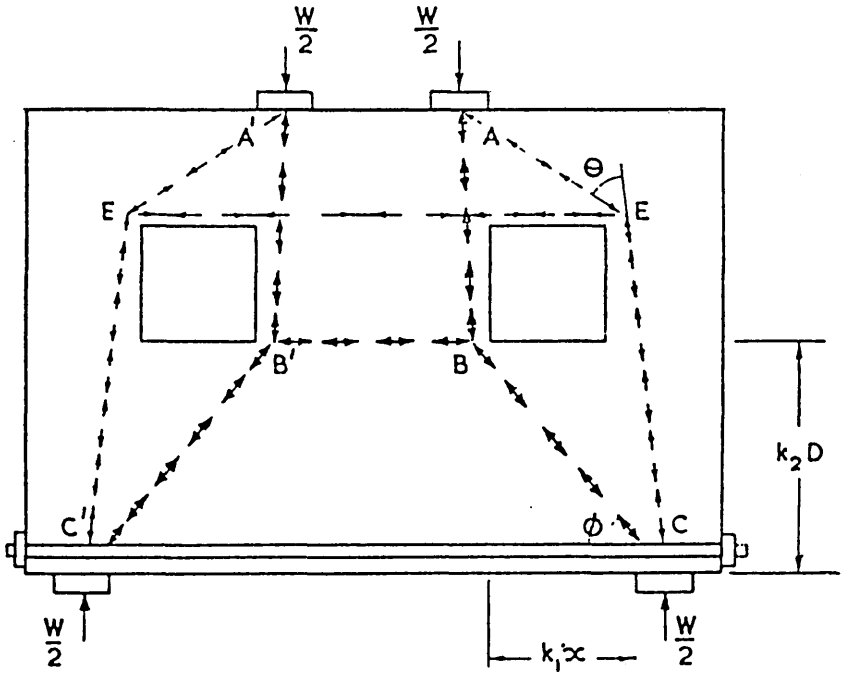

Figure(2.10) The structural idealization (Truss model)

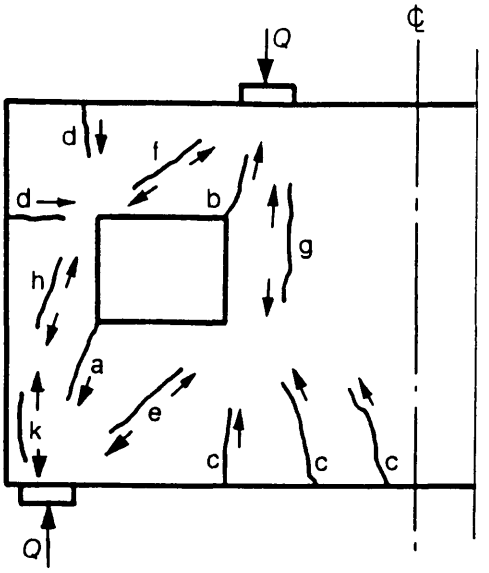

Figure(2.11) Typical crack pattern in deep beams with web with web opening

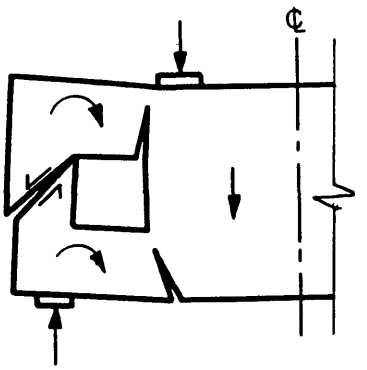

(a)

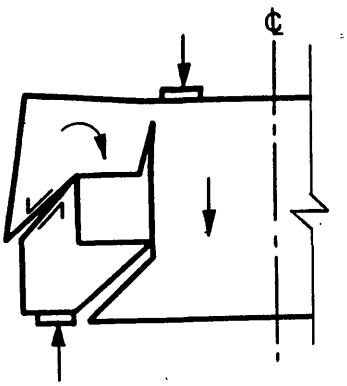

(b)

Figure(2.12) Failure modes for deep beam with opening.

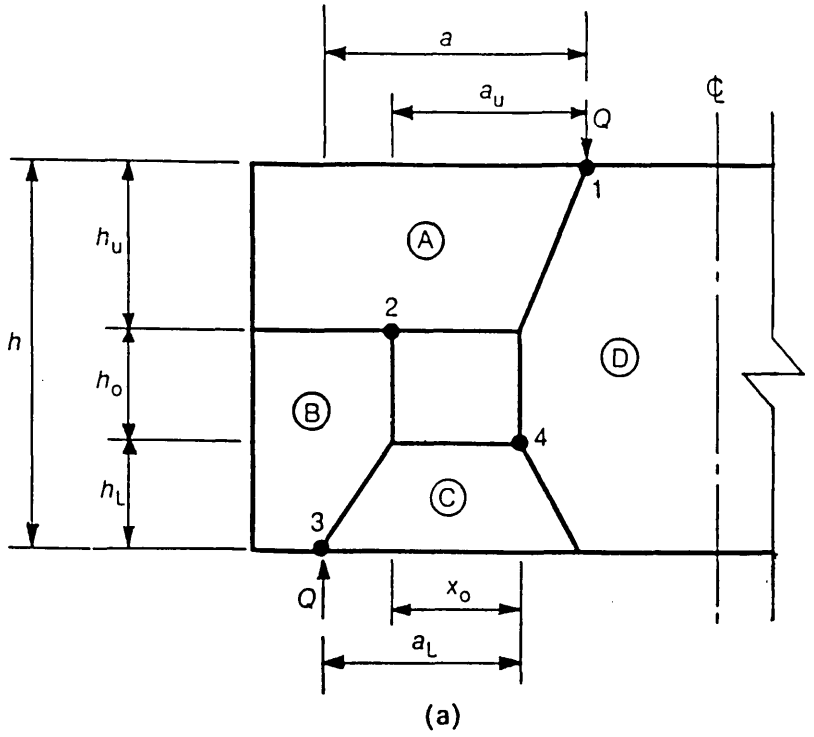

Figure(2.13) Idealization for deformation of beams with web opening

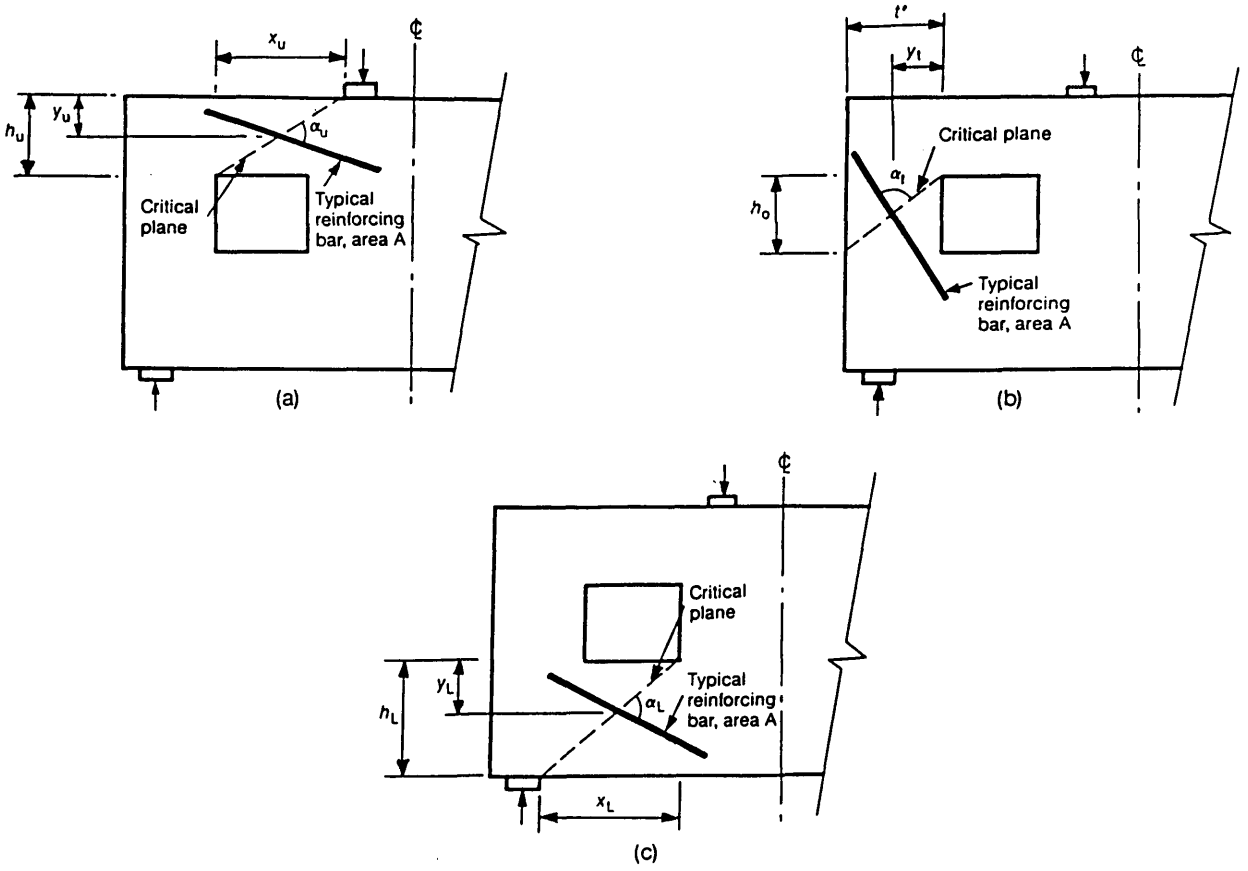

Figure(2.14) Typical planes of shear failure.

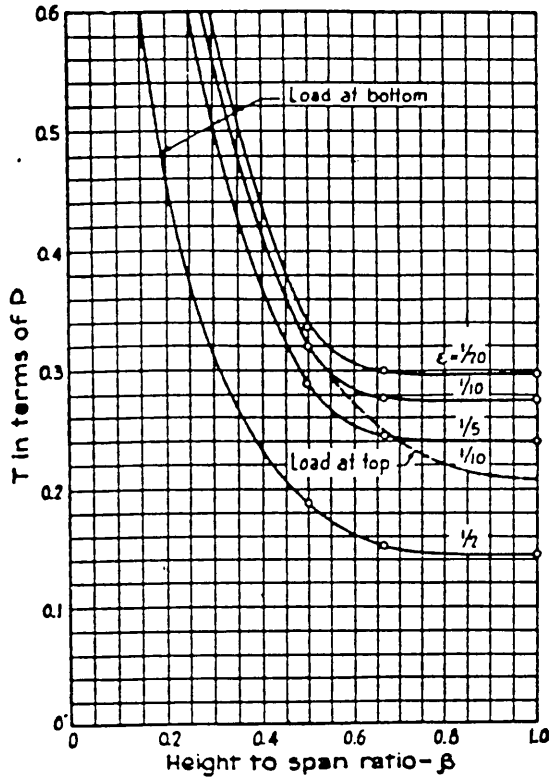

Fig.(2.15) Resultant, T, of tensile stresses in girders having concentrated loading at mid—span.

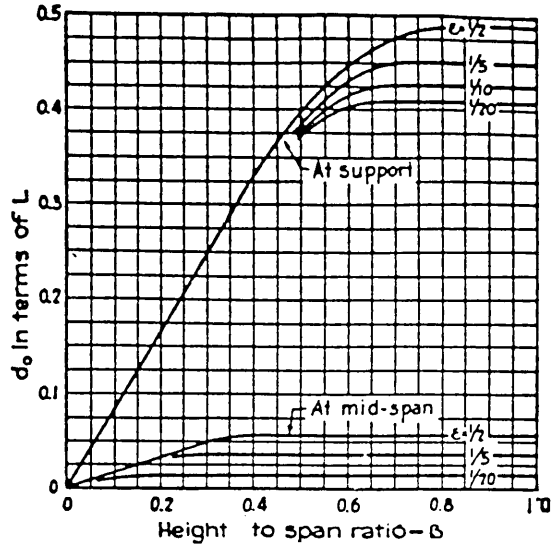

Fig.(2.17) Distance *do*, from resultant of tensile stresses to bottom edge of girders having concentrated loading at mid— span.

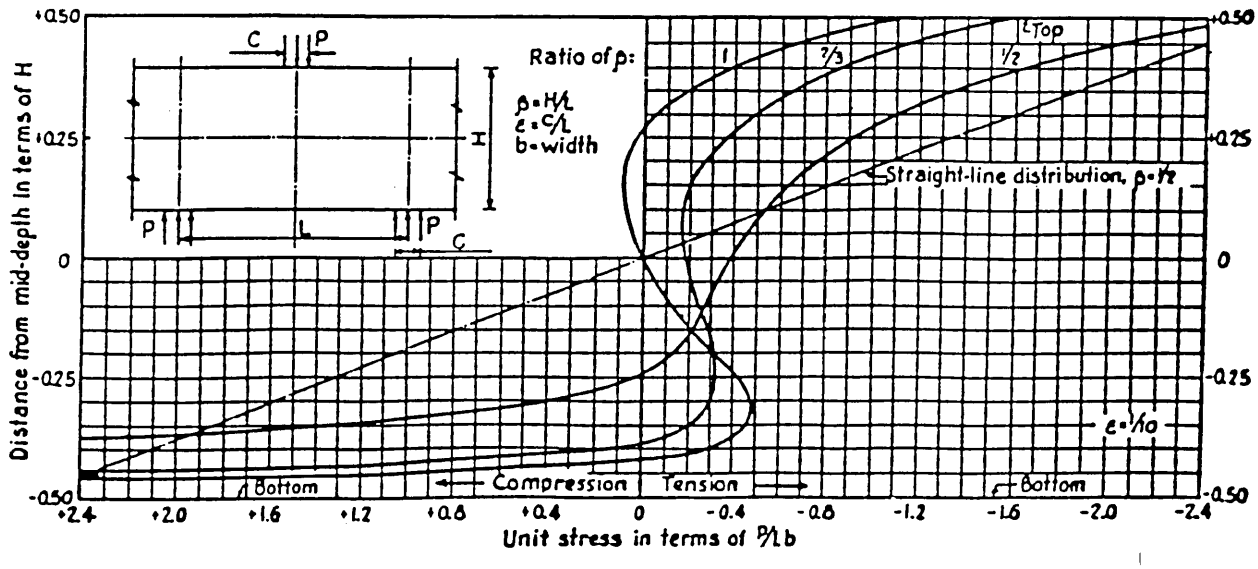

Fig.(2.16) Moment stresses at centre—line of support of girders having concentrated loading at top edge.

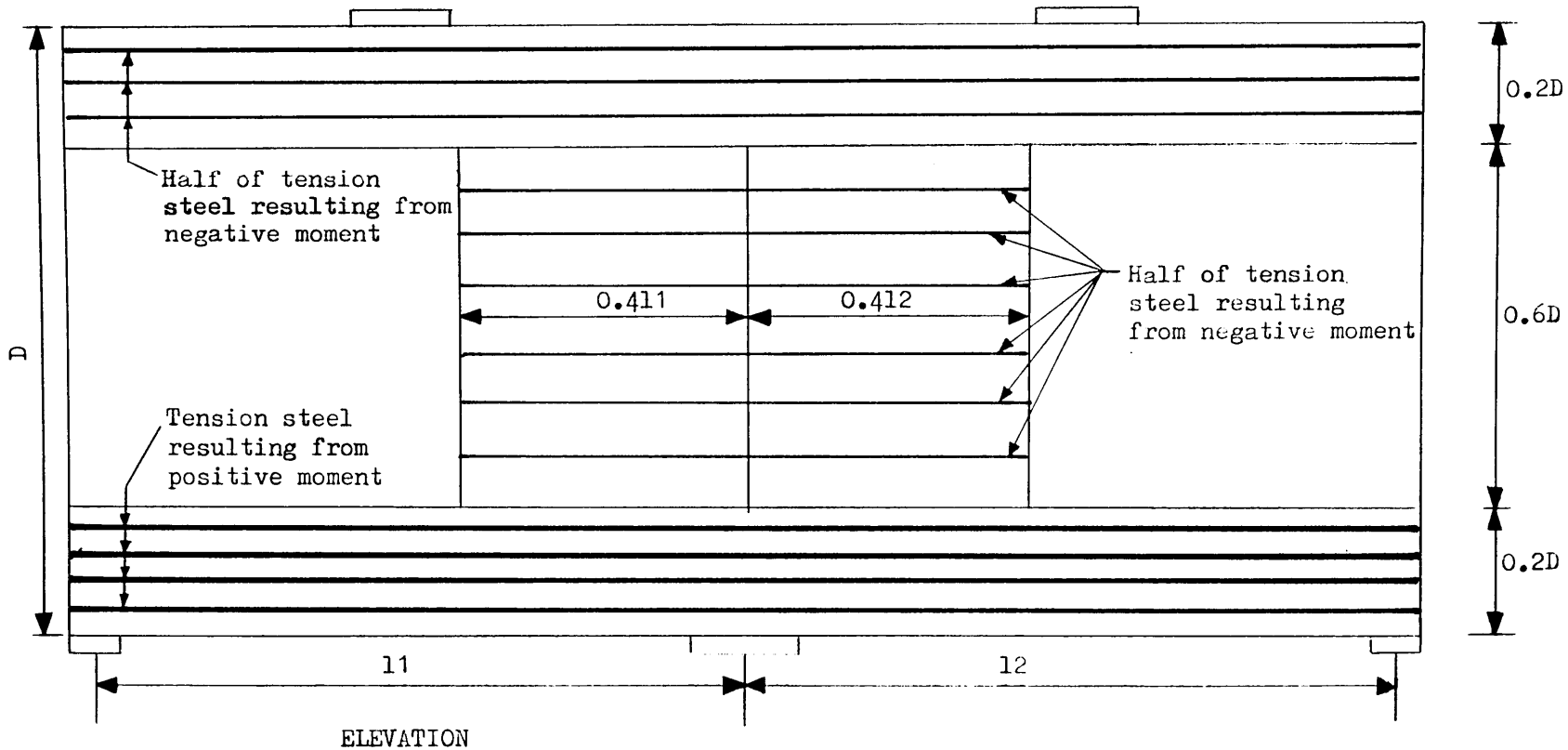

ELEVATION

Fig.(2.18) Steel distribution given by CEB-FIP and CIRIA Guide 2.

References

1 ALBRITTON, G.E., "Review of literature pertaining to the analysis of deep beams", Technical report No. 1–701, U.S. Army engineer waterways experiment station, Vicksburg, Miss, Nov. 1965, (80PP).

2. ROBINS, P.J., "Behaviour of reinforced concrete deep beams studied experimentally and by finite element methods", Ph.D. thesis, University of Nottingham, 1971.

3. LIN, C.K., "Ultimate strength design of deep beams", M.Sc. thesis, University of Glasgow, 1979.

4. MEMON, G.H., "Ultimate shear strength design of perforated deep beams", M.Sc. thesis, University of Glasgow, 1982.

5. CIRIA Guide 2, "The design of deep beams in reinforced concrete", London, CIRIA publication, 1977.

6. DISCHINGER, F., "Beitragzur theorie der halbscheibe und des wandartingen balken", Int. Asso. for bridge and structural engineering publications, Zurich, Vol. 1, 1932, (PP. 69–93).

7. PORTLAND CEMENT ASSOCIATION, "Design of deep girders", Concrete information, No. ST66, 1946, (10PP).

8. ACI STANDARD 318–77, "Building code requirements for reinforced concrete (ACI 318–77)", Detroit, Michigan 48219, American concrete institute, 1971.

9. CONWAY, H.D., CHOW, L. and MORGAN, G.W., "Analysis of deep beams", Journal of Applied mechanics, Trans., ASME, Vol. 18, No. 2, June 1951, (PP. 163–173).

10. CHOW, L., CONWAY, H.D. and WINTER, G., "Stresses in deep beams", Proc. American society of civil engineering (ASCE), Structural division, Vol. 78, Separate No. 127, May, 1952, (17PP).

11. UHLMANN, H.L.B., "The theory of girder walls with special reference to reinforced concrete design", The structural engineer, Vol. 30, No. 8, August, 1952, (PP. 172–181).

12. ARCHER, F.E. and KITCHEN, E.M., "Strain energy methods for the solution of

deep beams", Civil engineering and public works review, Vol. 52, No. 618, Dec. 1957, (PP. 1375–1378).

13. KAAR, P.H., "Stresses in centrally loaded deep beams", Proc. of the society for experimental stress analysis (SESA), Vol. XV, No. 1, 1975, (PP. 77–84).

14. ARCHER, F.E. and KITCHEN, E.M., "Stress distribution in deep beams", Civil engineering and public works review, Volume 55, No. 643, Feb. 1960, (PP. 230–234).

15. VARGHESE, P.C. and KRISHNAMOORTHY, C.S., "Strength and behaviour of deep reinforced concrete beams", Indian concrete journal (Bombay), Vol. 40, No. 3, Mar. 1966, (PP. 104–108).

16. RANGAN, B.V., "Ultimate strength of reinforced concrete deep beams", Indian concrete journal, Feb. 1969, (PP. 50– 54)

17. SUNDARA RAJA IYENGAR, K.T. and RANGEN, V.B., "A new theory for the shear strength of reinforced concrete beams", Indian concrete journal, Mar. 1967, Vol. 41, (PP. 102–109).

18. SHAIKH, M.A., DE PAIVA, H.A.R. and NEVILLE, A.M., "Flexure–shear strength of reinforced concrete deep beams", The structural engineer, Vol. 49, No. 8, August 1971, (PP. 359–363).

19. SHAIKH, M.A., DE PAIVA, H.A.R, and NEVILLE, A.M., "Flexure–shear strength of prestressed concrete beams", Journal of prestressed concrete institute, Vol. 13, No. 1, Feb. 1968, (PP. 68–85).

20. KUMAR, P., "Collapse load of deep reinforecd concrete beams", Magazine of concrete research, Vol. 28, No. 94, Mar. 1976, (PP. 30–36).

21. MARTI, P., "Basic tools of beam design", ACI Journal, Proceedings, Vol. 82, No. 1, Jan.–Feb. 1985, (PP. 46–56).

22. COLLINS, M.P., and MITCHELL, D., "A rational approach to shear design – The 1984 Canadian Code provisions", ACI Journal, Nov.–Dec. 1986, (PP. 925–933).

23. KOTSOVOS, M.D., "Design of reinforced concrete deep beams", The structural engineer, Vol. 66, No. 2, Jan. 1988 (PP. 28–32).

24. DE PAIVA, H.A.R. and SIESS, C.P., "Strength and behaviour of deep beams in

shear", Journal of the structural division, ASCE, Vol. 91, No. ST5, Oct., 1965, (PP. 19–41).

25. DE PAIVA, H.A.R. and AUSTIN, W.J., "Behaviour and design of deep structural members (Part 3): Tests of reinforced concrete deep beams", Structural research series No. 194, Civil engineering studies, Depatrment of civil engineering, University of Illinois, Urbana, I11, March, 1960.

26. WINEMILLER, J.R., AUSTIN, W.J. and SIESS, C.P. "Behaviour and design of deep structural members (Part 2): Tests of reinforced concrete deep beams with web and compression reinforcement", Structural research series No. 193, Civil engineering studies, Department of civil engineering, University of Illinois, Urbana I11, Aug. 1960.

27. UNTRAUER, R.E., "Strength and behaviour in flexure of deep reinforced concrete beams under static and dynamic loadings", Ph.D. thesis, Department of civil engineering, University of Illinois, Urbana, I11, 1961.

28. DE PAIVA, H.A.R., "Strength and behaviour in shear of deep reinforced concrete beams under static and dynamic loadings", Ph.D. thesis, Department of civil engineering, University of Illinois, Urbana I11, 1960.

29. DIAZ de COSSIO, R., and SIESS, C.P., "Behaviour and strength in shear of beams and frames without web reinforcement", Journal of ACI, Vol. 56, Feb., 1960 (PP. 1062–1064).

30. LAUPA, A. SIESS, C.P., and NEWMARK, N.M., "Strength in shear of reinforced concrete beams", Bulletin No. 428, Engineering experiment station, Uinversity of Illinios, Urbana III, Mar., 1959.

31. RAMAKRISHNAN, V., ANANTHANARAYANA, Y. and OBLI, S., "Strength and behaviour of deep reinforced concrete beams", Ultimate load design of concrete structures, Proceedings of symposium, 1967 Session II (PP 1–7).

32. RAMAKRISHNAN, V. and ANANTHANARAYANA, Y., "Ultimate strength of deep beams in shear", Proceedings of the american concrete institute (ACI), Vol. 65, 1968, (PP. 87–98).

33. LEONHARDT, F. and WALTHER, R., "Wandartige trager, Deutscher ausschuss fur stahlbton, Vol. 178, Wilhelm ernst und sohn, Berlin, West Germany, 1966.

34. CRIST, R.A., "Static and dynamic shear behaviour of uniformly loaded reinforced concrete deep beams, Ph.D. thesis, University of New Mexico, Albuquerque, New Mexico, 1971.

35. KONG, F.K., ROBINS, P.J. and COLE, D.F. "Web reinforcement effects on deep beams" Proceedings of American concrete institute, Volume 67, Dec. 1970 (PP 1010–1017).

36. KONG, F.K., ROBINS, P.J. "Web reinforcement effects on lightweight concrete deep beams" Proceedings of American concrete institute, Volume 68, July 1971 (PP 514–520).

37. KONG, F.K., ROBINS, P.J., KIRBY, D.P. and SHORT, D.R. "Deep beams with inclined web reinforcement" Proceedings of American concrete institute, Volume 69, Mar. 1972 (PP. 172–176).

38. KONG, F.K., and SINGH, A. "Diagonal cracking and ultimate loads of lightweight concrete deep beams" Proceedings of American concrete institute, Volume 69, Aug. 1972 (PP. 513–521).

39. KONG, F.K., and ROBINS, P.J. "Shear strength of reinforced concrete deep beams" Concrete magazine Mar. 1972 (PP. 34–36).

40. KONG, F.K., and ROBINS, P.J., SINGH, A. and SHARP, G.R. "Shear analysis and design of reinforced concrete deep beams", The structural engineer, Volume 50, No. 10, Oct. 1972 (PP. 405–409).

41. MANUEL, R.F., SLIGHT, B.W. and SUTER, G.T, "Deep beam behaviour affected by length and shear span variations", ACI Journal, Dec. 1971, (PP. 954–958).

42. SUTER, G.T. and MANUEL, R.F., "Diagonal crack width control in short beams", ACI Journal, Jun. 1971, (PP. 451–455).

43. MANUEL, R.F., "Failure of deep beams", Proc. Symposium on shear in reinforced concrete, Ottawa, ACI and ASCE, SP 42–19, Oct. 1973 (PP. 425–440).

44. SMITH, K.N. and VANTSIOTIS, A.S., "Shear strength of deep beams", ACI Journal, May–June 1982 (PP. 201–213).

45. ROGOWSKY, D.M., MACGREGOR, J.G. and ONG, S.Y "Tests of reinforced

concrete deep beams", Structural engineering report No. 109, Department of civil engineering, University of Alberta, Canada 1983.

46. ROGOWSKY, D.M. and MACGREGOR, J.G. "Shear strength of deep reinforced concrete continuous beams", Structural engineering report No. 110, Department of civil engineering, University of Alberta, Canada 1983.

47. RICKETTS, D.R. and MACGREGOR, J.G. "Ultimate behaviour of continous reinforced concrete deep beams", Structural engineering report No. 126, Department of Civil engineering, University of Alberta, Canada 1985.

48. THURLIMANN, B., "Plastic analysis of reinforced concrete beams",IABSE Colloquim, Copenhagen (Sesion II Plasticity), 1978 (PP. 71－89).

49. JENSEN, J. F., "Plastic solution for reinforced concrete beams in shear", IABSE Colloquim, Copenhagen, 1979 (Session II Plasticity), (PP. 71－79).

50. NIELSEN, M. P., "Some examples of lower－bound design of reinforcement in plane stress problems", IABSE Colloquim, Copenhagen 1979 (Session II Plasticity), (PP. 317－324).

51. SUBEDI, N.K., VARDY, A.E. and KUBOTA, N., "Reinforced concrete deep beams－some test results", Magazine of concrete research, Volume 38, No. 137, Dec. 1986 (PP. 206－219).

52. SUBEDI, N.K., "Reinforced concrete deep beams:a method of analysis", Proceedings of Institute of civil engineers, Part 2, 1988 (PP. 1－30).

53. CEB－FIP Committee, "International recommendation for the design and construction of concrete structures", Principles and recommendations", Prague, FIP sixth congress, Jun. 1970.

54. BRITISH STANDARDS INSTITUTION, "The Structural use of concrete, Code of practice", CP 8110, 1985.

55. KONG, F.K., and SHARP, G.R. "Shear strength of lightweight reinforced concrete deep beams with web openings", The structural engineer, Volume 51, No. 8, August 1973 (PP. 267－275).

56. KONG, F.K., ROBINS, P.J. and SHARP, G.R. "The design of reinforced concrete deep beams in current practice", The structural engineer, Volume 53, No. 4,

April 1975 (PP. 173–180).

57. KONG, F.K. and SHARP, G.R., "Structural idealization for deep beams with web openings", Magazine of concrete research, Vol. 29, No. 99, June 1977, (PP. 81–91).

58. KONG, F.K., SHARP, G.R., APPLETON, A., BEAUMONT, C.J. and KUBIK, L.A., "Structural idealization for deep beams with web openings: Further evidence", Magazine of concrete research, Vol. 30, No. 103, Jun. 1978, (PP. 89–95).

59. KONG, F.K. and KUBIK, L.A.,"Large scale tests on reinforced concrete deep beams with web openings", Department of engineering, Cambridge University, Technical report, CUED/C–Strut/TR80,1979.

60. KUBIK, L.A., "Predicting the strength of reinforced concrete deep beams with web openings", Proceedings of Institute of civil engineers, Part 2, No. 69, 1980.

CHAPTER THREE

FINITE ELEMENT MODELLING

3.1 Introduction

The finite element method (FEM) is now firmly established and accepted as the most powerful general numerical technique for structural analysis. It has provided engineers with a tool of very wide applicability, including the realistic analysis of reinforced concrete members and structures. The application of the finite element technique can provide new insights into the behaviour of ordinary reinforced concrete structures, such as beams, columns, slabs, shearwalls, transfer girders and panels. But it is also an essential tool for the analysis and design of complex structures like offshore oil platforms, hyperbolic cooling towers and nuclear containment structures.

Scientists and engineers are often faced with practical physical problems whose solution by conventional methods is either too difficult or even impossible in one operation. The process of subdividing systems into their individual components or 'elements', whose behaviour is readily understood, and then rebuilding the original system from such components to study its behaviour, is a natural way in which scientists, engineers, or even economists proceed[1,2,3,4]. This process is often referred to as discretization.

In any continuum the actual number of degrees of freedom are infinite and unless a close form solution is available an exact analysis (within the assumptions made) is impossible. However, numerical techniques can provide an approximate solution by assuming that the behaviour of the continuum can be represented by a finite number of unknowns. The finite element method is one such method, and is an extension of the matrix analysis of skeletal structures. However, unlike skeletal structures, there are no well defined joints in a continuum where equilibrium of forces can be established.

In the finite element method a continuous body is divided into small finite subregions called elements, each element possessing a finite number of unknown parameters. The elements are interconnected to each other by a finite number of common points existing on their boundaries, a process independent of the linear or non– linear nature of the problem. These common points are termed 'nodes'. A set of functions are chosen to define the variation of the required field variables within each element in terms of its unknown values at the nodes. These functions are also subject to certain constraints to ensure inter– element compatibility and correct convergence characteristics.

In continuum mechanics problems, the unknown variables can be displacements, stresses or both. This gives rise to the displacement (stiffness) method, the force (flexibility) method or the hybrid method respectively. Because of the ease of formulation, the displacement method is widely used, and has also been developed in this research.

Nowadays there are numerous texts, for example[1,2,3,4,5,6], which describe finite element methods and their applications, so no attempt will be made to describe it in great detail. The elastic design program developed in this research was based on Owen and Hinton's[4,5] work and full details are given in their texts. But in order to define basic terms, a brief résumé of two dimensional finite element theory using isoparametric elements is presented in the following sections, however only those aspects which are relevant to the needs of this research will be described. Although the representation of steel reinforcement is not necessary in the design program, it is necessary in the nonlinear analysis and so its formulation is also briefly described in this chapter.

The linear elastic finite element program was modified and extended to include the Direct Design equations. These equations used the elastic stress field produced by the

analysis to determine design reinforcement ratios, and is described in this chapter. All the transfer girders studied in this research were designed using this program and will be described in detail in Chapter Five.

The nonlinear finite element modelling is based on the program of Phillips[7] for reinforced concrete, and this is described in Chapter Four.

The use of the finite element method to obtain the elastic stress field was chosen because:

(i) Any shape of continuum including bodies with holes such as deep beams with openings, can be simulated without difficulty.
(ii) The finite element analysis is now well tested and proved as a reliable tool for analysis. Also, nowadays, it is cheap in terms of cost and time to obtain an internal elastic stress field of a continuous body.
(iii) A finite element analysis can produce a realistic elastic stress field throughout the continuum.
(iv) Variable material and geometrical representation can be made according to the real behaviour of the structure, such as different properties for support and loading points which are reinforced by steel load cages.
(v) Boundary conditions can be dealt with easily.

3.2 General procedures and discretization by finite elements

For structural applications, the governing equilibrium equations can be obtained by minimising the total potential energy of the system[1,2,4,5]. The total potential energy, Π, can be expressed as:

$$\Pi = 1/2\int_V \{\sigma\}^T\{\epsilon\}dV - \int_V \{\delta\}^T\{p\}dV - \int_S \{\delta\}^T\{q\}dS \qquad (3.1)$$

where σ and ϵ are the stress and strain vectors respectively, δ is the displacements

at any point, p is the body force per unit volume and q is the applied surface tractions. Integrations are taken over the volume, V, of the structure and loaded surface areas S.

The first term on the right hand side of equation (3.1) represents the internal strain energy and the second and third terms are the work contributions of the body forces and distributed surface loads respectively.

In the displacement method, the displacements are assumed to have unknown values at the nodal points so that the variation within any element is described in terms of the nodal values by means of interpolation functions. Thus

$$\{\delta\} = [N].\{\delta^e\} \qquad (3.2)$$

where N is the interpolation functions often termed shape functions, and δ^e is the vector of the nodal displacements of the element. The strains within the elements can be expressed in terms of the element nodal displacements,

$$\{\varepsilon\} = [B].\{\delta^e\} \qquad (3.3)$$

where B is the strain matrix generally composed of derivatives of the shape functions. The stresses may be related to the strains by making use of elasticity matrix, D, as follows:

$$\{\sigma\} = [D]\{\varepsilon\} \qquad (3.4)$$

Ensuring that the element shape functions have been chosen so that no singularties exist in the integrands of the function, the total potential energy of the continuum will be the sum of the energy contributions of the individual elements. Thus:

$$\Pi = \sum_e \Pi e \qquad (3.5)$$

where Πe is the potential energy of element e, by using equation (3.1) we get

$$\Pi e = 1/2 \int_{Ve} \{\delta^e\}^T [B]^T [D]^T [B] \{\delta^e\} dV -$$

$$\int_{Ve} \{\delta^e\}^T [N]^T \{p\} dV - \int_{Se} \{\delta^e\}^T [N]^T \{q\} dS \qquad (3.6)$$

where Ve is the element volume and Se is the loaded surface area of the element. The performance of minimisation for element, e, with respect to the nodal displacements, δ^e, of the element results in:

$$d\Pi/d\delta^e = \int_{Ve} [B]^T [D][B]\{\delta^e\} dV - \int_{Ve} [N]^T \{p\} dV - \int_{se} [N]^T . \{q\} dS$$

$$= [K^e]\{\delta^e\} - \{F^e\} \qquad (3.7)$$

where

$$\{F^e\} = \int_{Ve} [N]^T \{p\} dV + \int_{Se} [N]^T \{q\} dS \qquad (3.8)$$

are the equivalent nodal forces for the element and

$$[K^e] = \int_{Ve} [B]^T [D][B] dV \qquad (3.9)$$

is termed the stiffness matrix. The summation of terms in equation (3.7) over all the elements, when equated to zero, results in a system of equilibrium equations for the complete continuum, i.e,

$$\{F\} = [K]\{\delta\} \qquad (3.10)$$

where $\{F\}$ is the equivalent nodal forces for the continuum, $[K]$ is the stiffness matrix of the continuum and $\{\delta\}$ is the nodal displacements of the continuum.

After the insertion of the necessary boundary equations, these equations are then solved by any standard technique to yield the nodal displacements. Once the displacements are determined, the strains and thereafter the stresses in each element can be evaluated by using equations (3.3) and (3.4) respectively.

3.3 8– Noded parabolic isoparametric element

In the development of any finite element model, the first step is to decide the type

of element. The efficiency of any particular element depends on how well the defined shape functions are capable of representing the true displacement field.

In the last two decades many elements have been investigated and tested by various researchers; from simple ones to complex, for example [1,2,4,5]. Of these, the isoparametric family of elements has appeared to be greatly beneficial. These are a group of elements in which the shape functions are used to define the geometry as well as displacement field. Isoparametric elements are known for their better accuracy, versatility and efficiency over simpler types of elements. Savings in computer effort is obtained, because, even though complex elements require more time to formulate, fewer elements are required. In this study, a two dimensional version of the parabolic isoparametric element, shown in Figure (3.1), has been used throughout, and further description will be limited to this.

3.3.1 Shape functions

As mentioned earlier a shape function defines the variation of the field variables and its derivatives, through an element in terms of its values at the nodes. Therefore, the shape functions are closely related to the number of nodes and the type of element. Hence, in the displacement finite element approach

$$\delta = \sum_{i=1}^{n} N_i \ \delta i \qquad (3.11)$$

where N_i is the interpolation functions termed as shape functions and δ_i is the vector of the nodal displacements.

In the distorted and curved isoparametric elements, the shape functions N_i define the geometry and finite element analysis, i.e the unknown values at the nodal points. The shape functions are dependent on the local coordinate directions ξ and η. In the distorted elements, a given point is defined by coordinate ξ and η by means of two intersecting curves, called curvilinear coordinates. Moreover, these coordinates

represent better shape functions of isoparametric elements. Such curvilinear coordinates are so chosen, that on the faces of an isoparametric element the values of ξ and η are $+1$ and -1.

For two dimensional applications, the displacement field at a particular point with local coordinates (ξ,η) are $u(\xi,\eta)$, $v(\xi,\eta)$ and at each nodal point the displacement degrees of freedom are ui, vi. For the quadratic interpolation scheme used with parabolic isoparametric elements, there are eight nodes, i.e. $n=8$.

Therefore, for the displacements $u(\xi,\eta)$ and $v(\xi,\eta)$ at any point within the element, we make use of the expressions

$$u(\xi,\eta) = \sum_{i=1}^{8} Ni(\xi,\eta).ui$$

$$v(\xi,\eta) = \sum_{i=1}^{8} Ni(\xi,\eta).vi \qquad (3.12)$$

Global coordinate values $x(\xi,\eta)$ and $y(\xi,\eta)$ make use of the isoparametric concept and at any point within the element are defined in a similar manner:

$$x(\xi,\eta) = \sum_{i=1}^{8} N_i(\xi,\eta)\ x_i$$

$$y(\xi,\eta) = \sum_{i=1}^{8} N_i(\xi,\eta)\ y_i \qquad (3.13)$$

where (x_i,y_i), are the global coordinates of node i, and $N_i(\xi,\eta)$ are the quadratic shape functions for the 8-noded isoparametric element, given by[5]

$$N1(\xi,\eta) = -1/4(1-\xi)(1-\eta)(1+\xi+\eta)$$

$$N2(\xi,\eta) = 1/2(1-\xi^2)(1-\eta)$$

$$N3(\xi,\eta) = 1/4(1+\xi)(1-\eta)(\xi-\eta-1)$$

$$N4(\xi,\eta) = 1/2(1+\xi)(1-\eta^2)$$

$$N5(\xi,\eta) = 1/4(1+\xi)(1+\eta)(\xi+\eta-1)$$

$$N6(\xi,\eta) = 1/2(1-\xi^2)(1+\eta)$$

$$N7(\xi,\eta) = 1/4(1-\xi)(1+\eta)(-\xi+\eta-1)$$

$$N8(\xi,\eta) = 1/2(1-\xi)(1-\eta^2) \qquad (3.14)$$

The functions require that the node numbering is anticlockwise as shown in Figure (3.2). Each of these shape functions has a value of unity at the node to which it is related. They also have the property that their sum at any point within an element is also equal to unity, which satisfies the requirement that rigid body displacements of the element results in no element straining.

3.3.2 Strain matrix

Once the shape functions are evaluated the strain within the element can be expressed in terms of displacements or their derivatives. In plane stress and plane strain situations the strain is expressed as:

$$\epsilon x = \partial u/\partial x$$

$$\epsilon y = \partial v/\partial y$$

$$\gamma xy = \partial u/\partial y + \partial v/\partial x \qquad (3.15)$$

in which ϵx, ϵy are normal strain components and γxy is the shear strain component. Equation (3.15) can be written in matrix form as follows:

$$\begin{Bmatrix} \partial u/\partial x \\ \partial v/\partial y \\ \partial u/\partial y+\partial v/\partial x \end{Bmatrix} = \begin{bmatrix} \partial/\partial x & 0 \\ 0 & \partial/\partial y \\ \partial/\partial y & \partial/\partial x \end{bmatrix} \begin{Bmatrix} u \\ v \end{Bmatrix} \qquad (3.16)$$

Substituting for u and v from equation (3.15)

$$[\epsilon] = \sum_{i=1}^{8} \begin{bmatrix} \partial N_i/\partial x & 0 \\ 0 & \partial N_i/\partial y \\ \partial N_i/\partial y & \partial N_i/\partial x \end{bmatrix} \begin{Bmatrix} u_i \\ v_i \end{Bmatrix} = \sum_{i=1}^{8} [B_i]\{\delta_i\} \qquad (3.17)$$

where $[B_i]$ is 3x2 strain matrix which contains the cartesian derivatives of the shape functions.

Since the shape functions, N_i, are defined in terms of local coordinates, ξ,η of the element, transformation from local to global coordinates is required to obtain the B matrix in equation (3.17) . This is done through the well known Jacobian matrix which is written as:

$$J = \begin{bmatrix} \partial x/\partial\xi & \partial y/\partial\xi \\ \partial x/\partial\eta & \partial y/\partial\eta \end{bmatrix}$$

$$= \sum_{i=1}^{8} \begin{bmatrix} (\partial N_i/\partial\xi).x_i & (\partial N_i/\partial\xi).y_i \\ (\partial N_i/\partial\eta).x_i & (\partial N_i/\partial\eta).y_i \end{bmatrix} \qquad (3.18)$$

The inverse of the Jacobian matrix can be readily obtained using standard matrix inversion techniques

$$[J]^{-1} = \begin{bmatrix} \partial\xi/\partial x & \partial\eta/\partial x \\ \partial\xi/dy & \partial\eta/\partial y \end{bmatrix} = (1/\det J) \begin{bmatrix} \partial y/\partial\eta & -\partial y/\partial\xi \\ -\partial x/\partial\eta & \partial x/\partial\eta \end{bmatrix} \qquad (3.19)$$

3.3.3 Stress– strain relationships

From basic theory of elasticity for elastic materials, the stress– strain relationship is given by:

$$\{\sigma\} = [D]\{\epsilon\} \qquad (3.20)$$

where $[D]$ is the elasticity matrix. For a two dimensional isotropic material this takes the form for plane stress situations

$$[D] = \frac{E}{(1-\nu^2)} \begin{bmatrix} 1 & \nu & 0 \\ \nu & 1 & 0 \\ 0 & 0 & (1-\nu)/2 \end{bmatrix} \qquad (3.21)$$

whereas for plane strain situations

$$[D] = \frac{E(1-\nu)}{(1+\nu)(1-2\nu)} \begin{bmatrix} 1 & (\nu/(1-\nu)) & 0 \\ (\nu/(1-\nu)) & 1 & 0 \\ 0 & 0 & (1-2\nu)/(2(1-\nu)) \end{bmatrix} \qquad (3.22)$$

where E is Young's modulus of elasticity and ν is Poisson's ratio. The change in material properties due to concrete nonlinearity are entered through the material

property matrix [D] but this will be discussed in the next chapter. Here, we will limit ourselves to linear behaviour.

3.3.4 Element stiffness matrix

We now have all the information necessary to evaluate the element stiffness matrix ,K^e, from equation (3.9), i.e

$$K^e = \int \int [B]^T[D][B]dv \qquad (3.23)$$

A typical submatrix K^e_{ij} linking nodes i and j may be evaluated from the expression

$$K^e{}_{ij} = \int \int [B_i]^T[D][B_j]t.det.J.d\xi.d\eta \qquad (3.24)$$

where t is element thickness and

$$dv = det.J.d\xi.d\eta.t \qquad (3.25)$$

and the limits of integration becomes -1 to 1 in each one of the two directions.

3.3.5 Numerical integration

It is difficult or perhaps impossible to perform the closed form integrations required in evaluating the element matrix and thus numerical integration is essential. This choice of numerical integration will replace the exact integral by evaluating the integrand at various sampling points and then by making a weighted summation of these values. In this study Gauss–Legendre quadrature values have been used because of their higher accuracy over other forms of quadrature and the ease with which these can be implemented. They can integrate a polynomial $f(\xi)$ of degree$(2n-1)$[1,4,5].

In general, the one dimensional Gaussian quadrature formula is written as

$$I_n = \int_{-1}^{+1} \Phi(\xi)d\xi = \sum_{i=1}^{n} a_i.\Phi(\xi_i) \qquad (3.26)$$

where a_i is a weighting factor, ξ_i is the coordinate of the ith integration point and

n is the total number of integration points. In two dimensions where a double integral exists, then

$$In,n = \int_{-1}^{+1}\int_{-1}^{+1} \Phi(\xi,\eta)d\xi.d\eta = \int_{-1}^{+1}\left[\int_{-1}^{+1} \Phi(\xi,\eta)d\xi\right]d\eta \qquad (3.27)$$

The inner integral is evaluated first keeping η constant and then the outer integral is evaluated.

These Gaussian Legendre rules are particularly suitable for isoparametric elements since the limits of integration are $+1$ to -1 which coincide with the local coordinate system $+1$ to -1 on element boundaries. Table 3.1 shows the symmetrical positions of Gauss points ξi and the corresponding weighting factors a_i for n= 1,2,3, and 4[5]. However in this work the 3x3 Gauss rule has always been used for designing the reinforcement.

3.4 Steel representation

Since steel reinforcement is comparatively thin, it is generally assumed to be capable of transmitting axial force only; thus steel stress– strain behaviour is assumed to be uniaxial and therefore it is not necessary to introduce the complexities of multiaxial constitutive relationships.

In the finite element modelling there are at least three different representations which have been used[7,8,9,10,11]. These are:

(a) Distributed representation

(b) Embedded representation

(c) Discrete representation

(a) Distributed representation

In distributed steel representation, steel is assumed to be distributed (i.e as a

membrane) over the concrete element with a particular orientation θ as shown in Figure (3.3). Composite concrete and reinforcement constitutive relations are required in this case. In order to derive such a relation, perfect bond between steel and concrete has to be assumed. Although this approach is easy to implement, it is unrealistic in the sense that reinforcing bars are no longer discrete uniaxial members embedded in the concrete [9,10,11], additionally, dowel action mechanisms cannot be modelled adequately[10,11].

(b) Embedded representation

Embedded representation is shown in Figure (3.4) and is often used in connection with higher order isoparametric concrete elements. The reinforcing bars are considered as axial members built into the isoparametric concrete element, such that, its displacements are consistent with those of the element. Again in this type of representation perfect bond has to be assumed[7,9].

(c) Discrete representation

A discrete representation of reinforcement using a one dimensional element as shown in Figure (3.5), has been widely used by various researchers, for example[10]. Axial force members are effectively pin connected with two degrees of freedom at nodal points for two dimensional problems and are simply superimposed onto a two dimensional finite element mesh representing concrete. This approach is simple and has a significant advantage, that it can take into account possible relative displacements of reinforcement with respect to the surrounding concrete. However, a serious drawback is that the location of steel often dictates the concrete mesh. This may result in slender elements, when the reinforcing bars are close together, violating the ideal of aspect ratios being as close to unity as possible [8,9]. This representation can be particularly unsatisfactory when used with the higher order isoparametric elements often used to represent concrete.

3.4.1 Method of steel representation used in this study

Embedded representation of steel was considered to be a reasonable approach to take in this work. This approach takes a proper account of dowel action and can be incorporated without any difficulty into a finite element model, regardless of the type of nonlinear material models used. In order to take into account skew steel, skew elements can be used to represent the actual line of the steel. Although, in general the reinforcing steel can be placed along any constant local coordinate line in an element, here for ease of data input, the choice was restricted so that the bars can be positioned on the boundaries of the element and or along a line joining the midside nodes as shown in Figure (3.6).

4.5 Embedded bar element derivation

Consider a bar lying along a direction parallel to the local coordinate ξ as shown in Figure (3.7) i.e lying along the line of constant $n = \eta c$. Bars along constant ξ will obviously follow a similar derivation. It is further assumed that the bars are capable of transmitting in-plane forces only. The line of the bar is defined by using the same shape functions as the main element. Thus the cartesian coordinate of any point, P, are given by:

$$x = \sum_{i=1}^{8} N_i(\xi) x_i \qquad (3.28)$$

Full compatibility between the bars and basic element is assumed, therefore, the displacements of the bar are obtainable from the displacement field of the basic element[7,8,9].

$$\{f\} = \begin{Bmatrix} u \\ v \end{Bmatrix} = [N(\xi)]\{\delta^e\} \qquad (3.29)$$

For bars only one component of strain contributes to the strain energy and is defined locally by:

$$\epsilon p = \partial u'/\partial x' \qquad (3.30)$$

where x', y' are a local coordinate system at point, P, with y' being normal to the line of the bar, and u', v' are the corresponding displacements.

Now at any point it is possible to define a distortion matrix [j] as:

$$[j] = \begin{bmatrix} \partial u/\partial x & \partial v/\partial x \\ \partial u/\partial y & \partial v/\partial y \end{bmatrix} = \begin{bmatrix} \partial N_i/\partial x & \partial N_j/\partial x & \partial Nm/\partial x \ldots \\ \partial N_i/\partial y & \partial Nj/\partial y & \partial Nm/\partial y \ldots \end{bmatrix} \begin{Bmatrix} ui & vi \\ uj & vj \\ um & vm \\ . & . \\ . & . \\ . & . \\ . & . \end{Bmatrix} \quad (3.31)$$

and, as mentioned earlier, a Jacobian matrix given by:

$$[J] = \begin{bmatrix} \partial x/\partial \xi & \partial y/\partial \xi \\ \partial x/\partial \eta & \partial y/\partial \eta \end{bmatrix} = \begin{bmatrix} \partial N_i/\partial \xi & \partial N_j/\partial \xi & \partial Nm/\partial \xi \ldots \\ \partial N_i/\partial \eta & \partial Nj/\partial \eta & \partial Nm/\partial \eta \ldots \end{bmatrix} \begin{Bmatrix} xi & yi \\ xj & yj \\ xm & ym \\ . & . \\ . & . \\ . & . \\ . & . \end{Bmatrix} \quad (3.32)$$

Therefore from the relation

$$\begin{bmatrix} \partial N_i/\partial \xi & \partial N_j/\partial \xi & \partial Nm/\partial \xi \ldots \\ \partial N_i/\partial \eta & \partial Nj/\partial \eta & \partial Nm/\partial \eta \ldots \end{bmatrix} = [J] \begin{bmatrix} \partial N_i/\partial x & \partial N_j/\partial x & \partial Nm/\partial x \ldots \\ \partial N_i/\partial y & \partial Nj/\partial y & \partial Nm/\partial y \ldots \end{bmatrix} \quad (3.33)$$

it follows that

$$[j] = [J]^{-1} \begin{bmatrix} \partial N_i/\partial \xi & \partial N_j/\partial \xi & \partial Nm/\partial \xi \ldots \\ \partial N_i/\partial \eta & \partial Nj/\partial \eta & \partial Nm/\partial \eta \ldots \end{bmatrix} \begin{Bmatrix} ui & vi \\ uj & vj \\ um & vm \\ . & . \\ . & . \\ . & . \\ . & . \end{Bmatrix} \quad (3.34)$$

As [j] is a second order tensor, it transforms on co-ordinate rotation from x, y to x', y' according to

$$[j]' = \begin{bmatrix} \partial u'/\partial x' & \partial v'/\partial x' \\ \partial u'/\partial y' & \partial v'/\partial y' \end{bmatrix} = [R][j][R]^T \quad (3.35)$$

where [R] is the rotation matrix of direction cosines at point P, given by

$$[R] = \begin{bmatrix} \partial x/\partial x' & \partial y/\partial x' \\ \partial x/\partial y' & \partial y/\partial y' \end{bmatrix} \tag{3.36}$$

and by noting that x' and ξ coincide, and differ only in magnitude, it can be shown by:

$$[R] = 1/\sqrt{(\partial x/\partial \xi)^2+(\partial y/\partial \xi)^2} \begin{bmatrix} \partial x/\partial \xi & \partial y/\partial \xi \\ -\partial y/\partial \xi & \partial x/\partial \xi \end{bmatrix} \tag{3.37}$$

Finally from equation (3.30), (3.35) and (3.37), it follows that

$$\partial u/\partial x' = 1/h^2 \left[\{c1\partial Ni/\partial x + C2\partial Ni/\partial y\}\{C2\partial Ni/\partial x + C3\partial Ni/\partial y\} \ldots . \right] \begin{Bmatrix} ui \\ vi \\ uj \\ vj \\ . \\ . \\ . \\ . \end{Bmatrix} \tag{3.38}$$

where

$$h = \sqrt{(\partial x/\partial \xi)^2+(\partial y/\partial \xi)^2}$$

$$C1 = (\partial x/\partial \xi)^2,\ C2 = (\partial x/\partial \xi . \partial y/\partial \xi),\ C3 = (\partial y/\partial \xi)^2 \tag{3.39}$$

The stiffness matrix $[K']^e$ of the bar can be calculated by using equation (3.9).

$$[K']^e = \int_V [B']^T [D'][B'] \, d(vol) \tag{3.40}$$

where $[B']$ is strain matrix obtained from equation (3.38). For plane stress and strain case $[D'] = Es$, where Es is the modulus of elasticity of steel and the elemental volume is given by

$$d(vol) = As.dx' = As.h.d\xi \tag{3.41}$$

where As is the cross-sectional area of the bar and h is to be taken from equation (3.39).

Clearly numerical integration must be used again, but now applied in one dimension only.

The value of the stress which will be induced in the bar will be

$$\sigma p' = \epsilon p' . Es \tag{3.42}$$

The equivalent nodal loads contributed by the steel bar will be:

$$\{P1\}_{STEEL} = \int_V [B']^T \{\sigma p'\} d(vol) \qquad (3.43)$$

where $\{\sigma p'\}$ are the bar stresses.

3.6 Evaluation of loads

In the displacement method, the only permissible form of loading, other than initial stressing, is by the prescription of concentrated loads at the nodal points. Consequently, forms of loading such as gravity action and pressure applied to the element surfaces, must be reduced to equivalent nodal forces before a solution can proceed[5].

It would be very difficult in general to calculate manually the equivalent nodal forces using the isoparametric element principle, since area or volume integrations over arbitrary shaped regions are generally involved. Therefore, a subroutine for doing this function is used and is explained in detail in the referenced text[5] only a summary is given here.

3.6.1 Point loads

Consider a point load, P, acting on an edge of the element as shown in Figure (3.8). Applying virtual displacements, δ^*, in the x and y directions to each node in turn, so that for node i we have virtual displacement components u^* and v^* respectively then,

$$P_{xi}u^* = P_x N_i(\xi_p, \bar{\eta})u^*$$

$$P_{yi}v^* = P_y N_i(\xi_p, \bar{\eta})v^* \qquad (3.43)$$

where Pxi and Pyi are the corresponding forces in the x and y directions, Px and Py are the components of load, P, acting in the x and y directions respectively and ξ_p is the ξ coordinate of the point and $\bar{\eta}$ is the constant value of η at the edge in question i.e $\bar{\eta} = -1$ or $+1$.

By invoking the arbitrary nature of the virtual displacement then

$$\begin{Bmatrix} P_{xi} \\ P_{yi} \end{Bmatrix} = N_i(\xi_p, \bar{\eta}) \begin{Bmatrix} P_x \\ P_y \end{Bmatrix} \qquad (3.45)$$

This is the equation from which the equivalent nodal forces can be calculated as soon as the load component Px and Py and its points of application, as defined by $(\xi_p, \bar{\eta})$, are specified.

If the x and y coordinate of the point of application are specified as x_p and y_p respectively, and the nodal point coordinates are (x_i, y_i) along the element edge then using the isoparametric concept

$$\begin{Bmatrix} x_p \\ y_p \end{Bmatrix} = \sum_{i=1}^{3} N_i(\xi_p, \bar{\eta}) \begin{Bmatrix} x_i \\ y_i \end{Bmatrix} \qquad (3.46)$$

The shape functions, N_i, are in this case quadratic expressions in ξ and η and therefore equation (3.46) is quadratic in ξ and can be solved to yield ξ_p. The equivalent nodal forces can then be determined from (3.45) (This, of course implies that the point of application of the load is known to coincide with a particular mesh line).

Point loads which act on a node are handled more conveniently by inputting directly their values at the appropriate nodal points[5].

3.6.2 Body forces

Gravity forces are equivalent to the body force per unit volume acting within the solid in the direction of the gravity axis. It is not necessary that gravity loading should coincide with either of the coordinate axes. Gravity force components may act in both the x and y directions. The direction of the gravity force is defined by the angle which it makes with the y axis.

In order to obtain the equivalent nodal forces similar procedures are followed as in the previous section. Referring to Figure (3.8) once again, if g is the gravitational acceleration and the material mass density is p then the gravity force dG acting on an elemental volume dV is

$$dG = pg.dV \tag{3.47}$$

The components acting in the x and y directions will be

$$dG_x = pg.dV.\sin\theta$$

$$dG_y = -pg.dV.\cos\theta \tag{3.48}$$

Applying the principle of virtual displacements, the equivalent nodal force in the x and y directions are

$$P_{xi}u^* = \int_{Ve} N_i u^* pg.\sin\theta.dV$$

$$P_{yi}v^* = -\int_{Ve} N_i v^* pg.\cos\theta.dV \tag{3.49}$$

where N_i are the shape functions, and the integration is taken over the volume of the element. Noting the arbitrary nature of the virtual displacements these equations can be replaced in matrix form as

$$\begin{Bmatrix} Pxi \\ P_{yi} \end{Bmatrix} = \int_{Ve} N_i pg \begin{Bmatrix} \sin\theta \\ -\cos\theta \end{Bmatrix} dV \tag{3.50}$$

Finally, this equation requires the Gaussian numerical quadrature to perform the integration over the volume, i.e

$$\begin{Bmatrix} P_{xi} \\ P_{yi} \end{Bmatrix} = \sum_{n=1}^{NGAUS} \sum_{m=1}^{NGAUS} \rho g \begin{bmatrix} \sin\theta \\ -\cos\theta \end{bmatrix} N_i(\xi_n, \eta_m) a_n.a_m.t.\det J \tag{3.51}$$

where t is the thickness of the element and J is the Jacobian matrix and a_n, a_m are the Gaussian weighting functions.

3.6.3 Normal and tangential distributed edge loads

In some cases, element edges will have distributed loading per unit length in either the normal or tangential directions. In the parabolic isoparametric element shown in Figure (3.9), an edge of an element is represented by three nodes listed in an anticlockwise direction with respect to the loaded element.

The intensity of distributed load at any point along the loaded edge is given by

$$\begin{Bmatrix} P_n \\ P_t \end{Bmatrix} = \sum_{i=1}^{n} N_i \begin{Bmatrix} (P_n)_i \\ (P_t)_i \end{Bmatrix} \qquad (3.52)$$

where p_n and p_t are the normal and tangential distributed loads and N_i are the shape functions as defined before.

By applying the principle of virtual work to each nodal point of the element in turn, the equivalent nodal forces can be calculated. The components of forces acting in the x and y directions respectively, on an incremental length dS are

$$dP_x = (p_t.dS.\cos\alpha - p_n.dS.\sin\alpha) = (p_t.dx - p_n.dy)$$

$$dP_y = (p_n.dS.\cos\alpha + p_t.dS.\sin\alpha) = (p_n.dx + p_t.dy) \qquad (3.53)$$

By using the following relations in equation (3.53)

$$dx = (\partial x/\partial\xi).\partial\xi$$

$$dy = (\partial y/\partial\xi).\partial\xi \qquad (3.54)$$

and integrating along the element edge in terms of the curvilinear variable ξ then finally the expressions for equivalent nodal forces become

$$P_{xi} = \int_{Se} N_i(p_t(\partial x/\partial\xi) - p_n(\partial y/\partial\xi)).\partial\xi$$

$$P_{yi} = \int_{Se} N_i(p_n(\partial x/\partial\xi) - p_t(\partial y/\partial\xi)).\partial\xi \qquad (3.55)$$

where integration is taken along the loaded element edge Se and is again carried out using numerical integration.

3.6.4 Temperature loading

Sometimes stresses can be induced in a solid by temperature change. As thermal effects are only a particular case of initial straining, they are easily accommodated. In this situation, first the initial stresses, σ^o, corresponding to the initial thermal strains, ϵo, are calculated using $\sigma o = D\epsilon o$ and then converted to equivalent nodal forces. Later on, these stresses are added to stresses from other sources such as applied loads etc.

For the plane stress situation the initial strains are

$$\epsilon xo = \alpha T$$

$$\epsilon yo = \alpha T$$

$$\gamma xyo = 0 \qquad (3.56)$$

where α is the coefficient of thermal expansion and T is the temperature increase from an arbitrary datum.

For plane strain, the initial strains are

$$\epsilon xo = (-\nu\sigma zo/E) + \alpha T$$

$$\epsilon yo = (-\nu\sigma zo/E) + \alpha T$$

$$\gamma xyo = 0$$

$$\epsilon zo = (\sigma zo/E) + \alpha T = 0 \qquad (3.57)$$

By eliminating σzo in the above equation (3.57) we get

$$\epsilon xo = (1+\nu)\ \alpha T$$

$$\epsilon yo = (1+\nu)\ \alpha T$$

$$\gamma xy = 0 \qquad (3.57)$$

and $\sigma zo = -E\alpha T \qquad (3.58)$

3.7 The equation solution technique

There are various equation solution techniques which can be used to solve a given set of linear simultaneous equations. In this study direct Gaussian elimination

algorithims have been used in conjunction with the frontal method of equation assembly and reduction,[5] and is applicable here only for symmetric systems of linear equations. The main features of this technique are:

1:– It assembles the equations and eliminates the variables at the same time, hence the complete structural stiffness is never formed, only the upper triangle of a square matrix containing parts of the equations which are being assembled at a particular time.

2:– The frontal solver does not store as many zero coefficients as a banded solver does. Once an equation has been completely assembled and eliminated, it reduces space which can be used for subsequent equations.

3:– The storage allocation in a banded solver is determined by the order in which the nodes are presented for assembly. But, in front solver the storage is determined by the order, in which the elements are presented. It can handle any order of node numberings. Hence, at any stage, if a mesh of a problem is found to be too coarse in some regions, its modification does not require extensive nodal point renumbering. In this sense, the frontal solver is easier to use than banded solvers.

4:– The frontal solver tends to be more economical than banded solvers, especially for higher order elements with midside nodes.

3.8 Brief description of the developed model for design

The finite element model described in this chapter was basically developed from the work of Owen and Hinton[5] and was used to obtain the elastic admissible stress field for in–plane structures. The program was modified and extended by incorporating the Direct Design equations. The working order of the program is presented in Figure (3.10).

The Direct Design equations, originally presented by Nielson[12] and later extended by Clark[13], were programmed in two subroutines called Orthogonal and Skew to

carry out each particular type of reinforcement design. In order to design reinforcement for a particular beam, first an elastic stress field was obtained using the assumed material properties of cracked concrete. Secondly, this elastic stress field was transfered to the Design Module and, according to the type of reinforcement required i.e orthogonal or skew, the reinforcement was calculated.

Reinforcement ratios in each direction were obtained at the 9 Gaussian integration points of a 3x3 rule. As the stresses throughout the continuum were continuously varying, the resulting steel ratios also varied from point to point in both directions. To assist in the selection of discrete bars, the first step was to average steel ratios in each direction in each element. Then, steel areas were calculated from these steel ratios through some simple mathematical manipulations.

Once the steel areas for each element were determined for a particular load, the program calls the Plotting Module.

The Plotting Module was built into the finite element program to present the designed reinforcement as three dimensional and contour plots, and also in tabular form. This allows the designer to visualise the designed reinforcement profile of the structure, so that at any stage, decisions are more easily made about whether to change material properties or the geometry, if they do not satisfy intended design aims. This Plotting Module also helps in checking the mesh boundary conditions and loading points, which is also important in avoiding errors in the analysis. Three subroutines **MESHPL, STEELP, BCPLOT** carry out these functions as follows:

MESHPL– Plots the finite element mesh used in the analysis with nodal point and element numbers.

STEELP– Plots the finite element mesh with the average steel areas required in both directions in each element. It also plots a three dimensional view of the main and shear reinforcement ratios and also plots contours of both

reinforcements ratios.

BCPLOT– Plots boundary conditions on the finite element mesh and the nodal loads as arrows in the appropriate direction.

A demonstration of the use of this Program can be seen in the Chapter Five when designing the transfer girders.

TABLE 3.1

Weighting factors and Gaussian sampling point positions

n	i	ξ_i	a_i
1	I	0	2
2	I	$+1\sqrt{3}$	+1
	II	$-1\sqrt{3}$	+1
3	I	0	8/9
	II	$+\sqrt{0.6}$	5/9
	III	$-\sqrt{0.6}$	5/9
4	I	$\sqrt{\frac{3+\sqrt{4.8}}{7}}$	$\frac{1}{2} - \frac{\sqrt{30}}{36}$
	II	$-\sqrt{\frac{3+\sqrt{4.8}}{7}}$	$\frac{1}{2} - \frac{\sqrt{30}}{36}$
	III	$\sqrt{\frac{3-\sqrt{4.8}}{7}}$	$\frac{1}{2} + \frac{\sqrt{30}}{36}$
	IV	$-\sqrt{\frac{3-\sqrt{4.8}}{7}}$	$\frac{1}{2} + \frac{\sqrt{30}}{36}$

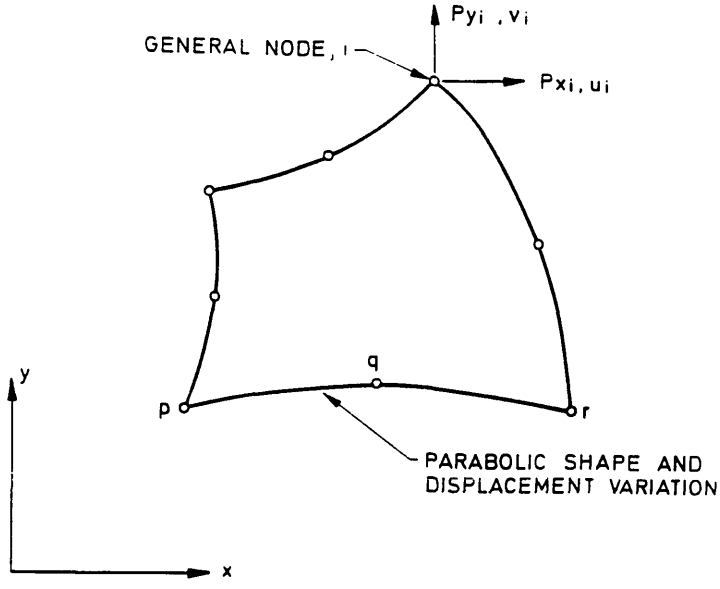

Figure (3.1) Typical two dimensional parabolic isoparametric element.

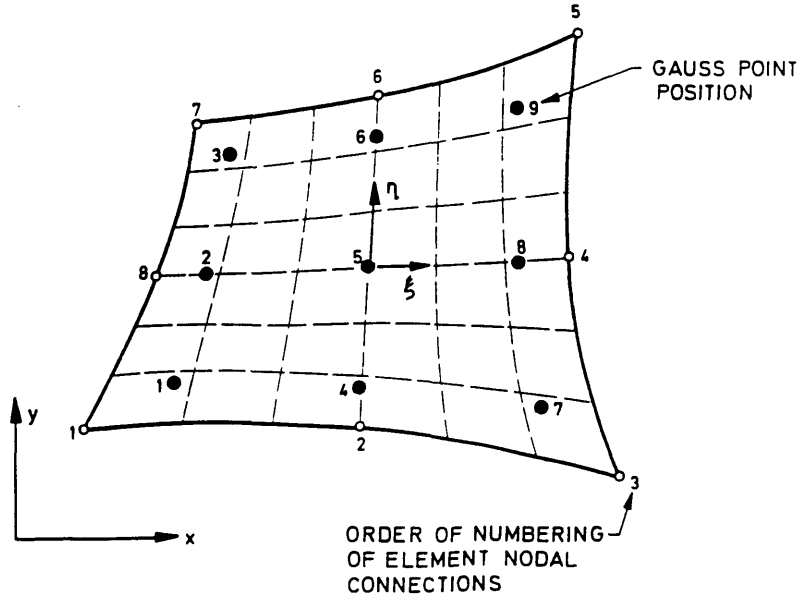

Figure (3.2) Orientation of local axes ξ, η, and order of Gauss point for two dimensional parabolic isoparamatric elements

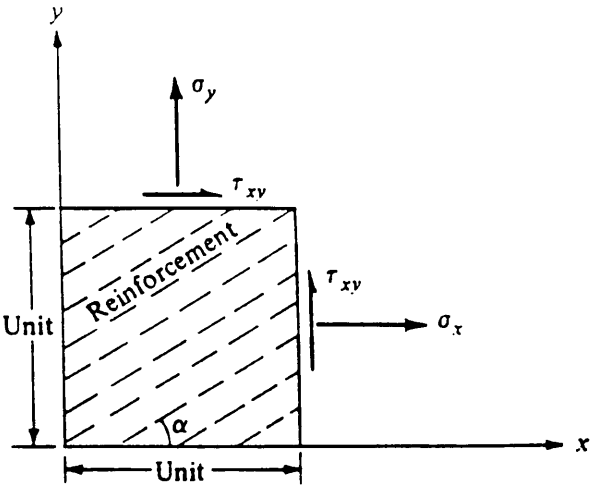

Figure (3.3) Distributed representation of steel.

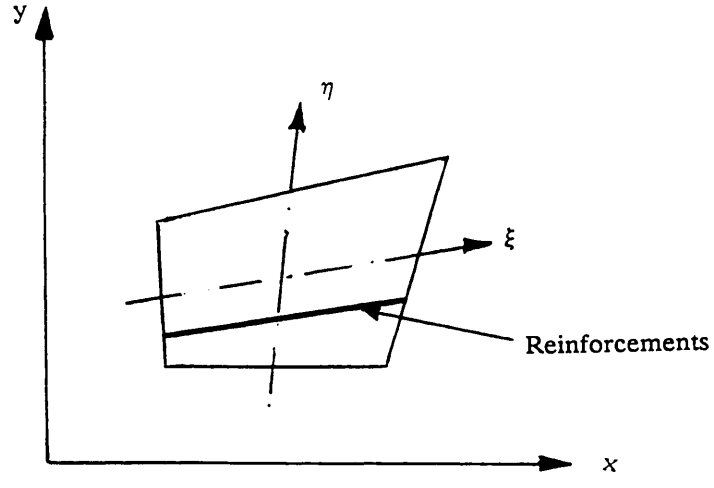

Figure (3.4) Embedded representation of steel.

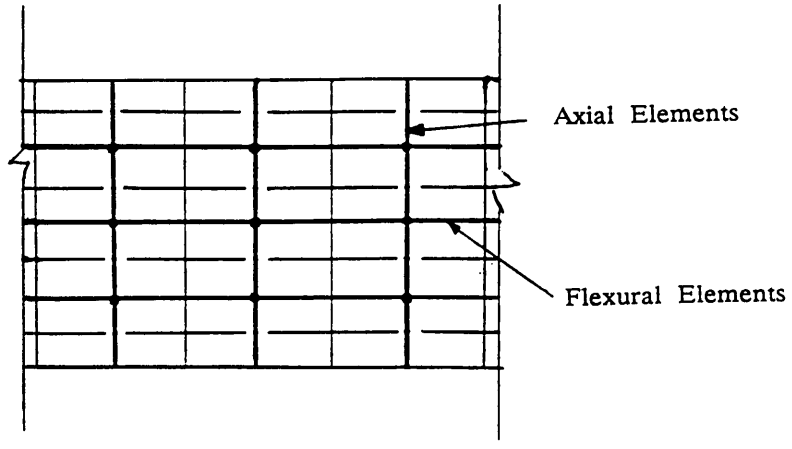

Figure (3.5) Discrete representation of steel

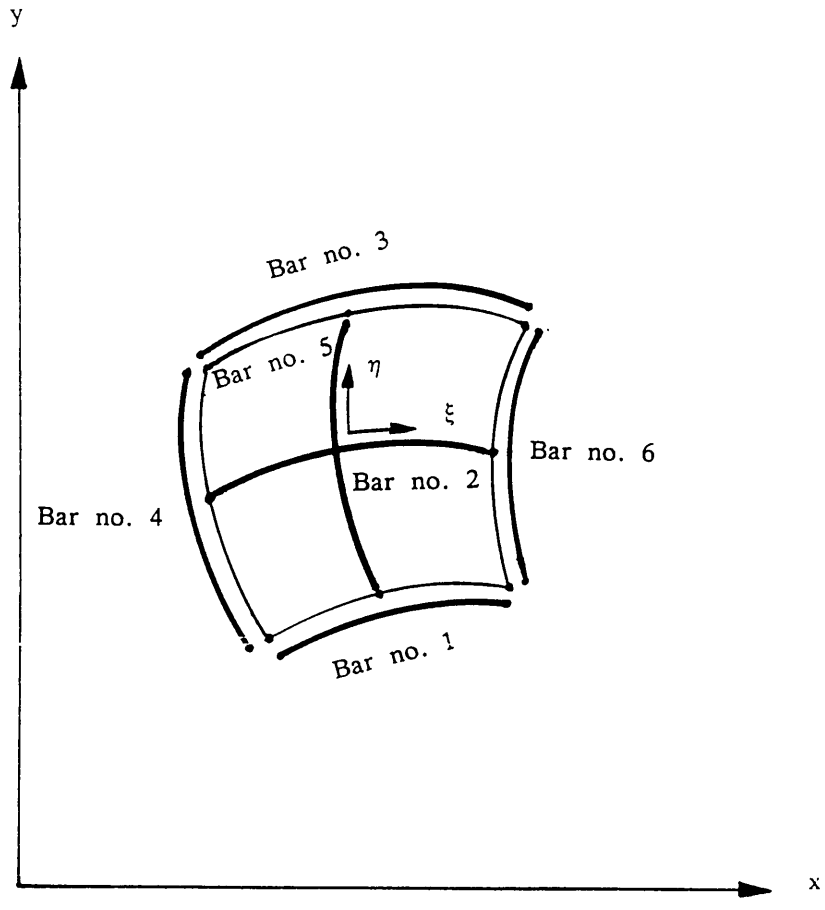

Figure (3.6) Bar element positions on the isoparametric element.

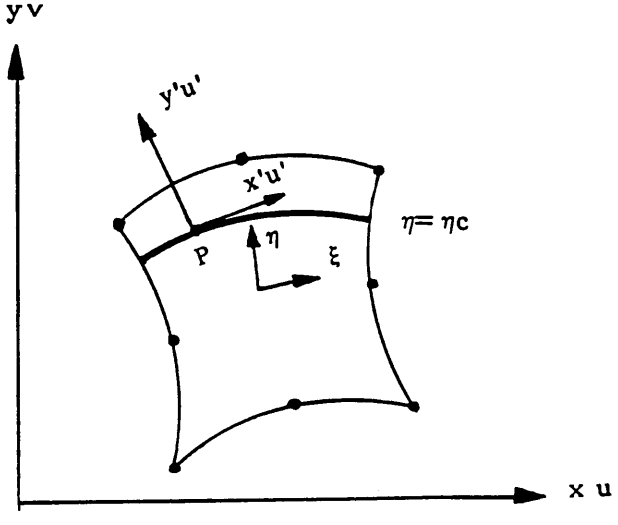

Figure (3.7) Bar element.

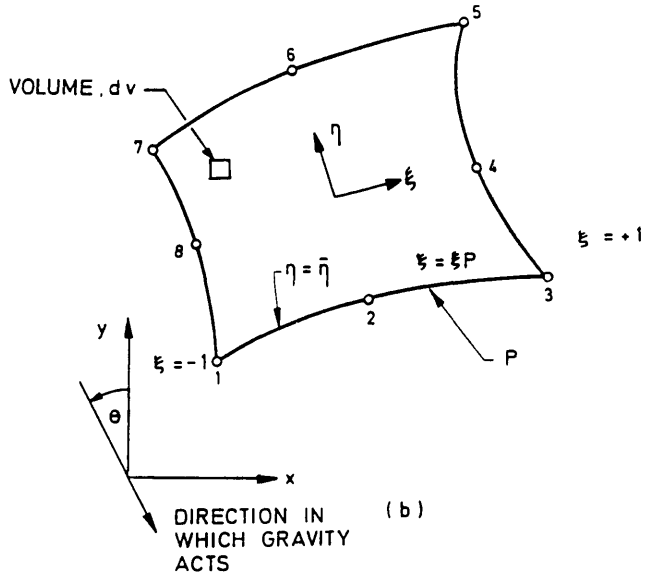

Figure (3.8) Application of point loads to two dimensional parabolic isoparametric elements.

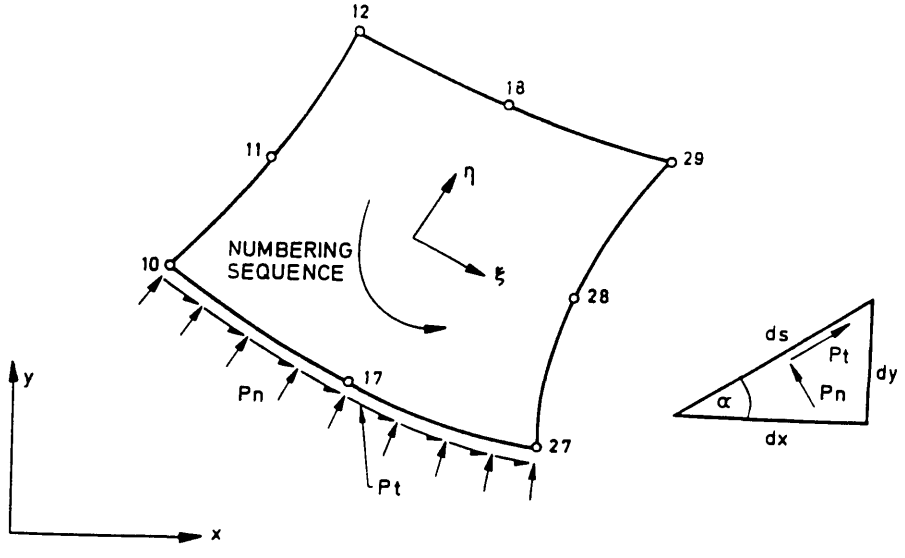

Figure (3.9) Normal and tanential load per unit length applied to a parabolic isoparametric element.

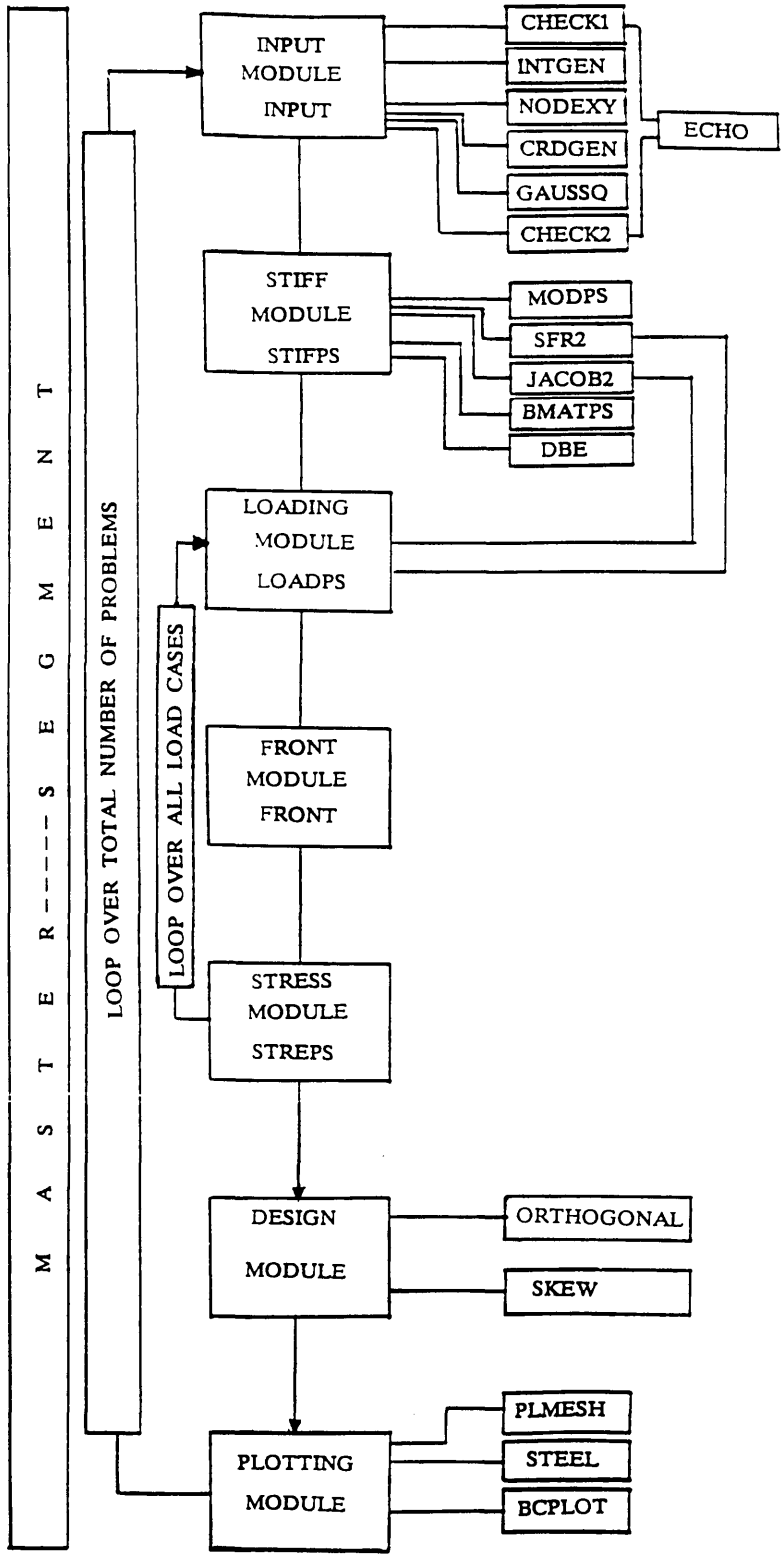

Figure (3.10) Flow chart of developed model

References

1. ZIENKIEWICZ, O.C., "The finite element method", McGrawhill, 3rd Edition, 1977.

2. COOK, R.D., "Concepts and applications of finite element analysis", Wiley, 1981.

3. NATH, B., "Fundamentals of finite elements for engineers", The athone press of the University of London, 1974.

4. OWEN, D.R.J. and HINTON, E., "Finite element in plasticity, Theory and practice", Pineridge press limited, Swansea, U.K.

5. HINTON, E. and OWEN, D.R.J., "An introduction to finite element programming", Academic press, 1977.

6. BHATT, P., "Programming the matrix analysis of skeletal structures", John willey & sons, Chichester, 1986.

7. PHILLIPS, D.V., "Nonlinear analysis of structural concrete by finite element methods", Ph.D. Thesis, University of Wales 1972.

8. Al- MANSEER, A.A., "A nonlinear finite element study of reinforced concrete beams", Ph.D. Thesis, University of Glasgow 1983.

9. MOHAMED, M.S., "A finite element and experimental study of reinforced concrete in torsion", Ph.D Thesis, University of Glasgow 1969.

10. AL- MAHAIDI, R.S.H., "Nonlinear finite element analysis of reinforced concrete deep members", Report No. 79-1, Cornell University, Itheca, New York, 1979.

11. ASCE, "Finite element analysis of reinforced concrete", State- of- the- art report 1982.

12. NIELSON, M.P., "Yield conditions for reinforced concrete shells in the membrance state", non- classical shell problems, IASS Symposium, Warsaw, 1963, (PP 1030- 1038)

13. CLARK, L.A., "The provision of tension and compression reinforcement to resist in- plane forces", Magazine of concrete research, Vol. 28, No. 94, March 1976 (PP 3- 12).

CHAPTER FOUR

NONLINEAR MODELLING OF REINFORCED CONCRETE

4.1 Introduction

The challenges in designing complex concrete structures has prompted analysts to acquire a sound understanding of reinforced concrete structural behaviour. In many cases conventional and code prescribed methods cannot be relied upon to provide realistic information, such as load deformation response, crack patterns, strengths, distorted shapes of structural elements, and failure mechanisms. This is primarily because of the complex behaviour of reinforced concrete under short term loadings.

Concrete is much weaker in tension than in compression. Hence, even at relatively low loads in many problems of practical consequence, concrete starts cracking and linearity is no longer preserved. Material nonlinearity is also caused by the yielding of steel and the "plasticity" of concrete in compression. Other nonlinearities arise from the complex action of the individual constituents of reinforced concrete e.g bond–slip between steel and concrete, aggregate interlock of a cracked concrete, tension stiffening between cracks and dowel action of reinforcement. Time–dependent effects such as creep, shrinkage, and temperature change also contribute to the nonlinear response. However, the major material nonlinear response is caused by cracking of the concrete, plasticity of reinforcement and the inelastic compressive response of concrete and any nonlinear procedure should include these as a minimum.

A structure may also exhibit nonlinear behaviour due to geometric nonlinearities; however, these tend to be associated only with certain special structural elements and systems in which the effects of displacements on internal forces must be considered in the analysis. Reinforced concrete transfer girders have small deflections, thus geometric nonlinearities have not been considered in this study. In order to study

more accurately the behaviour of such structures throughout the entire load range, it is important to extend the numerical process described in the previous chapter to include the nonlinearties described above.

A nonlinear finite element solution is obtained by a sequence of linear approximations using some iterative process which produces an overall response at any stage that satisfies the constitutive laws, compatibility and equilibrium conditions to some degree of tolerance. The obtained solution then represents the approximate nonlinear behaviour of reinforced concrete .

The progress made in the field of nonlinear analysis over the last two decades with the finite element technique has provided a reasonable method of prediction of the overall behaviour of a structure. In particular a variety of models have been proposed for predicting the nonlinear response of reinforced concrete. The ASCE Task Committee's state–of–the–art report[1] provides a useful summary of the various models up to 1982, whilst Chen[2] has provided a broad review of the various nonlinear material modelling techniques. A recent text edited by Hinton and Owen[3] also describes various models and their applications. For completeness, in this chapter the mathematical modelling of the material and nonlinear solution methods will be briefly explained and is based on earlier work and programs developed by Phillips[4,5].

It has been customary to consider the two constituents, concrete and steel reinforcement, as separate contributors to the overall stiffness and strength of the structure and this approach is also adopted here. Isoparametric elements have been used to model the concrete whilst a reinforcing element embedded in the main element is used to simulate the reinforcement. In this embedded reinforcement representation, full bond is assumed between steel and concrete. An advantage of

this representation is that bars can be more or less placed in positions corresponding to those in the real structure, leading to a more accurate analysis.

4.2 Numerical techniques for nonlinear analysis

The general basis of each method of nonlinear analysis is similar. For problems where only material behaviour is nonlinear, as considered in this study, the relationship between stress and strain is assumed to be of the form:

$$f(\sigma, \epsilon) = 0 \qquad (4.1)$$

The element stiffness matrix $[K]$ is a function of the material properties and can be written as:

$$[K] = k(\sigma, \epsilon) \qquad (4.2)$$

The external forces $\{R\}$ are related to nodal displacements $\{\delta\}$ through the stiffnesses of the element and can be expressed by:

$$\{R\} = [K]\{\delta\} \qquad (4.3)$$

Which on inversion becomes:

$$\{\delta\} = [K]^{-1}\{R\} \qquad (4.4)$$

Putting values of $[K]$ from equation (4.2) into (4.4) we get

$$\{\delta\} = [k\ (\sigma, \epsilon)]^{-1}\ \{R\} \qquad (4.5)$$

This derivation illustrates the basic nonlinear relationship between $\{\delta\}$ and $\{R\}$ due to the influence of the material laws on $[K]$.

The solutions of nonlinear problems by the finite element method are usually attempted by one of the following three basic techniques:

(i) Incremental (Step by Step)

(ii) Iterative (Newton Method)

(iii) Incremental– Iterative (Mixed Method)

These three methods will be briefly explained, but detailed discussion is presented by the state–of–art report[1], Chen[2], Al–Manaseer[6], Owen and Hinton[7] and Al–Mahadi[9].

4.2.1 Incremental method

In this method the intended or assumed total load on the structure is divided into small divisions called load increments. During each load increment, equation (4.3) is assumed to be linear i.e a fixed value of the new structural stiffness [K] is assumed using material data existing at the end of the previous increment in the updated material matrix [D]. Nodal displacements resulting from the loading of each increment are then added to the previously accumulated displacements. This process is repeated until the total load is reached[1,6,7,8,9].

The accuracy of this procedure depends on the increment size, the smaller the increments the better the accuracy, but at the same time more computational effort is needed. A modified version of this scheme is the "mid point Runge–Kutta" method[6,7]. In this, the first step is to apply half of the load increment and to evaluate new stiffnesses corresponding to the total stresses at this value. These stiffnesses are utilized to compute an approximation for the full load.

The increment method in its original and modified form do not take into account the force redistribution during the application of the incremental load (i.e no iteration process exists to restore equilibrium).

4.2.2 Iterative method[10,11]

In this method, the full load is applied in one increment. The resulting internal stresses are evaluated at that load according to the given material law. This gives equivalent nodal forces which may not be equal to the external applied loads i.e

equilibrium is not necessarily satisfied. The portion of the total loading which is not balanced is called "unbalanced nodal forces". These unbalanced forces are then used to compute an additional increment of the displacements, and hence new stresses, which give a new set of equivalent nodal forces. This process is repeated until equilibrium is approximated to a certain degree of tolerance. At this stage the total displacement is taken as the sum of the accumulated displacements from each iteration.

There are several variations of this basic process and a solution depends in many ways on the method used for computation of the stiffness matrix $[K]$ and the unbalanced nodal forces $\{Fu\}$.

(i) Computation of unbalanced nodal forces

In general, the linear constitutive law can be written in the form:

$$\{\sigma\} = [D](\{\epsilon\} - \{\epsilon o\}) + \{\sigma o\} \qquad (4.6)$$

where $[D]$ is the rigidity matrix, and $\{\sigma o\}$ and $\{\epsilon o\}$ are the initial stress and strain vectors. Equation (4.6) is in essence a linear approximation of the nonlinear relation between stress and strain, i.e.

$$f(\sigma, \epsilon) = 0 \qquad (4.7)$$

Adjustments to any of the quantities $[D]$, $\{\sigma\}$, or $\{\epsilon o\}$ in equation (4.6) can be made to approximate equation (4.7). Adjustments to $\{\epsilon o\}$ and $\{\sigma o\}$ are called the "initial strain" method and "initial stress" method.

In this study an extension of the initial stress method was used, hence only this will be explained. Equation (4.6) will become:

$$\{\sigma\} = [D]\{\epsilon\} + \{\sigma o\} \qquad (4.8)$$

Assuming $\{\sigma o\} = 0$ initially, equation (4.8) is solved with an approximate $[D]$ matrix and strain $\{\epsilon_A\}$ to obtain a certain level of stress $\{\sigma_{A1}\}$ where

$$\{\sigma_{A1}\} = [D]\{\epsilon_A\} \qquad (4.9)$$

The stress which should have occurred is:

$$\{\sigma_{A2}\} = [D]^{-1}\{\epsilon_A\} \qquad (4.10)$$

The difference between the stresses

$$\{\sigma o\} = \{\sigma_{A2}\} - \{\sigma_{A1}\} \qquad (4.11)$$

can be introduced as an initial stress in equation (4.8). Thus equivalent unbalanced nodal forces $\{Fu\}$ can be calculated from

$$\{Fu\} = -\int_V [B]^T\{\sigma o\}.dV \qquad (4.12)$$

which are then removed by applying them to the structure to obtain a correction to $\{\delta\}$. This process is repeated until $\{\sigma o\}$ or $\{Fu\}$ becomes negligible. The steps in the initial strain method are very similar.

(ii) Method for computing stiffness[6,7,9,10,11]

The stiffness can be either constant or variable throughout the solution. In the constant stiffness method, the linear stiffness as given in equation (4.8) is used at every stage in the analysis.

Although this method has an advantage of calculating the stiffness only once, it still requires a high number of iterations to achieve the desired accuracy, especially when nonlinearity occurs due to the cracking of concrete and yielding of steel. This is due to the sudden large changes that are caused in the stiffness. Accelerator processes could be employed but improvement cannot be guaranteed, and in general there has been a poor rate of success.

In the variable stiffness method, a linear solution is performed but the material matrix $[D]$ is adjusted during each iteration. The adjustments can be done by using either a tangential or secant modulus approach.

This method is a form of the well known "Newton– Raphson" method and requires considerably less iterations than the constant stiffness method, although a full solution is much more expensive than a resolution with constant stiffness.

A cheaper version of the variable stiffness approach can be obtained by using the modified "Newton– Raphson" method, where the stiffnesses are updated only at certain iterations. Figure (4.1a) shows the different methods used for the iteration procedure.

4.2.3 Incremental– iterative (Mixed method)[1,3,5,6,11]

In this method a combination of incremental and iterative schemes are used. The load is applied in small increments and a solution at each increment is obtained iteratively until equilibrium is obtained to a certain degree of tolerance. This method combines the advantages of both the incremental and iterative methods, hence it tends to minimize the disadvantages of each, and so nowadays is used very widely. Figure (4.1b) shows the different methods of the mixed procedure.

4.3 Method used in this study

There have been significant improvements in nonlinear solution techniques in recent years leading to a wide choice of solution strategies, including modified Newton– Raphson techniques, quasi– Newton techniques, arc– length methods etc. These techniques can be applied in conjunction with line search algorithms, accelerators, self adaptive techniques which automatically adjust load steps and so on. To date, many of these techniques have been applied successfully to concrete structures; however, the modified Newton– Raphson technique still seems to be the most popular.

In this study basically the mixed method is used in conjunction with the modified "Newton– Raphson" approach to evaluate the stiffness, using a tangential elasticity material property matrix. Four different algorithms were available for updating the stiffness, which could be selected as options within the program[4], as follows:–

(a) KT0; the "initial stiffness" process

(b) KT1; where $[K]_T$ is recalculated at the start of each load increment only

(c) KT2; where $[K]_T$ is recalculated at the start of the first iteration only

(d) KTA; the general "variable stiffness" process.

In order to calculate the unbalanced nodal forces, a modification of the initial stress method is used. The basic aim is to check the applied loading system against the equivalent forces caused by the total stress level rather than calculating initial stresses. The difference between these two will give a set of residuals which are a measure of any lack of equilibrium. The residuals are then applied to the structure to restore equilibrium. The process is repeated until the residuals are sufficiently small. Thus, for equilibrium, it is required that

$$\{Fu\} = \int_V [B]^T \{\sigma\}.dV - \{R\} = 0 \qquad (4.13)$$

where $\{\sigma\}$ are the actual stresses depending on the constitutive law being used, $\{R\}$ lists all forces due to the external loads, initial stress etc, and $\{Fu\}$ are the residual forces which are a function of the displacements.

4.4 Convergence criterion

In order to identify the elimination of the "out of balance forces" and to terminate the iterative process, a reliable convergence criterion is required. The user specifies the accuracy by giving quantitative values known as convergence tolerances. The convergence tolerance must be realistic; if generally too loose, inaccuracy may result, if too tight, much expensive effort may be spent in obtaining needless accuracy.

A convergence criterion can be based on checking the residual decay of every degree of freedom, but this process is expensive. Therefore an overall check based on some norm is preferable and in this study convergence was assumed when the relation

$$Fui^*/Ri^* \leqslant C \qquad (4.14)$$

was satisfied, where $Fui^* = \sqrt{\{Fu\}i^T\{Fu\}i}$ is the norm of residuals, $Ri^* = \sqrt{\{R\}i^T\{R\}i}$ is the norm of applied loads and C is the preselected convergence factor usually about 0.01 to 0.05.

4.5. Brief review of reinforced concrete behaviour

4.5.1 Behaviour of concrete

A reliable prediction of the response of a reinforced concrete structure requires a knowledge of the behaviour of concrete in its elastic and nonlinear ranges under various combinations of stress. Despite widespread use of structural concrete over a considerable length of time, this knowledge is still incomplete. For instance, there is no universally accepted triaxial failure criterion under combinations of tensile and compressive stresses. Until recently most tests on biaxial and triaxial stress behaviour, have concentrated on strength characteristics rather than obtaining stress–strain relationships. However the availability of data regarding deformational characteristics for biaxial stress states is now beginning to improve whereas there has been a respectable body of experimental data pertaining to deformations for concrete under uniaxial conditions for a number of years.

In this section the work done on the stress–strain behaviour and strength of concrete under short term loading will be described for uniaxial and biaxial stress states. This will give sufficient background for the constitutive models for concrete which will be described in this chapter.

4.5.1.1 Uniaxial stress behaviour

A typical stress strain curve of concrete subjected to a monotonically increasing uniaxial compressive state of stress, is given in Figure (4.2) and illustrates that:

(i) There is an almost linear relationship to about 30% of its ultimate load. Microcracks exist in the concrete at this stage, primarily due to stress and strain concentrations resulting from its heterogeneous nature, however, these cracks are stable and have little tendency to propagate. Prior to loading, microcracks can exist at the aggregate paste interface, due to phenomena such as settlement of fresh cement, hydration of cement paste, differential volume changes due to shrinkage or thermal movements.

(ii) Up to 30–50% of ultimate load, micro–cracks begin to propagate, but at a very slow rate. Bond cracks around the aggregate start to extend due to stress concentrations at crack tips. Mortar cracks remain negligible until a later stage. For this stress range, the available internal energy is approximately balanced by the required crack release energy. The stress–strain curve begins to show increasing curvature.

(iii) At 50–75% of ultimate load, some cracks near aggregate surfaces start to bridge in the form of mortar cracks and a much more extensive and continuous crack system then propagates into the matrix. If the load is kept constant, the cracks continue to propagate with a decreasing rate to their final lengths.

(iv) For compressive stresses above 75%, the largest cracks reach their critical lengths. The available internal energy is now larger than the required crack release energy and crack growth becomes unstable and the stress strain curve becomes increasingly nonlinear towards ultimate stress and will begin to strain soften[2,4,12].

The uniaxial compressive strength of concrete is the most common measure for

assessing the quality of concrete. It is suggested that the cylindrical compressive strength of concrete is more meaningful than cube strength, since the ratio of the height to width of a cylinder is higher than the height to width ratio of a cube[1,3,5].

The uniaxial tensile stress–strain curve of concrete is much more linear than the uniaxial compressive stress–strain curve. Up to approximately 60% of the ultimate stress, the microcracks have negligible effect on the curve. This stress level corresponds to the limit of elasticity, above this level microcracks starts to grow. As the uniaxial tension stress tends to arrest the cracks much less frequently than the compressive stress, one can expect the interval of stable crack propagation to be relatively short. A reasonable value for the onset of unstable crack propagation will therefore be about 75% of f_t'.

4.5.1.2 Biaxial stress behaviour

A biaxial stress condition occurs when the principal stresses are acting in only two directions and the third principal stress is zero. Under different combinations of biaxial loading, concrete exhibits strength and stress–strain behaviour somewhat different from that under uniaxial conditions.

Typical stress–strain curves for concrete under biaxial stress in compression–compression, tension–compression and tension–tension states are shown in Figure (4.3) to (4.5). These curves were obtained from the classical experimental study by Kupfer et al[12]. The uniaxial compressive stress–strain curve is shown in these figures for comparison.

The figures show that the curves are mostly linear up to about 40% of the ultimate stress. There is also a small permanent deformation which might be due to

microcracking; this limit is called the "initial discontinuity point" or the "elastic limit". In two dimensional principal stress space this elastic limit is represented by envelope 1 in Figure (4.6). Beyond this stress state larger cracks form, internal disruption of the material takes place and substantial permanent deformations are produced. Figure (4.6) also illustrates the envelopes 2, 3,4 for other important points in the stress– strain relationship.

A detailed discussion of the experimental data given by Kupfer et al and that of other workers has been given by Phillips[4], Chen[2], and Hinton and Owen[3], for example, and only the main points relevant to this study are summarized here:–

(i) The behaviour can be broadly classified into two categories conveniently defined by its mode of failure, brittle or cleavage– type failures caused by biaxial tensile stresses, and "ductile" or shear– type failures under biaxial compressive stress.

(ii) The ultimate strength of concrete under biaxial compression is greater than that under uniaxial compression, mainly due to the confinement of the microcracks.

(iii) The ultimate strength increase in biaxial compression, fcb, is dependent on the ratio of principal stresses. The biaxial compressive strength, fcb, is 1.1 to 1.4 times the uniaxial compressive strength, fc'. The greatest increase in strength is given by a stress ratio $\sigma 1/\sigma 2$ of about 0.5; this diminishes somewhat as the ratio is increased to unity.

(iv) The variation in Poisson's ratio is small until the start of stable crack propagation at "critical load". The value of ν typically varies between 0.18 for biaxial tension to 0.2 for biaxial compression, this difference being negligible for practical purpose.

(v) In biaxial compression the volume decreases linearly up to 30– 50% of the ultimate load, after which the rate of reduction slowly increases. A point of inflection is reached at about the "critical load" level and a minimum value follows

shortly afterwards close to the maximum load (at 95% according to Kupfer). The volume then expands very rapidly and often becomes greater than the original unloaded volume. The volumetric concrete strain corresponding to maximum stress varies from 0.0008 (uniaxial compressive stress) to 0.0025 (biaxial compressive stress) as shown in Figure (4.7).

(vi) Biaxial and uniaxial tensile stress– strain curves are similar in shape.

(vii) The uniaxial tensile strength of concrete is slightly higher than the strength under biaxial tension.

4.5.2 Behaviour of steel

Since steel reinforcement is predominantly uniaxial, it is generally not necessary to introduce the complexities of multiaxial constitutive relationships. A typical uniaxial stress– strain diagram for steel is shown in Figure (4.8). It is clear that the relationship is linear and elastic until the "proportional limit" P is reached. For a further small range of stress increase the strain is still elastic but no longer linear. The "yield point" Y is then reached and this marks the start of plastic deformation. The difference between P and Y is small for most steels and is usually neglected in practical applications. Beyond the yield point, plastic flow occurs with strain increasing at a much greater rate.

Generally, stress must be increased to cause further deformation, a condition termed strain hardening. Finally, a maximum stress is reached at point V, after which a descending tail occurs to fracture at P.

For some steels, the yield point is poorly defined so that it is arbitrarily taken to be at some fixed value of permanent strain, as 0.001 or 0.002, where the corresponding stress is known as "proof strength". The value of strain at the yield point is usually of the order 0.001.

Some steels, like mild steel, exhibit a small but sharp drop in load after the yield point to a lower yield level. Strain then increases plastically at more or less constant load to about ten times the yield strain. At this point material begins to work harden. Clearly the lower yield point should be used for calculation purposes. It is noted that strains are now large at the ultimate strengths, but that the stress is usually referred to the original area. This point is well above any strain which can be developed in concrete structure, so we shall be concerned mainly with values at yield.

Similar behaviour is generally assumed for both tension and compression. Figure (4.9) shows four different finite element idealizations which are commonly used for reinforced steel behaviour. For each case it is necessary to define, experimentally, the value of the stresses and strains at the onset of yield, and the strain hardening modulus after yield up to the ultimate tensile strength as well as the elastic modulus.

4.5.3 Cracking and post– cracking behaviour of reinforced concrete

The tension failure of concrete is characterized by a gradual growth of cracks, which join together and eventually separate parts of the structure. It is a usual assumption that the forming of cracks is a brittle process.

Two main mechanisms develop after cracking through which shear is transferred across the cracked section. These are aggregate interlocking on the two adjacent surfaces of the crack and dowel action of any reinforcing bars crossing the cracks.

If the surface of the crack is rough, it is possible that the opposite faces of the crack will interlock when subjected to differential movement as shown in Figure (4.10). This depends on the texture of the cracked surface as well as any

restraining force that can keep the cracked surfaces from moving apart, allowing forces to transmit across the crack. The frictional resistance depends on the properties of aggregate and mortar, the condition of the crack surface, and the width of crack. If the cracked surface is smooth, frictional resistance would be small and if the crack width becomes large the surface would completely separate and interlocking would cease. The important effect of this phenomenon is that shear stress along the crack will not be zero.

This factor plays an important role in post–cracking behaviour of reinforced concrete. For example, in reinforced concrete beams after the initiation of inclined cracking, at least 40% to 60% of the shear force is carried by aggregate interlocking.

Reinforced bars also act as dowels as shown in Figure (4.11), where major shear deformation has occured after the development of the tension cracking and the reinforced bar will also resist the concentrated shear force[2,6]. There are various factors which effect the dowel action, such as the number of bars crossing the cracked concrete zone, diameters of the bars, the orientation of bars with respect to crack direction, specimen geometry, length of the reinforcement bars and its arrangements, and concrete cover to the bars.

Although a considerable amount of experimental research has been carried out to quantify the dowel action contribution to shear transfer, it is still very difficult to take into account dowel effect precisely for a particular problem. Much still remains to be done before any definitive formulae can be used in finite element analysis. In order to take into account shear transfer across cracks in the finite element analysis due to aggregate interlocking and dowel action of reinforcing bars, in this study a parameter known as shear retention factor to take equivalent shear stiffness and

strength of cracked concrete is used, and will be discussed in section 4.7.

In practice, the material between discrete cracks can exhibits a state of strain which sometimes causes the crack to close. The movement required to close the crack would be less than that needed for initial crack formation and it is also possible that the crack may not be able to close perfectly. In order to take account of crack closing, a formulation is incorporated in the finite element model, assuming as crack has closed perfectly and the shear is considered as like a uncraked concrete, although the plane would be weaker in reality, this will be discussed in this chapter later.

In plane stress situation, once a primary crack has occured, on the further loading a secondary crack could develop in the non–orthogonal direction to the first crack. This plays an impotant role in the nonlinear finite element analysis and have been taken into account in this study and will be discussed later in this chapter.

4.5.4 Bond–slip phenomenon between steel and concrete

Bonding between concrete and steel is created by chemical adhesion, friction and mechanical interlock between these two materials. Loads are very rarely applied directly to the reinforcement, steel receiving its share of the load from the surrounding concrete. Bond stress is a name given to shear stress at the steel–concrete interface, which, by transferring load between the bar and the surrounding concrete, modifies the steel stresses. It can be measured by the rate of change of force or stress in the reinforcing bars[20].

In simplified analysis of reinforced concrete structures, it is assumed that a perfect bond exists between the concrete and steel. But this assumption is not valid in those regions of the structure where considerable stresses are transferred between the

concrete and steel. Slip between concrete and steel occurs when cracks appear along the concrete–steel interface.

In finite element analysis, the bond–slip phenomenon can be accounted for by using linkage elements, or interface elements connecting the nodes of steel and concrete finite elements. The linkage element is composed of two orthogonal springs which connect and transmit shear and normal forces between separate nodes. Each spring must be given a certain value of interface shear stiffness obtained from experimental pull out tests. A very high stiffness is given to the spring, perpendicular to the bar, to prevent any separation between the bar and concrete. It is difficult to give realistic values for the stiffness of springs perpendicular to the bar. Details of this method are presented elsewhere[1,21,22,23].

The advantage of using linkage elements is that there are no physical dimensions, i.e two different deformations are allowed to occur at a common node. But it has the disadvantage of being an expensive process, especially when there are a high number of bars used at different layers.

An alternative method of taking into account the concrete–steel bond in the finite element analysis is to use a "tension stiffening" approach in which a gradual softening curve for concrete after cracking is defined. This approach is based on the fact that, as a crack occurs, the bond fails, causing some movement between the bar and concrete. This will then cause the shear force at the contact surface between the cracks to feed tension stresses into the concrete. The concrete attached to the bar will contribute to the overall stiffness of the system, and this is accounted for by the gradual stiffening curve.

The bond–slip phenomenon can only be modelled through linkage elements when

the reinforcement is represented by discrete elements. In this study embedded reinforcement representation is used, and as a result the use of linkage elements is not possible. Nevertheless, with embedded bar representation, the tension stiffening method has proved helpful in accounting for the bond– slip activity.

4.6 Development of material modelling

4.6.1 Cracking of concrete

Two fracture criterion are most commonly used: the maximum principal stress criterion and the maximum principal strain criterion. These state that when a principal stress or strain exceeds its limiting value a crack occurs in a plane normal to the crack direction of the offending principal stress or strain and the crack direction is fixed for all subsequent loading. The maximum stress criterion is more commonly used than the maximum strain criterion, although it has been reported that the maximum strain criterion can predict stiffer behaviour than the maximum stress criterion[4].

In finite element analysis three different approaches have been most commonly used for representation of the cracks. These are classified as follows:

(i) Smeared– cracking Model

The cracked concrete is assumed to remain a continuum i.e the cracks are smeared out in a continuous fashion. A crack is not discrete but is represented by an infinite number of parallel fissures across the applicable part of the element, as shown in Figure (4.12). Once concrete is cracked, the material is assumed to change from isotropic to an orthotropic with one of the material axes being oriented along the direction of the crack. The element stiffness matrix will be modified. Thus, the stiffness across the crack will not reduce to zero and cracked concrete will continue to carry tensile stresses. The stiffness and stresses will depend on many factors such

as the amount of reinforcement crossing a crack, local bond characteristics and the strain softening behaviour of concrete after fracture. Such a formulation easily allows a gradual drop of strength in direction perpendicular to the crack and any reserve shear strength due to aggregate interlocking can be taken into account by retaining a positive shear modulus.

The smeared– cracking model was used in this study, since it is capable of predicting load deflection behaviour and general stress– strain distribution. In addition the problem of continuously altering the topology of the structure as cracking progresses was avoided. Moreover the initiation, orientation and propagation of cracks at sampling points are automatically generated resulting in a general solution.

(ii) Discrete– cracking Model

In discrete– cracking models, the nodes of the adjacent elements are assumed to be separated when a crack occurs, as shown in Figure (4.13). The most obvious difficulty in this approach is that knowledge of the location and orientation of cracks are not known in advance. Thus, geometrical restrictions imposed by the preselected finite element mesh can hardly be avoided. The model also requires, the ability to redefine the element nodes, making this technique extremely complex and time consuming.

(iii) Fracture mechnaics Model

The success of fracture mechanics theory in solving various types of cracking problems in metals, ceramics, and rocks has lead to its use in finite element analysis of reinforced concrete structures. By assuming concrete is a notch– sensitive material, a cracking criterion based on tensile strength may be dangerously unconservative, and the use of this method will provide a more rational approach to concrete cracking[2]. However, in its current state of development, the use of this model in

reinforced concrete is still questionable and much remains to be done.

4.6.2 Crack simulation by fixed crack model

4.6.2.1 Opening of cracks

As mentioned earlier the cracking of concrete is generally modelled by linear elastic– fracture relationships as shown in Figure (4.14). The comparison of the most commonly used maximum principal stress and strain in the biaxial state of stress is shown in Figure (4.15). It is clear that both these theories are similar, in particular when $\nu = 0$, they became identical. According to the basic hypothesis of the fracture model, when a principal stress or strain exceeds its limiting value, a crack is assumed to occur perpendicular to the stress or strain and the crack direction, αc, is fixed for all subsequent loading[1,2,4,5]. This is known as a "fixed crack model".

Thus for cracking:–

$$\sigma i \geqslant ft'$$
$$\text{or } \epsilon i \geqslant \epsilon cr \quad i=1,2, \tag{4.15}$$

where σi is the principal stress in both directions, ft is tensile strength of concrete, ϵi is the principal strains in both directions, and ϵcr is the cracking strain of concrete.

It is assumed that material parallel to the crack is capable of carrying stresses according to the uniaxial condition prevailing parallel to the crack. On further increase in loading, cracks may occur at some angle to the first crack. For simplicity, it is commonly assumed that the second crack will be orthogonal to the first crack and is also predicted by tensile stress or strain parallel to the plane of the initial crack. This is known as the fixed, orthotropic smeared crack model.

Thus for a second crack:–

$$\sigma t^* \geqslant ft'$$
$$\text{or } \epsilon t' \geqslant \epsilon cr \tag{4.16}$$

4.6.2.2 Closing of cracks

A crack is assumed to close perfectly if the normal strain across the crack is compressive, and then the full compressive stress can again be transmitted across the crack.

$$\text{i.e } \sigma n^* < 0 \qquad (4.17)$$

The initial modulus of elasticity is then assumed and stress is calculated accordingly. The shear resistance on this closed, weakened plane will now depend on a number of factors similar to shear transfer on an open crack e.g normal compressive stress and interface characteristics. The shear stress can be calculated as:

$$\tau^* = \beta' G \gamma^* \qquad (4.18)$$

where β' is a preselected constant or given by another function such that $0 \leqslant \beta' \leqslant 1$. In this study β' was assumed equal to 1, implying a perfect "healing" of the crack.

The procedure for the reopening a crack is similar to the initial formation, except that instead of a limiting tensile stress or strain, any tensile strain will cause reopening.

$$\text{i.e } \epsilon n^* \geq 0 \qquad (4.19)$$

where ϵn^* is the stress perpendicular to the crack.

4.7 Modelling of post-cracking behaviour using quasi-material parameters

There are various numerical parameters involved in nonlinear finite element analysis. Two important parameters used frequently nowaday are the shear retention and tension stiffening factors. These parameters can be considered as material properties, since they try to represent actual physical phenomena but, in fact they tend to be used more as numerical parameters which are adjusted in sensitivity studies prior to a final solution. Therefore, they are not material parameters in the actual sense and hence, we call them quasi-material parameters here.

4.7.1 Shear retention

A considerable amount of work has been carried out on this activity experimentally, and various analytical expressions have been suggested. However, these equations cannot be used directly in finite element methods which use smeared crack models because of crack width measurements etc. To account for shear transfer across the cracks in finite element analysis, the shear retention factor, β, was introduced by Phillips[4] and Schnobrich[24]. This parameter can be defined as an assumed numerical factor (0.0−1.0), which is used in the theoretical cracking model to take into account the reduction in the shear modulus after the development of a crack. In the smeared−cracking model, shear transfer is modelled as:−

$$\beta = G'/G \qquad (4.20)$$

where G' is the reduced shear modulus for cracked concrete and G is the shear modulus of concrete.

There are two main methods using the shear retention factor, these are the constant shear retention factor method, where β is chosen rather arbitrarily and kept constant[4,13], and the variable shear retention factor method, where β is assumed to vary as a function of the strain normal to the crack[9,14]. Recent studies carried out by Al−Manaseer and Phillips[15] and Phillips and Mohamed[16] have shown that the variable shear retention factor method predicts the behaviour in deep beams more accurately than the constant shear retention factor method.

The use of β has provided satisfactory results in most cases and values greater than 0 were found necessary in order to prevent numerical difficulties. Unfortunately the shear retention factor would appear to be dependent on the type of structure being studied and its failure mechanism This is reflected in the different recommended values resulting from other research carried out on post−cracking behaviour activity.

Nevertheless, in this study, three different shear retention factor models have been incorporated into the program. These shear retention models are presented in Figure (4.15). and are given by:

$$\beta = G'/G \qquad (4.21)$$

$$\beta = 0.4.G/(\epsilon/\epsilon t') \qquad (4.22)$$

For $\epsilon<\epsilon t'<1$ $\quad \beta=1.0$

For $1<\epsilon<\epsilon t'\leqslant\beta 3$ $\quad \beta=\beta 1-\beta 4[(1-2\beta 3)+2\beta 3(\epsilon/\epsilon t')-(\epsilon/\epsilon t')^2]$

where

$\beta 4 = (\beta 1-\beta 2)/(1-\beta 3)^2$ and $\partial\beta/\partial\epsilon = 0$ at $\epsilon/\epsilon t' = \beta 3$

For $\epsilon>\epsilon t'>\beta 3\epsilon t'$ $\quad \beta=\beta 2$ (4.23)

where $\epsilon t'= ft'/Ec$, ft' is the uniaxial tensile strength of concrete and Ec is Young's modulus of concrete and ϵ is the current strain at a particular load level normal to the crack.

The $\beta 1$, $\beta 2$, and $\beta 3$ are the shear retention factor parameters defining the shape of the law[11]. $\beta 1$ represents the sudden loss of stiffness at the crack formation; $\beta 2$ represents a reserve of shear stiffness due to dowel action of any steel, $\beta 3$ represents the rate of decay of stiffness as the crack widens and the crack surface deteriorates. It is difficult, experimentally, to obtain values for $\beta 1$, $\beta 2$ and $\beta 3$, however, the values suggested by Mohamed[8] have been used in the program. From a study on deep beams, it was concluded that the value of $\beta 1$ could range from 0.4 to 0.5, the value of $\beta 2$ a could be 0.2 and for $\epsilon t.\beta 3$ a value of 0.003 to 0.0035.

4.7.2 Tension stiffening

Tension stiffening is a method of retaining some stress when a crack occurs. This phenomenon was first introduced into finite element analysis by Scanlon and Murray[17] who assumed that when concrete reaches its ultimate strength in tension, a primary crack will form, but that the cracked concrete will carry some tensile

stresses perpendicular to the crack direction. Since then, this method has been used by many researchers, who have shown that it can have a significant effect on load deflection behaviour of a structure.

Many approaches have been tried by many researchers for approximating tension stiffening, e.g a descending branch beyond the cracking point and the use of coarse tolerances[6] etc. Currently, the descending branch approach is most commonly used and that of Al– Manaseer and Phillips[15] was used in this study. The model is shown in Figure (4.17) and assumes that:

$$\text{For } \epsilon/\epsilon t' \leqslant 1 \qquad E_T = E \tag{4.24}$$

$$\text{For } \epsilon/\epsilon t' \geqslant 1 \leqslant \alpha 2 \qquad \sigma_T = [\alpha 1 . ft(\alpha 2-(\epsilon/\epsilon t'))]/(\alpha 2-1)$$

$$E_T = \sigma_T/\epsilon \tag{4.25}$$

$$\text{For } \epsilon/\epsilon t \geqslant \alpha 2 \qquad \sigma = 0$$

$$E_T = 0 \tag{4.26}$$

The value of E_T is evaluated from the above equation (4.25) at any iteration during the loading process and is used in the material property matrix $[D]^*$ depending on whether the crack is caused by principal stress $\sigma 1$ or $\sigma 2$.

$\alpha 1$ and $\alpha 2$ are difficult to select in practice because of the lack of experimental data. An increasingly accepted trend is that they should be related to fracture energy of the concrete, G_F, which is associated with strain softening behaviour of cracking concrete. This is also reduces the dependency of the model on element size. It can be done by relating fracture energy of an opening crack to a characteristic length lc of the crack which is in turn related to the volume represented by sampling point[15]. Thus, the relationship given by equation (4.25) can be presented in fracture energy form as:

$$G_F = 0.5\alpha 1\alpha 2 ft\, \epsilon t \tag{4.27}$$

from which $\alpha 1$ and $\alpha 2$ can be evaluated. Al–Manaseer and Phillips[15] suggested a first approximation for lc as $V^{1/3}$ where V is the volume of concrete represented by the sampling point. For a normal concrete G_F varies from 50 to 200N/m. However, the concept of fracture energy is only applicable to a single crack in plain concrete and therefore it does not account for tension stiffening effects between cracks, nor the presence of reinforcement, nor the fact that a sampling point represents the overall effect of a number of cracks.

Indeed it is difficult in practice to select appropriate values of $\alpha 1$ and $\alpha 2$, because there are no specifically accepted values for $\alpha 1$ and $\alpha 2$; studies, completed by various researchers, have shown that the values depend on the type of structure and the type of failure experienced, for example in flexural failure these factors have a greater influence. However, the use of tension stiffening appear to offer a reduction in computational effort and stabilizes the solution.

4.8 Constitutive relations

The material property matrix for uncracked isotropic concrete in the plane stress situation was given in the previous chapter. The incremental form in global directions is given by the relationship, for plane stress

$$\begin{Bmatrix} \Delta\sigma x \\ \Delta\sigma y \\ \Delta\tau xy \end{Bmatrix} = \frac{E}{(1-2\nu)} \begin{bmatrix} 1 & \nu & 0 \\ \nu & 1 & 0 \\ 0 & 0 & G/E(1-\nu^2) \end{bmatrix} \begin{Bmatrix} \Delta\epsilon x \\ \Delta\epsilon y \\ \Delta\gamma xy \end{Bmatrix} \qquad (4.28)$$

$$\text{and } \Delta\sigma z = -\nu/E(\Delta\sigma x+\Delta\sigma y) \qquad (4.29)$$

where E, ν and G may be tangential values according to the compressive constitutive relationships.

Thus $\Delta\{\sigma\} = [D_T]\,\Delta\{\epsilon\}$ (4.30)

where $[D_T]$ is the tangential elasticity matrix.

Once the crack has occurred, the form of the elasticity matrix is modified according to the given tension stiffening law and preserved. The shear term is retained to take account of shear transfer. The constitutive relationship in crack directions are then given by

for plane stress

$$\begin{Bmatrix} \triangle\sigma n^* \\ \triangle\sigma t^* \\ \triangle\tau^* \end{Bmatrix} = \begin{bmatrix} E_{T1} & 0 & 0 \\ 0 & E_{T2} & 0 \\ 0 & 0 & \beta G \end{bmatrix} \begin{Bmatrix} \triangle\epsilon n^* \\ \triangle\epsilon t^* \\ \triangle\gamma^* \end{Bmatrix} \qquad (4.31)$$

$$\text{and } \triangle\epsilon z^* = -\nu/E(\triangle\sigma t^*) \qquad (4.32)$$

$$\text{Thus } \triangle\{\sigma\}^* = [D_T]^* \triangle\{\epsilon\}^* \qquad (4.33)$$

where $[D_T]^*$ is the tangent elasticity matrix in the crack direction, E_T is the reduced modulus of elasticity due to the crack and β is the shear retention factor, detail is discussed in section 4.7.

In plane stress, the values of the normal strain ϵz^* are affected when a crack occurs, therefore, after crack formation the normal strains are adjusted to.

$$\epsilon z^* = \epsilon z + \nu/E.\sigma n \qquad (4.34)$$

where σn is the stress across the crack prior to formation

When using $[D_T]^*$ for the new stiffness calculations, it is essential, for numerical reasons, to avoid zero values on the diagonal terms, and so these are set to comparatively small positive values if no tension stiffening is in use, causing the stiffness normal to the cracked plane to effectively vanish. The value of the diagonal terms will be determined from the descending branch of the uniaxial stress–strain curve if tension stiffening is used.

As $[D_T]^*$ is constructed in a local co–ordinate system coinciding with the angle of crack, it is necessary to transform it back into the global co–ordinate system for

stiffness calculations.

The constitutive law in the global co-ordinate system is given by equation 4.30.

$$\Delta\{\sigma\} = [D_T]\,\Delta\{\epsilon\} \tag{4.35}$$

and in local crack directions by equation

$$\Delta\{\sigma\}^* = [D_T]^*\,\Delta\{\epsilon\}^* \tag{4.36}$$

The two sets of strains are related by transformation rules as follows (where αc is defined in Figure (4.18)).

$$\begin{Bmatrix} \Delta\epsilon x^* \\ \Delta\epsilon y^* \\ \Delta\gamma xy^* \end{Bmatrix} = \begin{bmatrix} \cos^2\alpha c & \sin^2\alpha c & \sin\alpha c.\cos\alpha c \\ \sin^2\alpha c & \cos^2\alpha c & -\sin\alpha c.\cos\alpha c \\ -2\sin\alpha c.\cos\alpha c & 2\sin\alpha c.co\alpha c & (\cos^2\alpha c-\sin^2\alpha c) \end{bmatrix} \begin{Bmatrix} \Delta\epsilon x \\ \Delta\epsilon y \\ \Delta\gamma xy \end{Bmatrix} \tag{4.37}$$

where $\Delta\gamma xy^*$, $\Delta\gamma xy$ are engineering shear strains

i.e $$\Delta\{\epsilon\}^* = [T]\,\Delta\{\epsilon\} \tag{4.38}$$

Assuming that work done must be independent of the co-ordinate system, then

$$\Delta\{\epsilon\}^{*T}\Delta\{\sigma\}^* = \Delta\{\epsilon\}^T\,\Delta\{\sigma\} \tag{4.39}$$

Substituting equation (4.35), (4.36) and (4.38) into (4.39)

it follows that

$$[D_T] = [T]^T\,[D_T]^*[T] \tag{4.40}$$

Calculation of angle of crack

The method of solution adapted in this model allows more that one crack to occur during the same increment. Also the calculated stress which is used to check against the tensile strength criteria could be well in excess of the tensile strength itself. Thus, the resulting angle of crack could be significantly different from that if the sufficient incremental quantities had been added, a discrepancy which might increase for larger increments. In order to minimise the effect of increment size, a more correct angle is calculated[4].

For maximum stress criterion, the calculation of the angle of crack is given by

$$\alpha c = \frac{1}{2} \tan^{-1}\left\{ \frac{2(\tau xy + \triangle \tau xy'')}{(\sigma x+\triangle \sigma x'')-(\sigma y+\triangle \sigma y'')} \right\} \qquad (4.41)$$

where

$$\triangle\{\sigma\}'' = F.\ \triangle\{\sigma\} \qquad (4.42)$$

are the proportion of incremental stresses sufficient to cause cracking, $\{\sigma\}$ are the previous total stresses, and

$$F = \frac{-\beta + \sqrt{\beta^2 - 4\alpha c.\lambda}}{2\alpha c} \qquad (4.43)$$

$$\alpha = (\triangle \gamma xy^2 - 4.\triangle \sigma x.\triangle \sigma y) \qquad (4.44)$$

$$\beta = 2\ \{\gamma xy \triangle xy + 2(ft-\sigma y)\triangle \sigma x + 2(ft-\sigma x)\triangle \sigma y\} \qquad (4.45)$$

$$\lambda = \{\gamma xy^2 - 4(ft-\sigma x)(ft-\sigma y)\} \qquad (4.46)$$

4.9 Concrete constitutive laws in compression zone

There have been various proposed concrete constitutive models[1,2,4]. In this study a compression model is used which is based on deviatoric and hydrostatic components of stress and strain. The examination of the work done by Kupfer et al[12] and Weigler and Becker[18] and Richart et al[19] showed that an approximately unique relationship exists between hydrostatic stress σm and volumetric ϵo strain, and between deviatoric stress and strain until close to ultimate conditions. Thus the deformational response can be simulated incrementally by assuming the tangent bulk modulus, K_T, and tangent shear modulus, G_T, to be functions of first and second stress invariants I_1 and J_2 respectively.

$$K_T = f1(I_1)$$
$$G_T = f2(J_2) \qquad (4.47)$$

This implies that concrete remains isotropic under multiaxial compressive stress.

Plotting K_T, against, I_1, and, G_T, against, $J_2^{1/2}$, demonstrated that the curves were

clustered fairly close together. Finally, a particular relationship was obtained between the ratio of $J_2^{1/2}$ to fc', and the ratio of G_T to Go for the case where Ko was constant which was satisfactory except for the weakest mix. This relationship is shown in Figure (4.19).

In order to obtain the distortional relationships, a uniaxial stress–strain curve was used and K was kept constant

$$\tau oct = \sqrt{2}/3\ \sigma 1$$

$$\gamma oct = \sqrt{2}/3\ (3\epsilon 1 - \sigma 1/3K) \qquad (4.48)$$

This procedure was assumed to give sufficient approximation for many practical purposes.

In the implementation of the law it is required that at the beginning of a load increment, values of K_T and G_T are evaluated from a knowledge of I_1 and $J_2^{1/2}$. Values of E_T and ν_T are then obtained by using the following expressions

$$E_T = (9K_T.G_T)/(3K_T+G_T)$$

$$\nu_T = (3K_T-2G_T)/(6K_T+2G_T) \qquad (4.49)$$

from which the current tangential elasticity matrix $[D_T]$ is evaluated. The estimation of incremental stress will be found by

$$\triangle \{\sigma\} = \{D\}_T \triangle \{\epsilon\} \qquad (4.50)$$

Therefore, the total stress will be calculated by adding the incremental stress to the previous level of stress.

$$\{\sigma\} = \{\sigma\}o + \triangle \{\sigma\} \qquad (4.51)$$

This procedure alone will lead to divergence of the calculated stresses and strains from specified law and a corrective procedure is necessary. Using the updated values of $\{\sigma\}$, temporary values of G_T and K_T are evaluated. Final values of G_T and K_T are then calculated using the weighted mean of the original values and the newly calculated ones, i.e

$$G_{i+1} = G_i + c' \ (Go - G_T)$$

$$K_{i+1} = K_i + c' \ (Ko - K_T) \qquad (4.52)$$

where Ko, Go are the initial values at the start of the increments, K_i and G_i are the intermediate values and G_{i+1} and K_{i+1} are the final values. $\triangle \{\sigma\}$ is recalculated by means of G_{i+1} and K_{i+1}, from which new values of total stress can be obtained. A value of $c' = 0.6$ has proved satisfactory.

4.10 Compressive failure theories

There have been a number of compressive failure theories proposed and used by various investigators over recent years. It appears that all theories deviate from each other and there is not one single failure theory which seems applicable to all cases. In the last decade, however, a great deal has been learned, and studies have been made towards developing a consistent failure theory for concrete[1,3].

In this study the octahedral shearing stress theory was used. Studies carried out by Phillips[4] showed that satisfactory agreement could be obtained between experimental and theoretical results, for practical applications, where compressive failure did not significantly control the response of the structure.

The Octahedral shear stress theory is based on the assumption that octahedral shearing stress is a function of the octahedral normal stress[1,2,4] at failure, i.e

$$\tau oct \geqslant f(\sigma oct) \qquad (4.53)$$

and satisfactory fits have been obtained by assuming a linear relationship. Assuming the law to be applicable only in pure compressive zones, then the linear form of equation (4.53) is written as

$$\tau oct + n\sigma oct + c \geqslant 0, \quad \sigma oct < -fc'/3 \qquad (4.54)$$

The values of n and c can be obtained from plots of τoct against σoct, available from test data. Alternatively, n and c can be obtained by substituting known

compressive strength data in equation (4.53). From Figure (4.20), for uniaxial compressive tests.

$$\sigma 1 = \sigma 2 = 0 , \qquad \sigma 3 = -fc', \; fc'>0 \tag{4.55}$$

for biaxial compressive tests

$$\sigma 1 = 0 , \qquad \sigma 2 = \sigma 3 = -mfc', \; m>0 \tag{4.56}$$

which give

$$\tau oct + \sqrt{2}(m-1)\sigma oct/(2m-1) - \sqrt{2}.m.fc/(2m-1)) \geq 0, \; \sigma oct < -fc'/3 \tag{4.57}$$

In principal stress space this equation represents a circular cone with axis $\sigma 1 = \sigma 2 = \sigma 3$ and truncated at the plane $\sigma 1 + \sigma 2 + \sigma 3 = -fc'$ as shown in Figure (4.21). The cone intersects the biaxial plane to give an ellipse, which passes through the uniaxial and equal biaxial compressive strength points, as shown in Figure (4.22). It is seen that the ellipse is a reasonable fit to the actual failure envelope.

The major objections to the use of this theory are that it does not take into account large changes in the third principal stress, which can have a significant influence on the mode of failure, and that the relationships are different for biaxial stress states and triaxial compression stress states. However, this theory is based on the concept of a type of shear being exceeded, and can be thought of as a natural extension of Mohr's theory[1,2,4]. However it gives a better biaxial approximation. In addition, the octahedral quantities are related to the stress invariants, and thus the criterion is a particular case of the general invariant law

$$f(I_1, I_2, I_3) \geq 0 \tag{4.58}$$

4.11 Steel–reinforcement constitutive laws

The steel behaviour is modelled by a uniaxial, bilinear stress–strain curve with strain hardening effects and elastic unloading and reloading as shown in Figure (4.23). Thus,

(i) Elastic–perfect plastic behaviour is given by the hardening angle $Ew = 0$

(ii) When the magnitude of stress in the steel is less than the yield stress, the stress

is given by:

$$fs = Es.\epsilon i \qquad (4.59)$$

(iii) When the steel stress reachs the yield, stress is given by.

$$fs = fy + (Ew/Es(fs'-fy)) \qquad (4.60)$$

where Es is Young's modulus of steel, Ew is the Work hardening angle of steel, fy is the yield stress of steel, fs' is the stress value if no yielding is assumed fy, and fs is the uniaxial stress of steel at strain ϵs

(iv) For stiffness calculations, Es is used when steel has not yielded or is unloading or by Ew if the steel is on the failure surface.

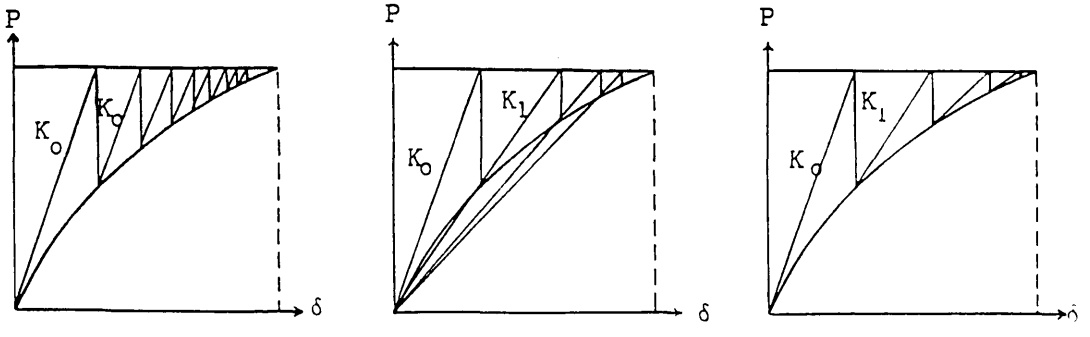

constant stiffness procedure

variable stiffness procedure

Secant Modulus Approach

variable stiffness procedure

Tangent Modulus Approach

Figure (4.1)a Iteration process

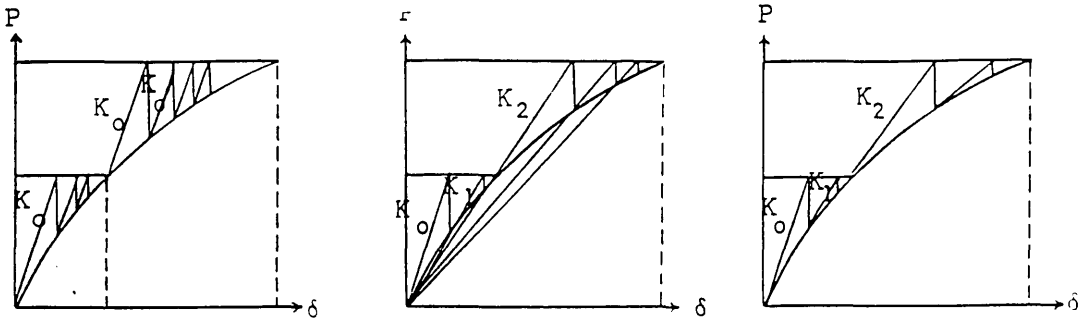

constant stiffness procedure

variable stiffness procedure

Secant Modulus Approach

variable stiffness procedure

Tangent Modulus Approach

Figure (4.1)b Mixed procedure

Figure (4.1) Basic procedure for nonlinear solution.

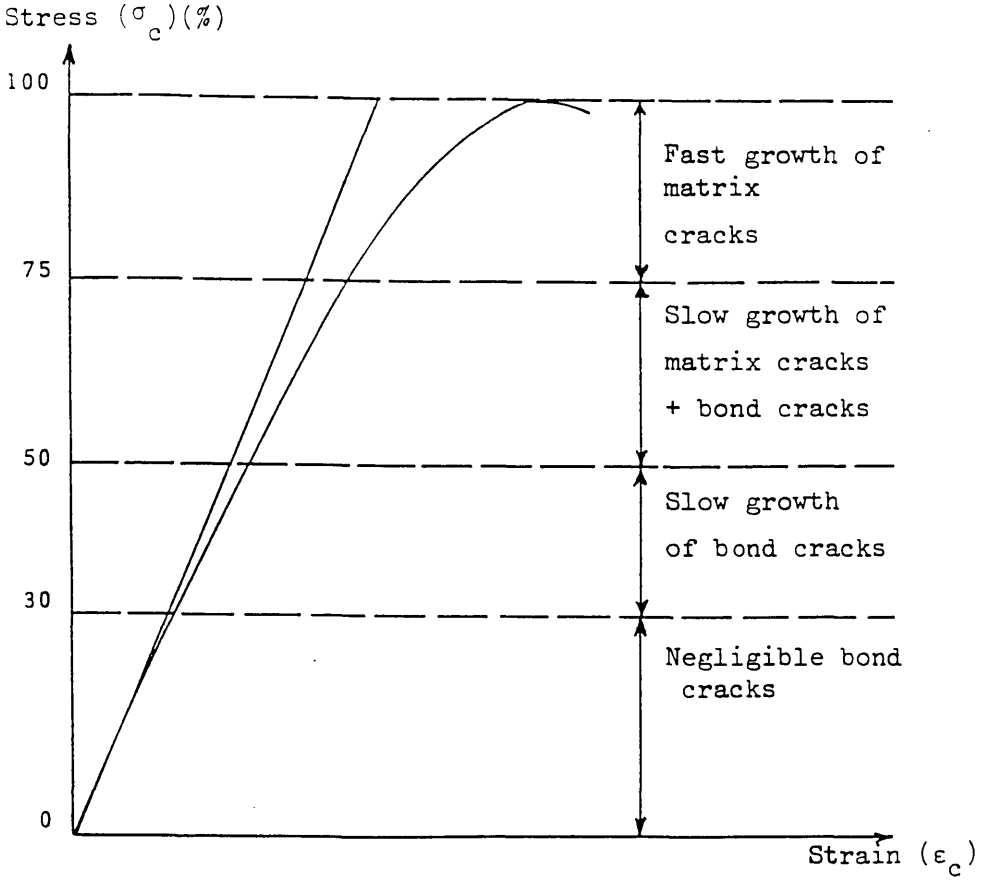

Figure (4.2) Typical stress–strain curve in uniaxial compression.

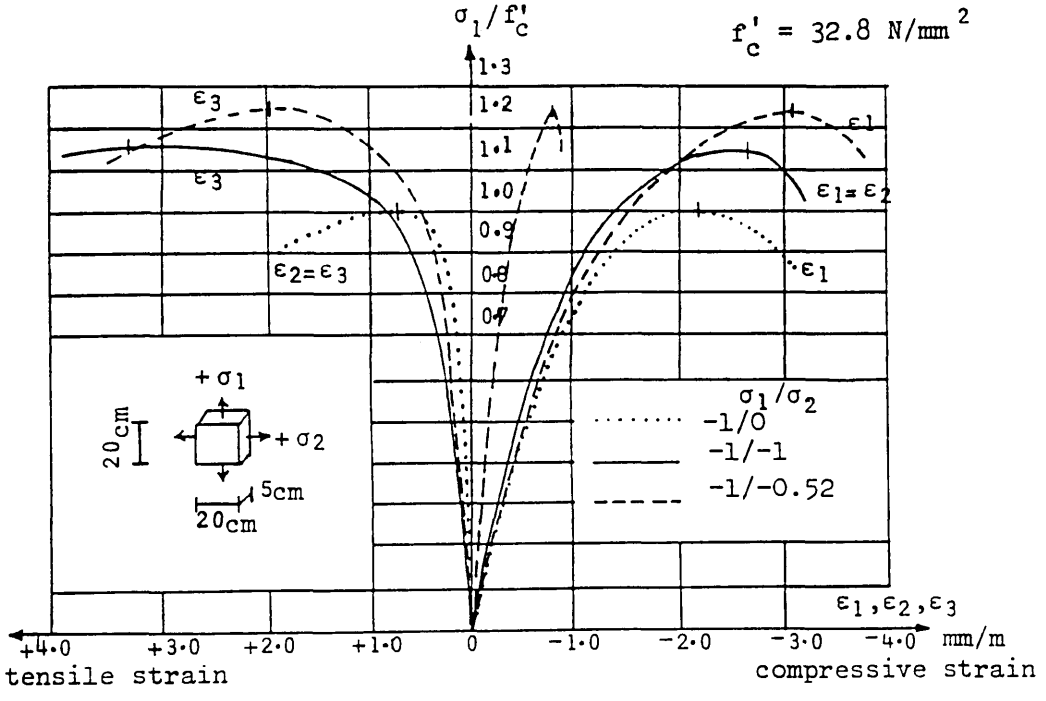

Figure (4.3) Experimental stress–strain curve for biaxial compression.

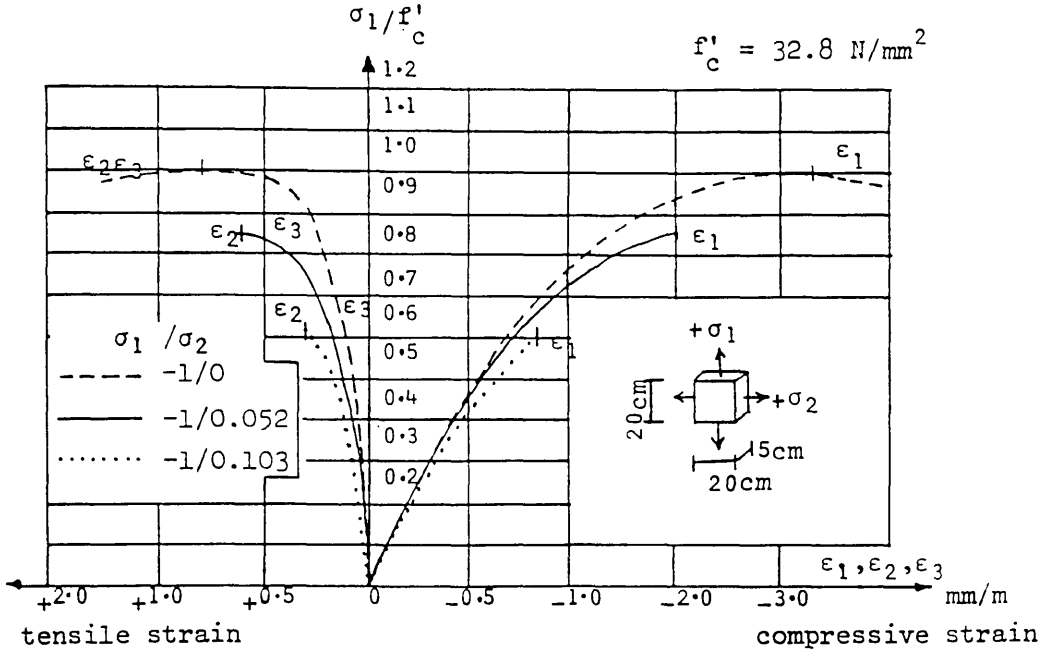

Figure (4.4) Experimental stress– strain curve for biaxial tension– compression.

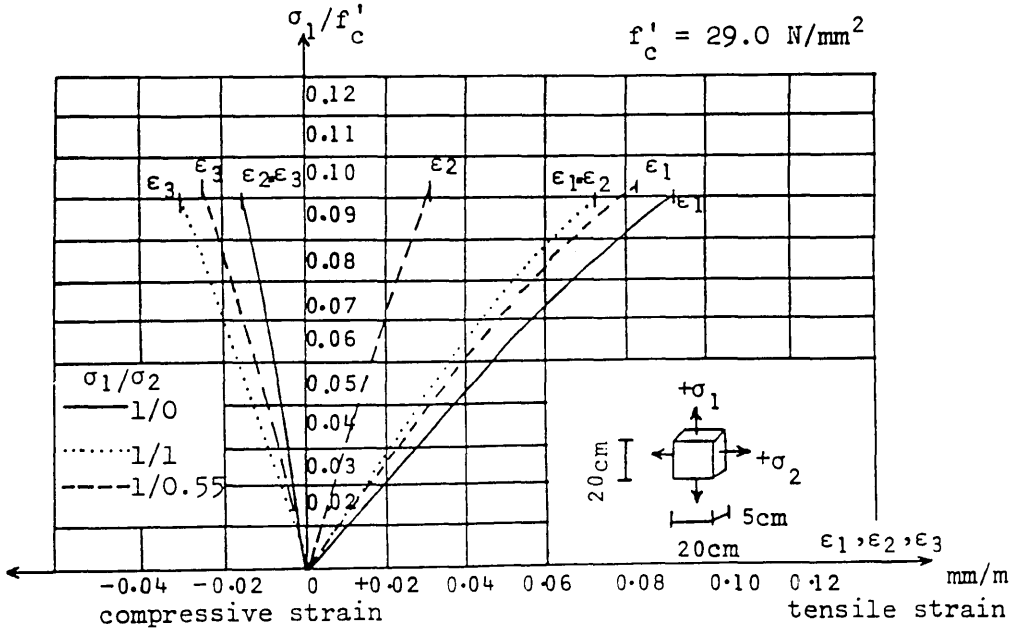

Figure (4.5) Experimental stress– strain curve for biaxial tension.

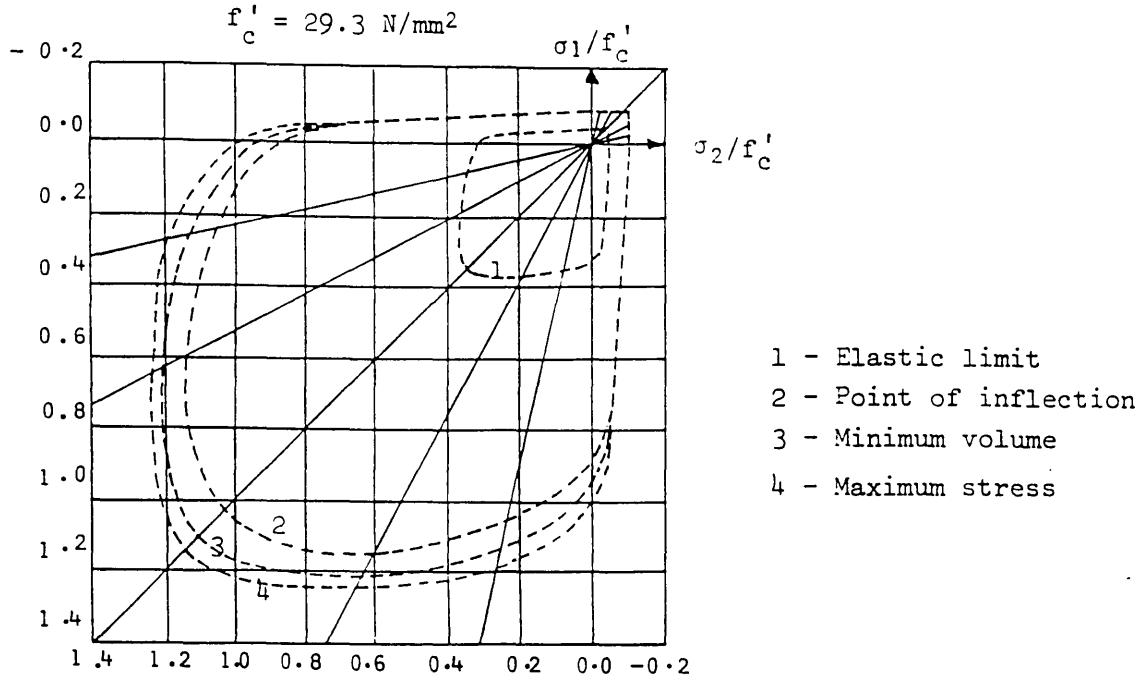

Figure (4.6) Deformational behaviour of concrete under biaxial state of stress.

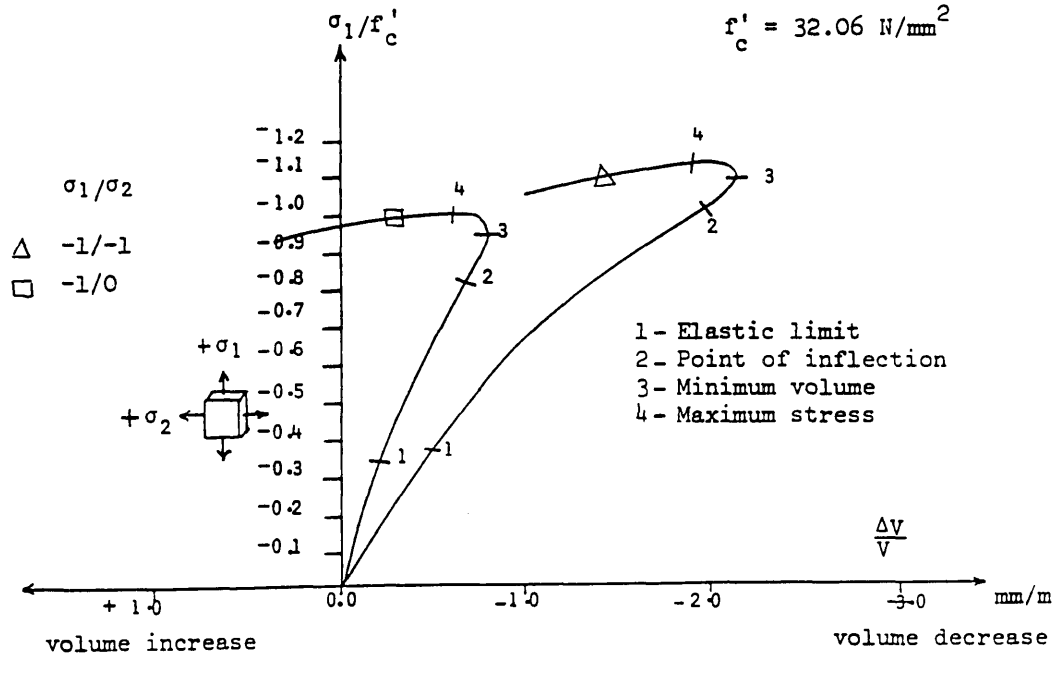

Figure (4.7) Volumetric strain of concrete under uniaxial and biaxial compression.

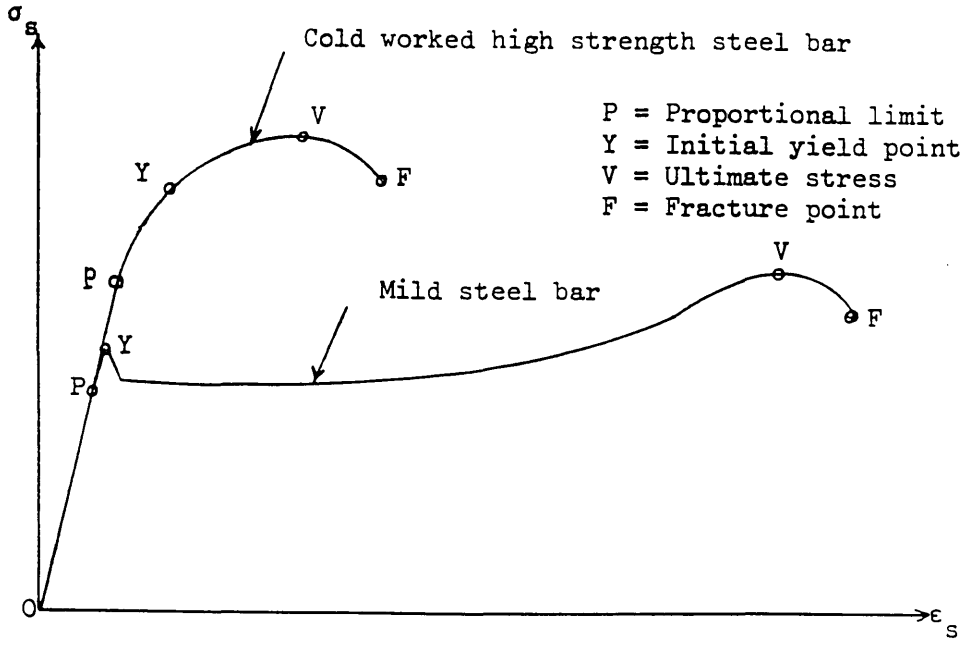

Figure (4.8) Typical steel stress– strain curve.

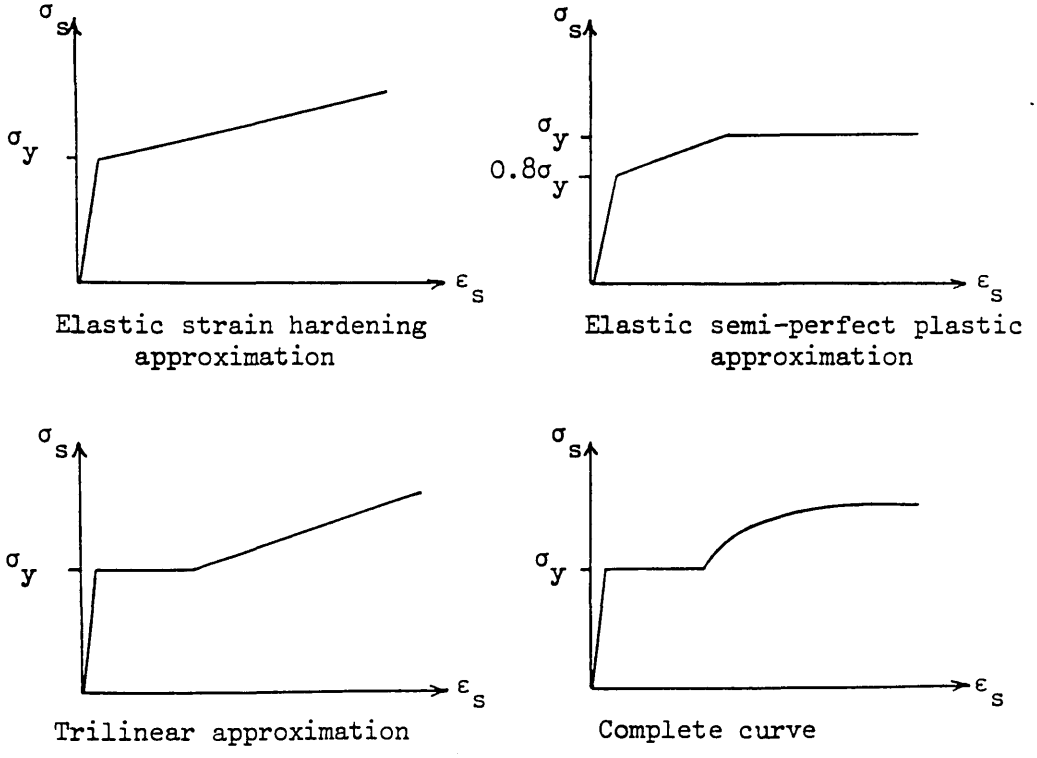

Figure (4.9) Idealized stress– strain curve for steel reinforcement.

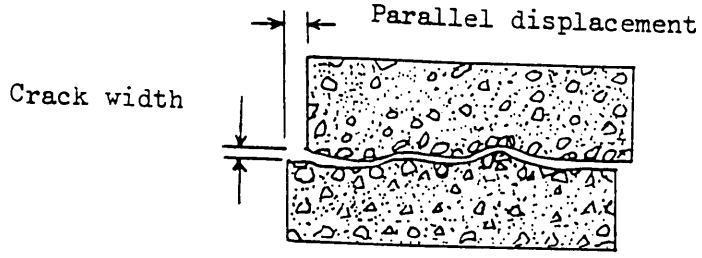

Figure (4.10) Aggregate interlocking of a cracked concrete.

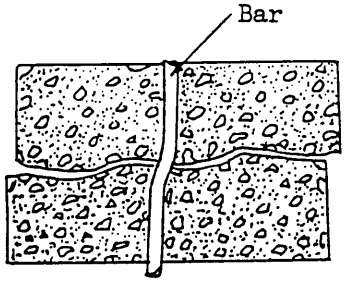

Figure (4.11) Dowel action of a reinforcing bar.

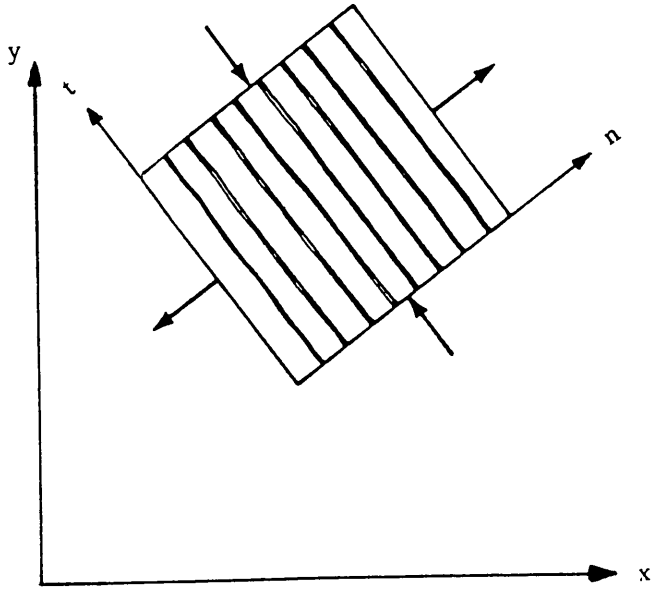

Figure (4.12) Smeared cracking model.

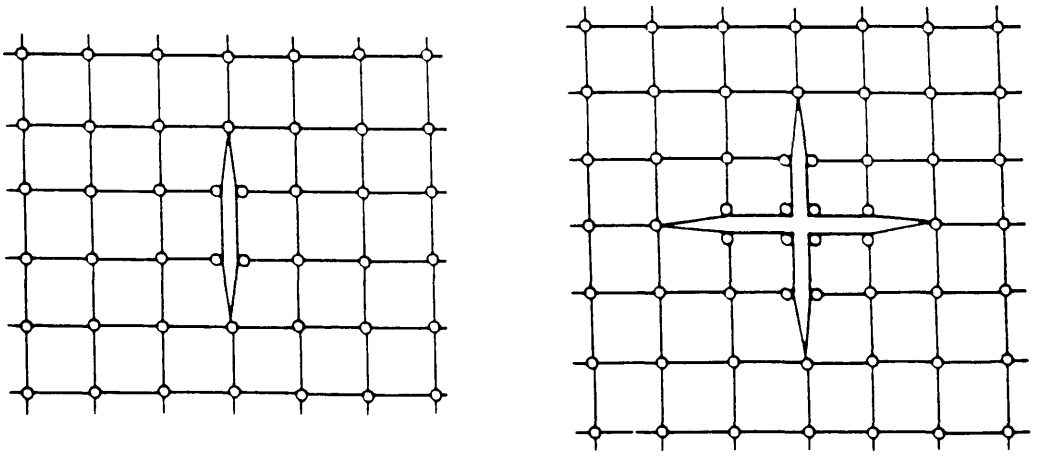

Figure (4.13) Discrete cracking model.

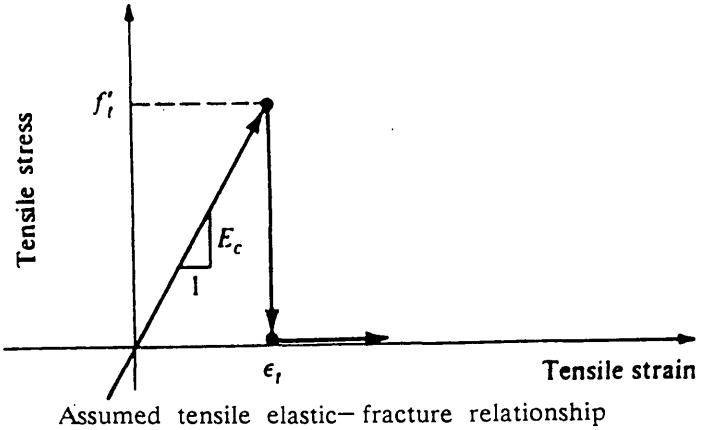

Assumed tensile elastic– fracture relationship

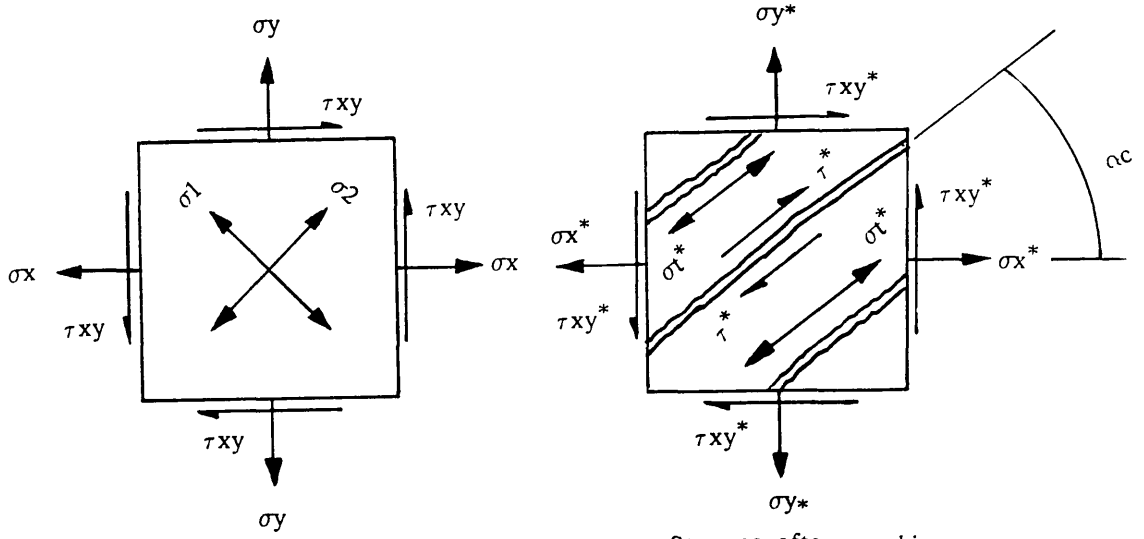

Stresses before cracking

Stresses after cracking

Figure (4.14) Cracking model.

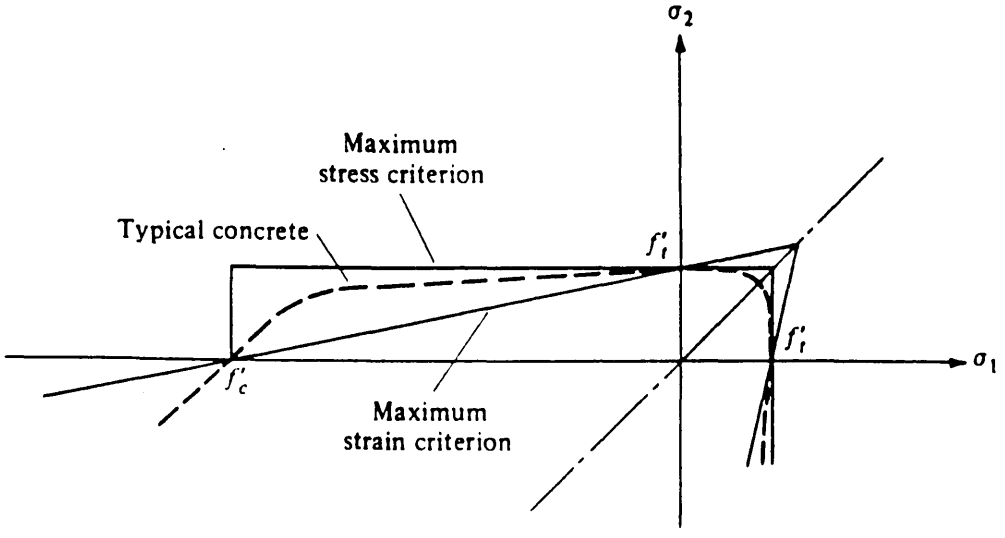

Figure (4.15) Comparison of biaxial failure criterion in tensile zone.

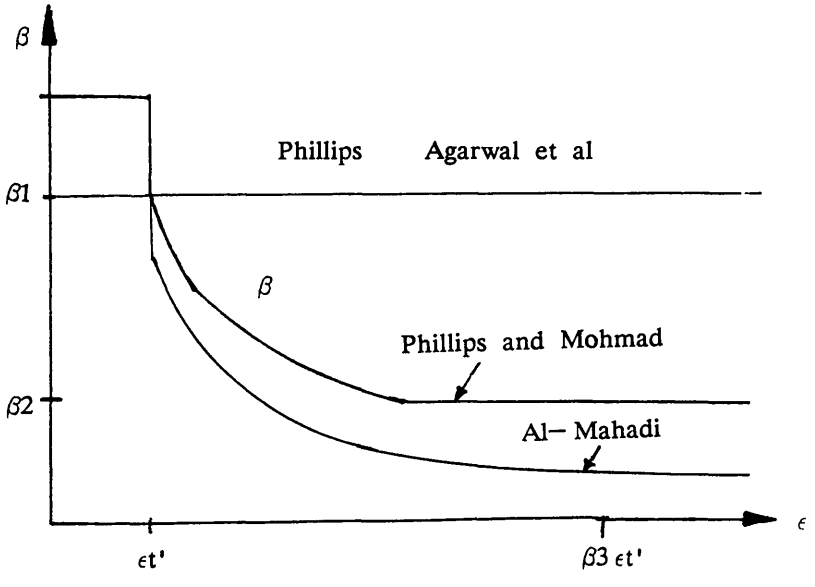

Figure (4.16) Various shear retention factor models.

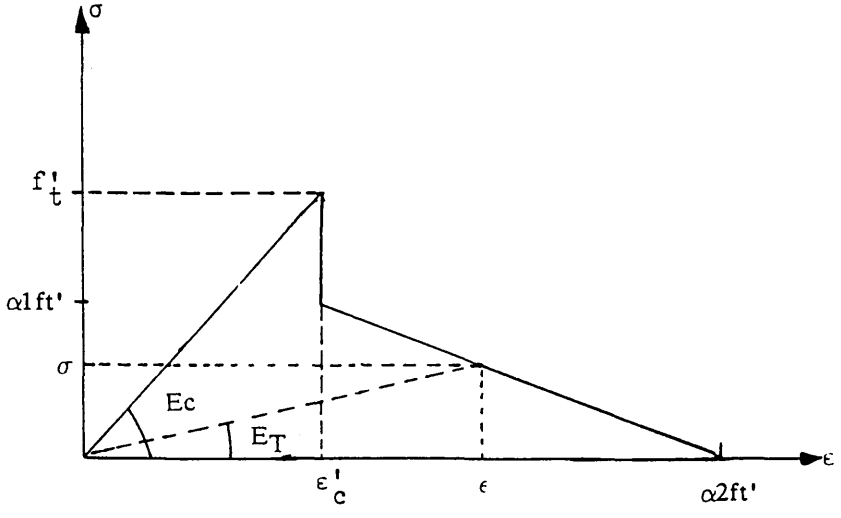

Figure (4.17) Tension stiffening model.

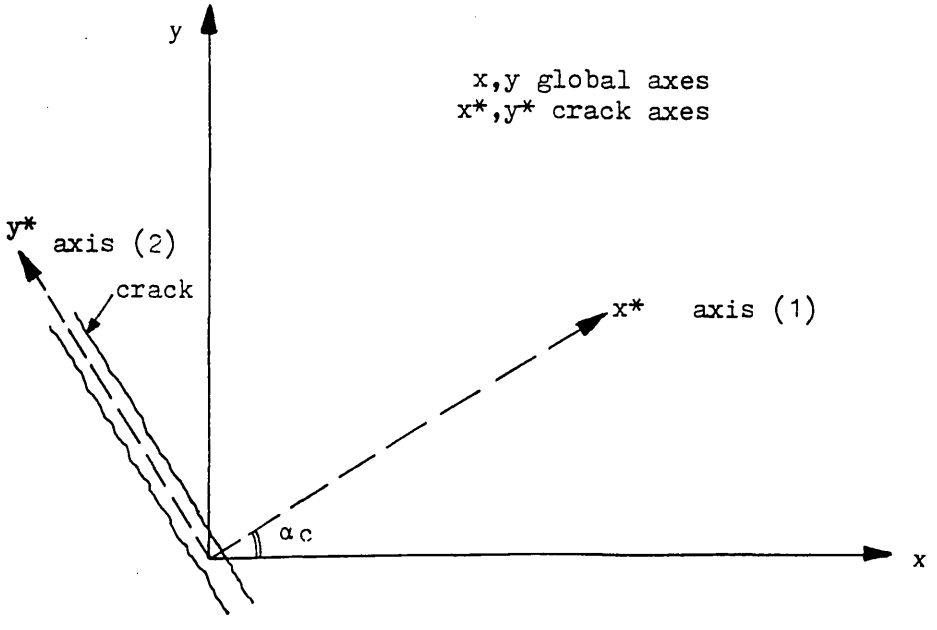

Figure (4.18) Rotation of axises.

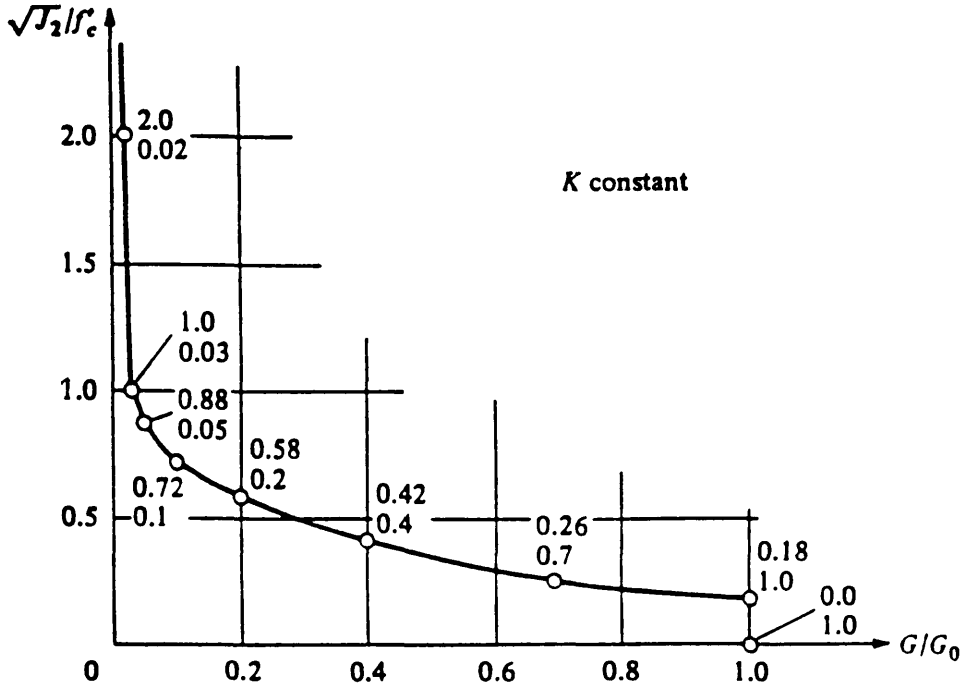

Figure (4.19) $J_2^{1/2}/fc'$ against G/Go.

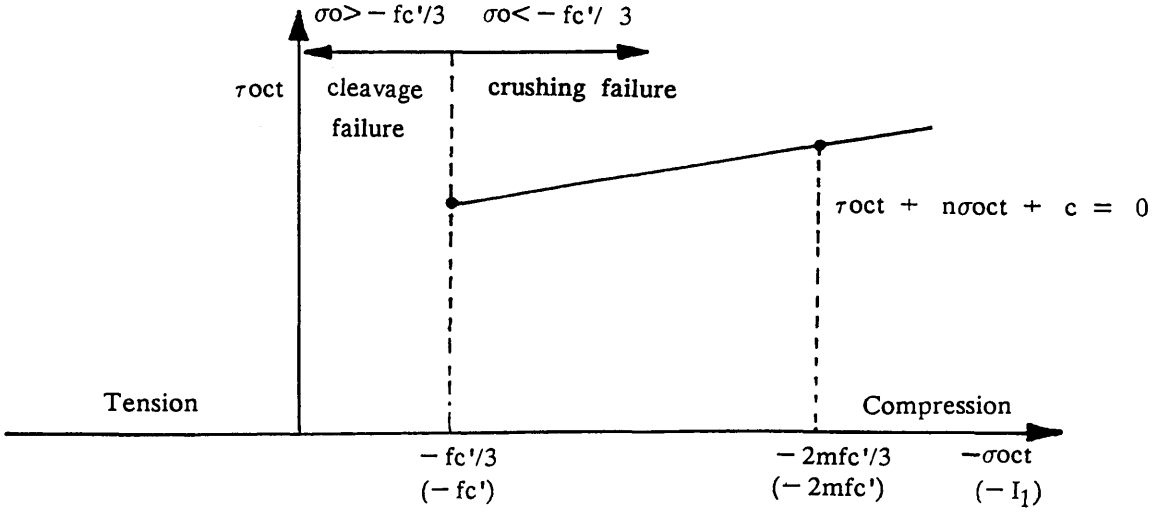

Figure (4.20) Linear octahedral shearing stress law.

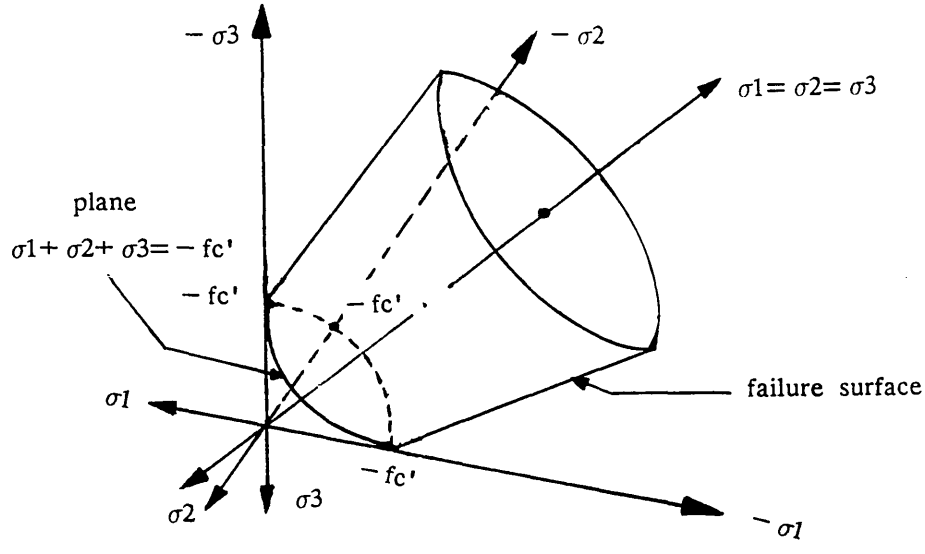

Figure (4.21) Octahedral failure surface.

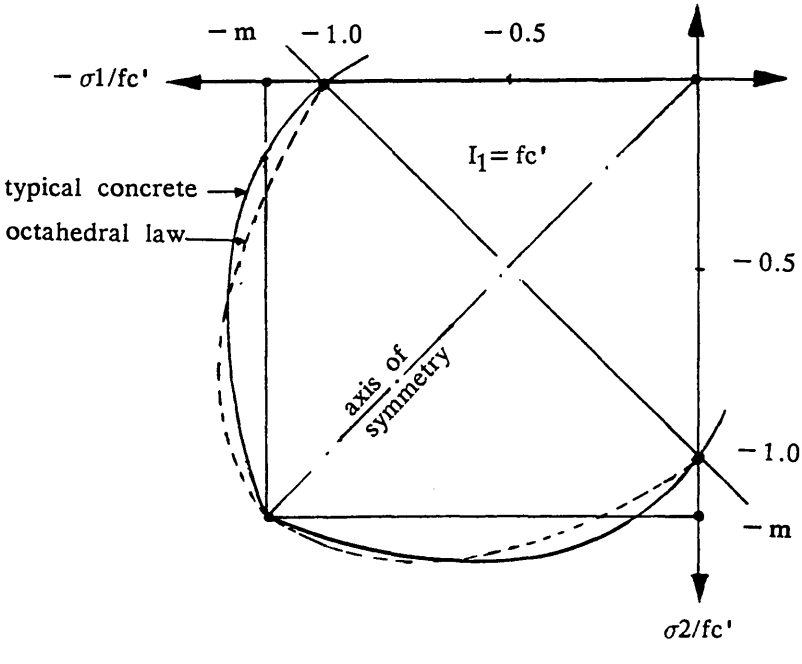

Figure (4.22) Biaxial octahedral failure envelope.

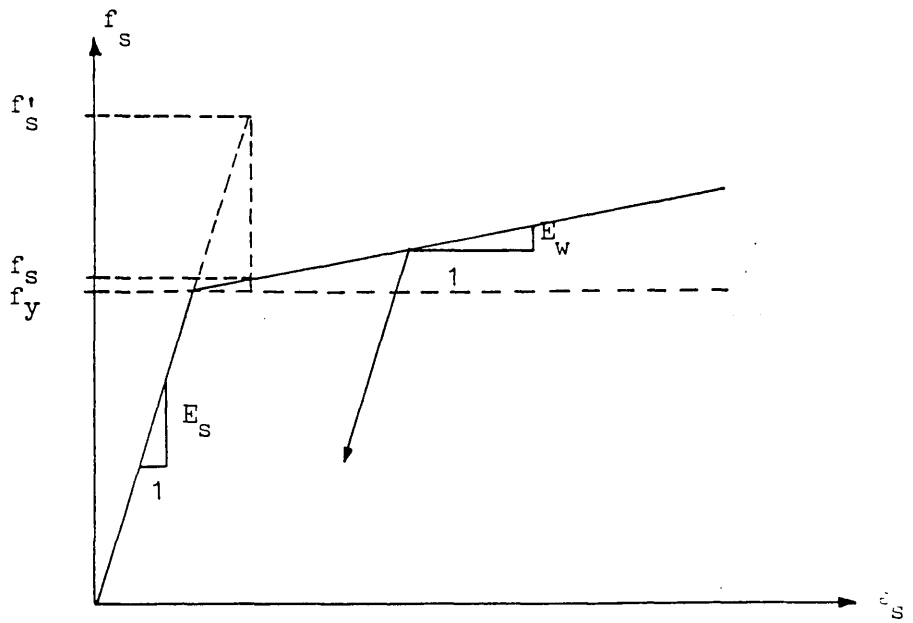

Figure (4.23) Mathematical uniaxial stress– strain curve for steel.

References

1. ASCE TASK COMMITTEE, "Finite element analysis of reinforced concrete", State– of– the– art, Report 1982.

2. CHEN, W.F., "Plasticity in reinforced concrete", McGraw– Hill London 1982.

3. HINTON, E. and OWEN D.R.J.(Editor) "Computational modelling of reinforced concrete structures", Pineridge, Swansea 1986.

4. PHILLIPS, D.V., "Nonlinear analysis of structural concrete by finite element methods", Ph.D Thesis, University of Wales, Swansea 1972

5. PHILLIPS, D.V, and ZIENKIEWCIZ, O.C, "Finite element nonlinear analysis of concrete structures", Proceeding of institute of Civil engineering, Part 2, March 1976, (PP 59– 88)

6. AL– MANSEER, A.A., "A nonlinear finite element study of reinforced concrete beams", Ph.D Thesis, University of Glasgow 1983.

7. OWEN, D.R.J. and HINTON, E., "Finite element in plasticity, Theory and practice", Pineridge, Swansea 1986.

8. MOHAMED, M.S, "A finite element and experimental study of reinforced concrete in torsion", Ph.D Thesis, University of Glasgow 1986.

9. AL– MAHADI, R.S.H, "Nonlinear finite element analysis of reinforced concrete deep members", Report No. 79– 1, Dept. of structural and enviroment engineering, Cornell University, Jan. 1979.

10. ZIENKIEWCIZ, O.C, "The finite element methods", Third edition McGraw– Hill London 1985.

11. COOK, R.D, "Concepts and applications of finite element analysis", Wily 1981.

12. KUPFER, H. et al, "Behaviour of concrete under biaxial stresses", Journal of ACI, 1969, 66, No. 8, (PP. 656– 666).

13. AGRAWAL, A.B., JAEGER, L.G. and MUFTI, A.A., "Crack propagation and plasticity of reinforced concrete shear– Wall under monotonic and cyclic loading", in

conference on cinite element methods in engineering 1976, University of Adelaide, Adelaide, Australia Dec.1976.

14. ABDEL–HAFEZ, L.M. "Direct design of reinforced concrete skew slabs", Ph.D. Thesis, University of Glasgow, 1986.

15. Al–MANSEER A.A. and PHILLIPS, D.V. "Numerical study of some post–cracking material parameters affecting nonlinear solutions in RC deep beams", Canadian Journal of civil engineering, Volume 14, Nov. 1987.

16. PHILLIPS, D.V and MOHAMED, M.S, "Analysis of reinforced concrete beams in torsion", Proceedings, 2nd international conference on civil and structural engineering Computing, Vol. 2, Institution of civil engineers, London, 1985, (PP. 305–311).

17. SCANLON, A. and MURRAY, A., "Time dependent reinforced concrete slab deflections", Journal, Structural division, ASCE, Vol. 100, No. ST9, 1979, (PP 1911–1924).

18. WEIGLER, H. and BECKER, G., "Untersuchungen uber des bruch und nuformungsver halten Von beton bei zweiachsiger beans pruchug, Des deutschan, Ausschusses fur stahlbeton 1963, 157, (PP 1–66).

19. RICHART, F. E et al, "A study of the failure of concrete under combined compressive stresses, Bull, Illinios University, Engng, Exp., Stn 1928, No. 185 (1–102).

20. PARK, R. and PAULAY, T. "Reinforced concrete structures", John Wiley 1975.

21. NGO, D. and SCORDELIS, A.C., "Finite element analysis of reinforced concrete beams", Journal of ACI, Vol. 64, Mar. 1967 (PP. 162–163).

22. NILSON, A. H., "Nonlinear analysis of reinforced concrete by finite element method", Journal of ACI, Vol. 65, 1968 (PP. 757–766).

23. MEHLHORN, G. and KEUSER, M., "Isoparametric contact elements for analysis of reinforced concrete", ASCE Task committee's Published report, Japan 1985.

24. SUIDAN, M., and SCHNOBRICH, W.C., "Finite element analysis of reinforced

Concrete", ASCE Journal of the Structural division, 99 (ST 10), 1973, (PP. 2109– 2122).

CHAPTER FIVE

DIRECT DESIGN METHODOLOGY FOR A CONTINUUM STRUCTURE

5.1 Introduction

In the United Kingdom, the design of reinforced concrete is largely based on the British Standards and BS Codes of Practice. Three basic methods are at present permitted, namely limit–state analysis, the load–factor method and elastic theory. Both the elastic theory and the load–factor method are permitted by CP 114[1]; all design to BSCP 8110[2] is undertaken on the basis of limit–state principles. All three methods employ certain basic common assumptions, e.g. that the distribution of strain across a normal beam section is linear and the strength of concrete in tension is neglected. Apart from assumptions of this nature, the methods differ traditionally from each other.

In order to choose a suitable design method for reinforced concrete structures, the following points must be considered:–

(a) The designed structure or part of it should not become unfit for the use for which it was designed during its intended life span. This is defined when it reaches a limit state beyond which it ceases to satisfy the function and conditions for its existence. Consequently, the structure should be designed to safely resist all loads likely to occur during construction and use, limit deformations and also have adequate durability.

(b) The designed structure must perform adequately all the intended functions in serviceability (i.e under normal working conditions).

(c) The designed structure should possess an appropriate factor of safety against collapse.

(d) The design procedure should be capable of handling any geometry and boundary conditions of the structure without any difficulty.

This chapter describes the proposed direct design methods for the ultimate limit state design of deep beams in general, and for two span continuous transfer girders in particular, using either orthogonal or skew reinforcement.

5.2 Limit state design

The current recommendations in British Practice for reinforced concrete are based on limit state design and are given in British Code of Practice BSCP 8110[2]. There are various limit states, but the two basic categories are summarized as follows:–

(a) Ultimate limit state : This state is primarly associated with the maximum load carrying capacity of the structure. Collapse of a structure, as a whole or as a part, may arise from the rupture of one or more critical sections, from buckling due to elastic or plastic instability (including the effects of sway), or from the loss of static equilibrium (e.g due to the transformation into a mechanism or due to loss of stability by overall tilting)[3,4].

(b) Serviceability limit state: This limit state requires that the structure should not suffer from excessive deflections, cracking or vibration under service loads.

The usual practice in the design of reinforced concrete structure is to design a structure for the ultimate limit state and check for the serviceability limit state.

5.3 Application of limit state design

During the last two decades, studies of plasticity in reinforced concrete have grown extensively. Limit analysis has been used to predict both upper and lower bound capacities of slabs, panels, beams etc under bending, shear, torsion and combined actions[5,6,7,8]. These techniques are based on the theorems of plasticity which demand that at collapse two of three conditions, i.e the equilibrium conditions, the yield criterion or the mechanism condition must be satisfied. Also it is required that the material should possess sufficient ductility so that areas which yield before collapse can deform plastically without loss of strength until ultimate conditions are reached. However, reinforced concrete structures generally exhibit limited plastic behaviour. Consequently, there is always a danger of unloading taking place in some parts of the structure whilst others are undergoing plastic deformation. One way of

overcoming this is to reduce ductility demands and to ensure a minimum redistribution of stress such that most of the critical sections of the structure yield simultaneously.

In the lower bound methods for reinforced concrete, the applied stresses are less, or equal to, the combined internal resistance offered by the concrete and steel. In upper bound systems, sufficient hinges or yield zones are formed in the structure which transform it into a mechanism. Upper bound methods are unsafe for design if the wrong mechanism is assumed, but are generally best suited for analysing an existing design. On the other hand, lower bound methods are safe and more suitable for design, but may be uneconomical.

5.4 Proposed direct design method

Recent computer developments have diverted the attention from design of reinforced concrete structures using conventional design methods in conjunction with code prescribed rules to more highly sophisticated computer aided design (CAD) procedures, using advanced analytical techniques such as the finite element method in conjunction with interactive graphic facilities. These developments have emphasized a need for the design procedures to be well supported by experimental verification both at service and ultimate behaviour. Equal emphasis is also required on automating the design procedures, so that a structure can be designed and redesigned with minimum intervention by the designer, its details automatically produced in a final drawing form.

Direct design is one of the more natural design–oriented procedures for the design of reinforcement because of the way it combines analysis and design into a single continuous operation. It uses a lower bound limit state approach in which a stress field in equilibrium with the ultimate load is used in conjunction with an appropriate yield criterion. The resultant design equations are based on the minimization of steel and provides reinforcement which theoretically satisfies equilibrium and yield at each point and causes simultaneous yielding throughout the structure at ultimate load.

Thus, this technique satisfies theoretically all four basic conditions of the theory of plasticity, since equilibrium, yield criterion, mechanism and ductility.

5.4.1 Equilibrium criterion

In classical approaches, the distribution of forces in reinforced concrete structures are found by elastic theory and the internal stresses are predicted by elastic theory until cracks are formed. This technique uses elastic stress field, obtained from a linear–elastic finite element analysis. In fact, any other stress field in equilibrium with the applied loads could be used. However, if the stress field departs significantly from linear–elastic stress field, then it is possible that the behaviour of the structure may not be satisfactory at working loads.

The elastic stress field for a structure is conveniently obtained by a linear–elastic finite element analysis of the unreinforced concrete structure, using the uncracked elastic material properties of concrete. The basic principals of finite element analysis and its modelling is presented in Chapter Three. This, incidentically, satisfies not only equilibrium but also compatability conditions.

5.4.2 Yield criterion

In reinforced concrete the resistance provided by concrete and steel at each point must be equal to, or greater than, the applied stresses. For reinforced concrete continuous structures, the resistance can vary quite widely by using different reinforcement arrangements. In the direct design technique, the combined resistance of steel and concrete at each point is matched as closely and as practically as possible with the applied stresses. Thus, for a particular ultimate load, the theoretical objective is for all parts of the structure to yield simultaneously. This will be discussed in detail in section (5.5).

5.4.3 Mechanism

The resistance offered by concrete and steel to take applied stresses at ultimate loads can be obtained by satisfying the conditions of equilibrium and yield. At the ultimate

stage, with minimum possible redistribution all the sections will yield simultaneously, thus, converting structure into a mechnasim.

5.4.4 Ductility

In classical plasticity theory, it is assumed that the material possesses unlimited ductility. This means that the early yielded regions in the structure will continue to deform plastically without any reduction in their strength.

For reinforced concrete this assumption must be treated with caution, since concrete is not a perfectly plastic material. However, this requirement can be sidestepped if the difference between the load at first yielding and the ultimate load is as small as possible, so that the regions which yield early can deform at constant stress before strain softening behaviour of the concrete has the opportunity to develop. If the ideal situation of simultaneous yielding occurs at all points, then this requirement is automatically satisfied. In practice, it is impossible to achieve this ideal situation, since there are constraints on bar sizes, bar spacing and steel provided for non–structural reasons etc. Nevertheless this departure from the requirement of simultaneous yielding is unlikely to be excessive and therefore the load range between first yielding and the final collapse should be sufficient to avoid violating the ductility requirements.

Although it seems to be a bit paradoxical in first instance, that elastic stress field should be used for ultimate limit state, but it is not expected that at ultimate load, the stress should necessarily be similar to the elastic stress. However, the strength determined by yield criterion and equilibrium at each point is tailored to elastic stress at that point, then minimum redistribution of stress takes place allowing ideally simultaneous yielding at all the points of the structure. In addition to that, since there is minimum redistribution of the stresses, therefore a further consequence of simultaneous yielding is that excessive deformation and cracking are unlikely at working loads, especially when taken in conjunction with the fact that the initial stress field is linear–elastic. So although the method gives no information about

behaviour at serviceability loads, there is an intrinsic safeguard against undesirable serviceability behaviour.

5.5 Direct design procedure equations

A number of design procedures have been developed for determining optimum arrangements of reinforcement in a concrete structure subjected to certain loading types[11−15]. The yield criterion for in−plane actions using known orthogonal isotropic or orthotropic reinforcement which can carry tension and is placed symmeterically with respect to the middle surface was originally presented by Nielsen[11,12]. He assumed that the provision of concrete of sufficient strength can preclude the use of compression reinforcement if both in−plane forces are compression. Later, Subedi[13] presented a graphical approach to design compression reinforcement when the compression forces in the structure are greater than the allowable compressive strength of concrete. Also Morley[14,15] presented design equations for skew reinforcement and highlighted its suitability on economical grounds. It was Clark[16] who finally extended the idea of Nielsen, Subedi and Morley by using Nielsen's yield criterion. He presented nine different cases for orthogonal and skew reinforcement. The designed reinforcement can be either tension or compression reinforcement for a given in−plane forces triad.

In order to establish the design equations, the following assumptions are adopted:

(i) A typical element cut from a deep beam shows the sign convention for in−plane direct and shear forces per unit length as shown in Figure (5.1). All the tensile forces are taken to be positive and compressive forces are considered negative.

(ii) The reinforcement is placed symmetrically about the middle surface of the section, as shown in Figure (5.2), and is in two non orthogonal directions, as shown in Figure (5.3). It only carries uniaxial stress in the original bar directions so kinking and dowel actions are neglected.

(iii) The reinforcement exhibits perfect elastic−plastic behaviour with a yield stress of fs in tension and fs' in compression as shown in Figure (5.4). The bar spacing is

small in comparison to the overall structure dimensions so that reinforcement can be considered in terms of area per unit length rather than individual bars.

(iv) Concrete has zero tensile strength, exhibits the square yield criterion shown in Figure (5.5), and is perfectly plastic.

(v) Instability failure and bond failure are assumed to be prevented by proper detailing and choice of section.

5.5.1 Yield criterion derivation

In Figure (5.6– b), the principal stresses in the concrete are σ_1 and σ_2 with the major principal stress σ_1 making an angle θ to the x– axis. In Figure (5.6– c) the original reinforcement directions coincide with the x and y directions. Let Ax and Ay be the areas per unit lemgth and fx and fy the associated yield stresses. Thus, the combined resistance of steel and concrete in the coordinate directions is given by

$$\sigma x = \sigma_1.\cos^2\theta + \sigma_2.\sin^2\theta + \sigma x^* \qquad 5.1$$

$$\sigma y = \sigma_1.\sin^2\theta + \sigma_2.\cos^2\theta + \sigma y^* \qquad 5.2$$

$$\tau xy = -\sigma_1 \sin\theta.\cos\theta + \sigma_2 \sin\theta.\cos\theta \qquad 5.3$$

where $\sigma x^* = \rho x fx$ and $\sigma y^* = \rho y fy$ are the steel resistances. The reinforcement ratios in x and y directions are given by $\rho x = Ax/t$ and $\rho y = Ay/t$ respectively. Now if σ_1 is tensile, the concrete will crack and $\sigma_1 = 0$. Hence, equations (5.1) to (5.3) become

$$\sigma x = \sigma_2.\sin^2\theta + \sigma x^* \qquad 5.4$$

$$\sigma y = \sigma_2.\cos^2\theta + \sigma y^* \qquad 5.5$$

$$\tau xy = \sigma_2.\sin\theta.\cos\theta \qquad 5.6$$

Now eliminating σ_2 and θ from these equations we obtain

$$(\sigma x^* - \sigma x).(\sigma y^* - \sigma y) - \tau xy^2 = 0 \qquad 5.7$$

This is the yield criterion for an in– plane forces triad derived origionally by Nielson[11,12]. He also assumed that concrete had sufficient compressive strength so that there was no need to provide compression reinforcement, he developed design equations for four cases of reinforcement design where either one or both stresses were tensile.

However Clark[16] later extended these four cases to nine cases to both orthogonal

and skew reinforcement and compression reinforcement also. Table 5.1 shows the nine possible combinations of reinforcement. It can be seen that a direct solution is available for all cases except 1 and 4 where four unknowns have to be determined from three equations of equilibrium. This can be solved by minimizing the total reinforcement in both directions of the section. The major principal stress $\sigma_1 = 0$ when tension reinforcement is required, and $\sigma_2 = fc'$ when compression reinforcement is provided. The derivation of these nine different cases for orthogonal reinforcement design is now explained.

5.5.2 Derivation of design equations for orthogonal reinforcement

CASE No. 1:

Both x and y direct applied stresses are tensile so that tension reinforcement will be required in both directions to carry tensile stress i.e Ax≠0.0 and Ay≠0.0. He also assumed that fx= fy= fs, and $0 > \sigma_2 > fc'$, then the number of unknowns are greater than the number of available equations and cannot be solved directly. In order to obtain a solution, the total steel voulme (Ax+ Ay) must be minimised.

From equations (5.1) to (5.3) then

$$\sigma x = \sigma_2 . \sin^2\theta + \sigma x^* \qquad 5.8$$

$$\sigma y = \sigma_2 . \cos^2\theta + \sigma y^* \qquad 5.9$$

$$\tau xy = \sigma_2 . \sin\theta . \cos\theta \qquad 5.10$$

Noting that $\sigma x^* + \sigma y^*$ is equal to (Ax+ Ay)fs/t and eliminating σ_2 from equation (5.8) and (5.9) using equation (5.10) then

$$(\sigma x^* + \sigma y^*) = \sigma x + \sigma y + \tau xy \ (\tan\theta + (1/\tan\theta)) \qquad 5.11$$

Using the minimization condition:

$$(d.(\sigma x^* + \sigma y^*))/(d.(\tan\theta)) = 0$$

Then

$$\tan^2\theta = 1 \quad \text{and} \quad \tan\theta = \pm 1$$

Thus from equation (5.10)

$$\tau xy = \pm \sigma_2/2$$

Now because $\sigma_2 < 0$, $\sigma_2 = -2|\tau xy|$

Now eliminating σ_2 and θ from equations (5.8) and (5.9) then

$$\sigma x^* = \sigma x + |\tau xy|$$

or

$$\text{i.e } \rho x = (1/fs)[\sigma x + |\tau xy|] \qquad 5.12$$

and similarly;

$$\rho y = (1/fs)[\sigma y + |\tau xy|] \qquad 5.13$$

Nielsen[11,12] suggested that if $\sigma_2 > fc'$ then the section should be redesigned. Note also for $\sigma_2 > fc'$ then $-2|\tau xy| > fc'$ i.e $|\tau xy| < fc'/2$.

CASE No. 2

When the direct applied stress in y direction is tensile and direct applied stress in x direction is compressive, but the compressive stress is smaller than the uniaxial compressive strength of concrete. Therefore only tension reinforcement is required in y direction to carry tensile stresses i.e $Ay \neq 0.0$ and $Ax = 0.0$. This also assumes $fy = fs$, $\sigma_1 = 0.0$ and $0 > \sigma_2 > fc'$.

Thus from equations (5.1) to (5.3) we obtain

$$\sigma x = \sigma_2 . \sin^2\theta \qquad 5.14$$

$$\sigma y = \sigma_2 . \cos^2\theta + (Ay.fy)/t \qquad 5.15$$

$$\tau xy = \sigma_2 . \sin\theta . \cos\theta \qquad 5.16$$

Now eliminating σ_2 and θ then

$$\sigma y^* = \sigma y - \tau xy^2/\sigma x$$

$$\text{i.e } \rho y = (1/fs)[\sigma y - \tau xy^2/\sigma x] \qquad 5.17$$

CASE No. 3

When the direct applied stress in x direction is tensile and direct applied stress in y direction is compressive, but the compressive stress is smaller than the uniaxial compressive strength of concrete. Therefore, only tension reinforcement is required in x direction to carry tensile stress i.e $Ax \neq 0.0$ and $Ay = 0.0$. This also assumes $fx = fs$, $\sigma_1 = 0.0$ and $0 > \sigma_2 > fc'$.

Thus from equations (5.1) to (5.3) we obtain

$$\sigma x = \sigma_2 . \sin^2\theta + \sigma x^* \qquad 5.18$$

$$\sigma y = \sigma_2 . \cos^2\theta \qquad 5.19$$

$$\tau xy = \sigma_2 . \sin\theta . \cos\theta \qquad 5.20$$

Now eliminating σ_2 and θ then

$$\sigma x^* = \sigma x - (\tau xy/\sigma y)$$

$$\text{i.e } \rho x = (1/fs)[\sigma x - (\tau xy/\sigma y)] \qquad 5.21$$

CASE No. 4:

Both applied direct stresses are compressive in x and y directions and are higher than the uniaxial compressive strength of concrete, fc', therefore compression reinforcement is required in both directions to carry the compressive stresses. Assuming that fx= fy= fs', σ_2= fc', then the unknown equations are greater than the number of available equations and cannnot be solved directly. In order to obtain a solution, the total steel volume (Ax+ Ay) must be minimized.

Thus from equations (5.1) to (5.3) we obtain

$$\sigma x = \sigma_1 . \cos^2\theta + fc' . \sin^2\theta + \sigma x^* \qquad 5.22$$

$$\sigma y = \sigma_1 . \sin^2\theta + fc' . \cos^2\theta + \sigma y^* \qquad 5.23$$

$$\tau xy = -\sigma_1 . \sin\theta . \cos\theta + fc' . \sin\theta . \cos\theta \qquad 5.24$$

Adding equations (5.22) to (5.23) and using (5.24) then

$$(\sigma x^* + \sigma y^*) = \sigma x + \sigma y + (\tau xy/\sin\theta . \cos\theta) \qquad 5.25$$

Minimization with respect to $\tan\theta$ then

$$(d.(\sigma x^* + \sigma y^*))/(d.(\tan\theta)) = 0$$

Therefore;

$$\tan^2\theta = 1 \text{ and } \tan\theta = \pm 1$$

Thus, from equation (5.24)

$$\sigma_1 = 2\ |\tau xy| + fc'$$

Now eliminating σ_1 and θ from equations (5.22) and (5.23) we obtain

$$\sigma x^* = \sigma xf - |\tau xy|$$

$$\text{i.e } \rho x = (1/fs)[\sigma xf - |\tau xy|] \qquad 5.26$$

and similarly;

$$\rho y = (1/fs)[\sigma yf - |\tau xy|] \qquad 5.27$$

where $\sigma xf = \sigma x - fc'$ and $\sigma yf = \sigma y - fc'$

CASE No. 5

Both direct applied stresses in x and y directions are compressive, but the compressive stress in the x direction is smaller than the uniaxial compressive strength of concrete, while in the y direction the compressive stress is higher. Therefore, only compressive reinforcement is required in the y direction and there is no need for reinforcement in the x direction. Assuming Ax= 0, Ay≠0.0, σ_2= fc' and fy= fs'.

Thus, from equation (5.1) to (5.3), we obtain

$$\sigma x = \sigma_1.\cos^2\theta + fc'.\sin^2\theta \qquad 5.28$$

$$\sigma y = \sigma_1.\sin^2\theta + fc'.\cos^2\theta + \sigma y^* \qquad 5.29$$

$$\tau xy = -\sigma_1.\sin\theta.\cos\theta + fc'.\sin\theta.\cos\theta \qquad 5.30$$

Adding equation (5.28) and (5.28) and using (5.30) them

$$\tan\theta = \tau xy/\sigma xf$$

knowing the value of $\tan\theta$ from equation (5.28) and inserting in (5.30), we obtain

$$\sigma_1 = \sigma x - \tau xy^2/\sigma xf$$

Now eliminating the σ_1 and θ from equation (5.29) we obtain

$$\sigma y^* = \sigma yf - (\tau xy^2/\sigma xf)$$

$$\text{i.e } \rho x = (1/fs)[\sigma yf - (\tau xy^2/\sigma xf)] \qquad 5.31$$

CASE No. 6

Both the direct applied stresses are compressive in x and y directions, but the compressive stress in the x direction is higher than the uniaxial compressive strength of concrete, while the compressive stress in the y direction is smaller. In such a case, compressive reinforcement is required in the x direction only and there is no need for reinforcement in the y direction i.e Ay= 0, σ_2= fc' and fx= fs'.

Thus from equation (5.1) to (5.3), we obtain

$$\sigma x = \sigma_1.\cos^2\theta + fc'.\sin^2\theta + \sigma x^* \qquad 5.32$$

$$\sigma y = \sigma_1.\sin^2\theta + fc'.\cos^2\theta \qquad 5.33$$

$$\tau xy = -\sigma_1.\sin\theta.\cos\theta + fc'.\sin\theta.\cos\theta \qquad 5.34$$

Adding equation (5.32) and (5.33) and using (5.34) then

$$\tan\theta = \sigma yf/\tau xy$$

Knowing the value of $\tan\theta$ and using in equations (5.33) and (5.34) then

Thus from equation (5.1) to (5.3) we obtain

$$\sigma x = fc'.\sin^2\theta + \sigma x^* \qquad 5.41$$

$$\sigma y = fc'.\cos^2\theta + \sigma y^* \qquad 5.42$$

$$\tau xy = fc'.\cos\theta.\sin\theta \qquad 5.43$$

Adding equations (5.41) and (5.42) and using (5.43) then

$$\tan\theta = -(2\tau xy/fc'(1-\beta)$$

where $\beta = \sqrt{1-(2\tau xy/fc')^2}$

Now eliminating θ from equation (5.41) and (5.42) we obtain

$$\sigma x^* = \sigma x - fc'/2(1+\beta)$$

$$\text{i.e } \rho x = (1/fs)\,[\sigma x - fc'/2[1+\beta]] \qquad 5.44$$

and similarly;

$$\rho y = (1/fs')[\sigma y - fc'/2[1-\beta]] \qquad 5.45$$

CASE No. 9:

Nielsen[11,12] and Clark[16] have assumed that when the both principal stresses are compressive i.e, $\sigma_1 \leqslant fc'$ and $\sigma_2 \leqslant fc'$, there is no need for reinforcement (i.e Ax= 0.0 and Ay= 0.0). However, it was suggested to know the principal stresses in the concrete. Therefore, in this case the derivation regarding σ_1, σ_2 and θ is presented. Thus from equations (5.1) to (5.3) we obtain.

$$\sigma x = \sigma_1.\cos^2\theta + \sigma_2.\sin^2\theta \qquad 5.46$$

$$\sigma y = \sigma_1.\sin^2\theta + \sigma_2.\cos^2\theta \qquad 5.47$$

$$\tau xy = (-\sigma_1 + \sigma_2).\sin\theta.\cos\theta \qquad 5.48$$

Adding equations (5.46) and (5.47) together we get:

$$\sigma x + \sigma y = \sigma_1 + \sigma_2$$

Now multiplying equations (5.46) by $\cos^2\theta$ and (5.47) by $\sin^2\theta$ and subtracting (5.47) from (5.46) and using (5.48) then

$$\tan\theta = ((\sigma x - \sigma y) - \sqrt{(\sigma x - \sigma y)^2 + 4.\tau xy^2})/2.\tau xy$$

Now eliminating θ from equations (5.46) and (5.47) and solving simulaneously, we obtain

$$\sigma_1 = ((\sigma x + \sigma y) + \sqrt{(\sigma x - \sigma y)^2 + 4.\tau xy^2})/2 \qquad 5.49$$

$$\sigma_2 = ((\sigma x + \sigma y) - \sqrt{(\sigma x - \sigma y)^2 + 4.\tau xy^2})/2 \qquad 5.50$$

$$\sigma_1 = \sigma y + (\tau xy^2/\sigma yf)$$

Now eliminating σ_1 and θ from equation (5.32) we obtain

$$\sigma x^* = \sigma xf - (\tau xy^2/\sigma xf)$$

$$\text{i.e } \rho x = (1/fs)[\sigma xf - (\tau xy^2/\sigma xy)] \qquad 5.35$$

CASE No. 7

When the direct applied stress in the x direction is tensile, and the direct applied stress in y direction is compressive and higher than the uniaxial compressive strength of concrete. In this situation, tensile reinforcement is required in x direction to take tension stress and compression reinforcement is required in y direction to take compressive stress. Assuming Ax≠0.0 and Ay≠0/0, $\sigma_1 = 0$, $\sigma_2 = fc'$, fx= fs, and fy= fs'.

Thus from equations (5.1) to (5.3), we obtain

$$\sigma x = fc'.\sin^2\theta + \sigma x^* \qquad 5.36$$

$$\sigma y = fc'.\cos^2\theta + \sigma y^* \qquad 5.37$$

$$\tau xy = fc'.\cos\theta.\sin\theta \qquad 5.38$$

Adding equation (5.36) and (5.37) and using (5.38) then

$$\tan\theta = -(2\tau xy/fc'(1+\beta)$$

where $\beta = \sqrt{1-(2\tau xy/fc')^2}$

Now eliminating θ from equations (5.36) and (5.37)) we obtain

$$\sigma x^* = \sigma x - fc'/2(1-\beta)$$

$$\text{i.e } \rho x = (1/fs)[\sigma x - fc'/2[1-\beta]] \qquad 5.39$$

and similarly;

$$\rho y = (1/fs')[\sigma y - fc'/2[1+\beta]] \qquad 5.40$$

CASE No. 8:

When the direct applied stress in x direction is compressive and higher than the uniaxial compressive strength of concrete, while direct applied stress in y direction is tensile. Therefore, compression reinforcement is required in x direction to take compressive stress and tensile reinforcement is required in the y direction to take tensile stress. assuming $\sigma_1 = 0$, Ax≠0, Ay≠0, fx= fs', fy= fs and $\sigma_2 = fc'$.

The above nine cases of reinforcement designs for orthogonal reinforcement are in graphically form in Figure (5.7). Table 5.2 summarizes the design equations for calculating steel ratios, principal concrete stresses and θ for each case. The following symbols are introduced in this Table.

$$\sigma xf = \sigma x - fc'$$

$$\sigma yf = \sigma y - fc'$$

$$\beta = \sqrt{(1-(2\tau xy/fc')^2}$$

5.5.3 Derivation of boundary curves for orthogonal reinforcement.

It is also necessary to establish a means of determining which set of equations should be used for a particular stress triad. This can be achieved by deriving the surfaces in stress space which form boundaries to regions pertaining to each case. Graphs of the boundaries have been plotted in Figure (5.8), using a reference frame where the vertical axis is $\sigma y/|\tau xy|$ and horizontal axis is $\sigma x/|\tau xy|$.

All these boundaries curves were derived by comparing the design equations of the two particular cases for a border line which separates them, for example, curve 4 is separating case 6 and 4, so the derivation will be:

$$1/fs'(\sigma xf-|\tau xy|) = 1/fs'(\sigma xf-(\tau xy^2/\sigma yf))$$

$$|\tau xy| = (\tau xy^2/\sigma yf)$$

$$|\tau xy| = \tau xy^2[(1/\sigma y)-(1/fc')]$$

$$\sigma y/|\tau xy| = [(fc'/|\tau xy|+1] \qquad 5.51$$

In this way all the boundary curve equations were derived and are given in Table 5.3 to 5.4.

In similar way, the design reinforcement equations for skew reinforcement can be derived. The summary of these design equations is given in Table 5.5. Figure (5.9) to (5.12) shows the graphs for skew reinforcement. Table 5.6 to 5.7 summarize the equations for boundary curves.

5.6 Design of transfer girders

5.6.1 Application of design program

In order to obtain an admissible stress field, a linear–elastic finite element model with isoparametric parabolic elements was developed, this model has been described in more detail in Chapter Three. The stress field was obtained for the the design ultimate load using elastic material data for the unreinforced concrete beam. The design equations for orthogonal and skew reinforcement of Clark[16] were codified and introduced into the program. Steel ratios were automatically calculated in two non–orthogonal directions. Before carrying out the final analysis, which was used for the designing of the reinforcement, a mesh convergence study was carried out to ascertain the most effective discretization. While designing the test girders in this study, a mesh convergence study was carried out each time when any change occured in the geometry of the girders.

5.6.2 Selection of reinforcing bars

Numerical analysis gives steel ratios which vary from point to point and from element to element. In order to simplify this, all the steel ratios for each element were averaged in each direction. Even doing this, steel ratios were varying from element to element continuously throughout the structure, since the test girders were small (i.e. (2.0x0.9x0.1m), (3.0x0.9x0.1m), (3.0x2.0x0.1m)) in comparison to usual practical dimensions, there was little possibility of varying the steel area (by curtailing the steel bars) to match the theoretical steel requirements. There are two possibilities to overcome these shortcomings:–

(a) To choose the maximum steel ratios at each level and place the required steel bar through this level.

(b) To take the average of all steel ratios at each level in both directions and placing the steel bars accordingly.

In the comparison between the two methods it was found that, method (a) appeared to be uneconomical but it provided a safe design, since it used higher steel areas in

some regions of the structure than the required theoretical steel areas. While the averaging procedure though more economical, might give an unsafe design, since some areas of the structure would be under– reinforced. At this stage a comprehensive study of steel behaviour and concrete behaviour was again revised to justify one of the above mentioned procedures. Finally, the average procedure with some constraints imposed on its use as described below was adopted:

(i) When high tensile strength steel is used in the structure, and the structural design is based on 0.2 percent of proof stress strength, by ignoring the work– hardening effect of steel. It is seen that steel can carry 30% to 40% of the ultimate strength after first yielding i.e the yield strength at 0.2% proof stress.

(ii) When the contribution of dowel action, kinking of bars and aggregate interlocking are ignored in the design process, since some researchers have found that they contribute a significant shear force to the strength of deep beams[2].

(iii) When the tensile strength of concrete is ignored in the design process.

(iv) When the variation between the maximum steel area in an element, at each level, in both directions is not higher than 20% of the average value at each level. When the difference between the maximum value of the steel area in an element and the average at the same level is higher than 20%. In such situation, other assumptions were made averaging the area over a certain length rather than the full length. This criteria was employed in all the test girders except girder TRGRAS11 which was reinforced with exact required steel areas as much as practically possible.

Aditionally, there are some other constraints concerning the bar spacing, bond anchorage and concrete cover, since all the codes of practice[1,2,23,24,25] in this respect are not fully aware of the experimental results on a deep beam subject, Some limitations are proposed following the various codes of practice and experimental results on deep members.

(i) The diameter of the bar used in a deep member, in particular deep beams should not be greater than one tenth of the thickness of the member.

(ii) The concrete cover should be at least 15 mm to the main reinforcement in the member.

(iii) The space between the two bars of a layer along the beam thickness should not be less than 4 times the diameter of the bars.

(iv) The concrete cover to the bottom steel from the beam soffit should not be greater than 40 mm.

(v) The spacing between two layers of steel bars along the beam depth should not be less than 40mm, to allow concrete compaction between the bar layers.

(vi) The thickness of the beam should not be less than 100mm to provide adequate side concrete cover and space for reinforcing bars.

(vii) The main reinforcement will be extended from one end of the beam to the other without curtailing since there is a point of contraflexure. This is currently recieving some attention from reaserches and codes of practice

A selection of transfer girder design is presented and described in this section. This includes finite element mesh, required steel ratios in a tabular form, three dimensional views of steel ratios, contours of steel ratios and the final reinforcement calculations based on the averaging procedure from the steel ratio envelopes in both directions for each girder. The selected design examples for girders TRGRAS1, TRGRAS4, TRGRAS7, TRGRAS9, TRGRAS10 and TRGRAS11 are given in Figures (5.13) to (5.42).

All the girders were designed for orthogonal reinforcement except TRGRAS7, which was designed with skew reinforcement; with the exception of reinforcement girder TRGRAS1 shared similar variables with TRGRAS7. For the skew reinforcement five different angles were studied i.e 5°, 10°, 15°, 20° and 25°. In comparison it was found that angles 10° and 15° were the best choice, producing 9% and 8% less volumetric reinforcement ratios compared to that orthogonal reinforcement. The comparison of volumetric ratios by excluding one fifth from bottom and top produced 11% reduction for 10° and 15% for 15°. Figure (5.43) shows the reduction trend of percentage of volumetric ratio of steel versus the various skew

angles. However, it was found that angles 10° and 15° were the most economical in both main and shear reinforcement. For girder TRGRAS7 the reinforcement was inclined at an angle of 15° to the x– axis.

The final details of reinforcement in the all transfer girders, which includes the selected sample, are shown in Figures (5.44) to (5.54).

5.7 Design of support bearing

Various authors have reported that local failure due to point load is the most common example of premature failure in deep beams. This is because, under the point load, a considerable force is transmitted to the support directly through the compression strut. Due to this phenomenon, a biaxial state of stress develops at the joint of the support and the compression strut, and at the loading point and two compression struts. The concentration of stresses may become higher than the permissible allowable bearing stress at the contact area. As a result, all the Codes of practice[1,2,23,24,25] and guides have proposed a criteria for checking bearing capacity.

In clause 5.2.5.4 of BSCP 8110[2], it states that the compressive stress in the contact area should not normally exceed 0.4fcu under ultimate loads. Stresses in excess of 0.8fcu of ultimate loads should only be used in laboratory conditions with proper provision of reinforcement.

A short column design (e.g a steel cage at support and loading point) was employed to ensure that there would be no premature failure due to bearing failure using clause 3.3.3 in BSCP 8110[2], that is

$$N = 0.4.fcu.Ac + 0.67.Asc.fy \qquad 5.52$$

where N is the applied force (i.e for support it is the reaction of the applied load and for the loading point it is the design load), fcu is the characteristic cube strength of concrete, Ac is the area of concrete (i.e bearing area), Asc is the required area of compression steel in the bearing area Ac and fy is the

characteristic strength of the compression reinforcement.

In a continuous beam, the distribution of the reactions is chosen according to BSCP 8110[2] for continuous beams based on elastic theory. The area, Asc, of reinforcement starts from the bearing plate and extends such that forces may be transmitted from the bearing area into the inner concrete zone. The required developed length can be calculated from the required anchorage length.

$$La = o.18.fy.\varphi/fba \qquad 5.53$$

where fba is the ultimate anchorage bond stress and φ is the diameter of the bar.

Additionally, links of minimum diameter size bars are also be provided to avoid buckling of the load or support cage, causing premature failure.

It is reported in previous studies by Lin[17] and Memon[18] that at the bearing point, bearing failure can also be caused by the effect of Poisson's ratio. Poisson's ratio effects results in a lateral force of one sixth in magnitude of the vertical force in the vicinity of the loading zone. In a real structure, sufficient concrete cover and reinforcement should also be provided to prevent this. In these tests to avoid congestion of reinforcement in the bearing area, the expansion force was resisted by using external plates clamped to the beam. A beam with such plates is shown in Figure (5.56).

5.8 Bond And Anchorage

Bond stress is the shear stress acting parallel to the reinforcement bars on the interface between the bars and the concrete. It is directly related to the change of stress in the reinforcement bars; there can be no bond stress unless the bar stress changes and conversely there can be no change in bar stress without bond stress[4,26]. When an effective bond stress exists, the strain in reinforcement, for design purposes, may be assumed to be equal to that in the adjacent concrete.

Bond strength is a more serious problem when only plain reinforcing bars are used.

Bars with a deformed surface provide an extra element of bond strength and safety. However, the designer must be aware of the bond stress and anchorage that critically effect the structural behaviour.

In this respect, clause 3.11.6.2, 3.11.6.7 and 8 of BSCP 8110[2] are followed. While considering the tied–arch behaviour in deep beams, the main reinforcement, which may reach its yield stress near the support due to the diagonal crack, should be securely anchored. It is suggested that full positive anchorage should be provided beyond the face of the support. There is some suggestion that bars should not be bent up within a region of 1/8 to 1/5 of the beam depth from the centre of support.

The local bond stress at a given section of a bar is the bond stress due to the rate of change of steel stress at that location. In fact only longitudinal bars in tension need to be checked for local bond stresses. The direct design technique assumes that bond and anchorage are perfect, and consequently in these examples the bond was assumed to be perfect. However, an additional anchorage was provided by using 180° hooks at the ends of the main bars. When these hooks were again fastened to the steel cages at the supports, they provided an additional positive anchorage. Hence bond stress does not necessarily have to be checked.

TABLE 5.1

Summary of various possible nine different cases of reinforcement design.

Case	Reinforcement description	Known values	Method of solution
1	Both tension	$f_x=f_y=f_s$, $\rho_x\neq0$, $\rho_y\neq0$, $\sigma_1=0$	Minimization of $(\rho_x+\rho_y)$
2	No X Y tension	$f_y=f_s$, $\rho_x=0$, $\rho_y\neq0$, $\sigma_1=0$	Direct solution
3	X tension No Y	$f_x=f_s$, $\rho_x\neq0$, $\rho_y=0$, $\sigma_1=0$	Direct solution
4	Both compression	$f_x=f_y=f_s'$, $\rho_x\neq0$, $\rho_y\neq0$, $\sigma_2=f_c'$	Minimization of $(\rho_x+\rho_y)$
5	No X Y Compression	$f_y=f_s'$, $\rho_x=0$, $\rho_y\neq0$, $\sigma_2=f_c'$	Direct solution
6	X compression No Y	$f_x=f_s'$, $\rho_x\neq0$, $\rho_y=0$, $\sigma_2=f_c'$	Direct solution
7	X tension Y compression	$f_x=f_s$, $f_y=f_s'$, $\rho_x\neq0$, $\rho_y\neq0$ and $\sigma_2=f_c'$	Direct solution
8	X compression Y tension	$f_x=f_s'$, $f_y=f_s$, $\rho_x\neq0$, $\rho_y\neq0$, and $\sigma_2=f_c'$	Direct solution
9	No reinforcement	$\rho_x=\rho_y=0$	Direct solution

TABLE 5.2

Equations for orthogonal reinforcement design.

Case	ρx	ρy	$\sigma 1$	$\sigma 2$	$\tan\theta$
1	$\frac{1}{fs}\left[\sigma x+\lvert\tau xy\rvert\right]$	$\frac{1}{fs}\left[\sigma y+\lvert\tau xy\rvert\right]$	0	$-2\lvert\tau xy\rvert$	$-\frac{\tau xy}{\lvert\tau xy\rvert}$
2	0	$\frac{1}{fs}\left[\sigma y\frac{\tau xy^2}{\sigma x}\right]$	0	$\sigma x+\frac{\tau xy^2}{\sigma x}$	$\frac{\sigma x}{\tau xy}$
3	$\frac{1}{fs}\left[\sigma x-\frac{\tau xy^2}{\sigma y}\right]$	0	0	$\sigma y+\frac{\tau xy^2}{\sigma y}$	$\frac{\tau xy}{\sigma y}$
4	$\frac{1}{fs'}\left[\sigma xf-\lvert\tau xy\rvert\right]$	$\frac{1}{fs'}\left[\sigma yf-\lvert\tau xy\rvert\right]$	$fc'+2\lvert\tau xy\rvert$	fc'	$-\frac{\tau xy}{\lvert\tau xy\rvert}$
5	0	$\frac{1}{fs'}\left[\sigma yf-\frac{\tau xy^2}{\sigma xf}\right]$	$\sigma x+\frac{\tau xy^2}{\sigma xf}$	fc'	$\frac{\tau xy}{\sigma xf}$
6	$\frac{1}{fs'}\left[\sigma xf-\frac{\tau xy^2}{\sigma yf}\right]$	0	$\sigma y+\frac{\tau xy^2}{\sigma yf}$	fc'	$\frac{\sigma yf}{\tau xy}$
7	$\frac{1}{fs}\left[\sigma x-\frac{fc'}{2}(1-\beta)\right]$	$\frac{1}{fs'}\left[\sigma y-\frac{fc'}{2}(1+\beta)\right]$	0	fc'	$\frac{2\tau xy}{fc'(1+\beta)}$
8	$\frac{1}{fs'}\left[\sigma x-\frac{fc'}{2}(1+\beta)\right]$	$\frac{1}{fs}\left[\sigma y-\frac{fc'}{2}(1-\beta)\right]$	0	fc'	$\frac{2\tau xy}{fc'(1-\beta)}$
9	0	0	$\frac{\sigma x+\sigma y+\sqrt{(\sigma x-\sigma y)^2+4\tau xy^2}}{2}$	$\frac{\sigma x+\sigma y-\sqrt{(\sigma x-\sigma y)^2+4\tau xy^2}}{2}$	$\frac{\sigma x+\sigma y-\sqrt{(\sigma x-\sigma y)^2+4\tau xy^2}}{2\tau xy}$

TABLE 5.3

Boundary curves for orthogonal reinforcement

Curve	Equation
1	$\frac{\sigma y}{\lvert\tau xy\rvert} = +\infty$
2	$\frac{\sigma y}{\lvert\tau xy\rvert} = \frac{1}{2}\left[\frac{fc'}{\lvert\tau xy\rvert} + \sqrt{(\frac{fc'}{\lvert\tau xy\rvert})^2 - 4}\right]$
3	$\frac{\sigma y}{\lvert\tau xy\rvert} = -1$
4	$\frac{\sigma y}{\lvert\tau xy\rvert} = \frac{fc'}{\lvert\tau xy\rvert} + 1$
5	$\frac{\sigma y}{\lvert\tau xy\rvert} = \frac{1}{2}\left[\frac{fc'}{\lvert\tau xy\rvert} - \sqrt{(\frac{fc'}{\lvert\tau xy\rvert})^2 - 4}\right]$
6	$\frac{\sigma y}{\lvert\tau xy\rvert} = -\infty$
7	$\frac{\sigma x}{\lvert\tau xy\rvert} = \frac{1}{2}\left[\frac{fc'}{\lvert\tau xy\rvert} - \sqrt{(\frac{fc'}{\lvert\tau xy\rvert})^2 - 4}\right]$
8	$\frac{\sigma x}{\lvert\tau xy\rvert} = -1$
9	$\frac{\sigma xf}{\lvert\tau xy\rvert}\ \frac{\sigma yf}{\lvert\tau xy\rvert} = 1$
10	$\frac{\sigma x}{\lvert\tau xy\rvert}\ \frac{\sigma y}{\lvert\tau xy\rvert} = 1$
11	$\frac{\sigma x}{\lvert\tau xy\rvert} = \frac{fc'}{\lvert\tau xy\rvert} + 1$
12	$\frac{\sigma x}{\lvert\tau xy\rvert} = \frac{1}{2}\left[\frac{fc'}{\lvert\tau xy\rvert} + \sqrt{(\frac{fc'}{\lvert\tau xy\rvert})^2 - 4}\right]$

TABLE 5.4

Modified boundary curves for orthogonal reinforcement

Curve	Equation
1	$E_1 = \frac{\sigma y}{\lvert\tau xy\rvert} = +\infty$
2	$E_2 = \frac{\sigma y}{\lvert\tau xy\rvert} = \frac{1}{2}\left[\frac{fc'}{\lvert\tau xy\rvert} + \sqrt{(\frac{fc'}{\lvert\tau xy\rvert})^2 - 4}\right]$
3	$E_3 = \frac{\sigma y}{\lvert\tau xy\rvert} = -1$
4	$E_4 = \frac{\sigma y}{\lvert\tau xy\rvert} = \frac{fc'}{\lvert\tau xy\rvert} + 1$
5	$E_5 = \frac{\sigma y}{\lvert\tau xy\rvert} = \frac{1}{2}\left[\frac{fc'}{\lvert\tau xy\rvert} - \sqrt{(\frac{fc'}{\lvert\tau xy\rvert})^2 - 4}\right]$
6	$E_6 = \frac{\sigma y}{\lvert\tau xy\rvert} = -\infty$
7	$E_7 = \frac{\sigma x}{\lvert\tau xy\rvert} = \frac{1}{2}\left[\frac{fc'}{\lvert\tau xy\rvert} - \sqrt{(\frac{fc'}{\lvert\tau xy\rvert})^2 - 4}\right]$
8	$E_8 = \frac{\sigma x}{\lvert\tau xy\rvert} = -1$
9	$E_{9X} = \frac{fc'}{\lvert\tau xy\rvert} + \frac{\lvert\tau xy\rvert}{\sigma yf}$ and $E_{9y} = \frac{fc'}{\lvert\tau xy\rvert} + \frac{\lvert\tau xy\rvert}{\sigma xf}$
10	$E_{10X} = \frac{\lvert\tau xy\rvert}{\sigma y}$ and $E_{10y} = \frac{\lvert\tau xy\rvert}{\sigma x}$
11	$E_{11} = \frac{\sigma x}{\lvert\tau xy\rvert} = \frac{fc'}{\lvert\tau xy\rvert} + 1$
12	$E_{12} = \frac{\sigma x}{\lvert\tau xy\rvert} = \frac{1}{2}\left[\frac{fc'}{\lvert\tau xy\rvert} + \sqrt{(\frac{fc'}{\lvert\tau xy\rvert})^2 - 4}\right]$

TABLE 5.5

Equations for skew reinforcement design.

Case	ρx	ρy	$\sigma 1$	$\sigma 2$	$\tan\theta$
1	$\frac{1}{fs}\left[\sigma x+2\tau xy\cot\alpha+\sigma y\cot^2\alpha + \left\lvert\frac{\tau xy+\sigma y\cot\alpha}{\sin\alpha}\right\rvert\right]$	$\frac{1}{fs}\left[\sigma y\operatorname{cosec}^2\alpha+\left\lvert\frac{\tau xy+\sigma y\cot\alpha}{\sin\alpha}\right\rvert\right]$	0	$-2(\tau xy+\sigma y\cot\alpha)(\cot\alpha\pm\operatorname{cosec}\alpha)$	$-(\cot\alpha\pm\operatorname{cosec}\alpha)$
2	0	$\frac{\operatorname{cosec}^2\alpha}{fs}\left[\frac{\sigma x\sigma y-\tau xy^2}{\sigma x+2\tau xy\cot\alpha+\sigma y\cot^2\alpha}\right]$	0	$\frac{(\sigma x+\tau xy\cot\alpha)^2+(\tau xy+\sigma y\cot\alpha)^2}{\sigma x+2\tau xy\cot\alpha+\sigma y\cot^2\alpha}$	$\frac{\sigma x+\tau xy\cot\alpha}{\tau xy+\sigma y\cot\alpha}$
3	$\frac{1}{fs}\left[\sigma x-\frac{\tau xy^2}{\sigma y}\right]$	0	0	$\sigma y+\frac{\tau xy^2}{\sigma y}$	$\frac{\tau xy}{\sigma y}$
4	$\frac{1}{fs'}\left[\sigma xf+2\tau xy\cot\alpha+\sigma yf\cot^2\alpha - \left\lvert\frac{\tau xy+\sigma yf\cot\alpha}{\sin\alpha}\right\rvert\right]$	$\frac{1}{fs'}\left[\sigma yf\operatorname{cosec}^2\alpha-\left\lvert\frac{\tau xy+\sigma yf\cot\alpha}{\sin\alpha}\right\rvert\right]$	$fc'+2(\tau xy+\sigma yf\cot\alpha)(-\cot\alpha\pm\operatorname{cosec}\alpha)$	fc'	$-(-\cot\alpha\pm\operatorname{cosec}\alpha)^{-1}$
5	0	$\frac{\operatorname{cosec}^2\alpha}{fs'}\left[\frac{\sigma x\sigma yf-\tau xy^2}{\sigma xf+2\tau xy\cot\alpha+\sigma yf\cot^2\alpha}\right]$	$fc'+\frac{(\sigma xf+\tau xy\cot\alpha)^2+(\tau xy+\sigma yf\cot\alpha)^2}{\sigma xf+2\tau xy\cot\alpha+\sigma yf\cot^2\alpha}$	fc'	$-\left[\frac{\tau xy+\sigma yf\cot\alpha}{\sigma xf+\tau xy\cot\alpha}\right]$
6	$\frac{1}{fs'}\left[\sigma xf-\frac{\tau xy^2}{\sigma y}\right]$	0	$\sigma y+\frac{\tau xy^2}{\sigma yf}$	fc'	$\frac{\sigma yf}{\tau xy}$
7	$\frac{1}{fs}\left[\sigma x+\tau xy\cot\alpha-\frac{fc'}{2}(1-\beta)\right]$	$\frac{1}{fs'}\left[\sigma y-\tau xy\cot\alpha-\frac{fc'}{2}(1+\beta)\right]$	0	fc'	$\frac{fc'(1-\beta)}{2(\sigma y\cot\alpha+\tau xy)}$
8	$\frac{1}{fs'}\left[\sigma x+\tau xy\cot\alpha-\frac{fc'}{2}(1+\beta)\right]$	$\frac{1}{fs}\left[\sigma y-\tau xy\cot\alpha-\frac{fc'}{2}(1-\beta)\right]$	0	fc'	$\frac{fc'(1+\beta)}{2(\sigma y\cot\alpha+\tau xy)}$
9	0	0	$\frac{\sigma x+\sigma y+\sqrt{(\sigma x-\sigma y)^2+4\tau xy^2}}{2}$	$\frac{\sigma x+\sigma y-\sqrt{(\sigma x-\sigma y)^2+4\tau xy^2}}{2}$	$\frac{\sigma x-\sigma y-\sqrt{(\sigma x-\sigma y)^2+4\tau xy^2}}{2\tau xy}$

Note: Case 1: alternative sign is the same as that of $(\tau xy+\sigma y\cot\alpha)$.
Case 4: alternative sign is the same as that of $(\tau xy+\sigma yf\cot\alpha)$.

TABLE 5.6

Boundary curves for skew reinforcement

Curve	Equation
1	$\frac{\sigma y}{\lvert\tau xy\rvert} = -\left[\pm \tan\alpha - \frac{fc'}{2\lvert\tau xy\rvert}(1-\lvert\sec\alpha\rvert)\right]$
2	$\frac{\sigma y}{\lvert\tau xy\rvert} = \frac{1}{2}\left[\frac{fc'}{\lvert\tau xy\rvert} + \sqrt{(\frac{fc'}{\lvert\tau xy\rvert})^2 - 4}\right]$
3	$\frac{\sigma y}{\lvert\tau xy\rvert} = -(\operatorname{cosec}\alpha \pm \cot\alpha)^{-1}$
4	$\frac{\sigma y}{\lvert\tau xy\rvert} = \frac{fc'}{\lvert\tau xy\rvert} - (-\operatorname{cosec}\alpha \pm \cot\alpha)^{-1}$
5	$\frac{\sigma y}{\lvert\tau xy\rvert} = \frac{1}{2}\left[\frac{fc'}{\lvert\tau xy\rvert} - \sqrt{(\frac{fc'}{\lvert\tau xy\rvert})^2 - 4}\right]$
6	$\frac{\sigma y}{\lvert\tau xy\rvert} = -\left[\pm \tan\alpha - \frac{fc'}{2\lvert\tau xy\rvert}(1 + \lvert\sec\alpha\rvert)\right]$
7	$\frac{\sigma x}{\lvert\tau xy\rvert} = -\frac{1}{2}\left[-\frac{fc'}{\lvert\tau xy\rvert} \pm 2\cot\alpha + \sqrt{(\frac{fc'}{\lvert\tau xy\rvert})^2 - 4(\frac{\sigma y \cot\alpha}{\lvert\tau xy\rvert} \pm 1)(\frac{\sigma yf \cot\alpha}{\lvert\tau xy\rvert} \pm 1)}\right]$
8	$\frac{\sigma x}{\lvert\tau xy\rvert} = -\frac{\sigma y}{\lvert\tau xy\rvert}\cot\alpha(\cot\alpha \pm \operatorname{cosec}\alpha) - \operatorname{cosec}\alpha \pm 2\cot\alpha$
9	$\frac{\sigma xf}{\lvert\tau xy\rvert}\ \frac{\sigma yf}{\lvert\tau xy\rvert} = 1$
10	$\frac{\sigma x}{\lvert\tau xy\rvert}\ \frac{\sigma y}{\lvert\tau xy\rvert} = 1$
11	$\frac{\sigma x}{\lvert\tau xy\rvert} = \frac{\sigma y}{\lvert\tau xy\rvert}\cot\alpha(-\cot\alpha \pm \operatorname{cosec}\alpha) + \operatorname{cosec}\alpha \pm 2\cot\alpha - \frac{fc'}{\lvert\tau xy\rvert}\operatorname{cosec}\alpha(-\operatorname{cosec}\alpha \pm \cot\alpha)$
12	$\frac{\sigma x}{\lvert\tau xy\rvert} = -\frac{\sigma y}{\lvert\tau xy\rvert}\cot\alpha(\cot\alpha \pm \operatorname{cosec}\alpha) - \operatorname{cosec}\alpha \pm 2\cot\alpha + \frac{fc'}{\lvert\tau xy\rvert}\operatorname{cosec}\alpha(\operatorname{cosec}\alpha \pm \cot\alpha)$
13	$\frac{\sigma x}{\lvert\tau xy\rvert} = \frac{\sigma y}{\lvert\tau xy\rvert}\cot\alpha(-\cot\alpha \pm \operatorname{cosec}\alpha) + \operatorname{cosec}\alpha \pm 2\cot\alpha$
14	$\frac{\sigma x}{\lvert\tau xy\rvert} = -\frac{1}{2}\left[-\frac{fc'}{\lvert\tau xy\rvert} \pm 2\cot\alpha - \sqrt{(\frac{fc'}{\lvert\tau xy\rvert})^2 - 4(\frac{\sigma y \cot\alpha}{\lvert\tau xy\rvert} \pm 1)(\frac{\sigma yf \cot\alpha}{\lvert\tau xy\rvert} \pm 1)}\right]$

Note: Alternative sign is the same as that of τxy.

TABLE 5.7

Modified boundary curves for skew reinforcement

Curve	Equation
1	$E_1 = -\left[\pm \tan\alpha - \frac{fc'}{2\lvert\tau xy\rvert}(1-\lvert\sec\alpha\rvert)\right]$
2	$E_2 = \frac{1}{2}\left[\frac{fc'}{\lvert\tau xy\rvert} + \sqrt{(\frac{fc'}{\lvert\tau xy\rvert})^2 - 4}\right]$
3	$E_3 = -(\operatorname{cosec}\alpha \pm \cot\alpha)^{-1}$
4	$E_4 = \frac{fc'}{\lvert\tau xy\rvert} - (-\operatorname{cosec}\alpha \pm \cot\alpha)^{-1}$
5	$E_5 = \frac{1}{2}\left[\frac{fc'}{\lvert\tau xy\rvert} - \sqrt{(\frac{fc'}{\lvert\tau xy\rvert})^2 - 4}\right]$
6	$E_6 = -\left[\pm \tan\alpha - \frac{fc'}{2\lvert\tau xy\rvert}(1 + \lvert\sec\alpha\rvert)\right]$
7	$E_7 = -\frac{1}{2}\left[-\frac{fc'}{\lvert\tau xy\rvert} \pm 2\cot\alpha + \sqrt{(\frac{fc'}{\lvert\tau xy\rvert})^2 - 4(\frac{\sigma y \cot\alpha}{\lvert\tau xy\rvert} \pm 1)(\frac{\sigma yf \cot\alpha}{\lvert\tau xy\rvert} \pm 1)}\right]$
8	$E_8 = -\frac{\sigma y}{\lvert\tau xy\rvert}\cot\alpha(\cot\alpha \pm \operatorname{cosec}\alpha) - \operatorname{cosec} \pm 2\cot\alpha$
9	$E_{9x} = \frac{\lvert\tau xy\rvert}{\sigma yf} + \frac{fc'}{\lvert\tau xy\rvert}$ and $E_{9y} = \frac{\lvert\tau xy\rvert}{\sigma xf} + \frac{fc'}{\lvert\tau xy\rvert}$
10	$E_{10x} = \frac{\lvert\tau xy\rvert}{\sigma y}$ and $E_{10y} = \frac{\lvert\tau xy\rvert}{\sigma x}$
11	$E_{11} = \frac{\sigma y}{\lvert\tau xy\rvert}\cot\alpha(-\cot\alpha \pm \operatorname{cosec}\alpha) + \operatorname{cosec}\alpha \pm 2\cot\alpha - \frac{fc'}{\lvert\tau xy\rvert}\operatorname{cosec}\alpha(-\operatorname{cosec}\alpha \pm \cot\alpha)$
12	$E_{12} = -\frac{\sigma y}{\lvert\tau xy\rvert}\cot\alpha(\cot\alpha \pm \operatorname{cosec}\alpha) + \operatorname{cosec}\alpha \pm 2\cot\alpha + \frac{fc'}{\lvert\tau xy\rvert}\operatorname{cosec}\alpha(\operatorname{cosec}\alpha \pm \cot\alpha)$
13	$E_{13} = -\frac{\sigma y}{\lvert\tau xy\rvert}\cot\alpha(-\cot\alpha \pm \operatorname{cosec}\alpha) + \operatorname{cosec}\alpha \pm 2\cot\alpha$
14	$E_{14} = -\frac{1}{2}\left[-\frac{fc'}{\lvert\tau xy\rvert} \pm 2\cot\alpha - \sqrt{(\frac{fc'}{\lvert\tau xy\rvert})^2 - 4(\frac{\sigma y \cot\alpha}{\lvert\tau xy\rvert} \pm 1)(\frac{\sigma yf \cot\alpha}{\lvert\tau xy\rvert} \pm 1)}\right]$

Note: Alternative sign is the same as that of τxy.

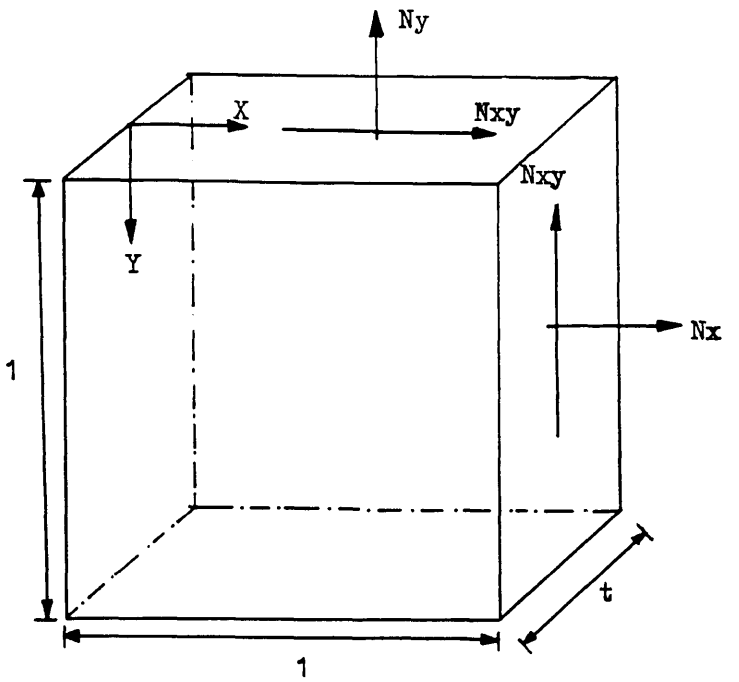

Figure (5.1) Sign convention for in– plane direct and shear stresses

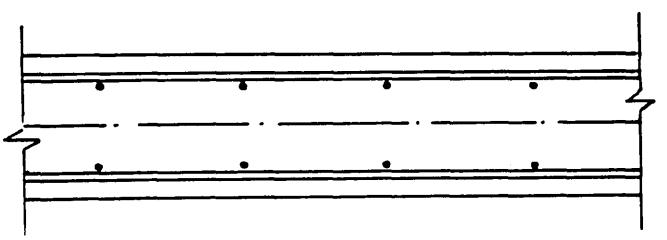

Figure (5.2) The symmetrical position of both reinforcement layers w.r.t the middle surface of the section.

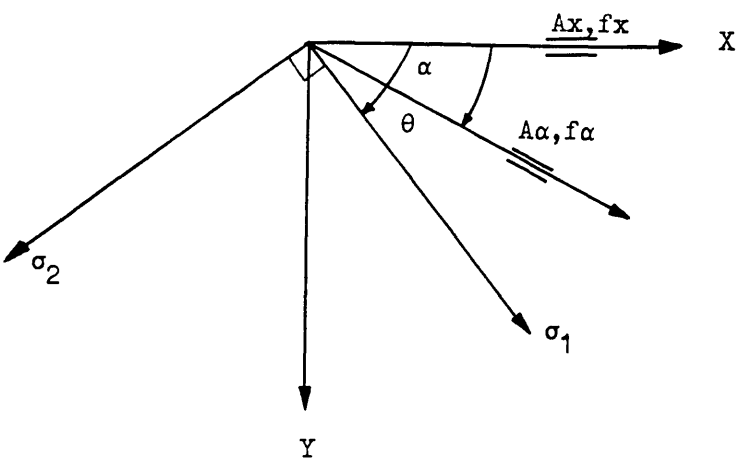

Figure (5.3) Principal concrete stresses and directions of reinforcement.

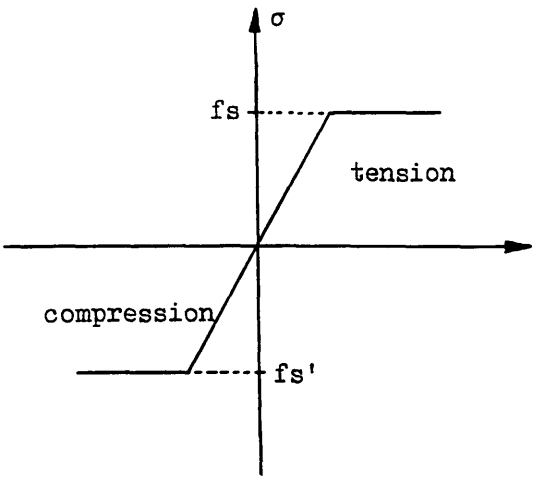

Figure (5.4) Yield criterion for steel in-plane stress.

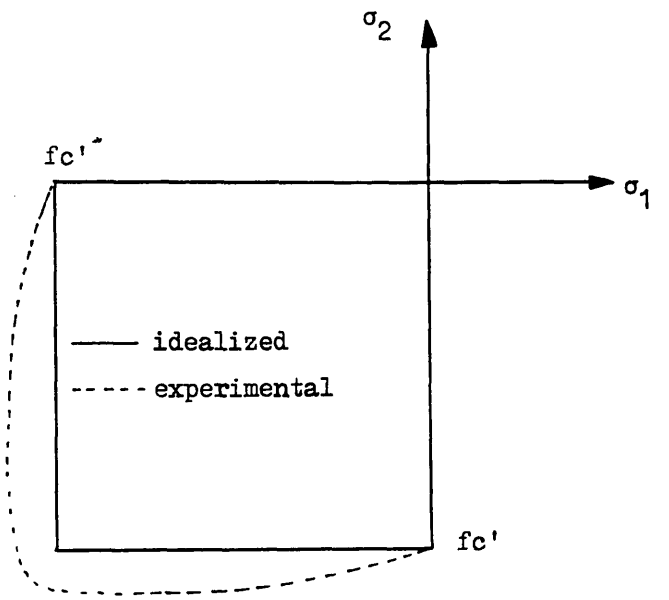

Figure (5.5) Yield criterion for concrete in plane stress.

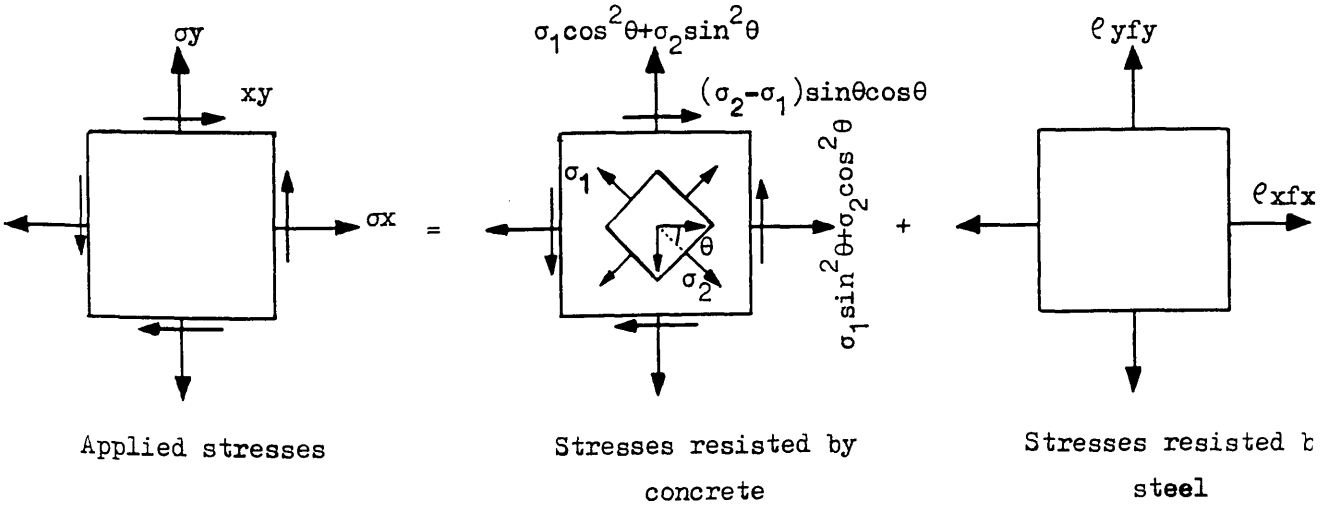

Figure (5.6) Combined resistance of concrete and steel against applied stresses.

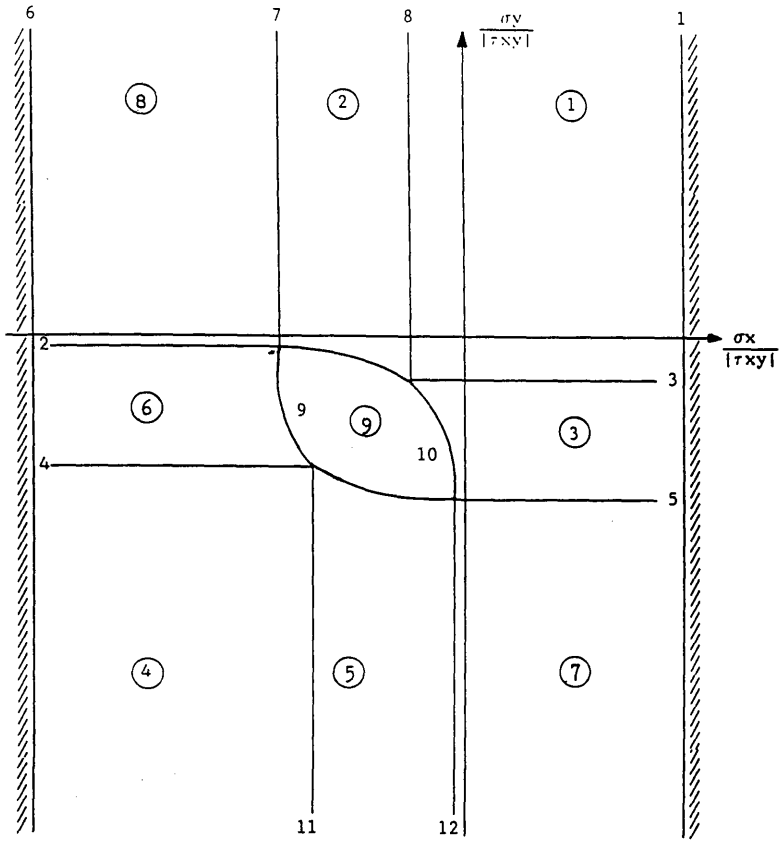

Figure (5.7) Boundary equation graph for orthogonal reinforcement design.

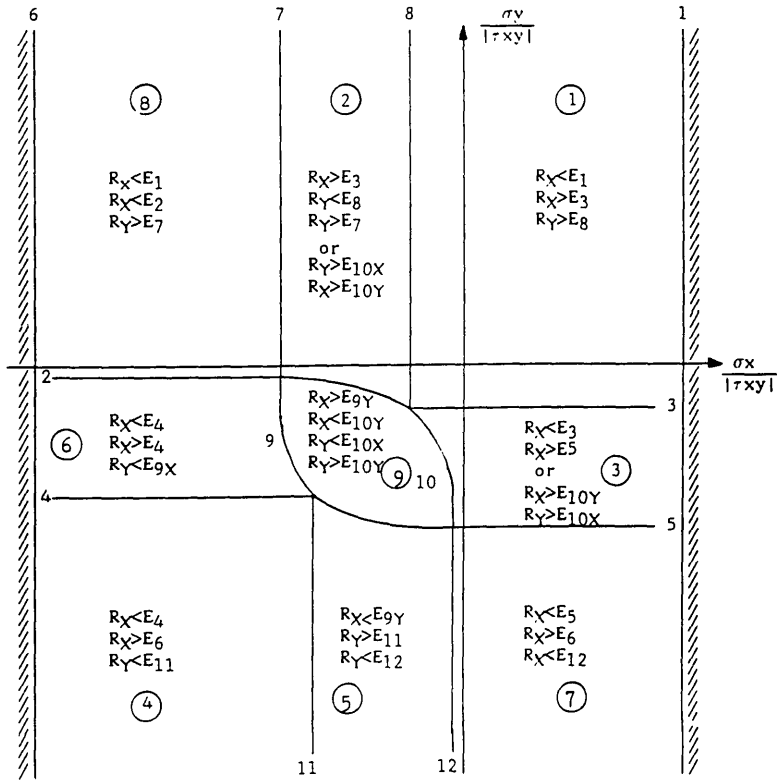

Figure (5.8) Conditions for chosen cases of boundary curves for orthogonal reinforcement design.

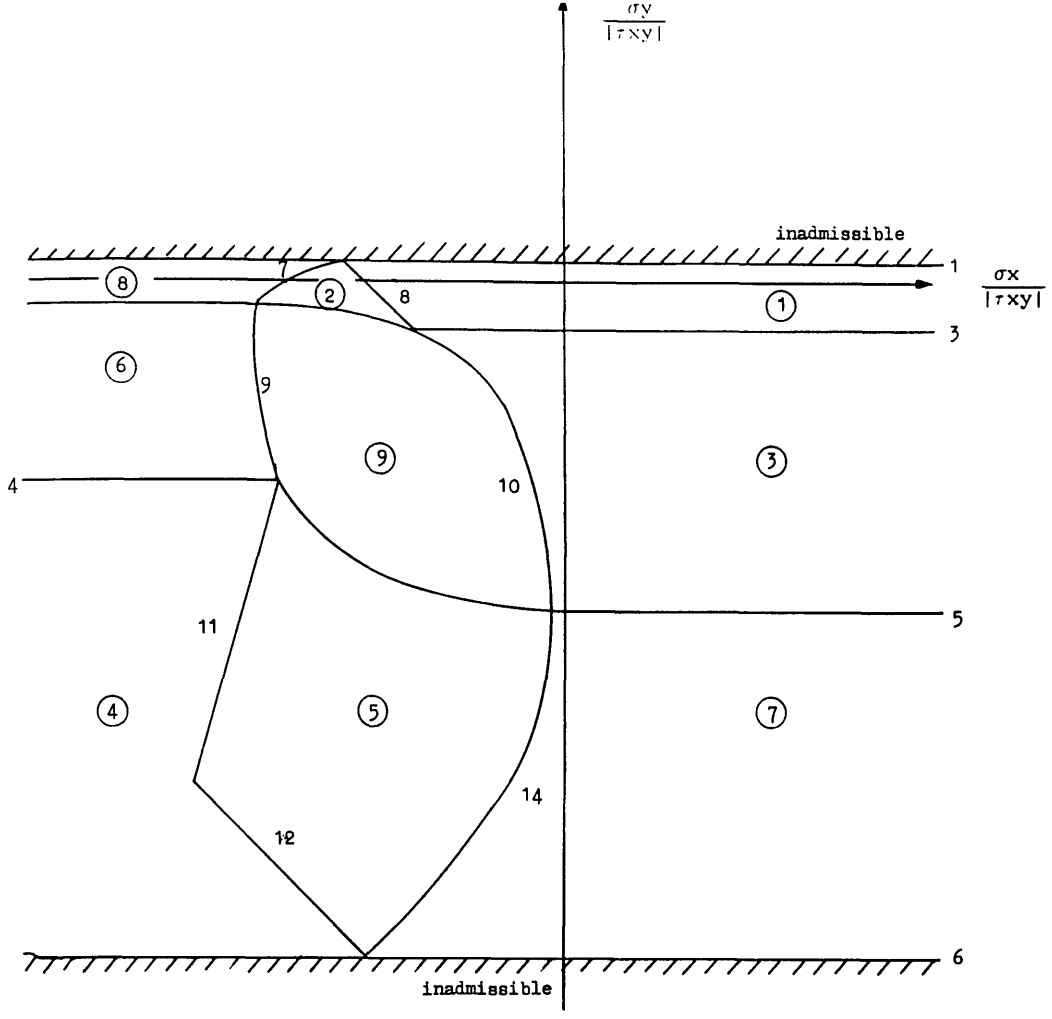

Figure (5.9) Boundary equations graph for skew reinforcement design when τxy is positive

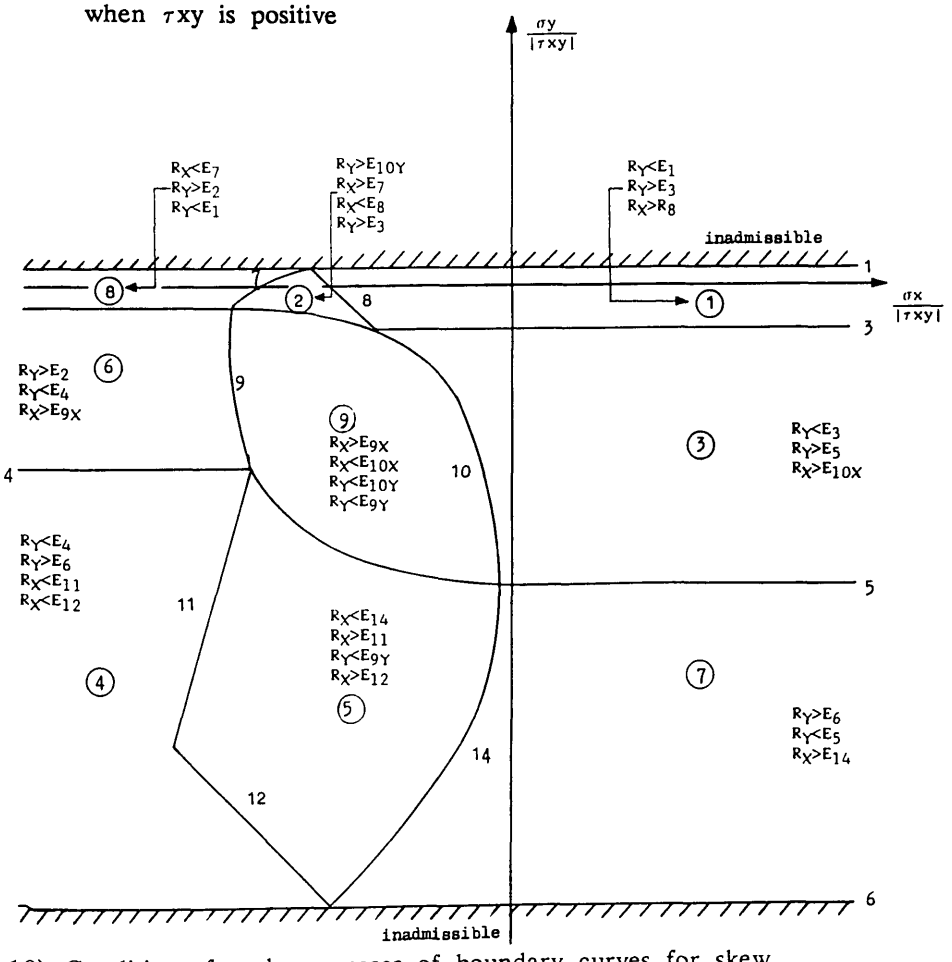

Figure (5.10) Conditions for chosen cases of boundary curves for skew reinforcement design when τxy is positive.

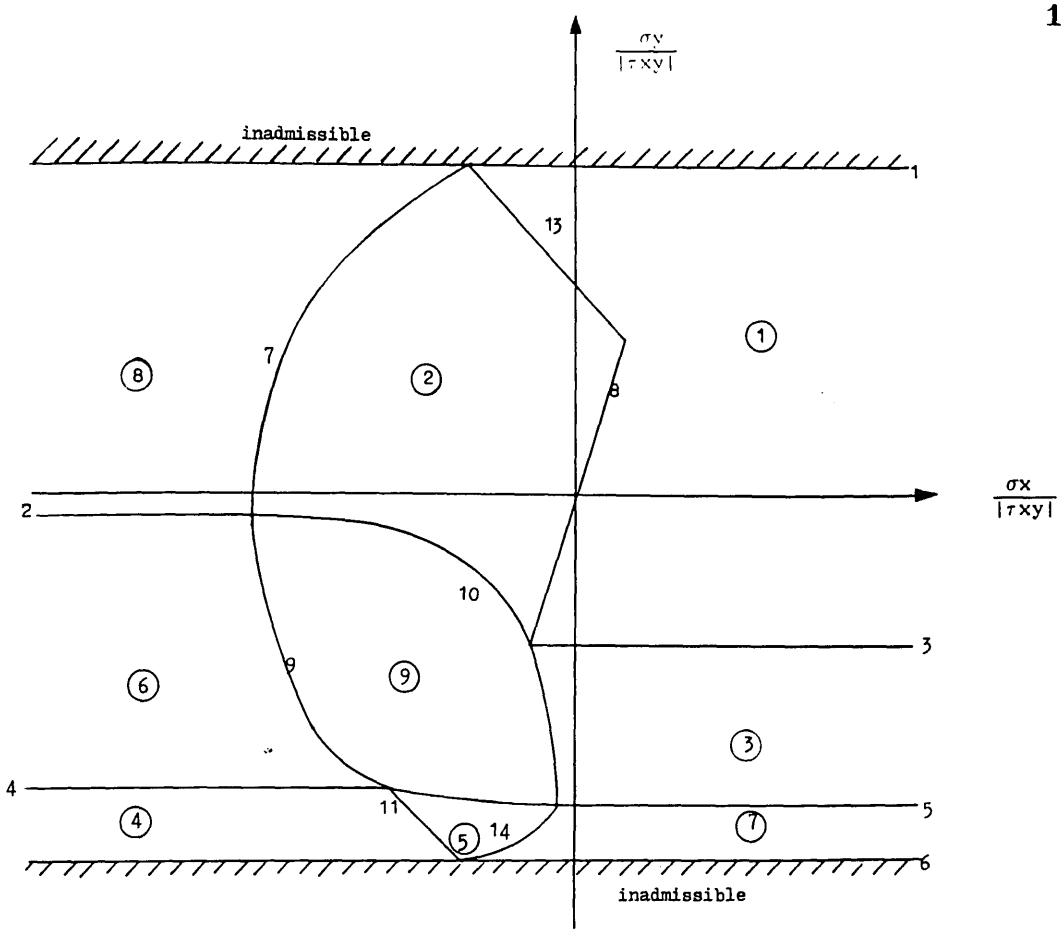

Figure (5.11) Boundary equations graph for skew reinforcement design when τxy is negative

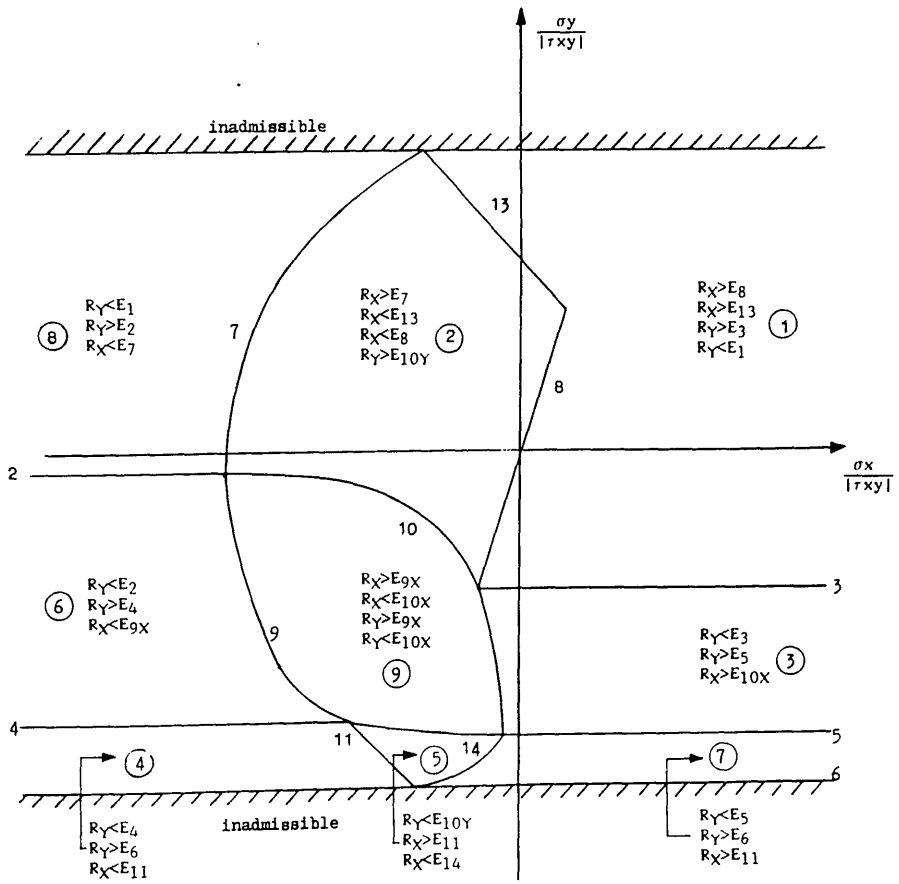

Figure (5.12) Conditions for chosen cases of boundary curves for skew reinforcement design when τxy is negative.

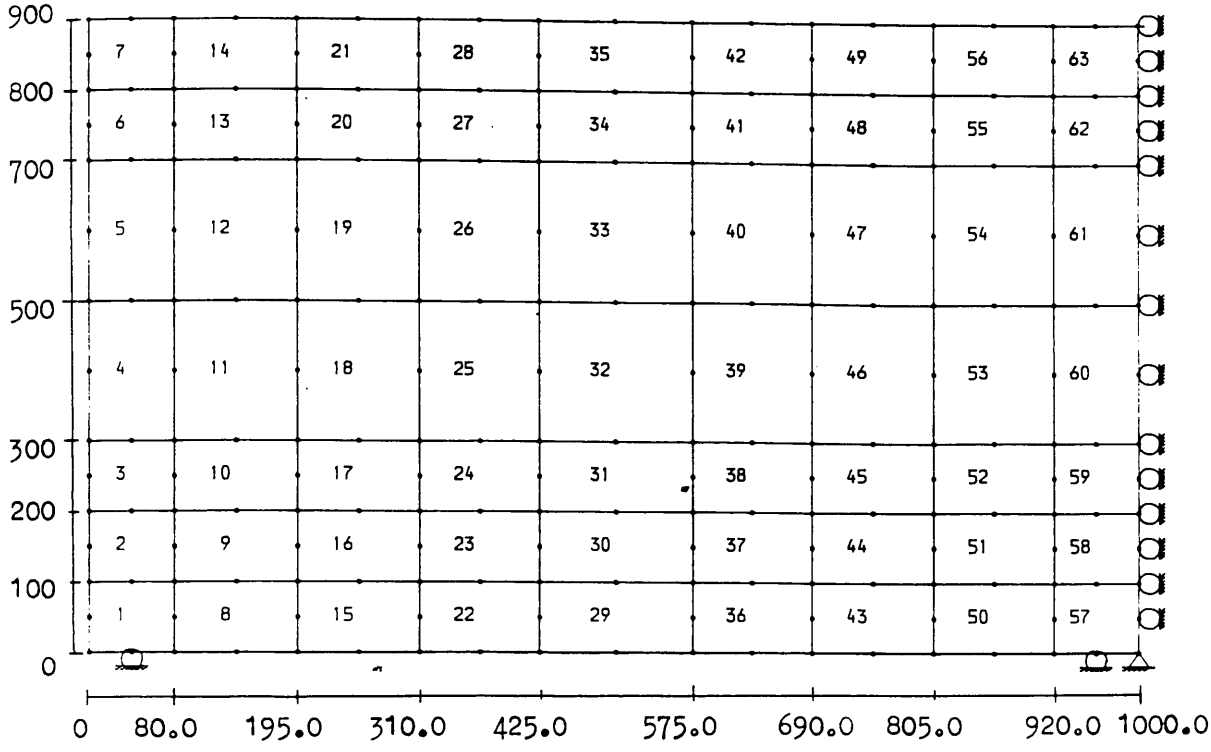

Figure(5.13) Finite element mesh of transfer girder TRGRAS1

0.03 0.04	0.05 0.01	0.04 0.03	0.11 0.13	0.04 0.00	0.18 0.18	0.24 0.11	0.42 0.06	0.47 0.01
0.01 0.04	0.01 0.01	0.04 0.07	0.11 0.04	0.09 0.00	0.30 0.07	0.21 0.22	0.17 0.10	0.10 0.00
0.06 0.01	0.20 0.00	0.28 0.00	0.17 0.00	0.12 0.00	0.32 0.00	0.41 0.03	0.18 0.02	0.01 0.00
0.05 0.00	0.27 0.00	0.37 0.00	0.15 0.00	0.07 0.00	0.36 0.00	0.53 0.00	0.38 0.00	0.22 0.00
0.06 0.00	0.29 0.00	0.40 0.06	0.26 0.01	0.25 0.00	0.52 0.08	0.72 0.09	0.67 0.00	0.52 0.00
0.06 0.00	0.39 0.03	0.48 0.10	0.53 0.02	0.60 0.03	0.65 0.15	0.65 0.25	0.79 0.08	0.55 0.00
0.73 0.00	1.08 0.12	1.12 0.02	1.17 0.01	1.15 0.03	1.04 0.07	0.83 0.12	0.56 0.26	0.29 0.00

Figure(5.14) Theoretical required steel ratios for girder TRGRAS1

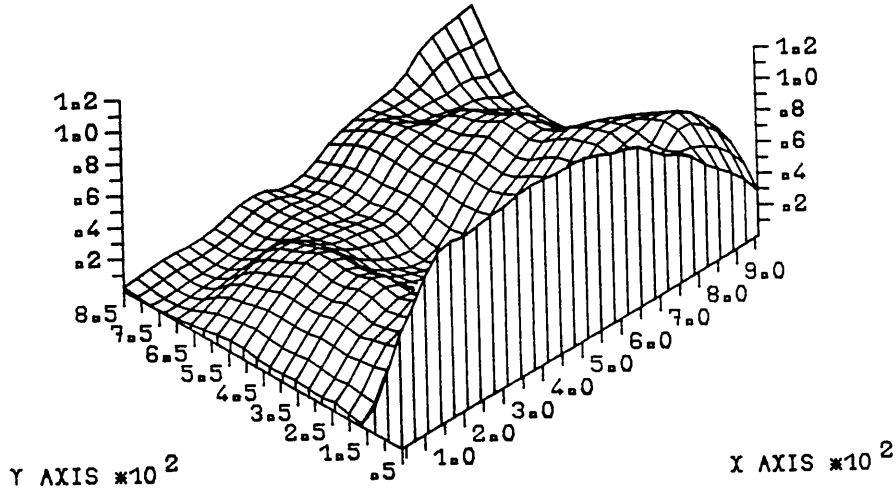

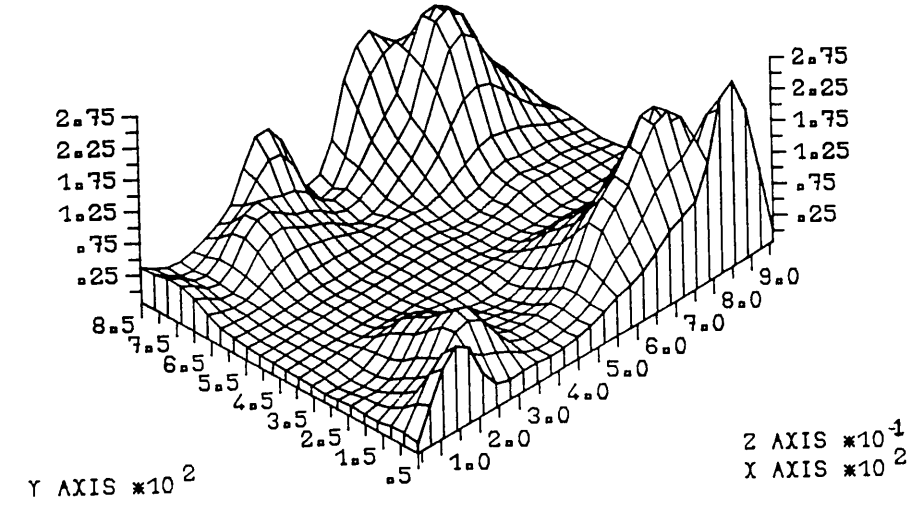

Figure(5.15) Isometric view of steel ratios for girder TRGRAS1

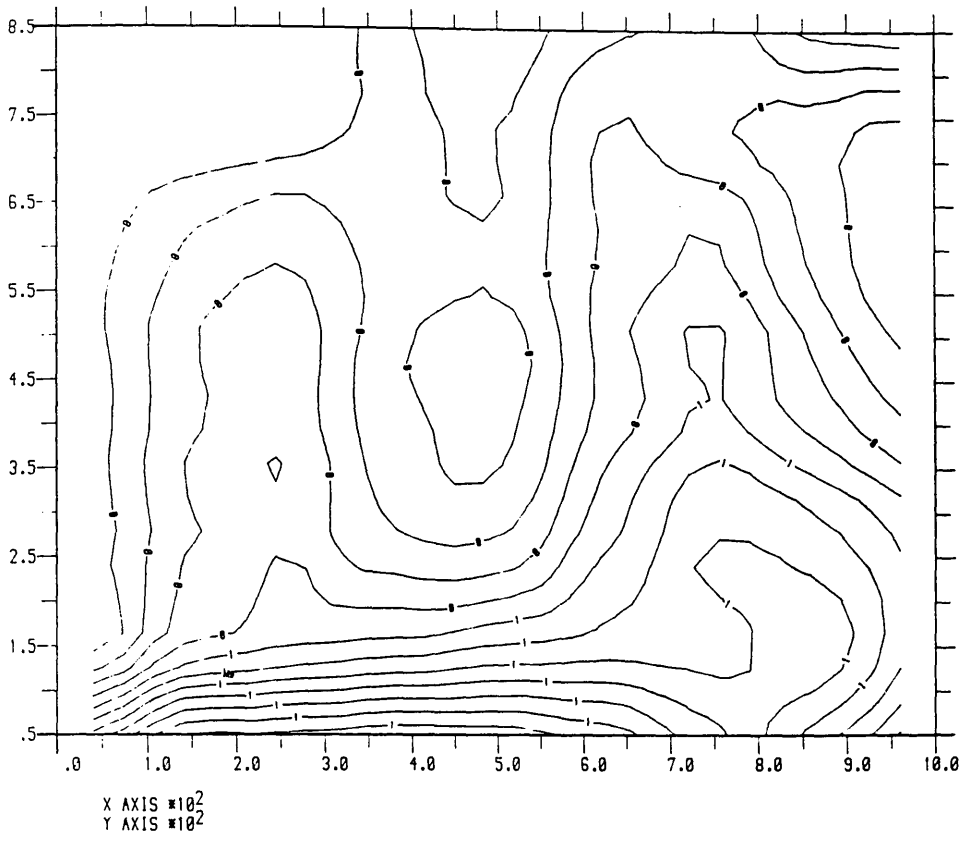

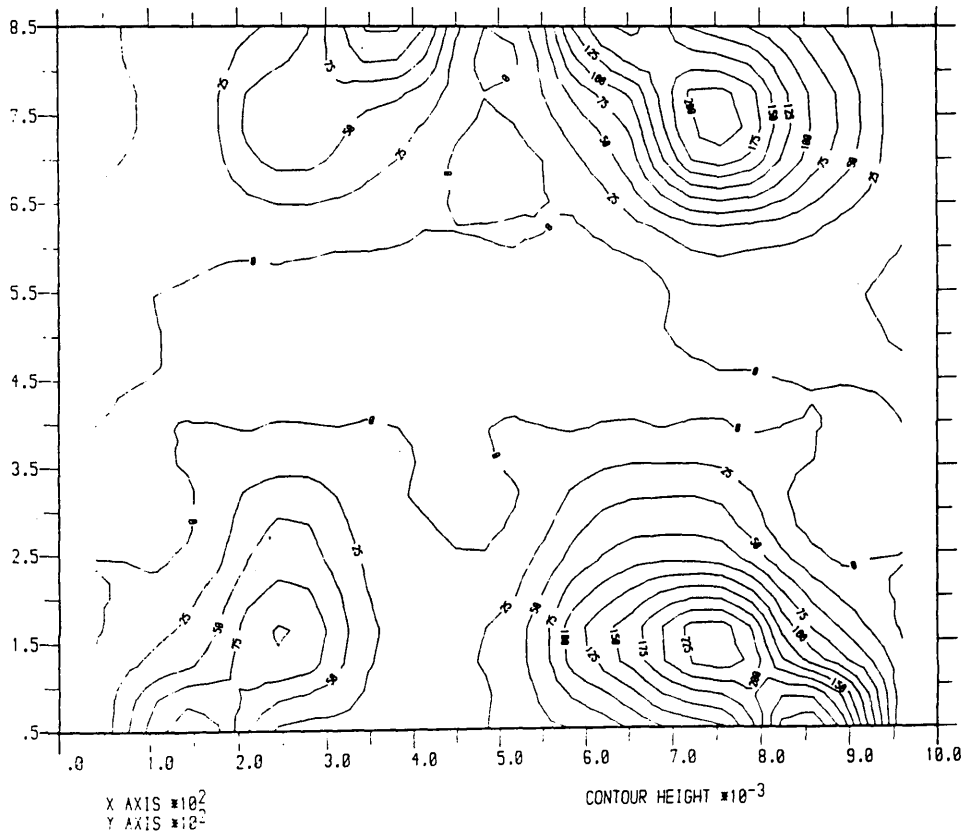

Figure(5.16) Contours of steel ratios for girder TRGRAS1

Main Steel Envelops

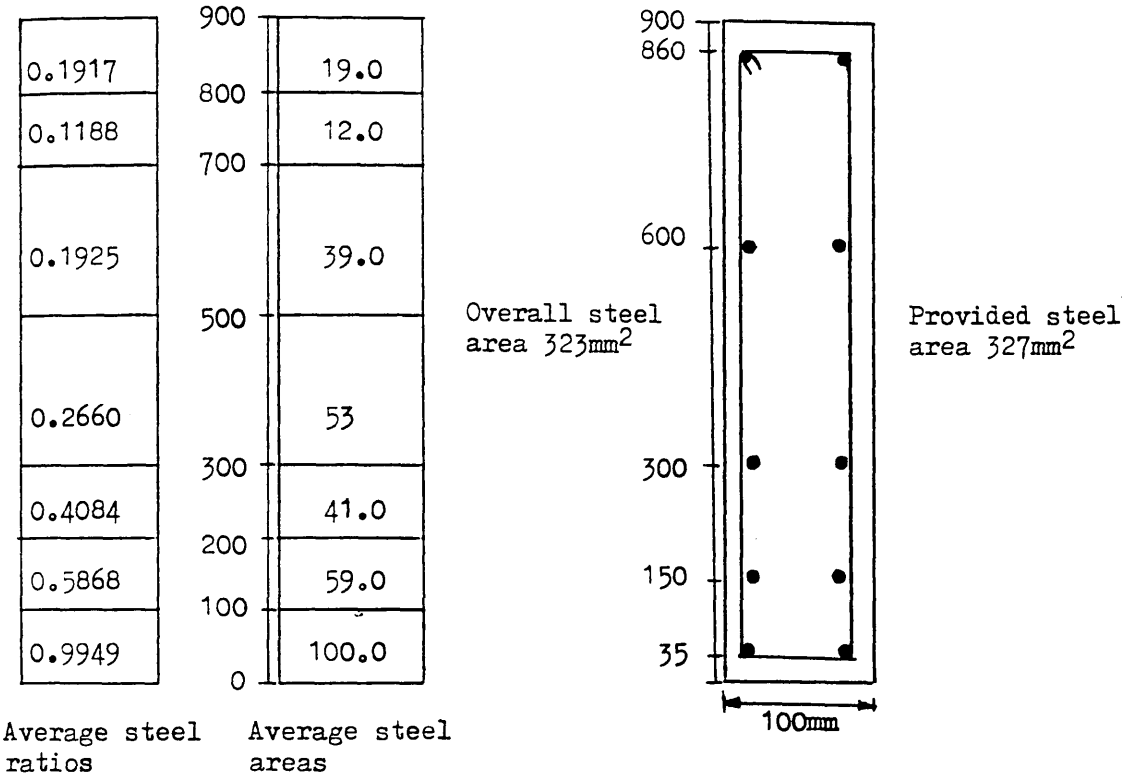

Shear Reinforcement Envelops

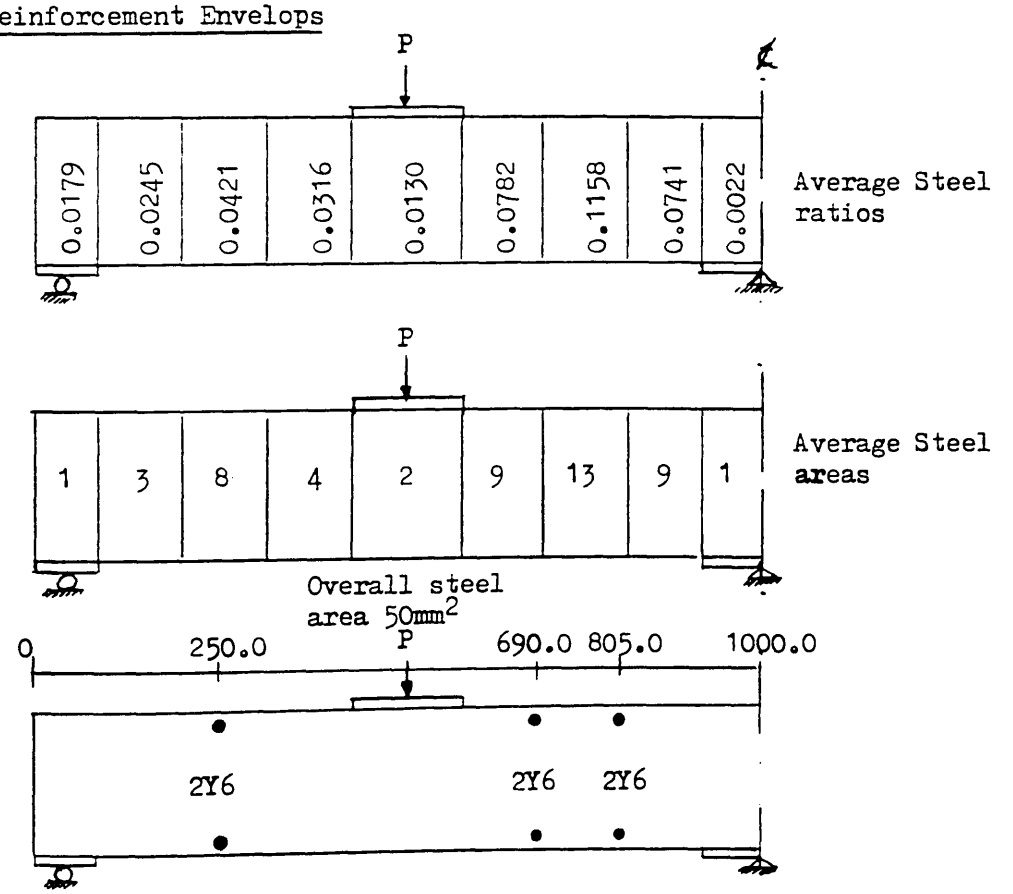

Fig. (5.17) Design of reinforcement of Transfer Girder TRGRAS1

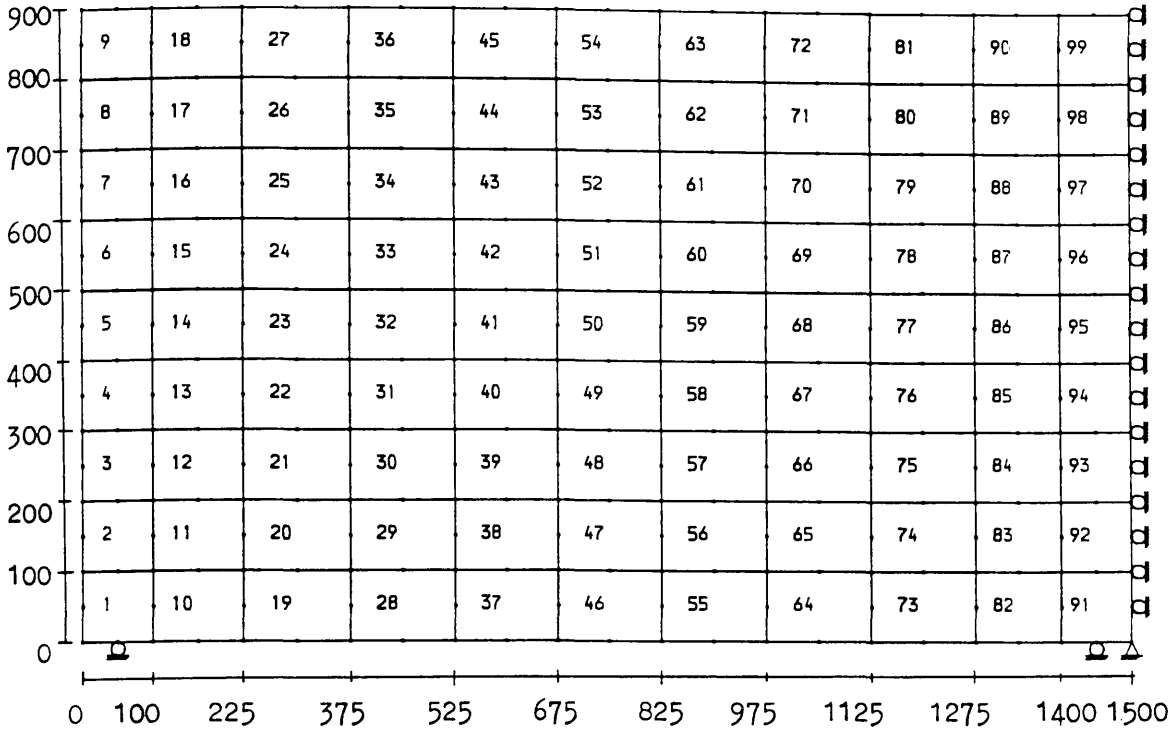

Figure(5.18) Finite element mesh of transfer girder TRGRAS4

0.01 0.01	0.00 0.01	0.00 0.03	0.00 0.02	0.01 0.12	0.00 0.00	0.05 0.18	0.11 0.12	0.49 0.12	0.74 0.07	0.81 0.01
0.01 0.00	0.02 0.05	0.00 0.13	0.00 0.13	0.00 0.05	0.00 0.00	0.17 0.16	0.20 0.42	0.44 0.31	0.55 0.13	0.49 0.01
0.04 0.00	0.13 0.08	0.09 0.26	0.07 0.25	0.06 0.02	0.03 0.00	0.40 0.10	0.48 0.47	0.52 0.39	0.49 0.11	0.30 0.00
0.06 0.00	0.25 0.07	0.27 0.29	0.28 0.23	0.13 0.00	0.09 0.00	0.52 0.08	0.66 0.45	0.64 0.39	0.51 0.07	0.23 0.00
0.06 0.00	0.33 0.06	0.41 0.30	0.40 0.22	0.22 0.00	0.20 0.00	0.60 0.09	0.74 0.44	0.74 0.37	0.55 0.04	0.24 0.00
0.06 0.00	0.37 0.05	0.48 0.30	0.49 0.22	0.36 0.01	0.36 0.00	0.67 0.14	0.75 0.45	0.78 0.39	0.62 0.03	0.30 0.00
0.07 0.00	0.39 0.06	0.53 0.29	0.61 0.21	0.56 0.02	0.59 0.01	0.76 0.19	0.73 0.44	0.69 0.43	0.64 0.06	0.32 0.00
0.11 0.00	0.48 0.06	0.63 0.20	0.83 0.14	0.88 0.02	0.90 0.02	0.92 0.18	0.74 0.33	0.48 0.42	0.49 0.17	0.15 0.00
0.62 0.00	0.96 0.13	1.06 0.04	1.23 0.05	1.31 0.01	1.31 0.02	1.19 0.08	0.90 0.12	0.48 0.15	0.22 0.26	0.10 0.00

Figure(5.19) Theoretical required steel ratios for girder TRGRAS4

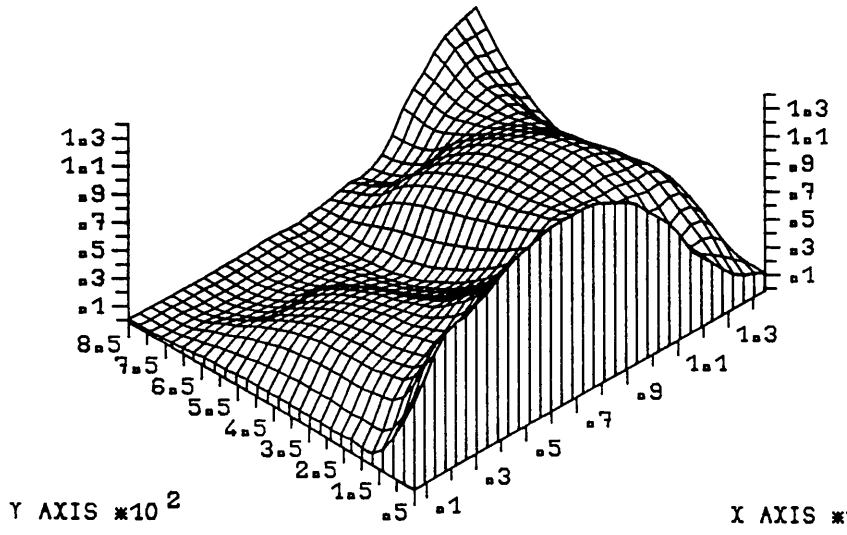

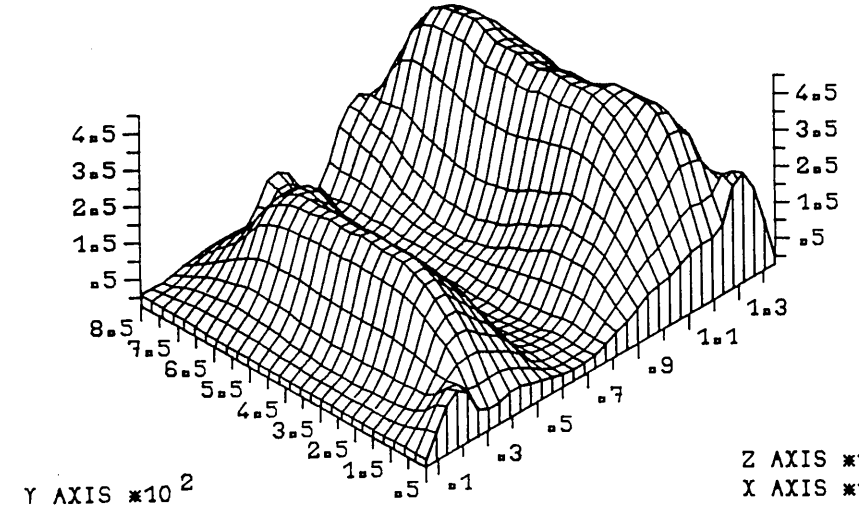

Figure(5.20) Isometric view of steel ratios for girder TRGRAS4

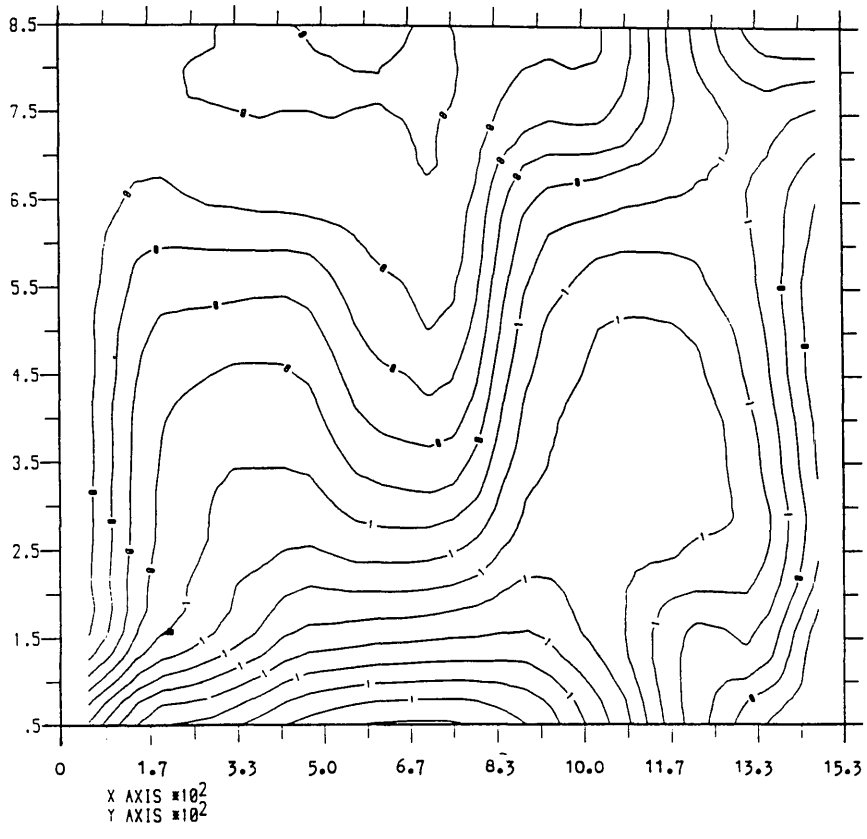

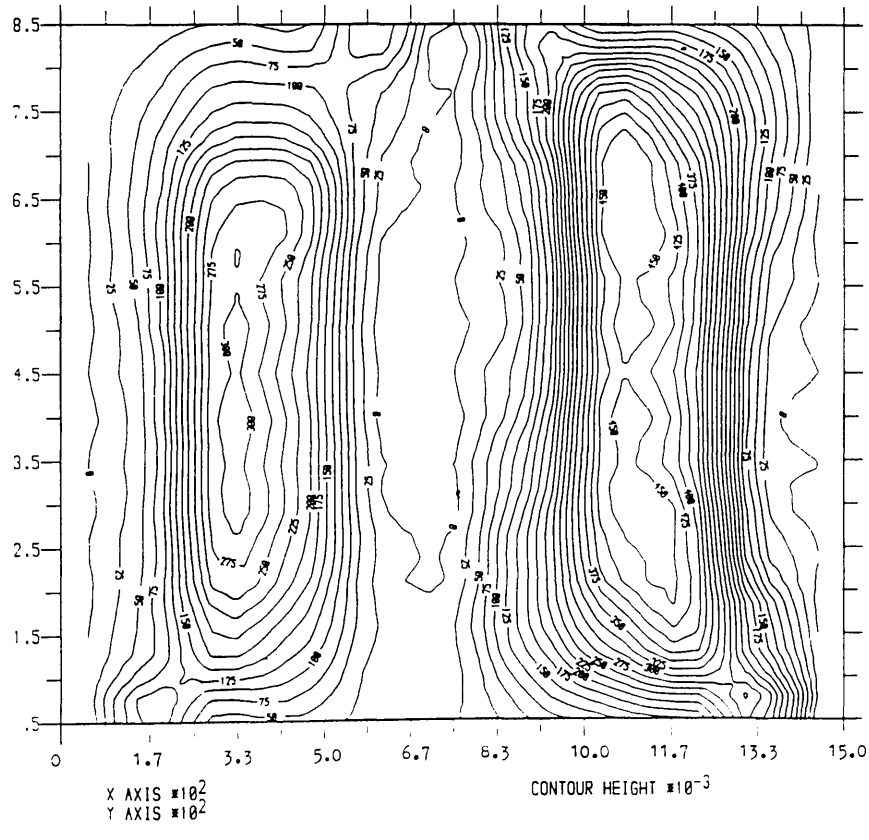

Figure(5.21) Contours of steel ratios for girder TRGRAS4

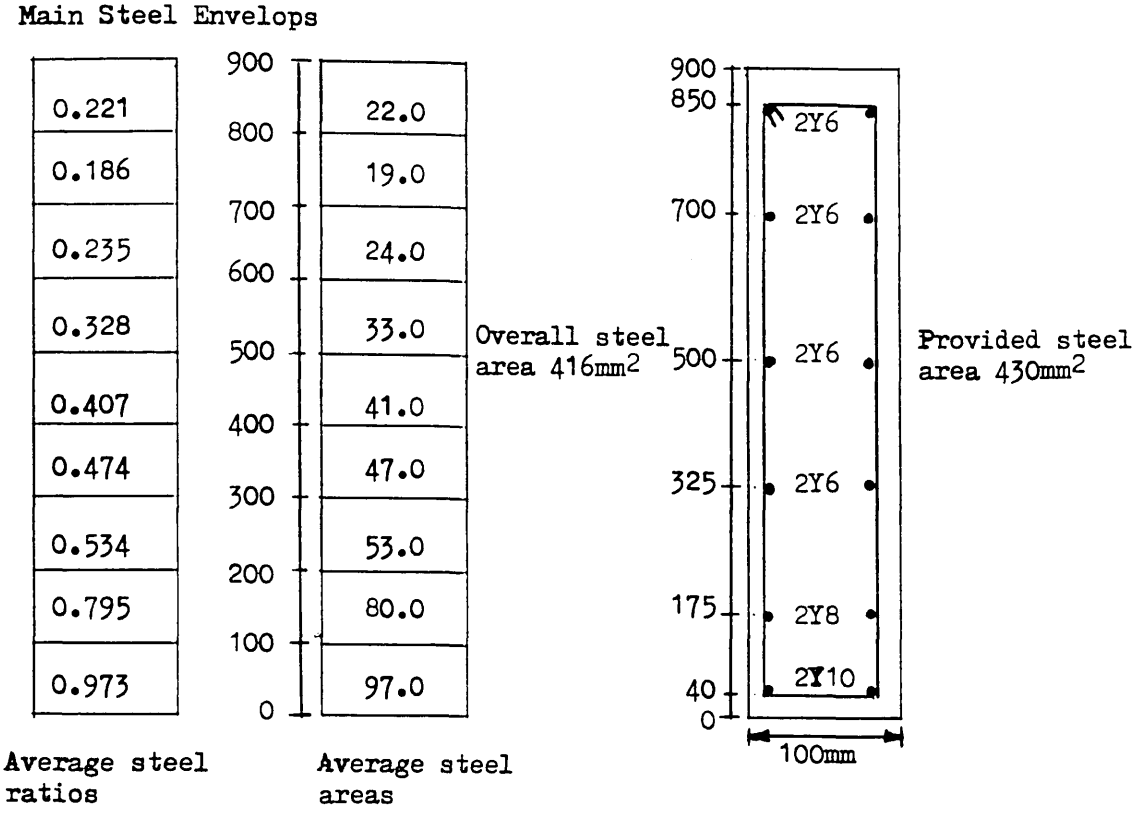

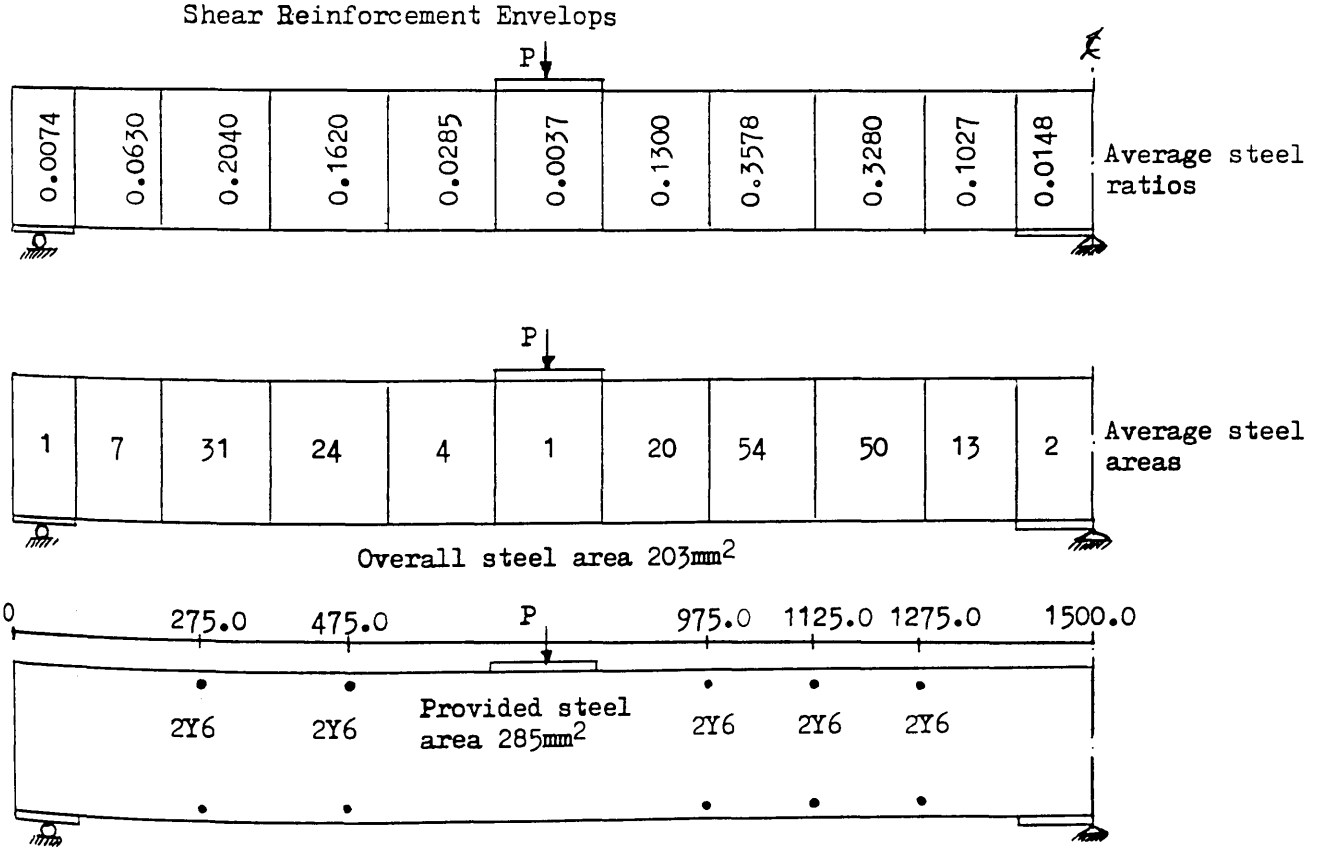

Fig. (5.22) Design of reinforcement of Transfer Girder TRGRAS4

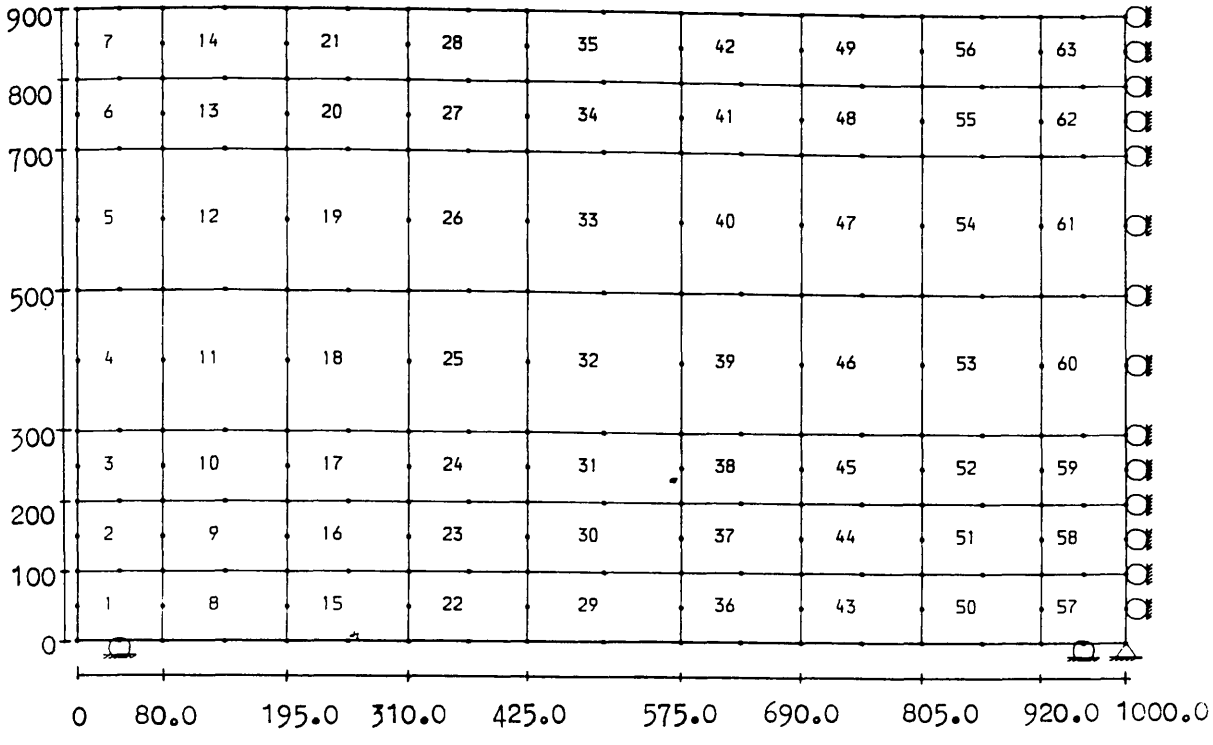

Figure(5.23) Finite element mesh of transfer girder TRGRAS7

0.03 0.05	0.06 0.03	0.05 0.04	0.13 0.12	0.04 0.00	0.21 0.15	0.28 0.08	0.46 0.08	0.57 0.12
0.01 0.04	0.02 0.00	0.06 0.03	0.11 0.01	0.09 0.00	0.26 0.01	0.26 0.06	0.17 0.01	0.08 0.00
0.04 0.01	0.14 0.00	0.20 0.00	0.13 0.00	0.12 0.00	0.25 0.00	0.30 0.00	0.14 0.00	0.00 0.00
0.04 0.00	0.20 0.00	0.26 0.00	0.11 0.00	0.07 0.00	0.26 0.00	0.38 0.00	0.30 0.00	0.21 0.00
0.05 0.00	0.22 0.00	0.30 0.00	0.20 0.00	0.24 0.00	0.39 0.00	0.53 0.00	0.53 0.00	0.50 0.00
0.06 0.00	0.30 0.00	0.41 0.01	0.57 0.07	0.59 0.03	0.54 0.00	0.58 0.02	0.62 0.00	0.51 0.00
0.66 0.00	1.16 0.24	1.43 0.35	1.52 0.41	1.11 0.03	1.18 0.21	0.85 0.12	0.61 0.19	0.24 0.00

Figure(5.24) Theoretical required steel ratios for girder TRGRAS7

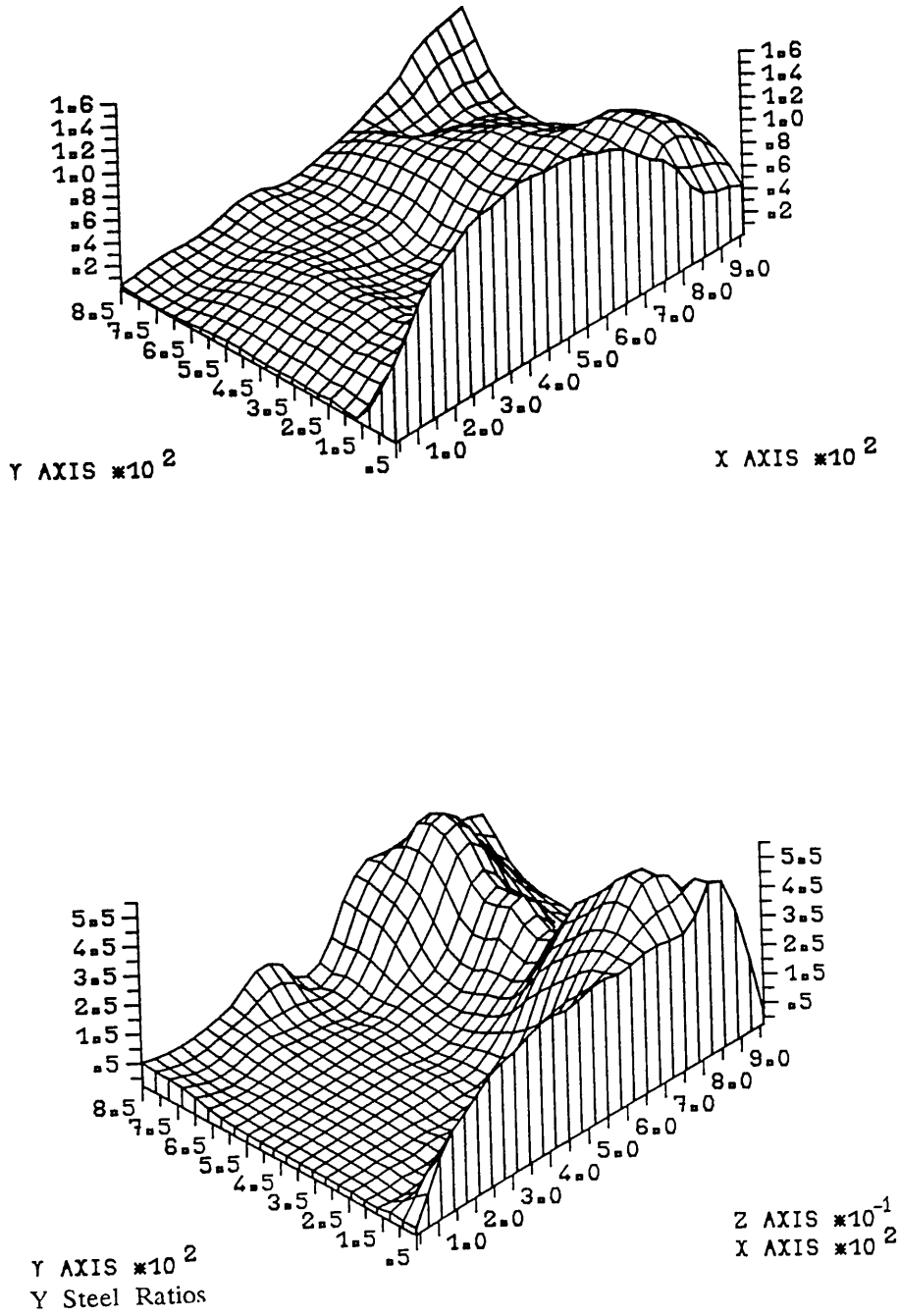

Figure(5.25) Isometric view of steel ratios for girder TRGRAS7

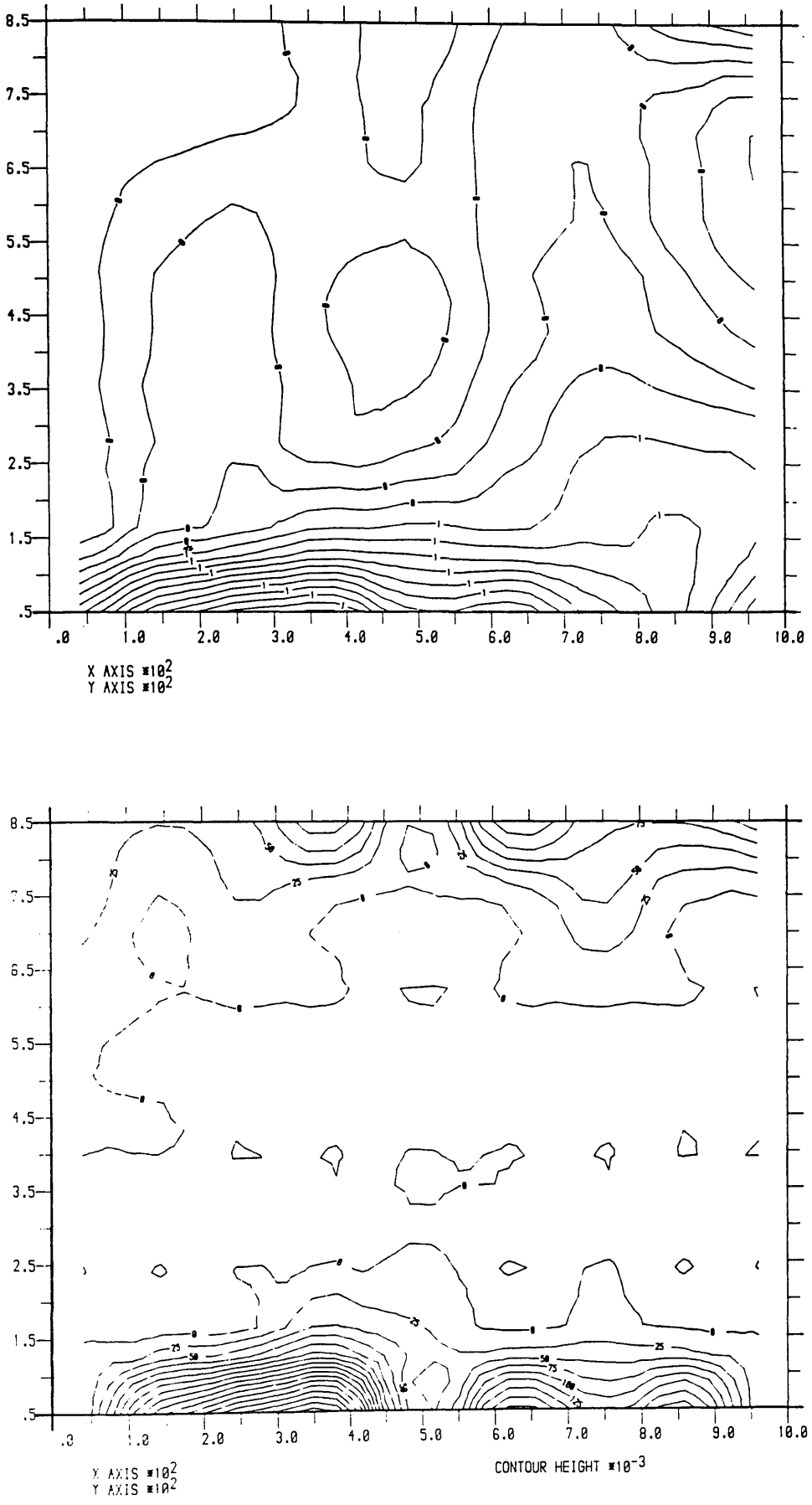

Figure(5.26) Contours of steel ratios for girder TRGRAS7

Main Steel Envelops

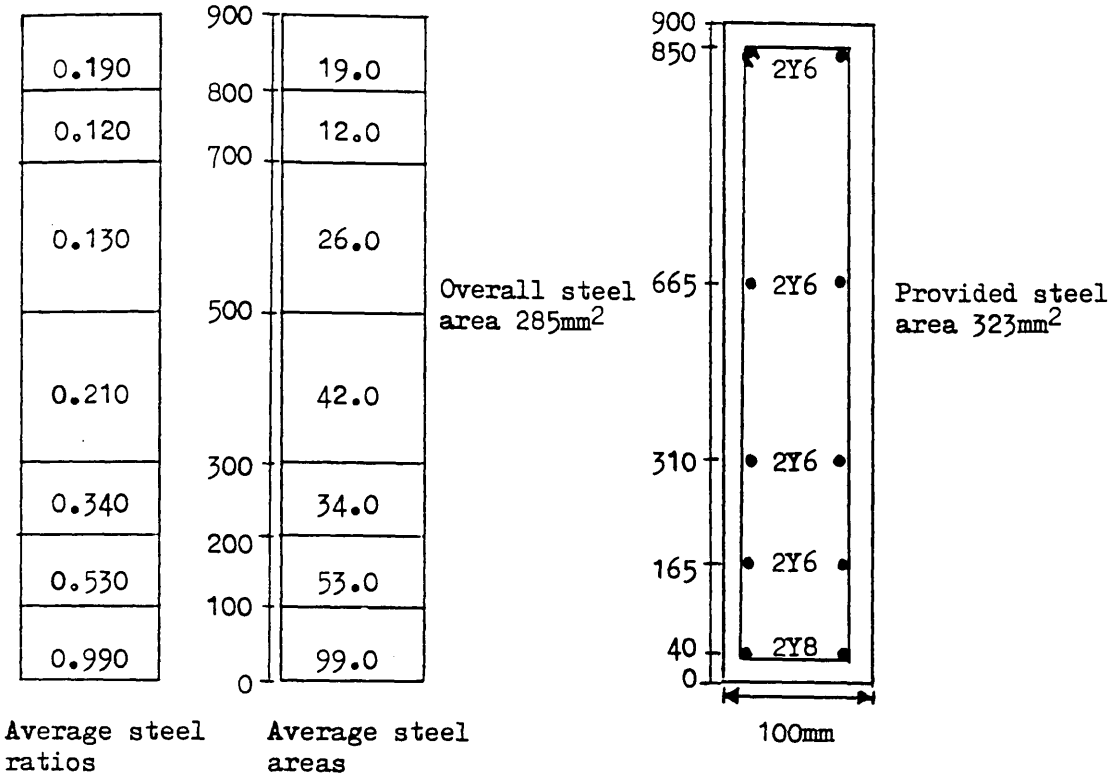

Shear Reinforcement Envelops

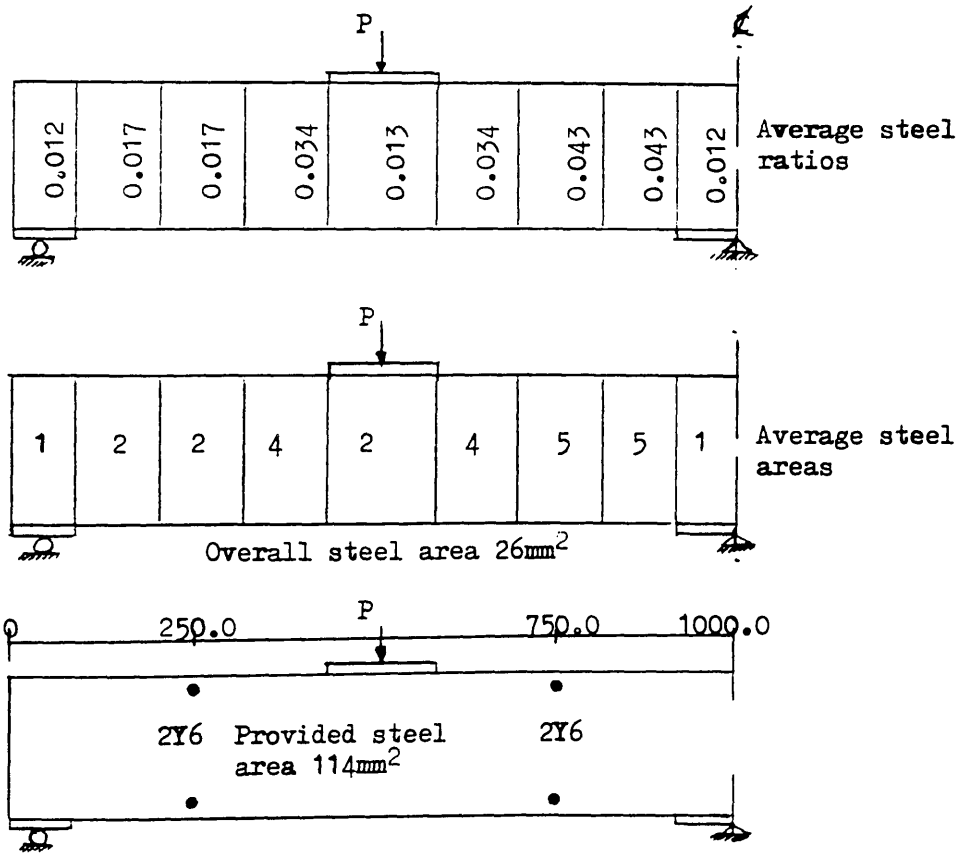

Fig. (5.27) Design of reinforcement of Transfer Girder TRGRAS7

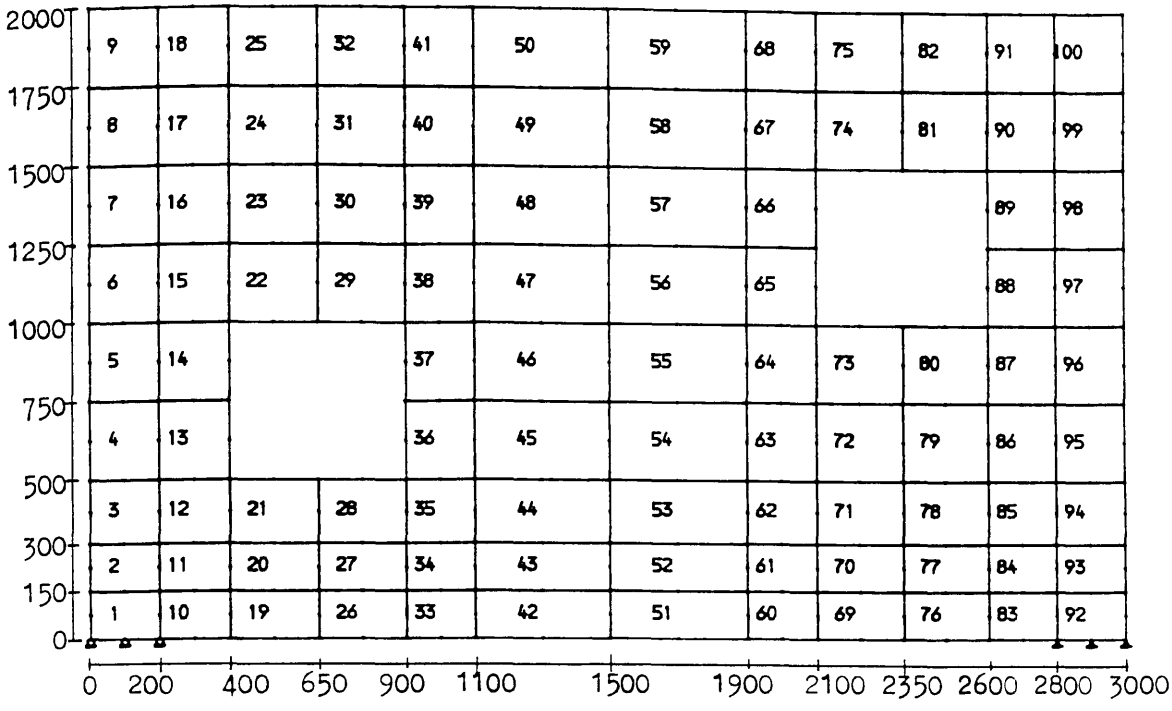

Figure(5.28) Finite element mesh of transfer girder TRGRAS9

0.01 0.02	0.01 0.04	0.00 0.11	0.01 0.13	0.00 0.00	0.00 0.05	0.02 0.05	0.01 0.00	0.08 0.32	0.23 0.35	0.29 0.02	0.22 0.24
0.03 0.00	0.20 0.04	0.31 0.31	0.22 0.16	0.00 0.00	0.00 0.00	0.03 0.00	0.47 0.00	1.11 0.60	0.36 0.40	0.02 0.00	0.09 0.46
0.05 0.00	0.35 0.00	0.83 0.28	0.59 0.39	0.10 0.02	0.01 0.00	0.08 0.00	0.50 0.03			0.21 0.02	0.31 0.32
0.02 0.00	0.10 0.00	0.67 0.28	1.34 0.78	0.74 0.16	0.18 0.00	0.00 0.00	0.02 0.00			1.01 0.39	0.44 0.04
0.12 0.00	0.14 0.00			0.95 0.56	0.47 0.14	0.00 0.00	0.02 0.00	0.38 0.31	1.08 0.94	0.52 0.14	0.11 0.00
0.35 0.00	1.03 0.30			0.18 0.09	0.33 0.33	0.20 0.02	0.45 0.02	0.84 0.45	0.63 0.63	0.13 0.03	0.00 0.00
0.23 0.00	0.84 0.12	1.53 1.07	0.55 0.31	0.15 0.00	0.44 0.14	0.72 0.03	0.95 0.10	0.96 0.41	0.75 0.36	0.32 0.00	0.07 0.00
0.29 0.00	0.47 0.11	0.95 0.83	1.41 0.46	1.15 0.01	1.19 0.05	1.31 0.03	1.34 0.12	1.19 0.27	0.91 0.27	0.77 0.04	0.32 0.00
0.21 0.00	0.46 0.16	0.90 0.29	1.85 0.25	2.14 0.03	2.06 0.05	1.91 0.02	1.82 0.05	1.60 0.09	1.30 0.19	1.04 0.16	0.61 0.09

Figure(5.29) Theoretical required steel ratios for girder TRGRAS9

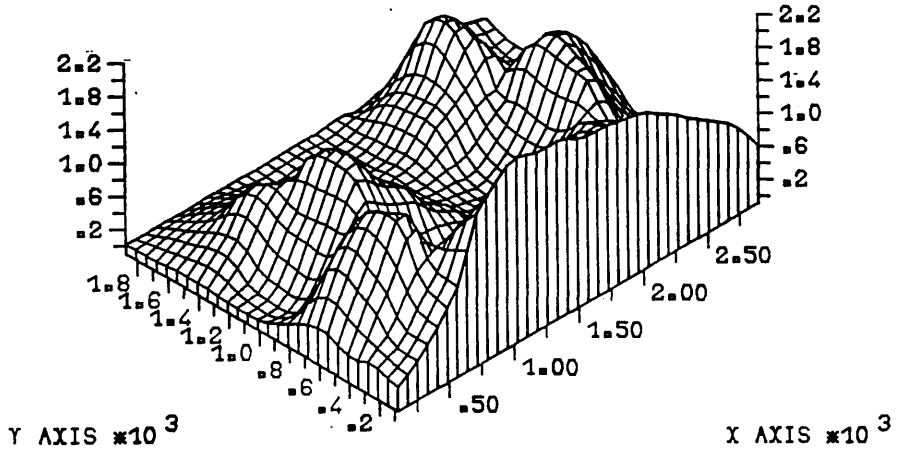

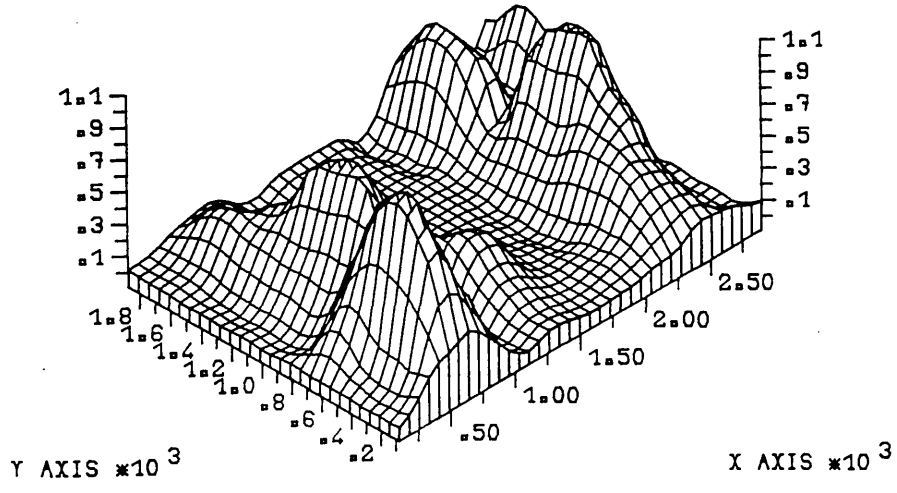

Figure(5.30) Isometric view of steel ratios for girder TRGRAS9

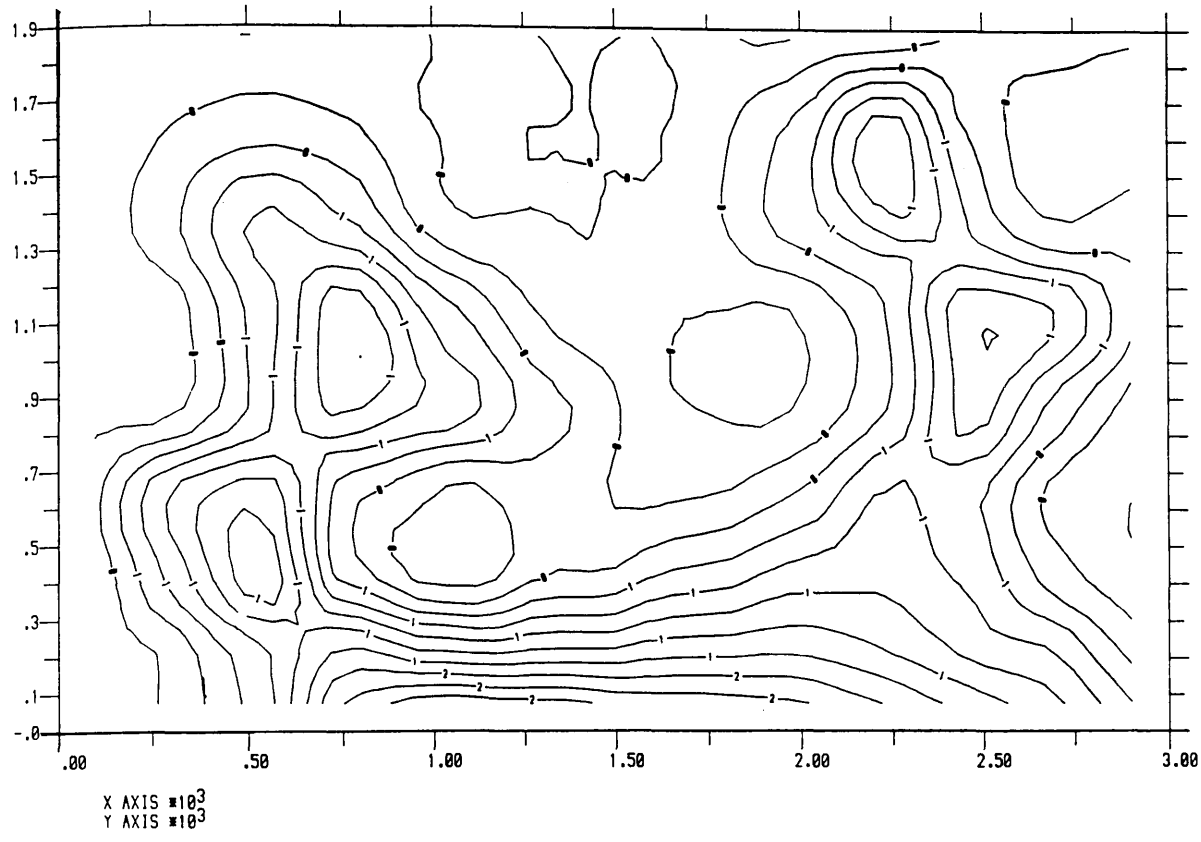

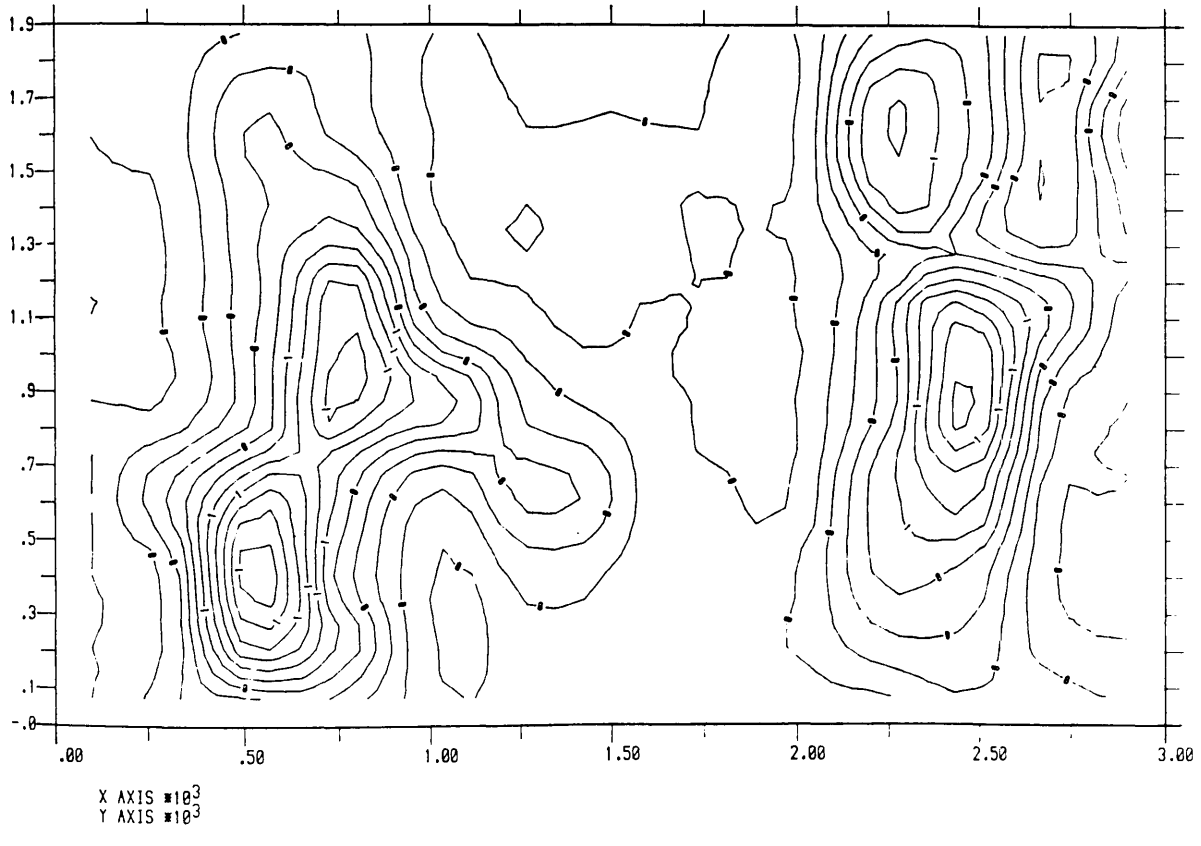

Figure(5.31) Contours of steel ratios for girder TRGRAS9

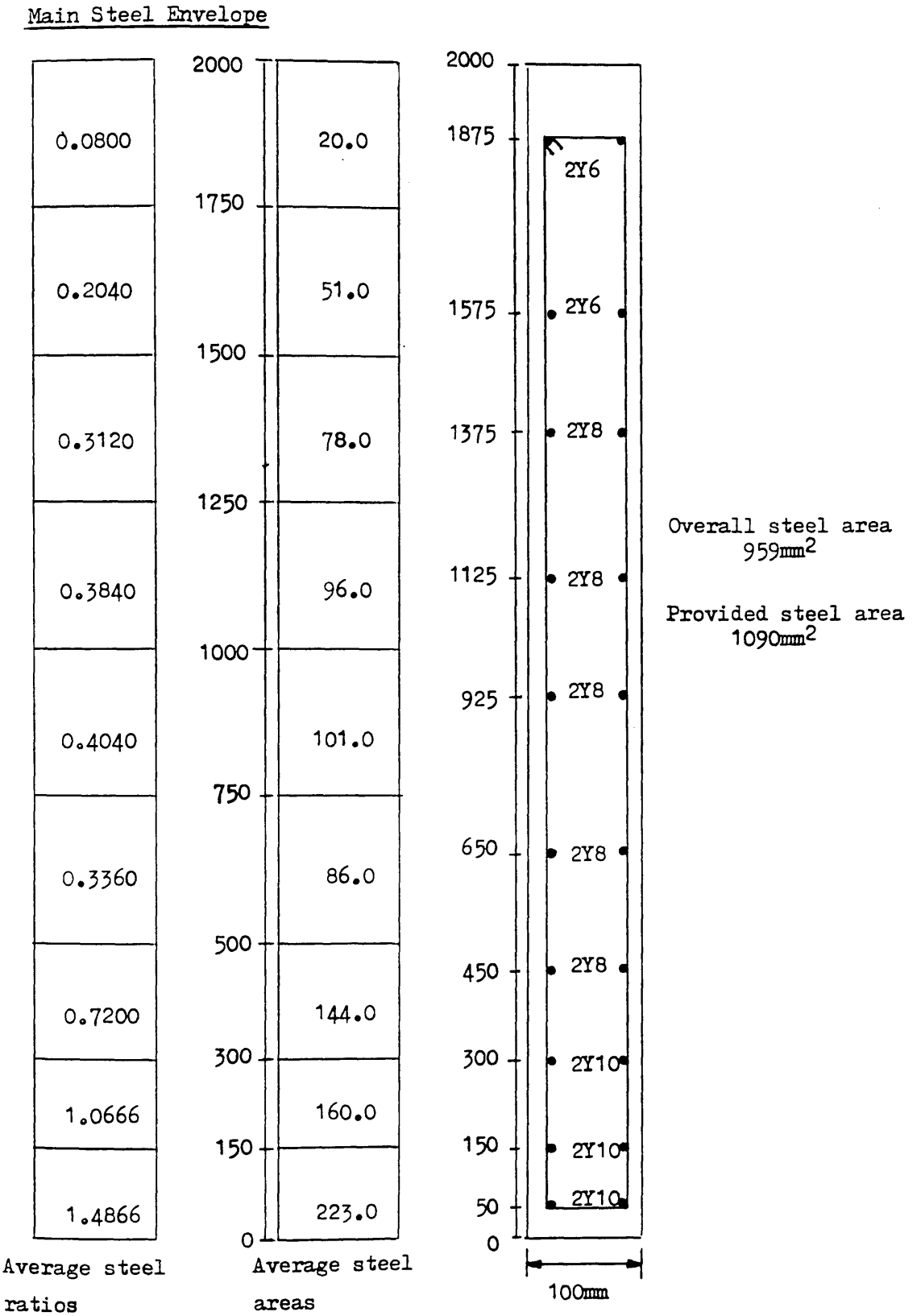

(a) Main steel envelops

Fig. (5.32) Design of reinforcement of Transfer Girder TRGRAS9

Shear Reinforcement Envelops

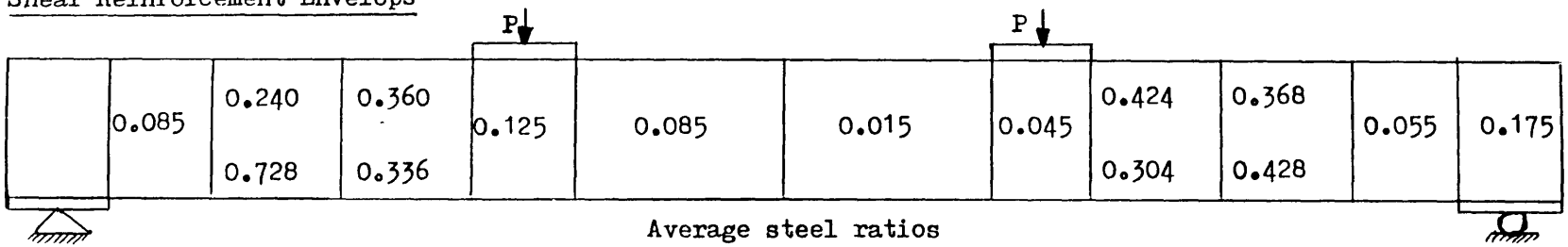

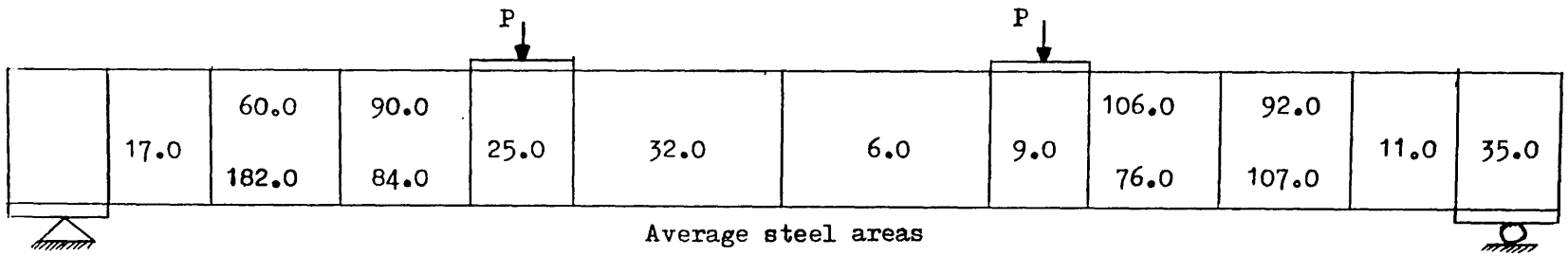

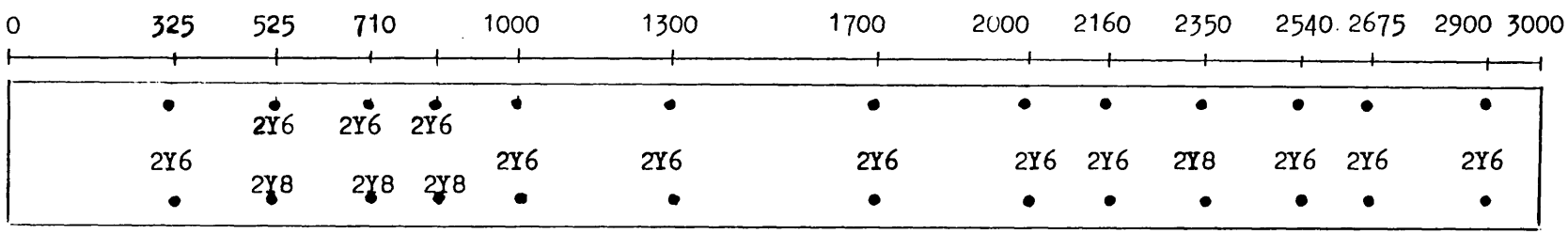

Overall steel area 534mm^2 Provided steel area 845mm^2

(b) Shear reinforcement envelops

Fig. (5.32) Continued

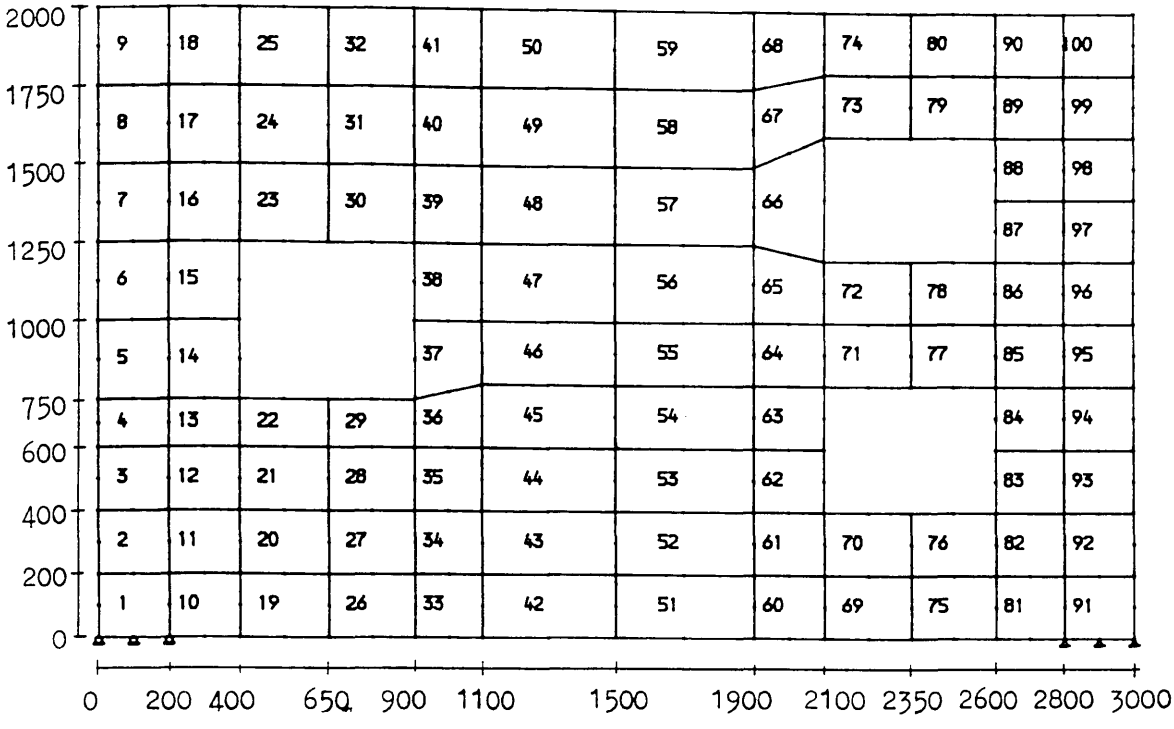

Figure(5.33) Finite element mesh of transfer girder TRGRAS10

0.03 0.04	0.05 0.03	0.03 0.19	0.02 0.17	0.00 0.00	0.00 0.05	0.03 0.05	0.08 0.00	0.04 0.42	0.36 0.44	0.51 0.07	0.33 0.32
0.04 0.09	0.18 0.01	0.54 0.39	0.36 0.35	0.02 0.00	0.00 0.00	0.02 0.00	0.62 0.00	1.23 0.80	0.22 0.44	0.02 0.01	0.09 0.53
0.04 0.19	0.06 0.00	0.60 0.32	1.25 0.61	0.59 0.00	0.11 0.00	0.00 0.00	0.21 0.00			0.24 0.06	0.30 0.46
										1.34 0.44	0.55 0.09
0.22 0.06	0.17 0.00			0.72 0.16	0.25 0.00	0.00 0.00	0.00 0.00	0.56 0.59	1.91 1.18	0.90 0.04	0.21 0.00
0.40 0.00	1.01 0.32			0.09 0.00	0.05 0.00	0.19 0.00	0.97 0.10	2.01 1.23	0.57 0.59	0.01 0.00	0.01 0.00
0.18 0.00	0.80 0.18	1.40 0.98	0.20 0.29	0.00 0.00	0.00 0.00	0.51 0.13	1.41 0.66			0.15 0.00	0.07 0.00
0.05 0.00	0.26 0.05	0.81 0.91	0.90 0.50	0.36 0.00	0.25 0.03	0.43 0.32	0.25 0.16			1.22 0.37	0.35 0.00
0.19 0.00	0.45 0.03	0.81 0.58	1.20 0.48	1.15 0.06	0.97 0.04	0.76 0.17	0.36 0.00	0.78 0.34	1.82 1.14	1.07 0.16	0.34 0.00
0.33 0.00	0.75 0.09	1.10 0.28	1.61 0.20	1.88 0.07	1.89 0.01	2.01 0.11	2.15 0.04	2.01 0.37	0.94 0.57	0.30 0.10	0.51 0.03

Figure(5.34) Theoretical required steel ratios for girder TRGRAS10

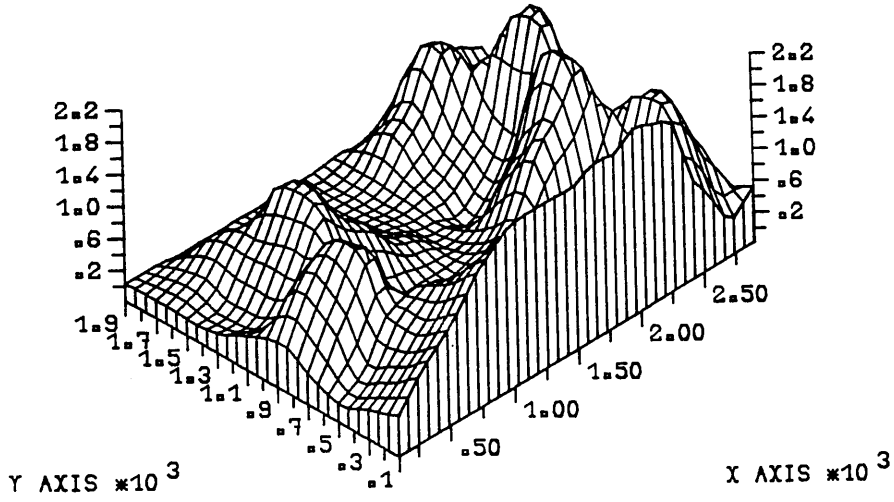

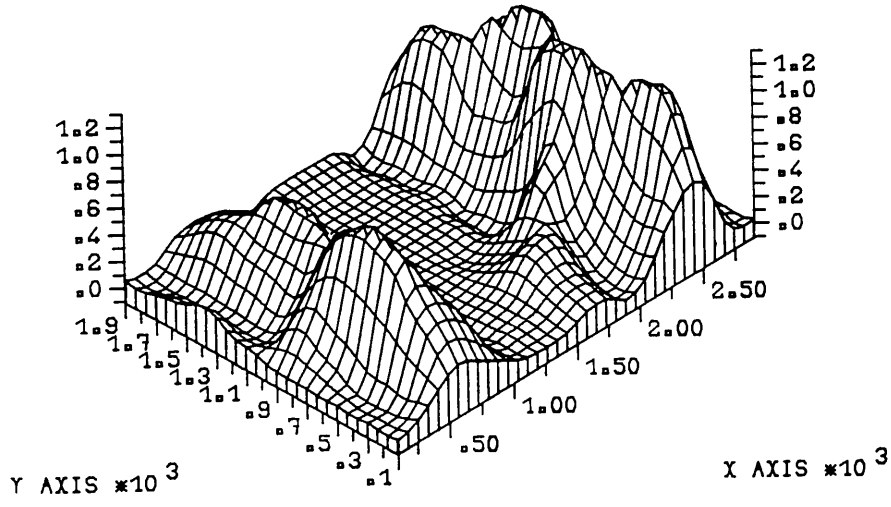

Figure(5.35) Isometric view of steel ratios for girder TRGRAS10

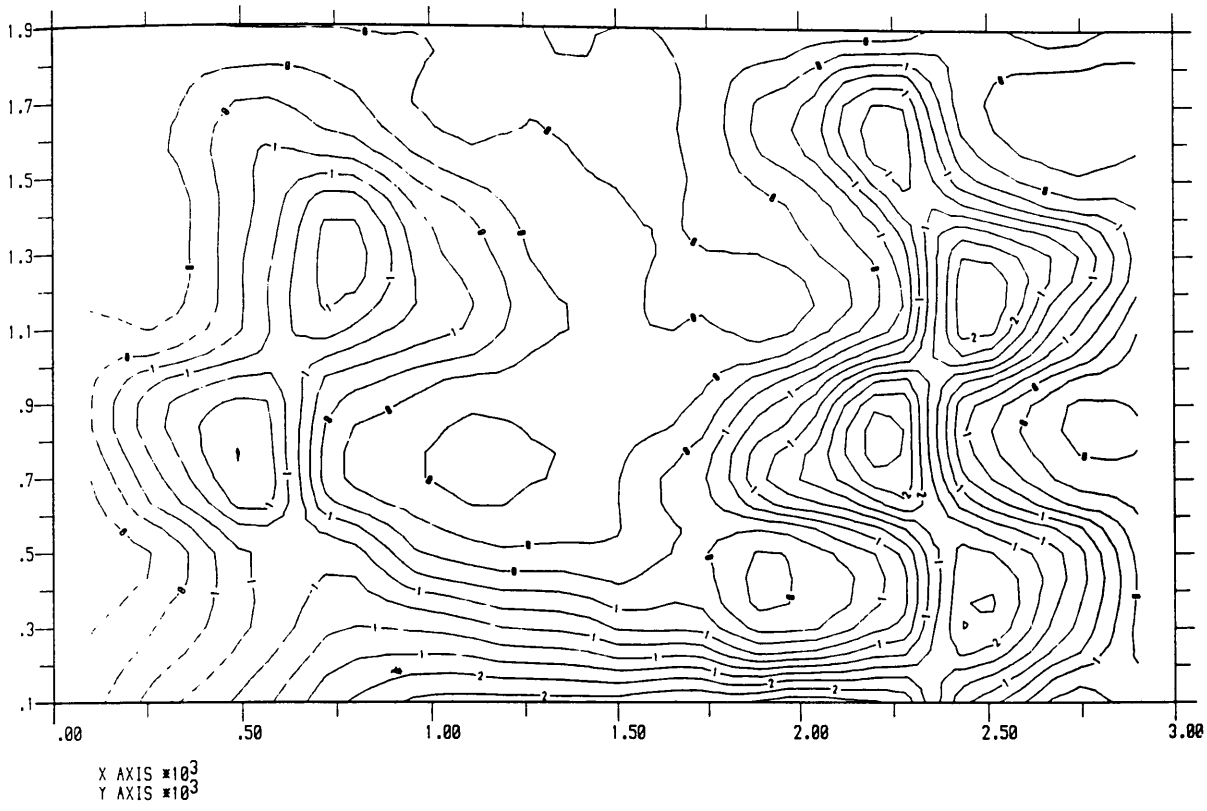

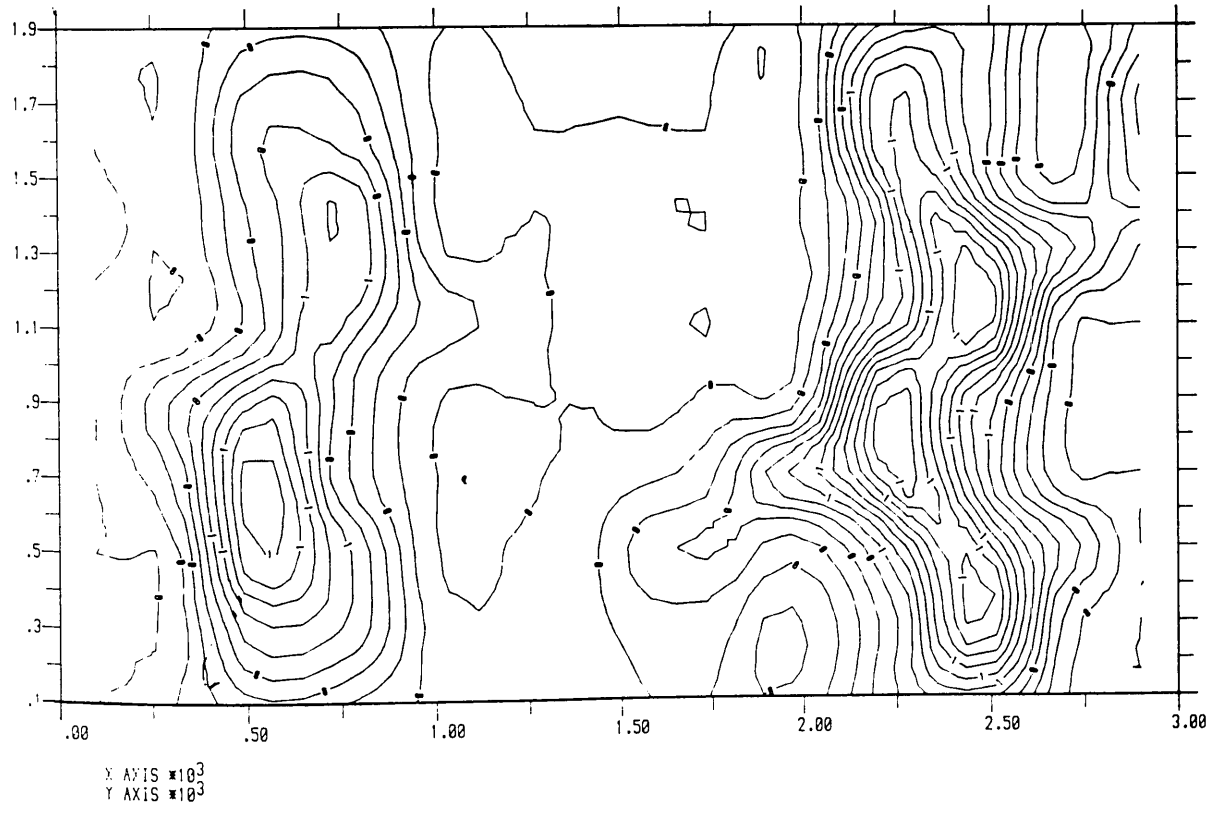

Figure(5.36) Contours of steel ratios for girder TRGRAS10

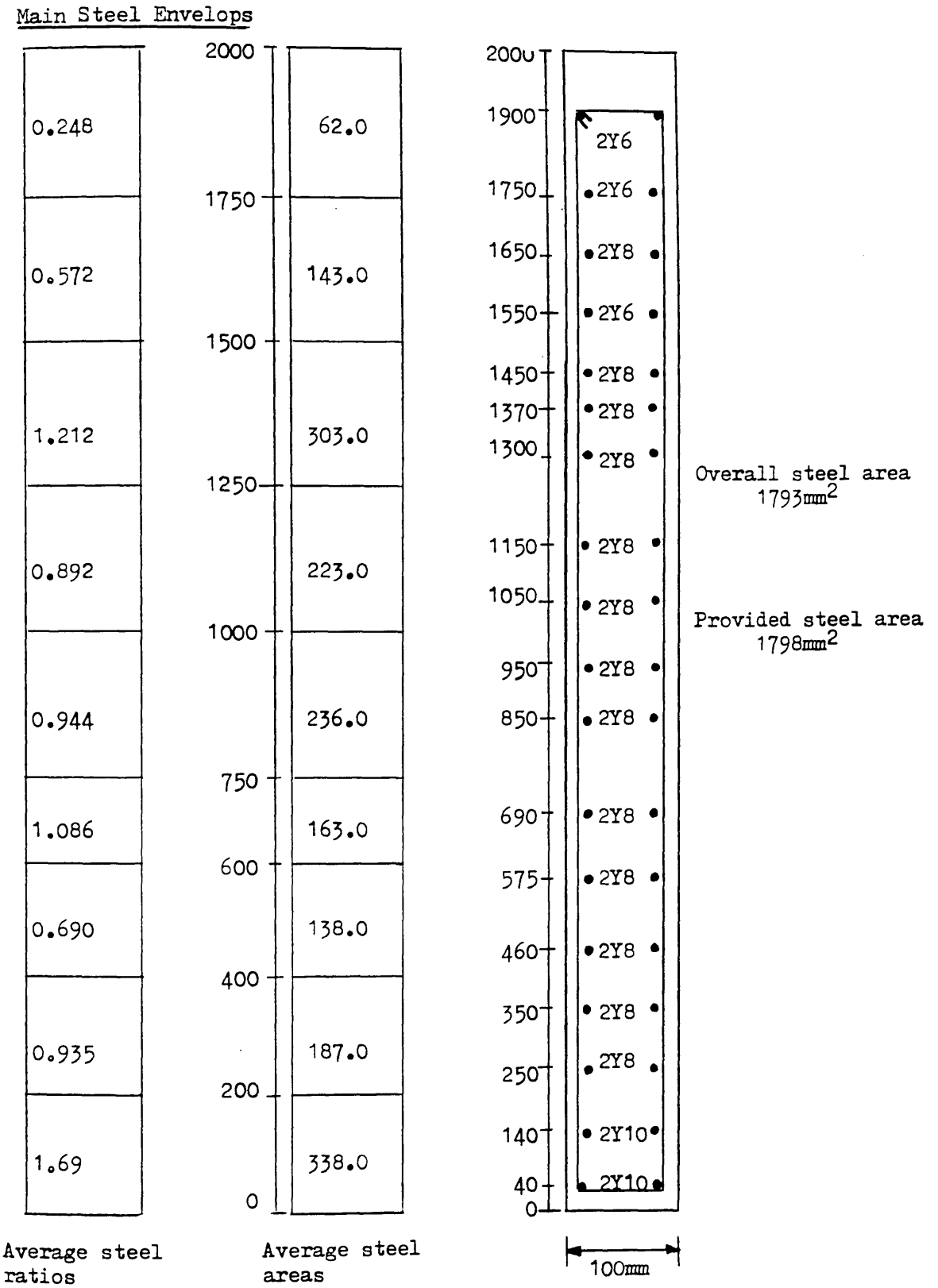

(a) Main steel envelops

Fig. (5.37) Design of reinforcement of Transfer Girder TRGRAS10

Shear Reinforcement Envelops

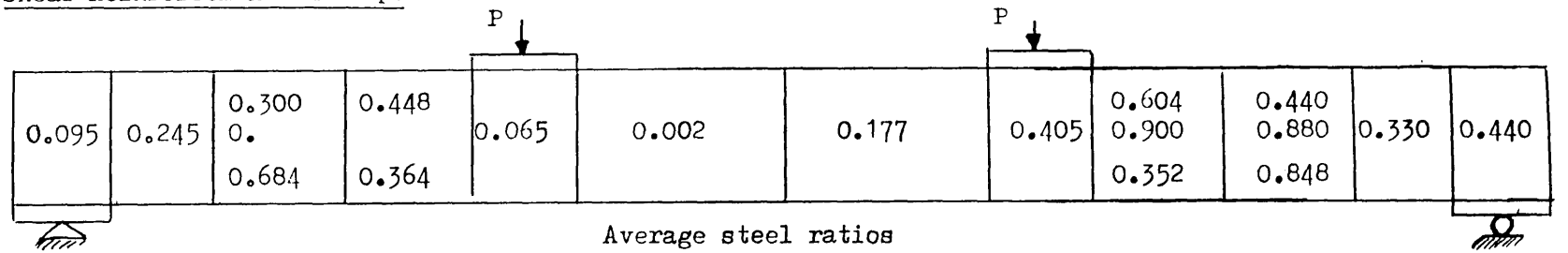

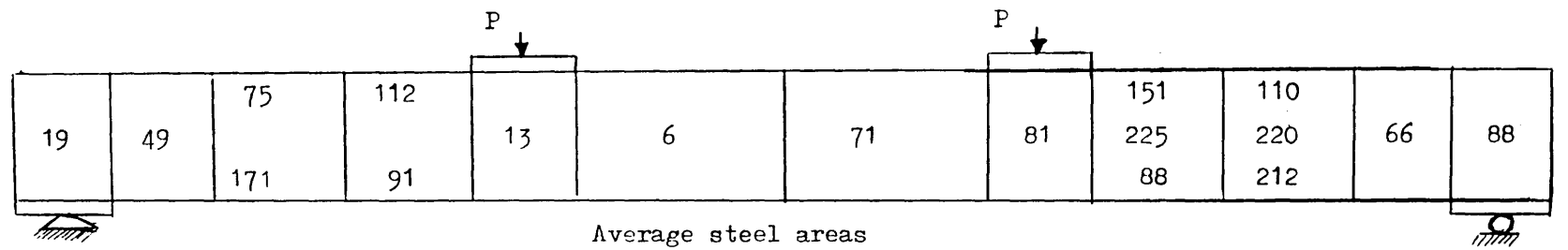

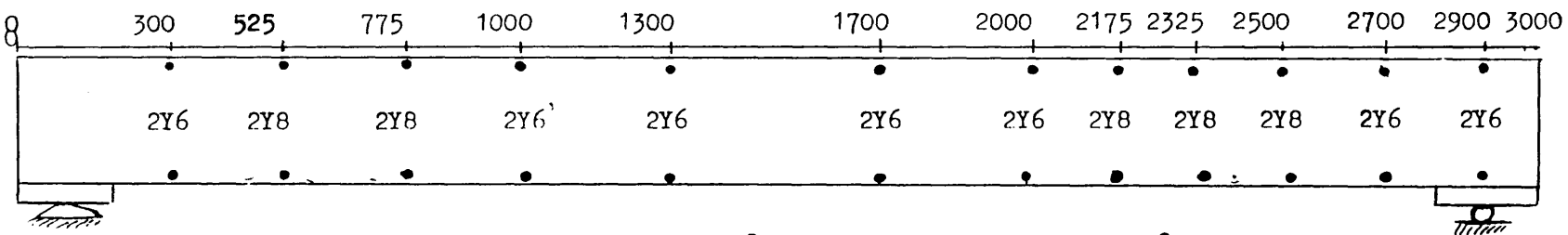

Overall steel area 841mm^2 Provided steel area 904mm^2

(b) Shear reinforcement envelops

Fig. (5.37) Continued

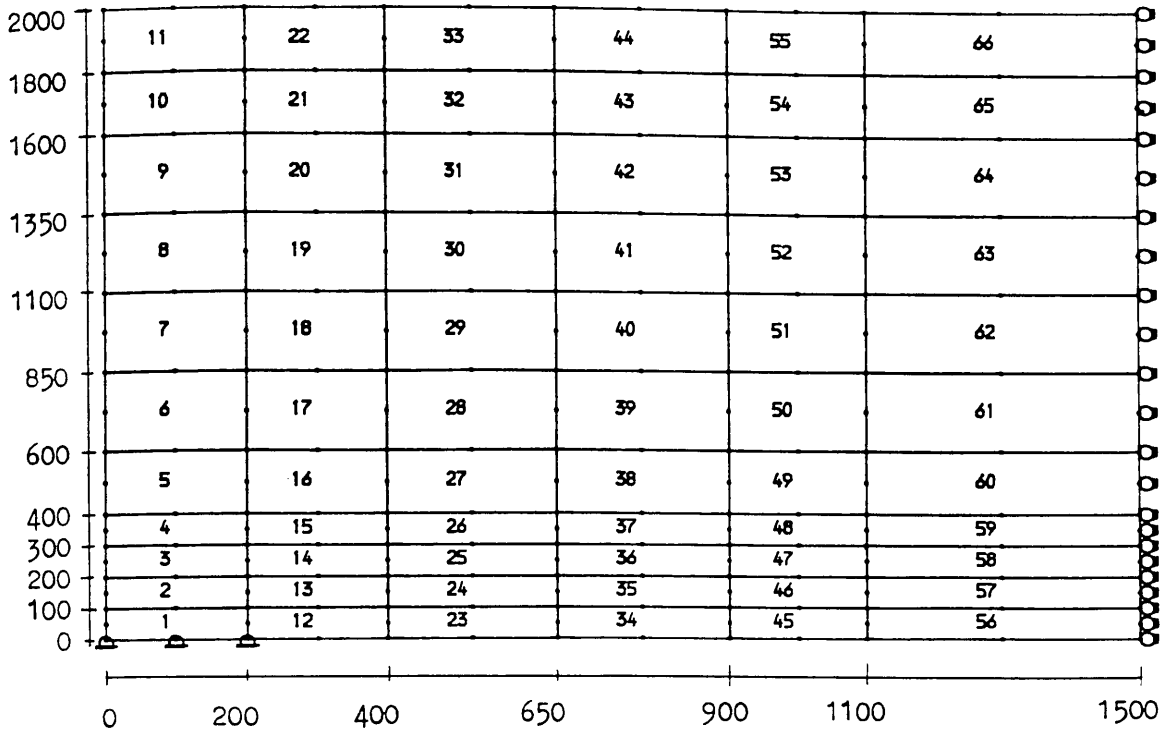

Figure(5.38) Finite element mesh of transfer girder TRGRAS11

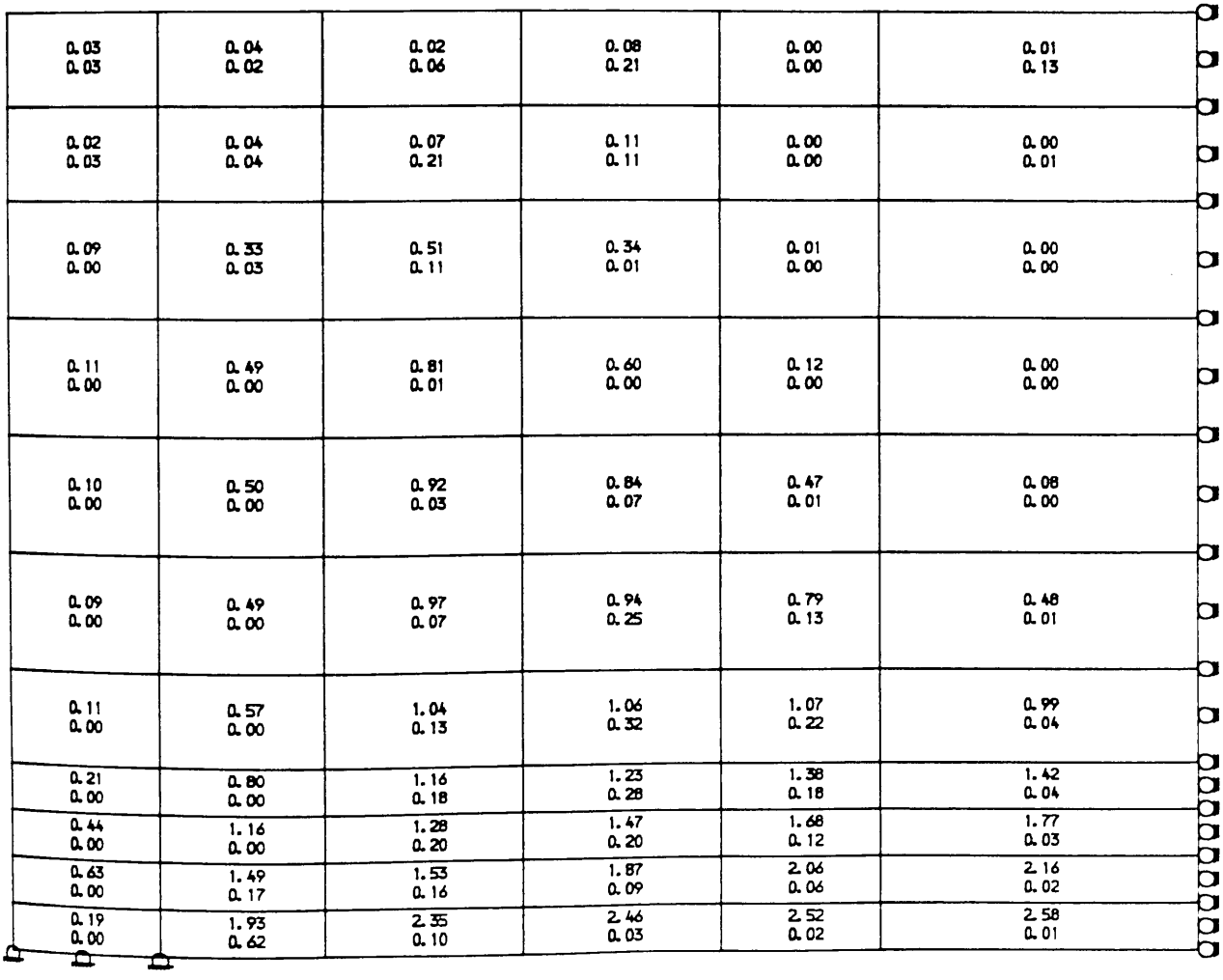

Figure(5.39) Theoretical required steel ratios for girder TRGRAS11

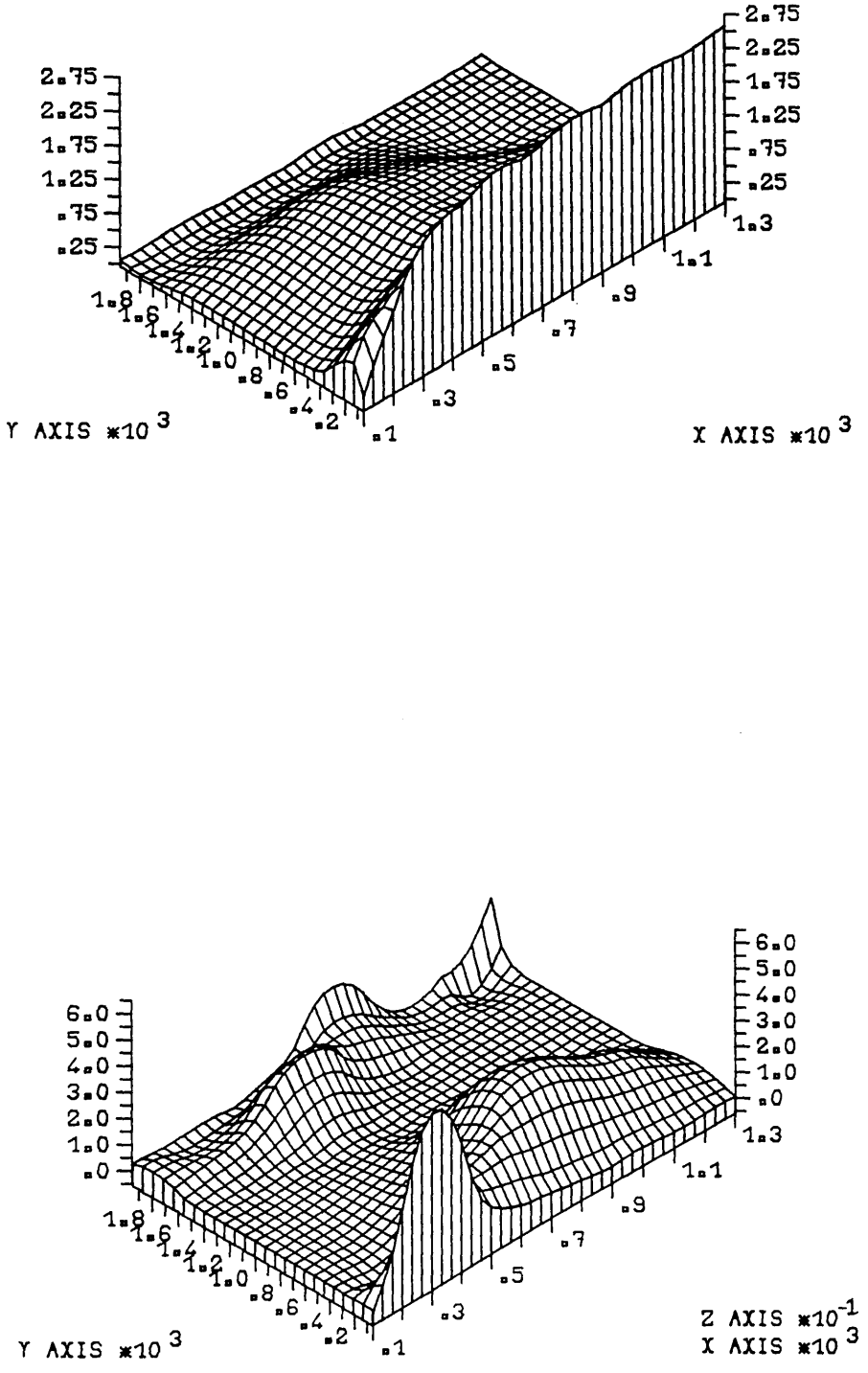

Figure(5.40) Isometric view of steel ratios for girder TRGRAS11

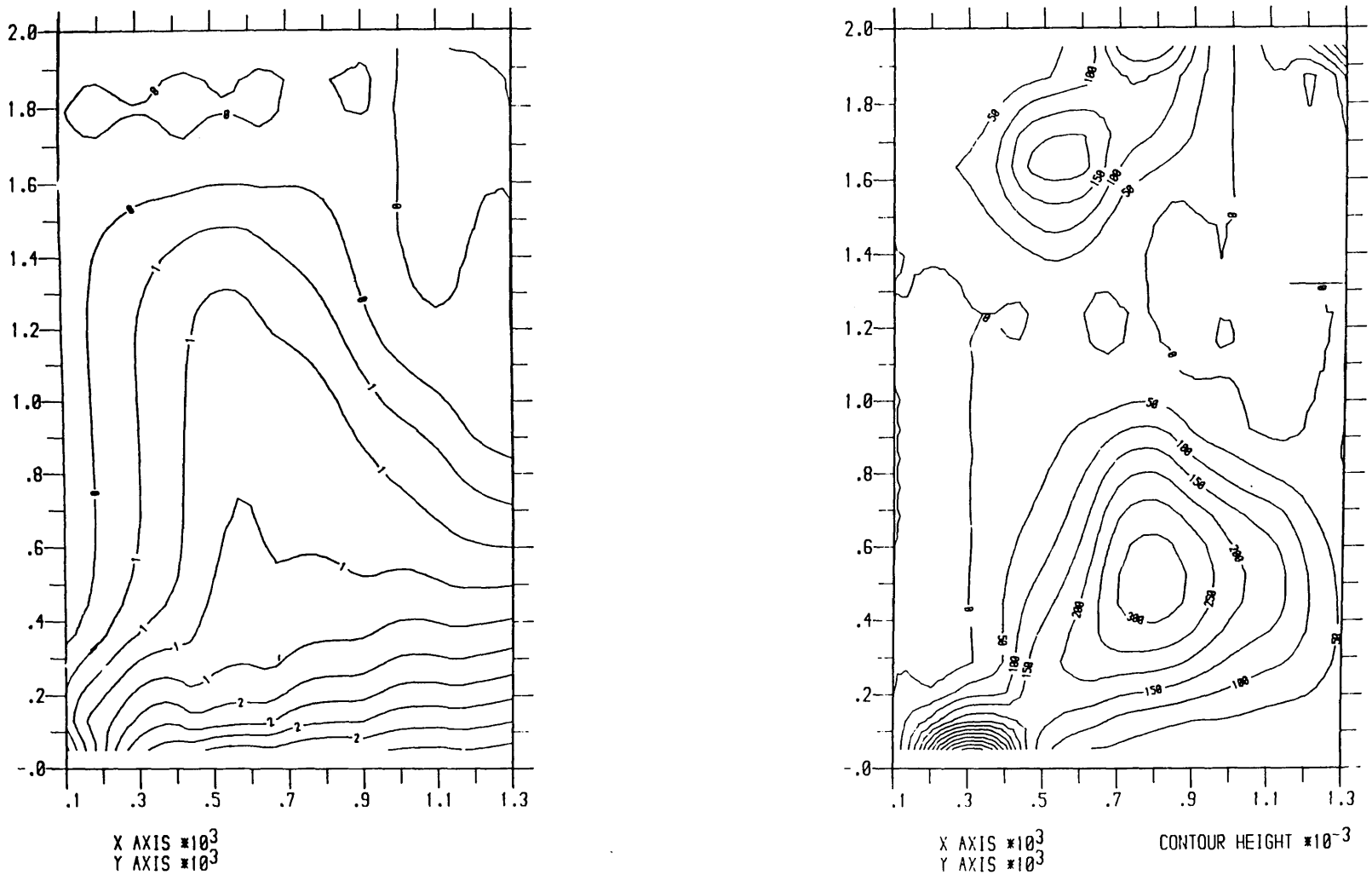

Figure(5.41) Contours of steel ratios for girder TRGRAS11

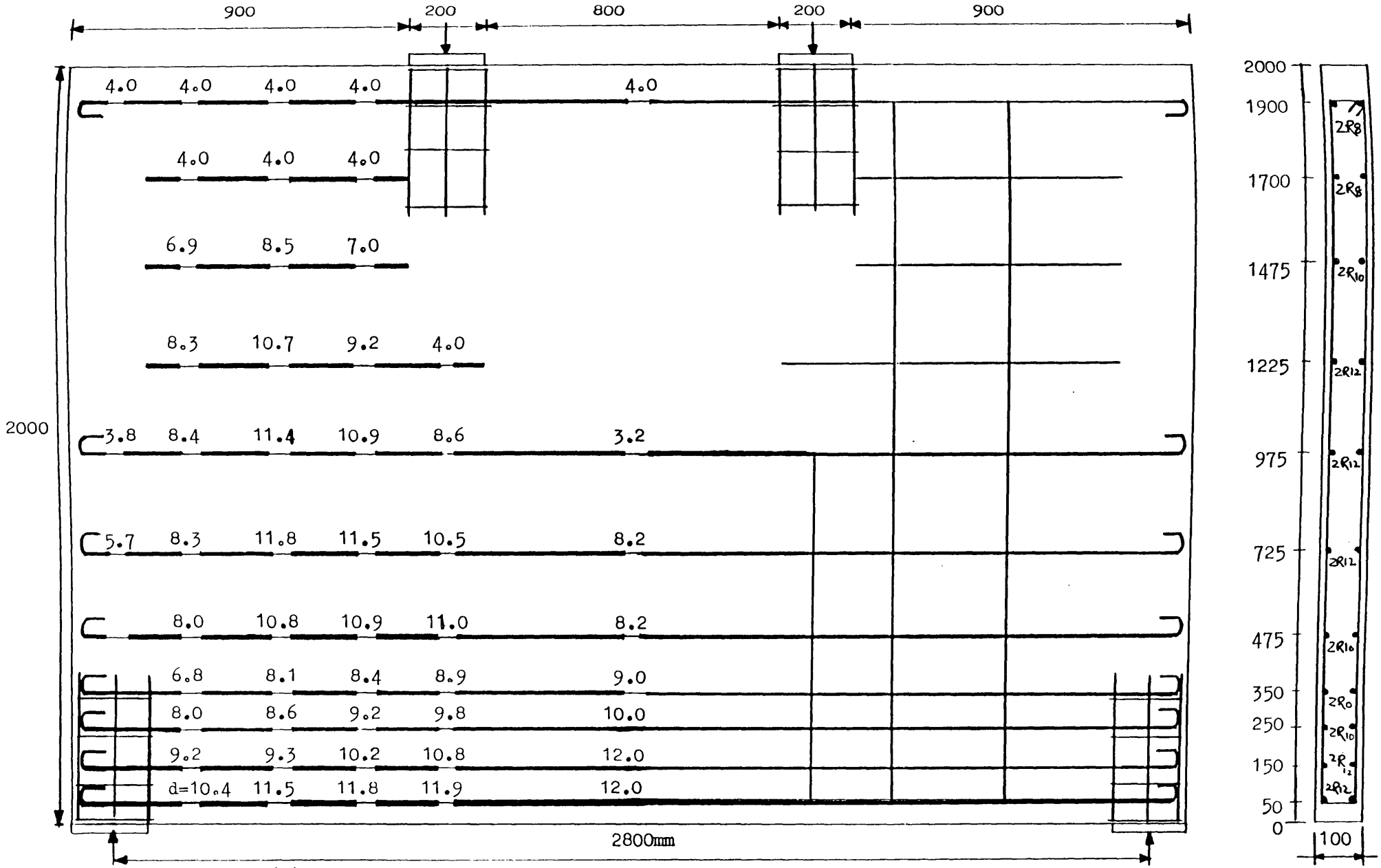

(a) Main reinforcement

Fig.(5.42) Design of reinforcement of Transfer girder TRGRAS11

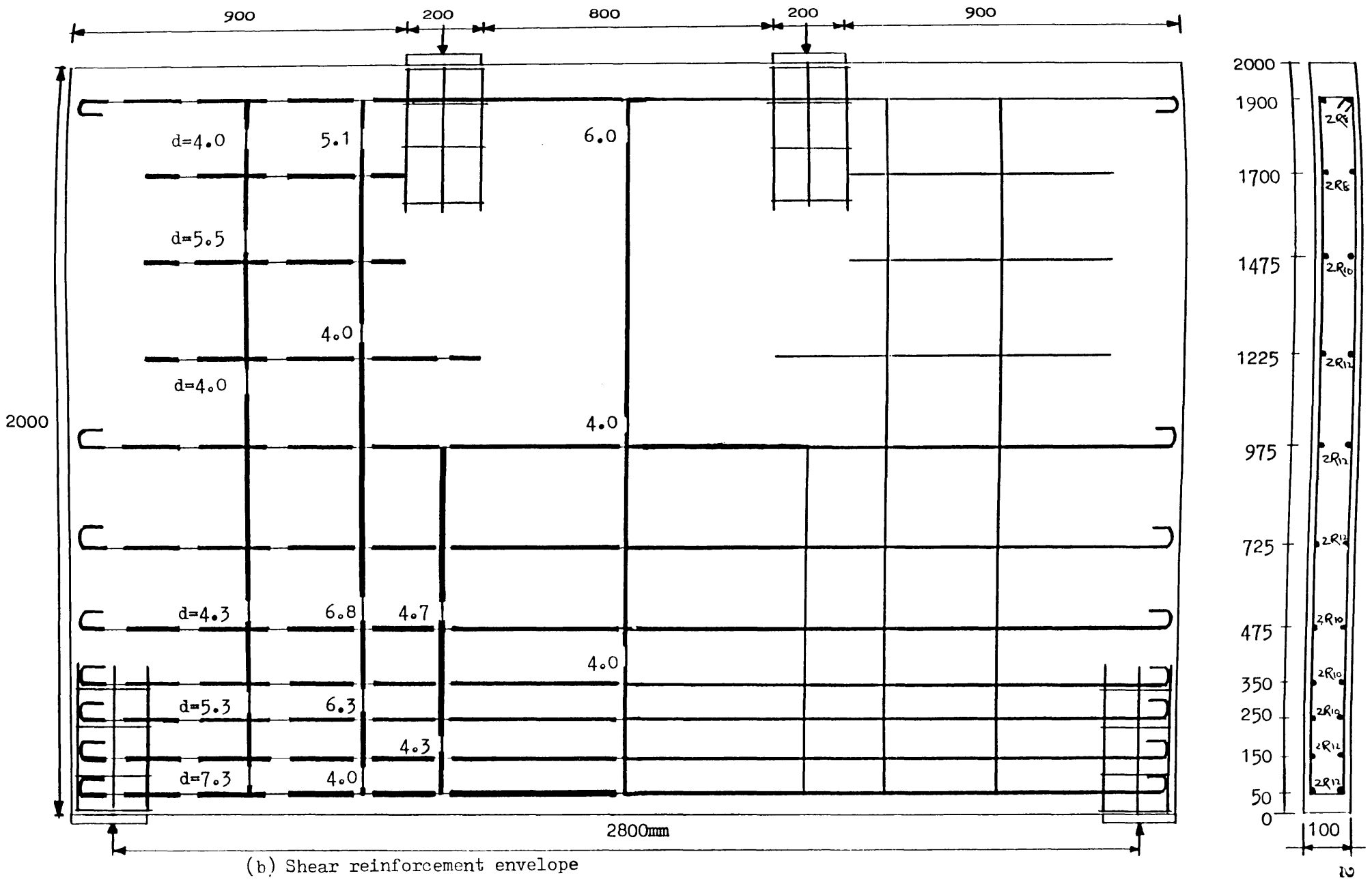

(b) Shear reinforcement envelope

Fig.(5.42) Continued

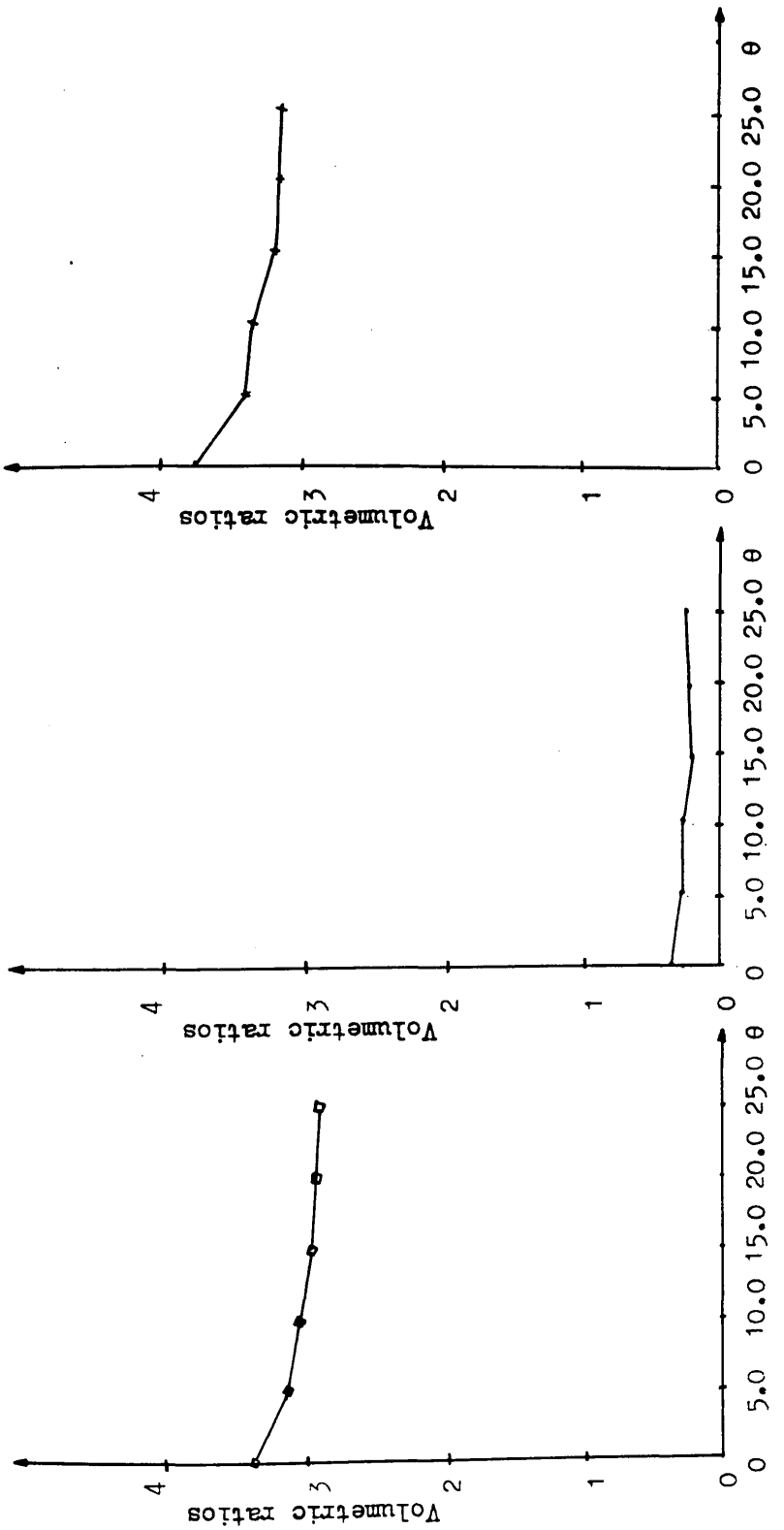

Figure(5.43) The behaviour of various skew angles w.r.t volumetric steel ratios

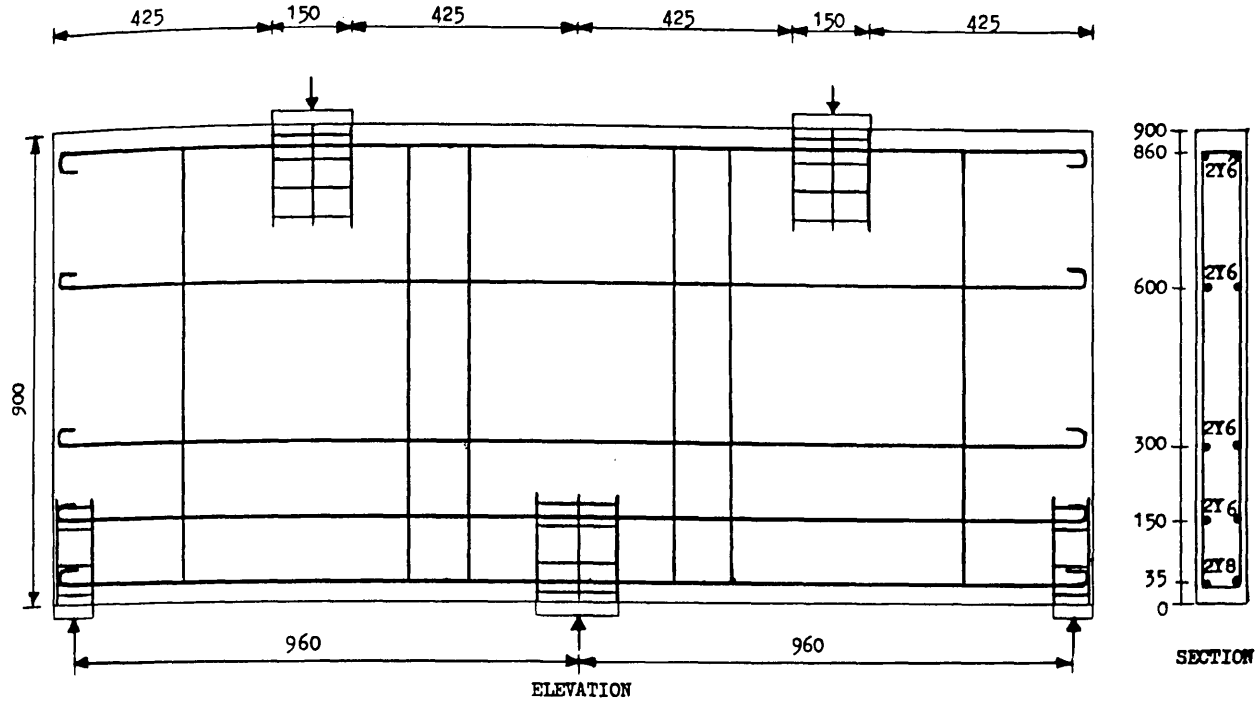

Figure(5.44) Dimensions and reinforcing details of girder TRGRAS1

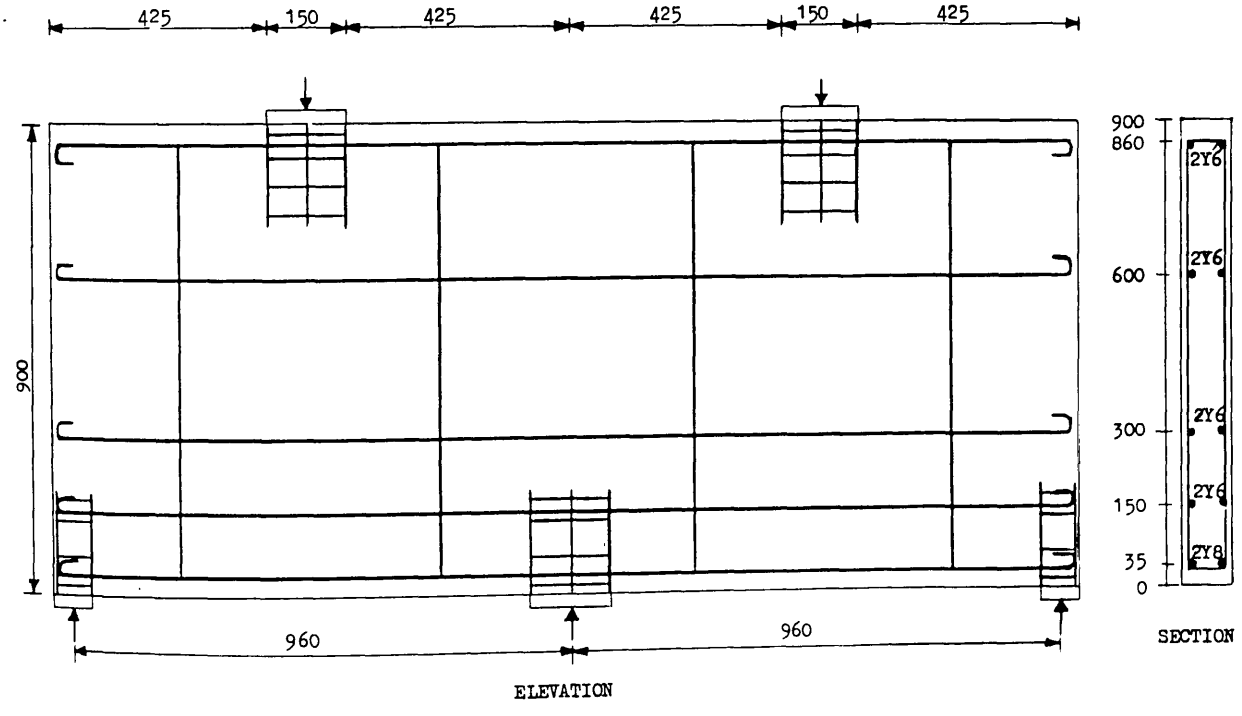

Figure(5.45) Dimensions and reinforcing details of girder TRGRAS2

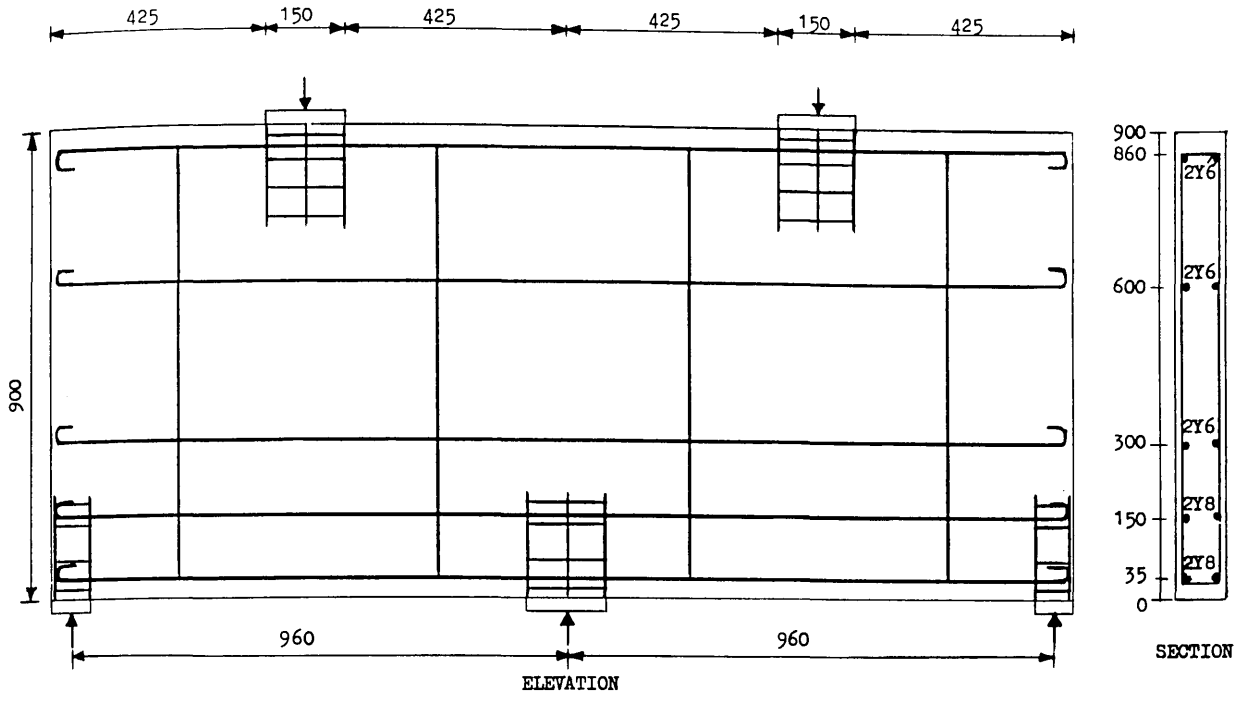

Figure(5.46) Dimensions and reinforcing details of girder TRGRAS3

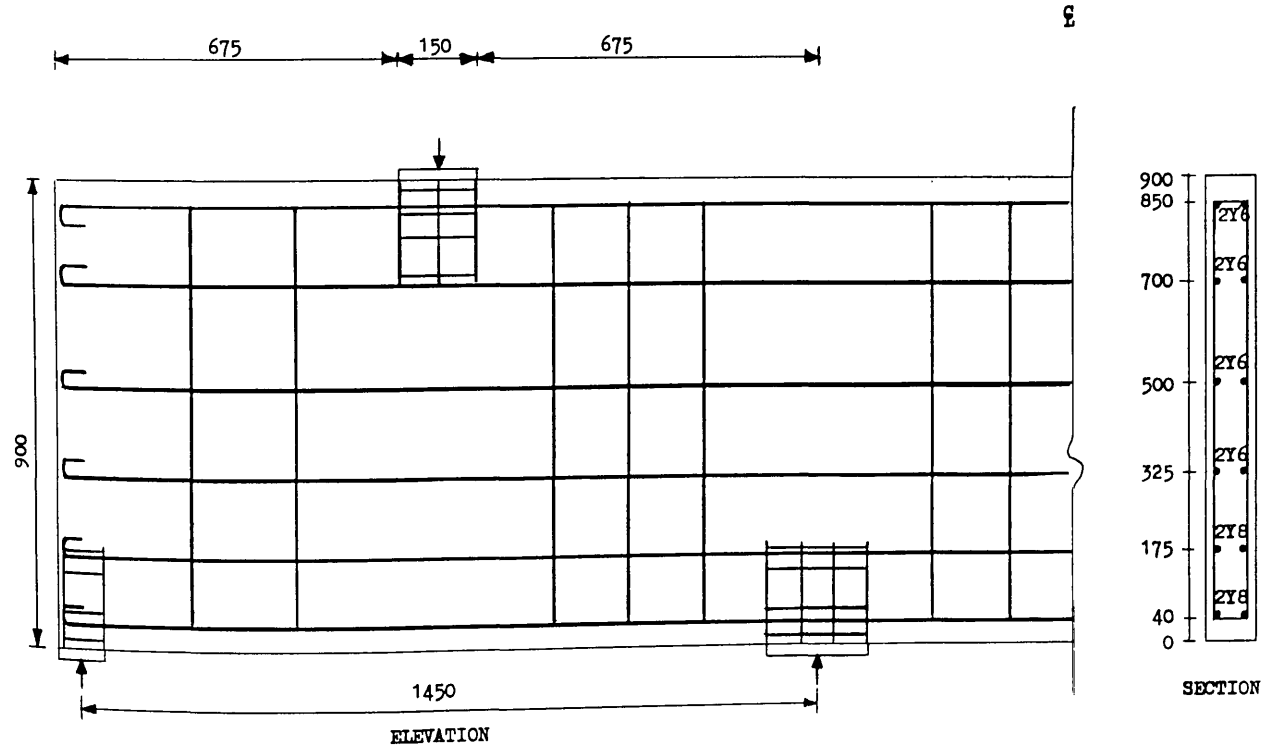

Figure(5.47) Dimensions and reinforcing details of girder TRGRAS4

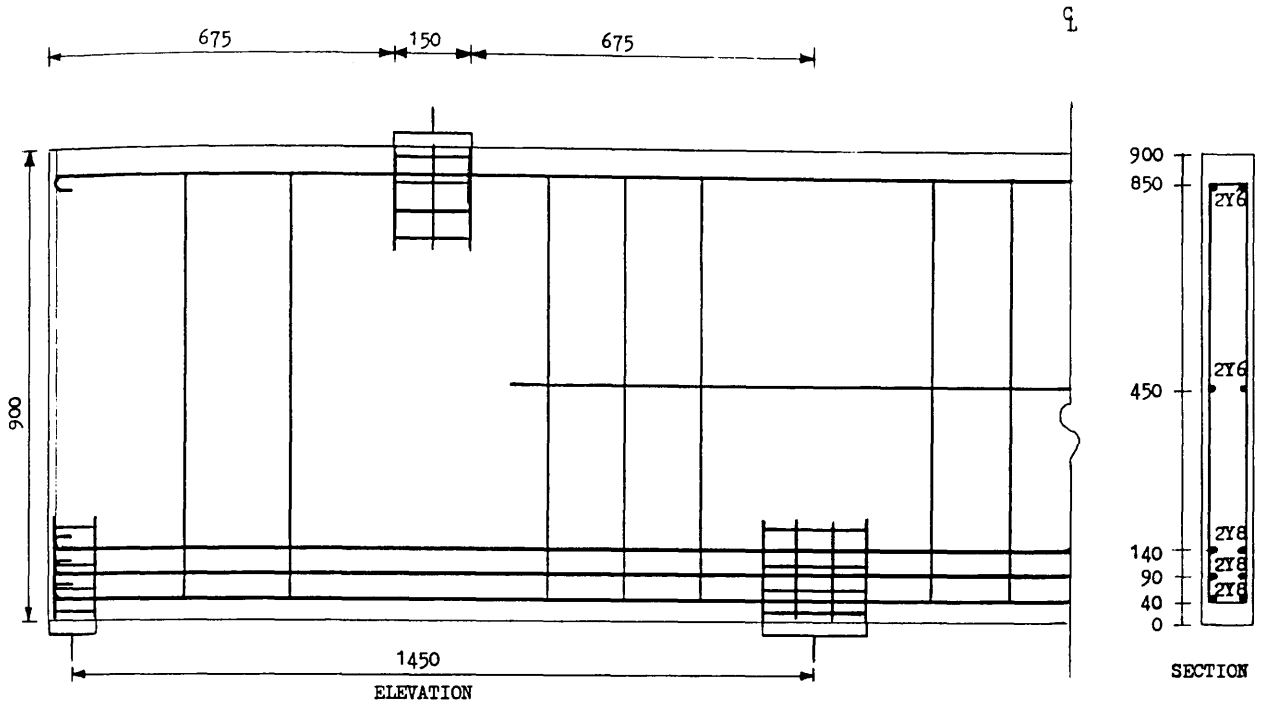

Figure(5.48) Dimensions and reinforcing details of girder TRGRAS5

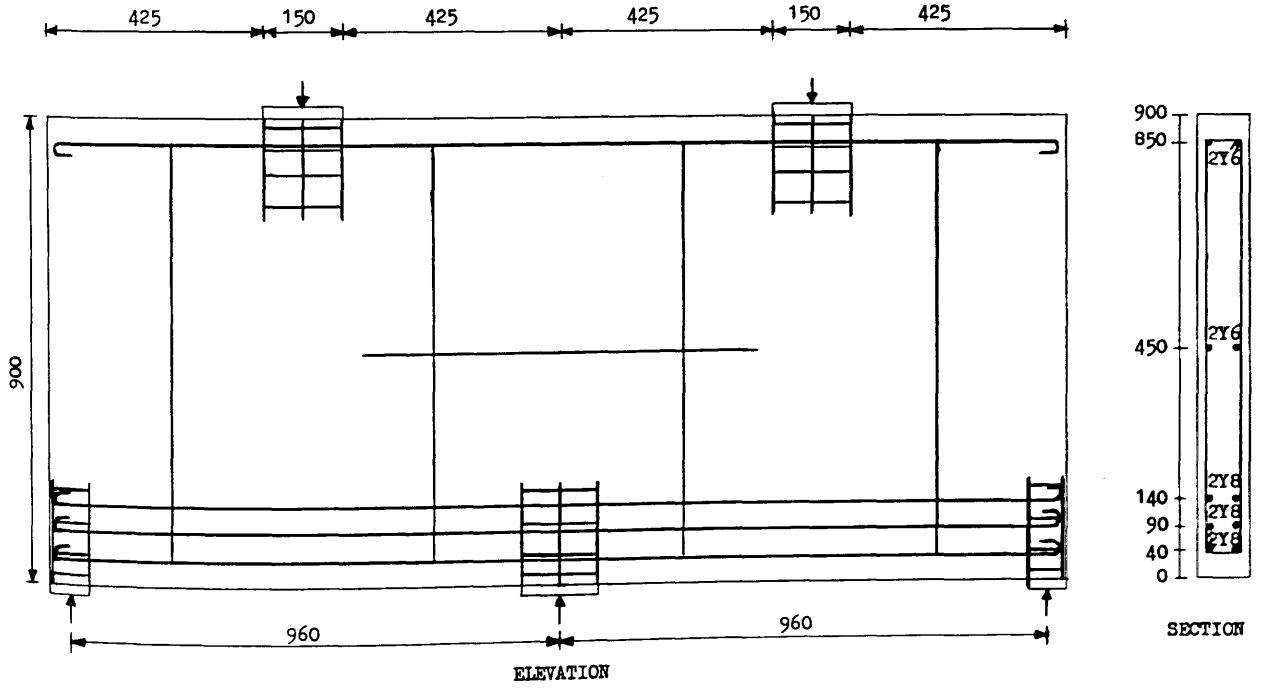

Figure(5.49) Dimensions and reinforcing details of girder TRGRAS6

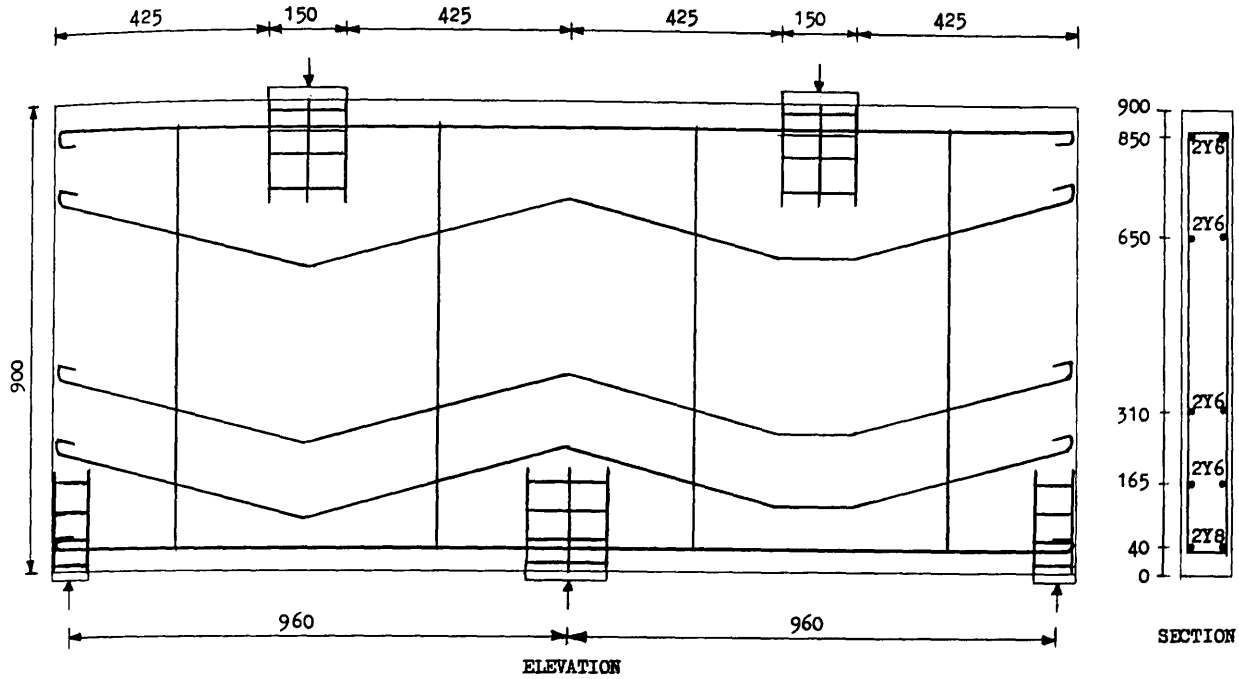

Figure(5.50) Dimensions and reinforcing details of girder TRGRAS7

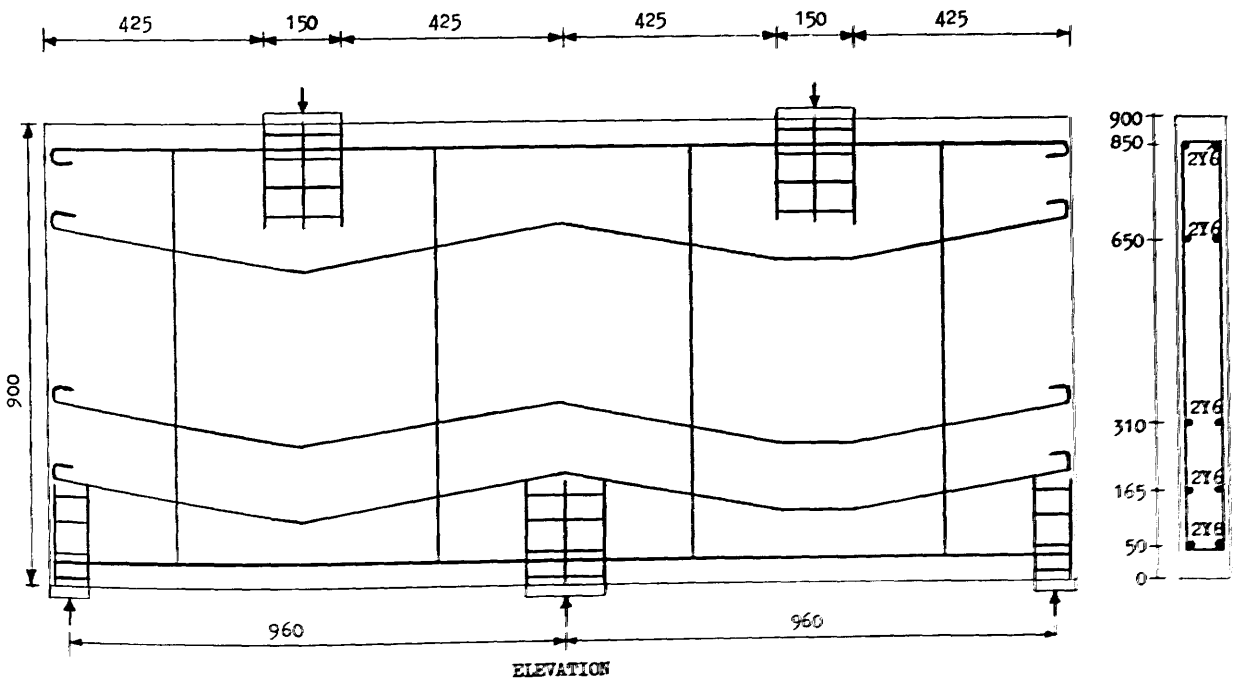

Figure(5.51) Dimensions and reinforcing details of girder TRGRAS8

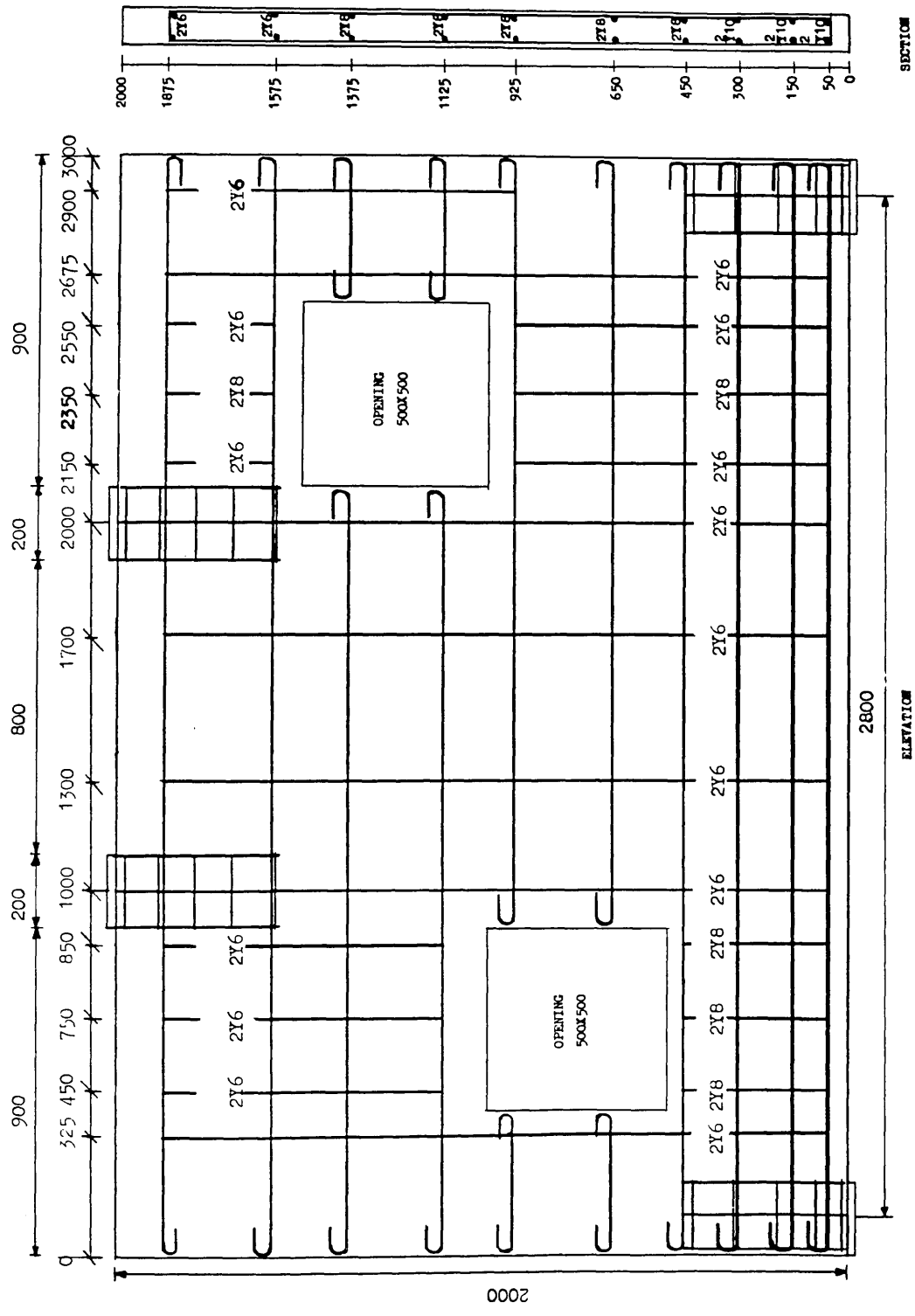

Figure(5.52) Dimensions and reinforcing details of girder TRGRAS9

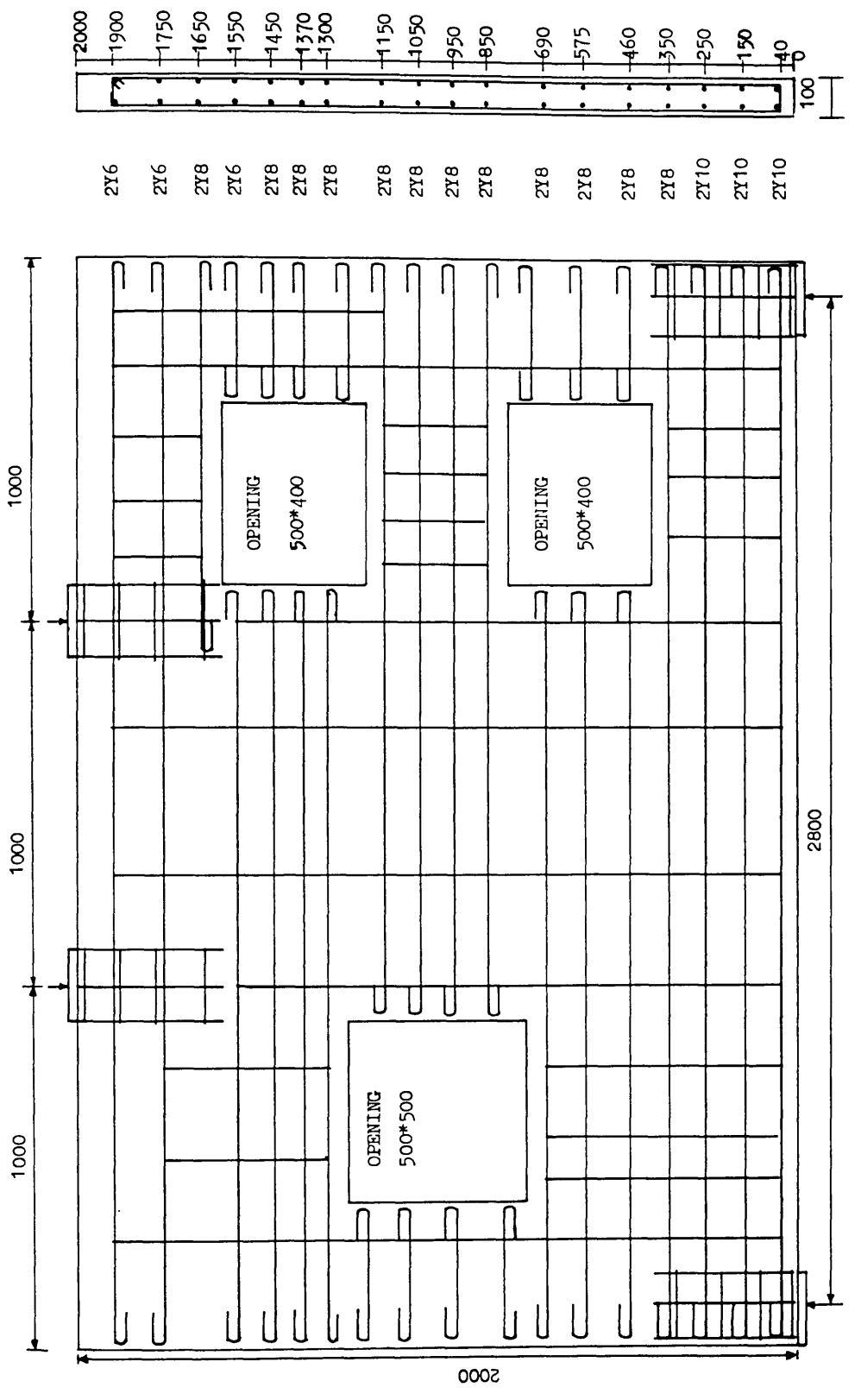

Figure(5.53) Dimensions and reinforcing details of girder TRGRAS10

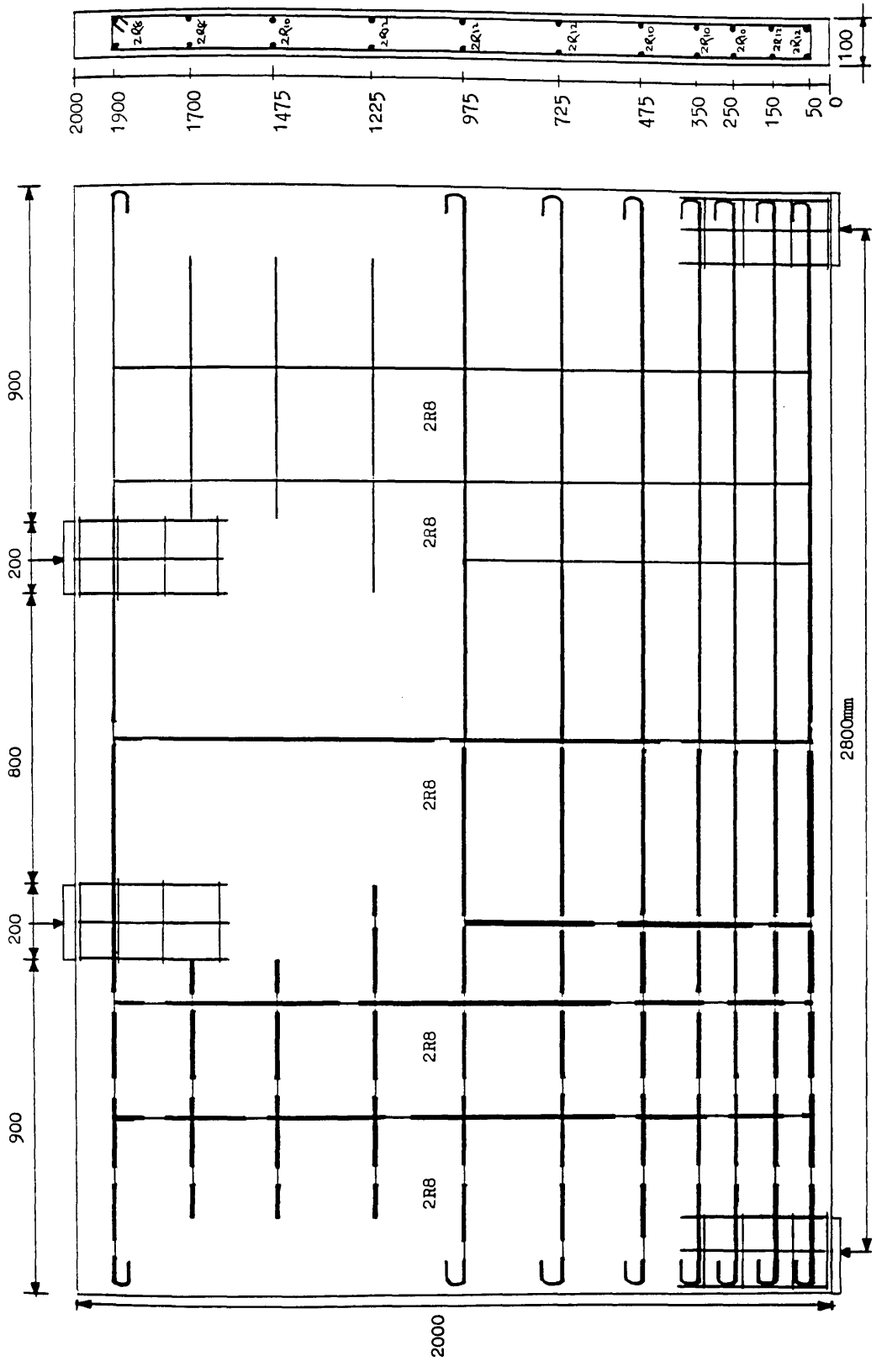

Figure(5.54) Dimensions and reinforcing details of girder TRGRAS11

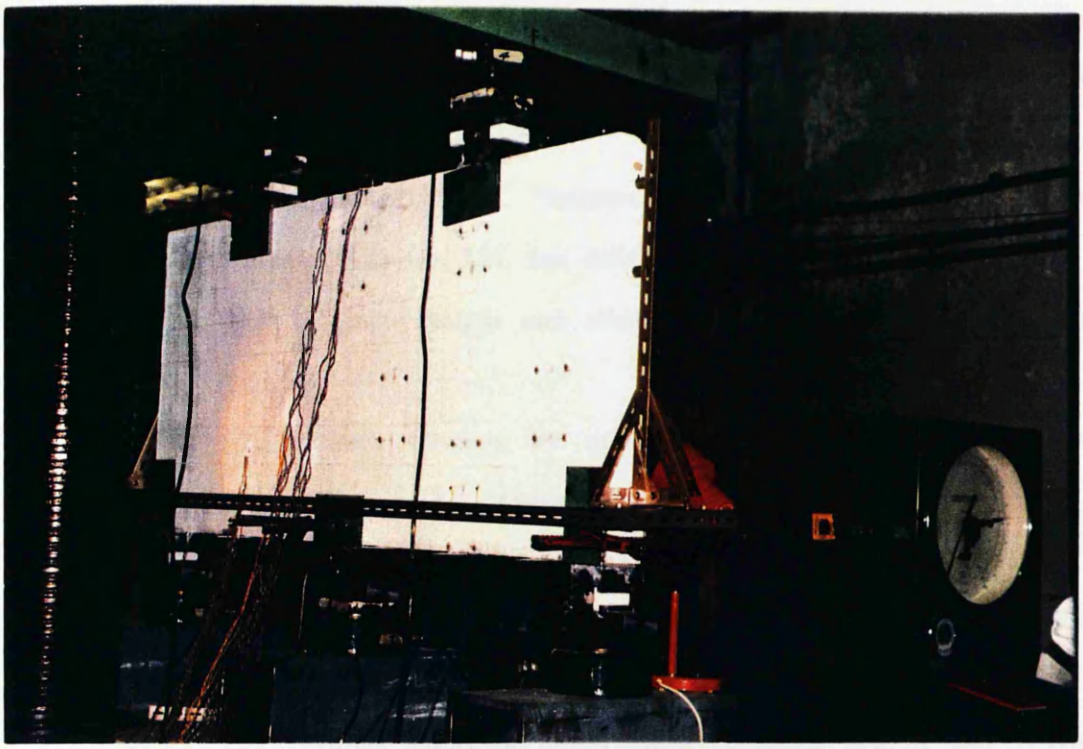

Figure(5.55) Typical test arrangements showing the use of steel plates clamped at bearing points.

REFERENCES

1. BSI, "Code of practice for the structural use of concrete in buildings", CP 114, London 1987.

2. BSI, "Code of practice for the structural use of concrete, (CP 8110, Part 2)", London 1985.

3. HUGHES, B.P., "Limit state theory for reinforced concrete design", Pitman, publishing ltd, London, 3rd Edition 1980.

4. KONG, F.K. and EVANS, R.H., "Reinforced and prestressed concrete design", Van nostrand reinhold (U.K) Co. Ltd, 2nd Edition, 1980.

5. NIELSEN, M.P., "Limit analysis and concrete plasticity", Prentice– hall, inc. New Jersey, 1984.

6. JENSEN, J.E., "Plastic solutions for reinforced concrete", IABSE Colloquium, Copenhagen, (Session II, Plasticity), August 1979.

7. CHEN, W.F., "Plasticity in reinforced concrete", Mc– Gravhill, 1982.

8. MARTI, P., "Basic tools of reinforced concrete beams design", ACI Journal, Jan.– Feb. 1985 (PP. 46– 56).

9. EBIRERI, J.O., "Direct design of beams under combined bending and torsion", Ph.D Thesis, University of Glasgow 1985.

10. PHILLIPS, D.V., GREEN, D.R. and KHASKHELI, G.B., "Design techniques for continuous deep beams using finite element modelling", IABSE Colloquium, Delft, Netherland 1987, (PP. 463– 472).

11. NIELSEN, M.P., "Yield condition for reinforced concrete shells in memberance state", Non– classical shells probelems, IASS Symposium Warsaw, 1963, (PP. 1030– 1038).

12. NIELSON, M.P., "Some examples of lower– bound design of reinforcement", IABSE Colloquium, Copenhagen, (Session II, Plasticity), August 1979.

13. SUBEDI, N. K., "Design of reinforced concrete sections subjected to memberance forces", The structural engineer, No. 7, Vol. 53, Jul. 1975, (PP. 289– 292).

14. MORLEY, C. T., "Optimum reinforcement of concrete slab elements" Against combinations of moments and memberance force", Mag. of con. res., Vol. 22, No. 72, Sept. 1970, (PP. 155– 162).

15. MORLEY, C. T., "Skew reinforcement of concrete slabs against bending and torsional moments", Proceedings of institution of civil engineers, Vol. 42, Jan. 1969, (PP. 57–74).

16. CLARK, L. A., "The provision of tension and compression reinforcement to resist in–plane forces", Mag. of con. res., Vol. 28, No. 94, Mar. 1976 (PP 3–12).

17. LIN, C. K., "Ultimate strength design of deep beams", M.Sc, Thesis, University of Glasgow 1979.

18. MEMON, G. H., "Ultimate strength of perforated deep beams", M.Sc. Thesis, University of Glasgow 1982.

19. MEMON, M.,"Strength and stiffness of shearwall–floor slab junction", Ph.D. Thesis, University of Glasgow 1984.

20. ELNOUNU, G. F., "Strength and stiffness of shearwall–slab junction", Ph.D. Thesis, University of Glasgow 1985.

21. HAGO, A. W., "Direct design of reinforced concrete slabs", Ph.D Thesis, University of Glasgow 1982.

22. ABDEL–HAFEZ, L.M., "Direct design of reinforced concrete skew slabs", Ph.D. Thesis, University of Glasgow 1986.

23. Comite, europeen du beton–federation Internationale de la precontriante, "International recommendations for the design and construction of concrete structures", Appendix 3, Deep beams, Cement and concrete association, London, June 1970.

24. ACI Committee 318, "Building code requirements for reinforced concrete (ACI 318–77)", American concrete institute, Detriot, Michigan 48219, 1977.

25. OVE ARUP and PARTNERS, "The design of deep beams in reinforced concrete", CIRIA Guide 2, London 1977.

26. PARK, R. and PAULY, T., "Reinforced concrete structures", John Wiley & Sons, U.S.A 1975.

CHAPTER SIX

EXPERIMENTAL INVESTIGATION

6.1 Introduction

Although considerable experimental research has been carried out on deep beam behaviour, research is still needed on large scale models which are close to actual practical situations, particularly in the provision of realistic reinforcement arrangements. Also, more experimental tests are needed to assess the applicability of the direct design technique for deep beams and continuous deep girders since little work has been done on this. The object of this experimental investigation was to meet these conditions by studying the ultimate strength, and general behaviour characteristics of a variety of two span continuous reinforced concrete transfer girders and simply supported girders, with and without openings, subjected to in-plane loads.

A total of eleven beams were tested of which eight were two span continuous deep beams, two were simply supported with openings, and one was a solid simply supported deep beam reinforced with steel areas as close as practically possible to that calculated by the direct design equations. The geometric details of all the girders and the concrete properties are given in Table 6.1, steel properties are given in Table 6.2, Figure (6.1) and Figure (6.2). The reinforcing details have already been given in a previous chapter.

The actual design of all the test girders has been described in the previous chapter, and the purpose of the next section in this chapter is to explain the reasons and objectives for studying these girders.

The loading arrangement for the two span deep girders were point loads acting at the top edge of the girder at the centre of each span. For the simple span girders

two point loads were applied on the top edge of the girder at the third points. The following characteristics were monitored in all tests:

1 :– Load deflection relationships

2 :– Strain distributions in the concrete and steel

3 :– Crack propagation and crack patterns

4 :– Failure mechanisms

6.2 Experimental programme

6.2.1 Description of experimental parameters

The tested girders were subdivided into five series and are explained in more detail below:

SERIES 1: This series consisted of four test girders, denoted TRGRAS1, TRGRAS2, TRGRAS3 and TRGRAS6. The aim of this series was to check the applicability of direct design for continuous deep beams, the effect of shear reinforcement and different distribution of reinforcement, other than those resulting from the direct design technique, on ultimate and serviceability behaviour. The geometry of all the girders in this series was kept constant. Discrete reinforcing bars were selected by taking arbitrary levels across and along the beams and calculating the average reinforcement ratios at each level. Reinforcement bars were selected and distributed using specified bar diameters, and limits and spacing.

The difference between the first girder, TRGRAS1, and the second girder, TRGRAS2, was in the provision of shear reinforcement, the main reinforcement and beam dimensions were same. This was because the shear reinforcement calculated according to the direct design equations was very small in comparison with even the minimum bar size recommended by CP110[1] and BS CP8110[2]. Thus, the provided shear reinforcement in girder TRGRAS1 was higher than the calculated shear

reinforcement according to the direct design procedure. In order to match theoretical and practical requirements closely, the provided shear reinforcement in girder TRGRAS2 was closer to (but higher than the) calculated value. Thus, the amount of shear reinforcement in girder TRGRAS1 was higher than TRGRAS2, this was to evaluate the effect of shear reinforcement on ultimate load.

The difference between girders, TRGRAS2 and TRGRAS3, was in the main reinforcement, while the shear reinforcement was kept constant. The aim of this comparison was to meet the minimum diameter size of shear reinforcement as required by BSCP 8110[2], which meant that the design ultimate load had to be increased and so consequently increased the amount of main reinforcement required. Hence, the design ultimate load of the girder TRGRAS3 was higher than that of TRGRAS2.

The design load for girders TRGRAS3 and TRGRAS6 was the same, but the calculated reinforcement for girder TRGRAS6 was distributed according to CIRIA Guide 2[3] and CEB– FIP[4]. The aim of this comparison was to evaluate the effect of different steel distribution on both ultimate and serviceability behaviour.

SERIES 2: This series consisted of two girders denoted TRGRAS4 and TRGRAS5. The general aim of this series was to check the applicability of the direct design procedure for continuous deep beams with increased span to depth ratio L/D, and clear shear span to depth ratio X/D, compared to the first series. These ratios are believed to be important parameters affecting the general behaviour of deep girders.

The difference between these two girders was in the steel distribution. In girder TRGRAS4, the steel was provided according to averaging procedure at each level, and so can be directly compared with girder TRGRAS2, thus deducing the effect of L/D and X/D ratios. In Girder TRGRAS5 the steel was distributed according to the

CIRIA Guide 2[3], CEB–FIP Model Cod[4] and Leonhardt and Walther's[5] recommendations and so can be compared with girder TRGRAS4.

SERIES 3: This series consisted of two deep continuous girders TRGRAS7 and TRGRAS8, reinforced with skew reinforcement.. The purpose of this study was to investigate the general behaviour of girders with skew reinforcement in terms of cracking control, ultimate and service loads. It has been reported in literature, that skew reinforcement can be highly beneficial despite its complexities in practice(4,6), (i.e. laborious work in bending and fabrication, etc). Two angles of skew 15^{o} and 10^{o} degrees to the horizontal were chosen for TRGRAS7 and TRGRAS8 respectively, in all other aspects they were identical. The behaviour of these two girders can be compared with girder TRGRAS2, an identical girder but reinforced with orthogonal reinforcement.

SERIES 4: This series consisted of two large scale single span girders with web openings. The aim of this series was to check the applicability of the direct design procedure in designing deep beams, when web openings interrupt the load path in the shear spans. The CIRIA Guide 2[3] only covers the design of beams with openings which do not interrupt the load path and suggests that the regions top and bottom of an opening are designed as deep beams. Another aim of this series was to assess the location of the opening in the shear spans of the deep beams.

The first girder, TRGRAS9, had two openings both 500*500mm in size. One was located above the mid–depth of the beam in one shear span, and the other was located below the mid–depth of the girder in the other shear span. The second girder, TRGRAS10, had two openings of dimensions 500*400mm in one shear span, one above mid–depth and the other below the mid–depth of the beam. It also had a third opening of dimensions 500*500mm in the other shear span of the beam, located at mid–depth of the beam. Figure (6.2) shows the general view of these

two beams.

SERIES 5: This series consisted of testing of a very large scale simply supported girder denoted TRGRAS11. It was tested to examine the accuracy of the direct design equations in detail. The direct design procedure produces a continuously varying reinforcement field as calculated at each Gauss point in the finite element analysis, but in practice the bars have to be provided either by using maximum steel ratios at a particular level, or by averaging steel areas. This leads to over and under–reinforced zones in the structure, and final design which has departed significantly from the original design assumptions.

In this beam, steel areas were provided as close as possible to those required by the theoretical calculations. This was achieved by reducing the bar diameters at selected points throughout the structure.

The direct design equations do not take into account the work–hardening effect. Hence, in this test, mild steel was used which has a small work–hardening effect as compared to high tensile strength steel. This test was designed to see that the simultaneous yielding of steel occurs at the ultimate load stage as theory provides, if theoretical steel areas are provided.

6.2.2 Beam notation

The letters 'TRGRAS' stands for Transfer Girder with Averaged Steel. The girders are numbered sequentially from the start of the investigation. For example, TRGRAS1 represents a Transfer Girder with Averaged Steel ratio Number 'TRGRAS1'. This notation is used for all the girders studied in this investigation.

6.3 Formwork

Since the geometries of all girders were not the same, it was necessary to design

and make several different formworks. However, only the construction of the formwork for girder, TRGRAS1, is described here, since it is essentially the same.

The formwork was made from 20mm thick plywood panels. To maintain the stability and strength of the mould during casting, 50mm*50mm timber battens were nailed at close spacing along the length of the mould. Battens were also nailed along the vertical walls of the mould (i.e soldiers) to make it more stable and some were nailed as stiffeners as shown in Figure (6.3). Prior to casting, the mould was oil coated in order to prevent the concrete sticking to the mould.

6.4 Test– rig

The test– rig was set up as shown in from Figure (6.4) to Figure (6.6). Figure (6.7) shows a photograph of one of the girders being tested. The test– rig was designed to be accommodated in a 10,000kN Losenhausen Universal Testing Machine and was capable of accommodating a girder of up to 3 metres long and up to 2.5 metres in height. It was designed for a total loading capacity of 2000kN. The main components of the test– rig are:

1:– Base Beam

2:– Support Girders

3:– Loading Girders

4:– Supporting Bearings

5:– Losenhausen Machine Platen

6.4.1 Base beam

This beam is made of two 356*406*287kg/m I– sections welded together to provide a firm base of up to 5000kN capacity. This beam was placed on the bottom platen of the Losenhausen Machine. Steel columns were bolted to this beam so that the girder could be positioned and placed accurately in the machine. During testing, these

columns were either dismounted or slackened and kept at least 20mm away from the beam plane, in order to avoid interference with the load transmission.

6.4.2 Support girders

Support girders of 250*250*16kg/m hollow square box cross section were used. The girders were designed as simply supported cross beams spanning the I-sections of the base beam and loaded at the centre by a maximum reaction of 2000kN from the test girder. Three girders were used for the two span continuous girders and two for the single span girders.

6.4.3 Loading girders

This loading girder was designed and used only for the two span continuous girders of 3 metre lengths because direct transmission of the load from the machine platen to the specified loading point locations on the top of beam was not possible. The loading girder was a 305*305*158kg/m I-section. To strengthen the girder at the loading points, extra steel web stiffeners were welded to the girder. BS449[7] was used to design this strengthening. Angle sections of 120*120*18.5kg/m were also designed to attach the loading girder to the machine platen safely. The bolts connecting the loading girder to the machine platen were also checked and designed accordingly.

6.4.4 Support bearings

All the support bearings were made of mild steel. Both exterior supports in the two span continuous girders were provided with rollers to allow free horizontal translation, and the mid-support was restrained horizontally and vertically. Under the loads, one bearing was roller supported and the other was fixed. The roller supports at the bottom and top of the girder were provided with two roller rods to avoid permanent deformation of the bearing block which would restrict the horizontal translation.

The support bearing dimensions for the two span continuous girders of two meters length were 80*100*50mm at each exterior support, 160*100*50mm for the intermediate support and 150*100*50mm for the load bearings. In the case of the two span continuous girders of three meters length, the exterior support bearing dimensions were 100*100*50mm, the interior support bearing dimensions were 200*100*50mm and the load bearing dimensions were 150*100*50mm. For the simply supported girders the dimensions for the support bearing and load bearing were both 200*100*50mm.

6.4.5 Losehausen machine platen

The detachable Losenhausen machine platens were used at the bottom for holding the base beam, and at the top to transmit the loads either directly onto the beam from the machine head, or for providing a uniformly distributed load on the loading girder for the beams of 3 metre length. In addition steel plates 50mm thick and of area 400*400mm were used in between the machine platen and the top of the loading support bearing block, to spread the load more effectively.

6.5 Material properties

6.5.1 Concrete

The same concrete mix was used for all specimens. It consisted of Rapid Hardening Portland Cement (RHPC), 10mm Hyndford uncrushed gravel of grading zone 2 and Hyndford sand obtained from Lanarkshire. A mix proportion of 1:1.5:3 and with 0.48 water/cement ratio was designed for an intended average cube strength of 45 N/mm^2 at 7 days. The weighed quantities of cement, sand, 10 mm gravel and water were mixed thoroughly in a 3 cu.ft capacity pan mixer. A minimum slump of 100 mm was specified.

All the girders were cast horizontally. The concrete was placed in the mould with shovels. The compacting of the mix during casting was achieved by using a 12mm

diameter poker vibrator. The vibration continued until a reasonably good compaction was achieved.

In addition to the main specimen, six 100*100mm cubes and at least four 150*300mm cylinders were cast as control specimens from all the different batches of material used for constructing the main specimen. These were compacted by using a vibrating table.

All the control specimens and the main specimen were cured under damp hessian for the first 24 hours. After that, the control specimens were taken out of the moulds and a few control specimens were cured in the water tank. All the remaining control specimens and the main specimen were kept under wet sacking for the first three days and then were cured dry under laboratory conditions.

The cubes were used to determine the cube strength of concrete, two cylinders were used to determine the splitting tensile strength, ft', and two for the concrete compressive strength, fc'. The remaining two cylinders were used to obtain the stress– strain curve and modulus of elasticity. All the control specimens were tested on the same day the transfer girder was tested. A typical compressive stress– strain curve for the concrete (girder TRGRAS3) is shown in Figure (6.8).

6.5.2 Reinforcing steel

High yield deformed bars of 6, 8 and 10mm diameter made by British Steel Corporation were used for the longitudinal and transverse reinforcement in all girders, except transfer girder TRGRAS11. Mild steel bars of 8, 10 and 12mm diameter were used for girder TRGRAS11. The yield stress of all different bar sizes were measured on samples cut from different batches of steel bars using a Tinus Olsen Universal Class A testing machine, fitted with a S– type electronic extensometer, and procedure laid down by British Standard BS18 [8] was followed.

Since high yield deformed bars have no definite yield point, the yield stress was assumed to be that at the 0.2 percent proof strain. Typical stress strain curves for all high tensile strength bars are shown in Figure (6.9) to (6.11) and for mild steel bars are shown in Figure (6.12) to (6.14).

When the bending of steel and cementing of strain gauges on the steel was completed, the fabrication of the steel commenced by placing the main and transverse steel at their required locations. All the reinforcement were then tied together by wires. Before casting, plastic spacers were attached to the longitudinal bars and the transverse steel, at certain intervals to ensure adequate cover to the reinforcement on both sides of the beam. In all the models, a 15mm concrete cover was provided to the reinforcement.

6.6 Instrumentation

All girders were connected to instruments to measure the load, the deflections, steel and concrete strains, and crack widths.

6.6.1 Loads

The intermediate support in two span continuous girders takes more than 60% of the total load. Therefore, the available Davy Limited K500 load cells were not suitable for the intermediate support because their maximum capacity is 500kN. Thus, for the two span continuous girders, only the exterior reactions and the applied loads at the top of each span were recorded by load cells. The total load was directly recorded by the machine. In the case of simply supported girders, all the reactions and loads were measured by load cells. It was found, that if the beam was positioned satisfactorily (i.e levelled horizontal) the reactions were within 2%– 4% of each other. The load cells were connected to an Orion 3530 type data logger.

The loads were applied by the Losenhausan Universal Testing Machine, at the centre of the two spans in the case of the two span continuous girders and at third point for the simply supported girders. Figure (6.15) shows the loading arrangements for one of the two span continuous test girders. Figure (6.16) shows the loading arrangement for a simple supported test girder.

6.6.2 Deflections

Net deflection measurements in deep girders is a challenging parameter. This is because these members take a very high load and failure is likely to be in shear, so that deflections are very small. The test floor is susceptible to vibrations and the plaster between the supports and the beam is subjected to a high load causing extra deflection. Thus, it was decided to try and isolate these effects by measuring the deflections using displacement transducers fixed to a frame, which could be mounted on the girder itself. The frame was thus constructed from handy angles.

The vertical deflections of two span continuous deep girders were measured by means of Novatech R101 type transducers located at the mid−span of the beam and at 200mm from the exterior and interior supports for each span on both sides of the girder as shown in Figure (6.17). For single span girders, vertical deflections were measured by means of transducers located at the mid−span of the beam and at 200mm from the each support of the girder on both sides of the girders as shown in Figure (6.18).

All the transducers were connected to the data logger and the deflections were recorded automatically at each load increment. These Novatech R101 type transducers were able to measure the deflection to an accuracy of 0.0001mm.

6.6.3 Steel strain gauges

EA−06−240LZ−120 Student type strain gauges were cemented to the longitudinal

and transverse steel at critical sections to record the strain history. Prior to fixing the strain gauges, the surface of steel was prepared by filling and then smoothning it with sand paper. During this process, care was taken not to remove a considerable area of steel which would weaken the steel bars. The surface was then treated with M– Prep conditioner A and M– Prep neutralizer 5 to remove any dirt and grease. Each strain gauge was checked with a voltmeter before cementing, and its proper position was located by making a very thin line on the steel bar. The strain gauge and terminal strip were cemented to the bar using M– Bond 200 adhesive. To protect the gauge from moisture and mechanical damage during fabrication and casting, an air drying protective coating type M– Coat D and expoy resin was applied to the gauge and terminal. Finally, a check using the voltmeter was carried out for each strain gauge after cementing.

At most positions on a bar, a pair of strain gauges were fixed on the opposite sides. Figure (5.19) to (6.29) shows the location and positions of the strain gauges in the all girders.

6.6.4 Concrete strains

To record the concrete surface strains, stainless steel demec gauges were used at critical sections. A gauge length of 100 mm was used as a sufficient length through which cracks could propagate. The points on the surface where demec gauges were to be fixed, were cleaned of dust and grease, and the points were correctly located using a standard setting bar provided for this purpose. The gauges were fixed with Araldite. The location and positions of the demec gauges in all girders are given in Figure (6.30) to (6.40). An average value of concrete surface strain of two demec gauges at the same point on either sides of the girder at each location was used in subsequent analysis of the results

6.6.5 Crack propagations and crack widths

Crack propagation and crack widths were monitored and measured throughout the loading history. The crack widths were measured by means of a microscope of accuracy up to 0.02mm. A few predominant cracks were selected and their crack widths were measured at each load level. The average of the crack width on two faces of the specimen were used as crack width.

6.7 Testing procedure

When each model was fully cured, it was manoeuvered on to wooden tressels and whitewashed with paint. A rectangular grid of 100*100mm lines was drawn in order to facilitate marking and locating crack propagation. After this process the demec gauges were fixed.

Using slings, placed through lifting hooks attached to the reinforcement, the girders were then taken to the test–rig by crane. 3mm of quick setting plaster was used between the bearing blocks and the beam, and in other critical places, so that any unevenness in the surface could be avoided.

Once the test girder was installed the various transducers were mounted on to a handy angle frame. The strain gauges, load cells, displacement transducer and a displacement transducer recording the overall displacement between the two machine platens, were connected to a 3530 Orion data logger for automatic recording. All the instruments were checked one day before starting the actual test. Additional steel plates were clamped to the loading and support points on the girders, in order to constrain local failure due to high bursting stresses.

The Losenhausen Universal Testing Machine was operated in displacement control mode using LVDT (Linear Variable Displacement Transducer). Loads were applied in small increments of about 50 kN up to the failure without unloading. It was

observed that in some girders that at small loads, there was a variation in loads and reactions of up to 4%, but as the load increased this became insignificant. This might be due to the unevenness in plaster thickness etc.

At each increment the displacements and strain in the steel and concrete demec gauges readings were recorded. Crack propagation and crack widths were marked and measured respectively. The duration of each load increment stage was usually about 15 minutes. In some cases when any major crack has occured during the test, load was considerably dropped. In such situations, prior to increasing the load according to intended increment, a set of readings was always taken. In some cases, beams were unloaded and reloaded, and similar procedures were adopted during reloading. For a few tests, photographs were taken at various loading levels when any major failure cracks or any new phenomenon occurred. For each test, photographs were taken of the crack pattern and failure type after the testing was over.

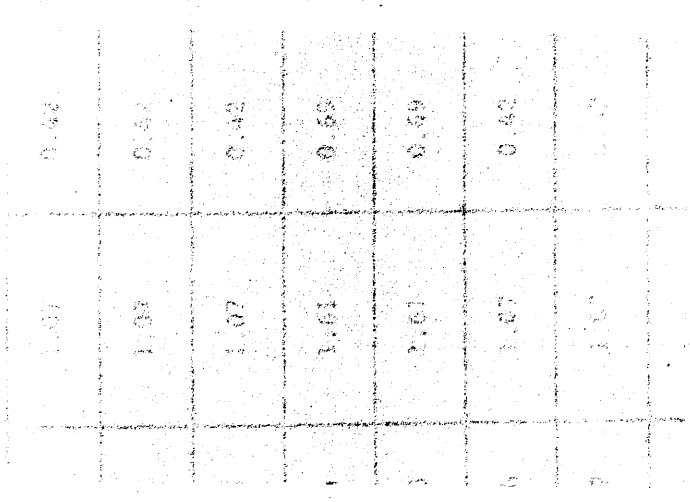

TABLE 6.1

Details of girder dimensions and properties of concrete of test girders

Girder No.	Span/depth ratio L/D	Shear-span/ depth ratio a/D	Clear-shear span/depth ratio X/D	Girder depth D	Girder width b	fcu N/mm^2	fc' N/mm^2	ft' N/mm^2	Ec kN/mm^2	Reinforcement type
TRGRAS1	1.07	0.42	0.38	900.0	100.0	63.0	41.8	3.2	19.3	Orthogonal
TRGRAS2	1.07	0.42	0.38	900.0	100.0	61.0	42.9	3.7	23.2	Orthogonal
TRGRAS3	1.07	0.42	0.38	900.0	100.0	61.0	39.6	3.4	20.8	Orthogonal
TRGRAS4	1.61	0.69	0.64	900.0	100.0	52.0	35.1	2.6	19.2	Orthogonal
TRGRAS5	1.61	0.69	0.64	900.0	100.0	61.0	40.5	4.1	22.4	Orthogonal
TRGRAS6	1.07	0.42	0.38	900.0	100.0	59.0	39.5	4.2	21.5	Orthogonal
TRGRAS7	1.07	0.42	0.38	900.0	100.0	59.0	38.3	2.6	19.1	Skew θ=15°
TRGRAS8	1.07	0.42	0.38	900.0	100.0	60.0	43.2	3.4	18.2	Skew θ=10°
TRGRAS9	1.40	0.40	0.35	2000.0	100.0	57.0	37.8	3.1	21.1	Orthogonal
TRGRAS10	1.40	0.40	0.35	2000.0	100.0	64.0	43.4	3.5	23.0	Orthogonal
TRGRAS11	1.40	0.40	0.35	2000.0	100.0	39.0	33.4	3.3	24.0	Orthogonal

TABLE 6.2

Steel properties of reinforcement used in this study.

Bar size mm	Area mm^2	Es kN/mm^2	fy N/mm^2	ϵy mm/mm	0.2% proof stress N/mm^2
6	28.0	199.0	——	——	513.0
8	50.0	195.0	——	——	520.0
10	79.0	200.0	——	——	471.0
8	50.0	210.0	290.0	0.0014	——
10	79.0	212.0	318.0	0.0015	——
12	113.0	198.0	336.0	0.0017	——

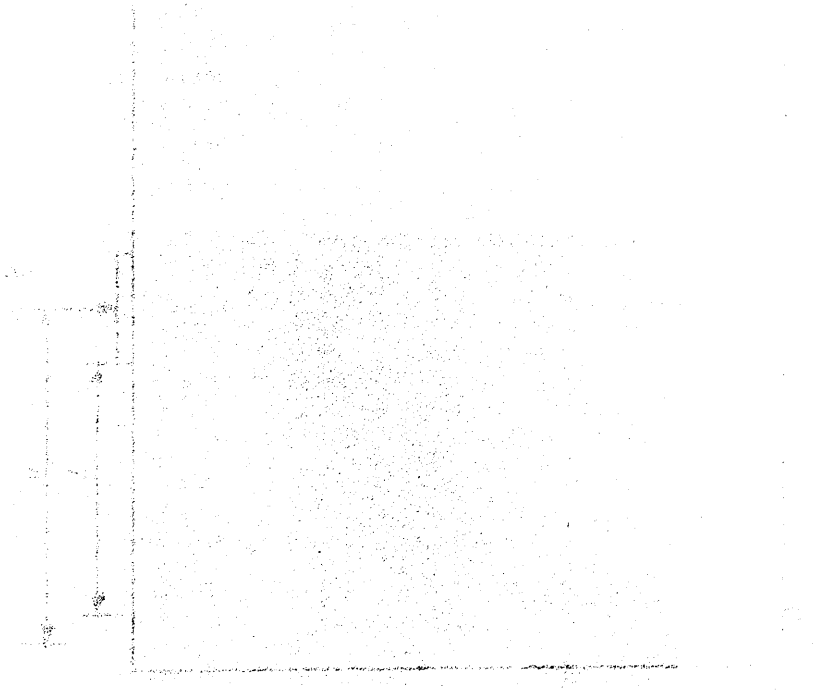

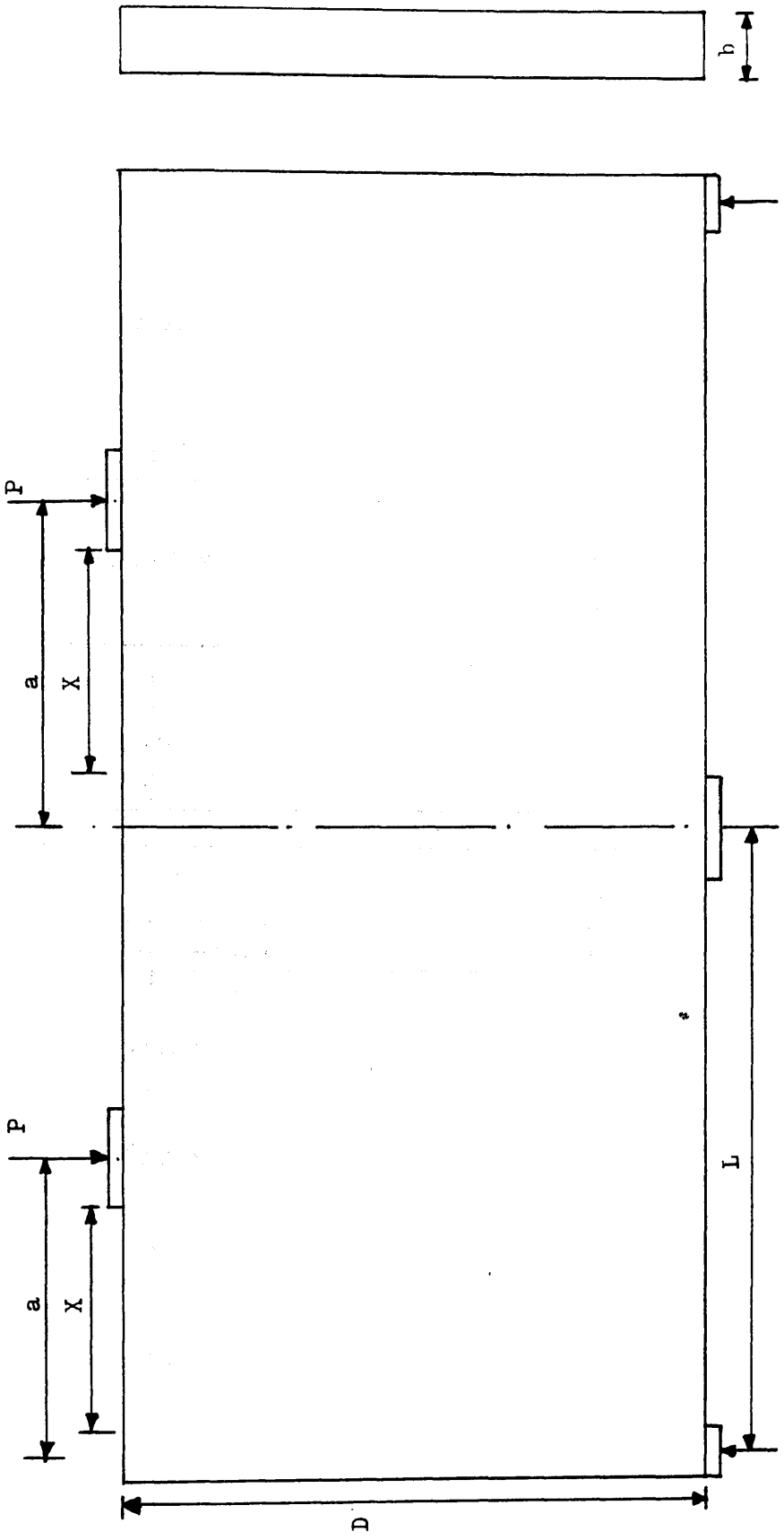

Figure (6.1) Details of the geometric governing parameters.

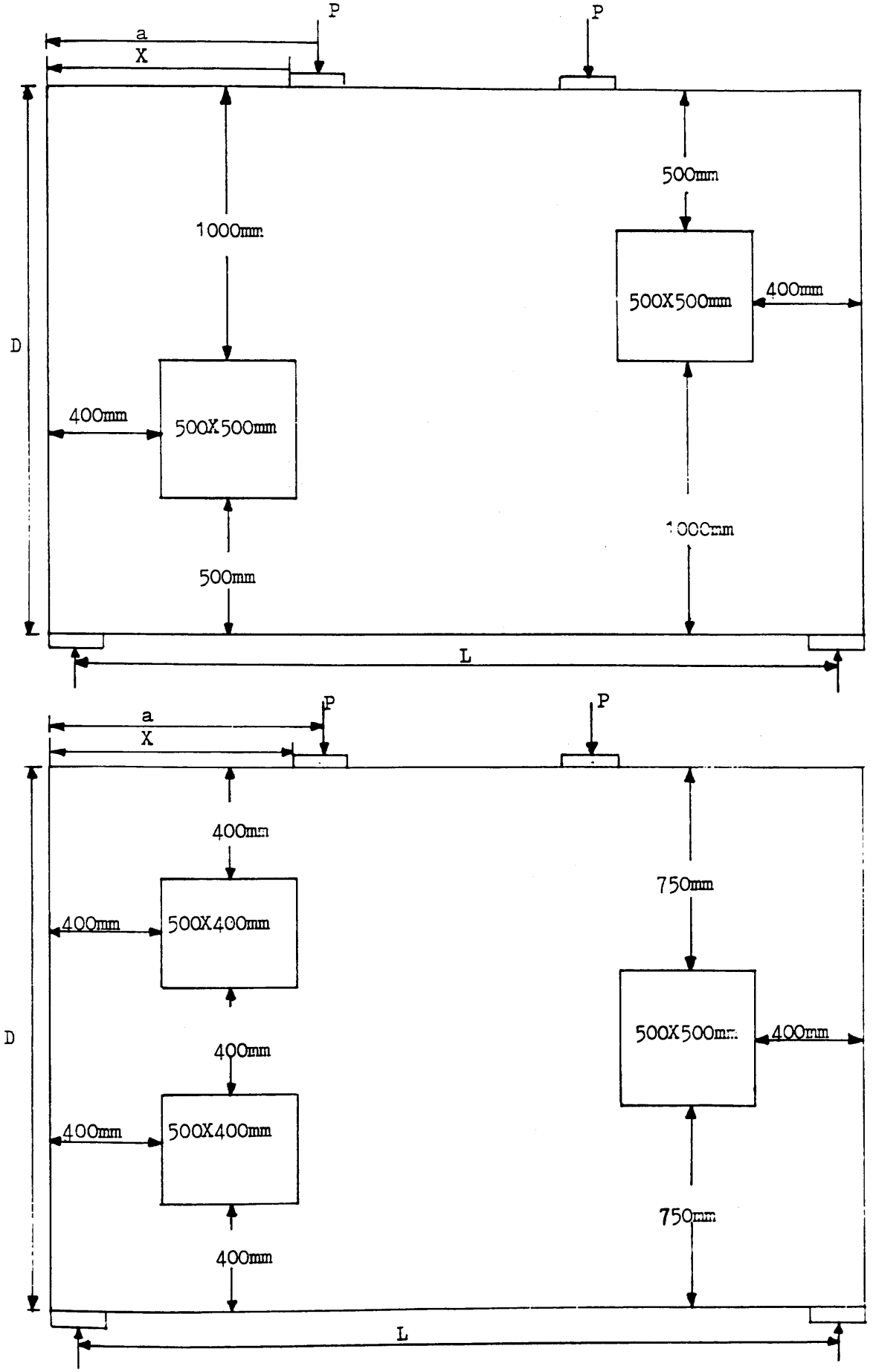

Figure (6.2) Geometric details of web opening girders

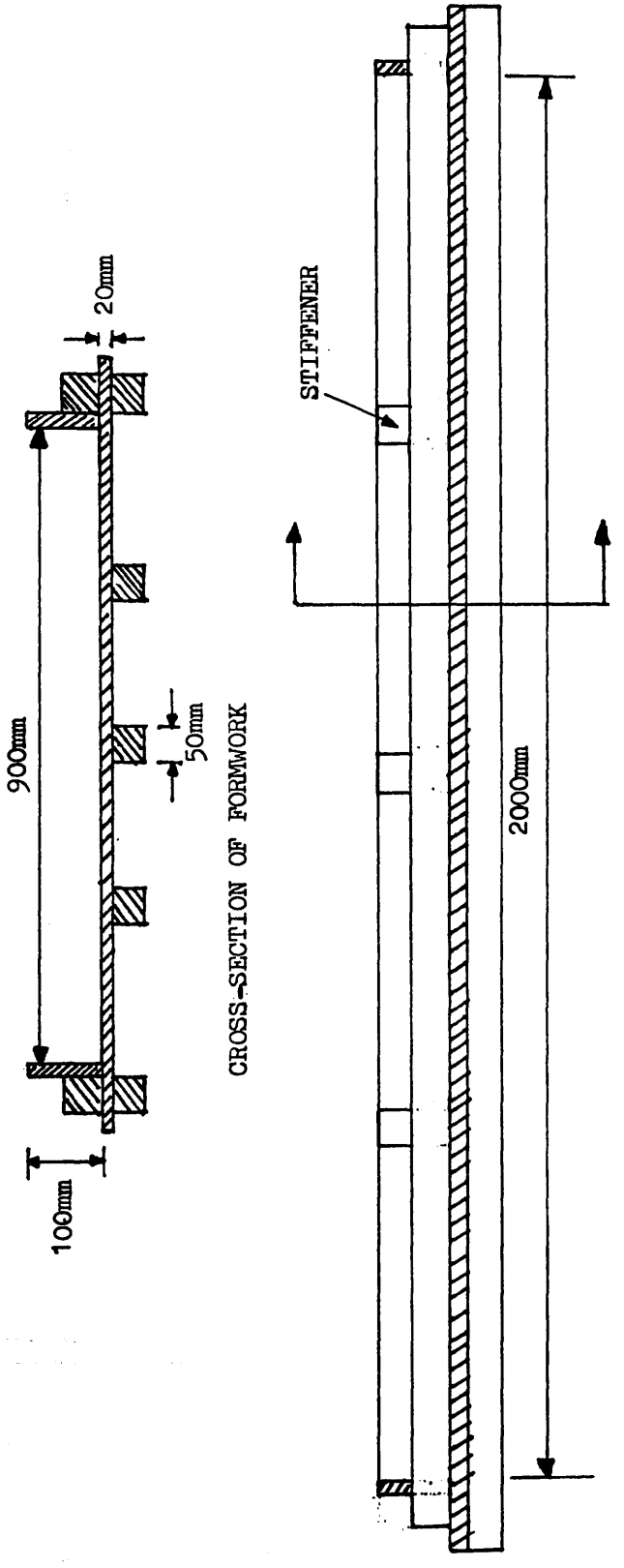

Figure (6.3) Typical formwork for the specimens

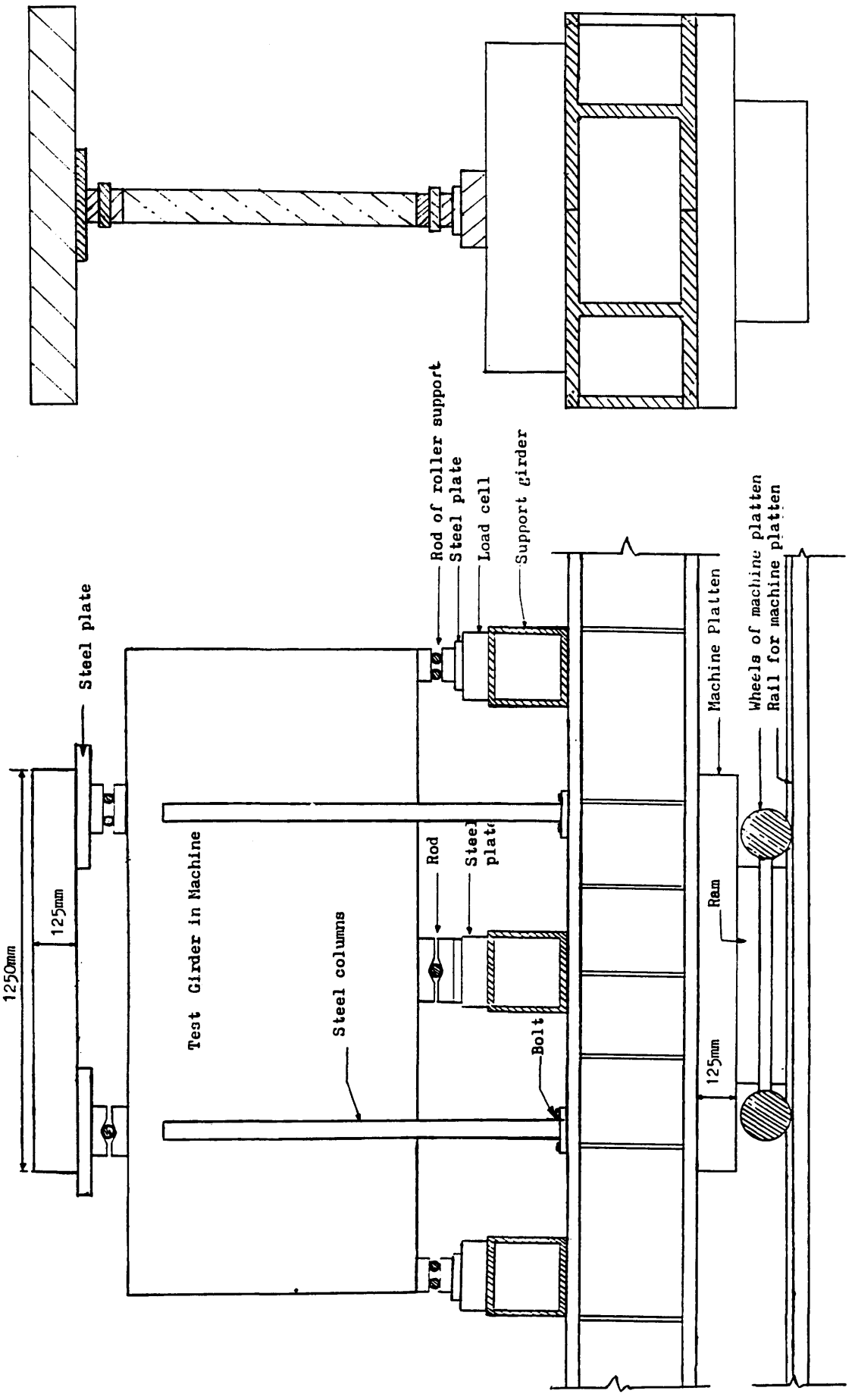

Figure (6.4) Test– rig for testing transfer girders (L= 2m, and D= 0.9m)

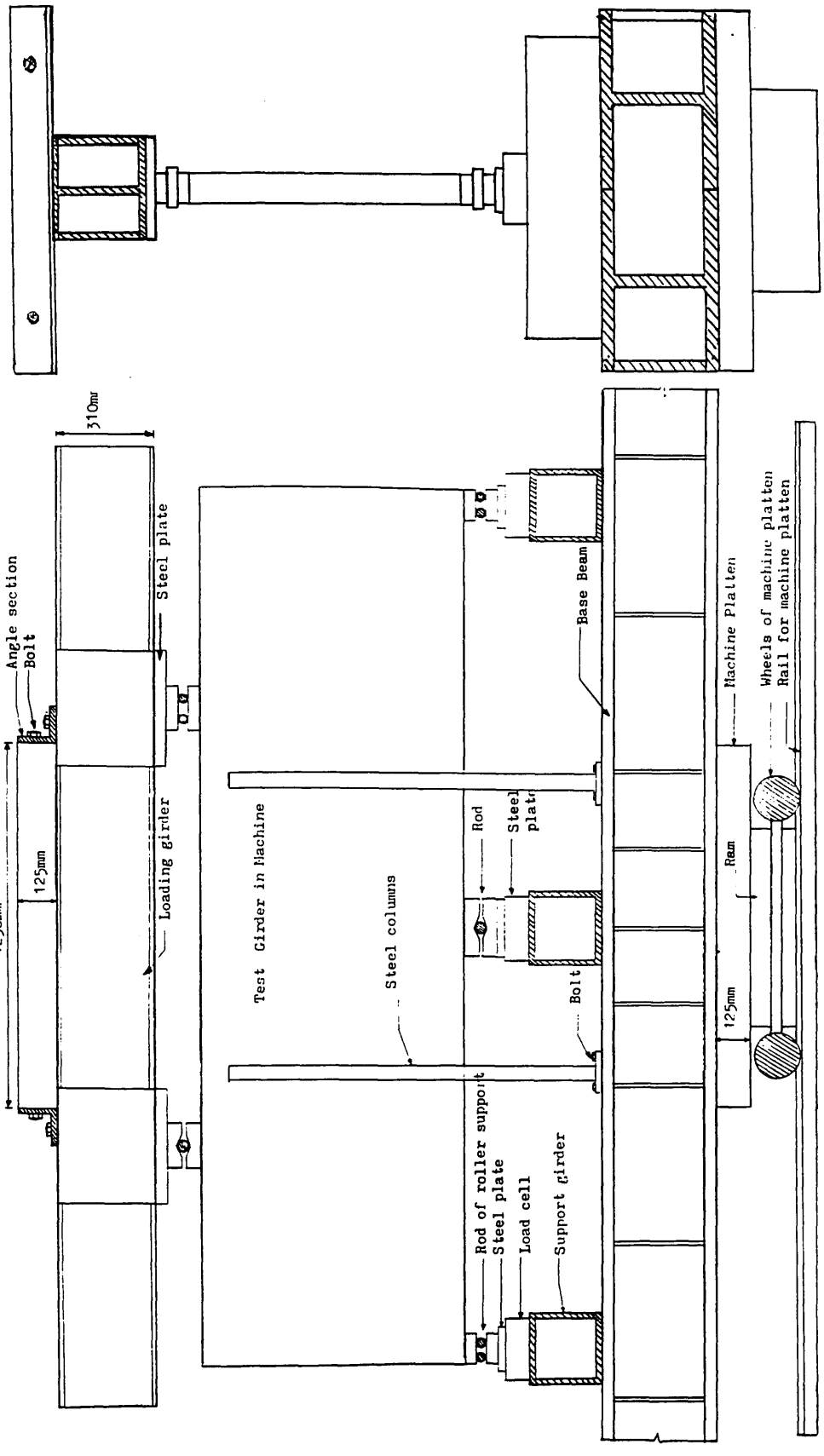

Figure (6.5) Test- rig for testing transfer girders (L= 3m, and D= 0.9m)

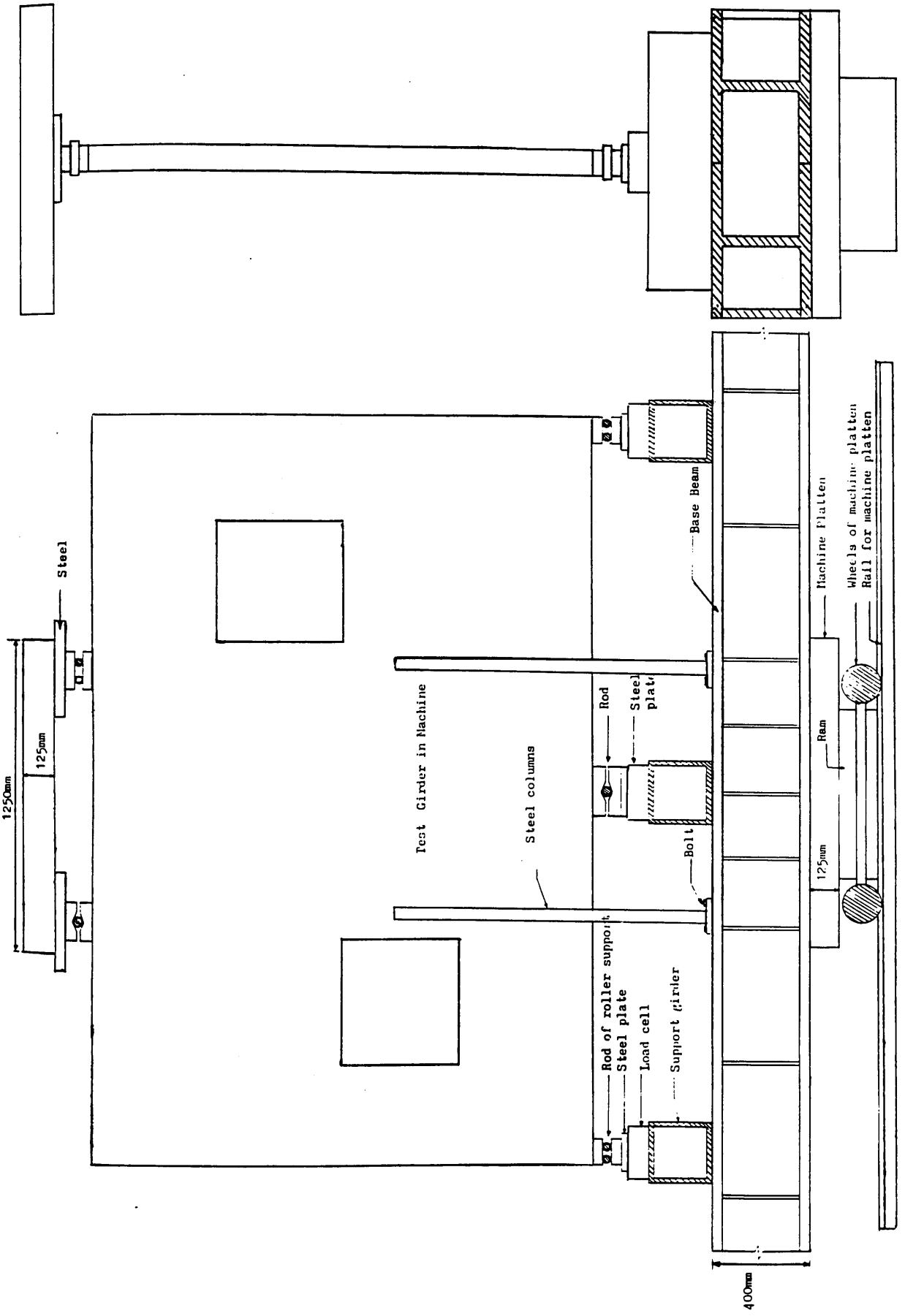

Figure (6.6) Test-rig for testing transfer girders (l = 3m and D= 2m)

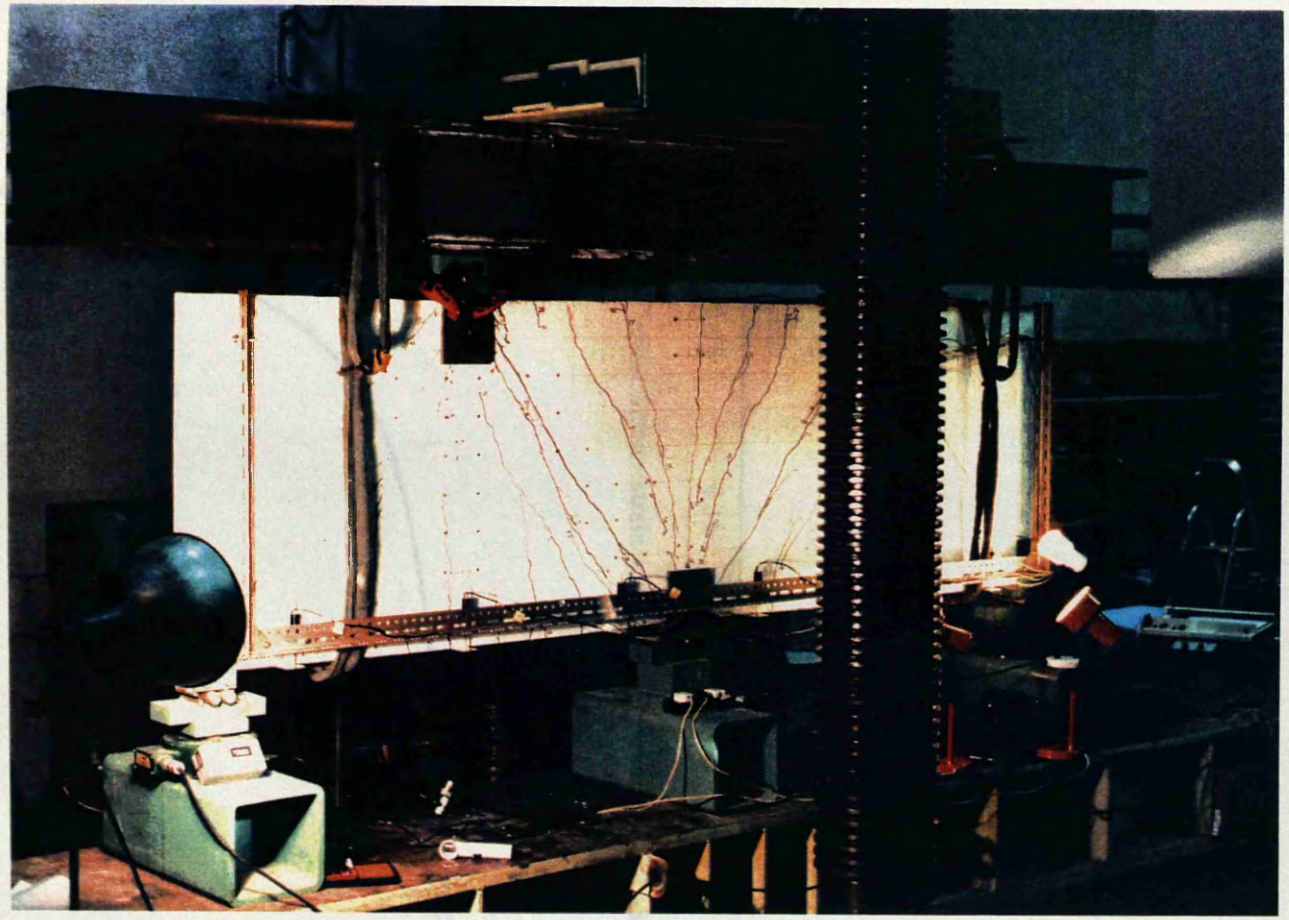

Figure (6.7) Test-rig shown during conducting the actual test of transfer girder TRGRAS4

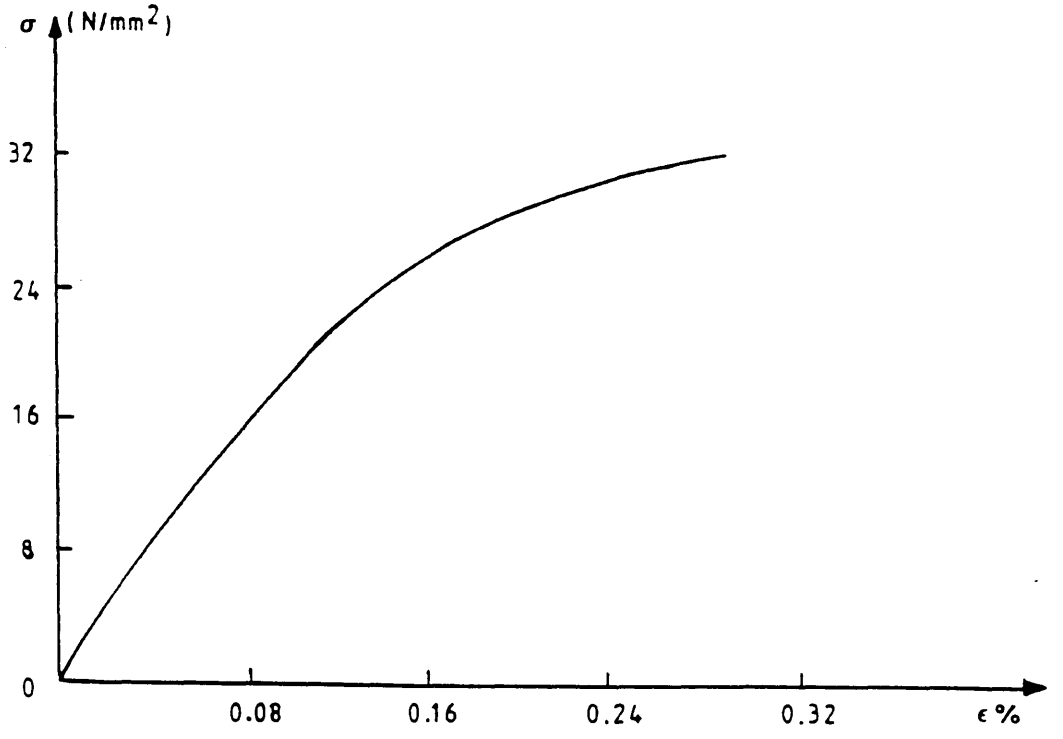

Figure (6.8) Typical stress– strain curve for concrete (TRGRAS3)

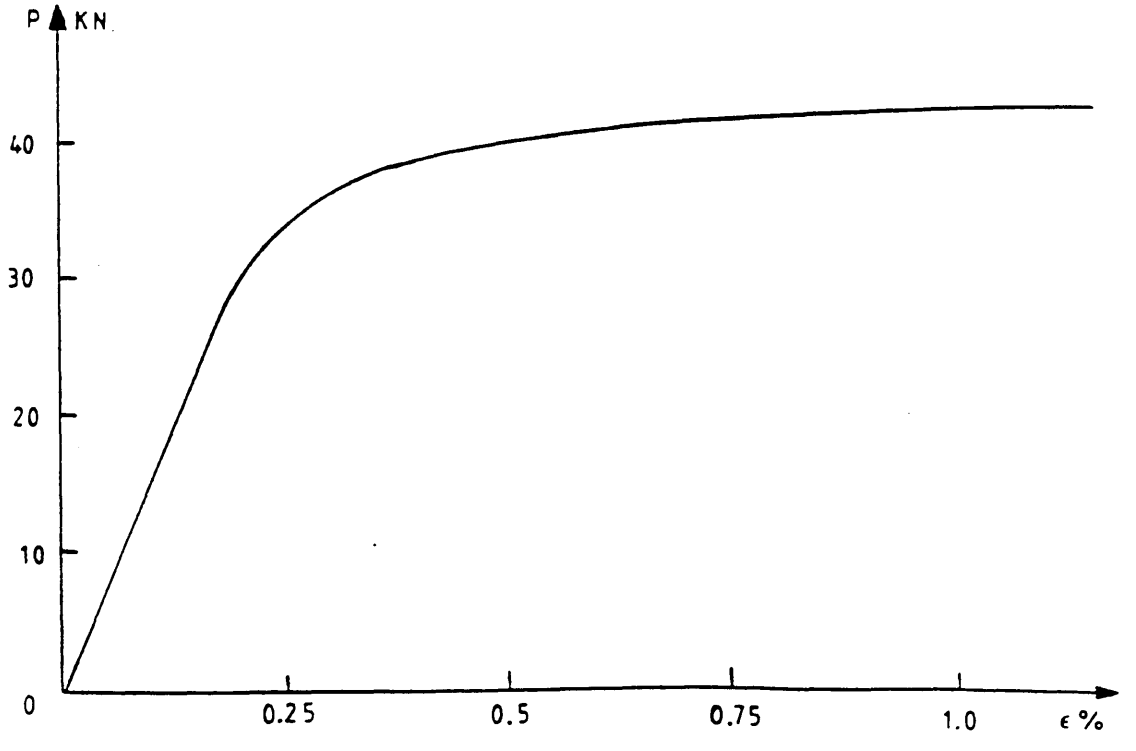

Figure (6.9) Typical stress– strain curve for 10mm dia. steel bar.

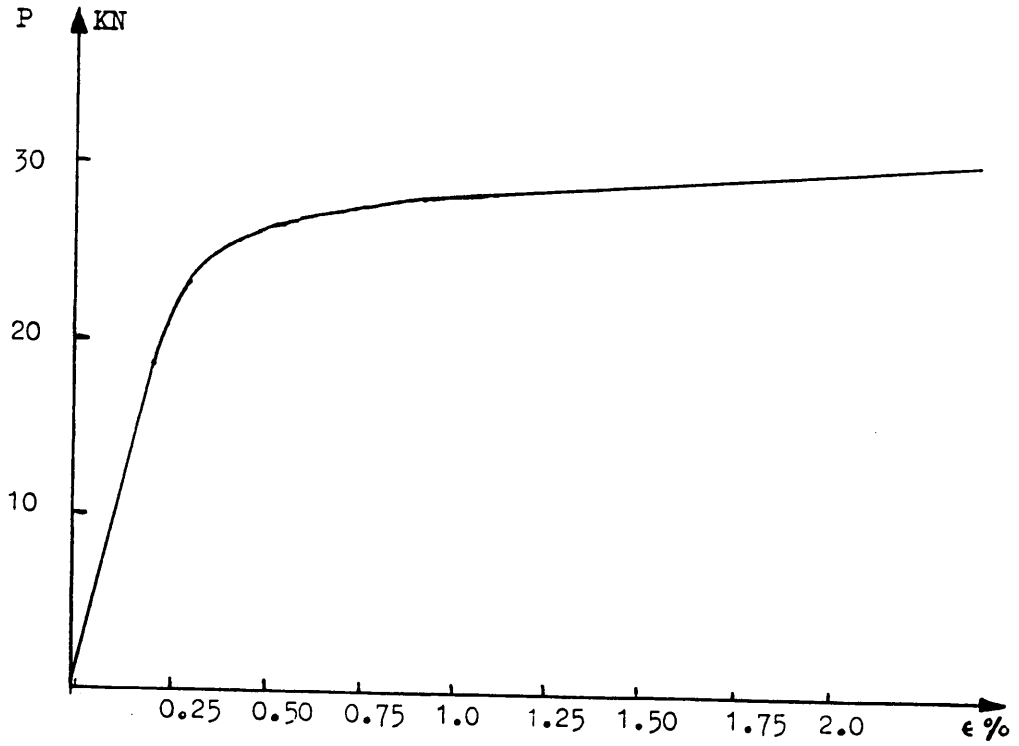

Figure (6.10) Typical stress– strain curve for 8mm dia. steel bar.

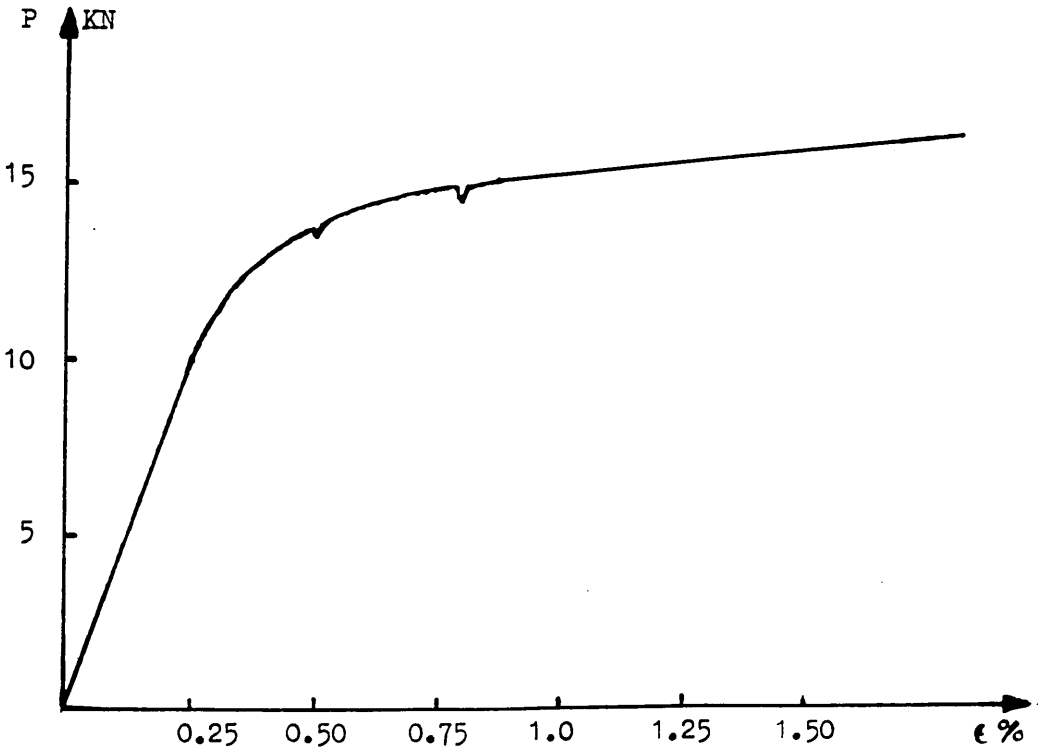

Figure (6.11) Typical stress– strain curve for 6mm dia. steel bar.

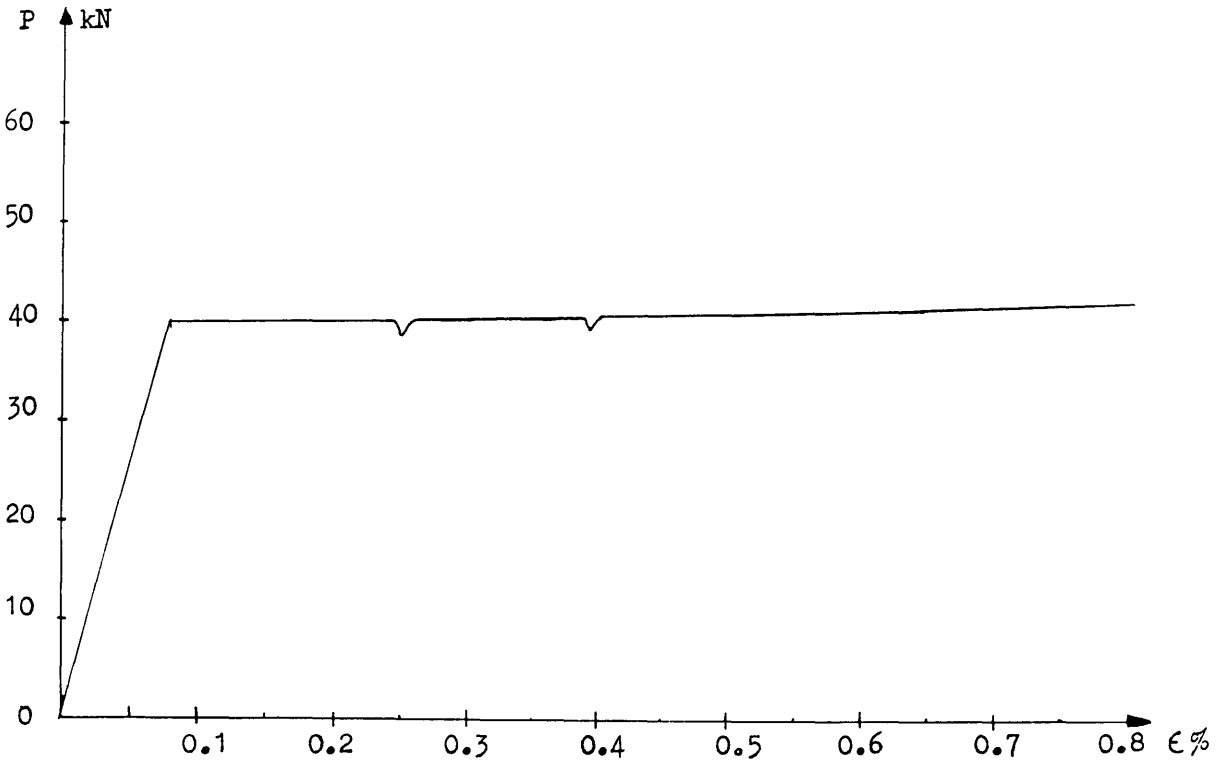

Figure (6.12) Typical stress– strain curve for 12mm dia. mild steel bar.

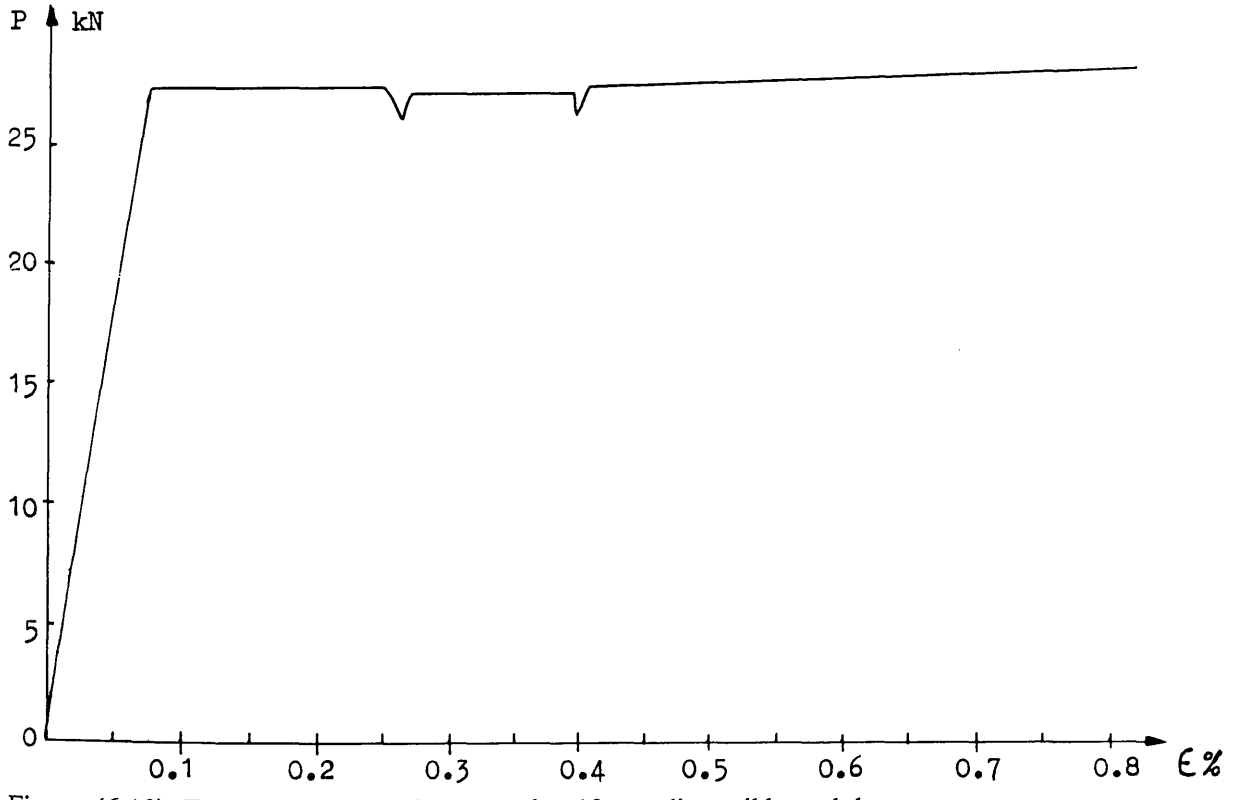

Figure (6.13) Typical stress– strain curve for 10mm dia. mild steel bar.

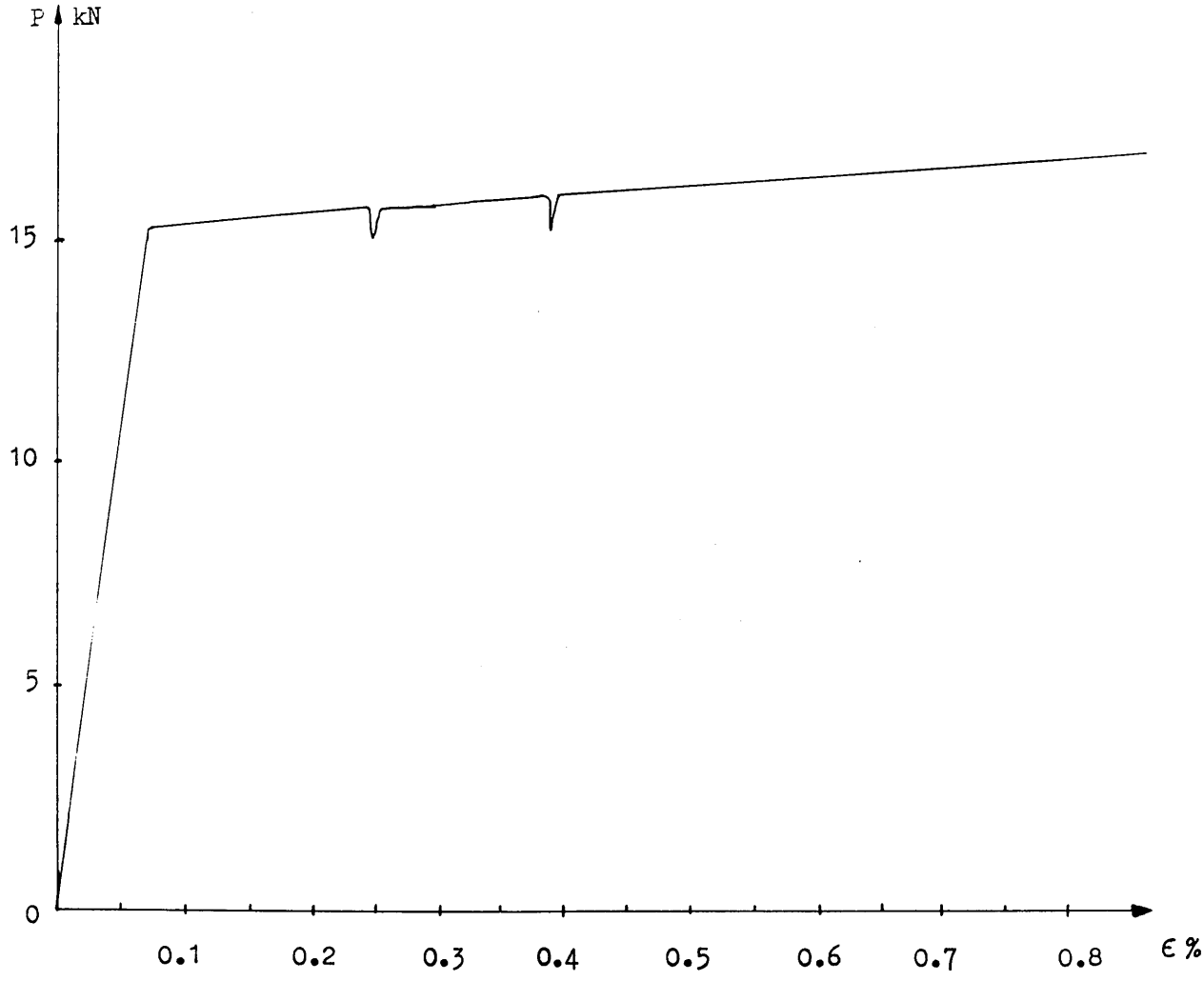

Figure (6.14) Typical stress– strain curve for 8mm dia. mild steel bar.

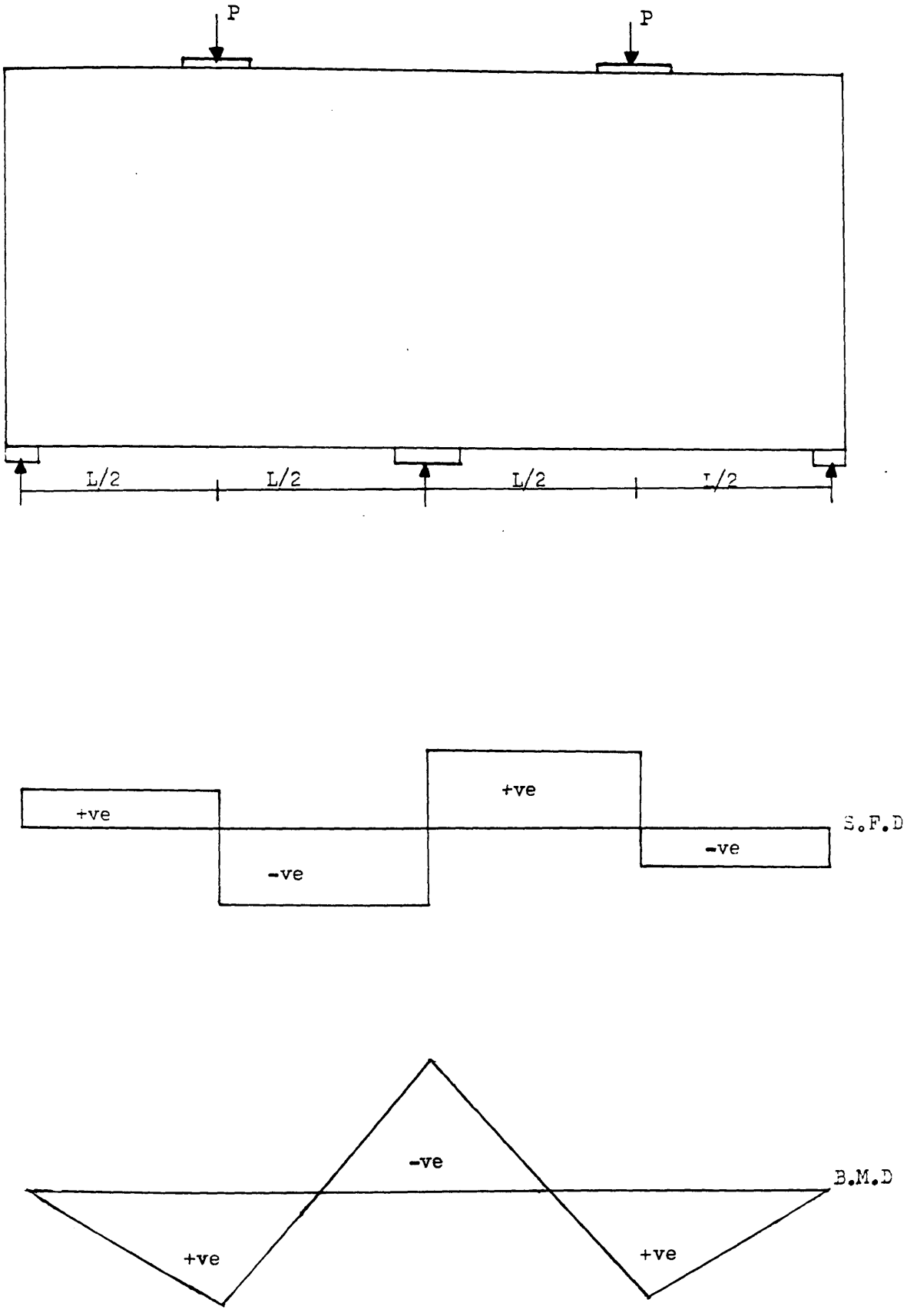

Figure (6.15) The arrangements of loading in a two span continuous girder

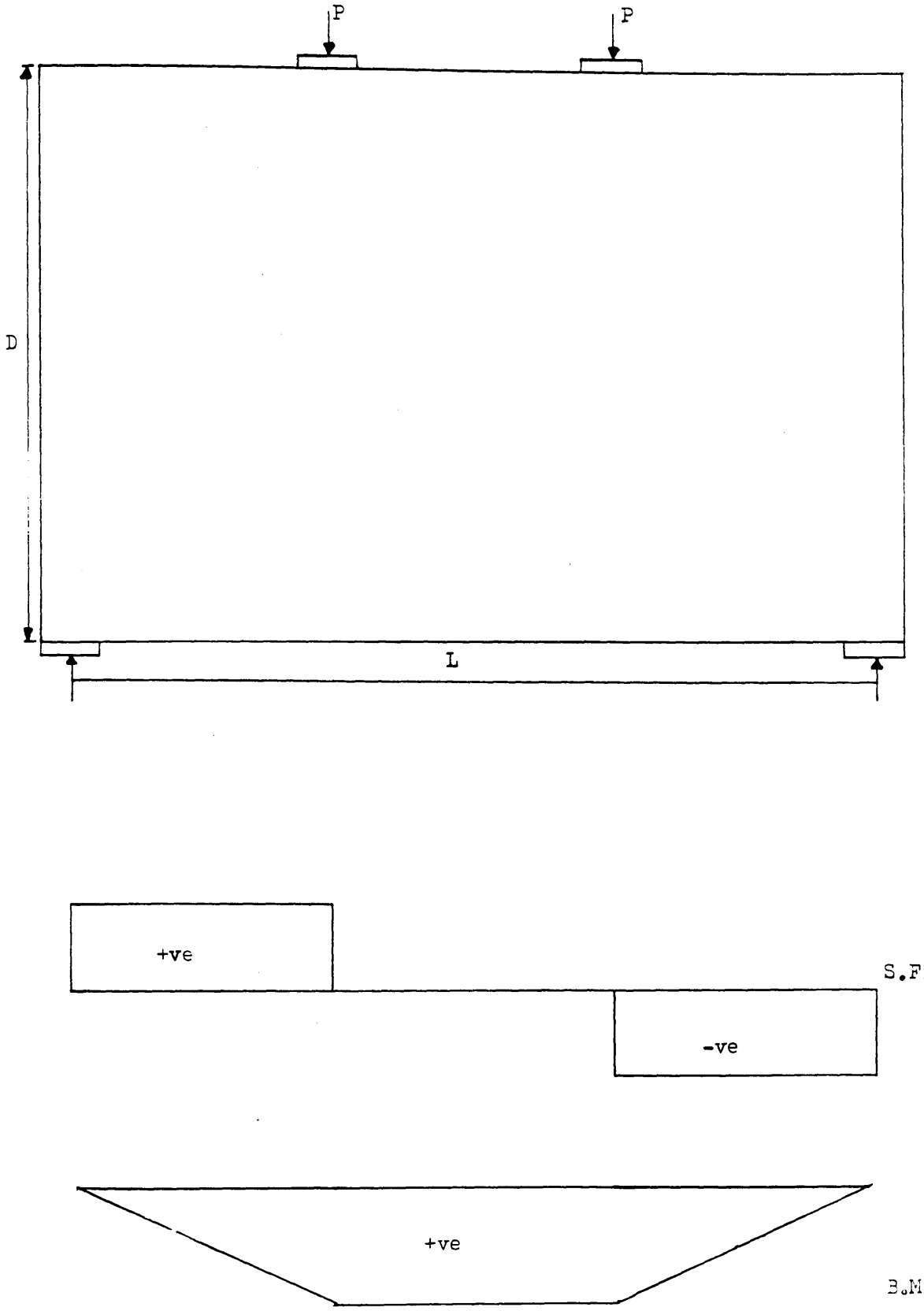

Figure (6.16) The arrangements of loading in a simply supported girder.

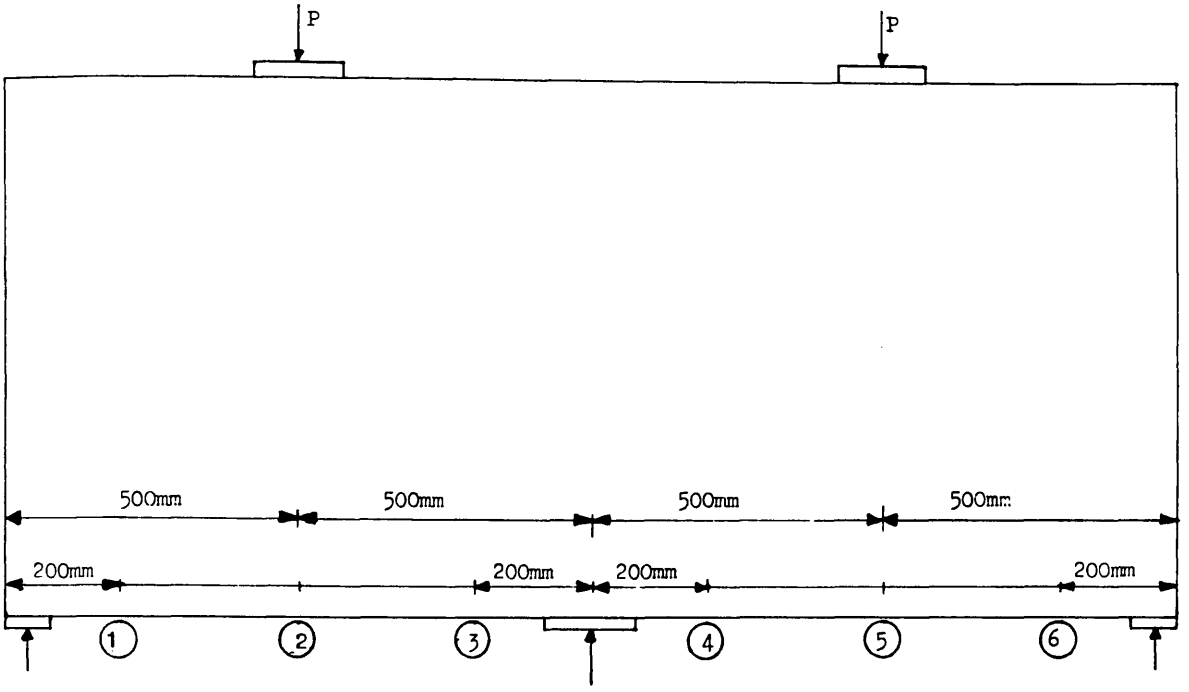

Figure (6.17) Transducer location and position in a continuous girder.

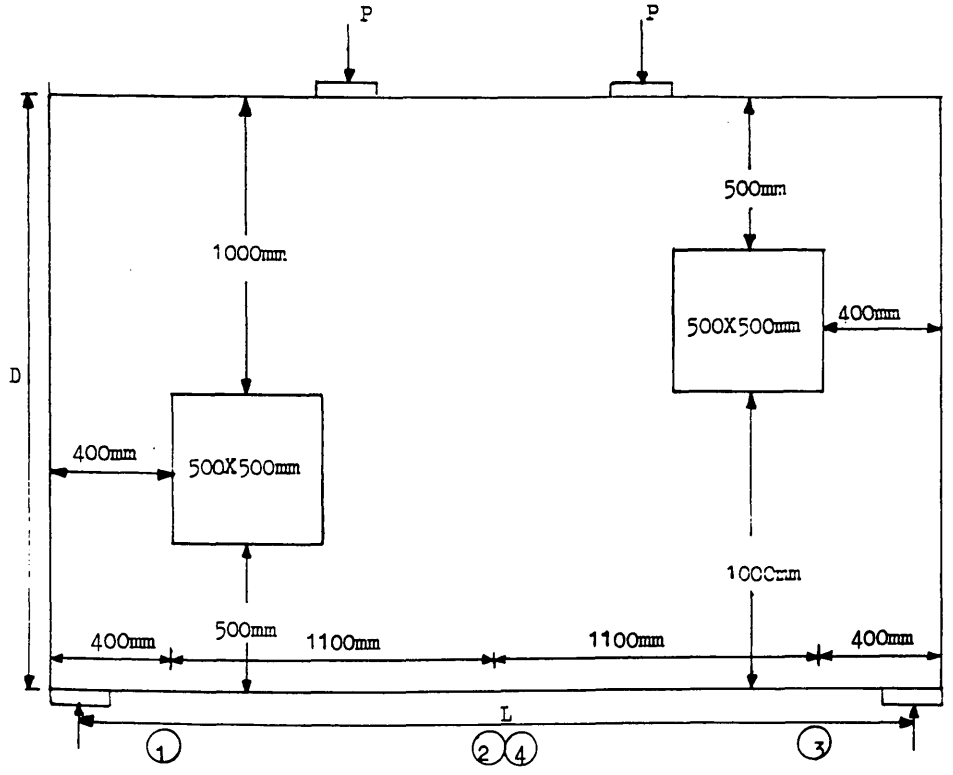

Figure (6.18) Transducer location and position in a single span girder.

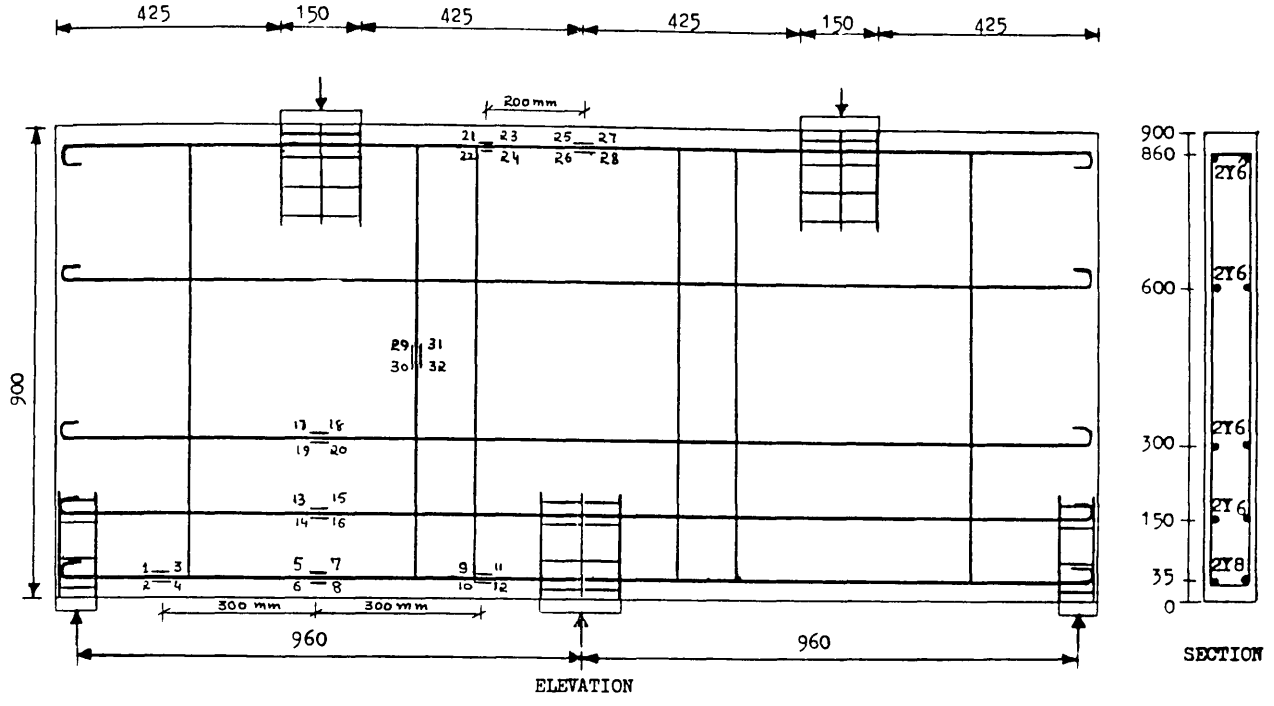

Figure (6.19) The location and position of steel strain gauges in transfer girder TRGRAS1

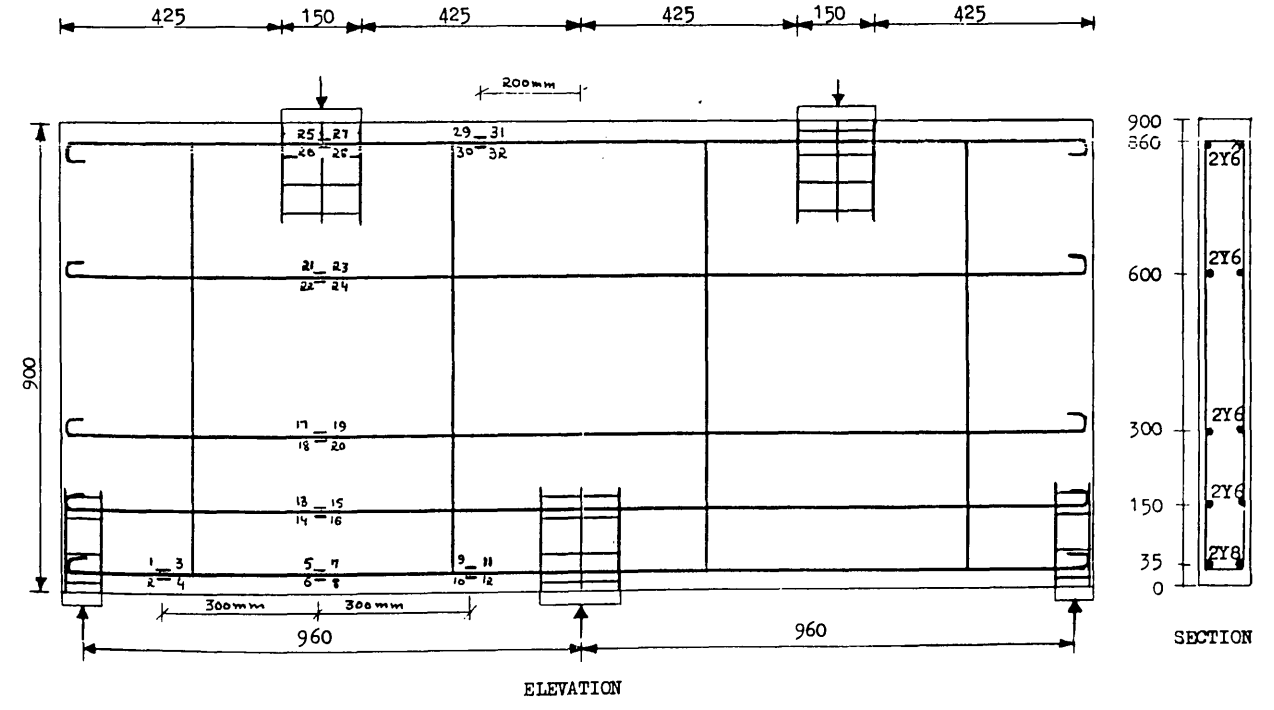

Figure (6.20) The location and position of steel strain gauges in transfer girder TRGRAS2

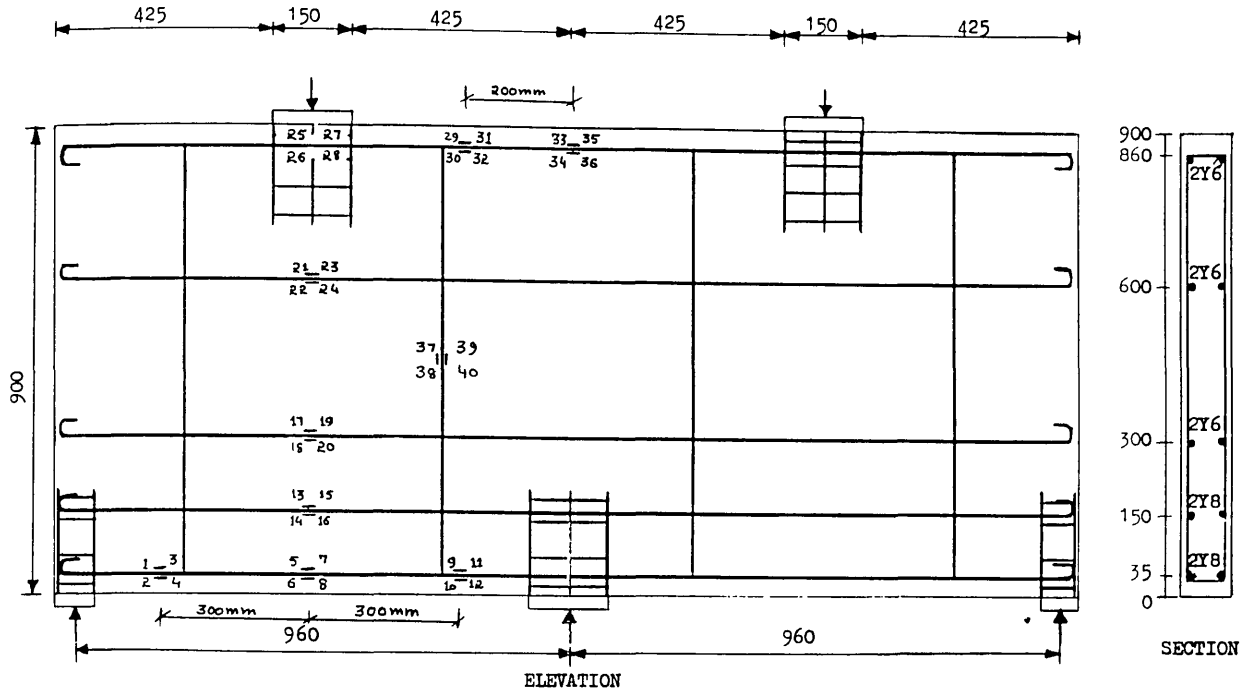

Figure (6.21) The location and position of steel strain gauges in transfer girder TRGRAS3

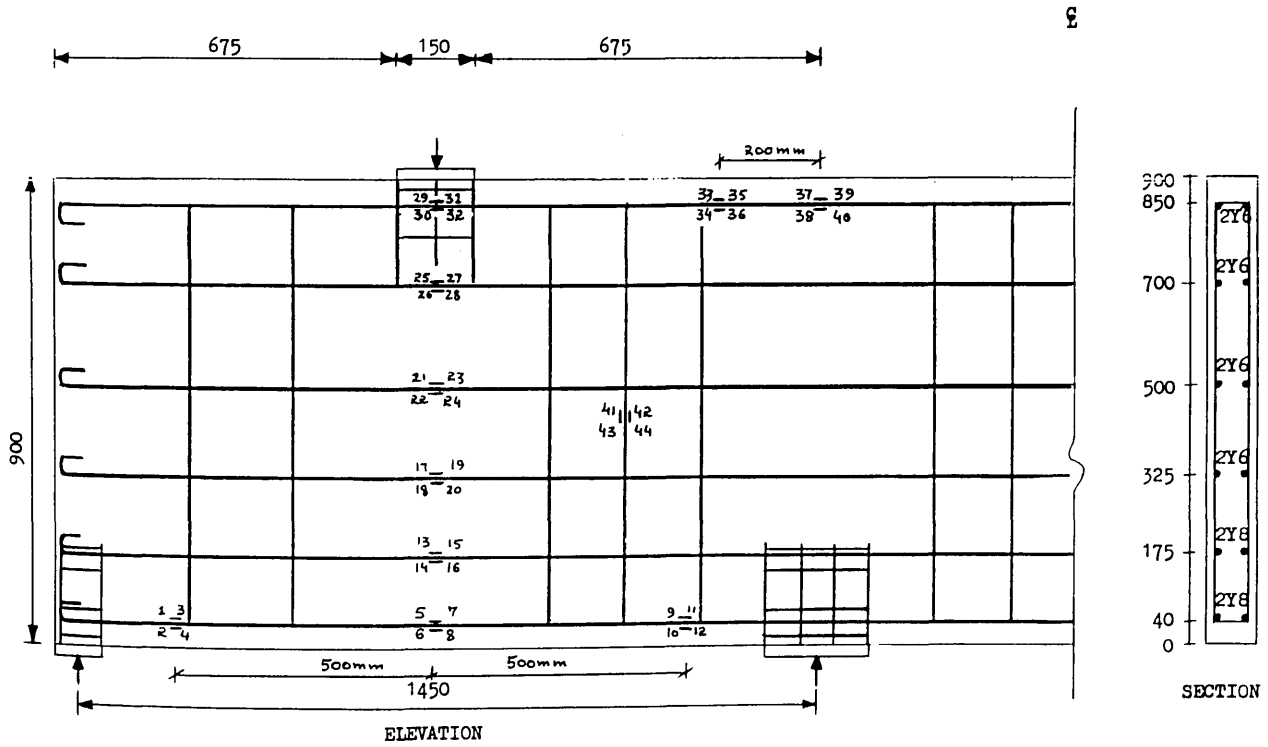

Figure (6.22) The location and position of steel strain gauges in transfer girder TRGRAS4

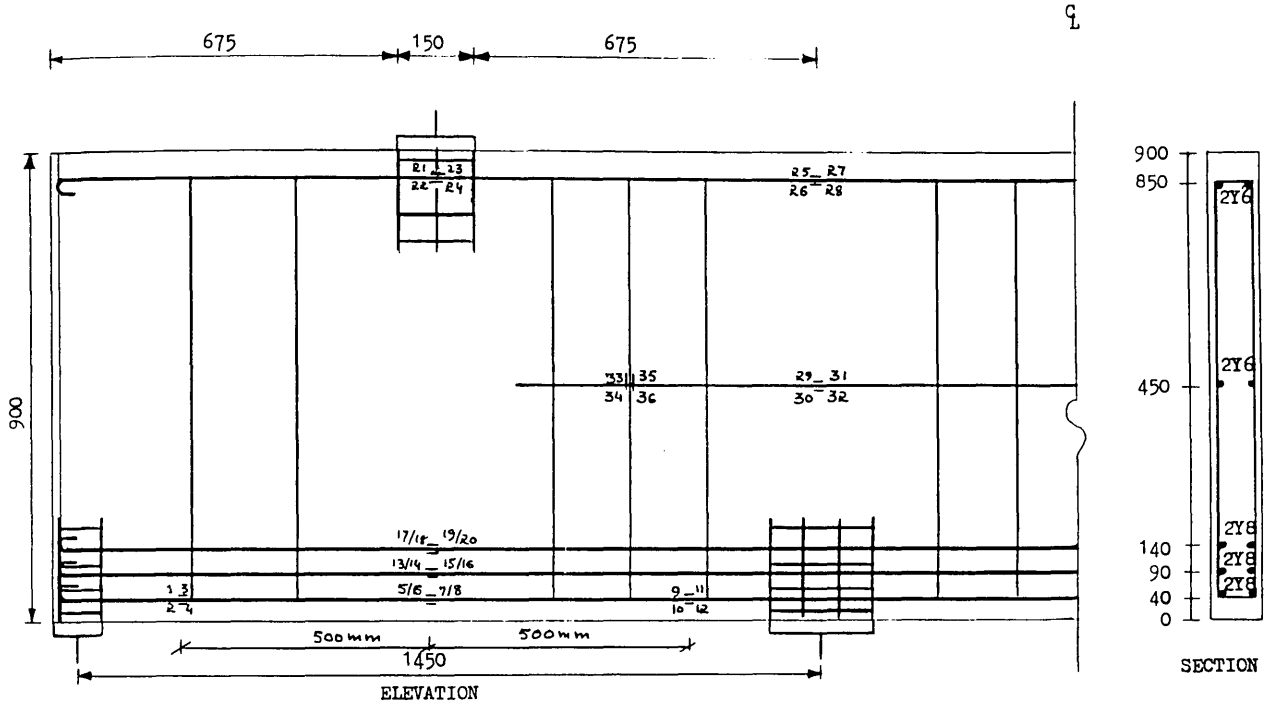

Figure (6.23) The location and position of steel strain gauges in transfer girder TRGRAS5

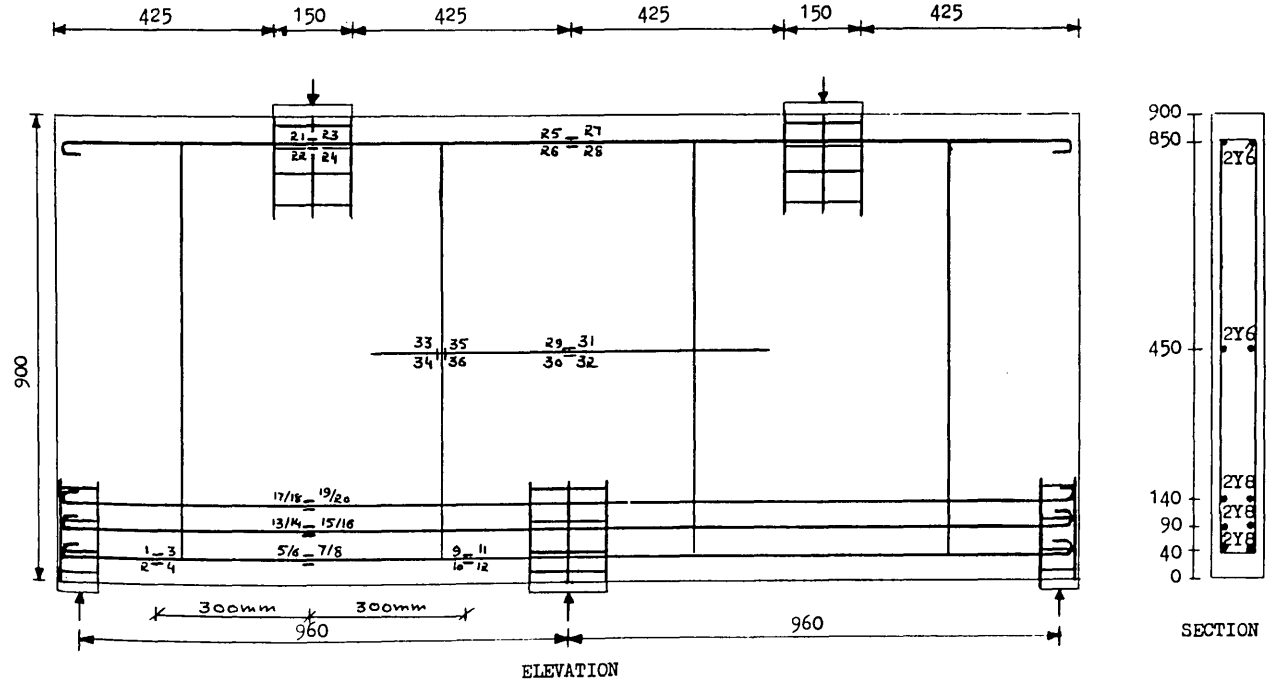

Figure (6.24) The location and position of steel strain gauges in transfer girder TRGRAS6

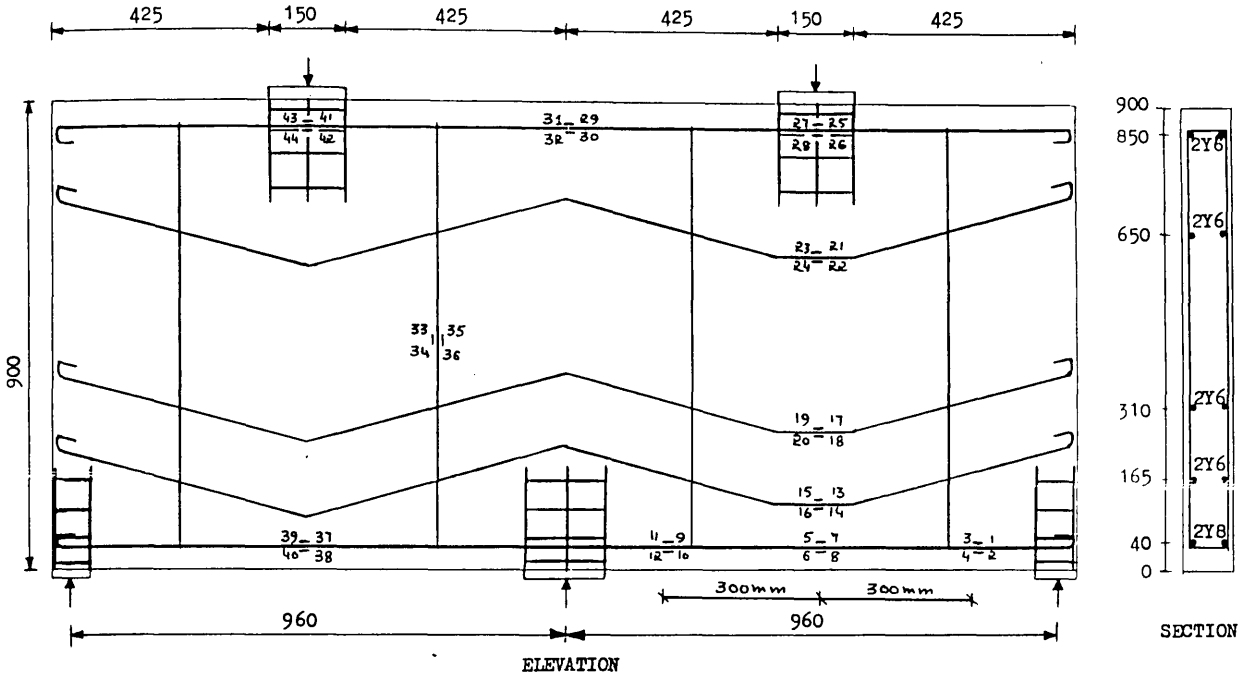

Figure (6.25) The location and position of steel strain gauges in transfer girder TRGRAS7

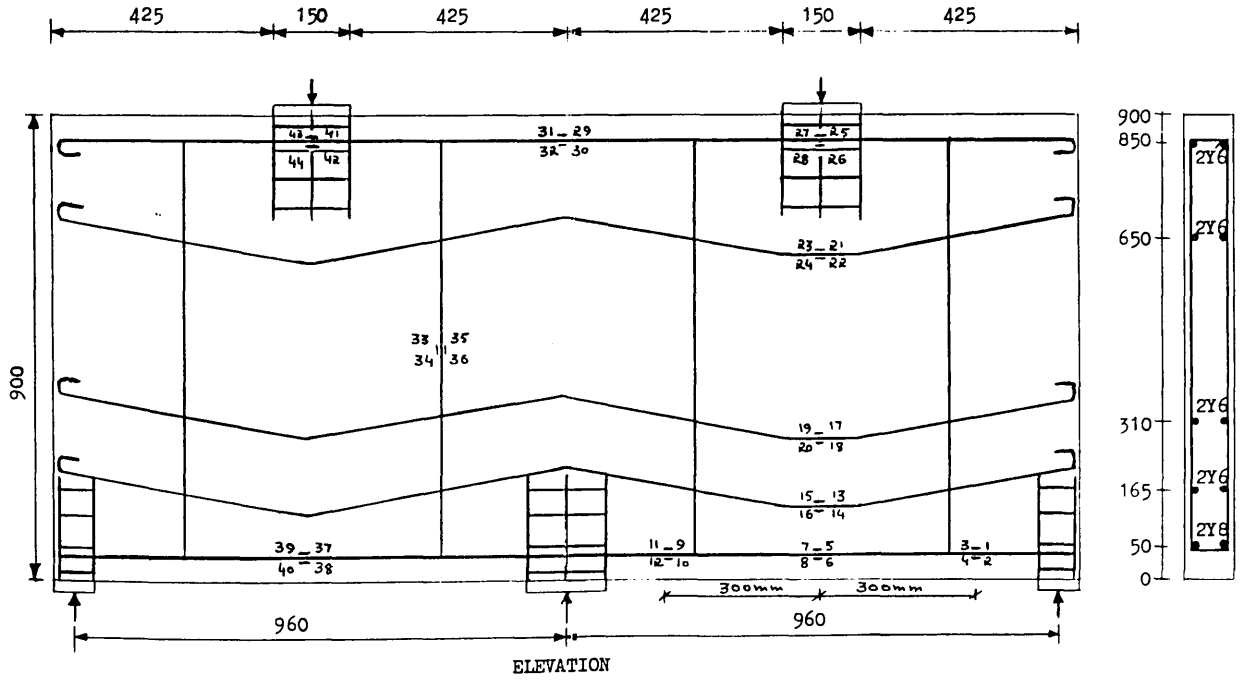

Figure (6.26) The location and position of steel strain gauges in transfer girder TRGRAS8

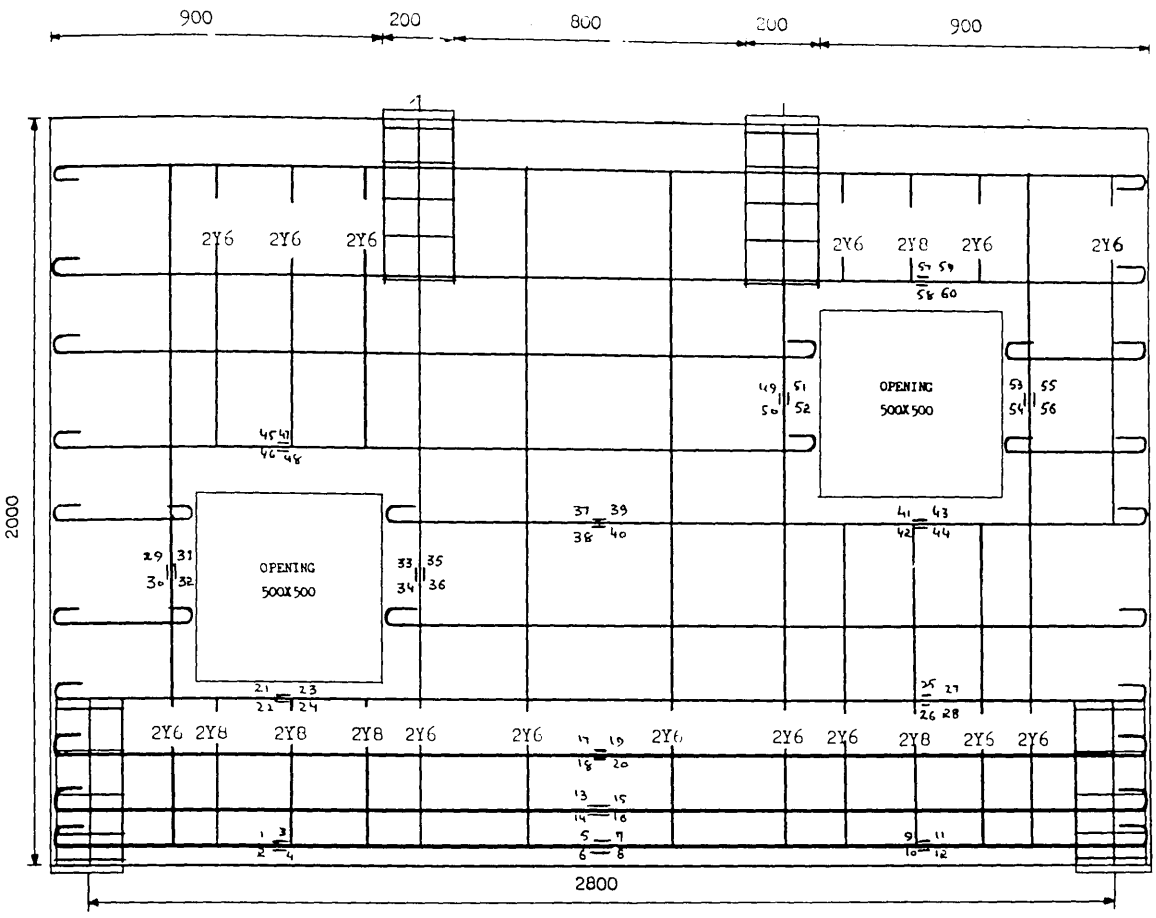

Figure (6.27) The location and position of steel strain gauges in transfer girder TRGRAS9

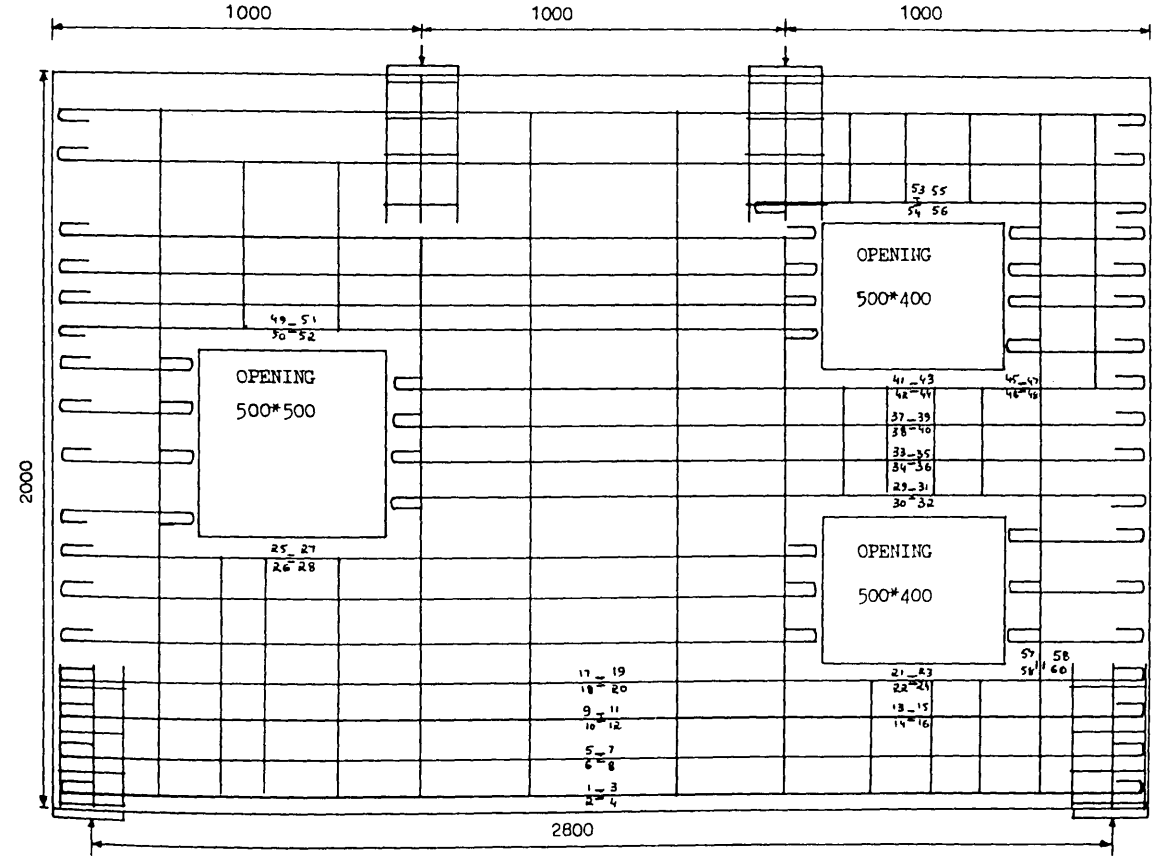

Figure (6.28) The location and position of steel strain gauges in transfer girder TRGRAS10

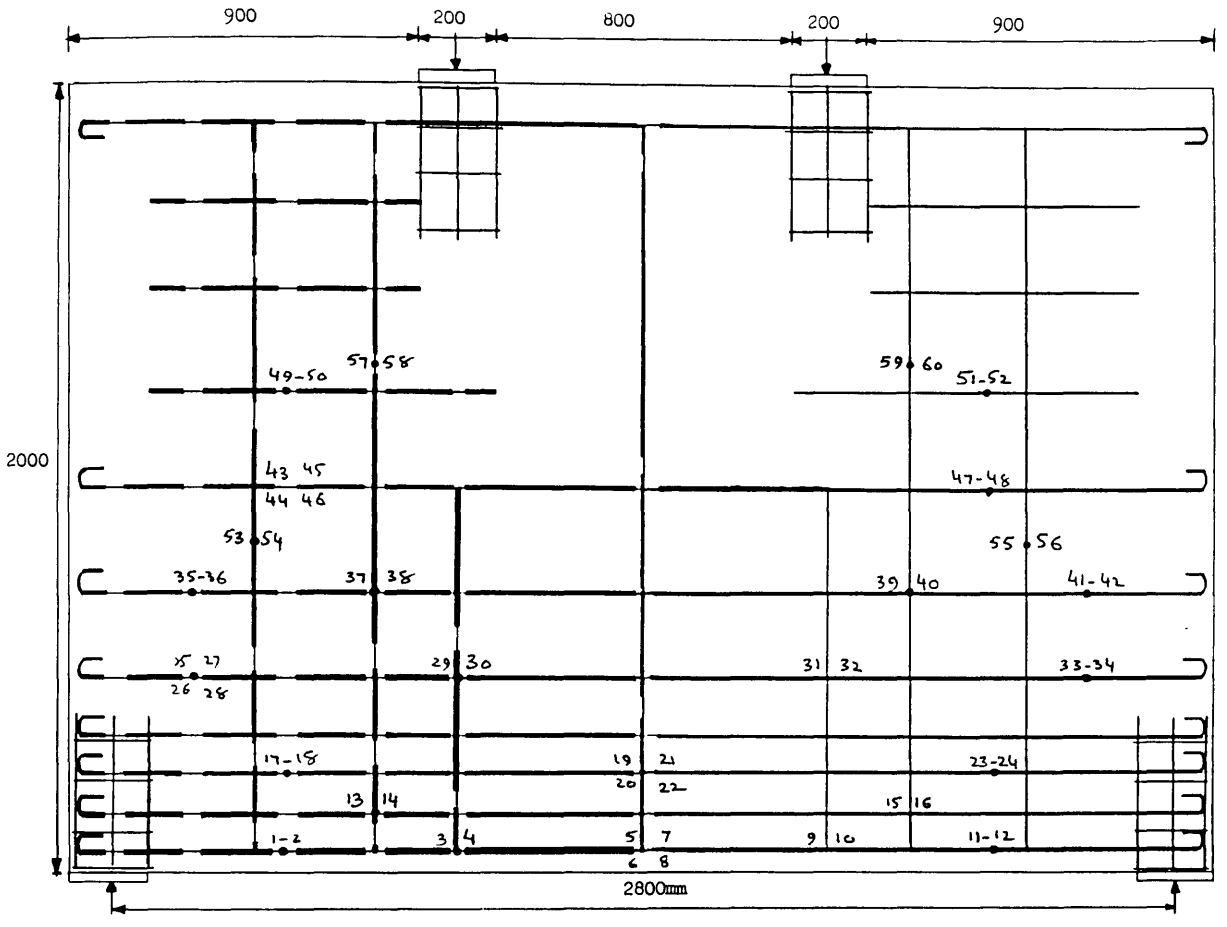

Figure (6.29) The location and position of steel strain gauges in transfer girder TRGRAS11

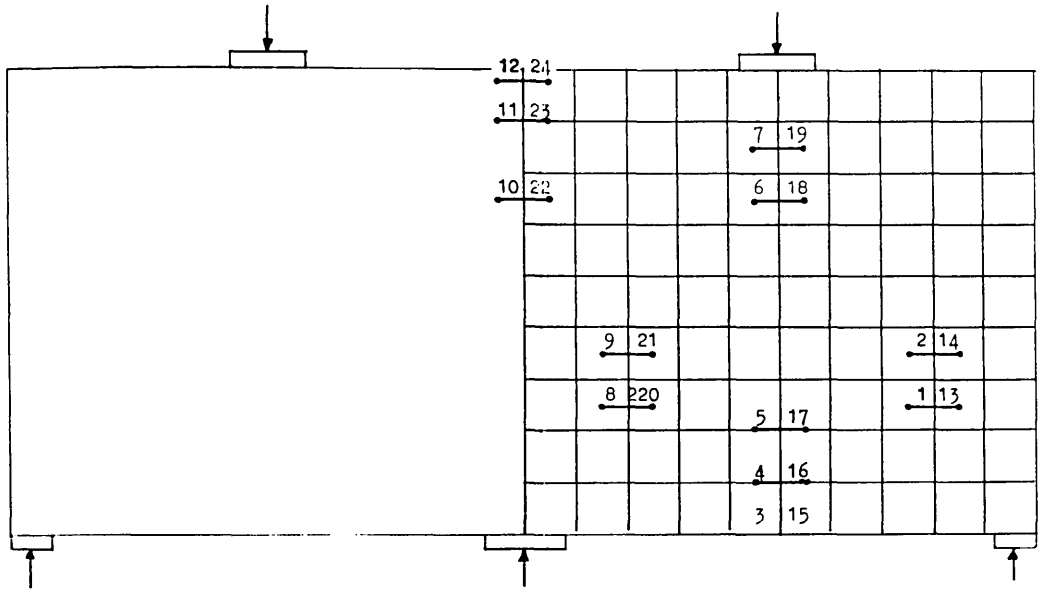

Figure (6.30) The location and position of demec gauges in transfer girder TRGRAS1

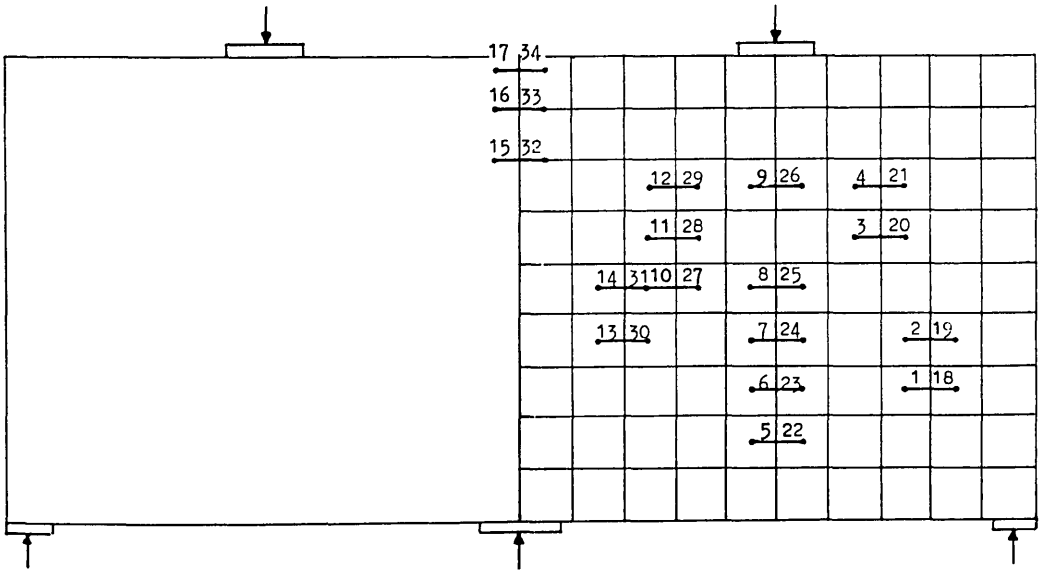

Figure (6.31) The location and position of demec gauges in transfer girder TRGRAS2

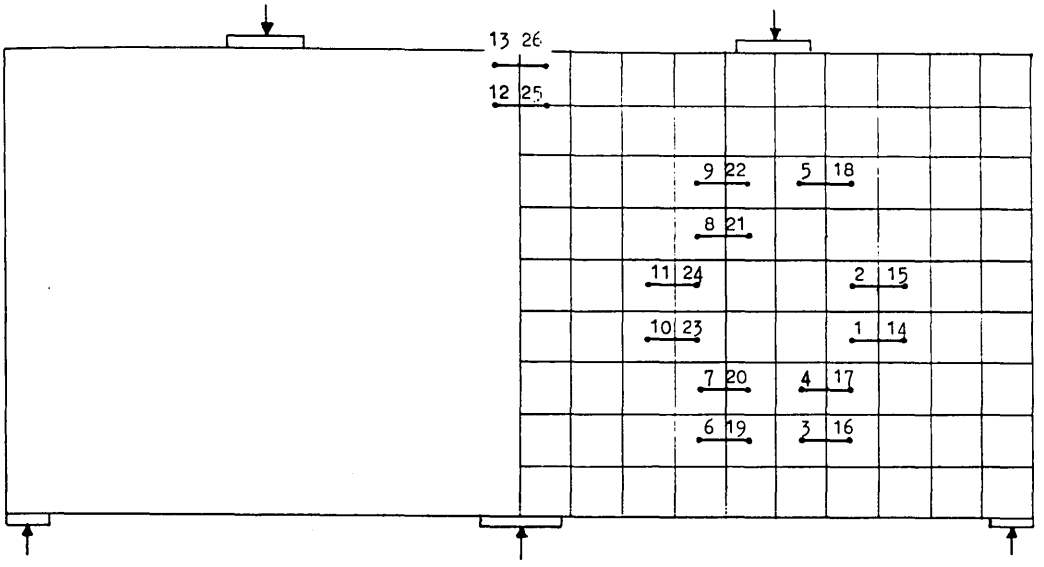

Figure (6.32) The location and position of demec gauges in transfer girder TRGRAS3

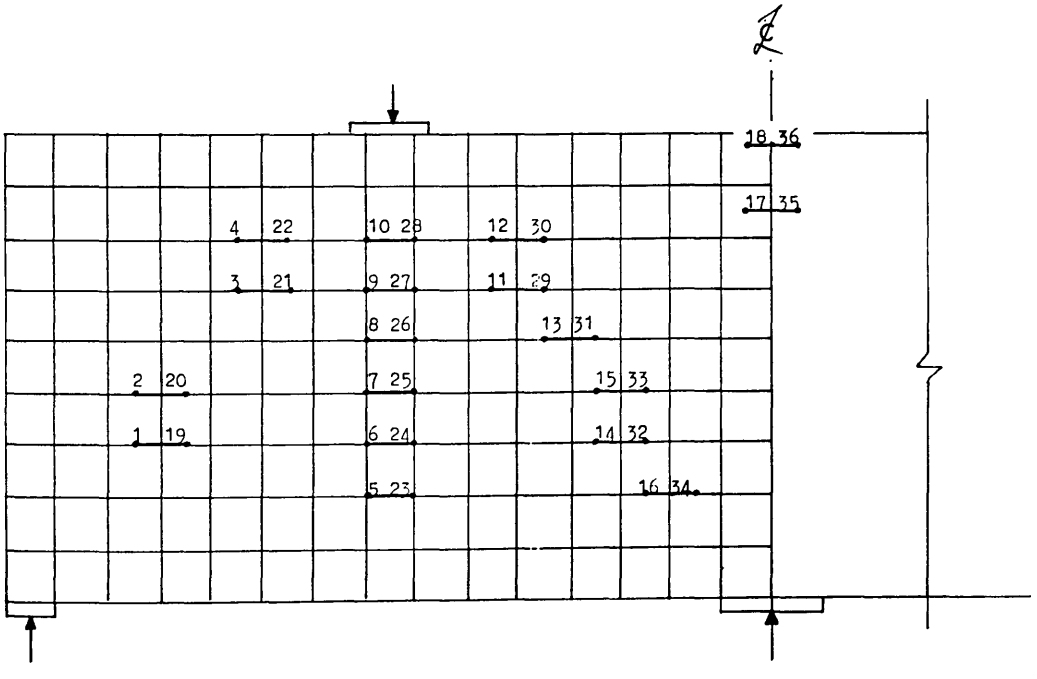

Figure (6.33) The location and position of demec gauges in transfer girder TRGRAS4

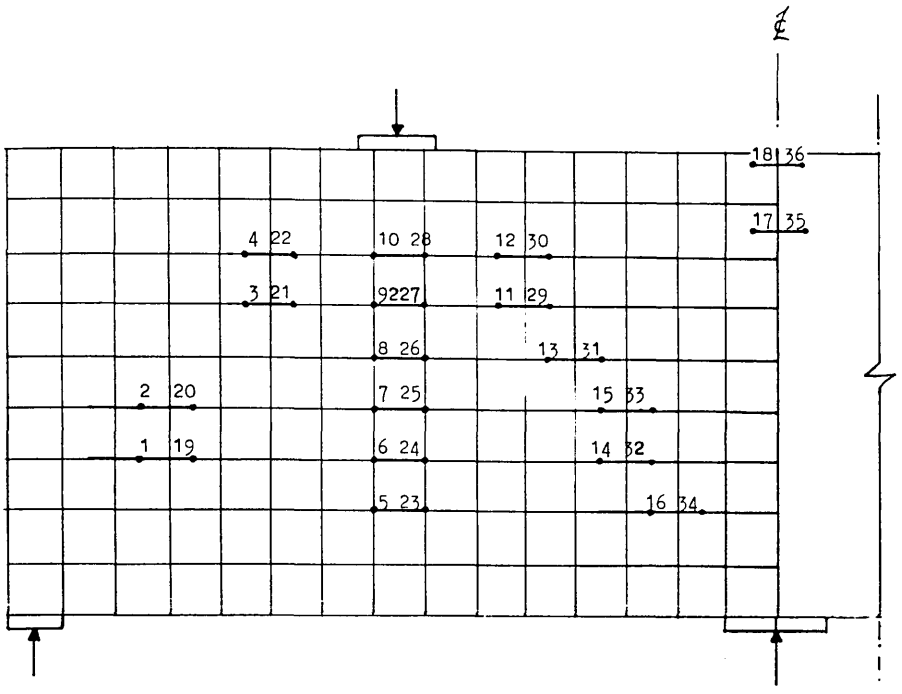

Figure (6.34) The location and position of demec gauges in transfer girder TRGRAS5

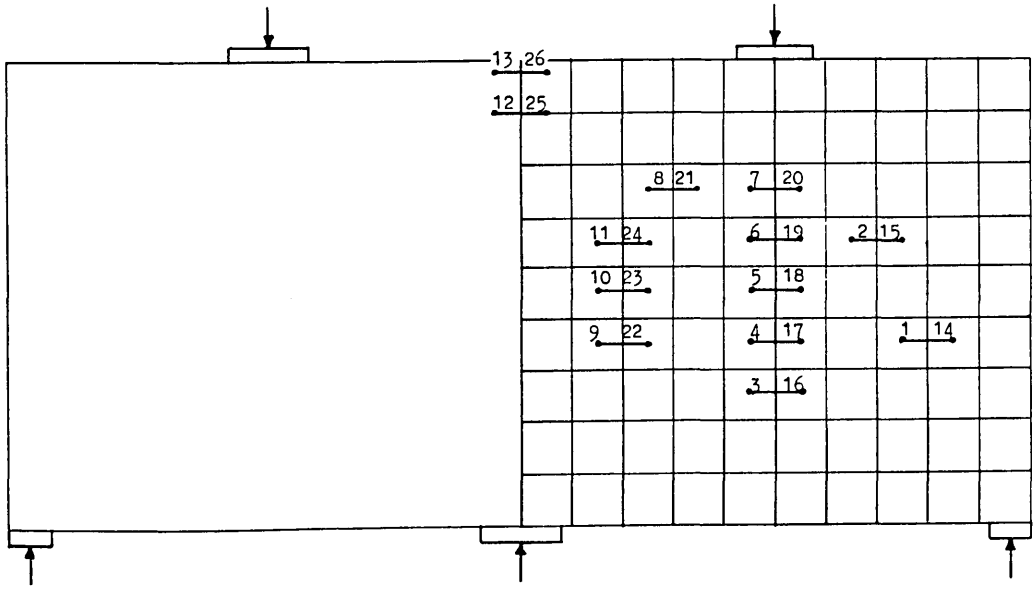

Figure (6.35) The location and position of demec gauges in transfer girder TRGRAS6

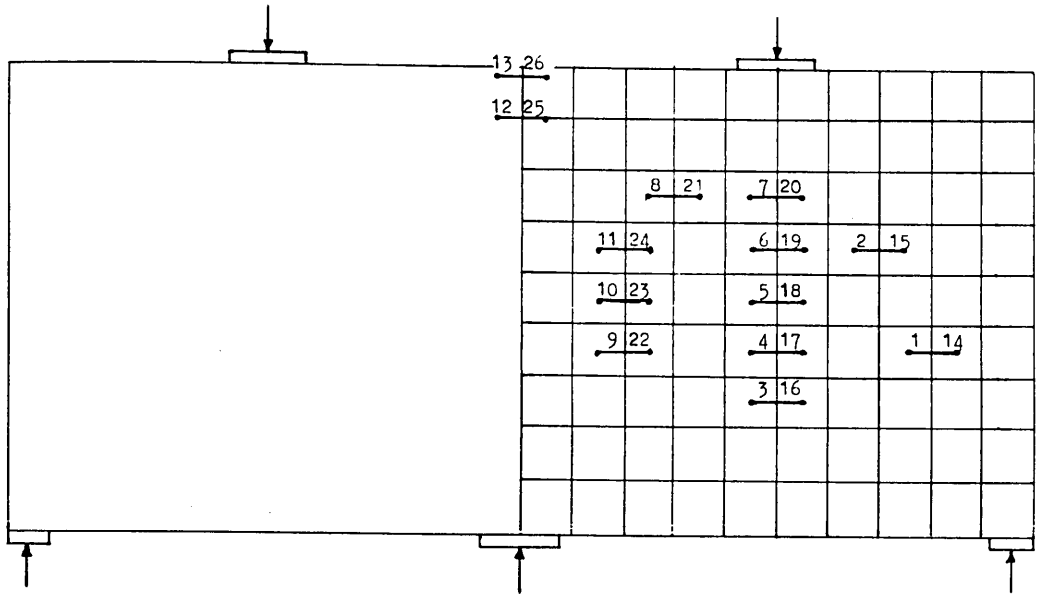

Figure (6.36) The location and position of demec gauges in transfer girder TRGRAS7

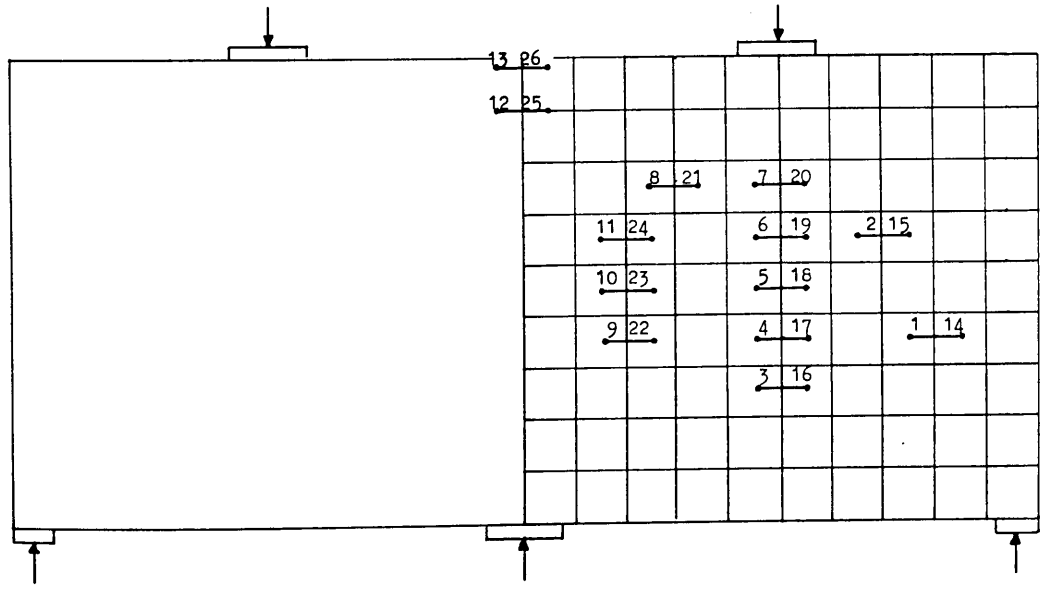

Figure (6.37) The location and position of demec gauges in transfer girder TRGRAS8

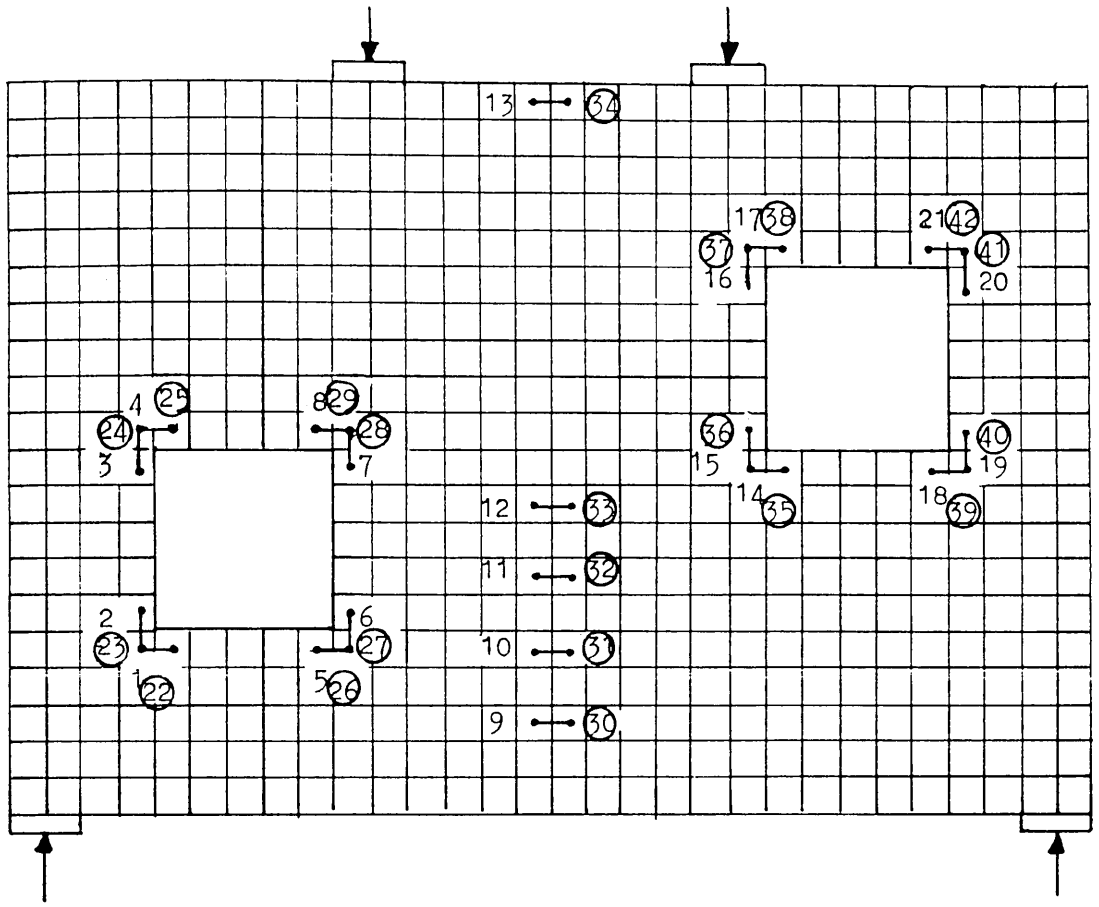

Figure (6.38) The location and position of demec gauges in transfer girder TRGRAS9

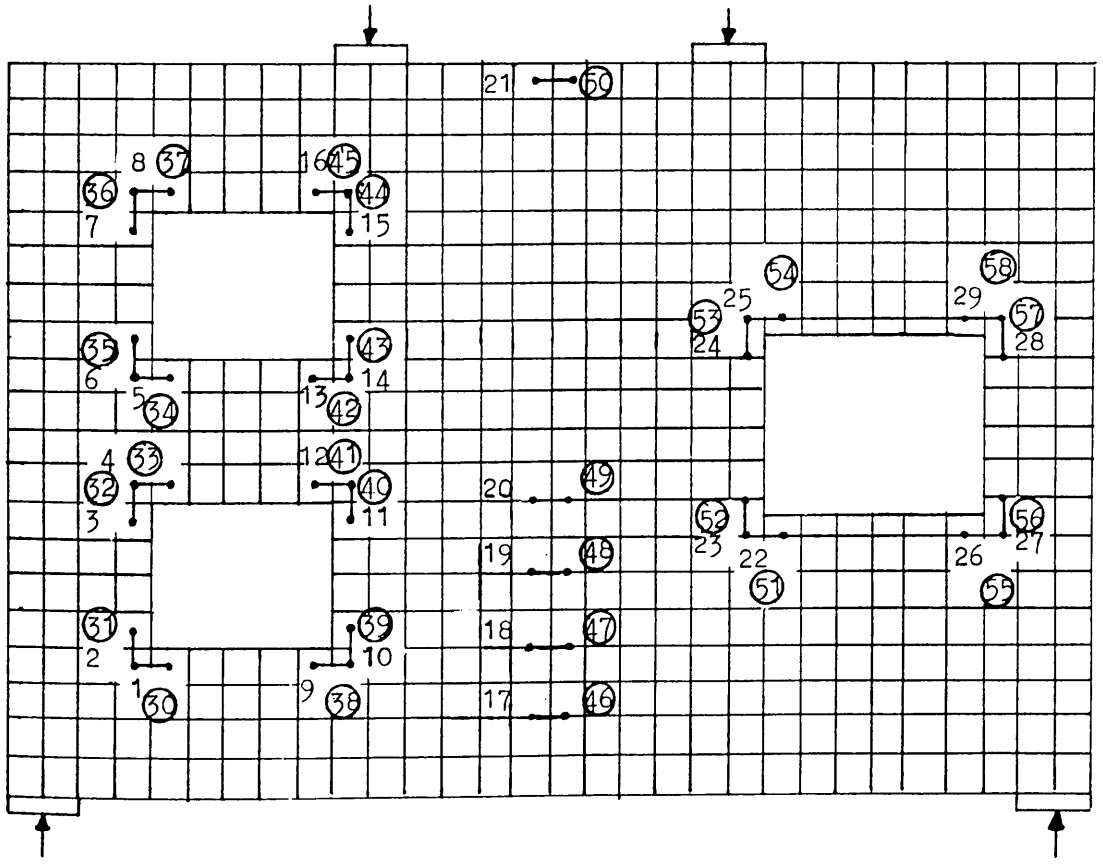

Figure (6.39) The location and position of demec gauges in transfer girder TRGRAS10

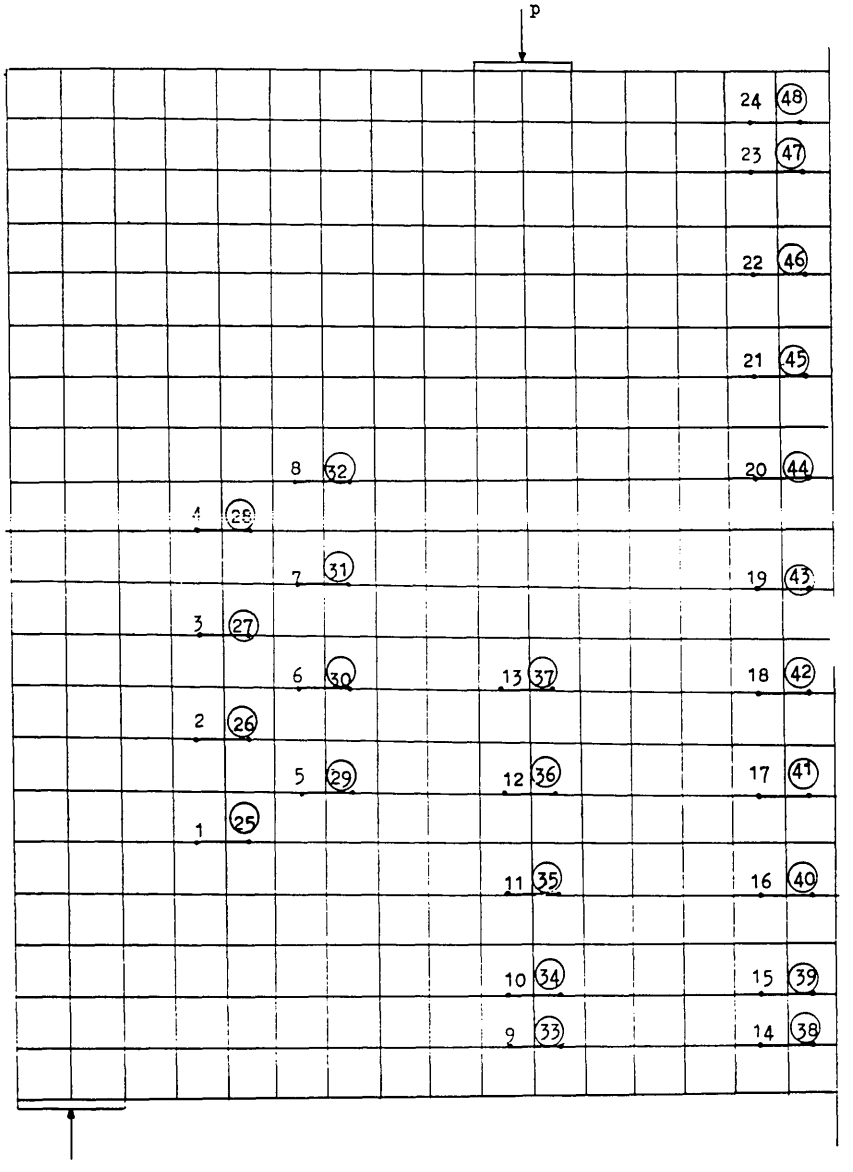

Figure (6.40) The location and position of demec gauges in transfer girder TRGRAS1

References

1. BRITISH STANDARDS INSTITUTION, "Code of practice for the structural use of concrete", CP110: Part 1, London 1972.

2. BRITISH STANDARDS INSTITUTION, "Code of practice for the structural use of concrete", BS8110: Part 1, London 1985.

3. OVE ARUP PARTNER, "The design of deep beams in reinforced concrete", Construction industry research and information association (CIRIA), Guide 2, London 1977.

4. LEONHARDT, F. and WALTHER, R., "Wandartige trager, Deutscher ausschuss fur stahlbton, Vol. 178, Wilhelm ernst and sohn, Berlin, West Germany, 1966.

5. Comite europen du beton– federation internationale de la precontrante, "International recommendations for the design and construction of concrete structures", Appendix 3, Deep beams, Cement and concrete association, London June 1970.

6. LIN, C.K., "Ultimate strength design of deep beams", M.Sc. Thesis, University of Glasgow, 1979.

7. BRITISH STANDARD INSTITUTION,"The use of structural steel in building", BS 449 Part 2, 1969.

8. BRITISH STANDARD INSTITUTION,"Methods for testing of metals", Part 1, Non– Ferrious Metals, BS 18, Part 1 1970

CHAPTER SEVEN

PRESENTATION OF EXPERIMENTAL RESULTS

7.1 Introduction

This chapter presents the results of the experimental tests on the transfer girders described in the previous chapter. The purpose of the experimental investigation was:

1. To validate the direct design procedures for designing deep beams in general, and continuous deep girders in particular, for serviceability and ultimate conditions.
2. For two span continuous girders, to study:

(i) the effect of shear reinforcement

(ii) the effect of the span to depth (L/D) ratio on the ultimate strength and the failure mechanism. Two span to depth ratios (L/D) were examined, 1.07 and 1.61.

(iii) the effect of placing the main reinforcement according to the CIRIA Guide 2[1] distribution (similar to the CEB– FIP Model Code[2]).

(iv) the effect of using skew reinforcement.

3. For single span girders with L/D ratio of 1.4, to study:

(i) the validity of the direct design approach when the web openings intercept the load path.

(ii) the behaviour of a very large scale solid deep girder with reinforcement which satisfies the design theory as close as possible, by reducing the bar size diameters to the required value.

A summary of all the results is presented in Table 7.1. The tests are classified into five series depending on the geometry, reinforcement type (i.e orthogonal or skew), reinforcement distribution or the continuity conditions. In all the tests the loads were applied under displacement control in small increments, average value of 50kN, up to failure. Each series will be discussed separately in the following sections.

7.2. Experimental observations

7.2.1 Series 1

This series was designed to test the validity of the direct design approach using

orthogonal reinforcement for two span continuous deep girders, whose span to depth (L/D) ratio was 1.07.

Four girders denoted TRGRAS1, TRGRAS2, TRGRAS3 and TRGRAS6 were tested and had similar cross-sections, span lengths and thicknesses, as shown in Figure (7.1). Girder TRGRAS1 and TRGRAS2 had the same amount and distribution of main reinforcement, but girder TRGRAS1 had twice the shear reinforcement in the interior shear spans. Test girders TRGRAS2 and TRGRAS3 had similar amounts of shear reinforcement, but TRGRAS3 had a higher amount of main reinforcement. Girders TRGRAS3 and TRGRAS6 were designed for the same design ultimate load, but the distribution of steel in girder TRGRAS6 was placed according to the rules of CIRIA Guide 2[1], which is the same as that suggested by the CEB-FIP Model Code[2] and Leonhardt and Walther[3]. The steel properties of girder TRGRAS3 were different from those of TRGRAS6, consequently the amount of steel provided was not exactly the same, otherwise a direct comparison in terms of steel area could have been made.

Transfer Girder TRGRAS1

Girder TRGRAS1 was designed for an ultimate design load of 850kN, but for practical reasons was reinforced with more shear reinforcement in the interior shear span than required by the direct design technique.

The first visible crack appeared at the bottom of the beam soffit at a load of 200kN. On further increase in loading, more cracks spread in the flexural zone of the beam and started propagating towards the loading points. Before cracking, steel strains were very small. As cracking progressed the steel strains started to increase and the displacements became considerably higher than the pre-cracking values. On a further increase in the load, cracks became wider and at 986kN inclined cracks appeared in both internal shear spans of the beam with a loud "thud" and the load suddenly dropped. The steel strains were also high, at some points the steel had yielded. The girder continued to take more load after the formation of the diagonal

cracks. The steel strains show that, at some points, forces in bars which originally took compression began to reduce and even became tensile.

The girder finally failed in a clear shear failure mode as shown in Figure (7.2). Failure occurred in one of the interior shear spans with a diagonal crack running from the inside edge of the support towards the outside edge of the loading point. The other span was severely cracked and looked as if it had also lost its stiffness and strength. Some crushing and spalling of concrete at the loading point was noticed as well. At failure all the steel except the stirrups had yielded at the measured points and was well above the yield stress.

Figure (7.3) illustrates the load deflection curve, and shows that the behaviour was linear up to the cracking of the concrete. This confirms that reinforced concrete beams behave much like plane concrete beams up to the concrete cracking or the yielding of the steel, whichever is first. The plots of longitudinal and transverse steel strains, shown in Figures (7.4) to (7.7), indicate that the bars carried relatively small strains before cracking. The steel strain in the bottom bars, along the span length, are plotted in Figure (7.8). This shows that the strains were more or less uniform along the beam length and did not behave according to the ordinary bending moment diagram of the beam.

The maximum crack width was monitored as shown in Figure (7.9). From this the 0.3mm crack width serviceability load was determined to be 900kN. Figure (7.10) shows the variation of concrete surface strains for increasing load. These tend to show a marked increase after the shear crack appeared at load 900kN.

It is worth noting that the beam was able to take a considerable increase in load after the diagonal crack formed. This is due to the development of arching action in conjunction with dowel action of the main reinforcing bars and interface shear transfer across the shear cracks. The ratio of the serviceability load to design ultimate load was 1.06 and the ratio of ultimate load to design ultimate load was

1.56. This confirms that serviceability behaviour of the design technique is good, whilst the measured ultimate load indicates a fair safeguard against collapse. The overall behaviour confirms the validity of the direct design technique.

Transfer Girder TRGRAS2

This girder was also designed for an ultimate load of 850kN. It was reinforced with the same amount of main reinforcement as TRGRAS1, but with half the shear reinforcement in the interior shear spans.

The first visible crack appeared at the bottom of the beam soffit at 250kN. As the load increased, the cracks started propagating and extending towards the loading point. Steel strains were very small before cracking, but as cracking progressed the steel strains increased. At 1050kN a diagonal crack occurred with a loud "thud", immediately reaching a width of 1.3mm and causing the deflections to increase drastically. At this load the steel started yielding at the centre of the girder span in the bottom bars, and the steel strains increased to almost twice the total at the previous increment. On further loading, cracks widened and the beam continued to take load. Finally, at a load of 1216kN the beam failed in a shear failure mode with some crushing of the concrete at the load and supporting points. At failure, all steel was carrying tensile forces and the strains in all steel bars were well above the yield value, except the top bars. The crack pattern at failure is shown in Figure (7.11).

The load deflection curve is shown in Figure (7.12). It illustrates that after the formation of the inclined crack, the stiffness of the girder reduced considerably. The steel strain in all bars at the centre of the span is shown in Figure (7.13), these demonstrate similar behaviour to the load deformation behaviour. The steel strains in the top bar, 200mm from the centre of the intermediate support, are illustrated in Figure (7.14). The distribution of strain along the bottom bar is shown in Figure (7.15) and is different from ordinary beam behaviour.

Crack widths were monitored at various points and are illustrated in Figure (7.16). From these, the 0.3mm crack width serviceability load was determined to be 1050kN. Finally, Figure (7.17) shows the variation of concrete surface strains for increasing load, these show a marked increase after the shear crack at load 1050kN.

Since concrete strength was higher in this girder, the shear crack appeared at a higher load, therefore, the 0.3mm crack width for serviceability also occurred at a higher load. The smaller amount of shear reinforcement, however, reduced the ultimate load, therefore, the ratio of serviceability load to design ultimate load (1.24) is higher than for girder TRGRAS1, and the ratio of ultimate load to design ultimate load (1.43) is smaller. However, the overall behaviour in serviceability and the ultimate stage is still satisfactory, indicating the suitability of the direct design technique. The comparison between TRGRAS1 and TRGRAS2 indicates that when the amount of reinforcement is closer to that required by the direct design equations, the range between serviceability limit state and ultimate limit state is smaller. This tends to confirm that the concept of simultaneous yielding is reasonable.

Transfer girder TRGRAS3

In the previous two girders, the required shear reinforcement was very small, but using the minimum bar size of 6 mm, the amount of shear reinforcement provided was substantially greater than this. In this girder an attempt was made to avoid this problem. The girder was designed to provide shear reinforcement which was closer to that required by the direct design equations. The idea was to provide the same minimum shear reinforcement as in girder TRGRAS2 and to calculate the design load which corresponds to this amount. It was not possible to calculate this precisely because of geometrical constraints and some other consequences relating to the test–rig. However, a design load of 1100kN was adopted. This higher design load obviously required a substantial increase in the amount of main reinforcement, but the shear reinforcement was the same as girder TRGRAS2.

The first visible crack occurred at 300kN at the centre of the beam span near the soffit. Some flexural cracks occurred in the central span region and propagated towards the loading points as the load was increased. When the load reached 1000kN, it dropped suddenly to 890kN but then started to increase again until, at 920kN, a shear crack suddenly appeared with a loud "thud" in one of the internal shear spans. At 1050kN, the steel started to yield in the centre of the span and the beam finally failed at 1500kN in a clear shear failure. At failure, some crushing of concrete was noticed at the load and support points. It was also observed that there had been about 7mm of relative displacement along the shear planes of the shear cracks, indicating that dowel action must have come into play. Also all the steel had yielded except in some of the top bars. The crack pattern at failure is shown in Figure (7.18).

The load deflection curve, in Figure (7.19), shows that behaviour was linear before cracking and that the girder exhibited a little ductility after diagonal cracking. Figures (7.20) to (7.23) illustrate the steel strain curves and show that some of the main bars started to depart from linear behaviour at about 600kN, whilst others did not start to behave nonlinearly until the shear cracks occurred at about 920kN. Steel strains along the bottom bars are presented in Figure (7.24), these show a different distribution from ordinary beam behaviour.

Crack widths were monitored at four crack points, as shown in Figure (7.25). From these the 0.3mm crack width serviceability load was determined to be 970kN. Finally, Figure (7.26) shows the variation of concrete surface strains for increasing load. These also tend to show a marked increase after the shear crack at about 920kN.

It is worth noting that the beam was able to take a considerable increase in load after the diagonal shear cracks formed. This is due to the development of arching action in conjunction with dowel action from the main reinforcement and interface shear transfer across the shear cracks.

The ratios of the serviceability load to design ultimate load (0.88) and measured ultimate load to the design ultimate load (1.36) are smaller than for girder TRGRAS2 (1.24 and 1.43 respectively). The comparison of TRGRAS2 and TRGRAS3 indicates that when the amount of reinforcement is closer to that required by the direct design equations, the ultimate load is closer to the design load. The overall behaviour in serviceability and ultimate stage is still satisfactory.

Transfer girder TRGRAS6

This girder was designed for the same load as the previous girder i.e 1100kN. The main difference was the placement of main steel. The amount of main steel calculated according to direct design was distributed following the procedure given by CIRIA Guide 2 [1].

The first visible crack occurred at 150kN at the centre of the span near the soffit. As the load was increased, more flexural cracks occurred in the central span region and propagated towards the loading points. Although cracks were spreading, the steel strains and deflections were approximately linear until 700kN. At 1100kN, shear cracks suddenly appeared with a loud "thud" in both shear spans of the beam, running from the loading point to the inside face of the support in both interior and exterior shear spans. After the shear cracks appeared, the steel strains showed an increase, but the steel did not yield. At 1300kN, the steel started to yield in the centre of the span and finally the beam failed at 1486kN in a clear shear failure mode. At failure, some crushing of concrete was noticed at the load and supporting points. All the steel had yielded at failure, except the top bars and stirrups and the top bars over the intermediate support. The crack pattern at failure is shown in Figure (7.27).

The load deflection curve is shown in Figure (7.28), and illustrates that the behaviour was linear before cracking. Figures (7.29) to (7.32) illustrate the steel strain curves and show that they started to depart from linear behaviour at about 700kN. The steel strain along the bottom bars, at various points, is shown in Figure

(7.33). These show a different distribution from ordinary beam behaviour.

Crack widths monitored at various points are illustrated in Figure (7.34). From these the 0.3mm crack width serviceability load was determined to be 900kN. Figure (7.35) show the variation of concrete surface strains for increasing load. These tend to show a marked increase after 1100kN.

Again the beam was able to take considerable increase in load after the formation of diagonal shear cracks due to the arching action, dowel action of reinforcing bars, and interface shear transfer across the shear cracks.

The ratio of serviceability to design ultimate load (0.8) is slightly smaller than for girder TRGRAS3 (0.88), whereas the ratio of ultimate load to design ultimate load (1.35) is practically equal. It would appear that when the reinforcement is distributed according to CIRIA Guide 2, behaviour is marginally worse than the direct design distribution.

7.2.2 Series 2

This series consisted of two continuous girders denoted TRGRAS4 and TRGRAS5, whose span to depth (L/D) ratio was 1.61.

Both girders had similar cross sections, span lengths, thicknesses, amount of shear and main reinforcements, loading conditions, but different distributions of the main reinforcement. Girder TRGRAS4 was reinforced according to the averaging procedure used in the direct design technique, while girder TRGRAS5 was reinforced using the distribution given by CIRIA Guide 2[1].

Transfer girder TRGRAS4

This girder was designed for an ultimate load of 850kN. Apart from the (L/D) ratio and the amount of reinforcement this girder was identical to girder TRGRAS2. The aim of this test was to ascertain the effect of the span to depth (L/D) ratio on the

ultimate and serviceability behaviour, and the failure mechanism.

The first visible crack occurred at 100kN in the beam soffit in the maximum tensile zone. On a further increase in the load, more flexural cracks occurred in the central span region and propagated towards the loading points. At 600kN, cracks started to appear over the top of the intermediate support in the tensile zone. A further load increase caused more cracks to appear in this region and extend towards the support. Up to 749kN the deflections and the steel strains were very small and were approximately linear. Steel started yielding at the centre of the girder span at a load of 789kN. At 900kN a shear crack appeared with a loud "thud" in one of the internal shear spans. Final failure of the beam was at 1143kN in a shear mode. All the steel had yielded except the stirrups and the top bars. The final crack pattern at failure is shown in Figure (7.36).

The crack pattern indicates that the cracks over the intermediate support are similar to those at the mid–span of the girder. This crack pattern was different to the pattern found in the girders of series 1 and confirms that as the span length of a girder increases, the behaviour changes from deep beams towards ordinary beams. However, the behaviour is still in the range of deep beams, because the flexural cracks appeared first in a positive bending moment region rather than in a region of negative bending moment existing over the intermediate support.

The load deflection curve in Figure (7.37) exhibited a different behaviour in comparison to the previous series. The deflections were higher which was according to expectations, but the shape of the curve suggests much greater ductility. The behaviour was linear before cracking, Figures (7.38) to (7.41) show that the steel strain curves were approximately linear up to 600kN. The steel strain in the bottom bars at various points along the beam length are shown in Figure (7.42). Although this beam has a larger length than the previous series, this strain distribution is still different from ordinary beam behaviour.

Crack widths were monitored at several points and are illustrated in Figure (7.43). From these, the 0.3mm crack width serviceability load was determined to be 800kN. Figure (7.44) shows the variation of concrete surface strains for increasing load, these tend to show a marked increase after about 600kN.

The ultimate load was closer to the design ultimate load than in the previous series, but as before the beam still took a considerable increase in load after the formation of inclined crack and behaved with an arching action.

The ratios of serviceability load to design ultimate load (0.90) and measured ultimate load to design ultimate load (1.27) indicate satisfactory serviceability and ultimate behaviour. Although the amount of reinforcement provided was higher than in girder TRGRAS2, the serviceability and ultimate strength are smaller. This can in part be attributed to different material properties. However, the trend of load deflection, steel strain curves and crack pattern indicate a different behaviour than girder TRGRAS2. In particular, the cracking over the intermediate support is much more extensive and the load deflection and steel strain curves suggest that ductility was considerably higher in TRGRAS4 than TRGRAS2.

Transfer girder TRGRAS5

This girder was also designed for an ultimate load of 850kN. It was reinforced with the same amount of reinforcement as TRGRAS4, but the reinforcement was placed according to CIRIA Guide 2.

The first visible crack occurred at 100kN, at the centre of the span near the soffit. As the load increased the cracks propagated and extended towards the loading points. The deflections and steel strains were very small before cracking. At a load of 650kN cracking started above the intermediate support. With a further increase in load, more cracks in this region spread and extended towards the intermediate support. At 800kN, a shear crack appeared with a loud "thud" in one of the internal shear spans. On the next load increment, another shear crack appeared in

the other internal shear span again with a loud "thud", along a line joining the support and loading point. However, the girder was able to sustain further increases in load and at an increment before failure, the flexural cracks over the intermediate support became approximately 8mm wide and extended to the intermediate support indicating that flexural failure was about to occur. The crack pattern indicates that the cracks over the intermediate support are severe and are responsible for the failure in the girder Finally, the beam failed at 1243kN in a flexure–shear failure mode. All the steel had yielded except the top bars at the centre of the beam span and the stirrups. The crack pattern at failure is shown in Figure (7.45).

The crack pattern is different from the crack patterns of girders in series 1, and suggests that the behaviour is changing from deep beam towards ordinary beam behaviour.

The load deflection curve in Figure (7.46) illustrates that the behaviour was linear up to cracking but after cracking there was a fair amount of ductility. The steel strain curves for all bars are shown in Figures (7.47) to (7.50). These demonstrate that the strains were very high in the steel over the top of the intermediate support as in ordinary beams, but the distribution was not the same as the ordinary beams. The steel strain in the bottom bars at various points along the span length is shown in Figure (7.51).

Crack widths were monitored at several points and are illustrated in Figure (7.52). From these, the 0.3mm crack width serviceability load was determined to be 650kN. Figure (7.53) shows the variation of concrete surface strains for increasing load, these show a marked increase after about 650kN.

The ratio of serviceability to design ultimate load (0.76) is smaller than for girder TRGRAS4 (0.90), whilst the ratio of measured ultimate load to design ultimate load is higher (1.38 to 1.27). This might be attributed to the higher concrete material properties of girder TRGRAS5. The comparison of these two girders indicates that

CIRIA Guide 2 distribution does not give as satisfactory a serviceability behaviour as that obtained by the direct design technique. Better crack control is achieved because the reinforcement is placed throughout the beam depth. In addition to that the failure mode changes from shear to flexural mode.

7.2.3 Series 3

This series was designed to test the validity of the direct design approach for skew reinforcement in two span continuous deep girders. It was expected that skew reinforcement would give better ultimate and serviceability behaviour.

Two girders, TRGRAS7 and TRGRAS8, were tested and had identical geometry, loading conditions, amount and distribution of main and shear reinforcement as girder TRGRAS2 but skew reinforcement was used instead. The skew reinforcement in girder TRGRAS7 had an angle of 15° with the x−axis and 10° in girder TRGRAS8.

Transfer girder TRGRAS7

This girder was designed for an ultimate load of 850kN. The required amount of reinforcement was smaller than for transfer girder TRGRAS2, but in order to make a direct comparison the same amount was provided as girder TRGRAS2. Each span had a different configuration of the skew angle. In one span a sharp bend was introduced at the centre of the span. In the other span a flat transition was introduced between the bends, the length of this transition being equal to the length of the load bearing block.

The first visible crack occurred at 250kN at the centre of the span near the soffit. As the load increased, more flexural cracks occurred in the central span region and propagated towards the loading point. It was observed that the cracking was more severe in the span which was reinforced with the sharp skew angle. Also, the deflections in this span were higher than the other. At 857kN, yielding started in the span which was reinforced with the sharp skew angle, and at 1050kN a shear

crack occurred in the same internal shear span. At 1250kN a shear crack appeared with a loud "thud" in the other internal shear span. When the load reached 1346kN the span with the sharp angle failed in a clear shear mode. From the crack pattern it was clear that the other span could take more load. Hence the load was released and the other span of the girder was tested on its own. The retesting was carried out in order to obtain the ultimate strength only, since the girder was already cracked and with repositioning the whole set–up, the load deflection behaviour would be different than the original. This span of the girder failed in shear at a load of 720kN (i.e overall beam load of 1440kN). At failure all the steel was well above the steel yield point except the top bars and stirrups. The crack pattern at failure is shown in Figure (7.54).

The load deflection behaviour of both spans of the girder was approximately similar. The load deflection curve in Figure (7.55) indicates that behaviour was linear before cracking. The steel strain curves are shown in Figures (7.56) to (7.58), and show that steel strain behaviour was linear up to 700kN. The comparison of the steel strains in the bottom bars at the centre of each girder span are given in Figures (7.59) and (7.60), which shows that behaviour is more or less identical. The steel strain in the bottom bars at various points along the span length (Figure (7.61)) indicates that for up to 60% of the ultimate load, the strain in the bottom bar was fairly constant.

Crack widths were monitored at several points and are illustrated in Figure (7.62). From these, the 0.3mm crack width serviceability load was determined to be 810kN. Figure (7.63) shows the variation of concrete surface strains for increasing load, these show a marked increase after about 1050kN.

The ratio of serviceability load to design ultimate load (0.95) is smaller in comparison to girder TRGRAS2 (1.23) this might be due to the higher material properties of TRGRAS2. However, the ratio of measured to design ultimate load (1.67) compared to girder TRGRAS2 (1.43) indicates that skew reinforcement allows

a higher load. The load deformation behaviour also indicates that even after the formation of diagonal cracks, the girder took considerably more load in comparison to TRGRAS2. This suggests that skew reinforcement, which is approximately perpendicular to the load path joining the load bearing block to the support points, is more efficient than horizontal reinforcement. Finally, it would appear that reinforcement which is gradually bent, is better than that with a sharp change in skew angle.

Transfer girder TRGRAS8

This girder was also designed for an ultimate load of 850kN and was reinforced with the same amount of reinforcement as the previous girder. The angle of skew, however, was 10° to the x–axis. In a similar fashion to girder TRGRAS7, this girder was reinforced with two different configurations of steel, i.e one span was reinforced with a sharp skew angle whilst the other span was reinforced with a gradual change of angle by introducing a flat transition length, equal in dimension to that of the load bearing block, at the centre of the beam span.

Prior to the test starting properly, a sudden load of 500kN was accidentally applied, which caused precracking of the beam and some permanent deformation in the girder. Because of this, there was no precise idea of the correct serviceability load and crack widths. Therefore crack widths were not recorded.

At 950kN the steel started yielding at the centre of the span which was reinforced with the sharp skew angle. This span finally failed at a load of 1300kN. After the failure of one span, the other span was retested alone, but it did not take a higher load. The yielding history of the steel showed that all the steel had yielded except for the top bars. The crack pattern at failure is shown in Figure (7.64).

The load deflection behaviour of both spans of the girder were approximately similar. The load deflection curve is shown in Figure (7.65) and the steel strain curves in Figures (7.66) to (7.68). Though the beam was initially cracked, the curves

still indicate that nonlinearity started after 900kN. Comparison of the strains in the bottom and top bars in both spans is presented in Figures (7.69) and (7.70) and show quite similar behaviour. The strain distribution in the bottom bar (Figure (7.71)) indicates that strain in the steel bar is fairly constant up to 80% of the ultimate strength.

Figure (7.72) shows the variation of concrete surface strains for increasing loading, a marked change is evident after 900kN.

The ratio of serviceability load to design ultimate load (0.36) is poor in comparison to girder TRGRAS2 (1.23); however this is not a true reflection of behaviour because of the accidental cracking before the test, so that there was no precise idea of the serviceability load. However, the ratio of measured ultimate load to design ultimate load (1.54) indicates that skew reinforcement takes higher loads than the orthogonal reinforcement. In addition, the comparison of this girder with TRGRAS7 indicates that the 15° angle of skew is better than 10° when considering the ultimate strength.

7.2.4 Series 4

This series consisted of single span deep girders with web openings, namely TRGRAS9 and TRGRAS10. Girder TRGRAS9 was designed with two openings. One opening (500*500mm) was placed in the upper mid–depth of the beam in one shear span and the other (500*500mm) was placed in the lower mid–depth of the beam in the other shear span. Girder TRGRAS10 was designed with three openings, two (400*500mm) were placed in one shear span in the upper and lower half, and one (500*500mm) was placed in the other shear span at the mid–depth. The aim of this series was to test the direct design technique when the load path is intercepted by perforations and to study the behaviour of such beams. Both beams were designed for a load of 1000kN.

Transfer girder TRGRAS9

The first visible crack occurred at 200kN at the beam soffit and the corners of the openings. The cracks mostly propagated around and widened at the corners of the openings. On further increase of load the concrete surface strains became higher at the corners of the upper opening. This opening, which interrupted the load path to a larger extent than the bottom one, was severely cracked. As the new cracks formed the load dropped considerably. However, attempts were made to continuously increase the load either from the dropped point to the next intended increment or by unloading to zero load and then increasing again. Several times the load was reduced to zero and applied again as cracking progressed around the openings.

At 437kN cracking became more severe in areas away from the holes, and steel strains started to increase more rapidly. At 796kN, yielding occurred at the centre of the span in the bottom bars and also in the bars underneath and above the top opening. Before failure shear cracks occurred in both shear spans over the top and bottom of the openings, indicating that the structure was converting into a mechanism at ultimate load by the rotation of the block between the shear crack at the exterior bottom corner of the top opening and the shear crack running from the load bearing block to the top corner of the opening (Figure 7.73). Finally the beam failed in a clear shear mode with a shear crack running from the loading point to the exterior corner of the top opening. Most of the steel had yielded except the transverse steel which took compressive stresses throughout the loading history. The crack pattern at failure is shown in Figure (7.74)

The load deflection curve showing the load drops is illustrated in Figure (7.75). The steel strains in longitudinal and transverse steel are shown in Figures (7.76) to (7.79), these show that most of the steel started nonlinear behaviour from 450kN. The strain distribution in the bottom bars is shown in Figure (7.80) which demonstrates that the behaviour is quite different from ordinary beams.

Crack widths were monitored at several points and are illustrated in Figure (7.81). From these, the 0.3mm crack width serviceability load was determined to be 400kN.

Figure (7.82) shows the variation of concrete surface strains for increasing load. These show a marked increase after about 300kN.

It should be noted that the serviceability load was based on a crack width which occurred in local zones around the openings. This may not represent true serviceability behaviour because stress concentrations at the corners of openings cause severe cracking, and normally such zones would be strengthened with extra diagonal reinforcement, provided on an ad hoc basis. Hence, the ratio of the serviceability load to the design ultimate load (0.40) is not satisfactory.

However the ratio of the measured ultimate load to the design ultimate load (1.05) is satisfactory. It would appear from the results that the opening in the upper part of the beam interrupted the load path to a greater extent, and so was more severely cracked.

Transfer girder TRGRAS10

The first visible crack occurred at 250kN near the top corner of the opening, in the shear span with the two openings. After that, the majority of crack propagation occurred around the top opening. At 550kN, a diagonal crack running from the outside edge of the loading point to the exterior corner of the top opening appeared, accompanied by a diagonal crack running between the inside corner edge of the top opening to the far side edge of the bottom opening. During the progression of these cracks, the load continuously dropped. Attempts were made to increase the load either from a dropped point to a new intended increment level or by unloading to zero and then loading in small increments until new cracks developed or failure occurred. Steel strains showed linear behaviour until the load reached 600kN. The failure mechanism was the rotation of the block in between the shear cracks above and below the top opening and a diagonal crack from the nearer corner of the bottom opening towards the support (Figure 7.83). Steel at the top of the upper opening started yielding at a load of 891kN, after which the load dropped to 600kN. After this the beam did not attain the higher load again. At failure the

bottom bars and the bars at the bottom and top of the upper opening had yielded, the remainder had not yielded. The crack pattern at failure is shown in Figure (7.84).

The load deflection curve including the load drops is shown in Figure (7.85). It illustrates that the behaviour was more flexible in comparison to the solid girders, due to the earlier severe cracking around the opening. The steel strains in the longitudinal and transverse steel are shown in Figures (7.86) to (7.90), these show that the curves are approximately linear up to 600kN.

Crack widths were monitored at several points and are illustrated in Figure (7.91). From these, the 0.3mm crack width serviceability load was determined to be 500kN. Figure (7.92) shows the variation of concrete surface strains for increasing load. These tend to show a marked increase after about 500kN except at points near the corners of the openings, which showed a slightly earlier increase.

The ratios of serviceability to design ultimate load (0.5) and ultimate to design ultimate load (0.89) are not satisfactory. This suggests that when the load path is severely intercepted, reinforcement design based on the averaging procedure is unsafe unless special precautions are taken around the openings. Both this and girder TRGRAS9 exhibited poor serviceability behaviour and although the ultimate behaviour of girder TRGRAS9 was just satisfactory but girder TRGRAS10 was not, which deals the greater extent of interception of the load path by opening, the less satisfactory the behaviour when the openings are not additionally strengthened over and above that required by the design procedure used here.

7.2.5 Series 5

This series consisted of one large scale solid deep girder, namely TRGRAS11. This girder was reinforced as close as possible to the amount required by the direct design theory by reducing bar diameters at selected points throughout the girder. The aim was to test the theoretical assumptions and to compare the behaviour of this

reinforcement field with those using the average or maximum stress envelopes. The girder was designed for a load of 1000kN.

Transfer girder TRGRAS11

The first visible crack occurred at a load of 250kN near the beam soffit. With increasing load, more cracks appeared in the maximum tensile zone at points where steel bar diameters were reduced to the required values. Initially cracks propagated vertically upwards from the beam soffit. At about the design load, some major cracks appeared along the line joining the support and the loading point. As cracking progressed the steel started taking more stress. At 1153kN, the steel started yielding in the bottom bars and the beam finally failed at a load of 1750kN in a clear shear failure. All the main and shear reinforcement had yielded throughout the structure and were well above the yield strain at failure except at points in the stirrups which were carrying compressive stresses. The crack pattern at failure is shown in Figure (7.93).

The load deflection curve of the girder in Figure (7.94) illustrates that, before cracking, behaviour was linear. The strain in steel is shown in Figures (7.95) to (7.96) and illustrates that nonlinearity starts after 500kN. The distribution of steel strain in various bars along the length of the girder is shown in Figures (7.97) to (7.103), these clearly show that the distribution is different from ordinary beams.

Crack widths were monitored at several points and are illustrated in Figure (7.104). From these, the 0.3mm crack width serviceability load was determined to be 1050kN. Figure (7.105) shows the variation of concrete surface strains for increasing load. These show a marked increase after the shear crack at a load of 1050kN.

The ratio of the serviceability to design load (1.05) is satisfactory, whereas the ratio of ultimate load to design load (1.75) is higher than expected. Some of this can be attributed to the contribution of the dowel action of main reinforcing bars and aggregate interlocking in transferring shear. However, the reinforcement reduction at

selected points throughout the girder means that at no point was the steel less than that required, and in some places it was much higher than required. The averaging procedure used elsewhere in this work produced ultimate loads on average 45% higher than the design load. This is less, because some regions are underreinforced and others are over–reinforced, producing less favourable load paths. Lin[4] used maximum stress envelopes and observed 100% higher ultimate loads than design ultimate loads.

7.3 General discussion of experimental results

The detailed discussion of experimental behaviour of individual girders was given in section 7.2. This section summarizes the results under the following headings.

(i) Deflections

(ii) Strains

(iii) Crack propagation and crack widths

(iv) Mode of failure

(v) Limit state behaviour

7.3.1 Deflections

The measurement of net deflections in deep beams is a challenging task because the deflections are always small and the isolation of effects due to the squeezing of plaster or support settlements are difficult to quantify. Neverthless Figures (7.106) and (7.107) attempt to compare the load deflection curves of groups of girders tested in this study.

In all two span continuous girders, prior to the initiation of cracks, very small deflections were observed and the load deflection relationships were approximately linear. After the initial flexural cracking, subsequent load increases caused increases in crack lengths and widths and accordingly the flexural stiffness of the section progressively deteriorated. After the occurrence of diagonal cracks, deflections increased rapidly and the final failure was imminent except for the girders with skew

reinforcement, in which case the final failure was considerably later. The deflections were larger in girders having span to depth (L/D) ratio equal to 1.61 (TRGRAS4 and TRGRAS5) than those girders having span to depth (L/D) ratio equal to 1.07.

In general, deflections were small in all continuous girders and were of the order of 1.0mm at 80% of the measured ultimate load. The serviceability limit state criterion, based on BSCP8110[5], was not attained in those girders whose span to depth ratio was 1.07, whereas girders having span to depth (L/D) ratio equal to 1.61 attained serviceability behaviour at about ultimate load stage. Thus, the serviceability limit state, with respect to deflection, is not a problem.

The load deflection curves of girders with perforations indicate that behaviour was linear up to 200kN, after which cracking started and the curves became nonlinear. The load deflection curves of both girders are more or less similar. The stiffness of girder TRGRAS10 in the post–cracking range is less than girder TRGRAS9, which is to be expected because it had a greater area of openings interrupting the load path.

The load deflection curve of girder TRGRAS11 has a similar form to two span continuous girders, but the deflections are smaller than the perforated girders. However the curve indicates a unique behaviour in that there is no sharp increase in deflection at the occurence of a diagonal shear crack. The deflection criterion for serviceability limit state was not attained in this case.

7.3.2 Strains

The concrete surface strains were not consistent and at some critical points, cracks appeared and the demec gauges came off. Hence a comprehensive comparison from girder to girder cannot be made and only the steel strain will be discussed.

In general, the behaviour of steel strain was similar to the load deflection behaviour.

In all continuous girders, before cracking the behaviour was linear and relatively small strains existed. As cracking started a gradual increase of strain was observed in all bars including the stirrups. After the formation of a diagonal crack the steel started to yield, the stress rapidly increasing well into the work– hardening range.

For loads up to 75% of ultimate strength, the strain distribution along the length for girders having span to depth (L/D) ratio of 1.07, is approximately constant on average. For girders having span to depth ratio equal to 1.61, the strain distribution is constant up to 52% of the ultimate strength. The distribution becomes more like that in the shallow beams as stress redistribution take place.

The data also suggests that the steel strains are larger for higher span to depth ratios at all load levels. The yielding in all two span continuous girders on average at the load approximately equal to design load.

For girders with perforations early yielding of steel depends on the extent to which the load path is intercepted by the openings. Figures (7.76) and (7.84) reveal that in girder TRGRAS10 yielding started earlier than girder TRGRAS9. The yielding of steel, in the perforated deep girders, occurrred at 80% of the design load on average, which is lower than the design load. This might be due to the perforation interception of the load path.

The strain distribution of girder TRGRAS11 shows evidence of arching action. The strain in reinforcement at various heights indicate that the main bars are carrying a constant force. The yielding of steel in a single span solid girder occurred at the design load

7.3.3 Crack propagation and crack widths

The formations of cracks can be conveniently classified into two major groups for two span continuous girders:

(i) Flexural cracks, which started from the beam soffit and propagated towards the loading point, or started at the top above the intermediate support and propagated towards this support. It was generally observed that cracks did not occur until a load of 0.20 to 0.35 of the design ultimate load had been applied except for girder TRGRAS8, which was accidentally cracked before testing. In girders TRGRAS4 and TRGRAS5 with span to depth (L/D) ratio of 1.61 these cracks reached 0.3mm crack widths before the formation of a diagonal shear crack.

(ii) Shear (i.e diagonal splitting) cracks occurred after about after 68% of the measured ultimate load, originating from the inside face of the support to the outside edge of the loading point. In some beams parallel cracks formed. The shear crack was more severe in the interior shear span than the exterior shear span, as was expected, since the interior shear span carries a higher shear load.

Crack width curves (Figure (7.108) show that the maximum crack widths were greater in girders having a span to depth (L/D) ratio of 1.61 and consequently the serviceability loads, based on the maximim crack width criterion, were lower than for girders having a span to depth (L/D) ratio of 1.07.

For the beams with web openings, the initial cracks appeared in the region of the maximum tensile strain around the openings, propagating from the corner of the opening towards the support and loading points. The shear cracks occurred at about 0.5 of the ultimate load running from the top exterior corner of the top opening towards the loading point. The monitored maximum crack width of TRGRAS9 and TRGRAS10 was of similar order. The maximum crack widths (Figure (7.109)) were wider than the solid girder, which is clearly due to the web openings.

7.3.4 Modes of failure

It was mentioned in Chapter Two that whatever the initial cracks in deep beams the eventual failure will be a type of shear failure, although it has been reported that premature failure such as bearing failure or the spalling and splitting of concrete near supports can occur. In this investigation all the tested girders exhibited a wide

range of cracking, but the final collapse was a shear (i.e diagonal splitting) mode, when the high force in the compression strut caused it to suddenly split. In the two span continuous deep girders shear failure always occurred in one of the interior shear spans.

The modes of failure in perforated girders were also shear type over the top of the top opening. The shear cracks always occurred from the exterior corner of the top opening to the loading point and from the nearer corner of the opening to the support. At failure a block between these two shear cracks rotated and the load path was destroyed. The summary of all the types of modes of failure is given in Table 7.2.

7.3.5. Limit state behaviour

7.3.5.1 Serviceability behaviour

Serviceability load according to BS 8110[5] is based on the one of the following criteria:

(a) Deflection limit of span/250

(b) Maximum crack width of 0.3mm

and normally, the minimum serviceability load of the two criterion is considered as the serviceability load for a particular section of the structure. Since deflections are small in deep beams only the crack width criterion has been used and these are summarized in Table 7.1. The average serviceability load for a two span continuous girder is 0.91 of the design ultimate load, for a single span girder with web opening it is 0.45, and for single span solid girder it is 1.05.

In order to gain an idea of serviceability load, the ratio of serviceability load to concrete compressive strength (Ps/fc') against X/D ratio is illustrated in Figure (7.110) for all the two span continuous girders. Because of the limited amount of data and the effect of other parameters on the data, it was difficult to suggest any equation for this relationship. However, the trend indicates that a larger shear span to depth (X/D) ratio produces lower serviceability behaviour.

7.3.5.2 Ultimate limit state

The measured ultimate loads for all the tested girders are presented in Table 7.1. The ultimate strengths are different for all girders due to differences in concrete strengths, difference of shear reinforcement, main reinforcement, L/D or X/D ratios or because of skew reinforcement. The ratio of ultimate strength to concrete compressive strength (Pu/fc') against percentage of main reinforcement (ρt), percentage of shear reinforcement (ρs) and shear span to depth ratio (X/D) for all continuous girders are illustrated in Figures (7.111) to (7.113). Again, because of the limited amount of data and the effect of other parameters on the data, it is difficult to suggest any relationship for predicting the ultimate strength of a girder. However, the ultimate strength would appear to be affected by the X/D ratio, when the span length of girder was increased the ultimate strength decreased considerably (i.e girder TRGRAS4 in comparison with girder TRGRAS2).

An examination of ultimate strength of both perforated girders reveals that the ultimate strength depends upon the extent to which an opening interrupts the load path joining the bearing block and the loading and support points. Serious strength reduction occurred in girder TRGRAS10 (which had two opening in one shear span) as compared to girder TRGRAS9 (which had one opening in each shear span). Also the comparison of the perforated girders with the solid girder indicates significant strength reductions, again because the load path is intercepted by the openings.

7.4 Appraisal of direct design method

Two span continuous girders

All the two span continuous deep girders designed by the direct design technique in conjunction with the proposed averaging procedure, produced satisfactory overall behaviour.

(a) The serviceability behaviour based on 0.3mm crack width always occurred at 80% to 125% of the design load.

(b) The measured ultimate loads were 25% to 60% higher than the design ultimate

loads, which gives an intrinsic safety factor against collapse.

(c) First yielding of steel occurred approximately at the design loads or in some cases later. Most of the steel had yielded near ultimate conditions. This suggests that redistribution of stresses was possible as that failure occurring in local regions, and that the ductility requirements were adequate.

(d) Crack widths were not severe because of the control given by the better distribution of reinforcement obtained using the direct design technique rather than CIRIA Guide 2.

(e) The use of skew reinforcement produced significantly higher ultimate and serviceability loads than the orthogonal reinforcement.

Perforated girders

When applying the direct design technique to deep girders in which the load path is intercepted by web openings the proposed averaging procedures leads to difficulties in coping with the corners of the openings, where a high concentration of stress exists. In these situations the corners should be considered as local zones with additional diagonal reinforcement being provided. The greater the extent of the load path by the web openings interception the less satisfactory the behaviour.

Special girder

The behaviour of the solid single span girder which at selected points was reinforced as closely as practically possible to that required by the direct design equations, provided an ultimate load 75% higher than the design load. This may be explained by the dowel action of the reinforcing bars and aggregate interlocking which contribute the shear transfer. Also the fact that reinforcement was provided higher than calculated due to the practical reasons. In comparison to reinforcement provided on averaging procedure, the ultimate behaviour is satisfactory.

TABLE 7.1

Summary of test Results

Girder No.	Design Load kN DL	First cracking load kN CL	Serviceability load kN SL	Ultimate load kN Pu	Ratio of SL/DL	Ratio of Pu/Dl	Ratio of CL/Pu	Ratio of SL/Pu	Type of Reinforce-ment
TRGRAS1	850	200	900	1330	0.94	1.56	0.15	0.67	Orthogonal
TRGRAS2	850	150	1050	1216	1.23	1.43	0.12	0.86	Orthogonal
TRGRAS3	1100	300	970	1500	0.88	1.36	0.20	0.65	Orthogonal
TRGRAS4	850	150	770	1143	0.90	1.27	0.09	0.67	Orthogonal
TRGRAS5	850	200	650	1243	0.76	1.38	0.16	0.52	Orthogonal
TRGRAS6	1100	150	890	1486	0.80	1.35	0.10	0.60	Orthogonal
TRGRAS7	850	250	810	1440	0.95	1.67	0.19	0.56	Skew
TRGRAS8	850	*	303	1312	0.36*	1.54	*	0.23*	Skew
TRGRAS9	1000	200	400	1046	0.40	1.05	0.19	0.38	Orthogonal
TRGRAS10	1000	200	500	891	0.50	0.89	0.22	0.56	Orthogonal
TRGRAS11	1000	250	1053	1750	1.05	1.75	0.14	0.60	Orthogonal

* indicates that this girder was accidentally cracked before test

TABLE 7.2

Failure modes of tested girders

Girder No.	Mode of failure
TRGRAS1	Shear failure
TRGRAS2	Shear failure
TRGRAS3	Shear failure
TRGRAS4	Shear failure
TRGRAS5	Flexure-shear failure
TRGRAS6	Shear failure
TRGRAS7	Shear failure
TRGRAS8	Shear failure
TRGRAS9	Shear failure
TRGRAS10	Shear failure
TRGRAS11	Shear failure

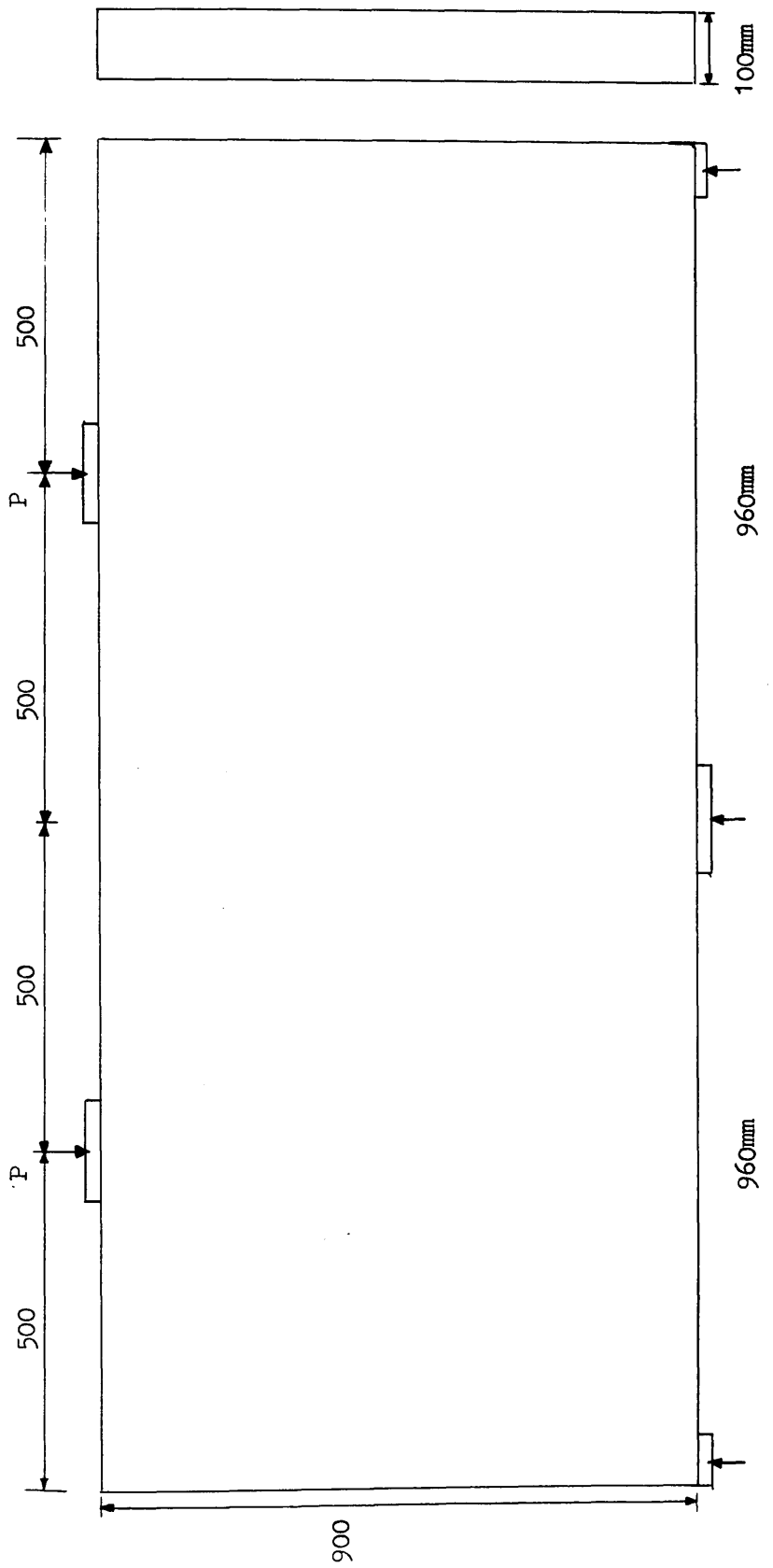

FIG(7.1) Dimensions of transfer girders TRGRAS1, TRGRAS2, TRGRAS3 and TRGRAS6

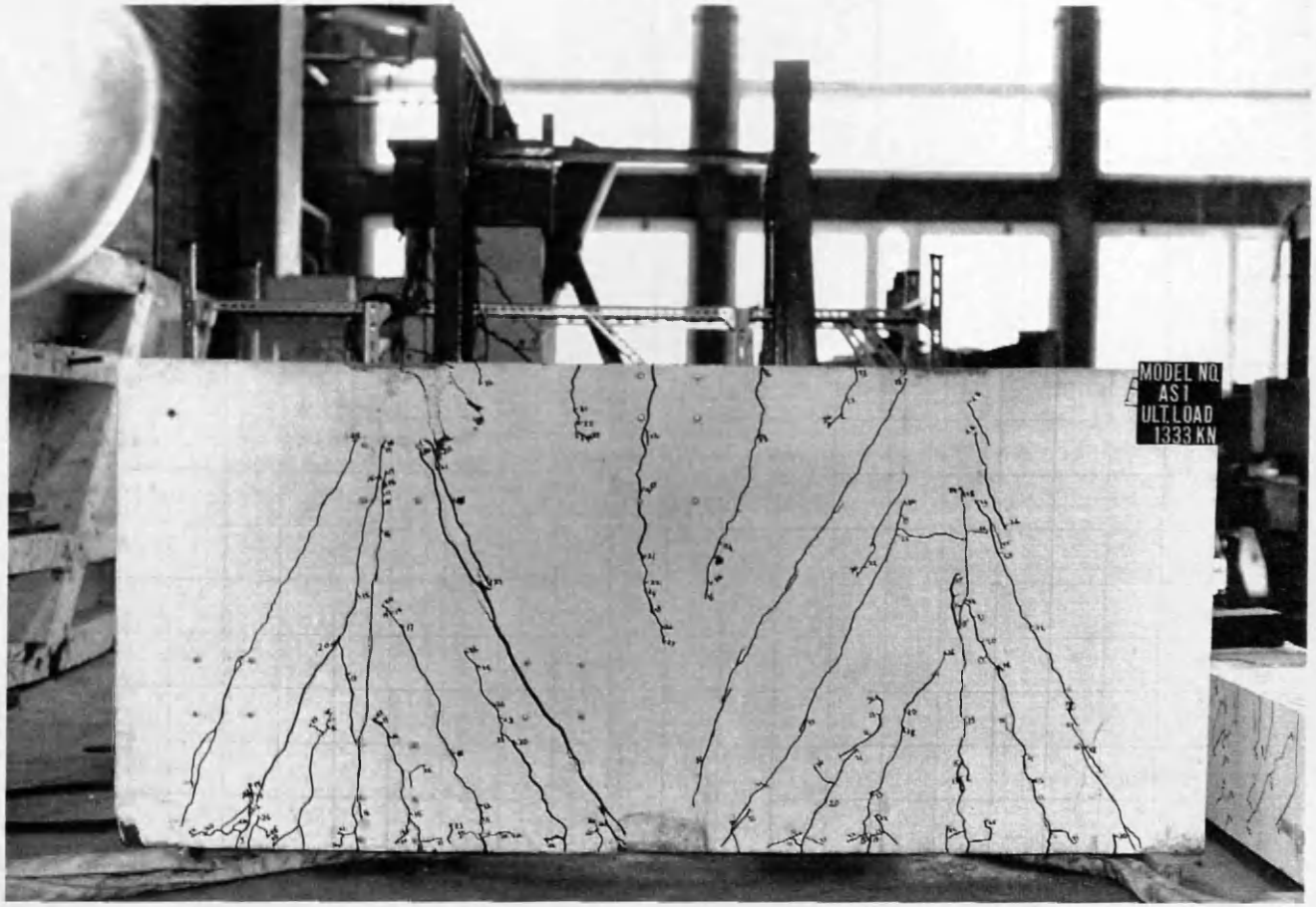

Figure(7.2) Final crack pattern of transfer girder TRGRAS1

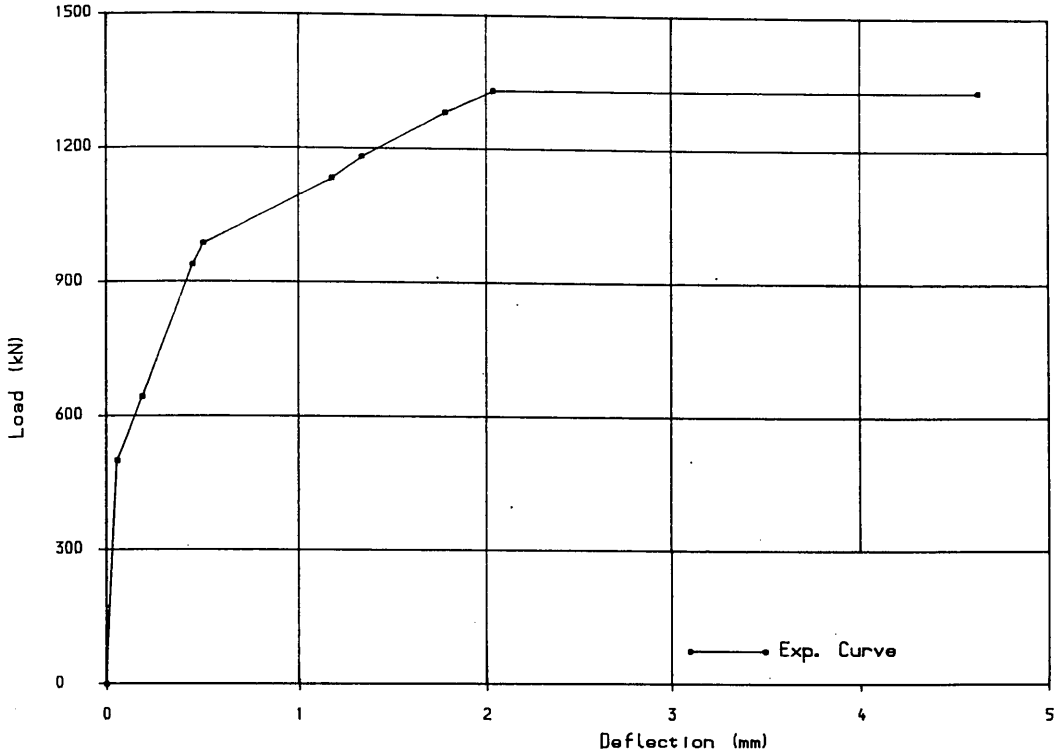

FIG(7.3) Load deflection curve for girder TRGRAS1

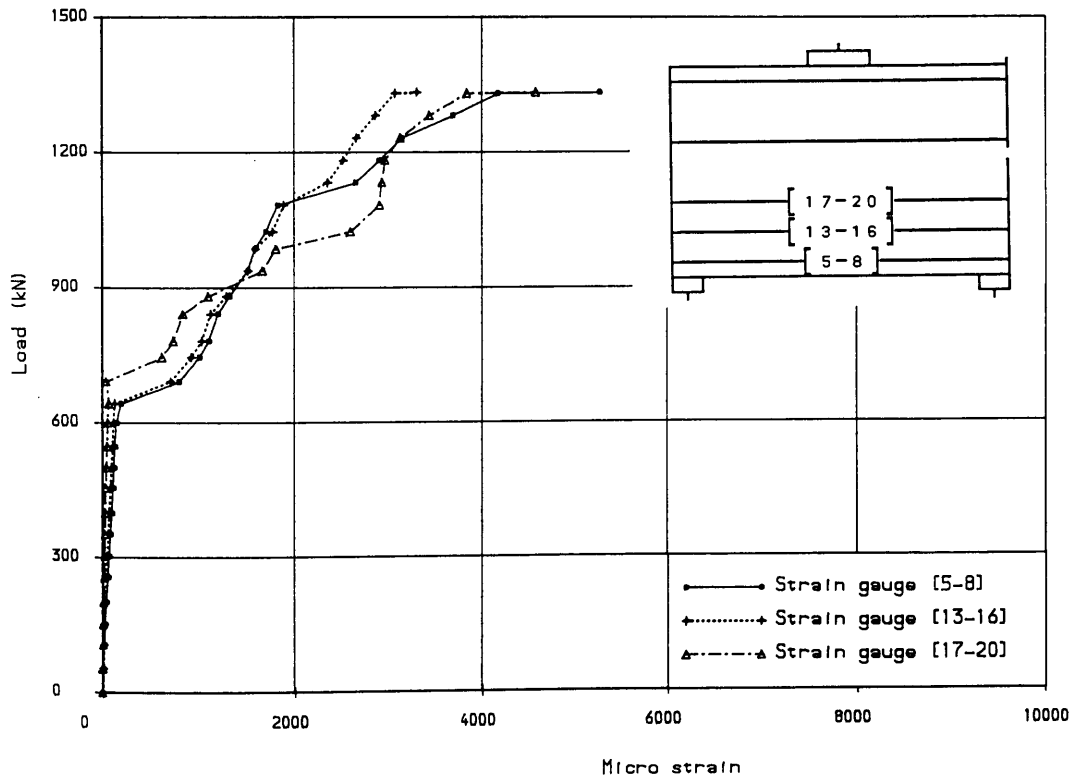

FIG(7.4) Load vs longitudinal steel strains at centre of girder span for girder TRGRAS1

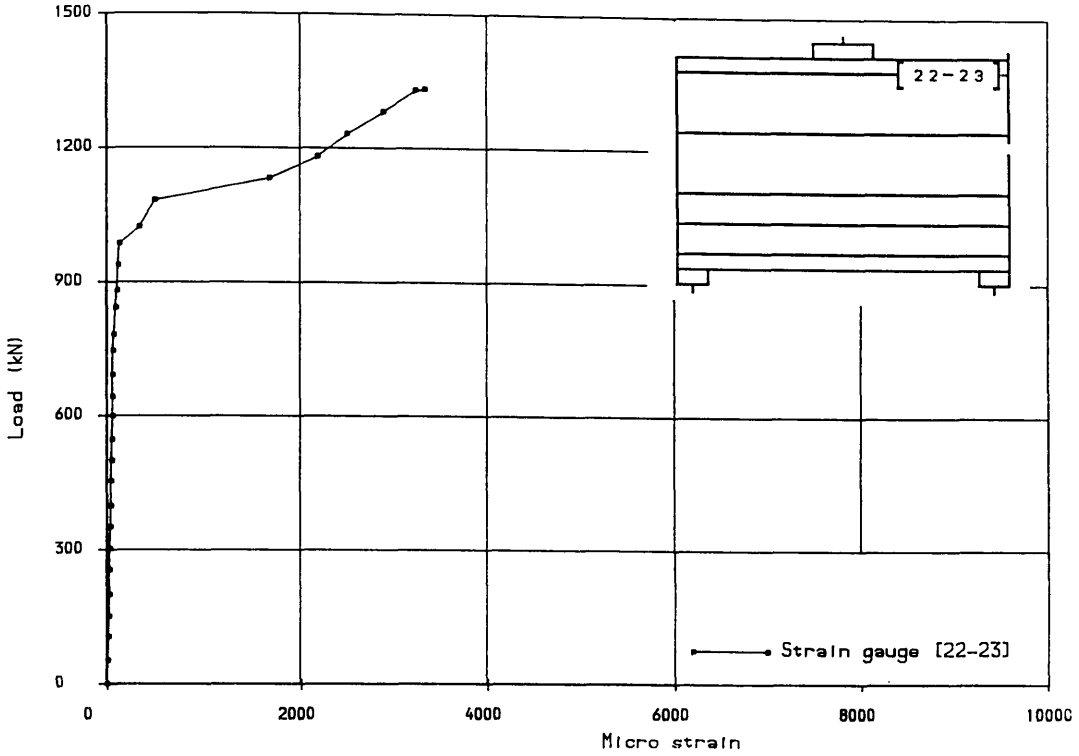

FIG(7.5) Load vs longitudinal steel strains in top bars at 200mm from beam span centre for girder TRGRAS1

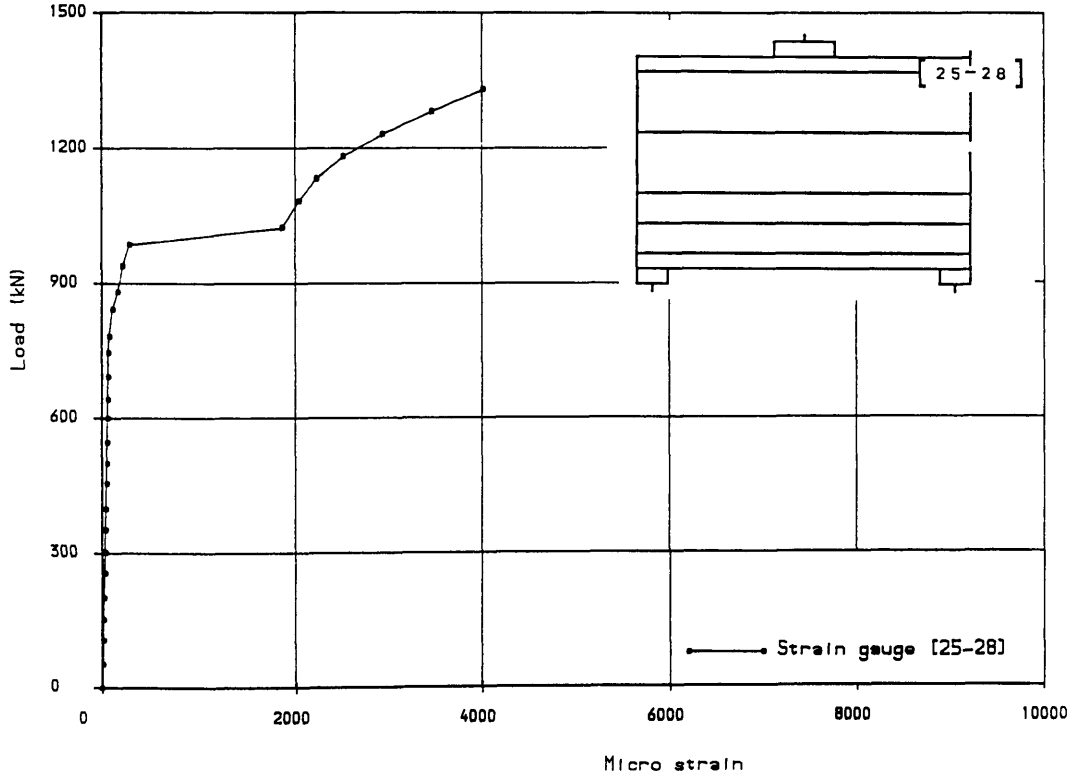

FIG(7.6) Load vs steel strains in top bars over intermediate support for girder TRGRAS1

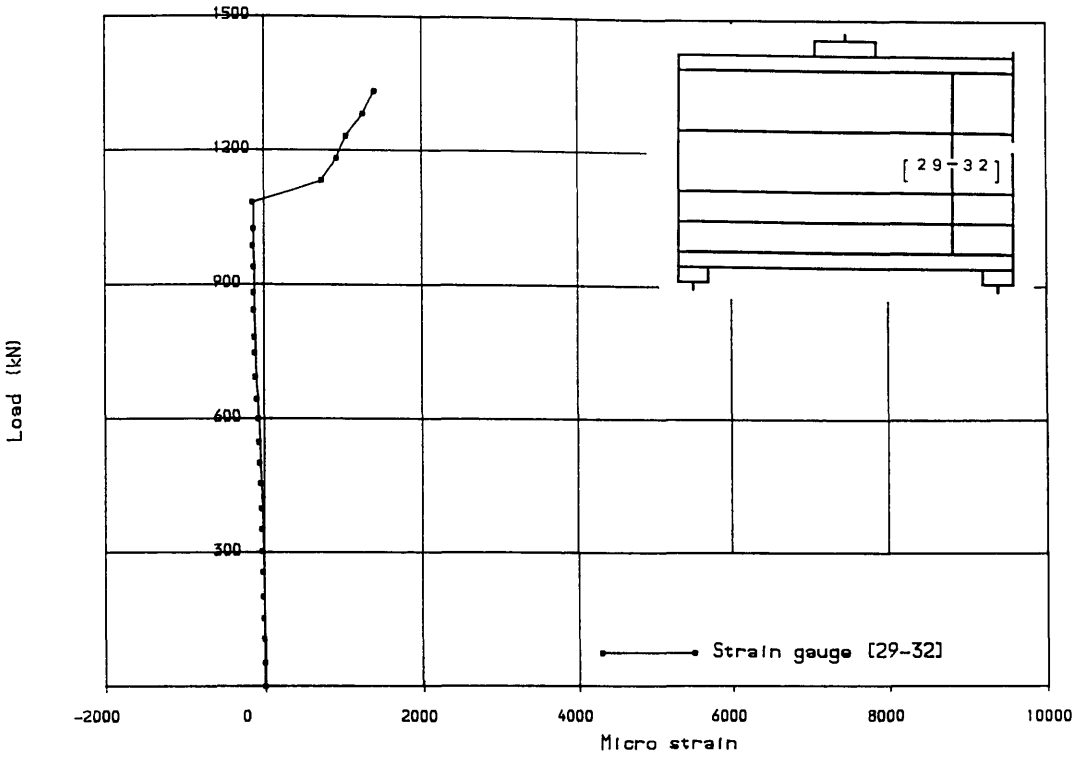

FIG(7.7) Load vs stirrup strains in interior shear span of girder for girder TRGRAS1

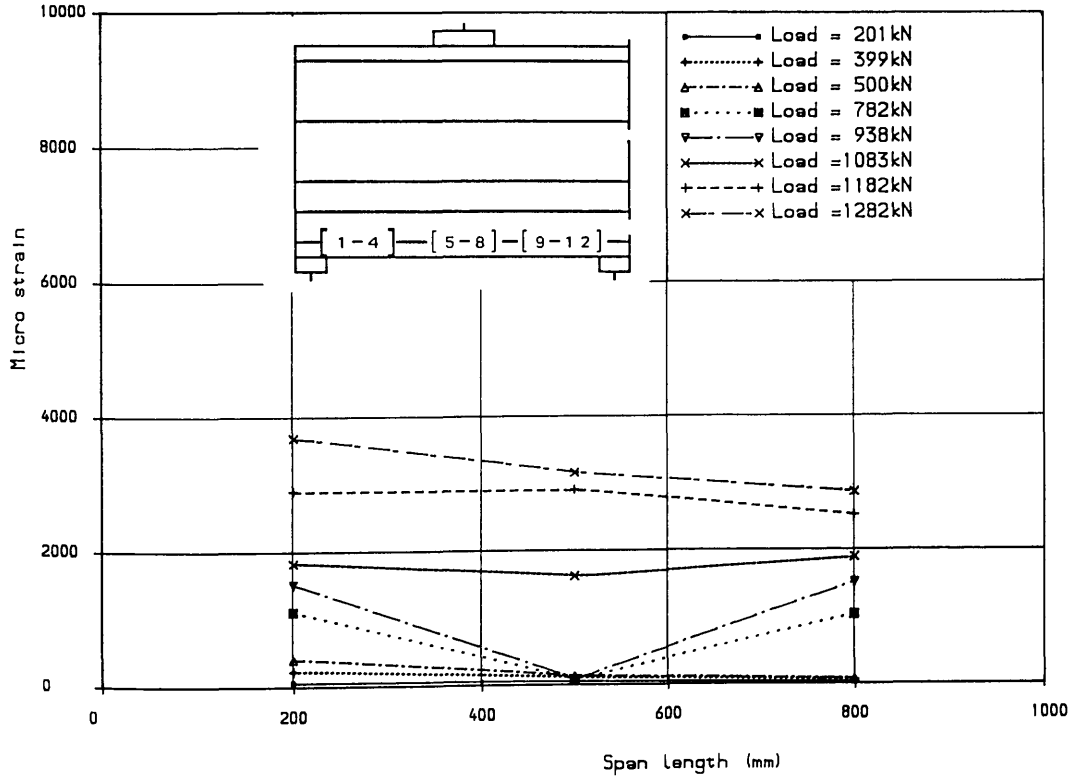

FIG(7.8) Steel strain distribution in bottom bars along girder length for girder TRGRAS1

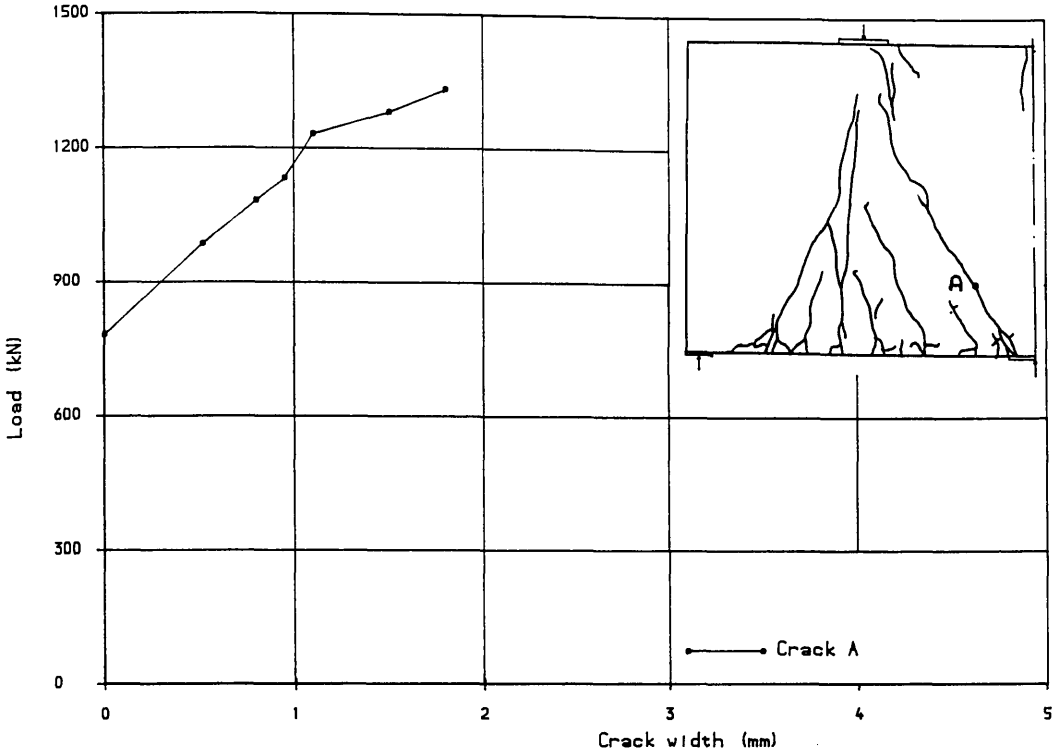

FIG(7.9) Load vs crack width for girder TRGRAS1

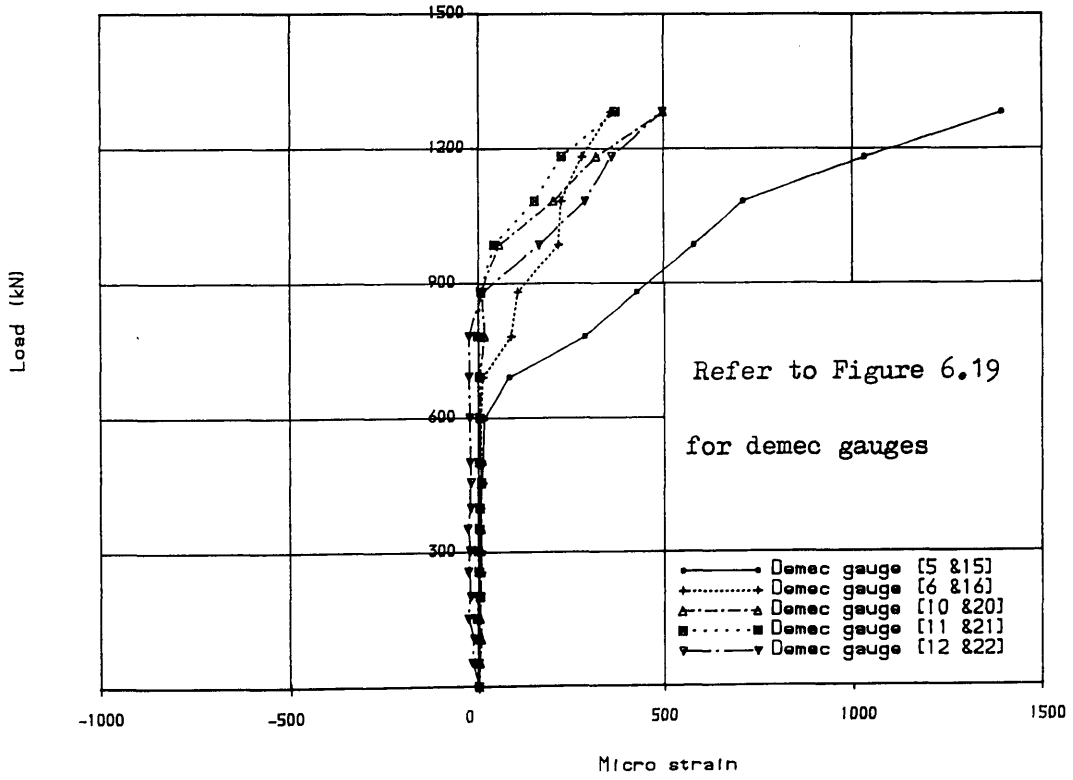

FIG(7.10) Load vs concrete surface strains for girder TRGRAS1

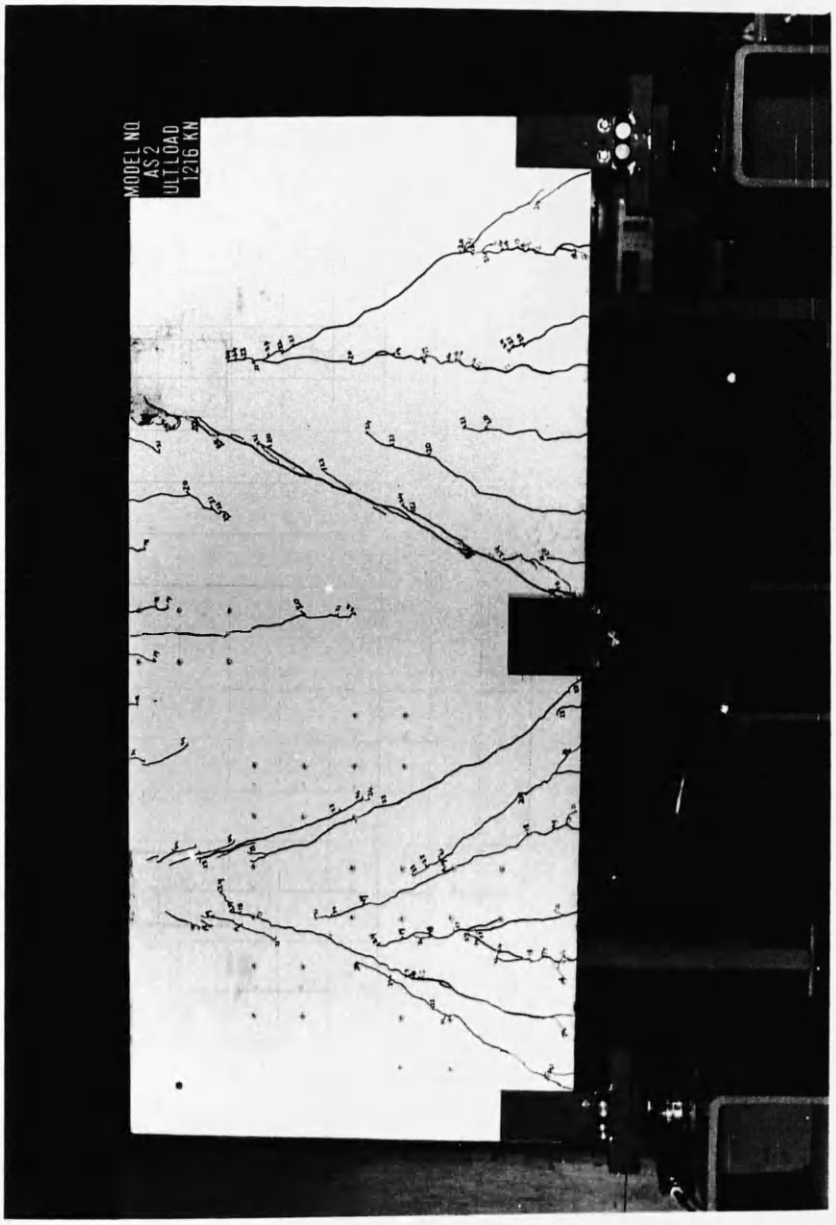

Figure(7.11) Final crack pattern of transfer girder TRGRAS2

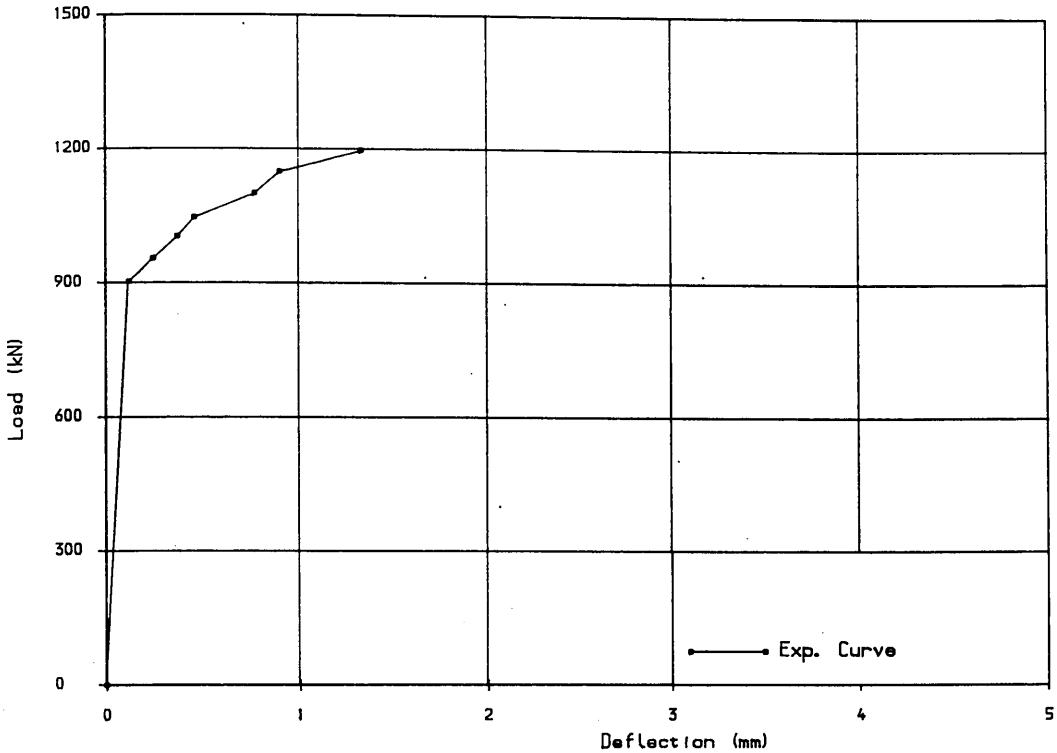

FIG(7.12) Load deflection curve for girder TRGRAS2

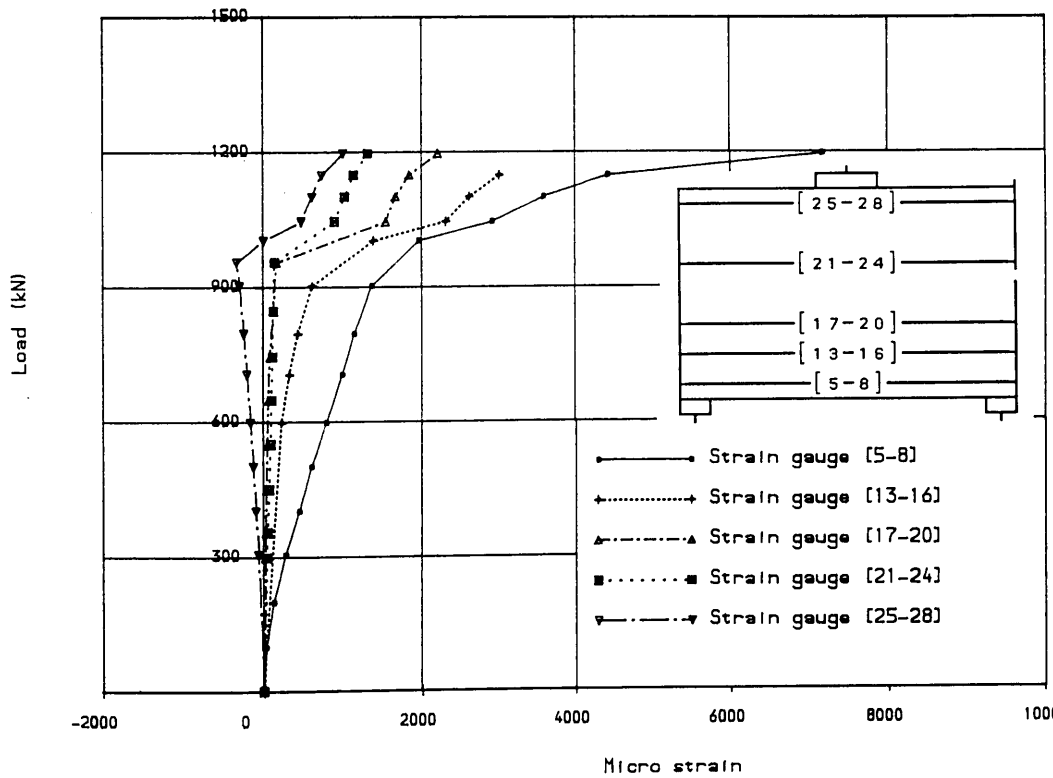

FIG(7.13) Load vs longitudinal steel strains at centre of girder span for girder TRGRAS2

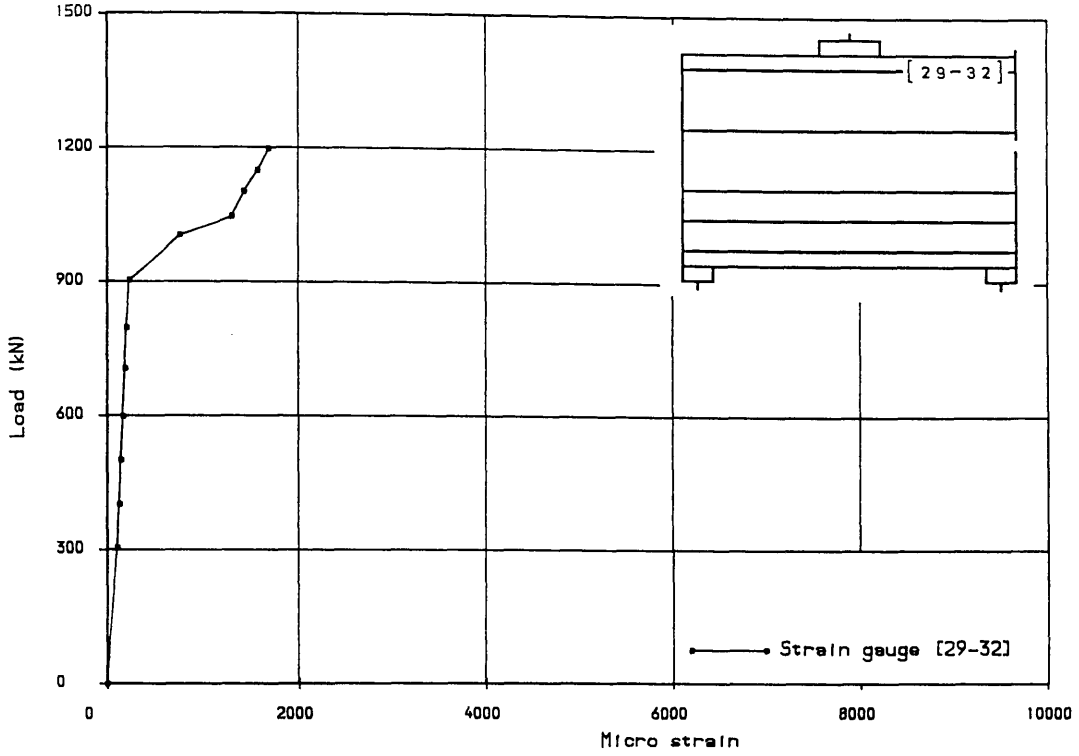

FIG(7.14) Load vs longitudinal steel strains in top bars at 300mm from beam span centre for girder TRGRAS2

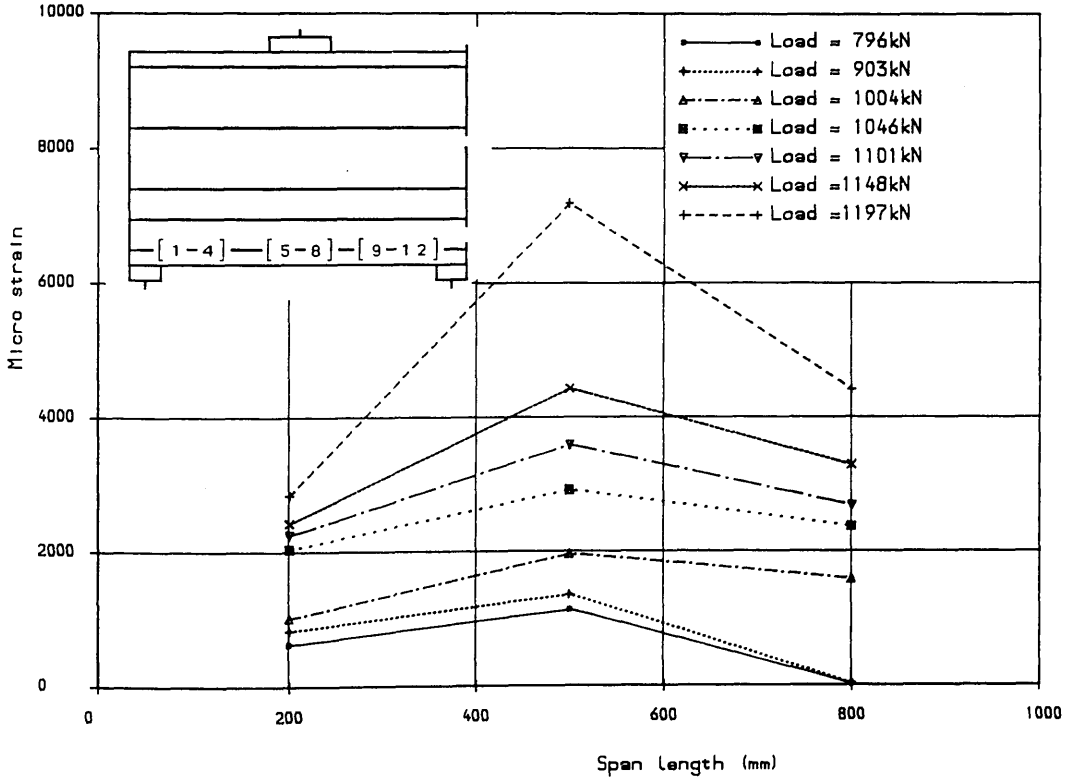

FIG(7.15) Steel strain distribution in bottom bars along girder length for girder TRGRAS2

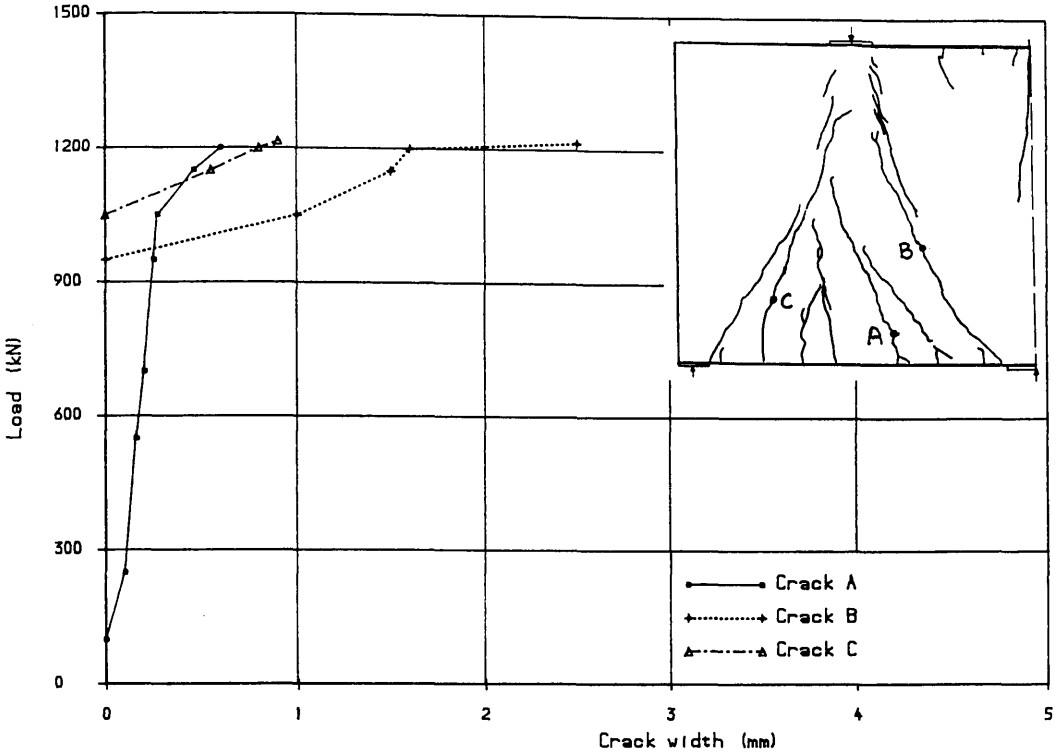

FIG(7.16) Load vs crack width for girder TRGRAS2

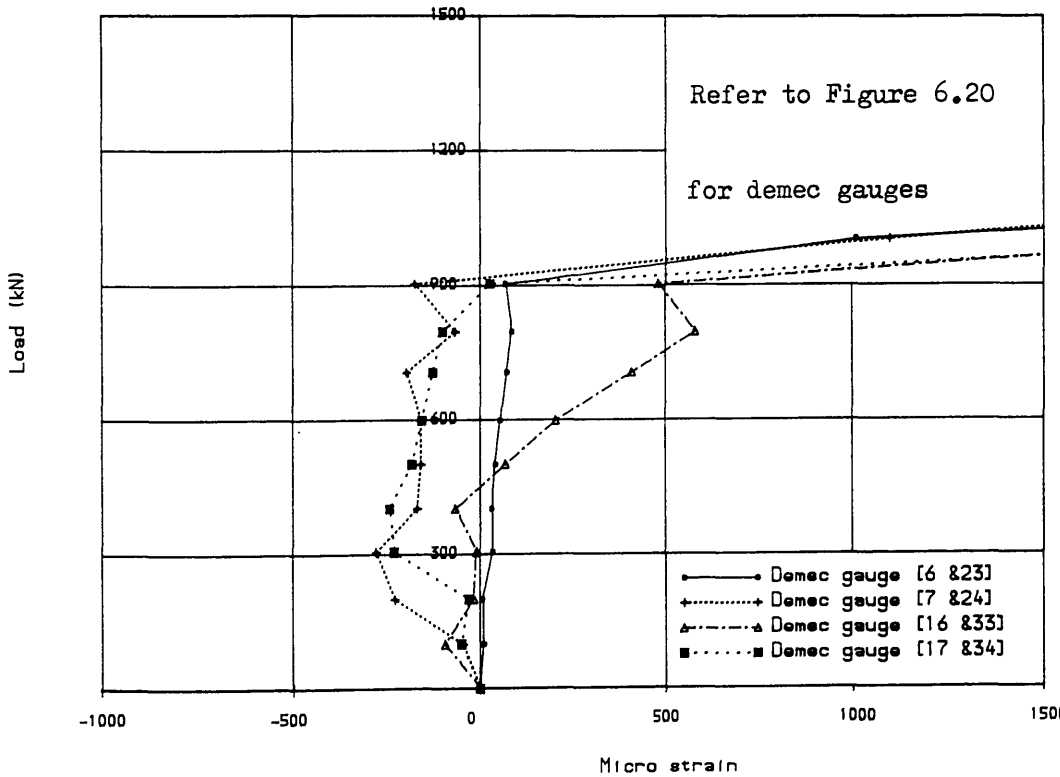

FIG(7.17) Load vs concrete surface strains for girder TRGRAS2

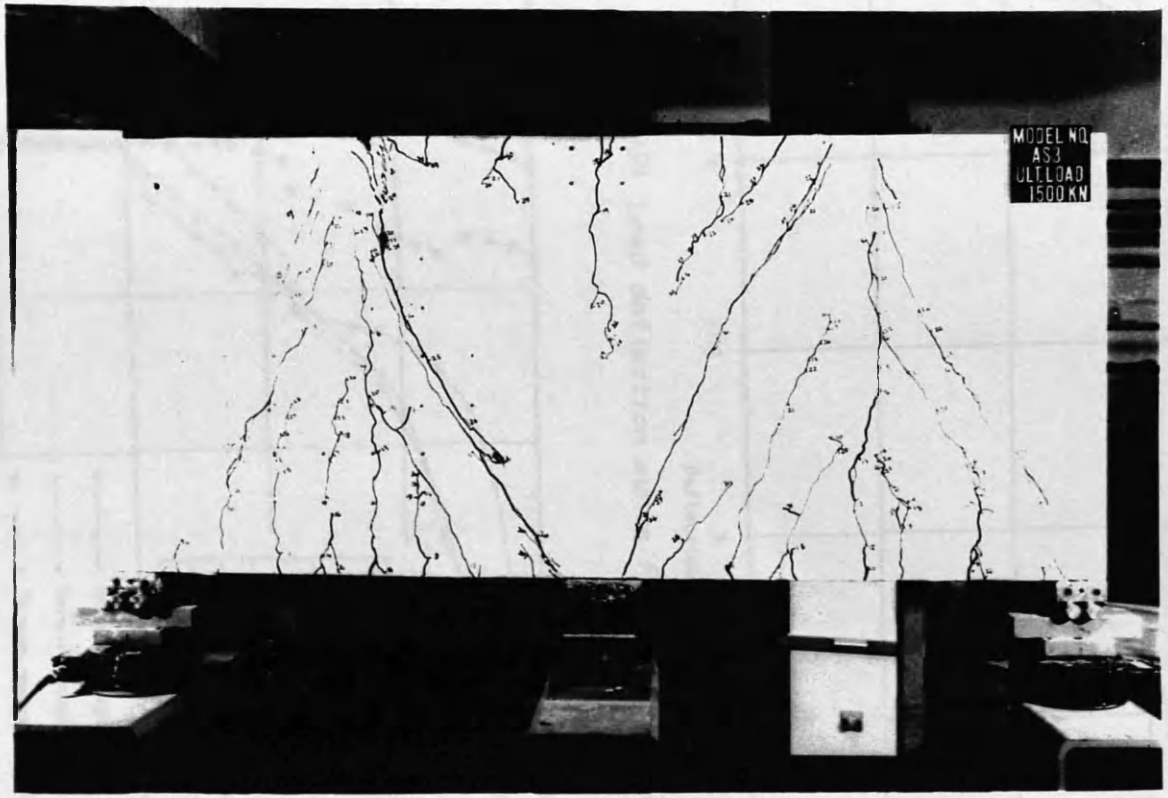

Figure(7.18) Final crack pattern of transfer girder TRGRAS3

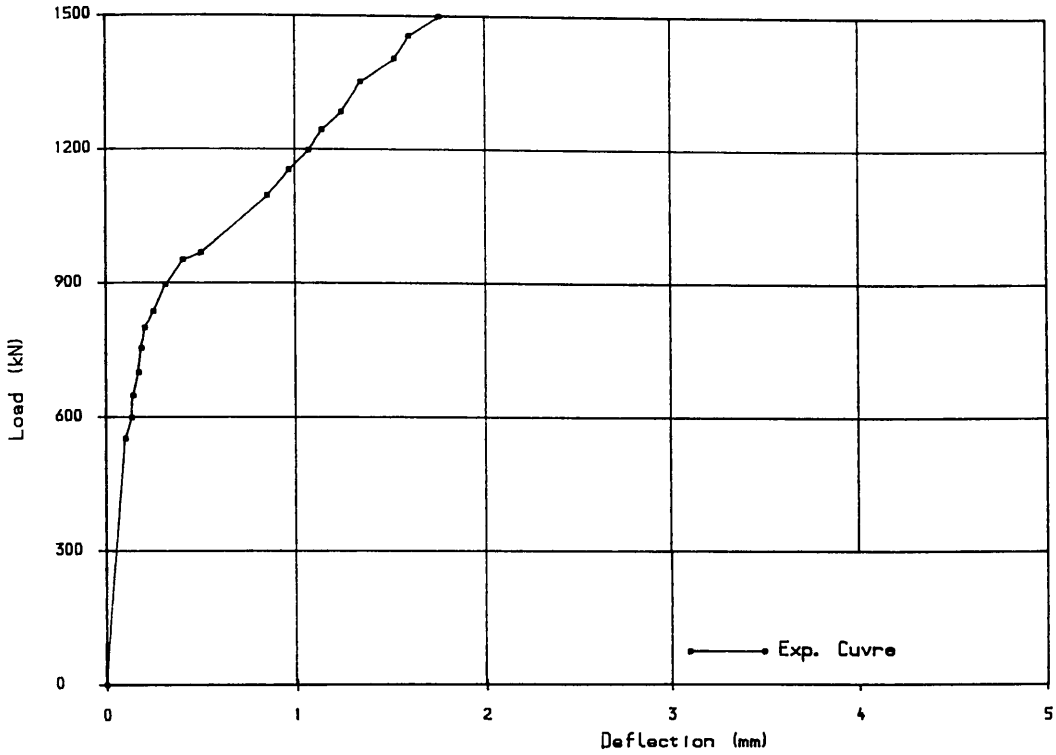

FIG(7.19) Load deflection curve for girder TRGRAS3

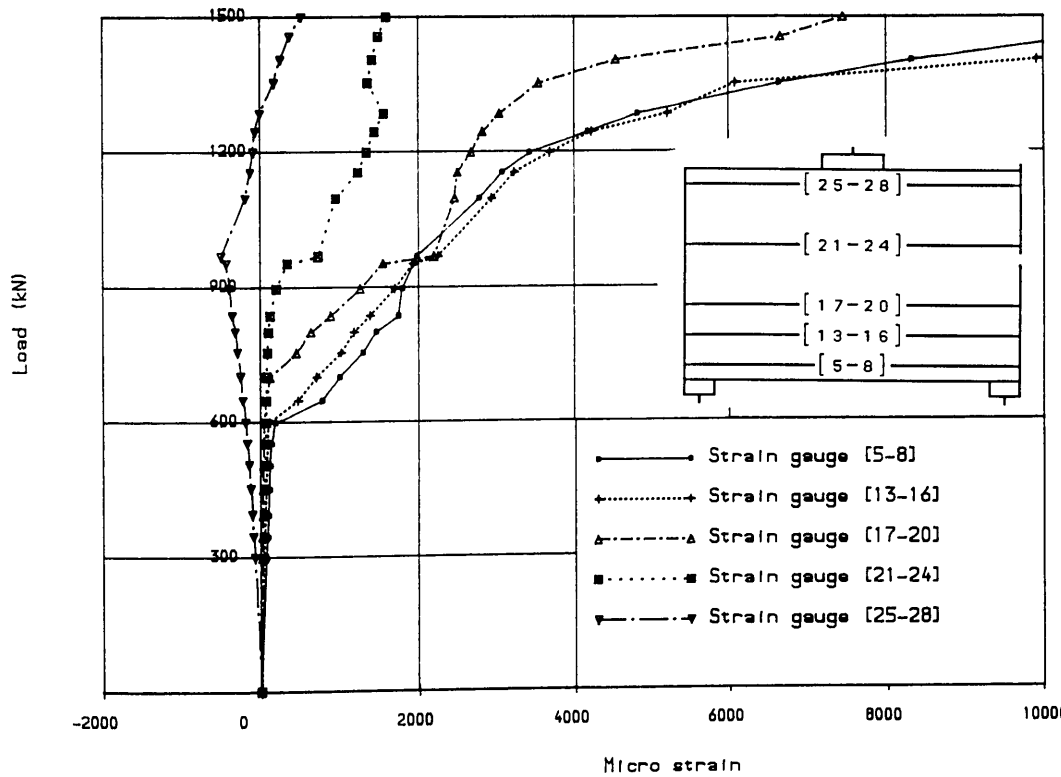

FIG(7.20) Load vs longitudinal steel strains at centre of girder span for girder TRGRAS3

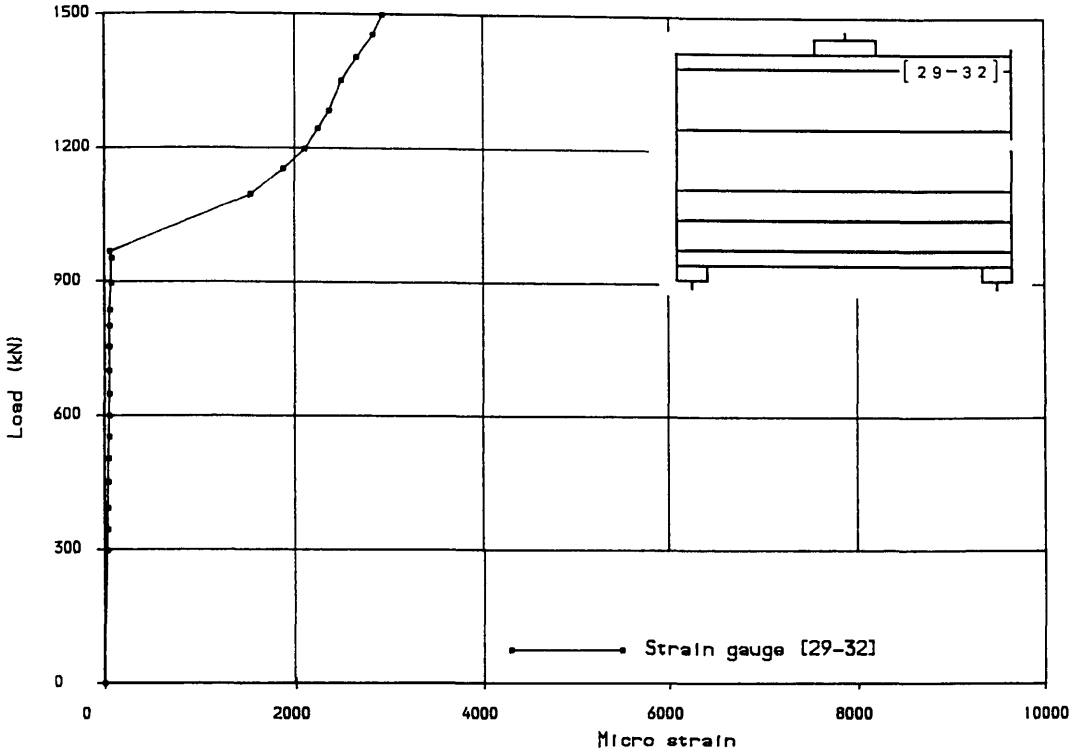

FIG(7.21) Load vs longitudinal steel strains in top bars at 300mm from beam span centre for girder TRGRAS3

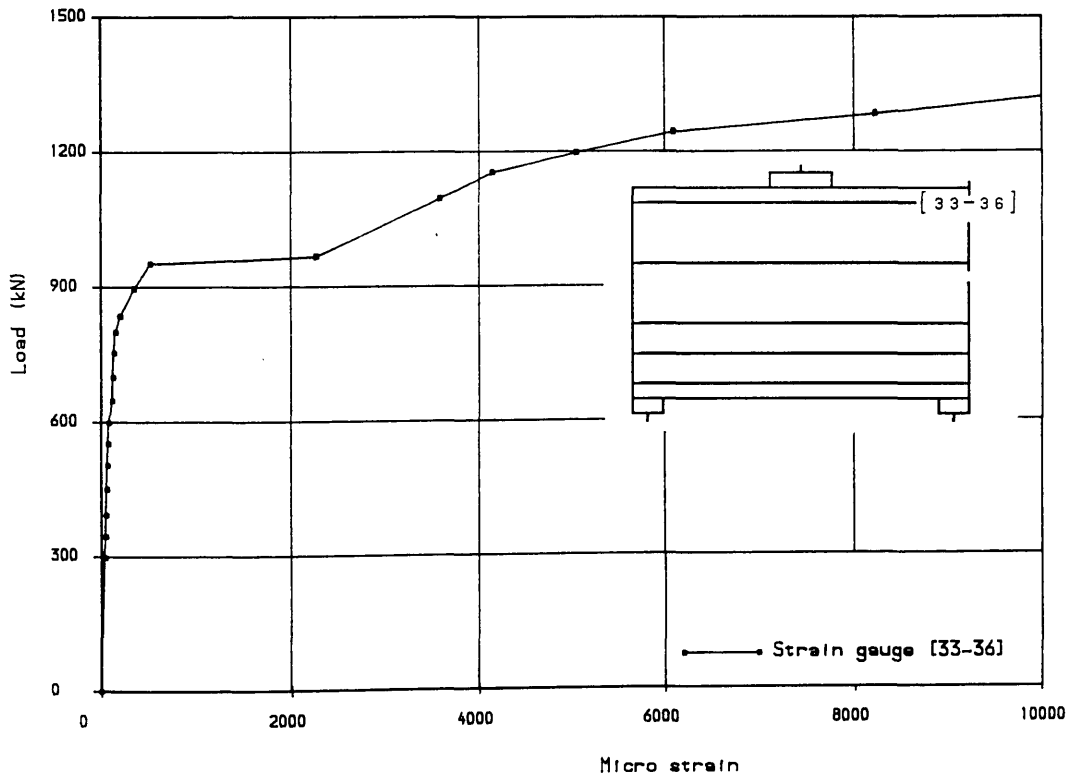

FIG(7.22) Load vs steel strains in top bars over intermediate support for girder TRGRAS3

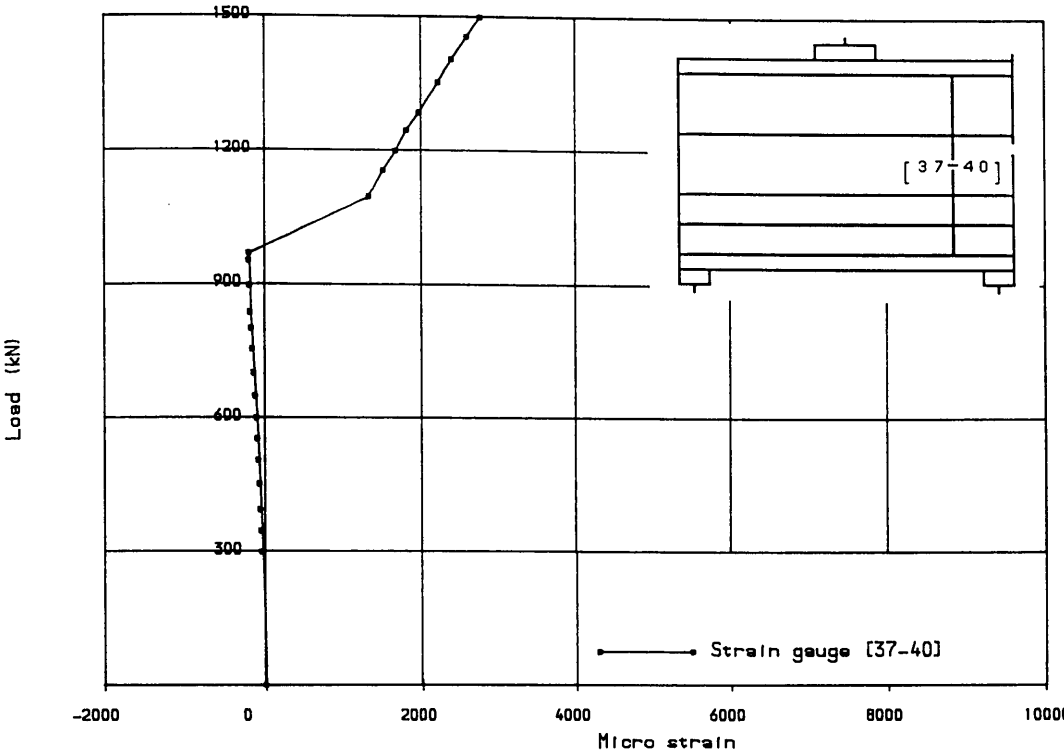

FIG(7.23) Load vs stirrup strains in interior shear span of girder for girder TRGRAS3

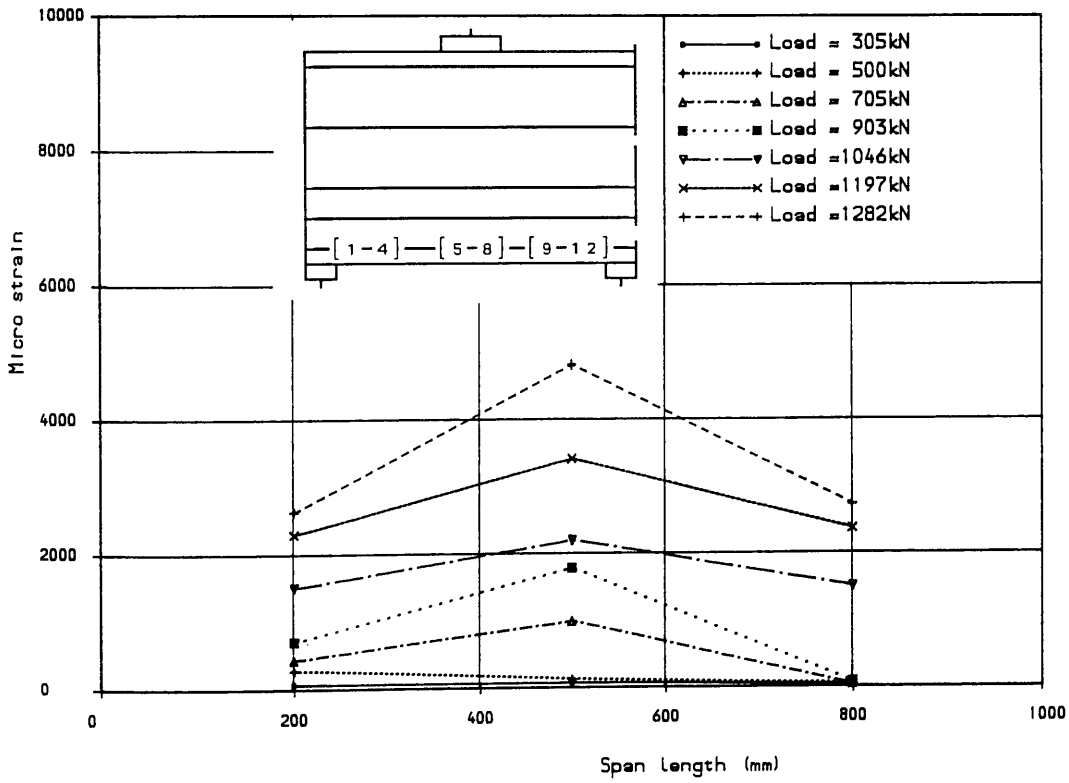

FIG(7.24) Steel strain distribution in bottom bars along girder length for girder TRGRAS3

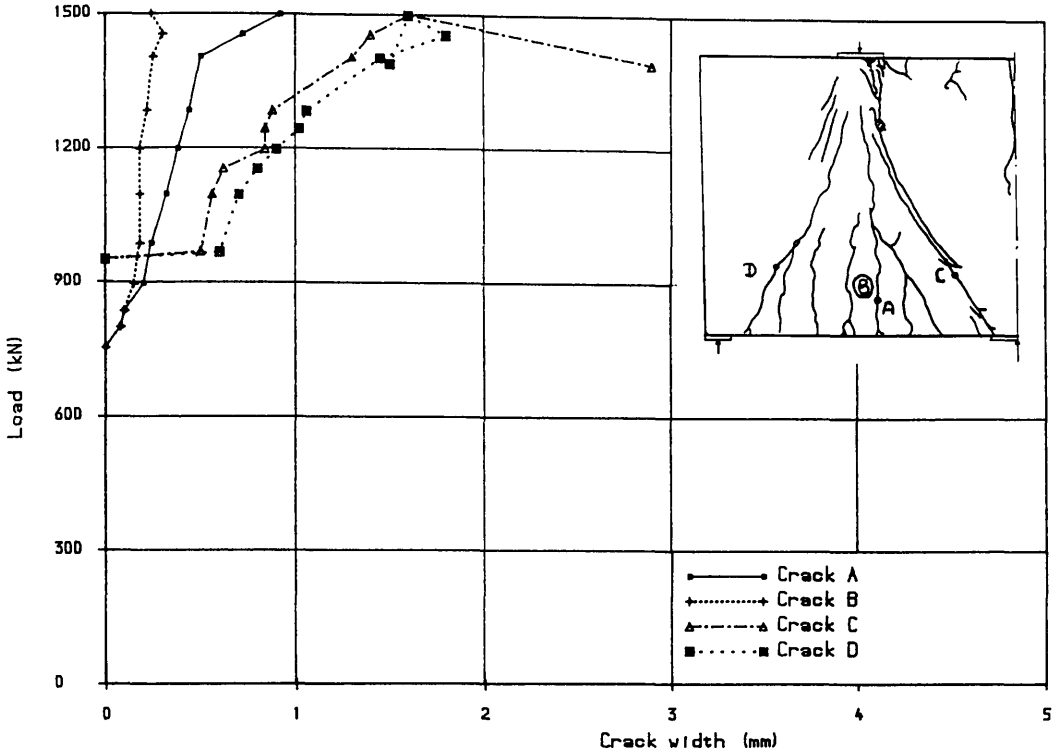

FIG (7.25) Load vs crack width for girder TRGRAS3

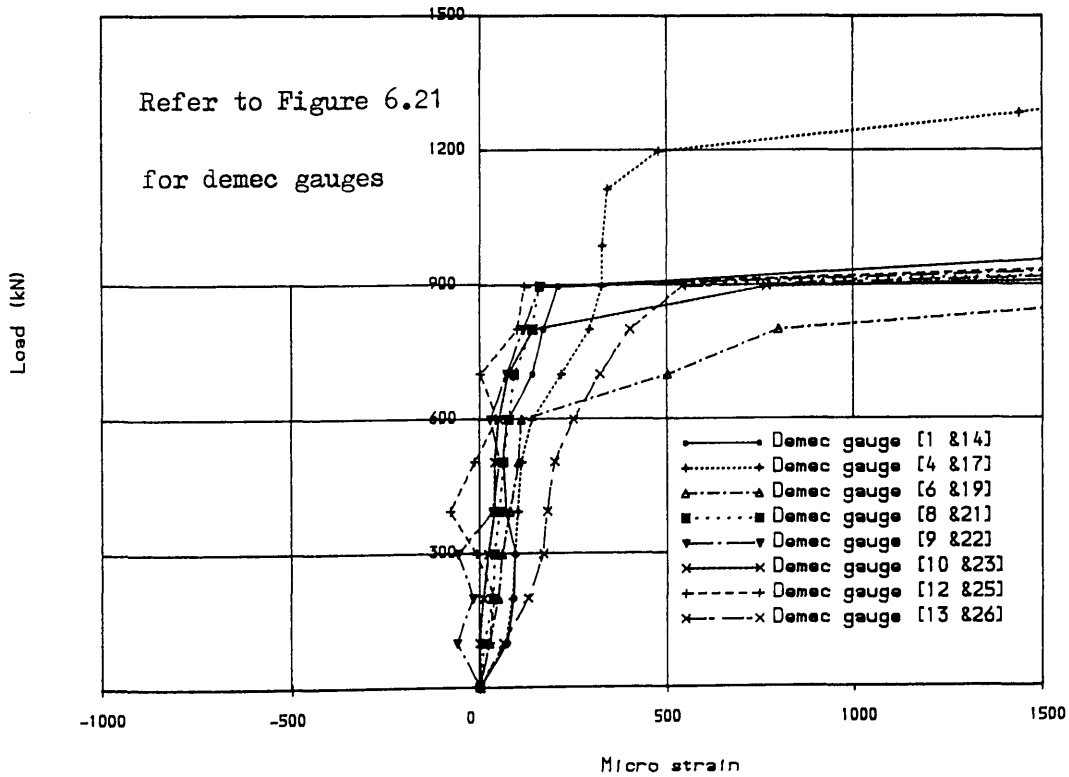

FIG (7.26) Load vs concrete surface strains for girder TRGRAS3

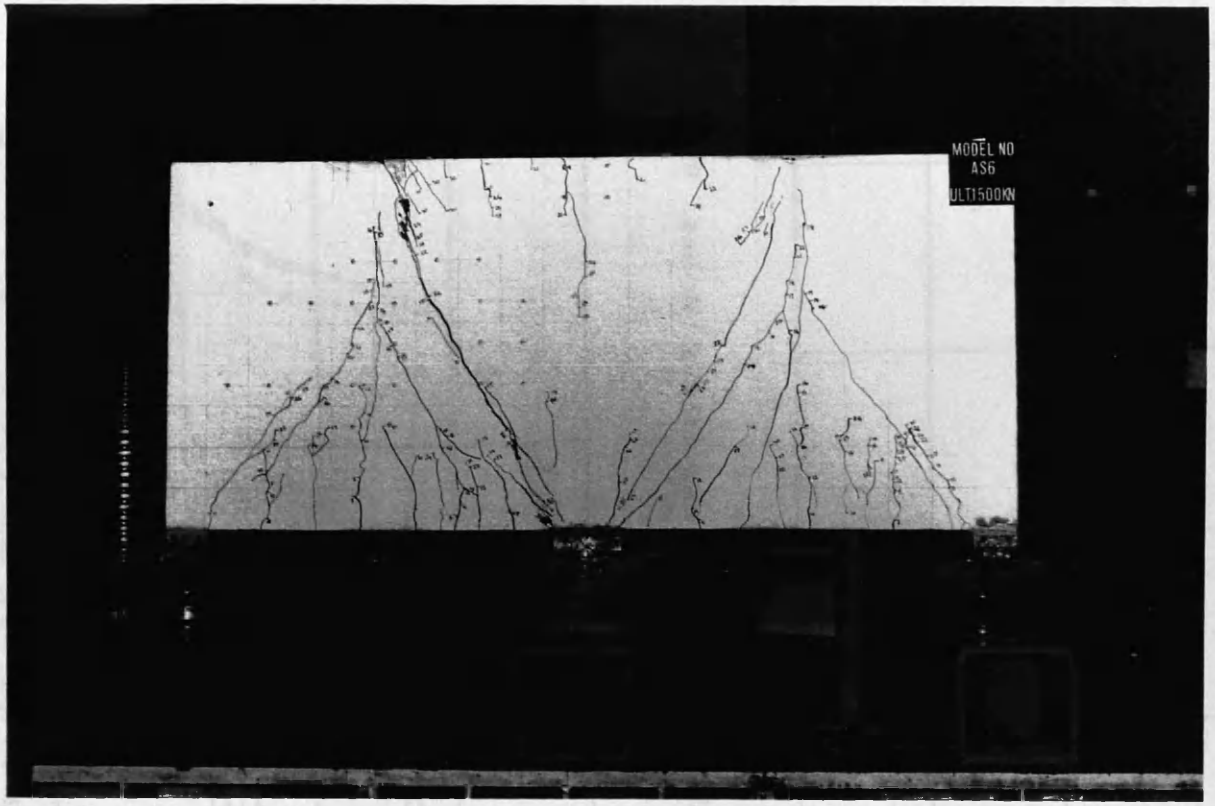

Figure(7.27) Final crack pattern of transfer girder TRGRAS6

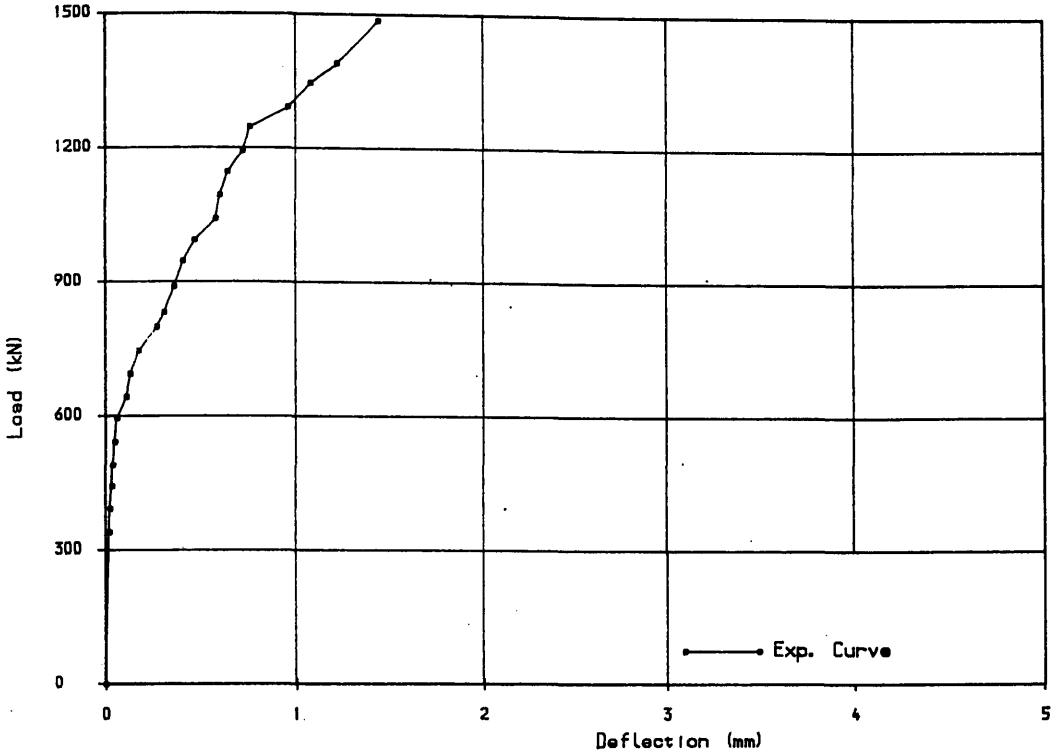

FIG(7.28) Load deflection curve for girder TRGRAS6

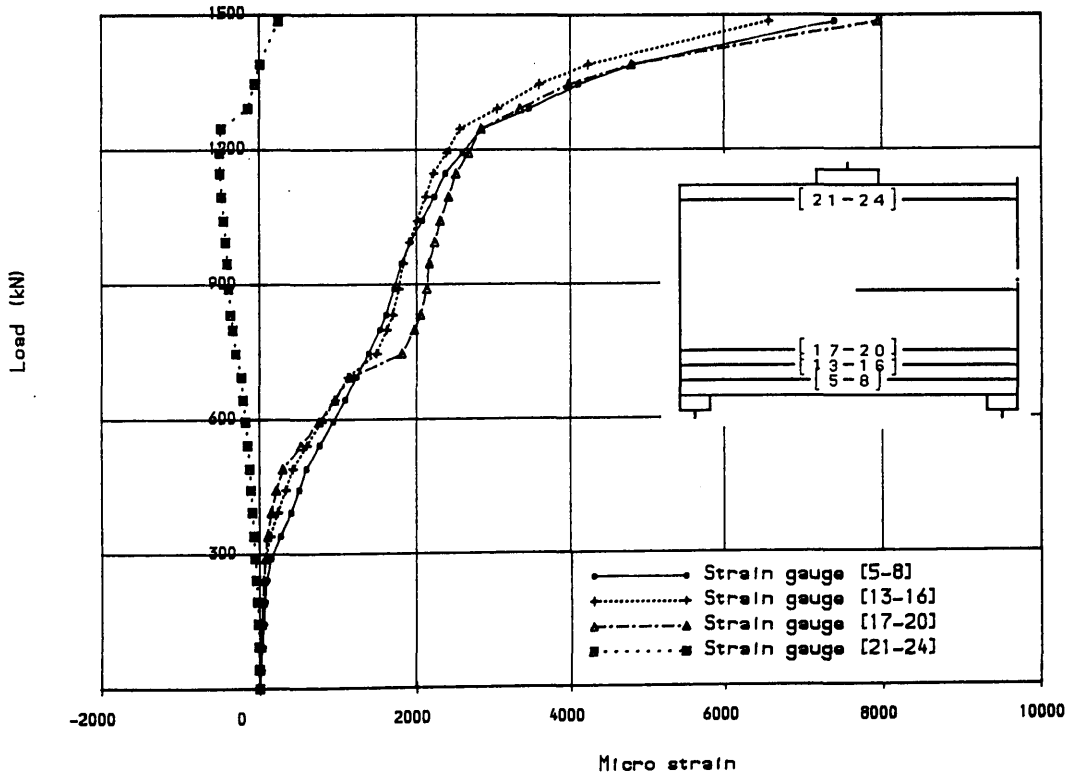

FIG(7.29) Load vs longitudinal steel strains at centre of girder span for girder TRGRAS6

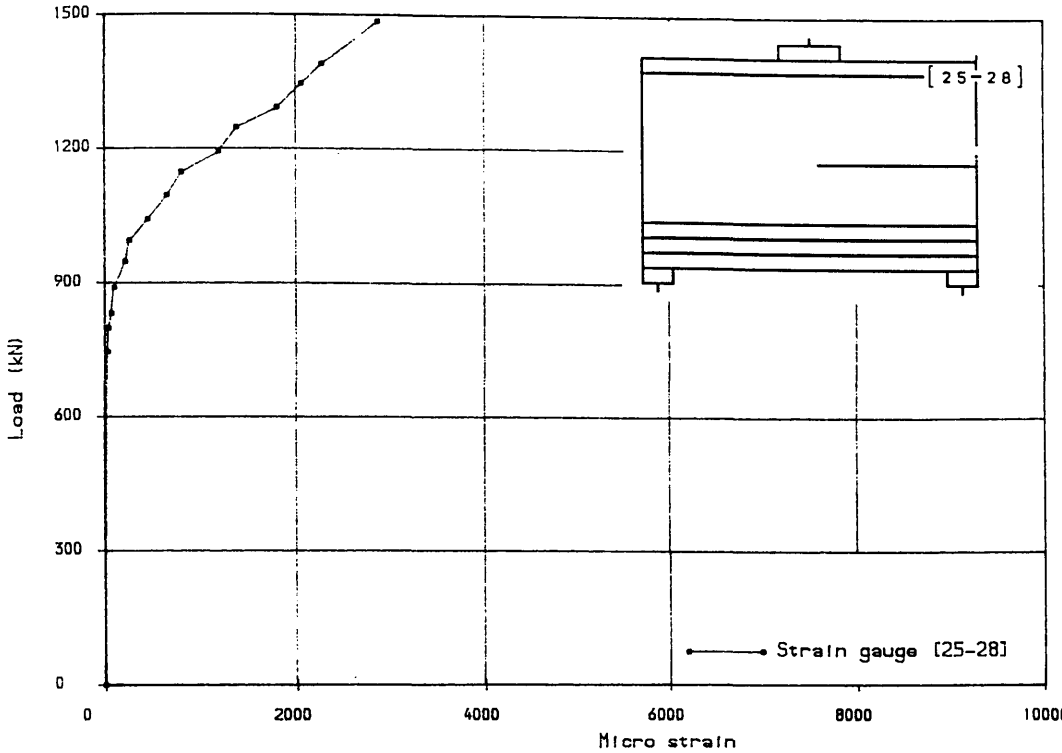

FIG (7.30) Load vs steel strains in top bars over intermediate support for girder TRGRAS6

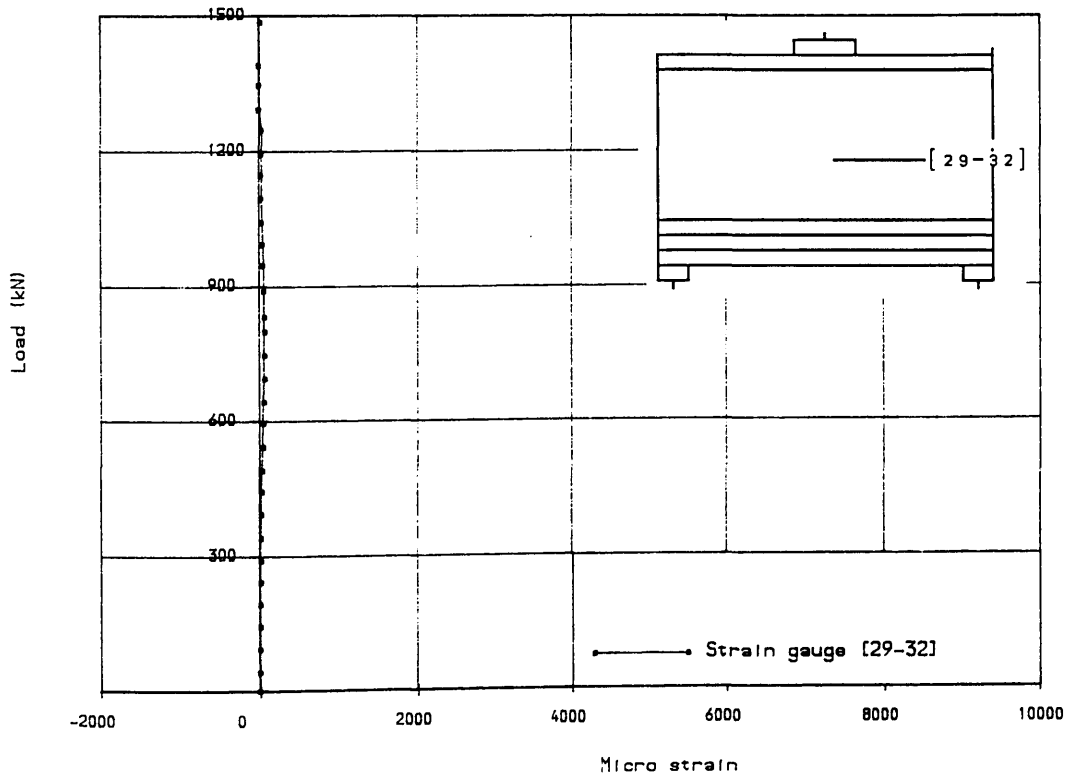

FIG (7.31) Steel strain in mid-depth steel layer over int. support of girder TRGRAS6

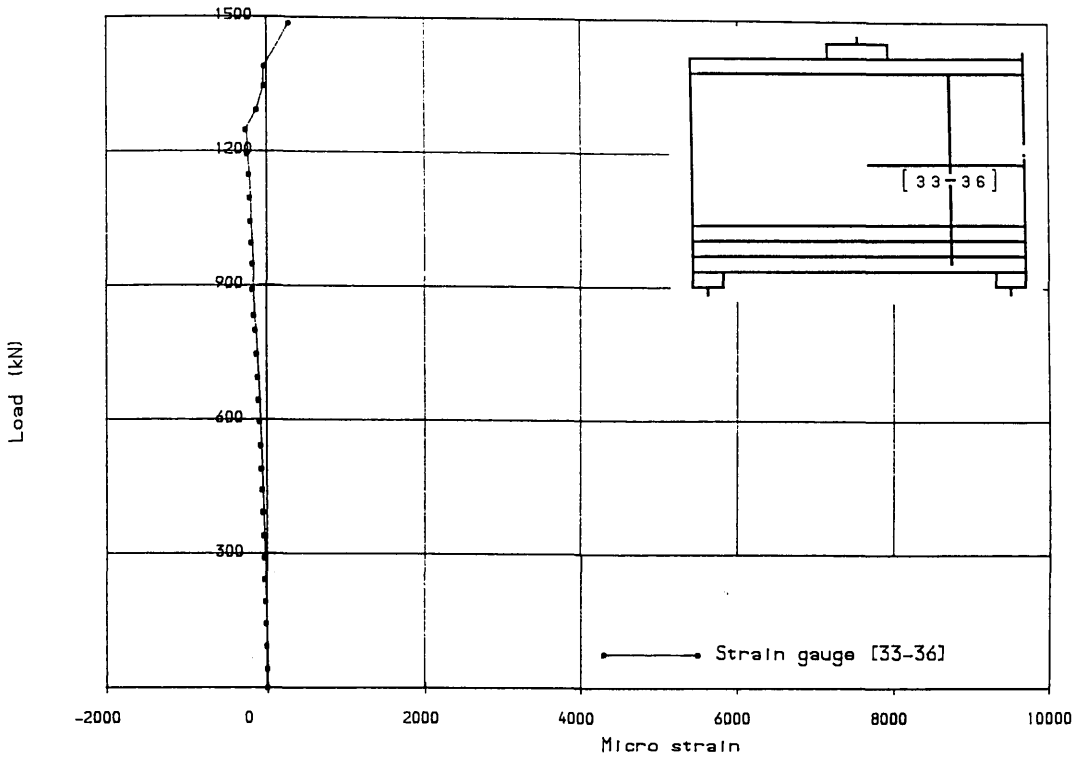

FIG(7.32) Load vs stirrup strains in interior shear span of girder for girder TRGRAS6

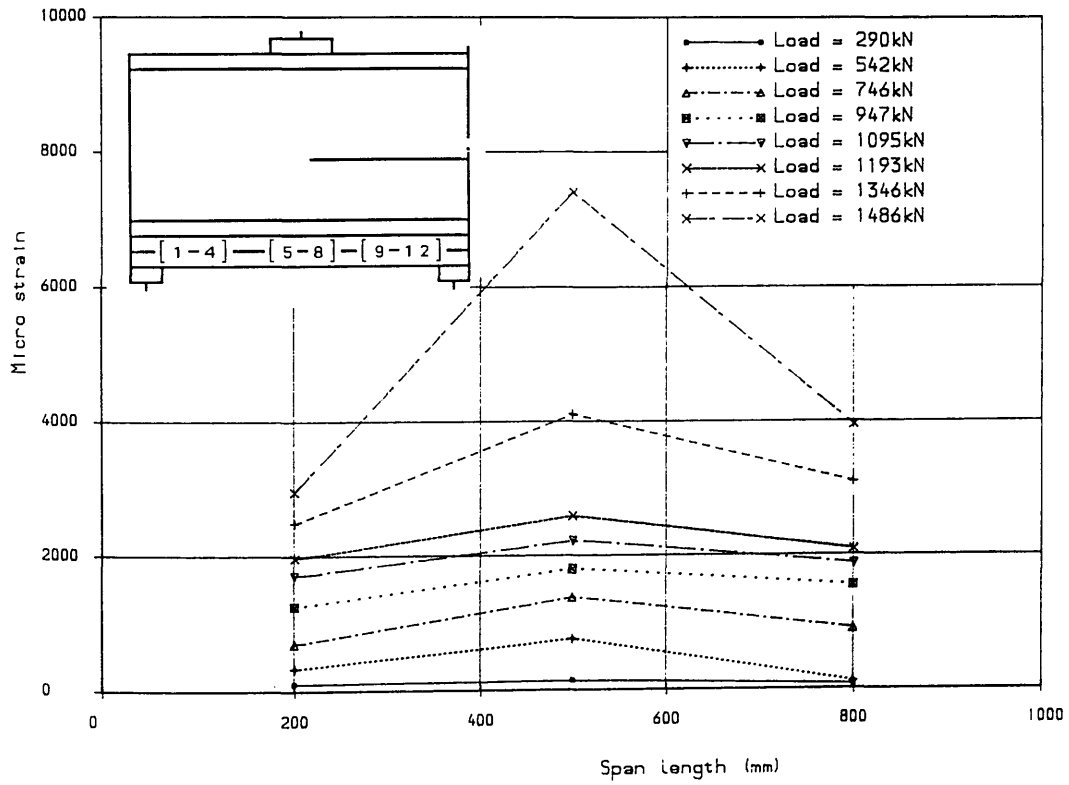

FIG(7.33) Steel strain distribution in bottom bars along girder length for girder TRGRAS6

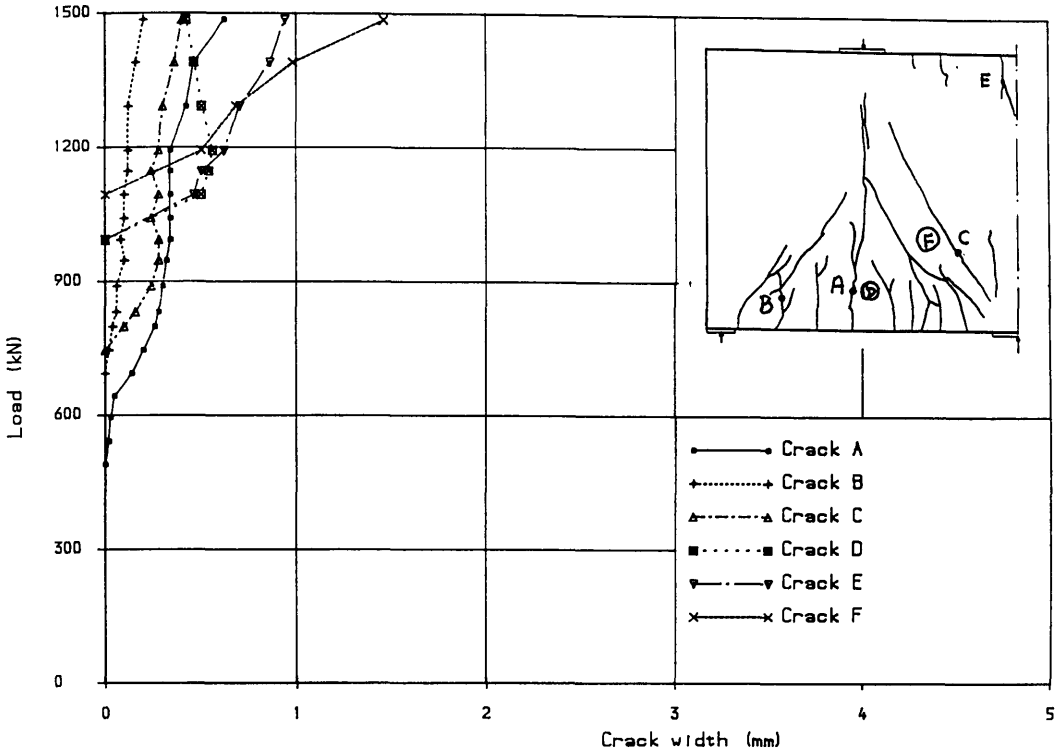

FIG(7.34) Load vs crack width for girder TRGRAS6

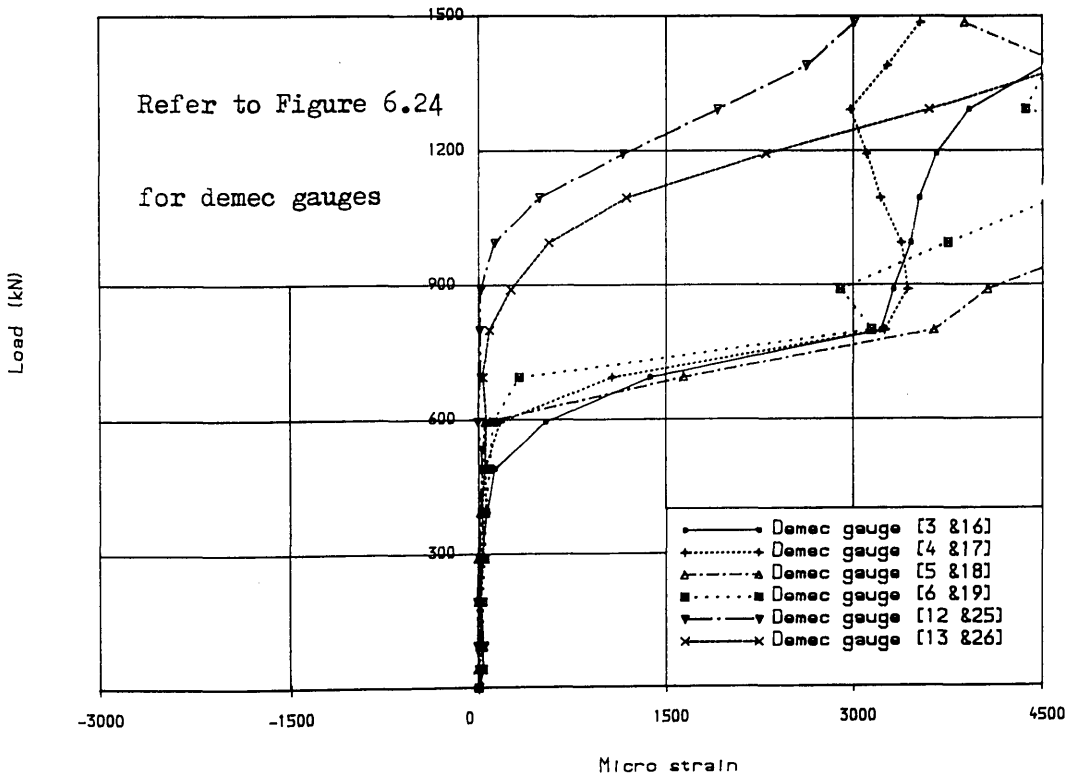

FIG(7.35) Load vs concrete surface strains for girder TRGRAS6

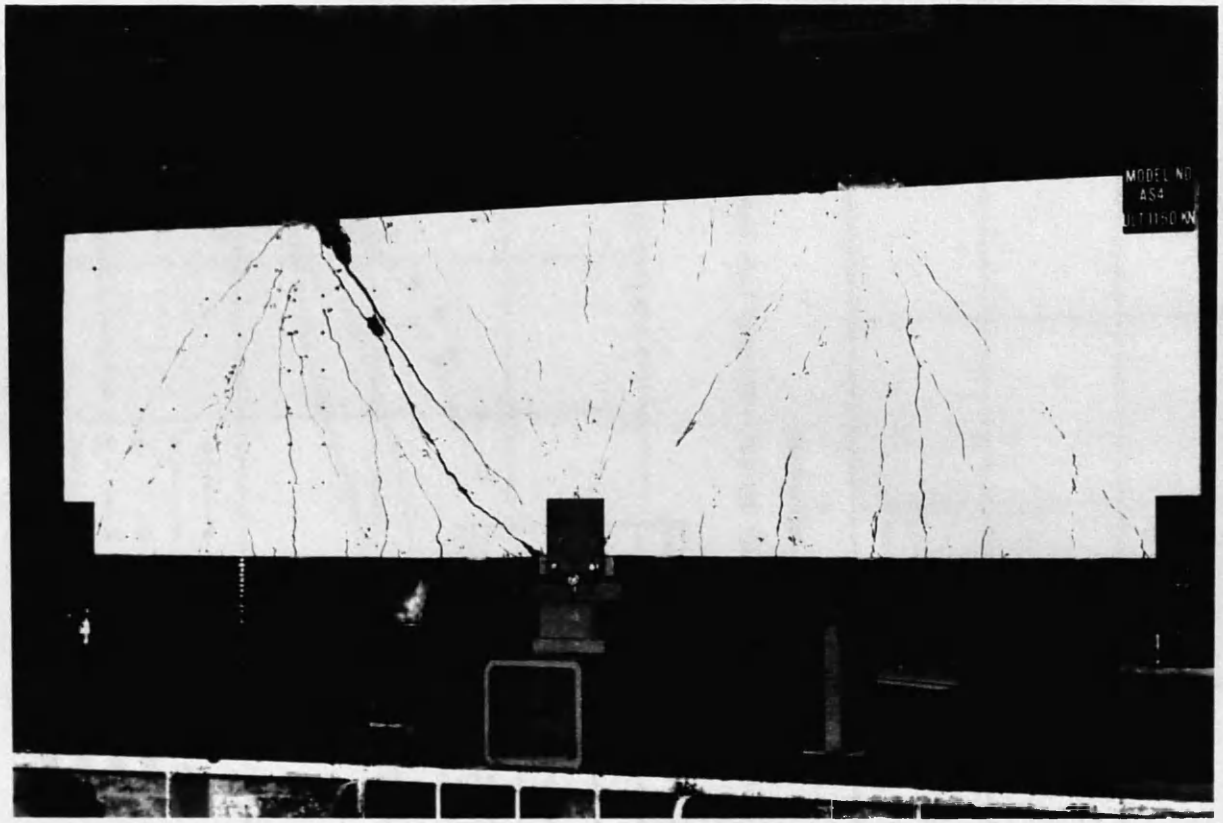

Figure(7.36) Final crack pattern of transfer girder TRGRAS4

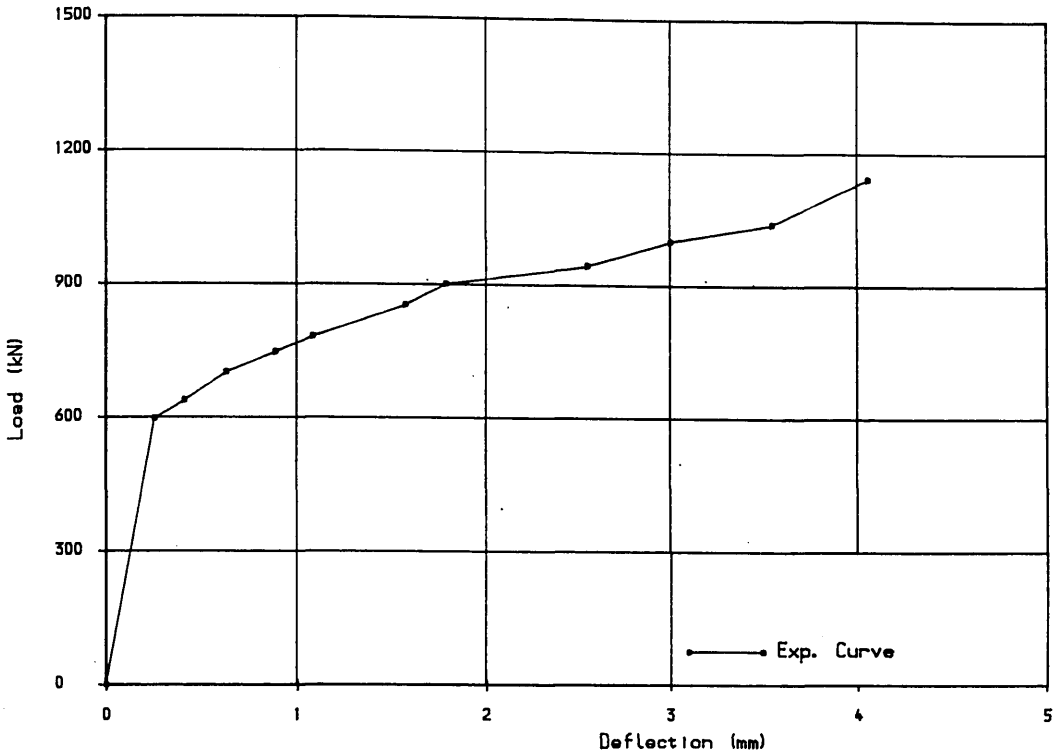

FIG (7.37) Load deflection curve for girder TRGRAS4

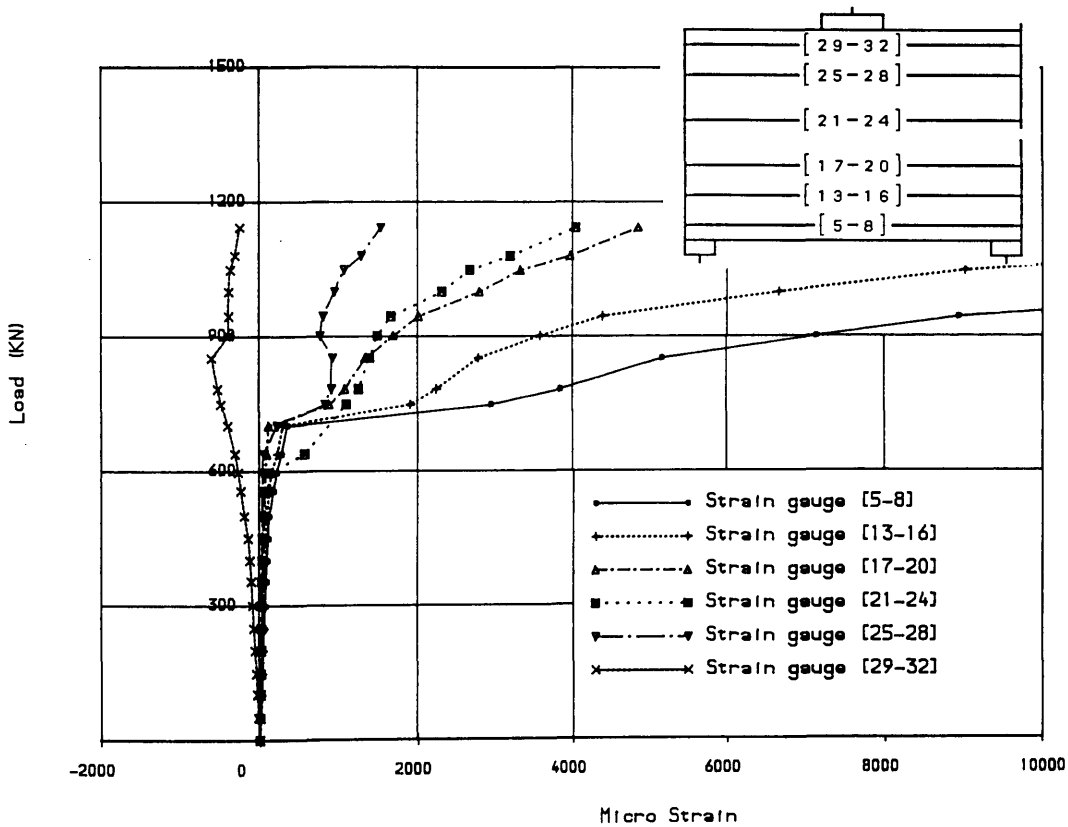

FIG (7.38) Load vs longitudinal steel strains at centre of girder span for girder TRGRAS4

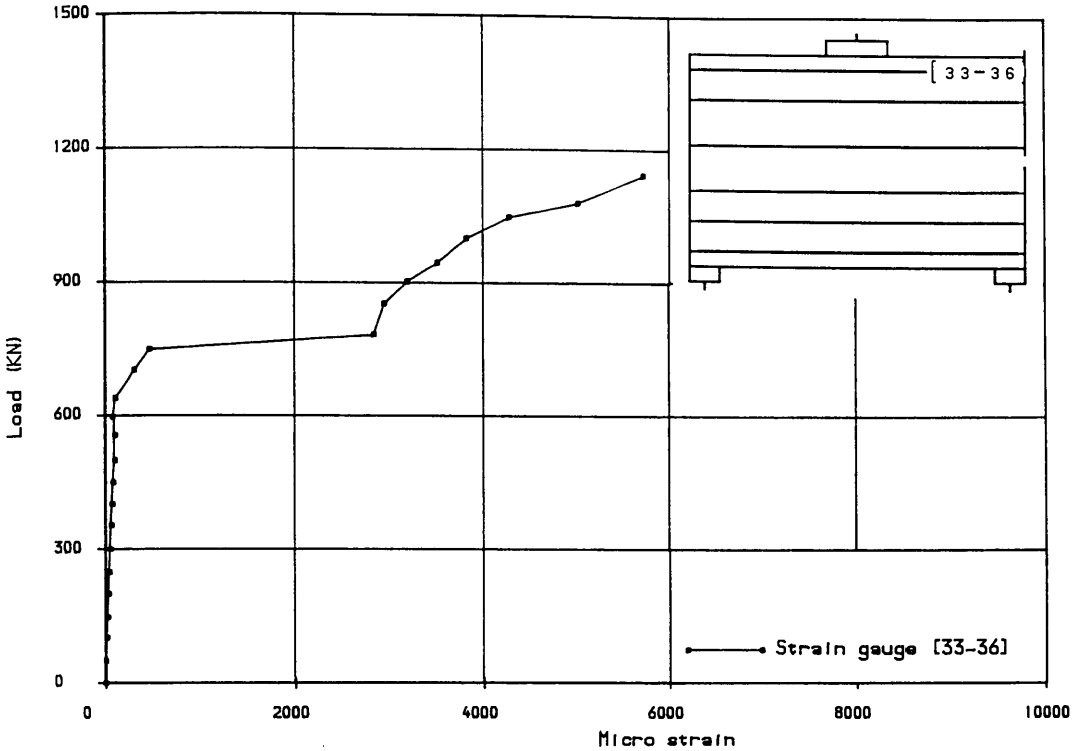

FIG(7.39) Load vs longitudinal steel strains in top bars at 500mm from girder span centre for girder TRGRAS4

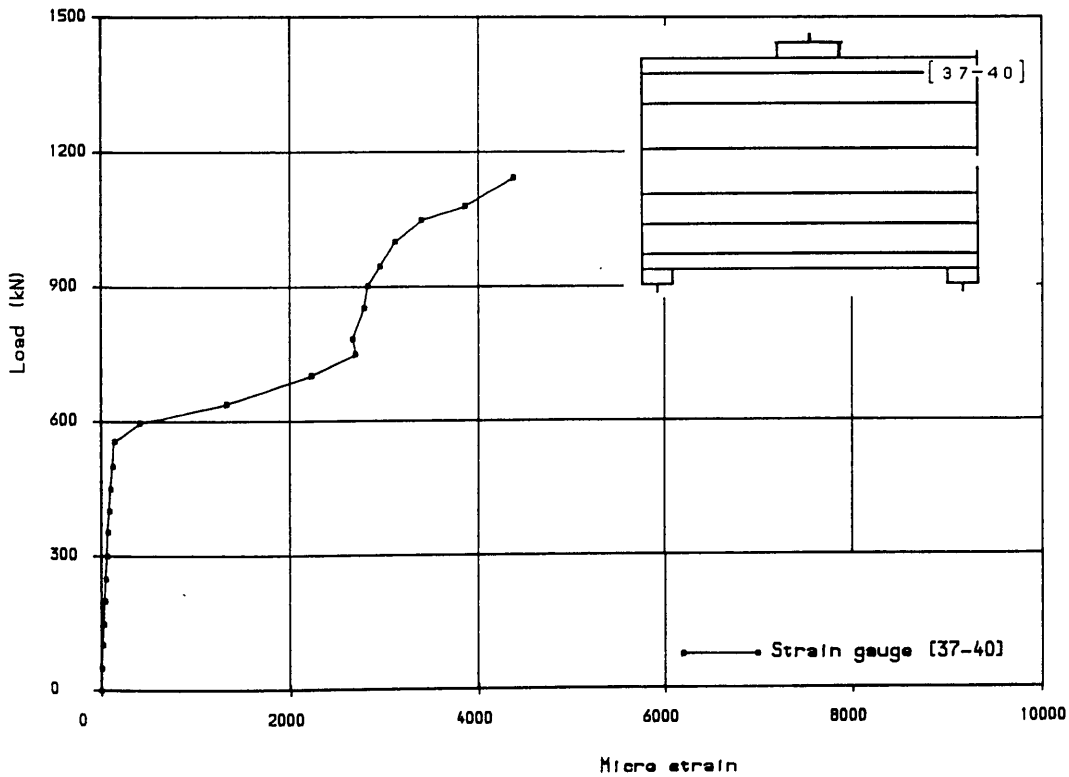

FIG(7.40) Load vs steel strains in top bars over intermediate support for girder TRGRAS4

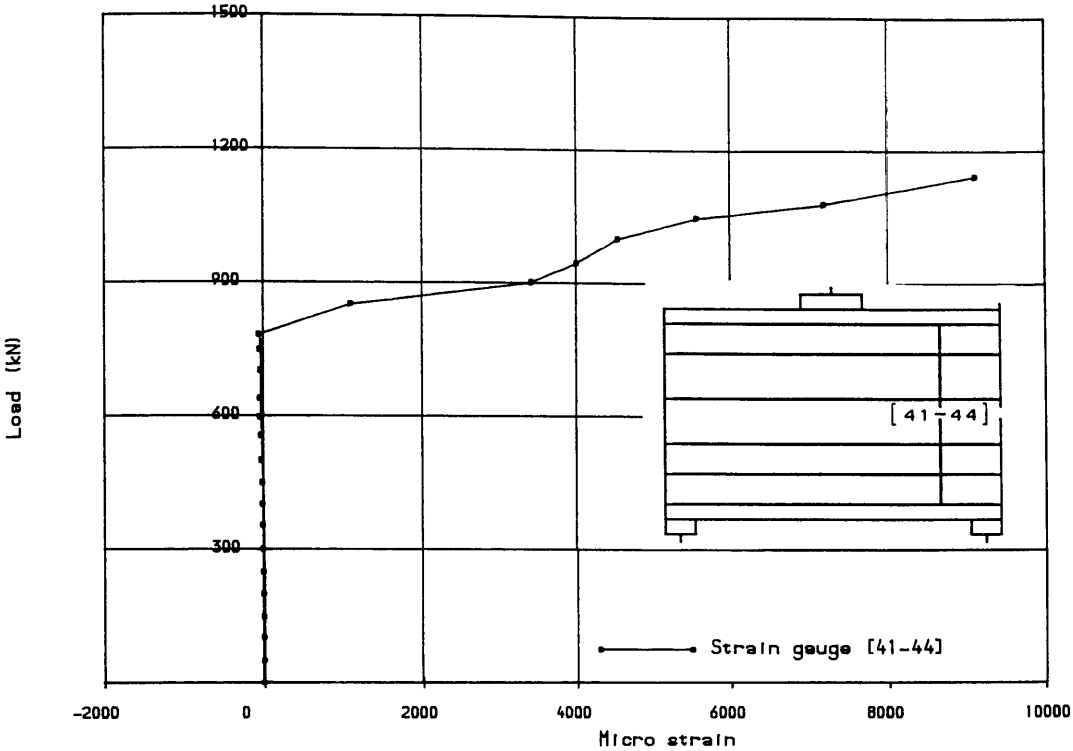

FIG(7.41) Load vs stirrup strains in interior shear span of girder for girder TRGRAS4

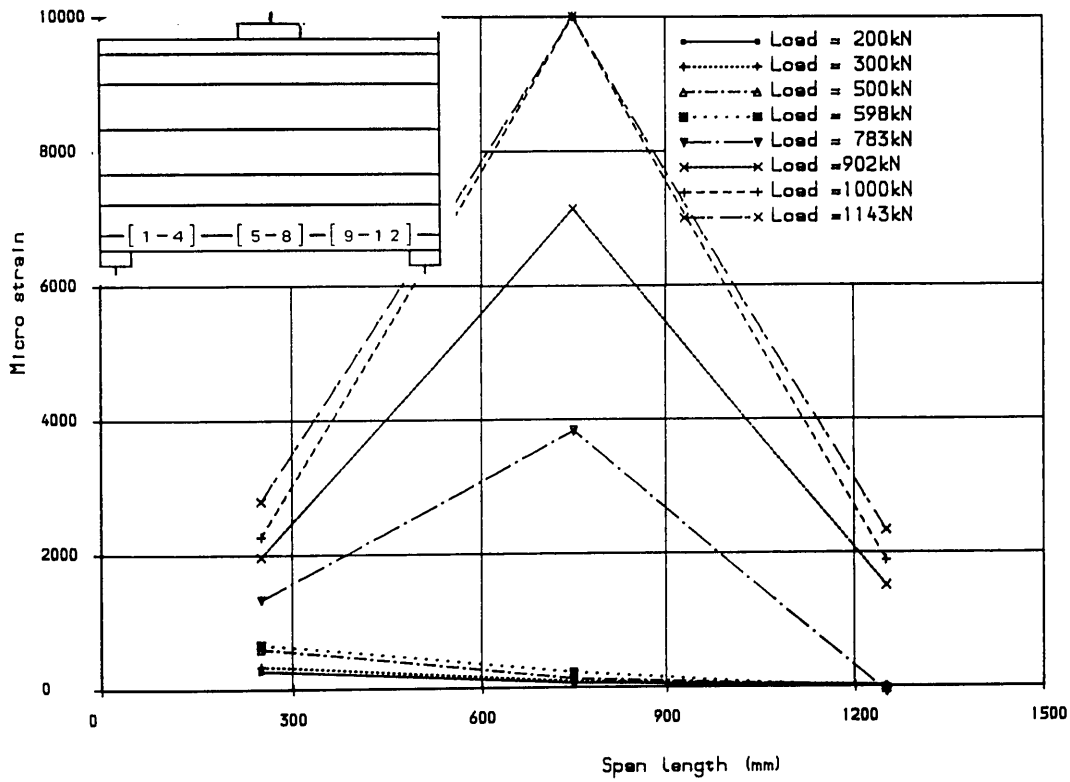

FIG(7.42) Steel strain distribution in bottom bars along girder length for girder TRGRAS4

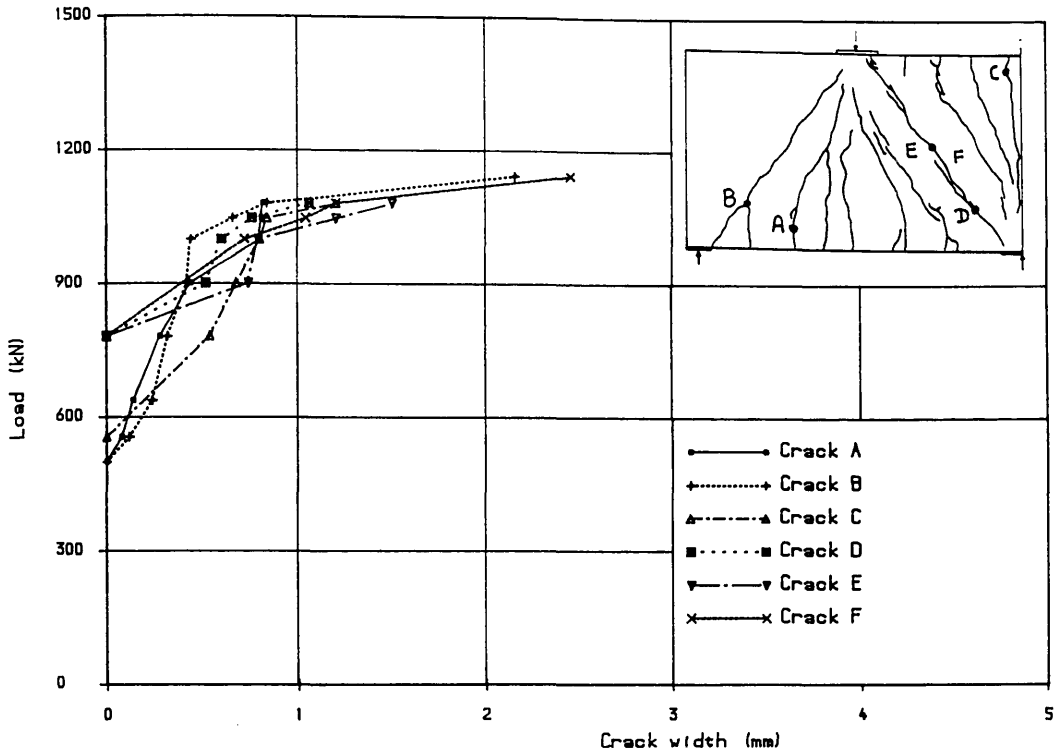

FIG (7.43) Load vs crack width for girder TRGRAS4

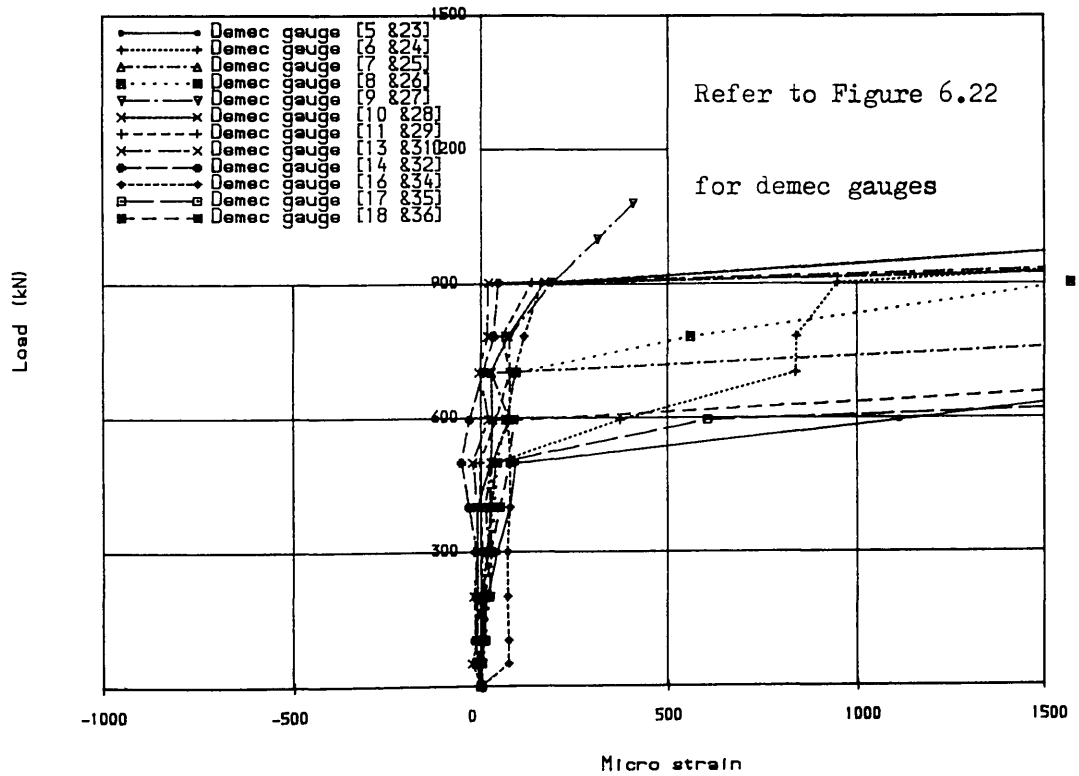

FIG (7.44) Load vs concrete surface strains for girder TRGRAS4

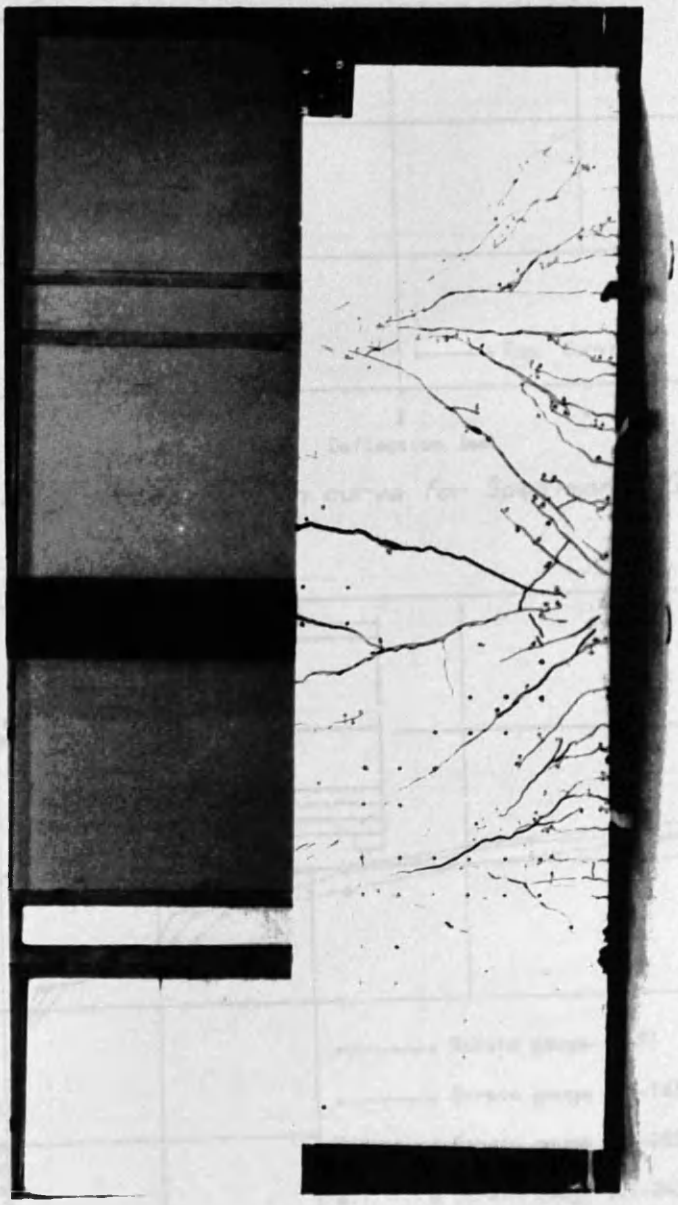

Figure(7.45) Final crack pattern of transfer girder TRGRASS

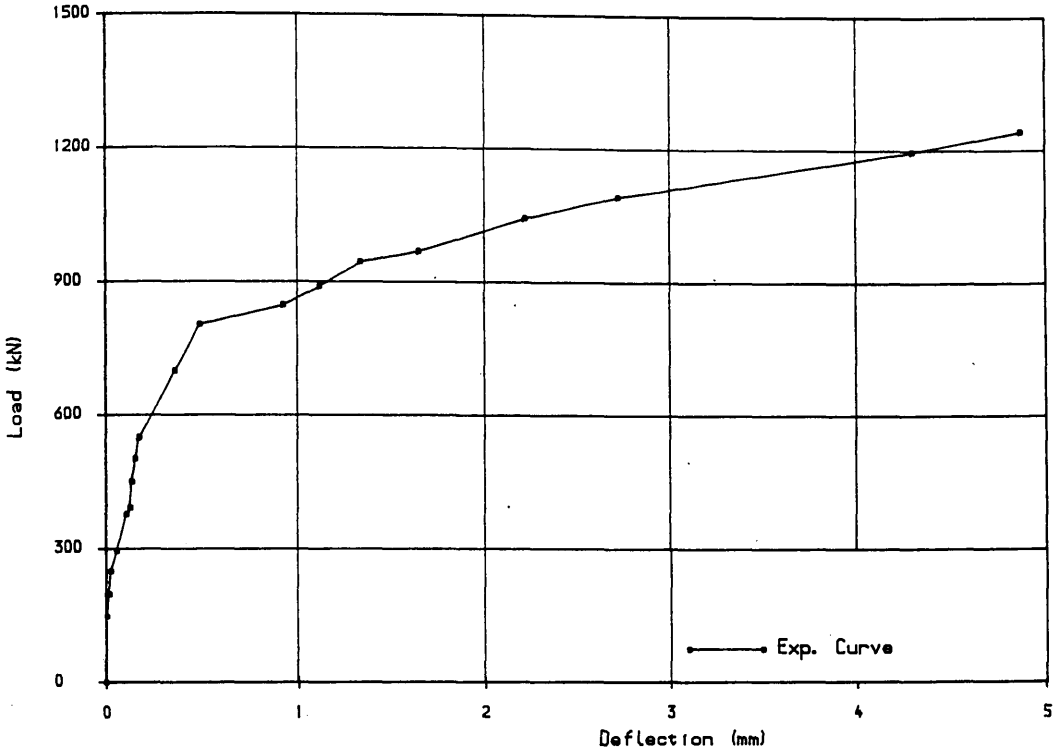

FIG(7.46) Load deflection curve for Specimen TRGRAS5

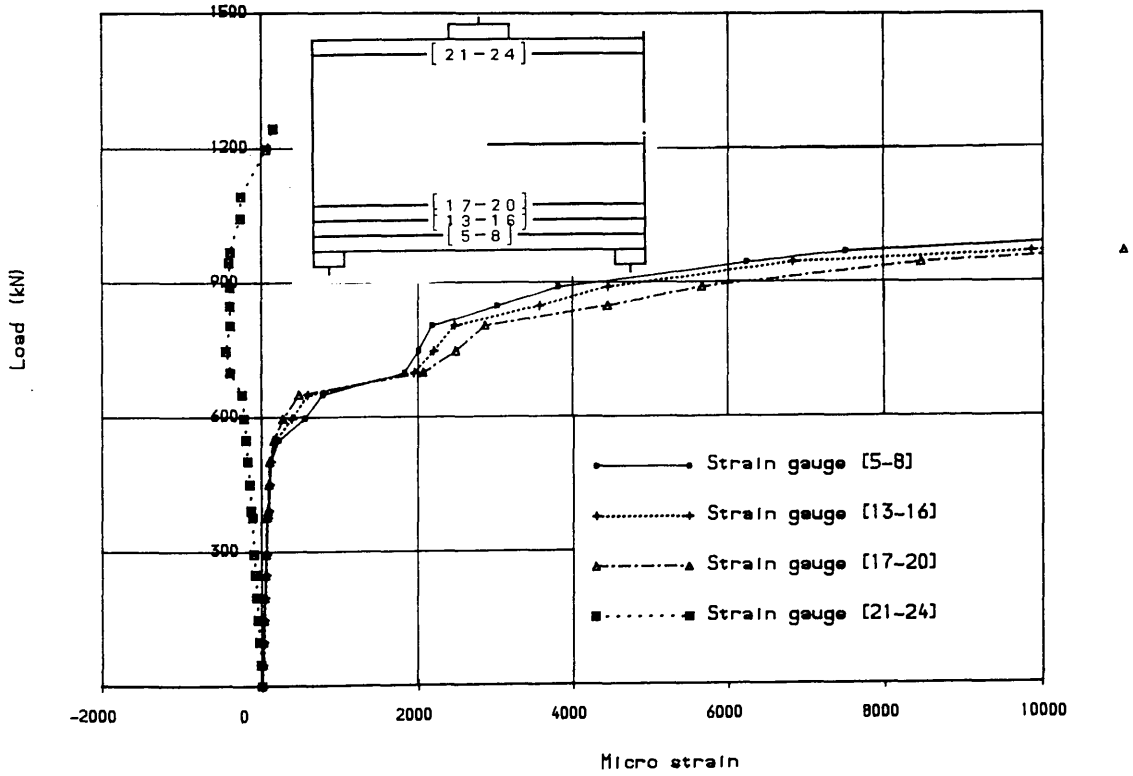

FIG(7.47) Load vs longitudinal steel strains at centre of girder span for girder TRGRAS5

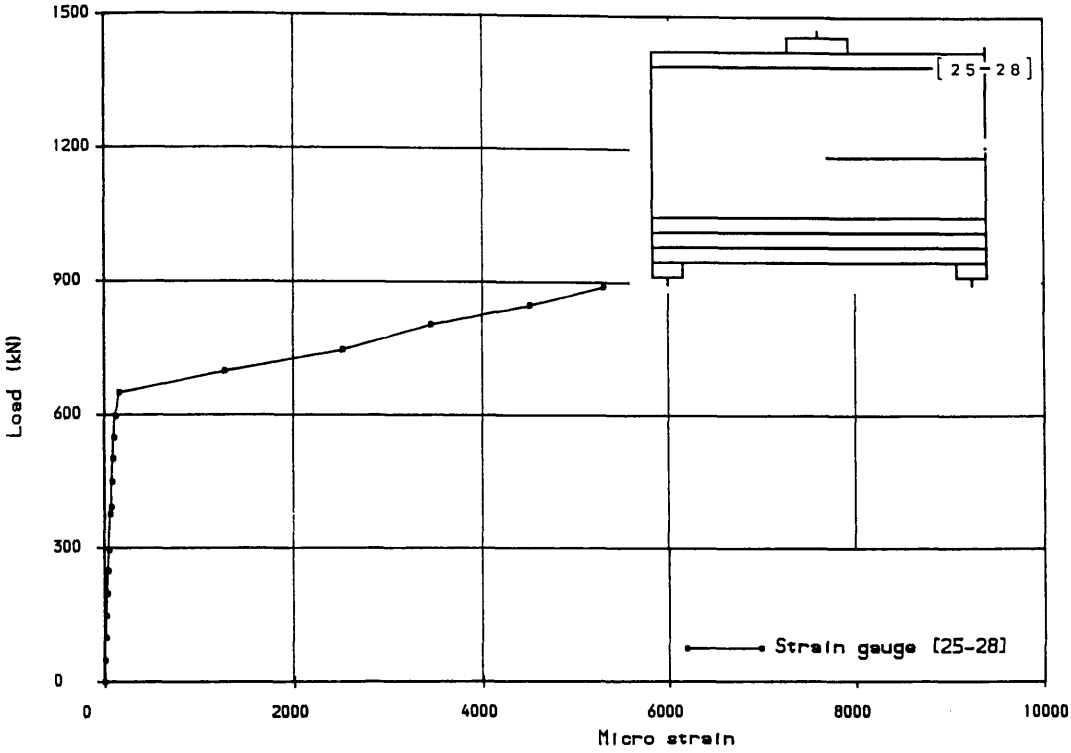

FIG (7.48) Load vs steel strains in top bars over intermediate support for girder TRGRAS5

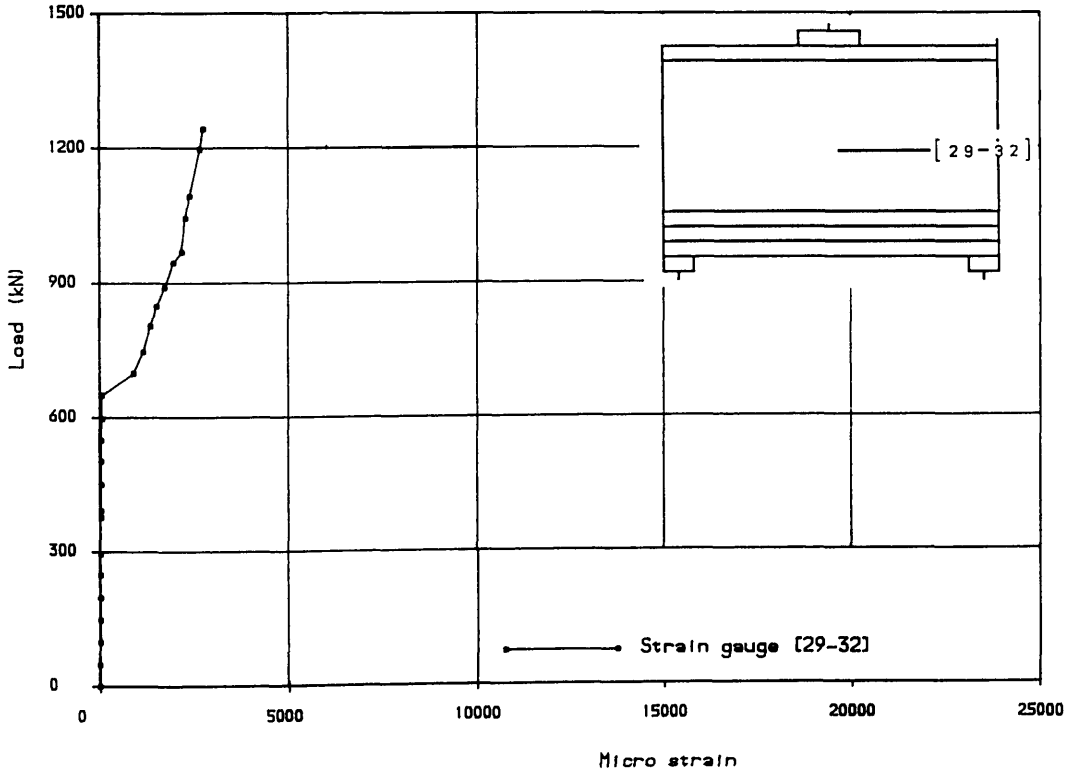

FIG (7.49) Steel strain in mid-depth steel layer over int. support of girder TRGRAS5

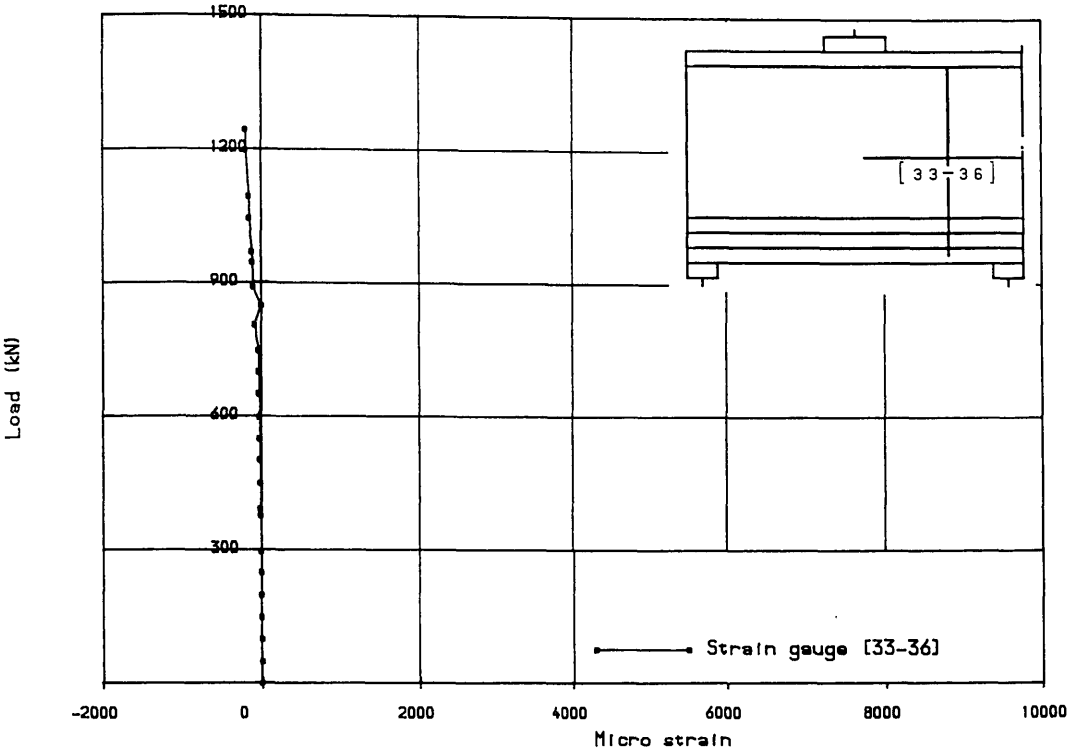

FIG(7.50) Load vs stirrup strains in interior shear span of girder for girder TRGRAS5

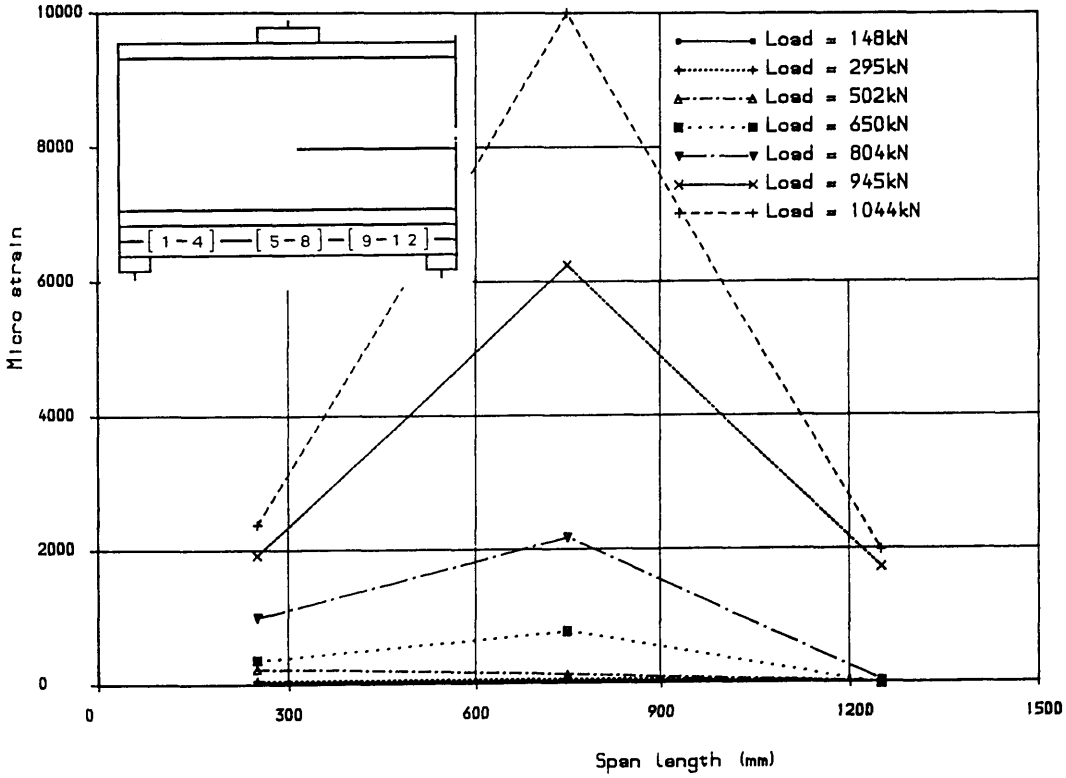

FIG(7.51) Steel strain distribution in bottom bars along girder length for girder TRGRAS5

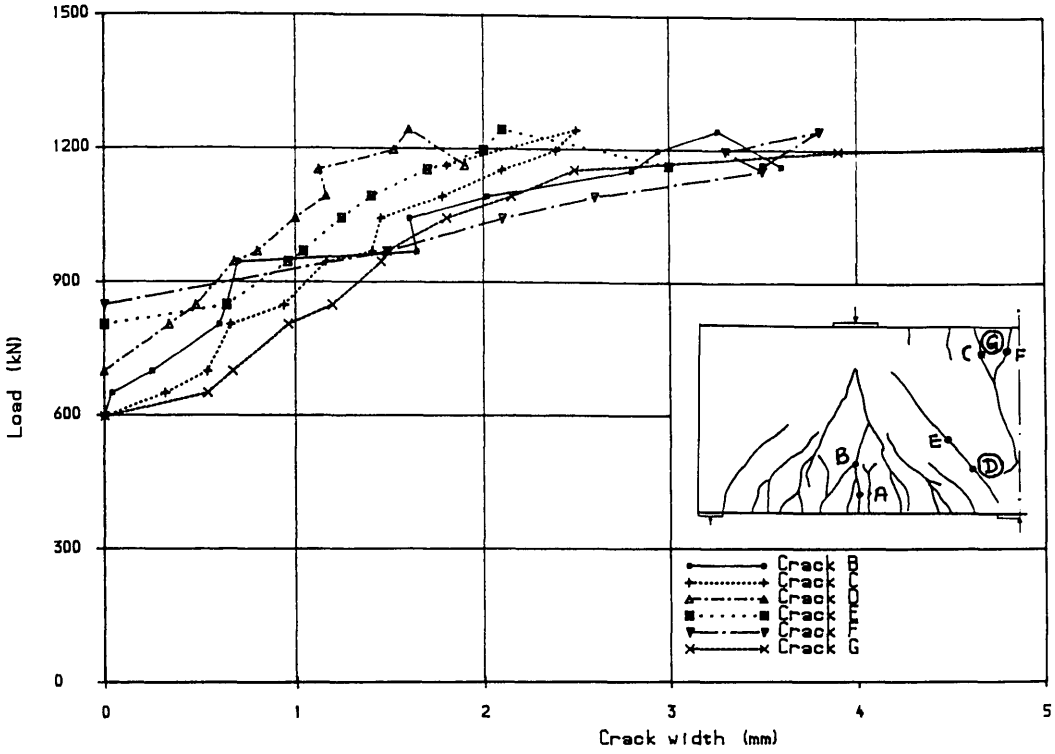

FIG(7.52) Load vs crack width for girder TRGRAS5

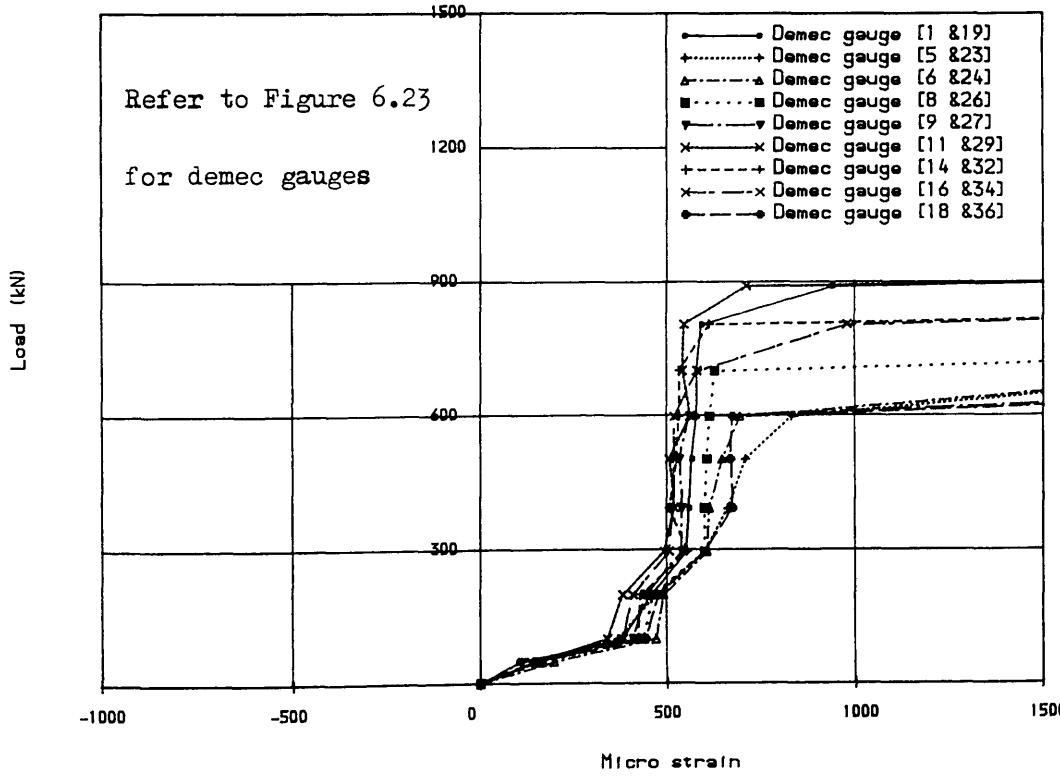

FIG(7.53) Load vs concrete surface strains for girder TRGRAS5

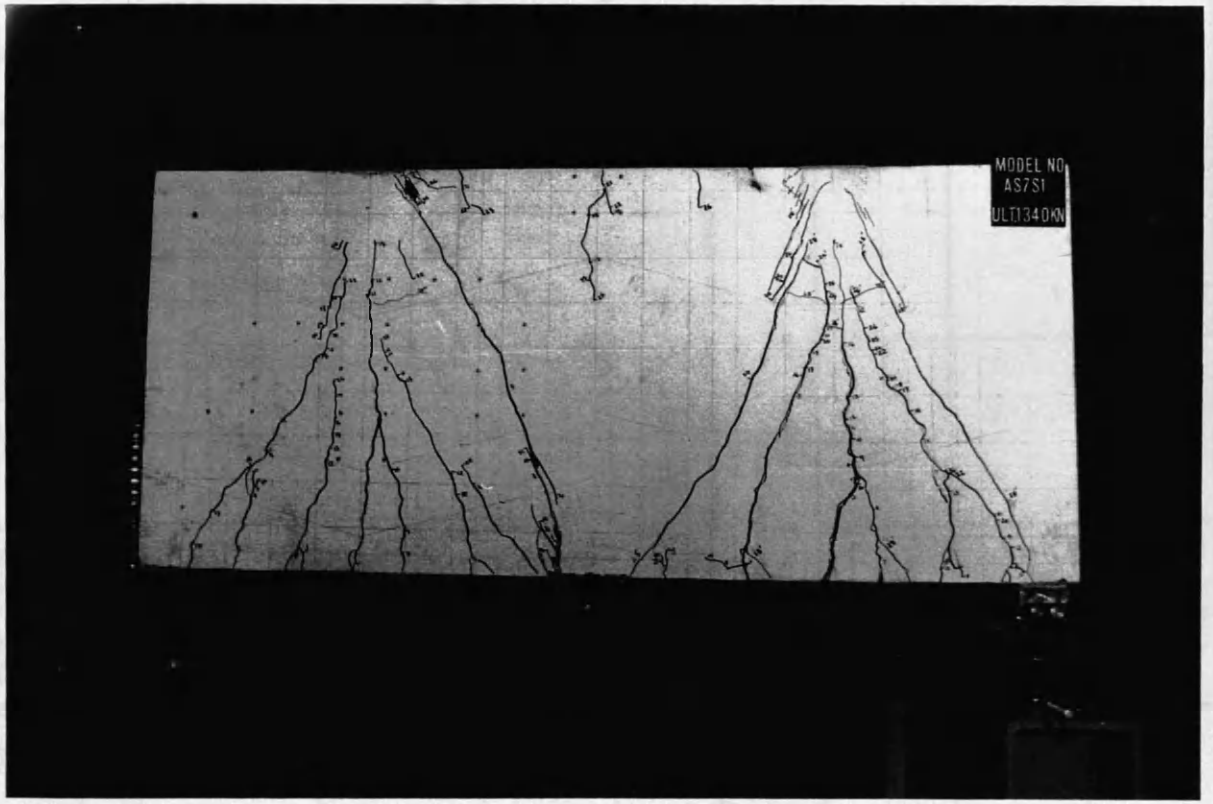

Figure(7.54) Final crack pattern of transfer girder TRGRAS7

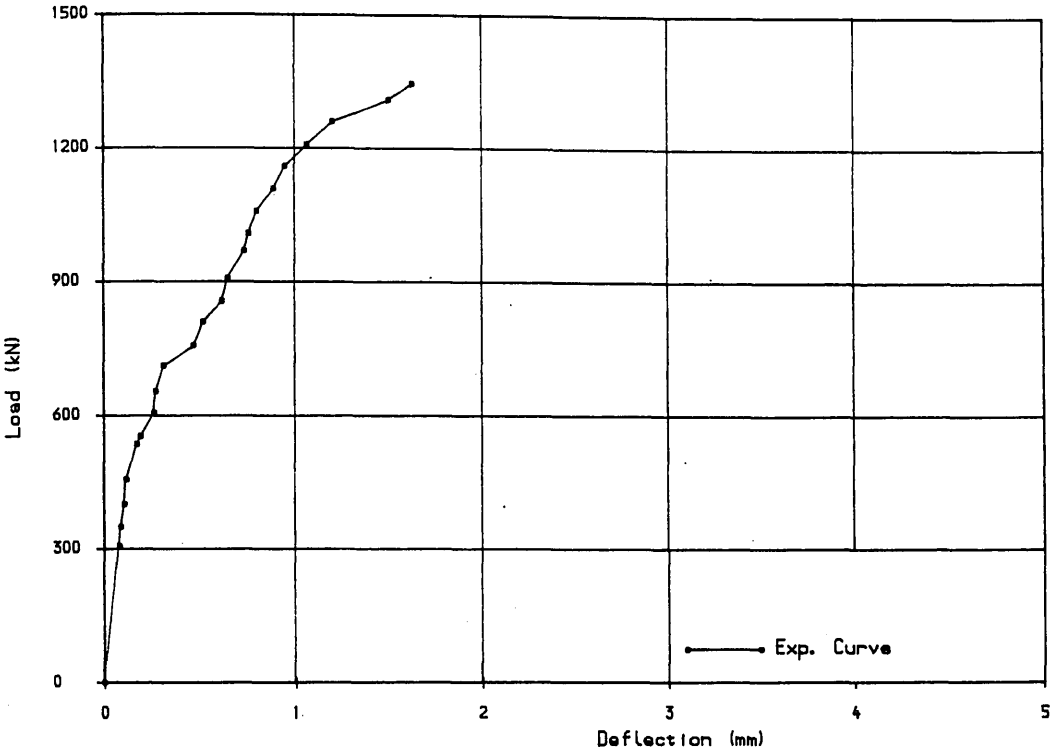

FIG(7.55) Load deflection curve for girder TRGRAS7

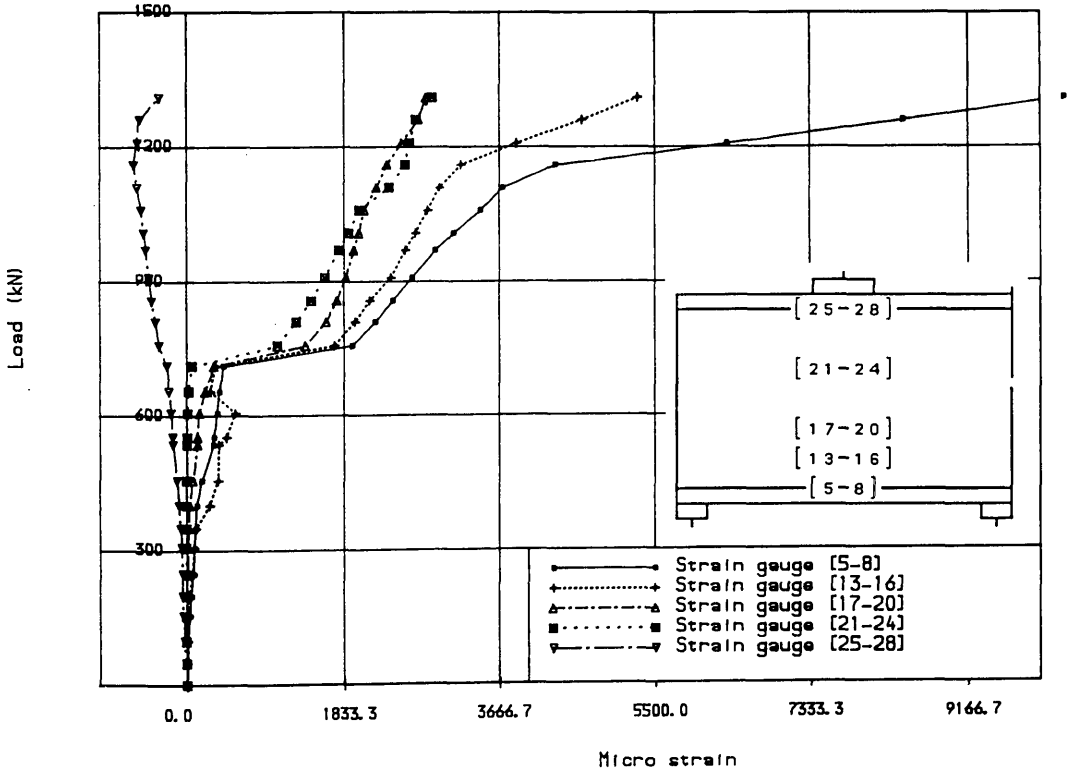

FIG(7.56) Load vs longitudinal steel strains at centre of girder span for girder TRGRAS7

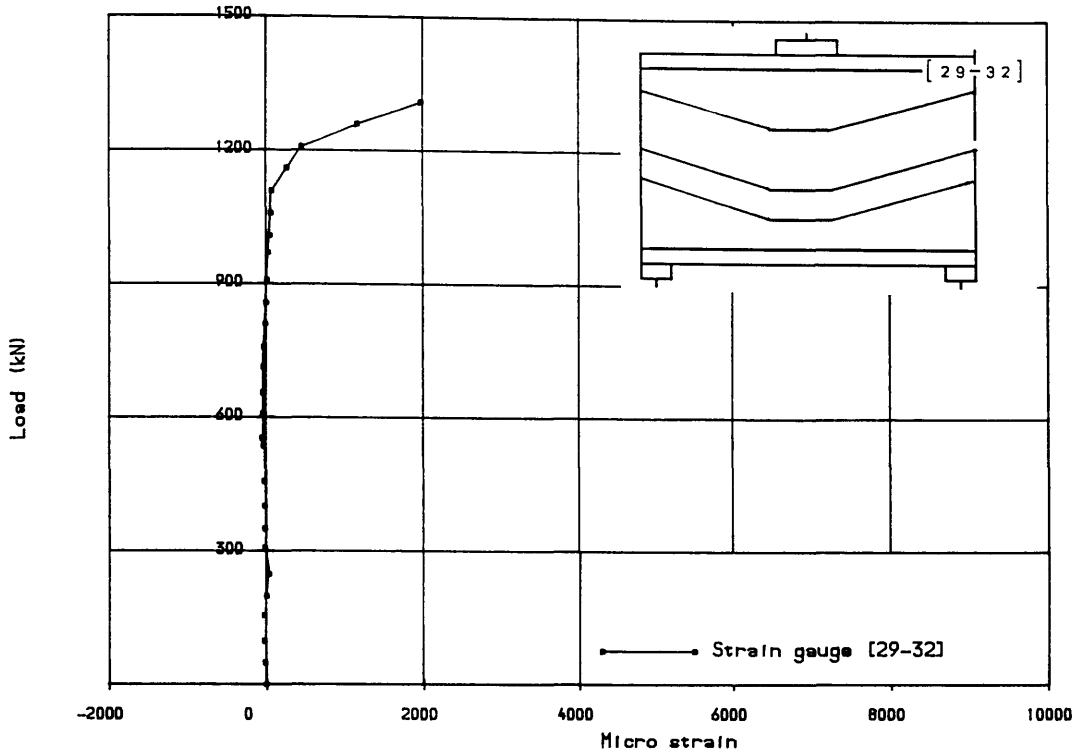

FIG(7.57) Load vs steel strains in top bars over intermediate support for girder TRGRAS7

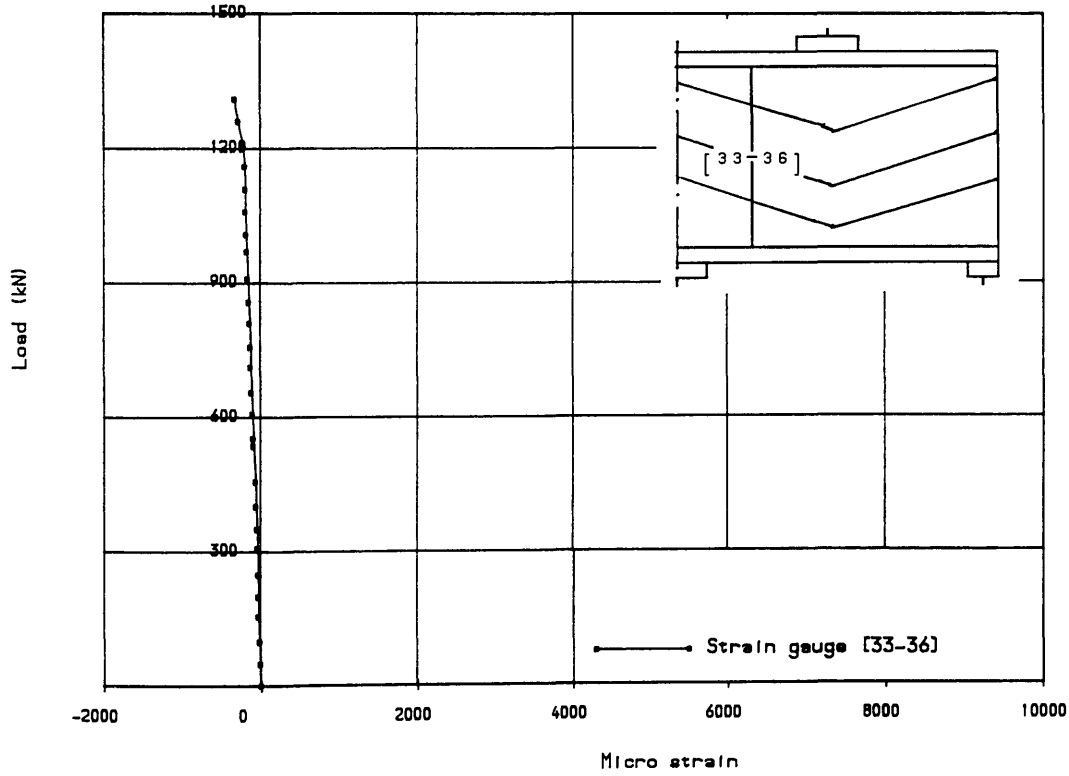

FIG(7.58) Load vs stirrup strains in interior shear span of girder for girder TRGRAS7

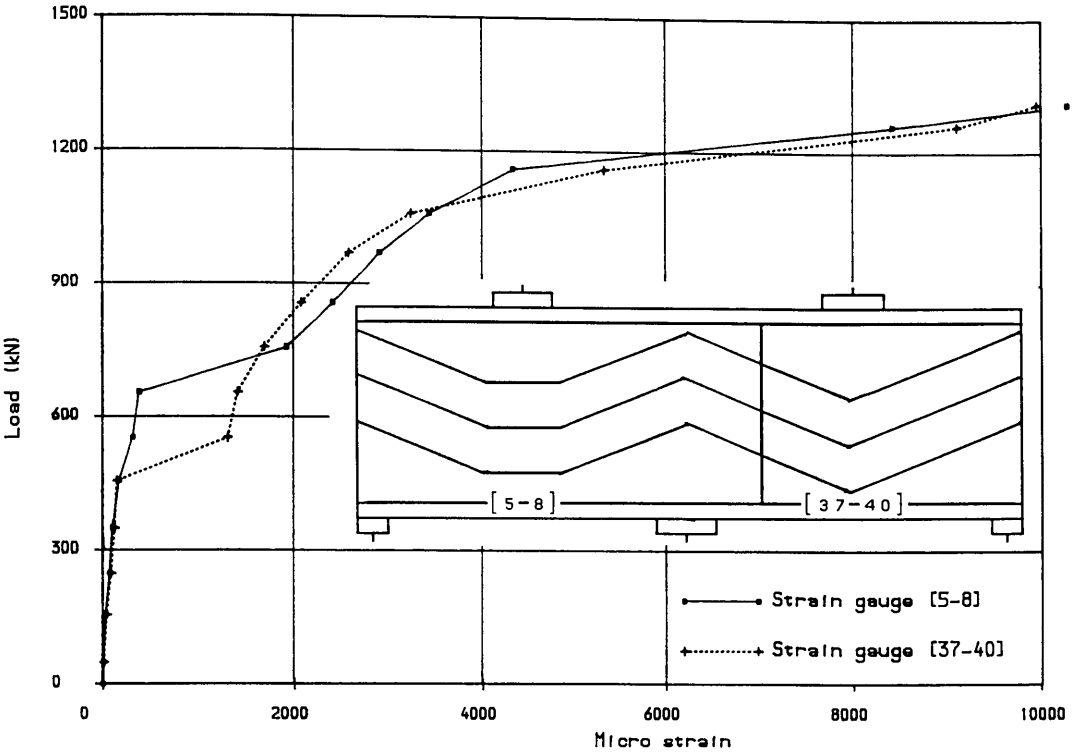

FIG (7.59) Comparison of steel strain in bottom bars of two spans of girder TRGRAS7

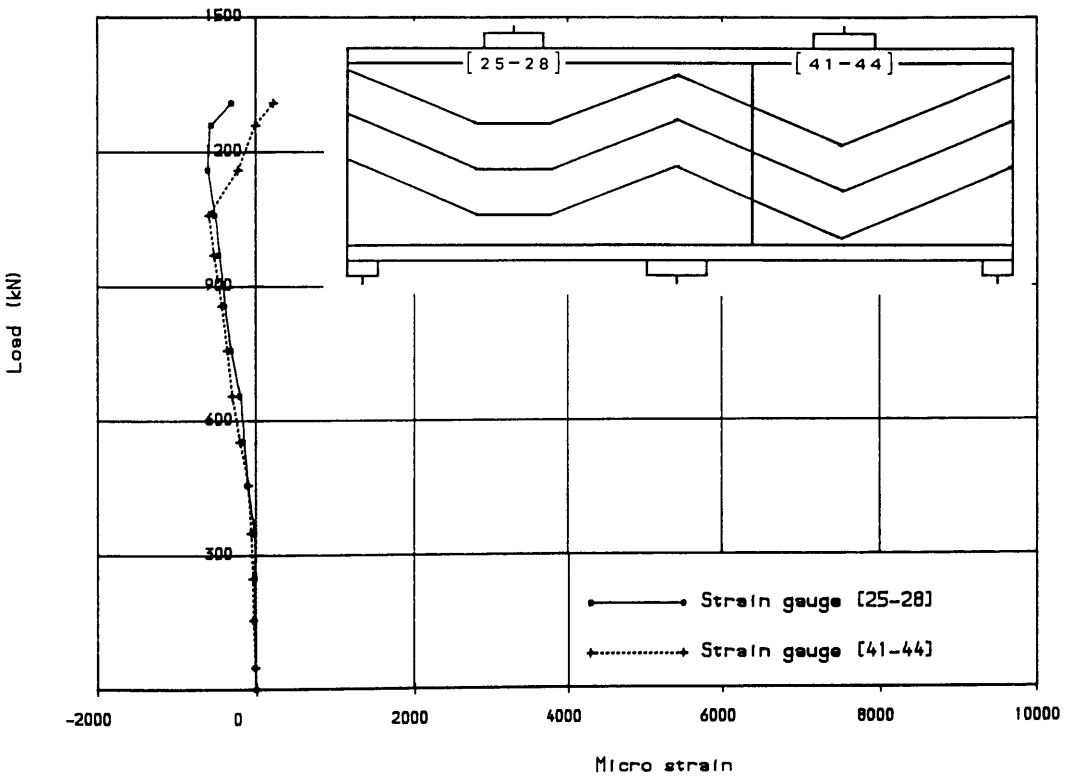

FIG (7.60) Comparison of steel strain in top bars of two spans of girder TRGRAS7

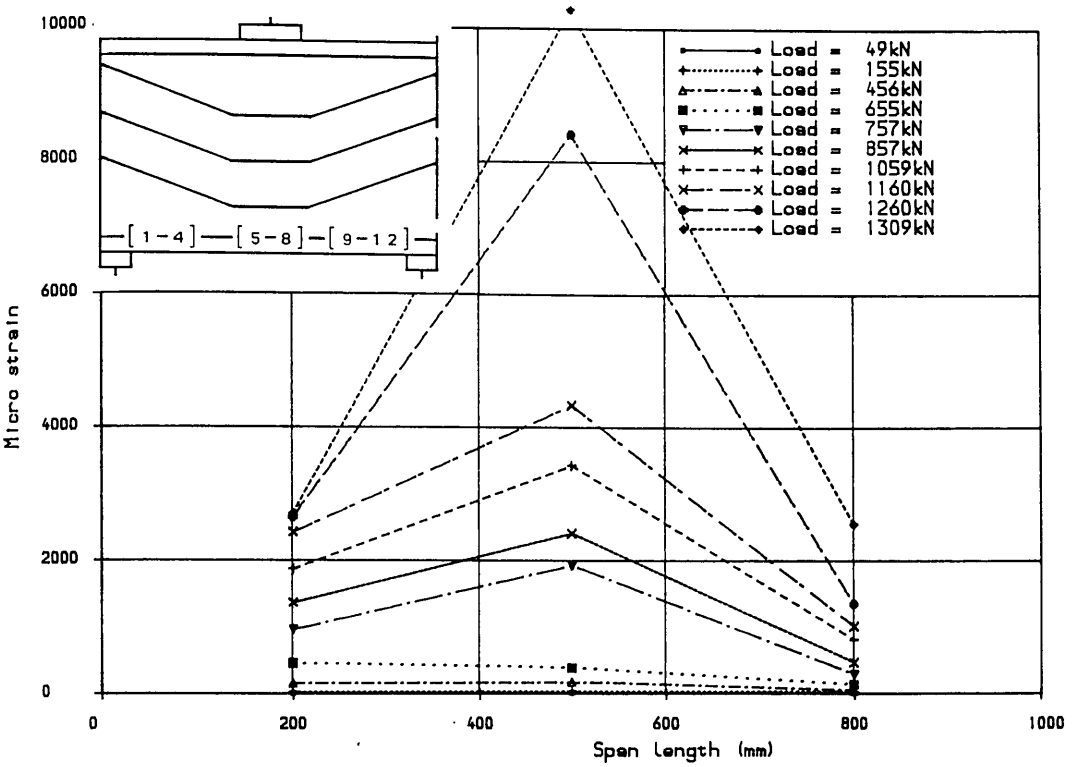

FIG(7.61) Steel strain distribution in bottom bars along girder length for girder TRGRAS7

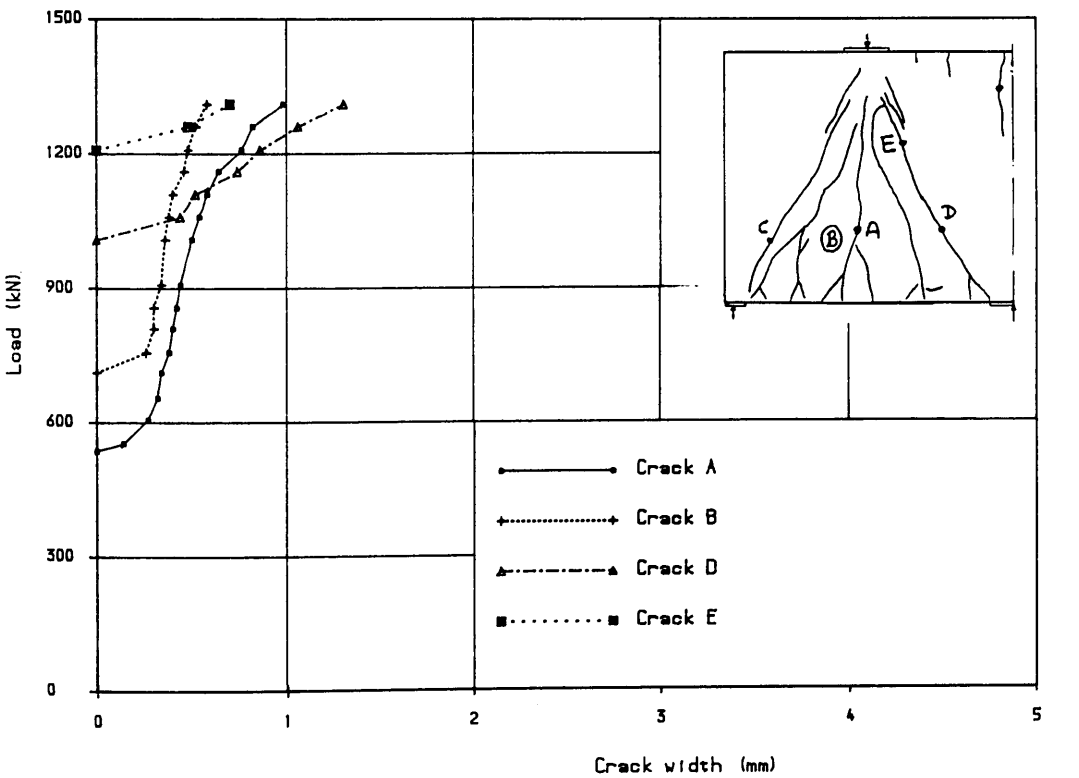

FIG(7.62) Load vs crack width for girder TRGRAS7

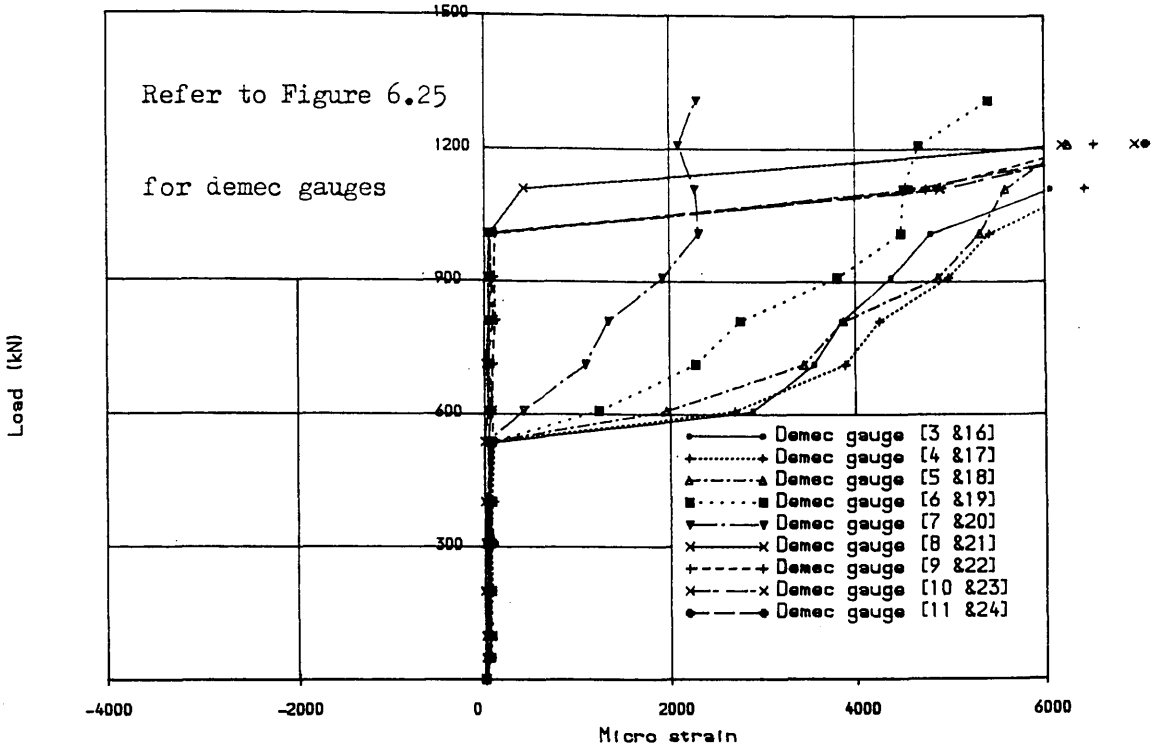

FIG (7.63) Load vs concrete surface strains for girder TRGRAS7

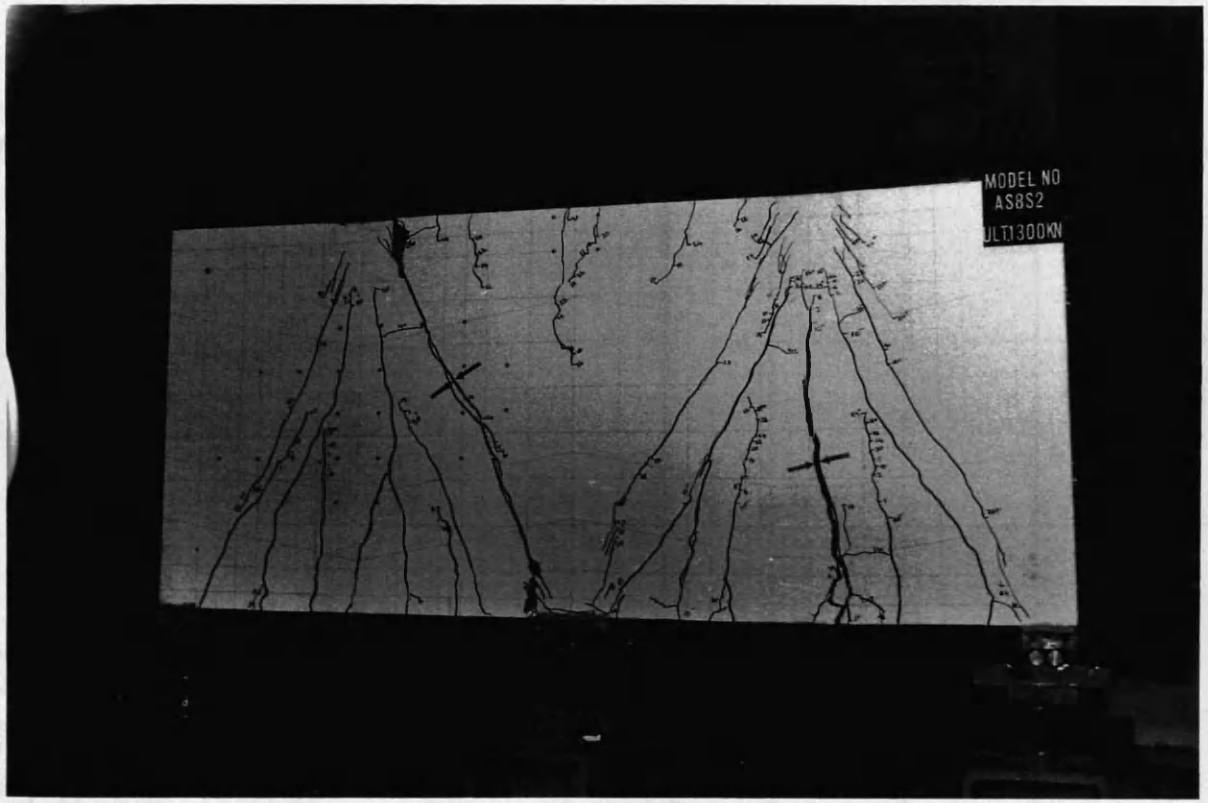

Figure(7.64) Final crack pattern of transfer girder TRGRAS8

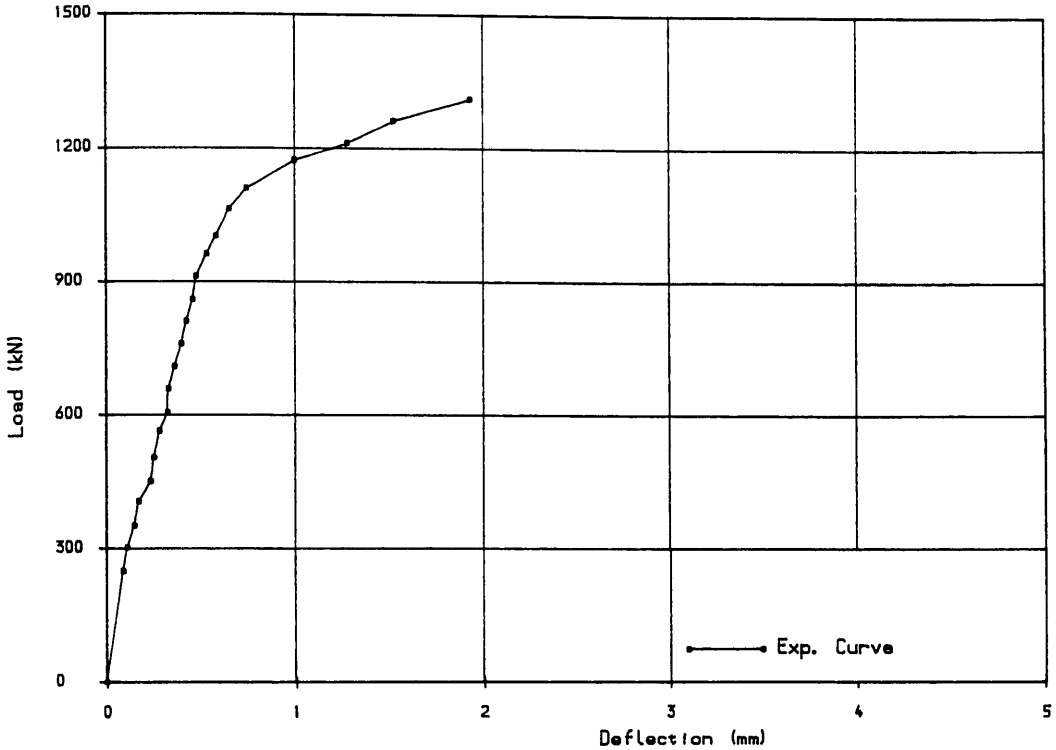

FIG(7.65) Load deflection curve for girder TRGRAS8

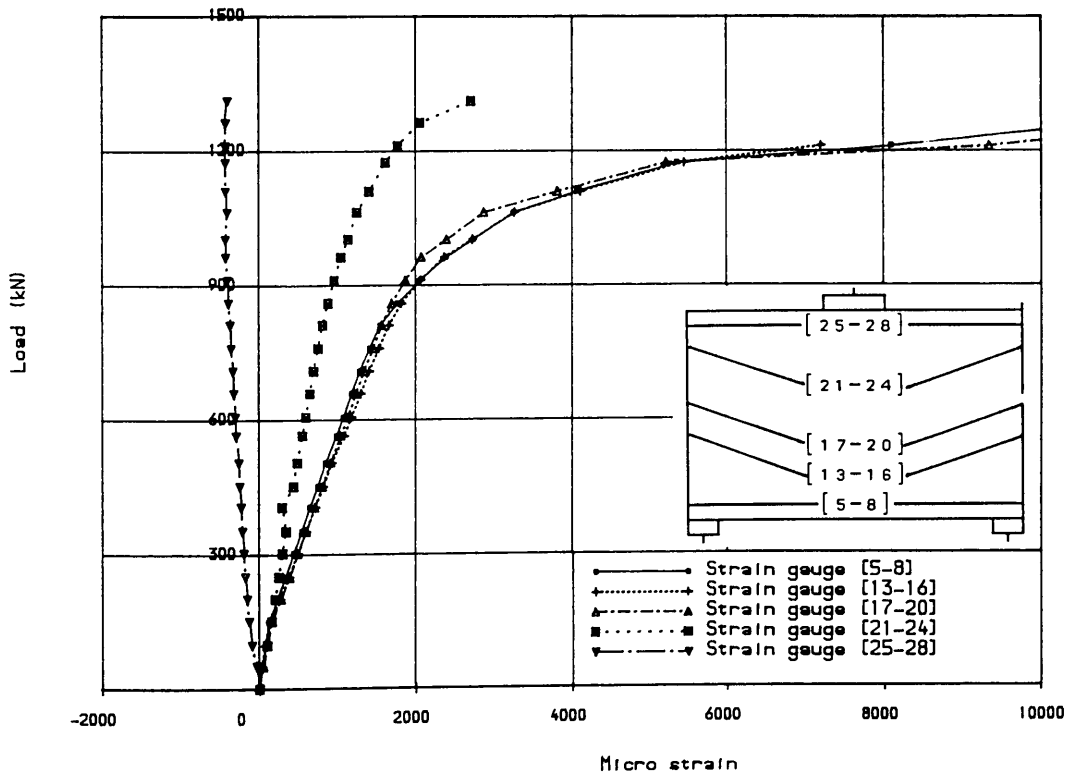

FIG(7.66) Load vs longitudinal steel strains at centre of girder span for girder TRGRAS8

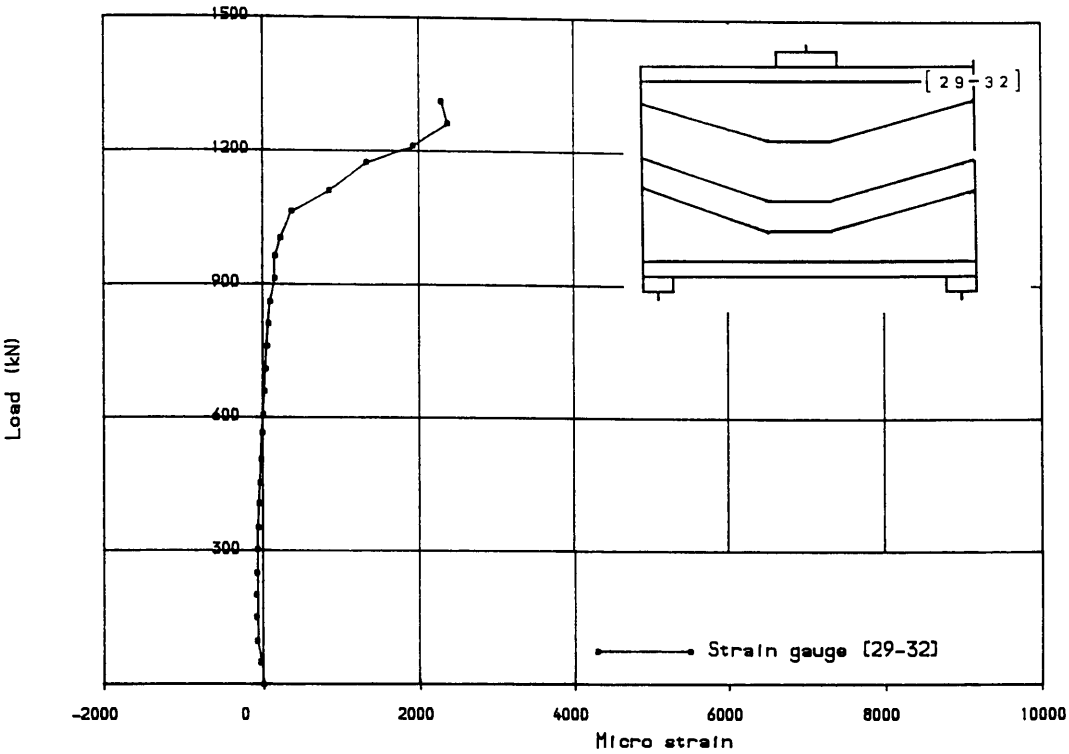

FIG(7.67) Load vs steel strains in top bars over intermediate support for girder TRGRAS8

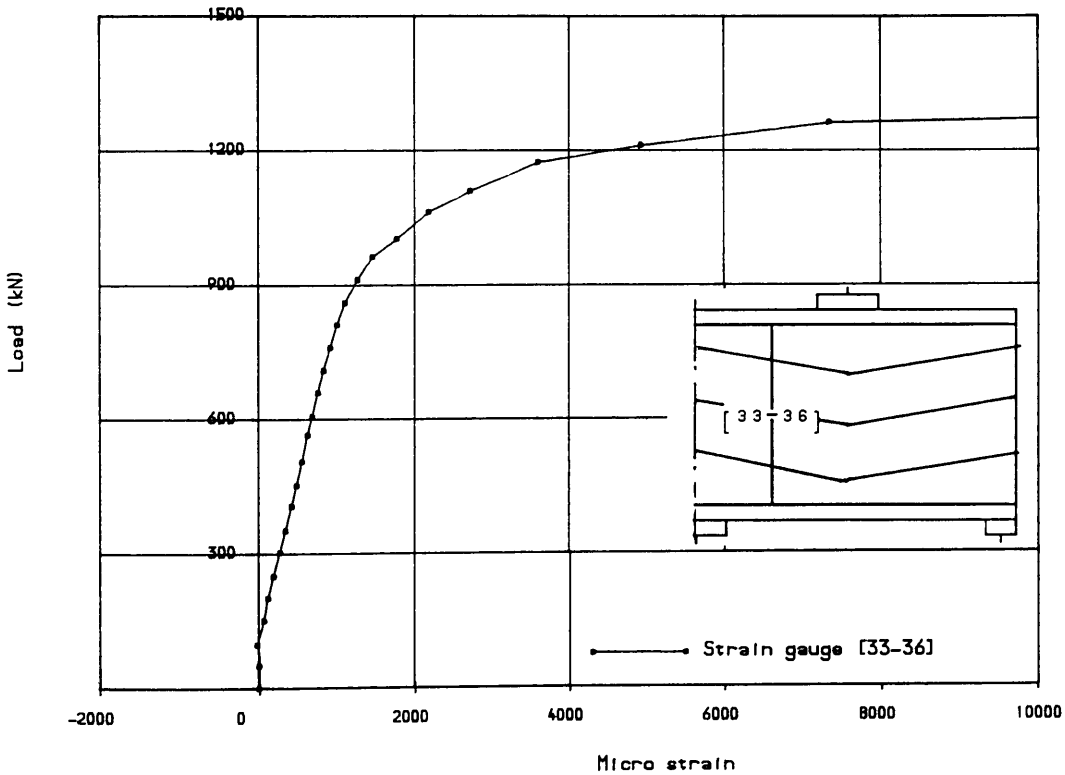

FIG(7.68) Load vs stirrup strains in interior shear span of girder for girder TRGRAS8

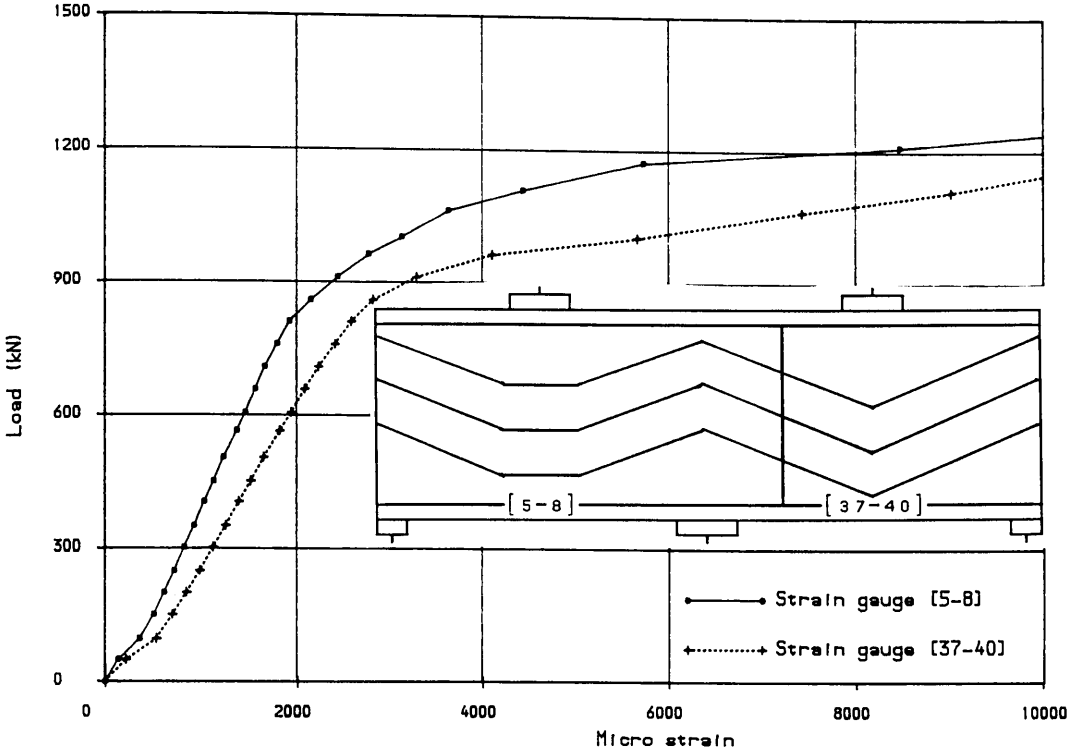

FIG (7.69) Comparison of steel strain in bottom bars of two spans of girder TRGRAS8

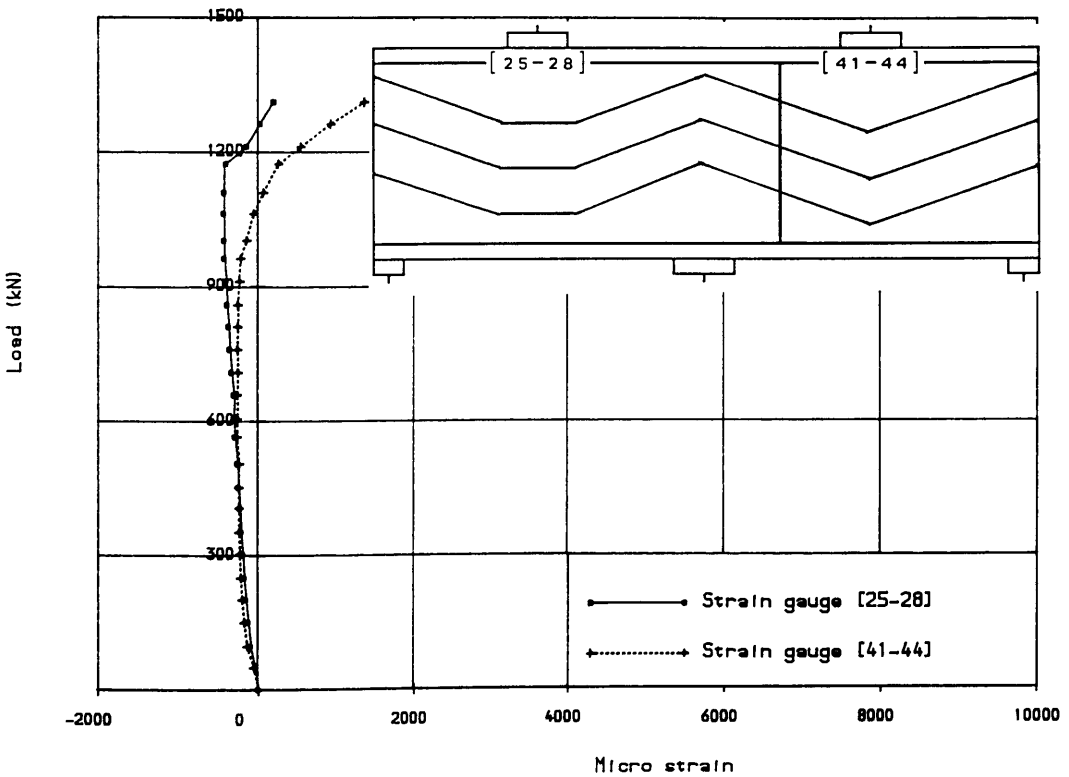

FIG (7.70) Comparison of steel strain in top bars of two spans of girder TRGRAS8

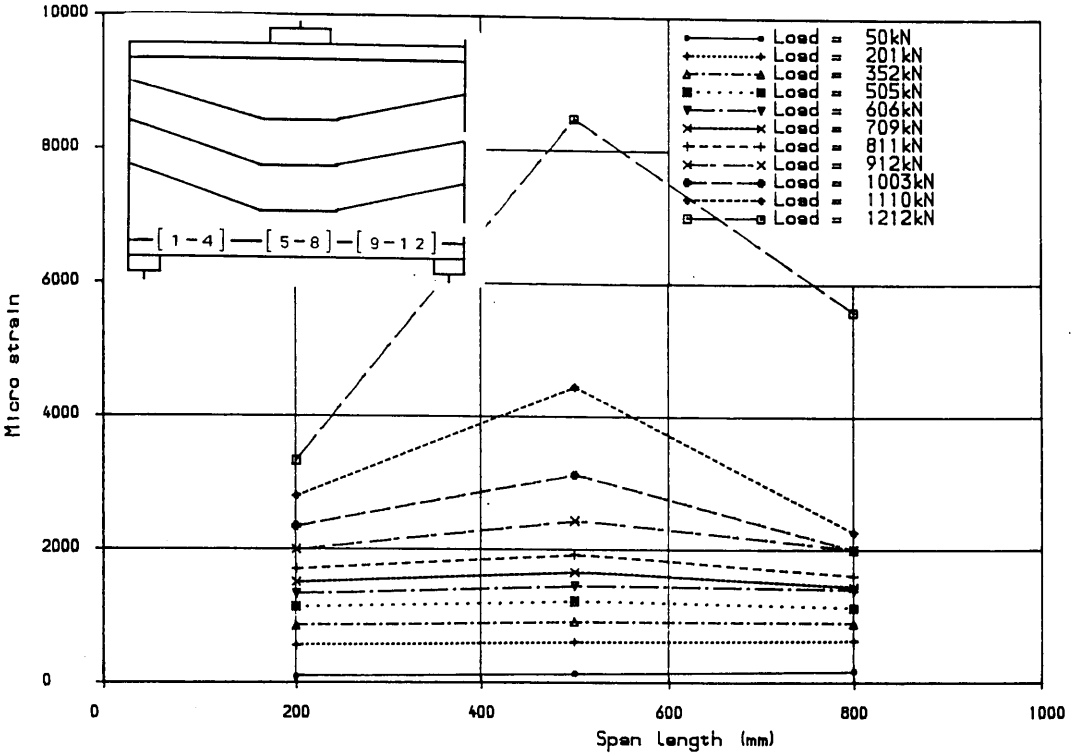

FIG(7.71) Steel strain distribution in bottom bars along girder length for girder TRGRAS8

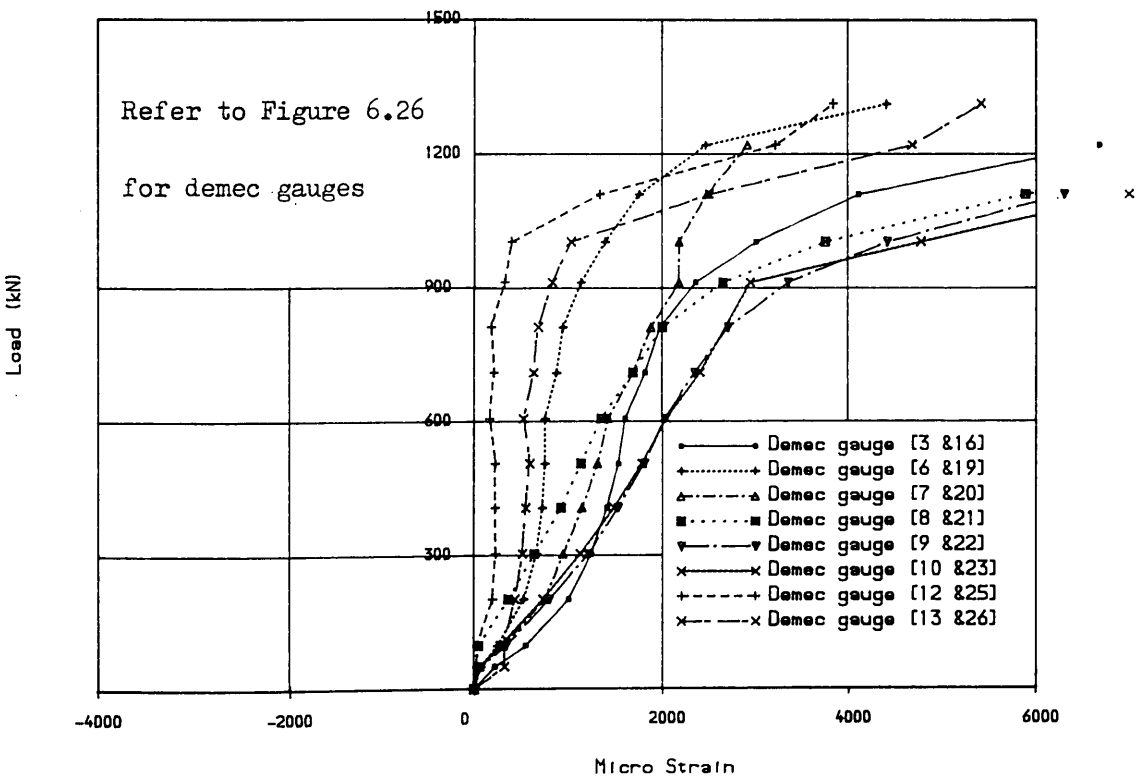

FIG(7.72) Load vs concrete surface strains for girder TRGRAS8

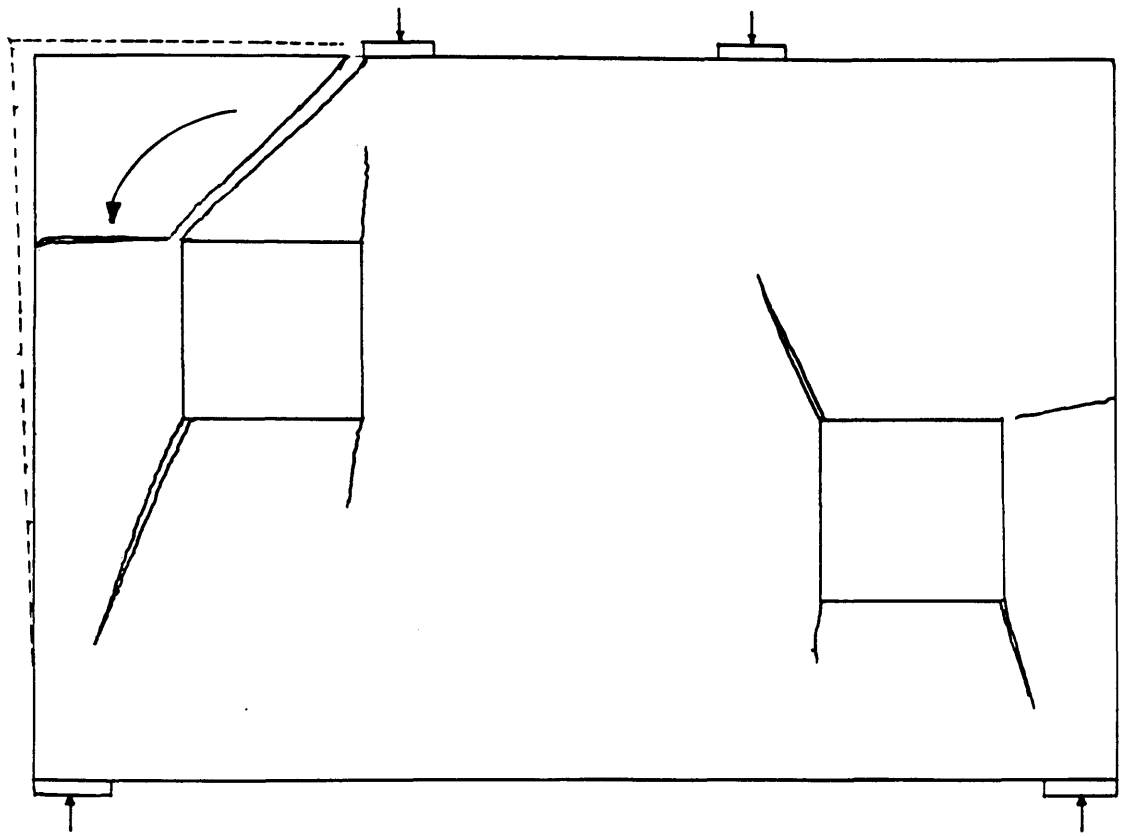

Figure (7.73) Failure mechanism of girder TRGRAS9

Figure(7.74) Final crack pattern of transfer girder TRGRAS9

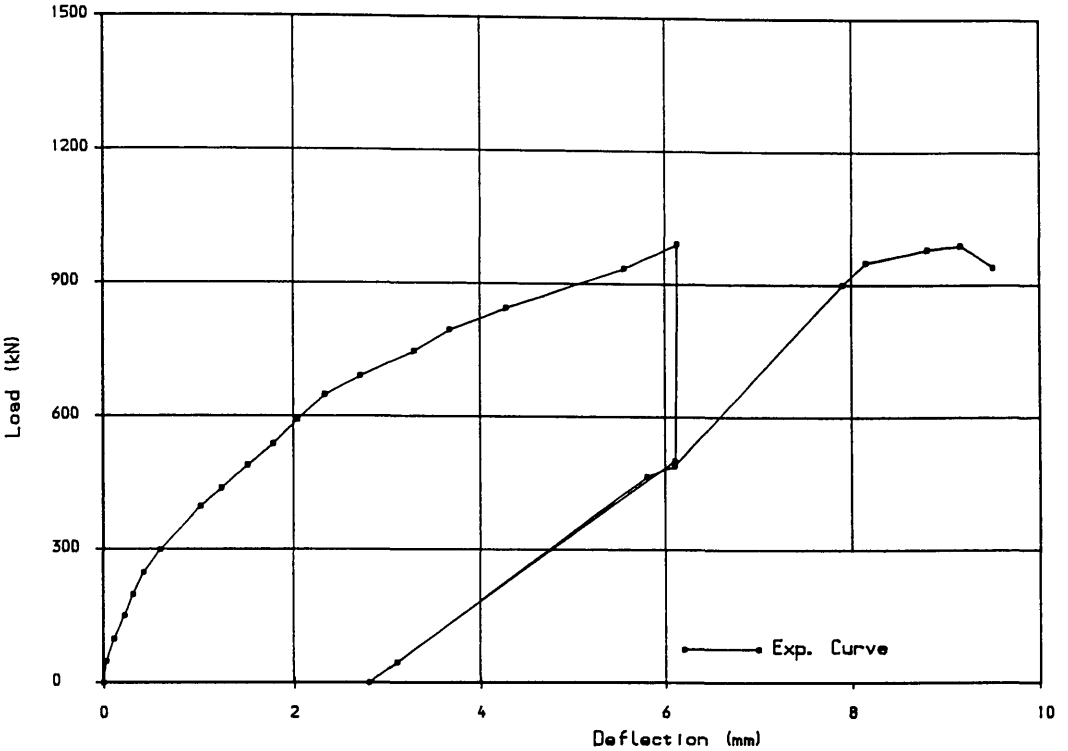

FIG (7.75) Load deflection curve of transfer girder TRGRAS9

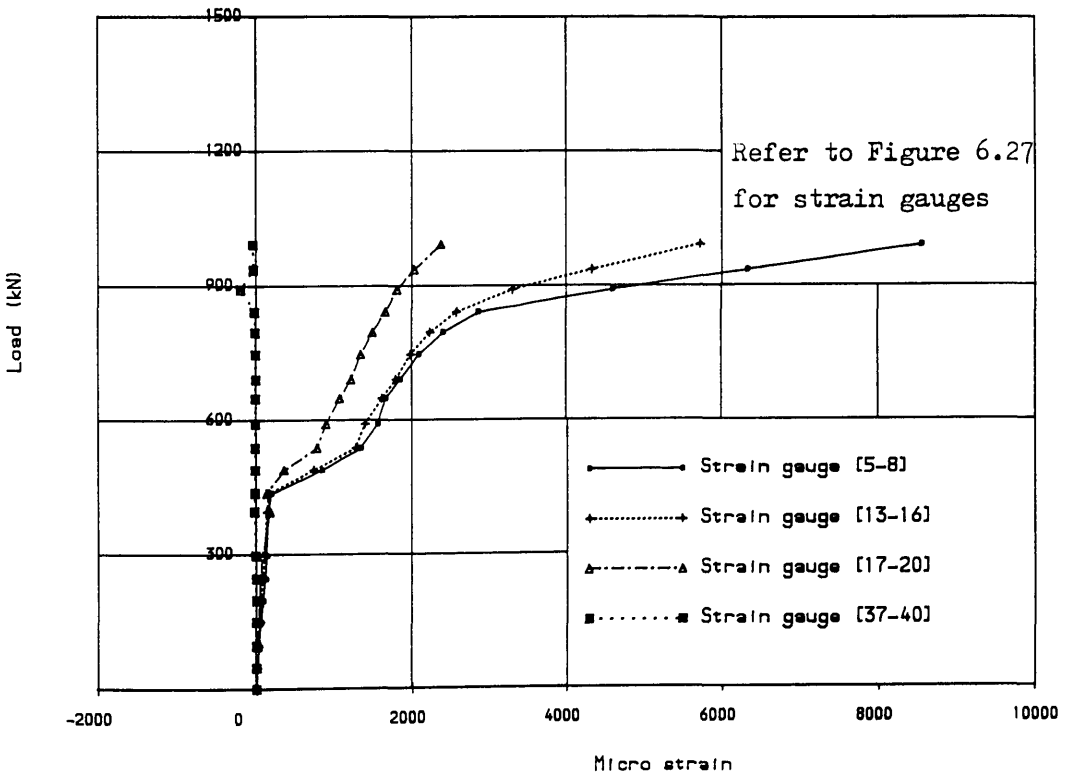

FIG (7.76) Load vs longitudinal steel strains at centre of girder span for girder TRGRAS9

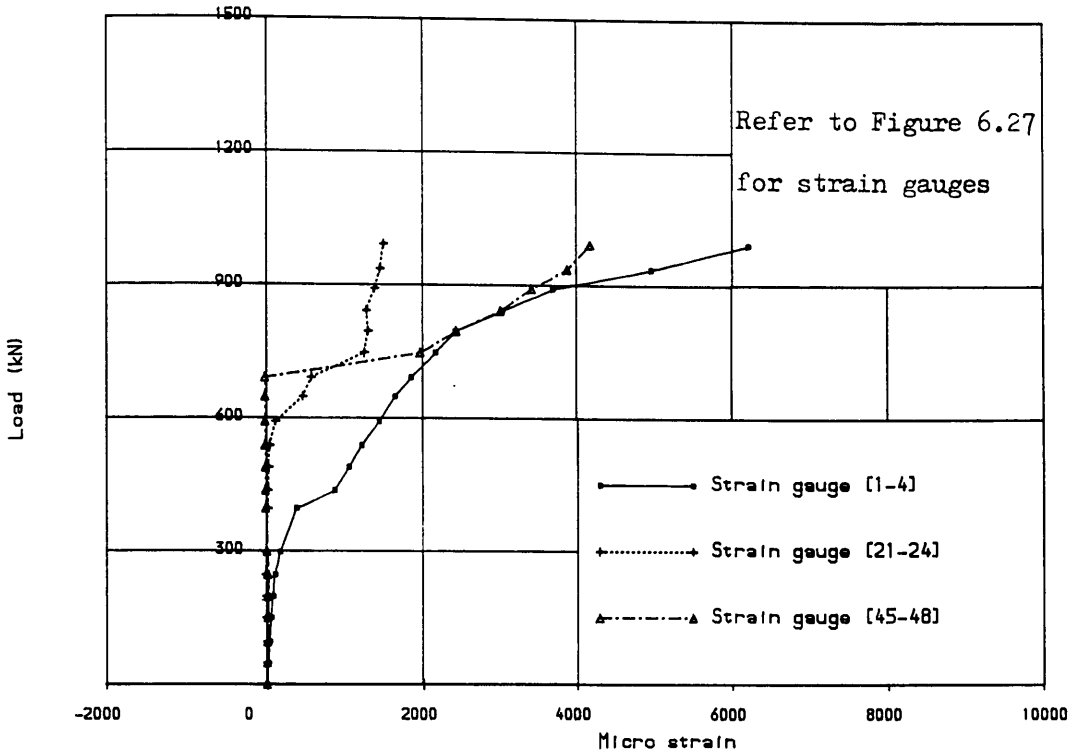

FIG(7.77) Load vs longitudinal steel strains at 450mm from the face of support for girder TRGRAS9

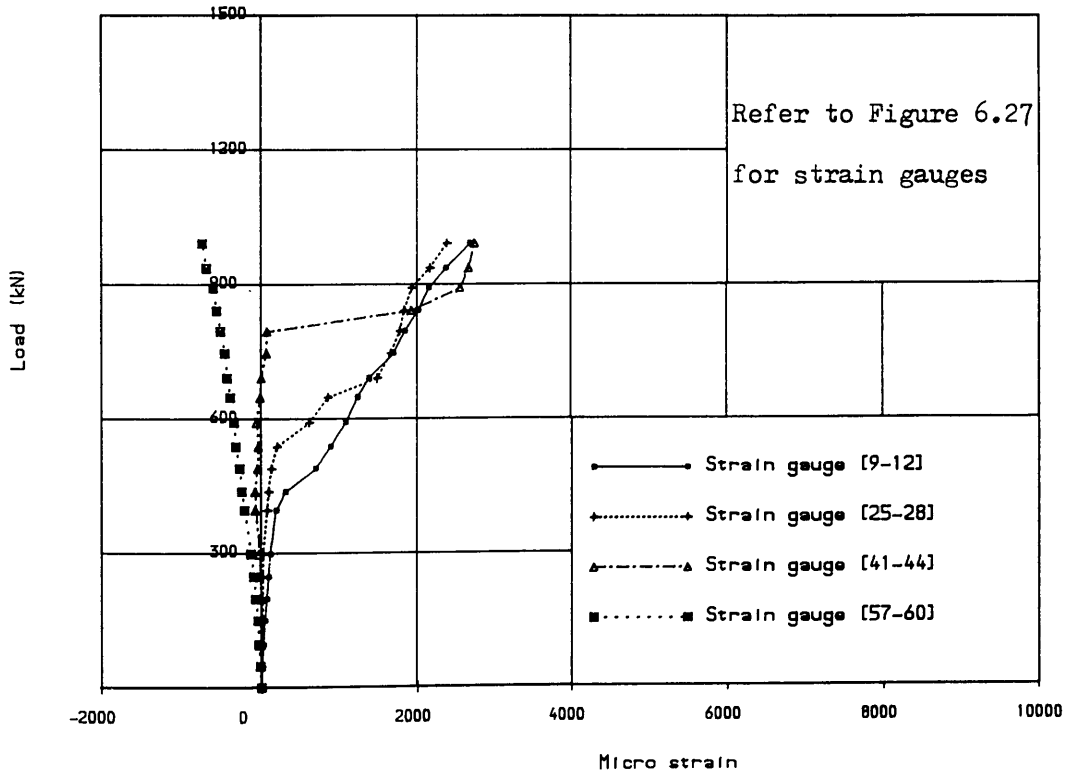

FIG(7.78) Load vs longitudinal steel strains at 450mm from the face of R.H.S. support for girder TRGRAS9

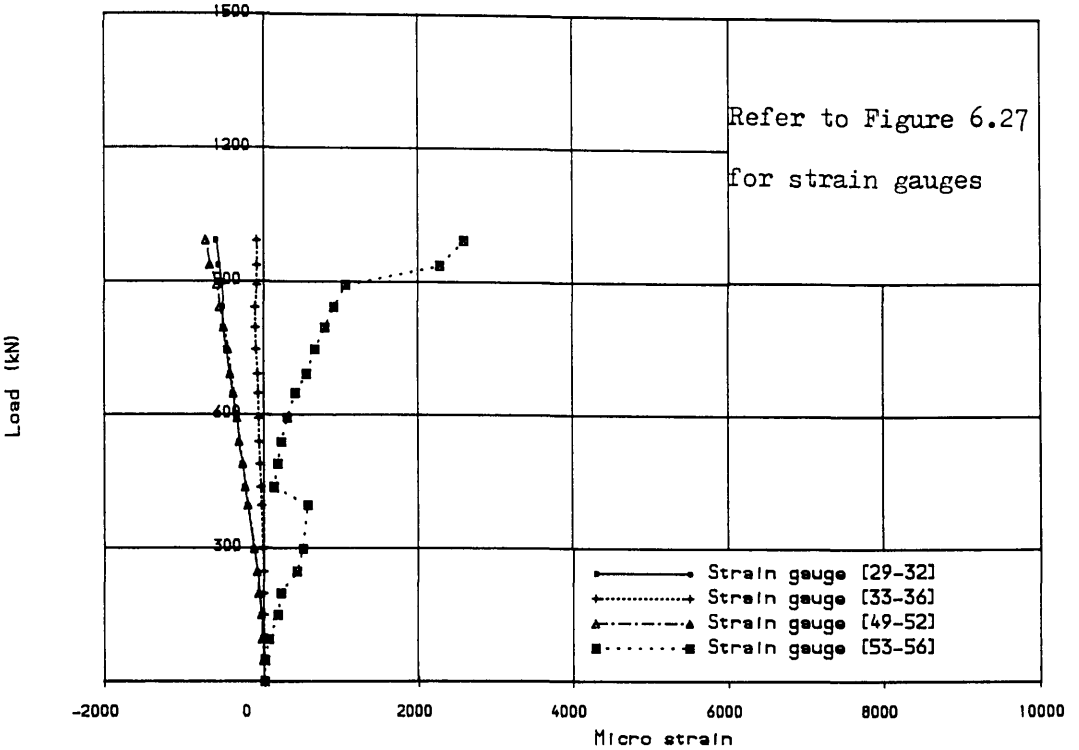

FIG (7.79) Load vs stirrup strains in interior shear span of girder for girder TRGRAS9

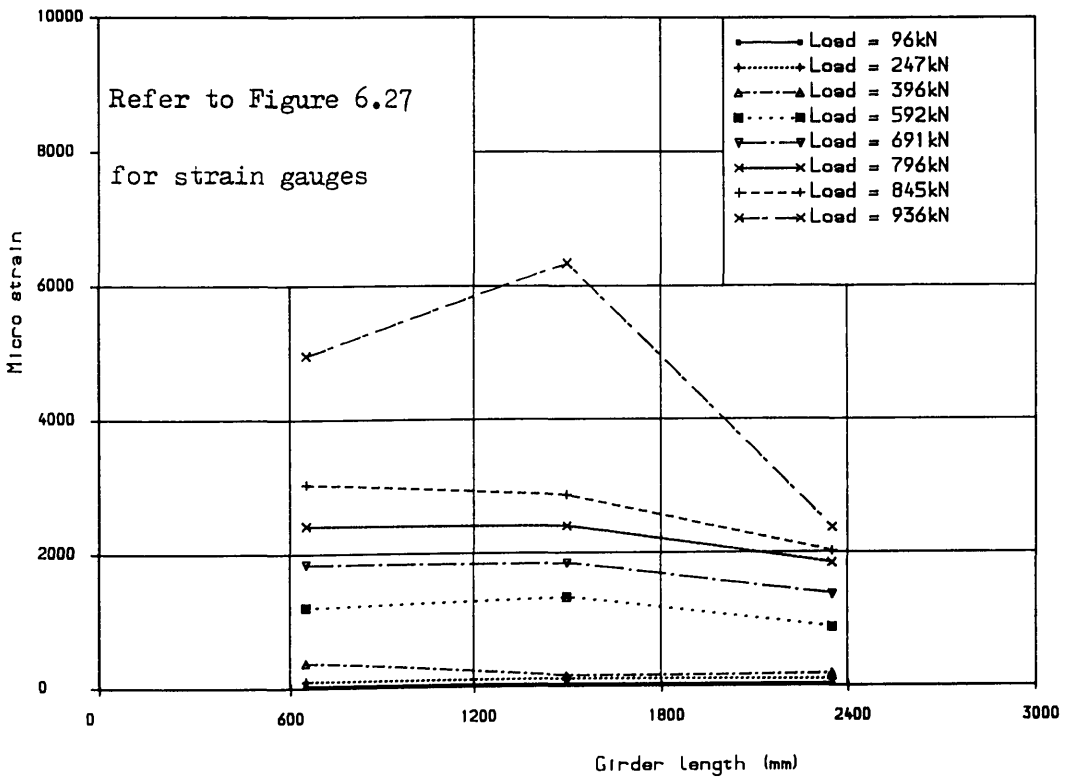

FIG (7.80) Steel strain distribution in bottom bars along girder length for girder TRGRAS9

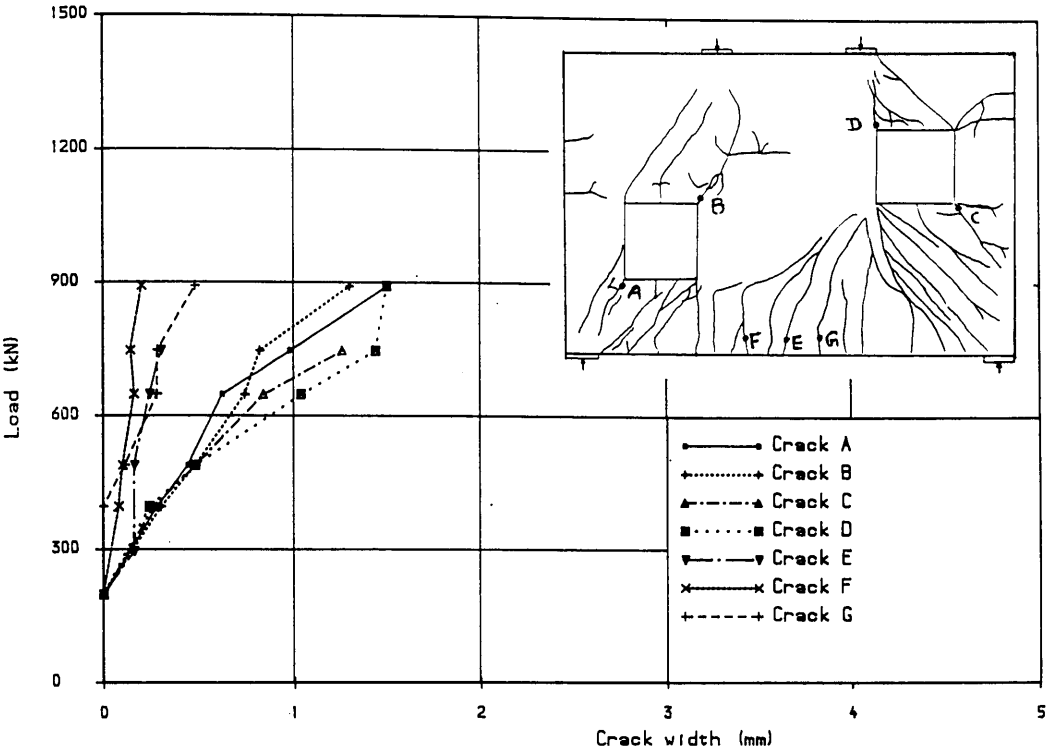

FIG(7.81) Load vs crack width for girder TRGRAS9

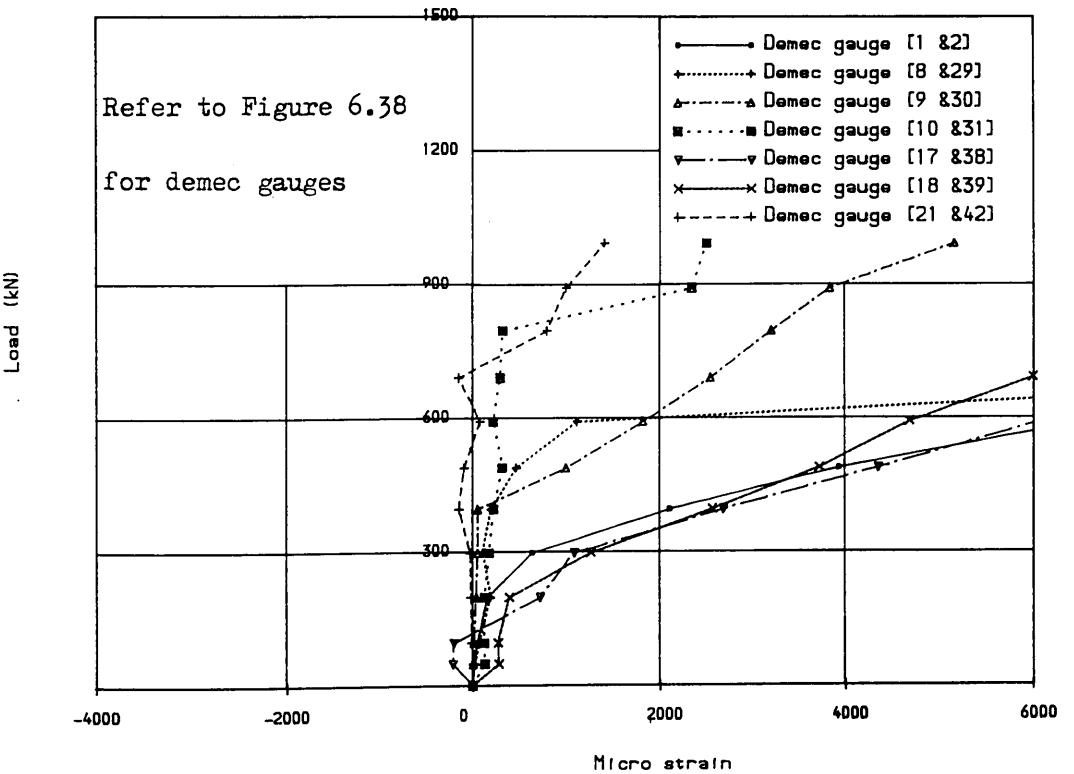

FIG(7.82) Load vs concrete surface strains for girder TRGRAS9

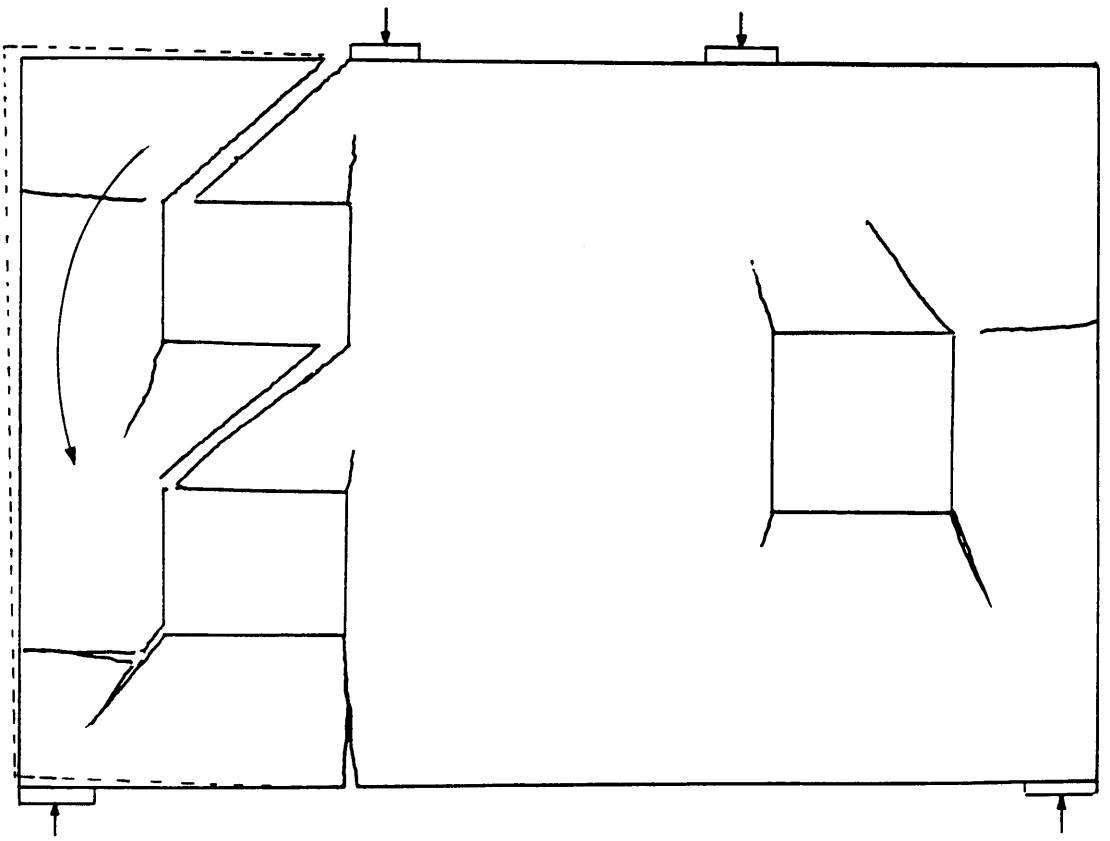

Figure (7.83) Failure mechanism of girder TRGRAS10

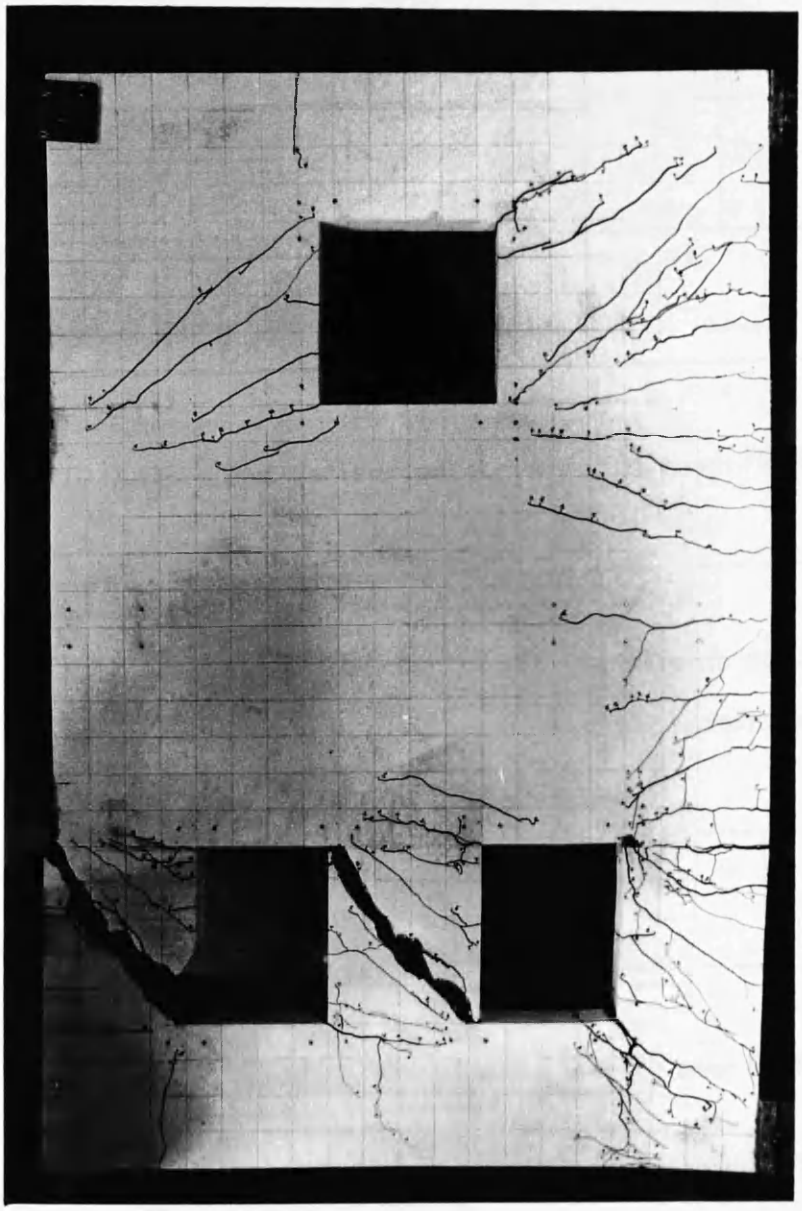

Figure(7.84) Final crack pattern of transfer girder TRGRAS10

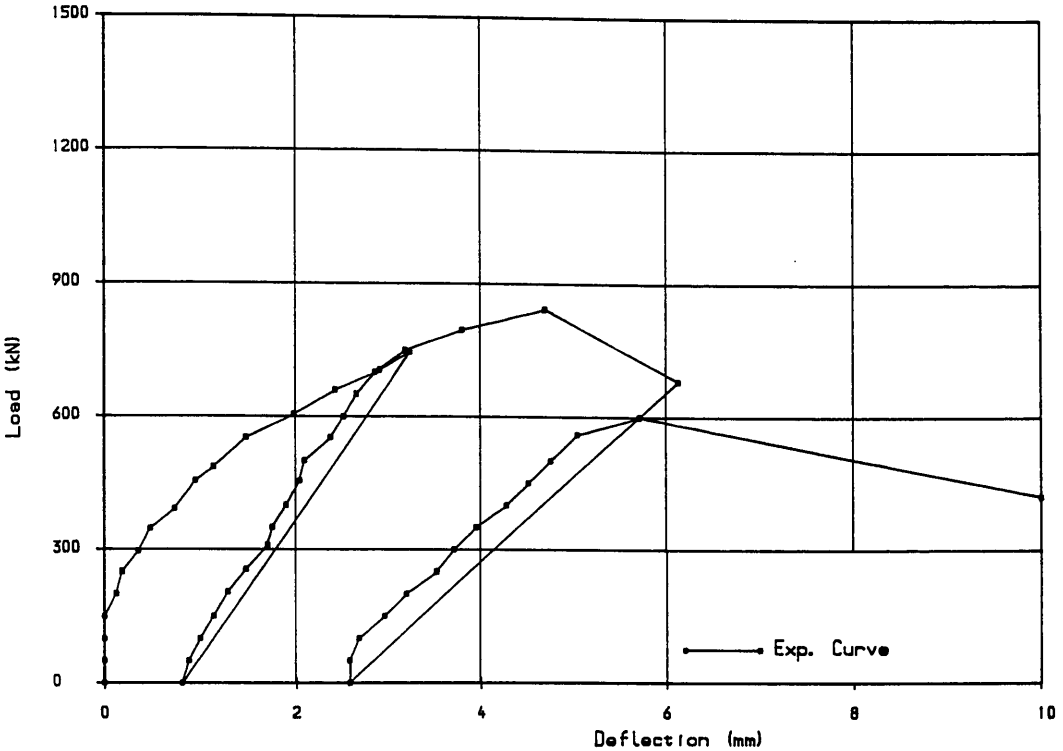

FIG(7.85) Load deflection curve for girder TRGRAS10

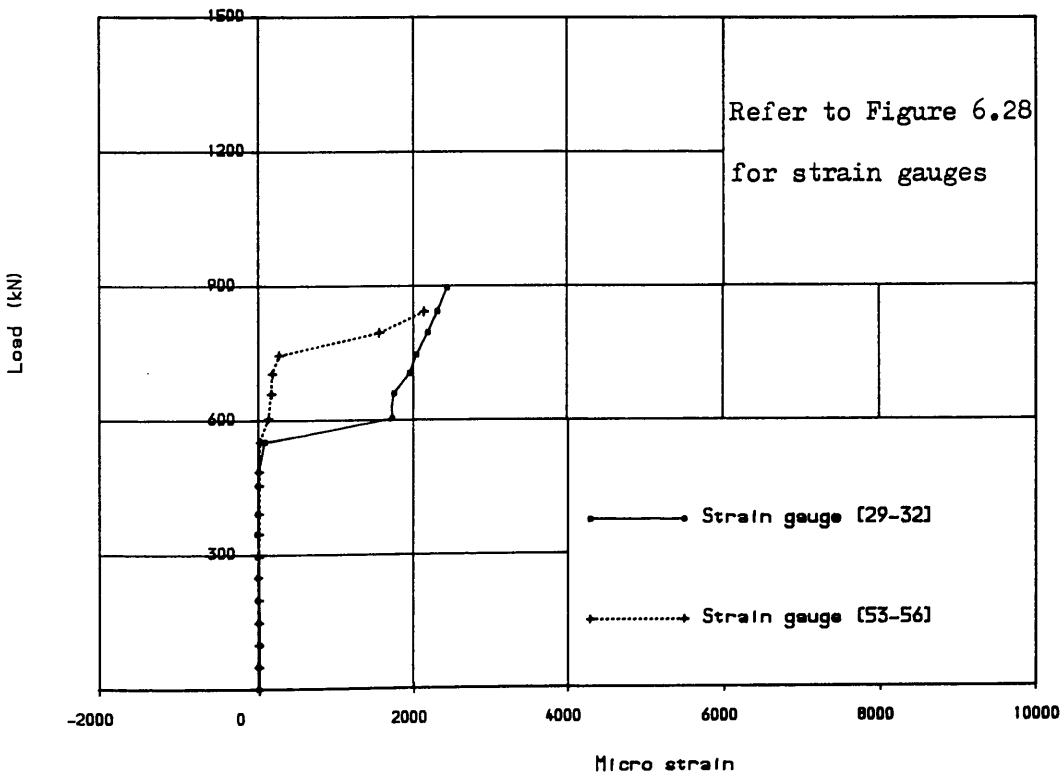

FIG(7.86) Load vs longitudinal steel strains at 450mm from the face of L.H.S support for girder TRGRAS10

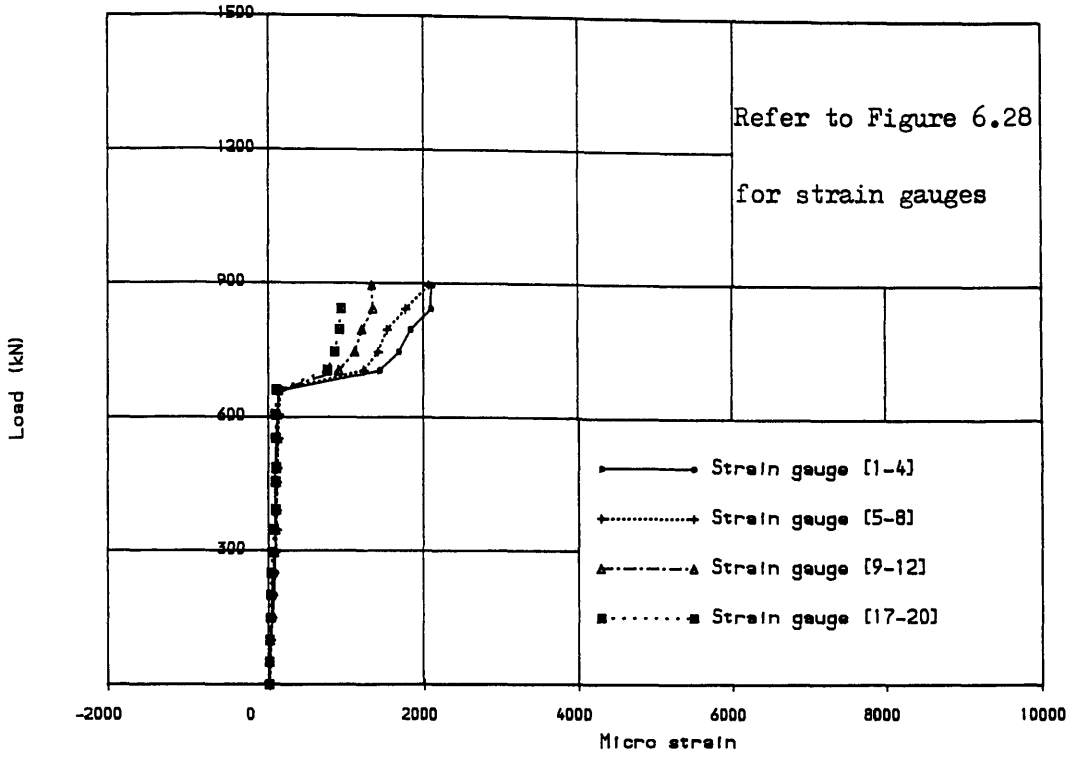

FIG (7.87) Load vs longitudinal steel strains at centre of girder span for girder TRGRAS10

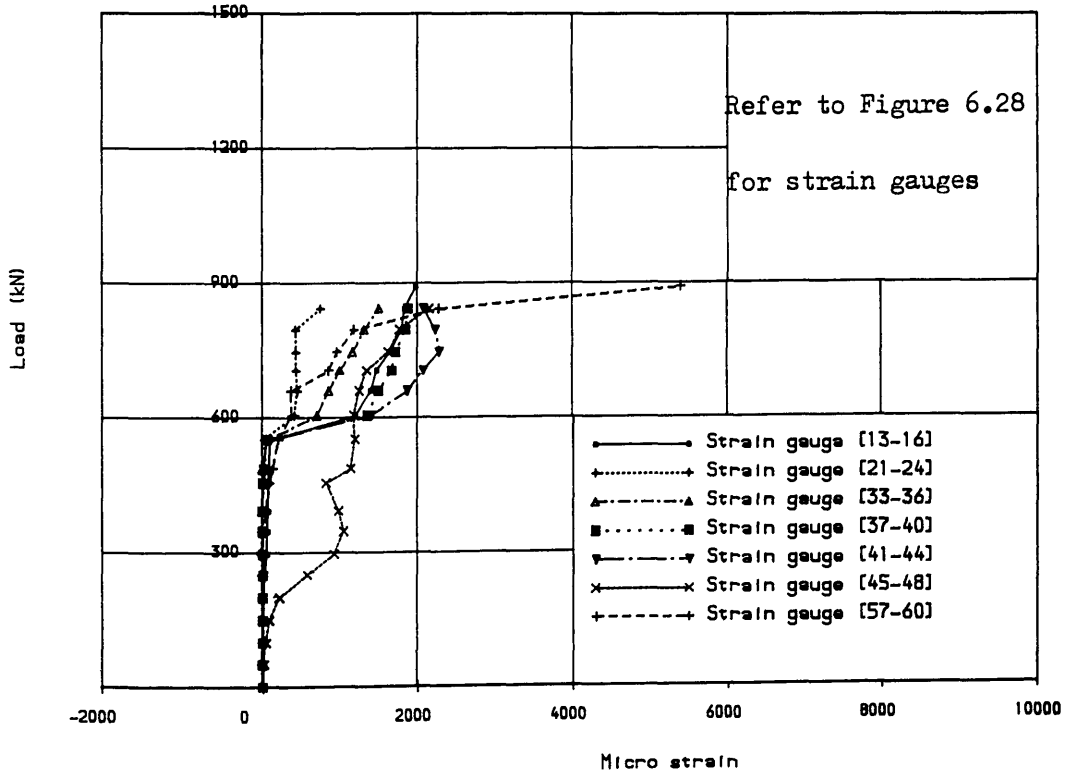

FIG (7.88) Load vs longitudinal steel strains at 450mm from the face of R.H.S support for girder TRGRAS10

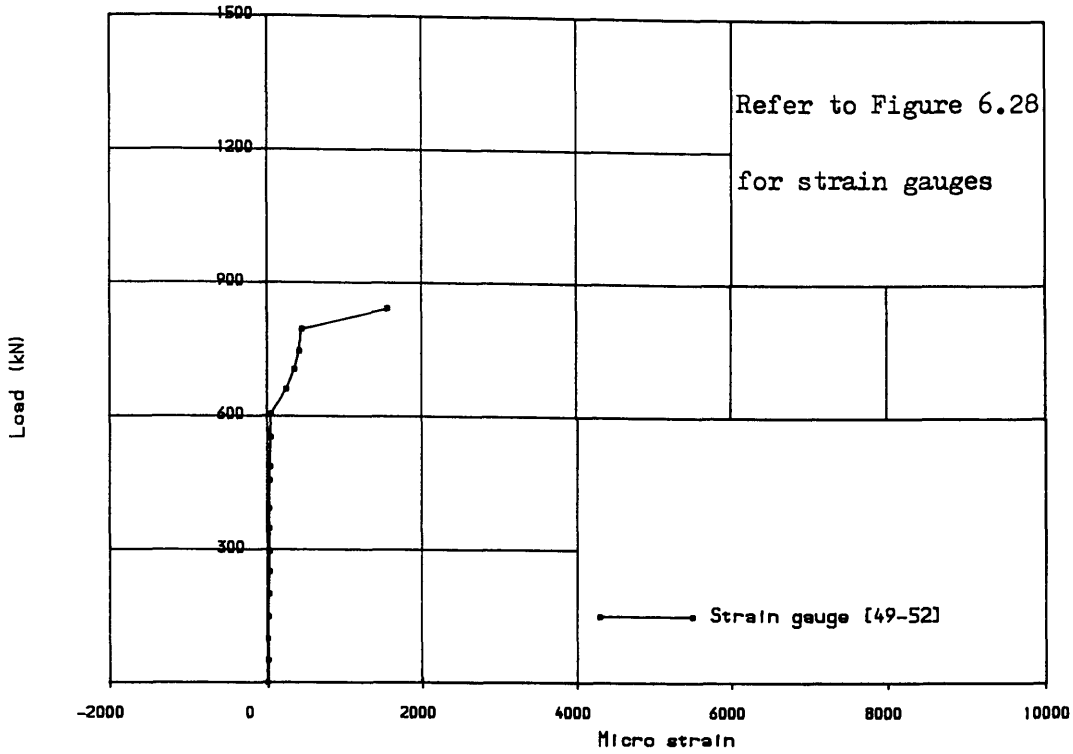

FIG(7.89) Load vs longitudinal steel strains at 150mm from the face of R.H.S support for girder TRGRAS10

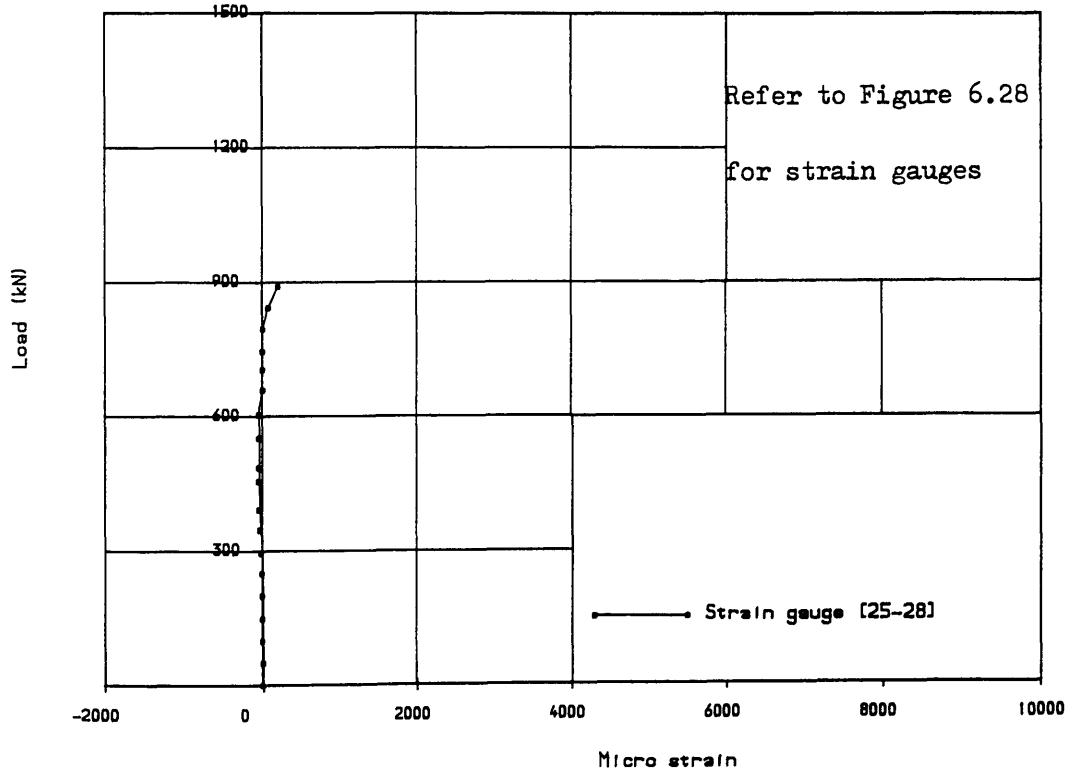

FIG(7.90) Load vs steel strains in stirrups for girder TRGRAS10

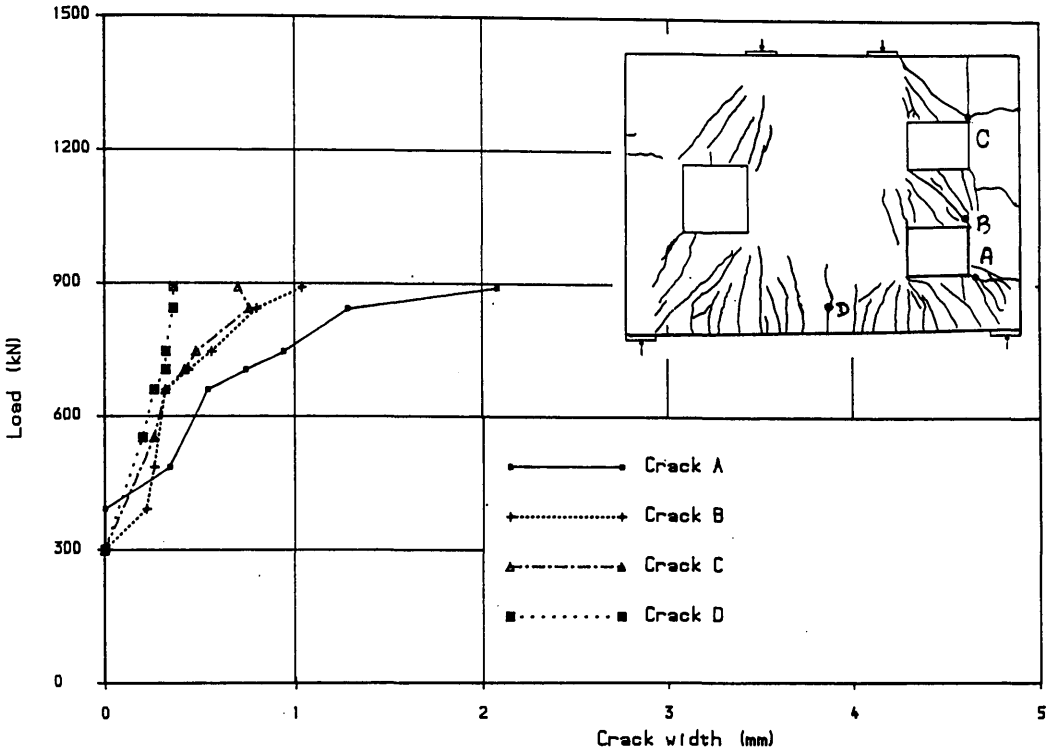

FIG(7.91) Load vs crack width for girder TRGRAS10

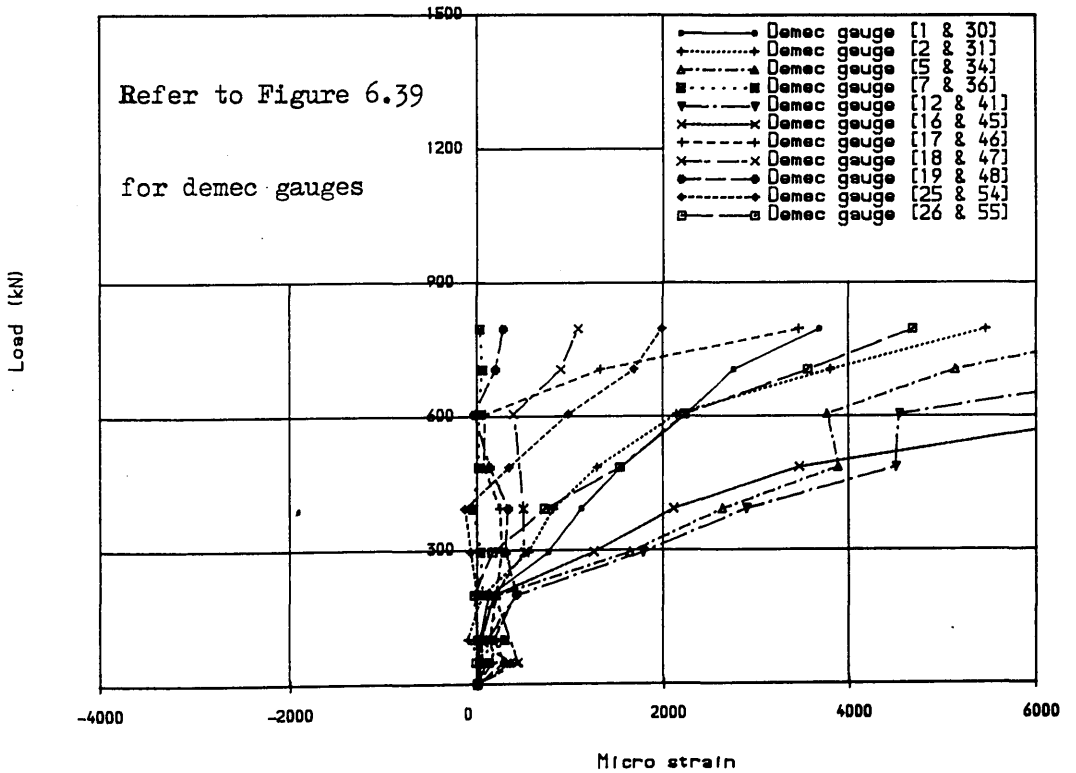

FIG(7.92) Load vs concrete surface strains for girder TRGRAS10

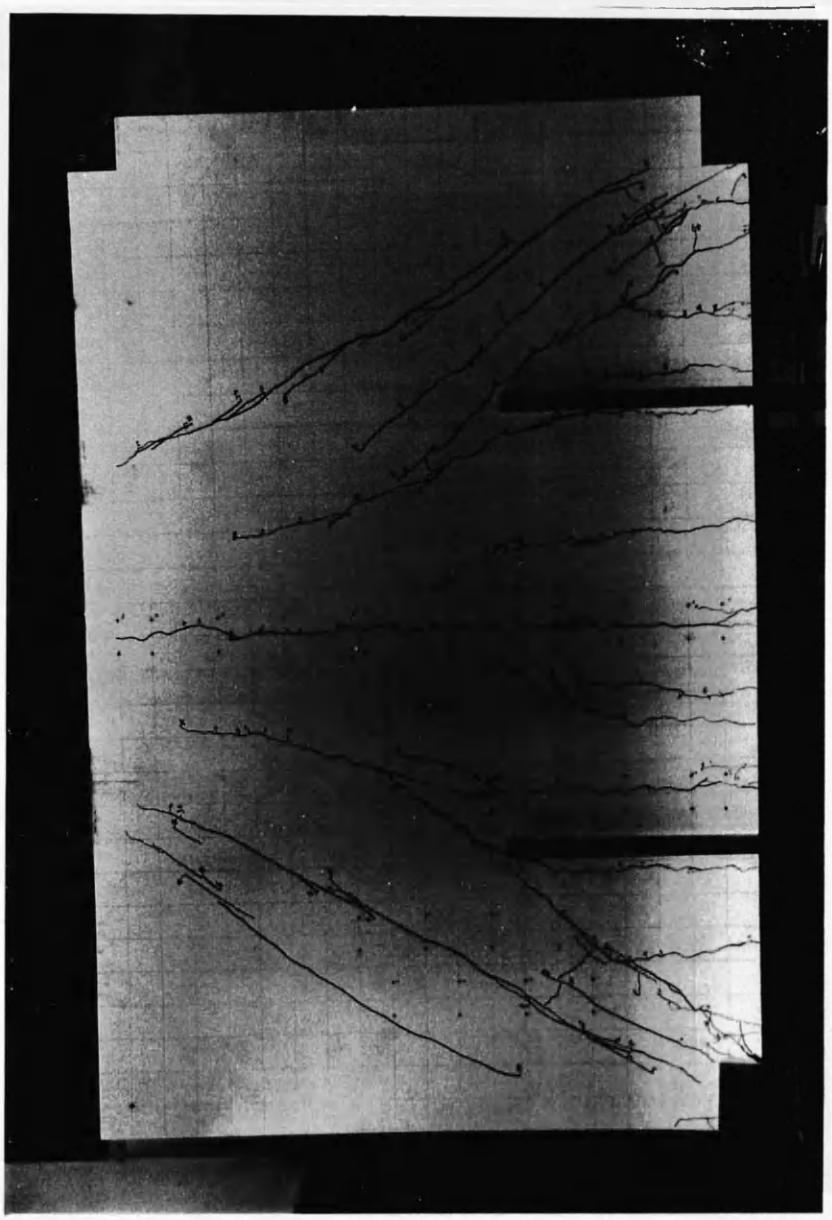

Figure(7.93) Final crack pattern of transfer girder TRGRAS11

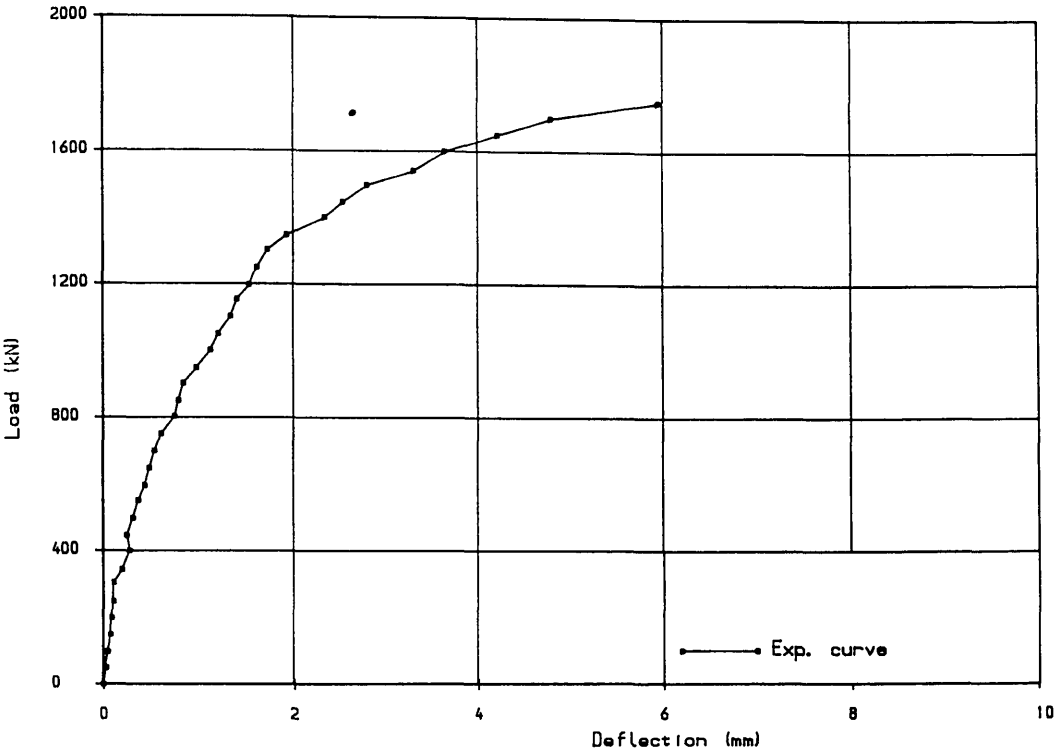

FIG(7.94) Load deflection curve for girder TRGRAS11

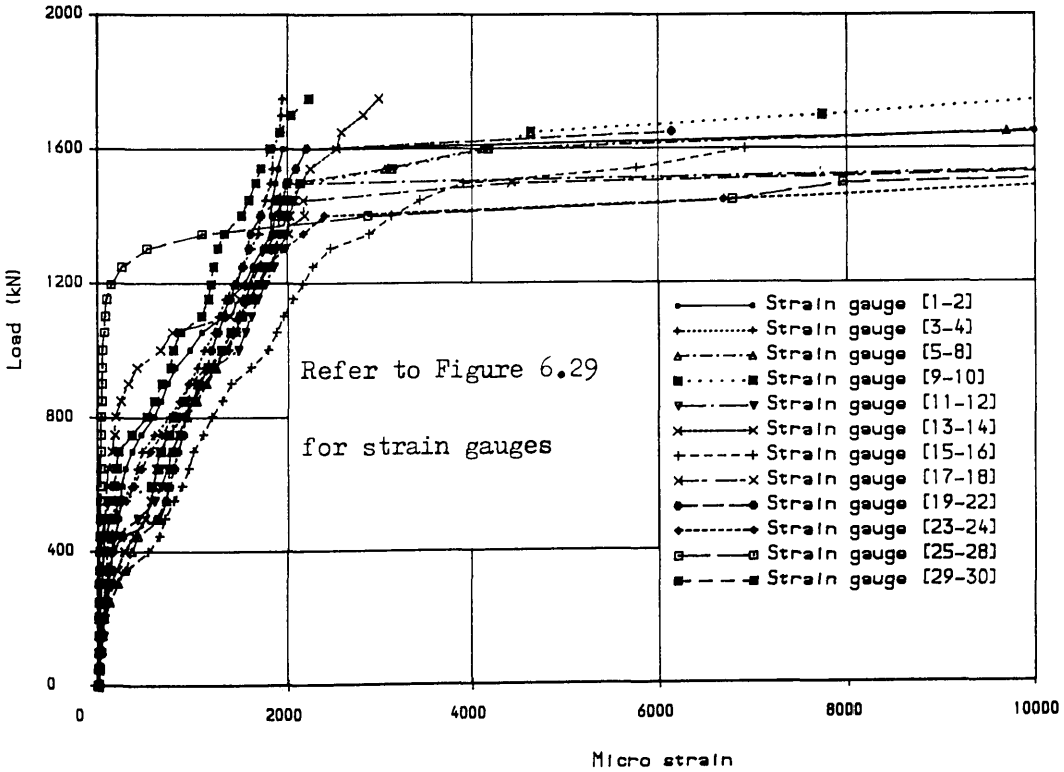

FIG (7.95) Steel strains at various points in transfer girder TRGRAS11

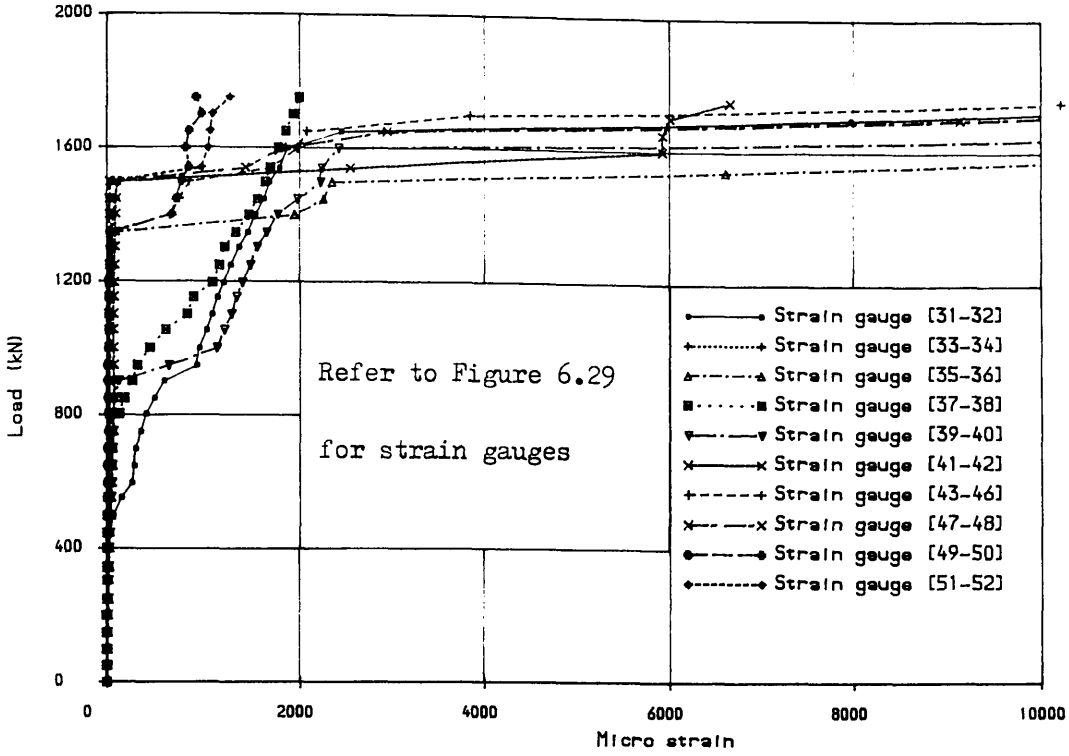

FIG (7.95) Continued

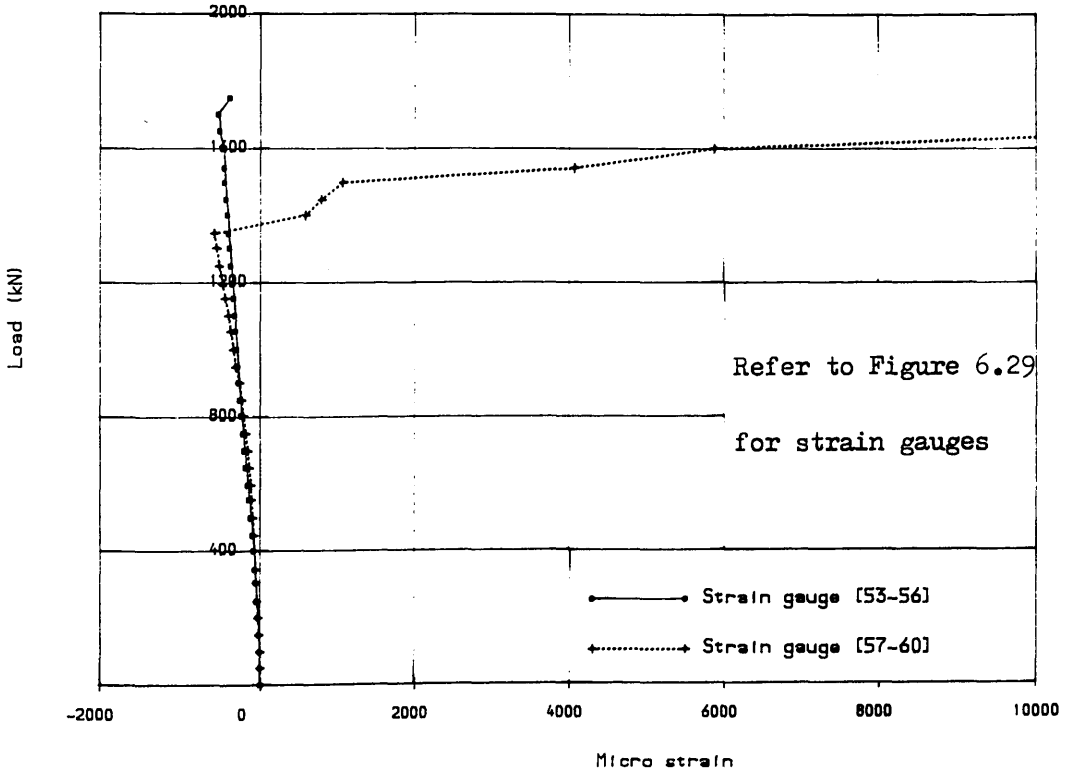

FIG (7.96) Steel strains in stirrups at various points in transfer girder TRGRAS11

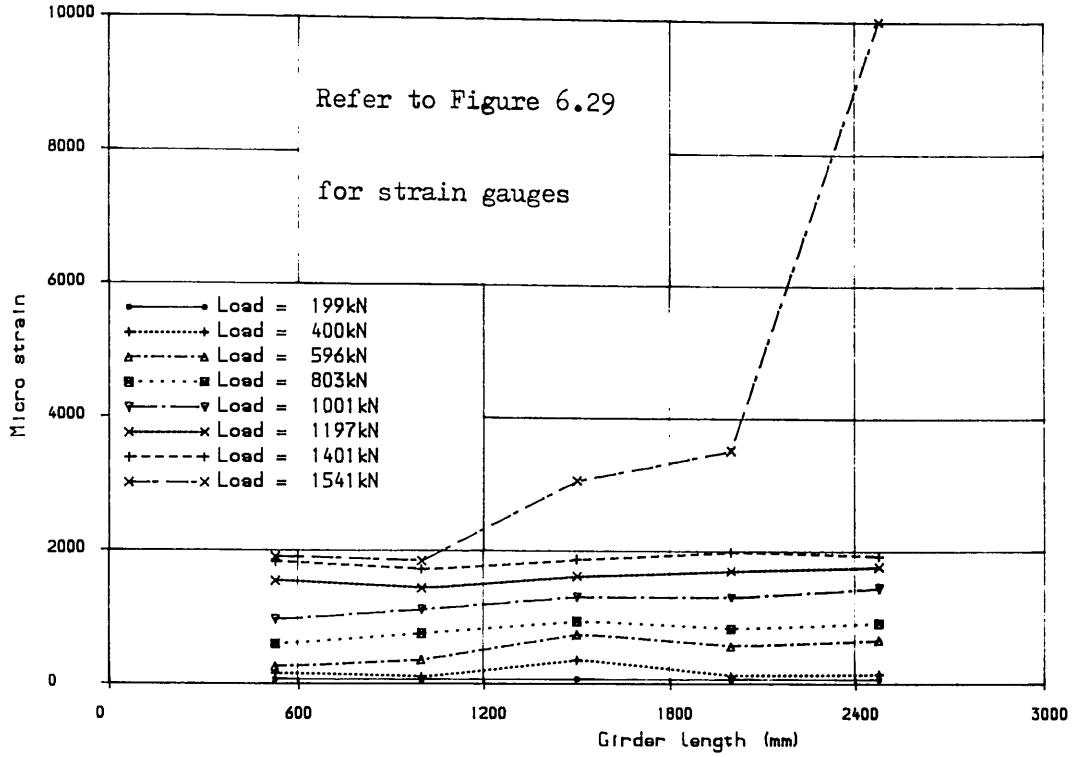

FIG (7.97) Steel strain distribution in bottom bar along girder length of girder TRGRAS11

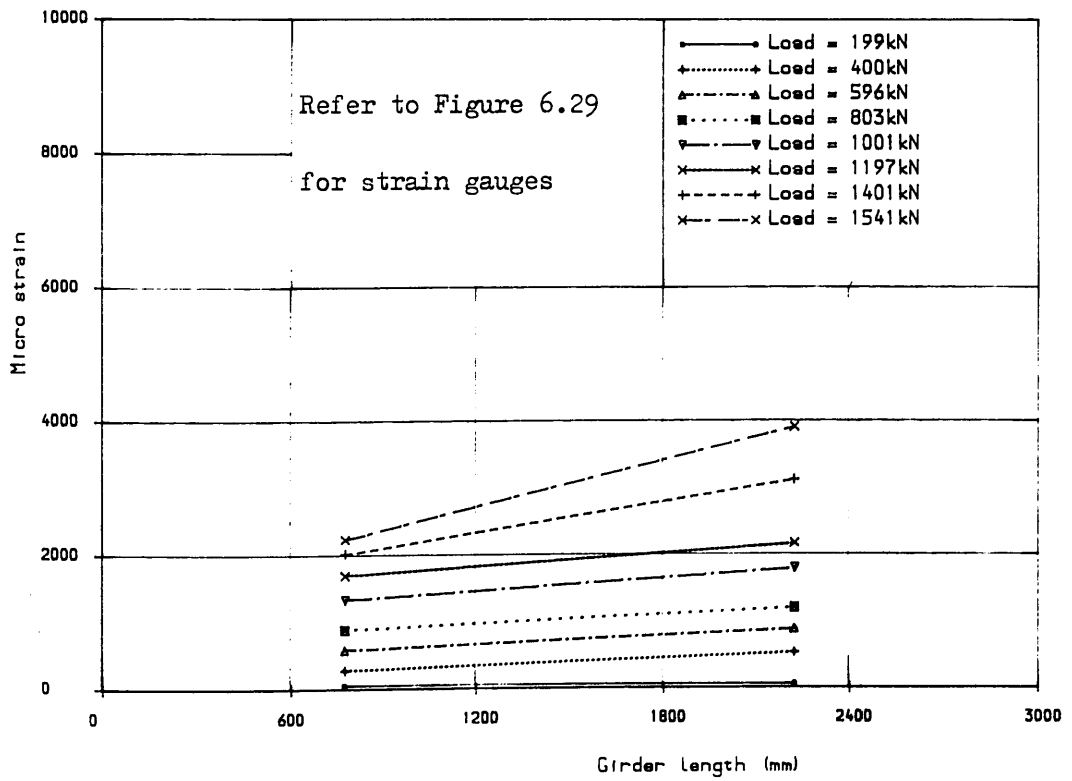

FIG (7.98) Steel strain distribution in second bar from bottom along girder length of TRGRAS11

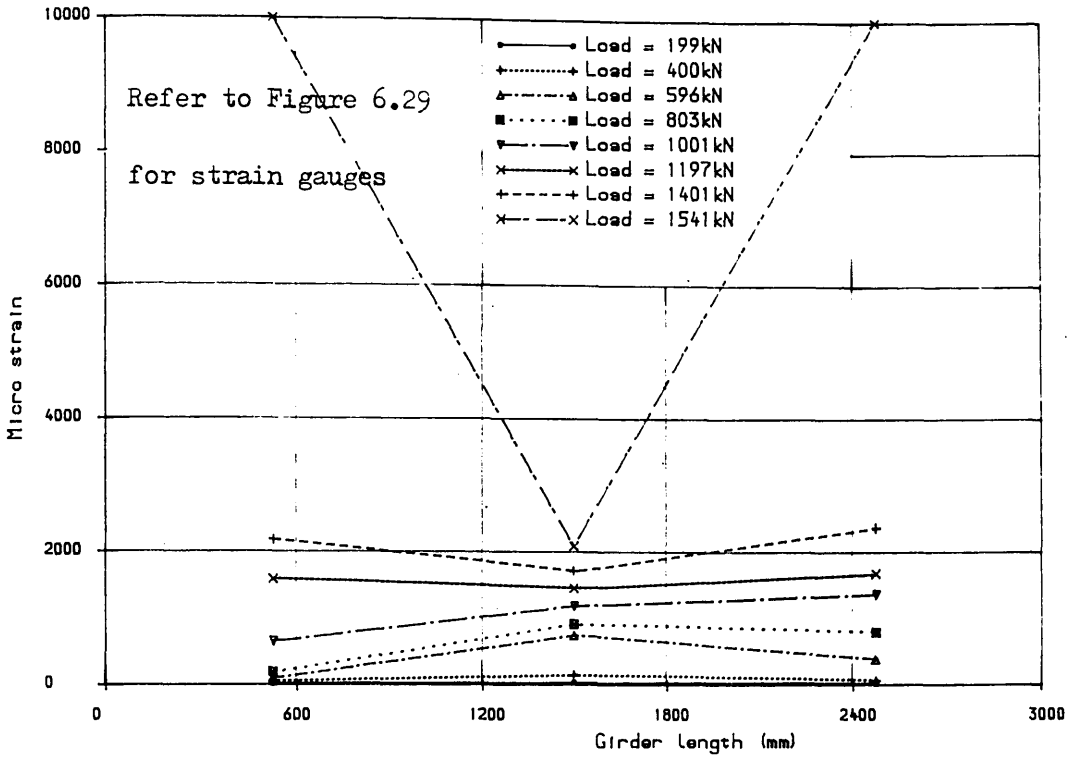

FIG (7.99) Steel strain distribution in third bar from bottom along girder length of TRGRAS11

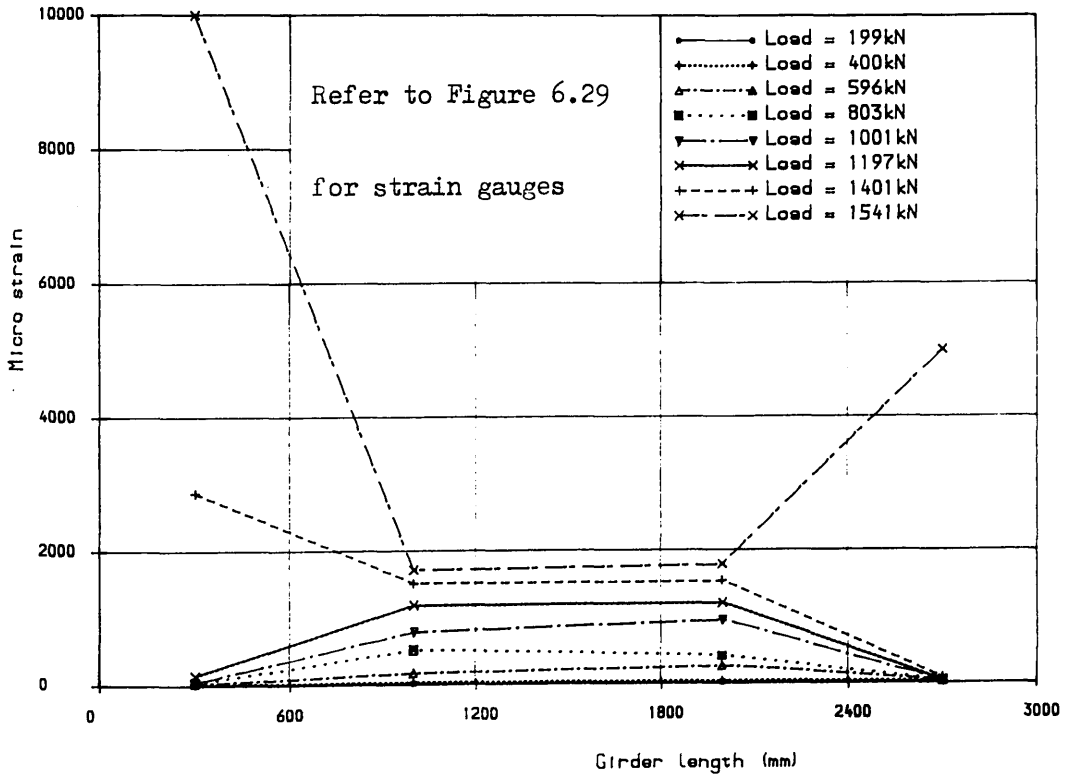

FIG (7.100) Steel strain distribution in fifth bar from bottom along girder length of TRGRAS11

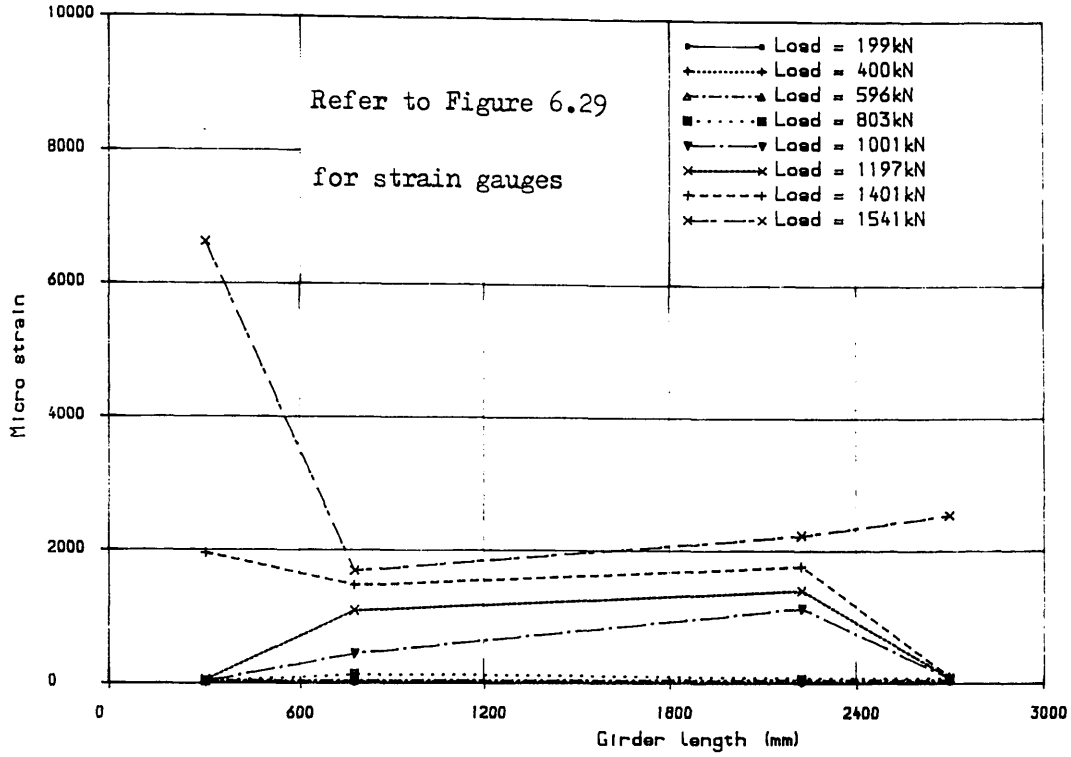

FIG (7.101) Steel strain distribution in sixth bar from bottom along girder length of TRGRAS11

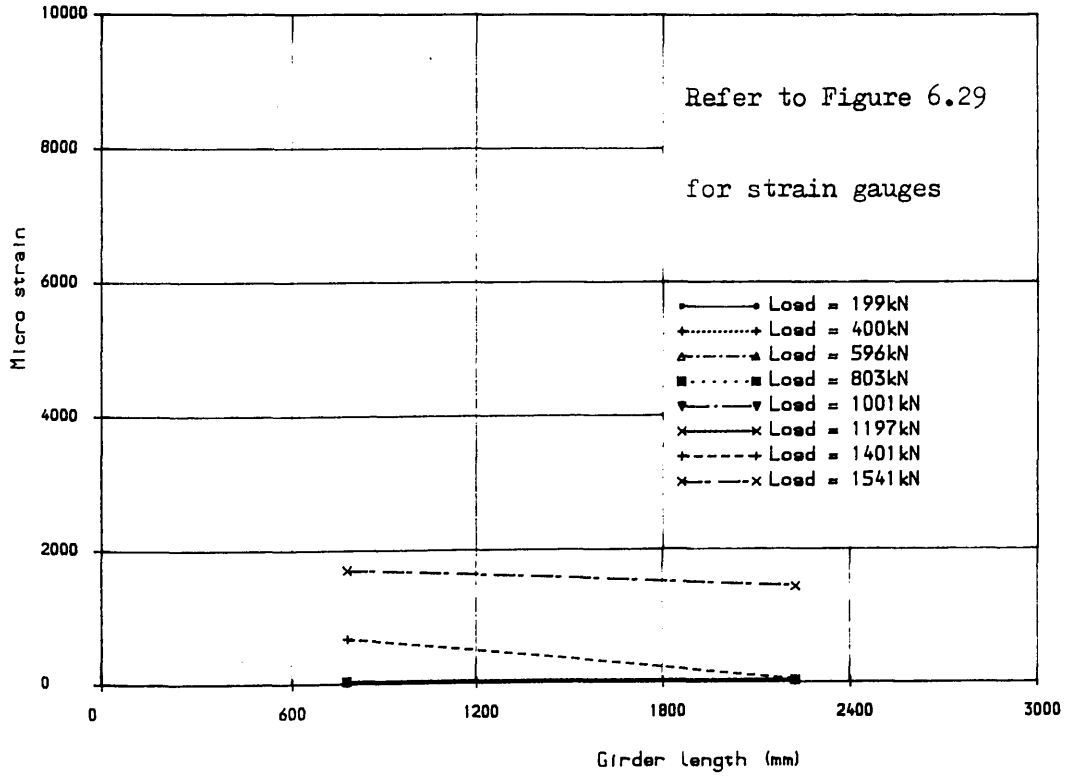

FIG (7.102) Steel strain distribution in seventh bar from bottom along girder length of TRGRAS11

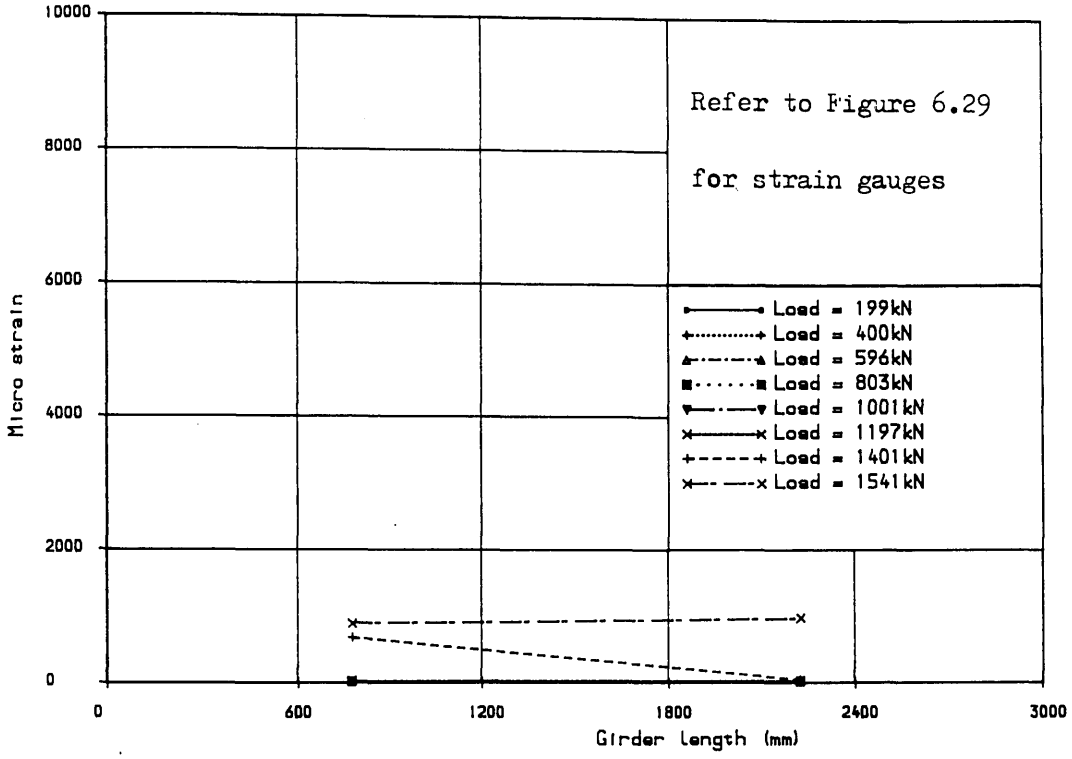

FIG (7.103) Steel strain distribution in 8th bar from bottom along girder length of TRGRAS11

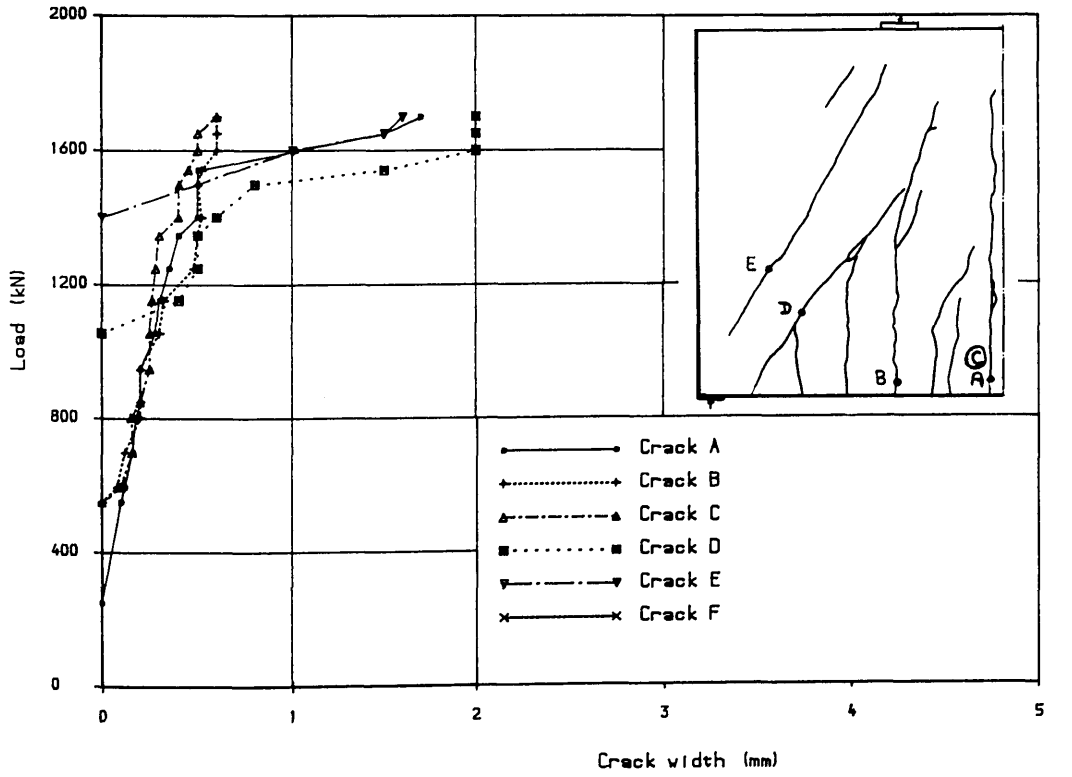

FIG(7.104) Load vs crack width for girder TRGRAS11

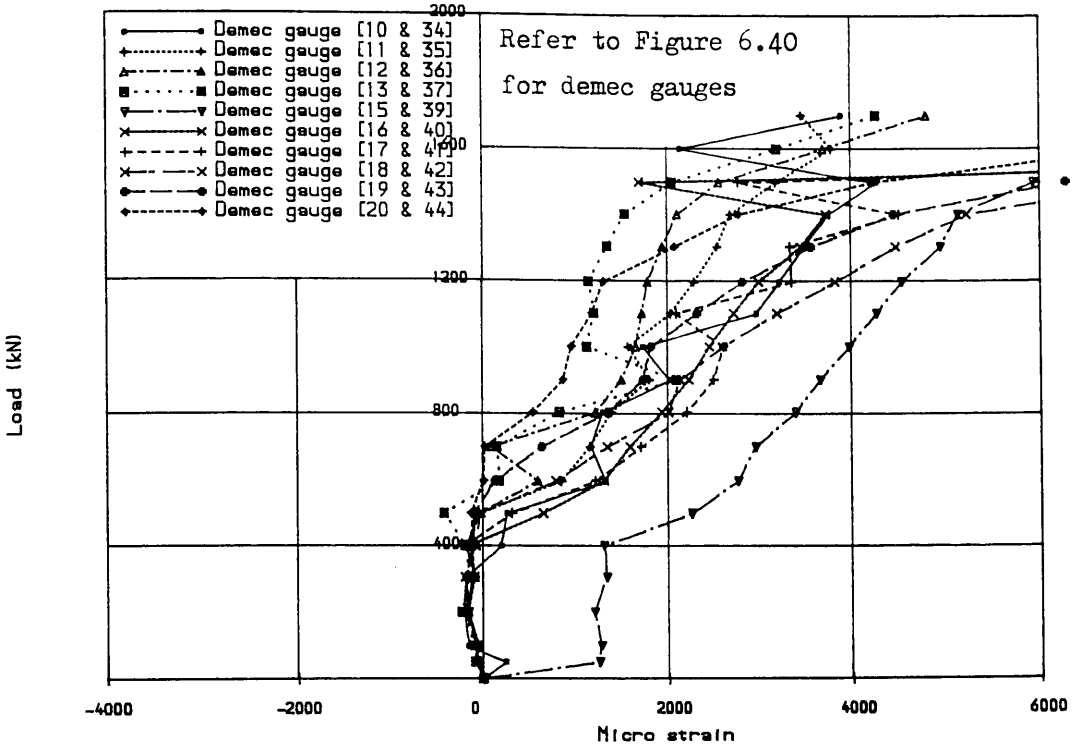

FIG (7.105) Load vs concrete surface strains for girder TRGRAS11

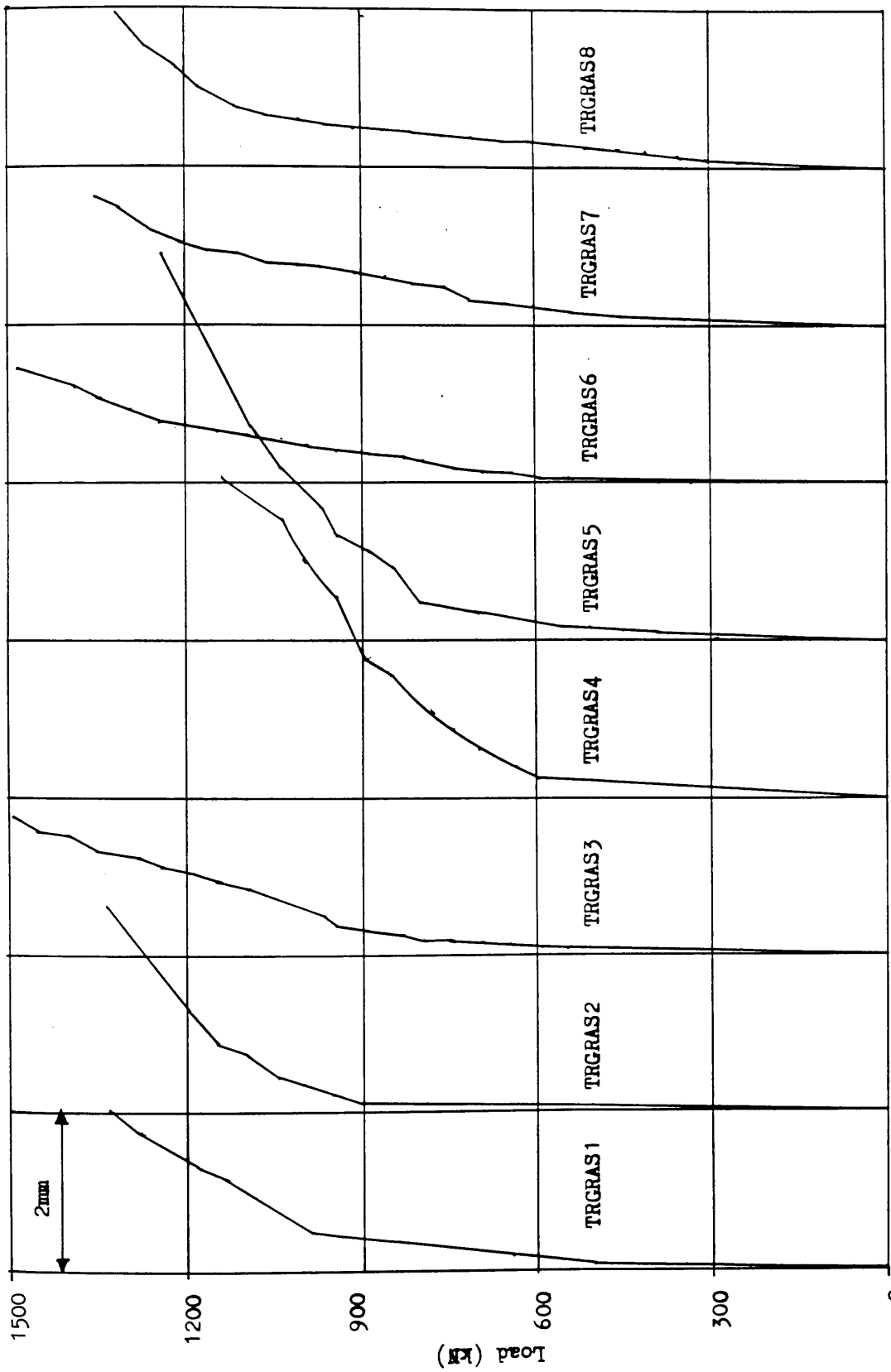

FIG(7.106) Comparison of load deflection curves for two span continuous girders

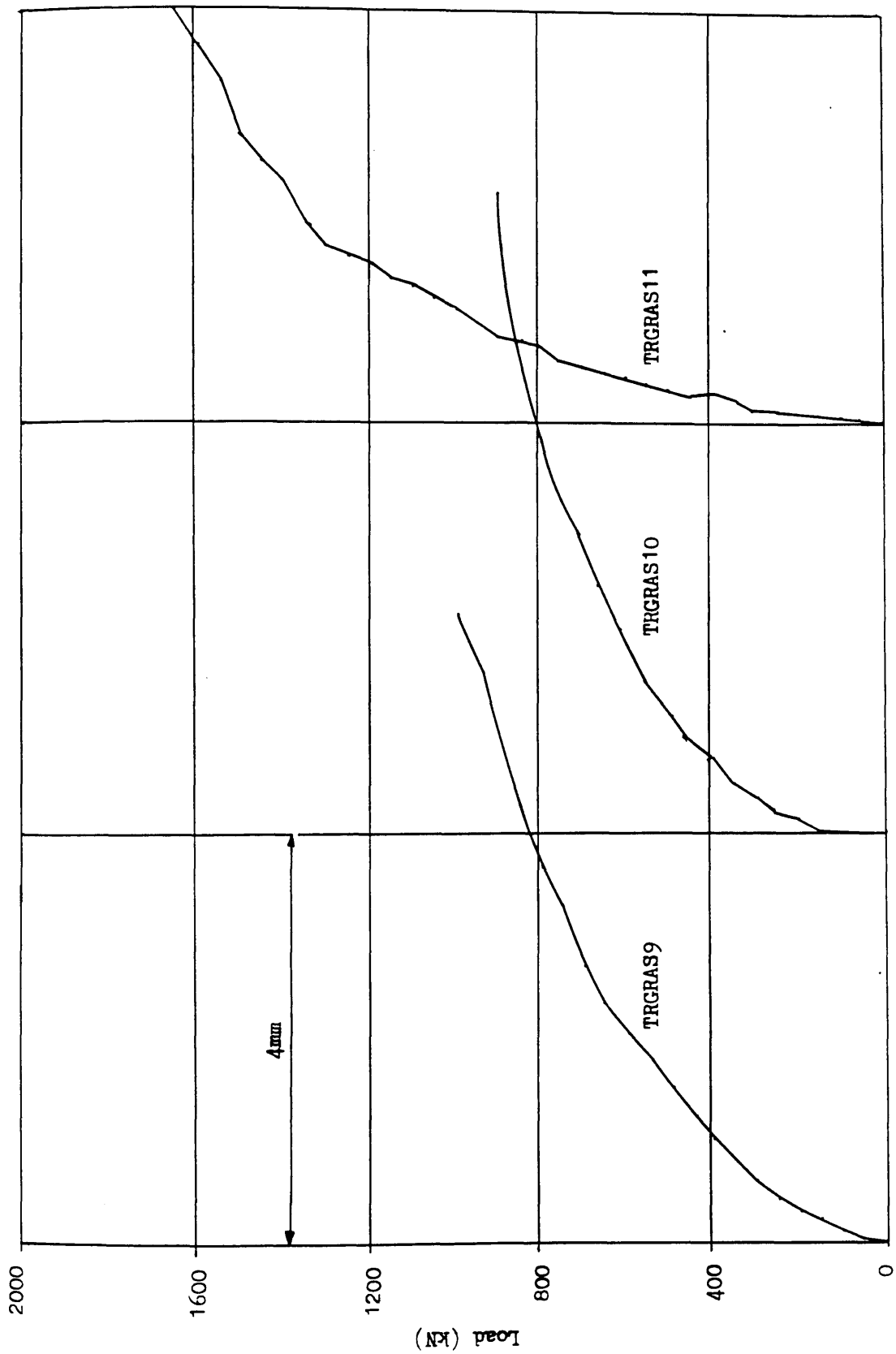

FIG(7.107) Load deflection curves for single span girders

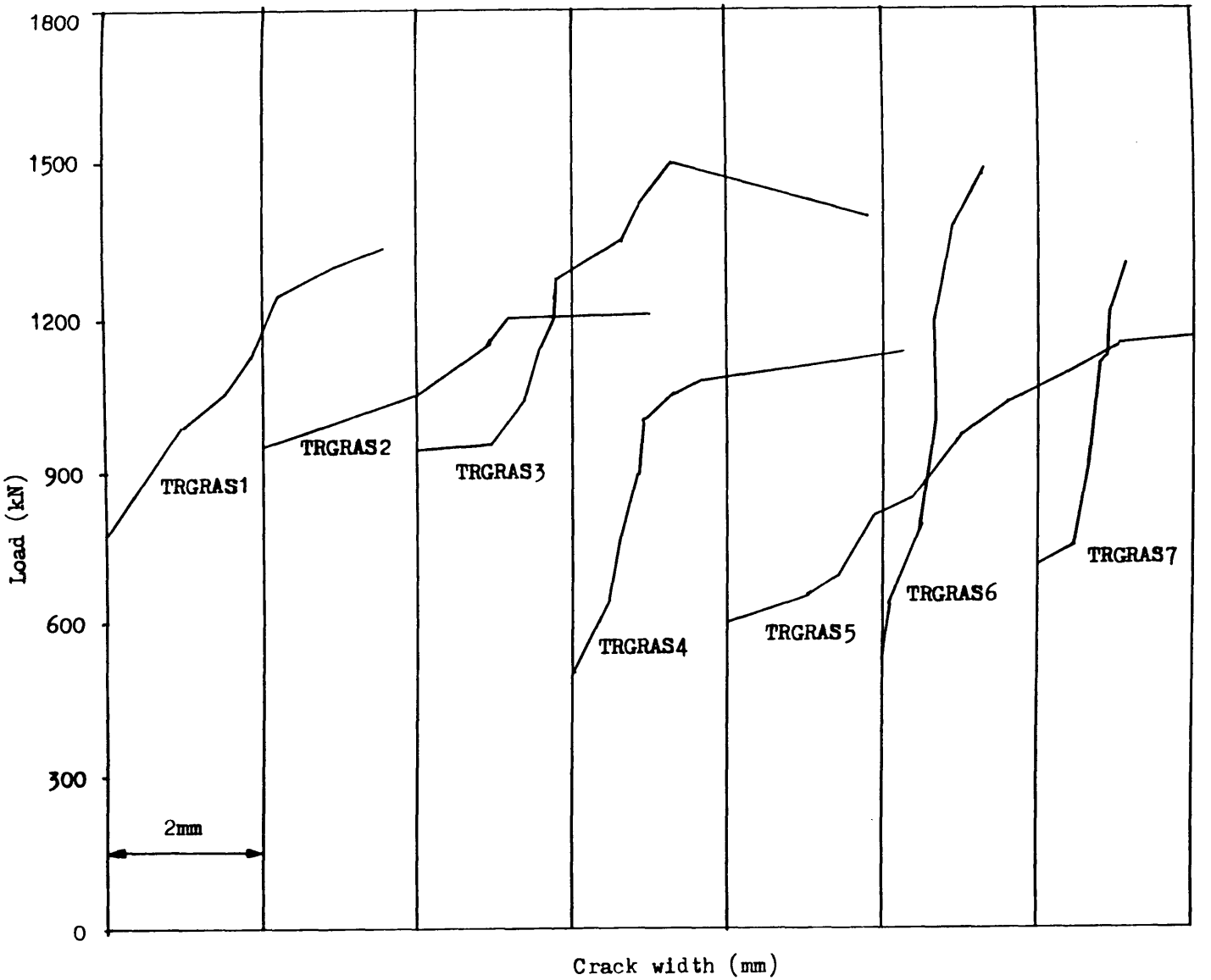

FIG(7.108) Load vs maximum crack width of all two span continuous girders

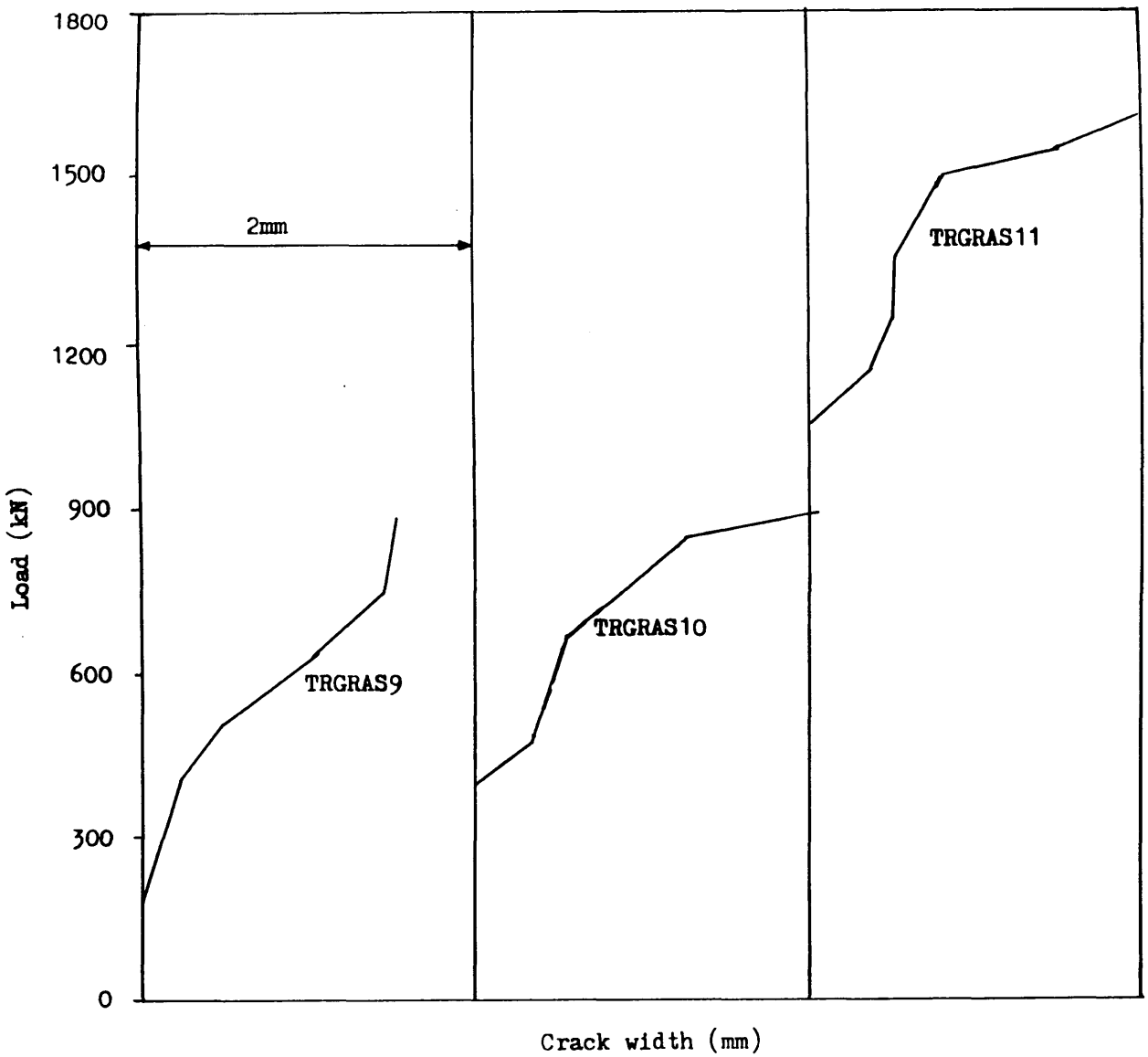

FIG(7.109) Load vs maximum crack width for single span girders

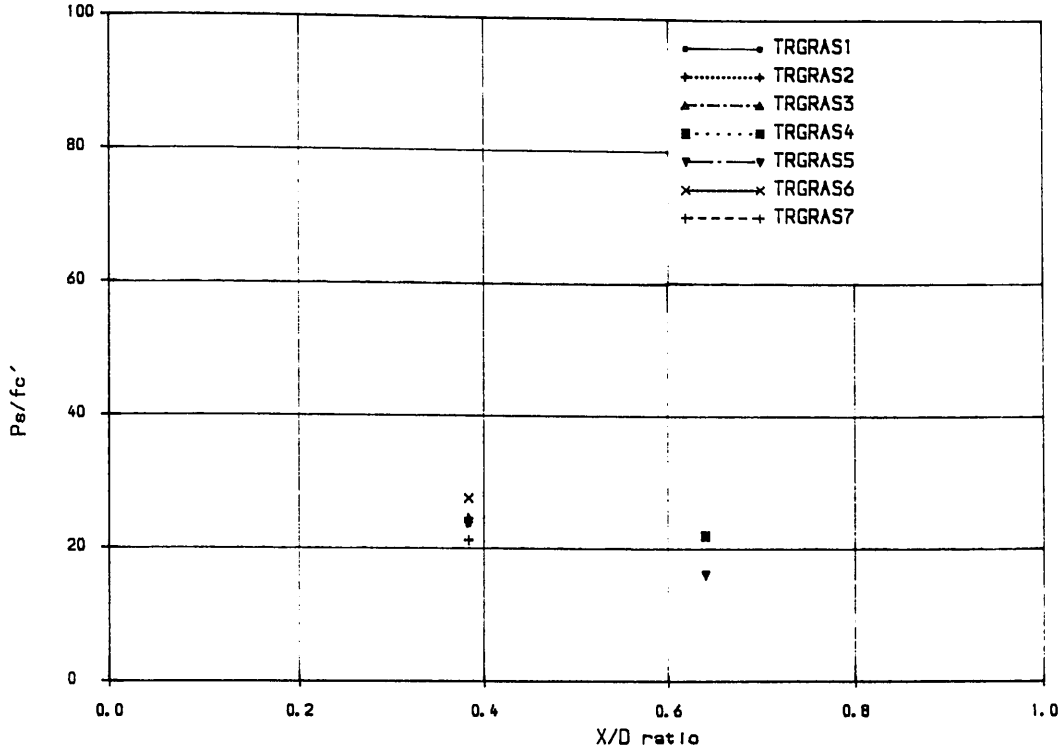

FIG(7.110) Serviceability strength of girder vs clear shear span to depth (X/D) ratio

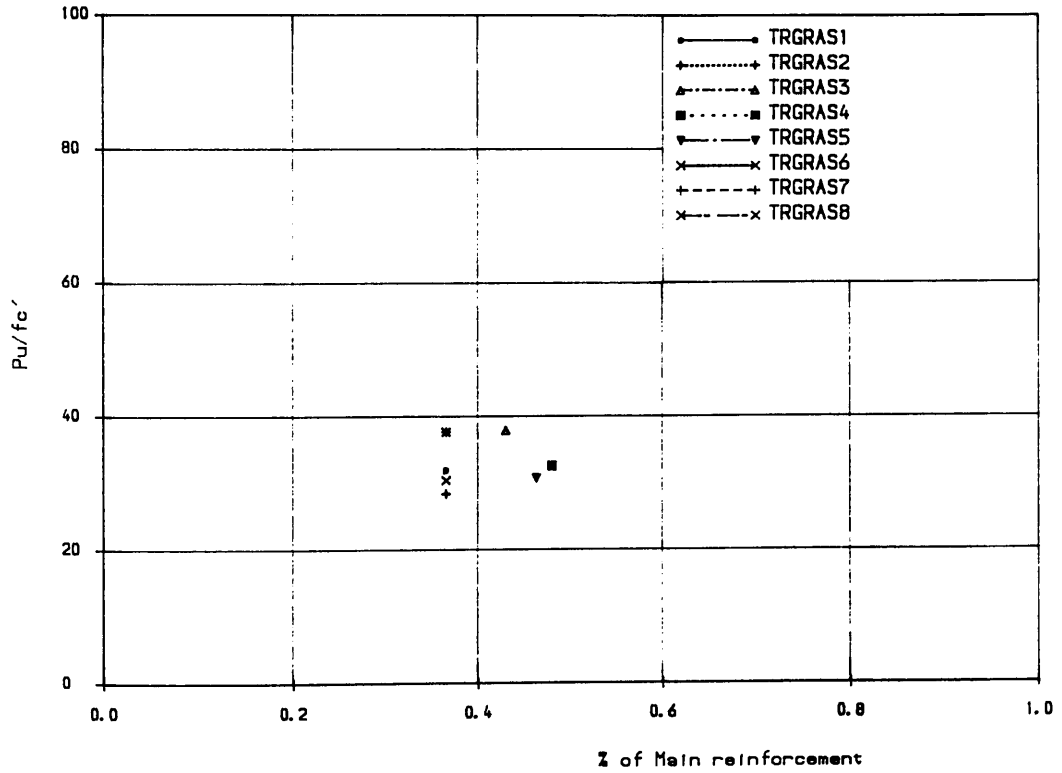

FIG(7.111) Ultimate strength of girder vs volume ratio of main reinforcement

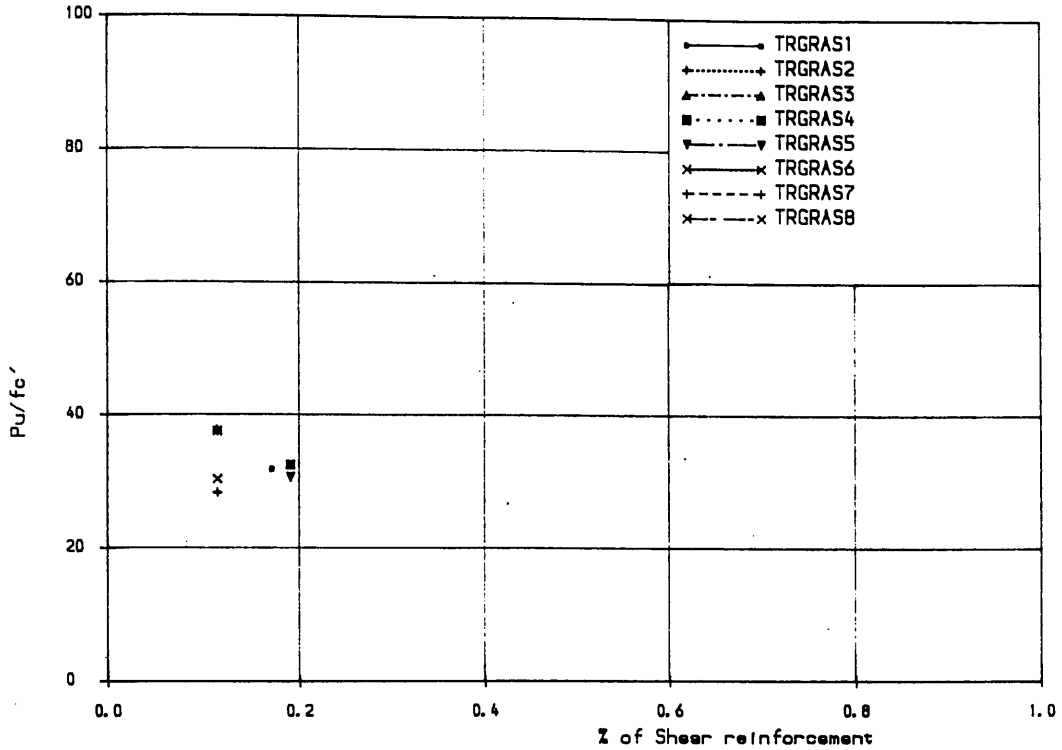

FIG(112) Ultimate strength of girder vs volume ratio of shear reinforcement

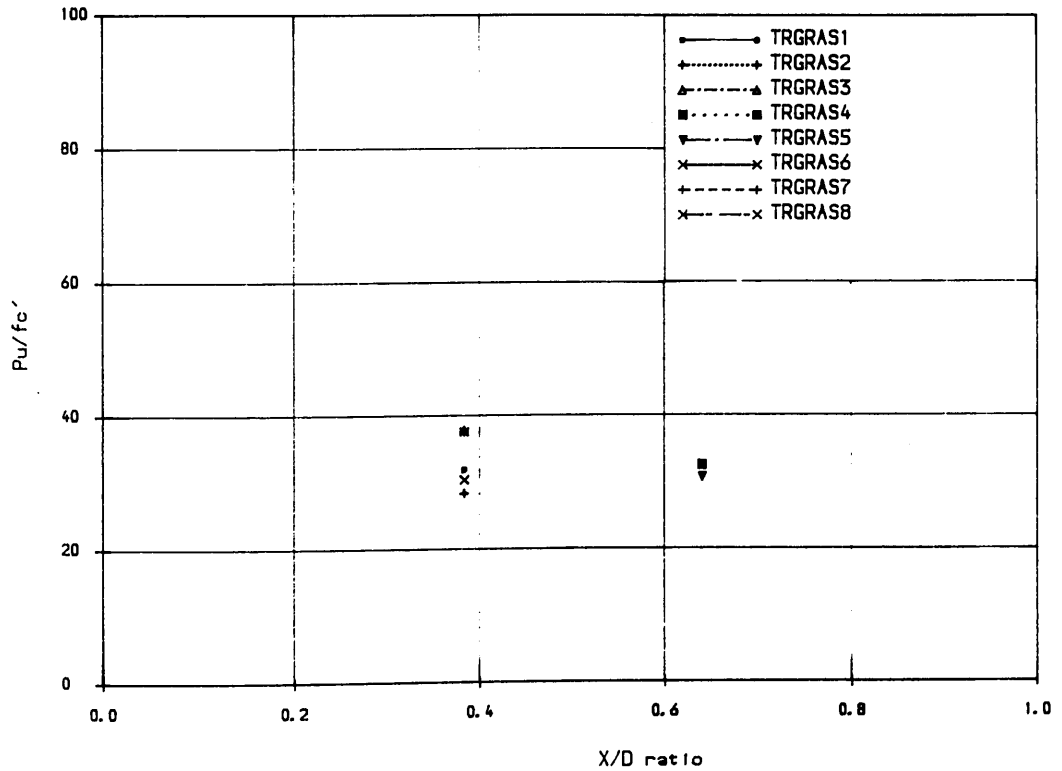

FIG(7.113) Ultimate strength of girder vs clear shear span to depth (X/D) ratio

References

1. CIRIA Guide 2, "The design of deep beams in reinforced concrete", London, CIRIA publication, Jan. 1977.

2. CEB– FIP committee, "International recommendation for the design and construction of concrete structures", Principles and recommendations", Prague, FIP sixth congress, Jun. 1970.

3. LEONHARDT, F. and WALTHER, R., "Wandartige trager, Deutscher ausschuss fur stahlbton, Vol. 178, Wilhelm ernst und sohn, Berlin, West Germany, 1966.

4. LIN, C.K. "Ultimate strength design of deep beams", M.Sc thesis, University of Glasgow 1979.

5. BRITISH STANDARDS INSTITUTION, "The structural use of concrete, code of practice", BS 8110, 1985.

CHAPTER EIGHT
THEORETICAL INVESTIGATION AND DISCUSSION

8.1 Introduction

The aim of this chapter is to provide some perspective on the application of the nonlinear finite element method to the tested girders. At present, this is the main technique for predicting the complete nonlinear behaviour of existing designs. Although in the last three decades, much has been learned about this technique, its reliability depends on the ingenuity and skill of the engineer. This is because it is an approximate iterative method based on various assumptions and, depending on their validity, it may or may not provide a true picture of behaviour. Experience gained in nonlinear analysis suggests that some experimental verification is essential when complex behaviour is to be analysed to give confidence for conducting parametric studies once the reliability of the developed model for a particular problem has been validated.

Finite element analysis of reinforced concrete predicts the general behaviour of the structure including load–deformation, stress flow, crack patterns, yielding of steel, and failure mechanism. It has so far been difficult, if not impossible, to predict accurately every aspect of the actual behaviour. Many comparisons have used the stiffness and ultimate load, that is the load deformation behaviour. However, a good agreement with experimental results is relatively straightforward to achieve, by adjusting certain factors, such as quasi–material parameters like the shear retention and tension stiffening factors. Other consequences resulting from adjusting these parameters on the general structural behaviour, such as crack pattern, yielding of steel, stress and strain history in the structure, and the failure mechanism, are not always considered thoroughly. For example, Al–Manaseer and Phillips[1] have recently demonstrated the effect of the quasi–material parameters on load deformation behaviour, cracking and failure mechanisms of the structure, which warns analysts not to rely solely on just load–deformation behaviour.

In this chapter, the results of the nonlinear finite element analysis are presented and verified using load deflection curves, steel strain history, crack patterns, deformational

behaviour of the structure in the form of distorted finite element mesh, and three dimensional views and contours of the maximum shear strains. Results for girder TRGRAS1 will be presented in detail, the behaviour of the other two span girders was similar and will only be discussed briefly. The comparison of ultimate loads is summarized in Table 8.1. A numerical parametric study of two span continuous girders was also carried out, and the results of these are presented in section 8.4. This study supplemented the experimental tests.

In addition, a comparison has been made with other empirical formulae developed for predicting the ultimate capacities of deep beams. These are presented in section 8.7.2 and Tables 8.10 to 8.14.

8.2 Sensitivity studies of the nonlinear finite element method

A sensitivity study was carried out on the following aspects:

(i) The finite element mesh

(ii) The shear retention factor

(iii) The tension stiffening factor

and this will be presented first. Girders TRGRAS1 and TRGRAS5 were used for this purpose.

Throughout the analysis a 3*3 Gauss integration rule was used. The element stiffnesses were recomputed at the first iteration of each load increment. The maximum number of iterations was kept to 10 for the two span continuous girders and for the solid single span girder and for perforated girders was kept to 30. The convergence tolerance was set to 5%. All the reinforcing bars were embedded as close as possible to their positions within the girders themselves.

8.2.1 Mesh sensitivity

Because of symmetry, only one span of the two span continuous girder was considered for nonlinear analysis. Five different meshes of 10, 20, 28, 42 and 54 elements were studied with a linear–elastic analysis as shown in Figure(8.1) using the same

boundary conditions and loading application point. The central displacement versus the number of degrees of freedom is plotted in Figure(8.2). The displacement increased about 8% when the mesh was refined from ten to twenty elements, about 2% from twenty to twenty eight, about 1.5% from twenty eight to forty two and 1% from forty two to fifty four. Thus it was concluded that a mesh containing a maximum of 42 elements was the best choice. For girder TRGRAS5, 48 elements were used in order to better simulate the reinforcing bars.

In the single span perforated girders, openings were placed at different locations in each shear span, so it was not possible to use symmetry. In this case, 100 and 108 elements were used, in both the elastic and nonlinear analysis, in order to represent the reinforcing bars accurately. For these girders, a mesh convergence study was not carried out because the number of elements were already high and were considered to be sufficient. For girder TRGRAS11 only one half was analysed as it was symmetrical and 60 elements were used.

8.2.2 Shear retention factor

A study was carried out to evaluate the effect of the shear retention factor on the ultimate strength and overall behaviour. Four different constant values of shear retention were used, 0.1, 0.25, 0.5 and 0.75 respectively, for girder TRGRAS1. The results are presented in Figures (8.3) to (8.5). It is clear from these figures that the shape of the deflection and steel strain curves are not greatly affected by various values of the shear retention factor, but the failure load is affected. The summary of results in terms of ultimate strengths is presented in Table 8.2. Although several researchers have proposed a constant shear retention factor of 0.5[2,3] as well as variable values[1,4,5] for deep beams, in this study 0.25 seemed satisfactory and so was used in the analysis of all girders.

8.2.3 Tension stiffening study

A study of tension stiffening models was carried out on girder TRGRAS5. Figures (8.6) to (8.8) show the comparisons of experimental and theoretical results using

different models and Table 8.3 summarizes the effect on the ultimate strength. It appears that tension stiffening has a tendency to:

(a) increase the ultimate load.

(b) improve the shape of load deformation curve.

(c) give a stiffer response for secondary behaviour i.e steel strains etc.

However an increase in the load would give a worst predictions for some of the other girders. Therefore, using tension stiffening parameters for girders designed by the direct design method in conjunction with the averaging procedure did not improve all aspects of behaviour. Since this was the intention rather than relying solely on the load deflection and ultimate strength, it was decided to omit tension stiffening from the analysis altogether.

8.3 Comparison of the theoretical and experimental results

Figure (8.9) shows the finite element mesh used for TRGRAS1 and Figure (8.10) illustrates the details of the reinforcement used in the analysis. Figure (8.11) shows the load deflection curve and demonstrates that general trends and ultimate strength were satisfactorily predicted. The ratio of predicted to experimental ultimate strength is 0.98. The theoretical curve is more flexible up to 40% of ultimate load, after which it is stiffer than the experimental curve. The discrepency between these curves might be attributed to the difficulties in measuring the experimental deflection by mounting a handy angle frame on the model itself. This is another reason why it is not wise to rely solely on the load deflection curve for verifying the analytical model. The post– cracking behaviour is predicted with reasonable accuracy.

The steel strain is examined for both longitudinal and transverse reinforcement in Figures (8.12) and (8.13). Reasonable agreement can be seen between predicted and experimental behaviour. These curves show that neither the longitudinal steel nor the stirrups recorded any significant strains prior to concrete cracking. After cracking, there is a considerable increase in the strains and this is well predicted. However,

the accuracy of these predictions vary between remarkable to fairly acceptable. The comparison of yielding of the main and transverse steel indicates that yielding in the finite element model occurred at a later stage than the experimental. This was due to the assumption of full bond between reinforcement and concrete in the finite element analysis, whereas in the real structure, as the cracking progressed, the bond would deteriorate and the steel would take over the load earlier than in the theoretical model.

The predicted deformational behaviour and crack progression for all girders tested in this study are given in detail in a departmental report . However, a resume' for girder TRGRAS1 is shown in Figures (8.14) to (8.16). The deformations are exaggerated ten times in these figures.

Cracks started in the local zones (i.e support points) and at the beam soffit at a load of 375kN. On a further increase in load, more cracks occurred at the centre of the beam span and started propagating towards the loading point (Figure (8.14), and continued to do so until 750kN (Figure (8.15)) when a few cracks occurred at the top of the intermediate support in the tensile zone. At 900kN (Figure (8.16)), shear cracks appeared running from the inside face of the support towards the loading point. The cracking in the interior shear span was more severe than the exterior shear span. Some secondary cracks also appeared at the beam soffit at the bottom tip of the shear crack. This illustrates the arching behaviour in both interior and exterior shear spans. More cracks occurred at loads of 1125kN and 1275kN and the formation of the shear crack in the interior shear span was then quite clearly evident. The final failure was at 1312kN, the crack pattern is not given at this particular increment, because of the numerical instability in nonlinear analysis which occurs at failure. The final crack pattern clearly indicates that the shear failure takes place in the interior shear span running through the intermediate support to the loading point.

The final predicted crack propagation is in reasonable agreement with experimentally

observed crack propagation, as shown in Figure (8.17), except in the local regions of the loading and support points. In the experiments these areas were clamped by external steel plates, as a result either the cracks were prevented from occuring or they could not be observed.

At an increment before failure, Figure (8.17) tends to show that the shear deformation were larger in the interior shear span suggesting that the beam was failing in a shear mode.

Maximum shear strains were small as cracking started as shown in Figure (8.18) for a load of 600kN. At 825kN, large shear strains were concentrating towards the loading points in both shear spans, but by 975kN the shear strains were clearly higher in the interior shear span and were concentrated along the line joining the support and the loading point. After this, the maximum shear strains became more significant in the other shear span, although they were still about half the value of the interior span. At 1275kN, the increment before failure, the maximum shear strains clearly indicate that the failure of the beam will be by shear along the line joining the support and the loading point in the interior shear span as shown in Figure (8.19). This agrees well with the experimental failure mechanism.

The above results tend to confirm the adequacy of the modelling approximations with regard to boundary conditions, load increment size, load application, material modelling, and the shear retention and tension stiffening parameters. These were then used for all other analysis.

The load deflection curves for the specimens in the first series, TRGRAS1, TRGRAS2, TRGRAS3 and TRGRAS6, are illustrated in Figure (8.20). The pre-cracking and post-cracking behaviour are reasonably predicted for all girders except the load-deflection curve for girder TRGRAS2, which might be attributed to the difficulties in measuring the experimental deflections by mounting handy angle frame on the model istself, although the predicted post-cracking behaviour gives a

slightly stiffer response. The predicted and measured ultimate strengths are within 4%, with a mean ratio of 0.98 which is very satisfactory.

Figures (8.21) to (8.25) compares steel strains for both longitudinal and transverse steel for girders TRGRAS2, TRGRAS3 and TRGRAS6. Again the predictions are similar to girder TRGRAS1 and are in reasonable agreement.

The predicted deformed shape and crack progression for girders TRGRAS2, TRGRAS3 and TRGRAS6 are similar to girder TRGRAS1 and compare well with experimental crack patterns as illustrated in Figures (8.26) to (8.34). Cracks always started at the beam soffit, and eventually lead to shear failure in the internal shear span. There was less cracking in the external shear span of girder TRGRAS6, due to the concentration of reinforcement at the bottom of the beam, and this was well predicted.

The maximum shear strains were similar to girder TRGRAS1 and are not presented here. However they also confirm that failure was due to shear in the interior shear span.

Figures (8.35) to (8.38) show the finite element meshes and reinforcement details for girders TRGRAS4 and TRGRAS5. Figure (8.39) shows the load deflection curves. The finite element model predicted the overall behaviour of TRGRAS4 quite reasonably, giving a predicted to measured ultimate strength ratio of 1.0 although the stiffness in the final 20% of loading was much higher than the experimental. However, for girder TRGRAS5, the ultimate strength was underestimated by 22% although the post–cracking stiffness was similar to the experimental value. This underestimate might be due to the fact that the reinforcement provided over the intermediate support was insufficient to control the severe cracking which occurred in this region in the numerical model. This would lead to sperious local mechanism, causing premature breakdown of the numerical solution, and hence underestimating the ultimate strength.

Figures (8.40) to (8.43) compare the steel strains curves for longitudinal steel and stirrups. These demonstrate that the theoretical response is stiffer than the experimental but, with one or two exceptions, general trends are on the whole satisfactorily predicted.

The deformed shape and crack progression were similar to girder TRGRAS1 except that deformations were larger because of the larger span length. Comparisons of experimental and theoretical crack patterns are given in Figures (8.44) to (8.49). Again satisfactory agreement is evident, except for local regions.

The maximum shear strains are illustrated in Figures (8.50) and (8.51) for TRGRAS4 and demonstrate the shear failure mechanism along the line joining the support and the loading point in the interior support.

Figures (8.52) and (8.53) show the finite element mesh and reinforcement details for the skew reinforced girder TRGRAS7. Similar details were used for girder TRGRAS8 except the different angle of skew. Figure (8.54) compares the load deformation curves for both girders and demonstrate reasonable predictions in both the pre–cracking and post–cracking ranges. The mean of the ratio of predicted to measured ultimate strengths is 1.02.

Figures (8.55) to (8.58) compares the steel strains for longitudinal and shear reinforcement. Generally speaking, there is reasonable agreement for TRGRAS7. However, the experimental behaviour of TRGRAS8 is much more flexible, which is probably due to the accidental load applied before starting the test.

The deformed shape and crack progression are illustrated for different load levels in Figures (8.59) to (8.64). Again, satisfactory agreement is evident except for local regions.

The maximum shear strains are illustrated in Figures (8.65) and (8.66) for TRGRAS7, and again suggest a shear failure mechanism as observed in the experimental study.

Figures (8.67) to (8.70) show the finite element meshes and details of reinforcement used for the perforated girders TRGRAS9 and TRGRAS10. Figure (8.71) compares the load deformation curves. The predictions are reasonably good, except for the stiffer post–cracking behaviour for TRGRAS9. In the test, failure was initiated locally by cracking around the opening which might have caused early bond deterioration. In the finite element analysis this was not the case and thus a more stiff response occurred. However the mean ratio of the predicted to measured ultimate strengths is 1.0, which is highly satisfactory.

The comparison of the experimental and theoretical steel strains are presented in Figures (8.72) to (8.75). The comparsion is generally satisfactory, however some strains were poorly predicted, particularly in the stirrups. This is probably due to the bond deteriorations which were not properly modelled in the finite element analysis. Also the predicted response tended to be stiffer than the experiment in the post–cracking stages.

Figure (8.76) shows the cracking in TRGRAS9 at 420kN. Cracking started at corner 2 of opening A at a load of 240kN. With increase in load to 300kN and beyond more cracks occurred at corner 2 and 4 of both openings, and near the beam soffit, extending towards the loading point. At a load of 420kN more cracks appeared, in particular a horizontal crack appeared from the end of the beam extending towards corner 1 of opening B. Figure (8.77) shows how the cracks had extended by 720kN. At 480kN, more flexural cracks at the beam soffit occurred, extending vertically, and also more cracks propagated around both openings. At 600kN, more cracks appeared from the beam soffit and joined the bottom of openings A and B, and propagated towards the loading points. The cracks which occurred at the centre of the beam were vertical.

Figure (8.78) shows the extent of cracks at 1020kN. At 800kN severe cracks occurred around opening B, and cracks which joined corner 1 and the loading point behaved like a shear crack. Similar behaviour was evident from the deformed shapes over the top of opening B. Also at this load the horizontal crack extended to corner 1 of opening B, after which the block above the opening bounded by the diagonal shear crack and the horizontal crack started to become more distorted. This indicates that the block is trying to rotate and that the diagonal shear crack over the top of opening B will cause failure, as can be seen in Figure (8.78).

The comparison of experimental and theoretical crack patterns illustrated in Figures (8.76) to (8.78) show good agreement and suggests that the finite element model is quite capable of handling the perforated deep beam analysis.

The maximum shear strain plots shown in Figures (8.79) and (8.80) show that as cracking progresses the maximum shear strains start to increase and concentrate in the shear crack zones particularly over the top of opening B, where failure occurred.

Figure (8.81) show the extent of cracking in TRGRAS10 at a load of 420kN. When the load was at 180kN, the first numerical cracking occurred at corner 1 and 3 of openings B and C; in addition some cracks also appeared in the beam soffit. On a further increment in the load more cracks appeared in the other shear span at corners 2 and 4 of opening A. At 360kN, cracks appeared at the beam soffit and extended vertically. At this load a horizontal crack also appeared from the end of the beam extending towards corner 4 of opening C. On a further increase in load, more cracks occurred extending around openings B and C.

Figures (8.82) and (8.83) show the growth of cracks at 720kN and 780kN respectively. At 600kN, more cracks appeared around all the openings and started extending towards the loading point, forming diagonal shear cracks between corner 4 of opening C and the loading point, and between corner 4 of opening B and corner

2 of opening C. Also a horizontal crack appeared at the end of the beam extending towards corner 3 of opening A. A further increase in load caused more cracks and some secondary cracks occurred in the zone between opening B and C close to corner 4 of opening B, and also at the top of opening C at corner 4. At this load, the deformed shape also showed the significant appearance of a shear crack over the top and at the bottom of opening C. At 840kN, a diagonal crack occurred over the top and bottom of opening C as is evident from the deformed meshes.
This description is essentially the same as occurred experimentally as can be seen in Figures (8.81) to (8.83).

The maximum shear strains (Figures (8.84) and (8.85)) also illustrate the high concentration of the shear strains around opening C and B and show that the failure mechanism is probably due to the diagonal shear crack over the top opening C and between openings C and B.

Figures (8.86) and (8.87) show the finite element analysis mesh and details of the reinforcement used in the analysis of girder TRGRAS11. Details of bar diameters were given in Chapter Five. Exact steel areas as used in the actual test were used in the nonlinear finite element analysis. Figure (8.88) shows the comparison of the experimental and theoretical load deflection curves. The predicted ultimate strength is satisfactory but the predicted stiffness is more flexible at low loads and becomes more stiffer than the experimental values at higher loads.

Figures (8.89) and (8.90) show the comparison of the steel strains in longitudinal steel and steel stirrups. The predicted pre–cracking and post–cracking behaviour is in reasonable agreement with experimental behaviour.

Figures (8.91) to (8.93) illustrate the crack development at loads of 640kN, 800kN and 1760kN in the nonlinear analysis. The first crack occurred at 400kN at the beam soffit in the tensile zone. On a further increase in load more flexural cracks occurred in the beam soffit extending in the vertical direction. Cracks already

existing between the loading point and the centre of the girder continued to extend in a vertical direction, but cracks in the shear span started to bend round towards the loading point, forming diagonal shear cracks. This confirms that failure was a flexural– shear type mechanism. Severe cracking occurred at a load 1454kN near the support face and extended towards the loading point. Similar behaviour was evident from the deformed meshes. The comparison between experimental and predicted crack patterns is good except in the local regions which were clamped with steel plates in the experimental tests.

Shear failure is very clear from the maximum shear strain contours shown in Figures (8.94) and (8.95). These indicate that failure took place along the plane joining the support to the loading point.

The finite element analysis also confirms the much higher ultimate strength compared to the design ultimate load.

8.4 Parametric study

Since satisfactory predictions were given by nonlinear finite element analysis in the previous section, further numerical experiments were conducted on two span continuous girders. The object of this exercise was to study the effect of various other factors on the ultimate strength of a transfer girder designed by the direct design technique which had not been examined experimentally. These results will be combined with experimental results of Chapter Seven in order to extend the experimental conclusions.

8.4.1 Parameters chosen for investigation

Table 8.4 shows the details of the numerical models. This includes three specimens of the experimental programme to aid comparison. The main variables investigated are given as follows and the results are given in Table 8.5.

(a) The effect of the shear reinforcement on the ultimate strength.

(b) The effect of clear shear span to depth (X/D) ratios on the ultimate strength.

(c) The effect of skew reinforcement on the ultimate strength.

(d) The effect of different reinforcement distribution on the ultimate strength.

(a) The effect of shear reinforcement on the ultimate strength.

The effect of the shear reinforcement on the ultimate strength was studied by using the material properties of girder TRGRAS2 to analyse girder T11 (i.e TRGRAS1) and T12 (i.e TRGRAS2) by nonlinear finite element analysis. The results are given in Table 8.5, and indicate that the ultimate strength increases with increase in the shear reinforcement. The addition of one extra 6mm diameter bar stirrup in the interior shear span increased the ultimate load by 6%.

(b) The effect of clear shear span to depth (X/D) ratio on the ultimate strength.

In order to study the effect of clear shear span to depth (X/D) ratio on the ultimate strength two more continuous girders were designed by the direct design technique to cover the ultimate strength ranges of X/D ratios varying from 0.3 to 0.64. The details of these girders are given in Figures (8.96) and (8.97).

These girders were then analysed by nonlinear finite element model. The results are given in Table 8.5, which indicates that increse in clear shear span to depth (X/D) ratio reduces the ultimate strength. However, a graph has been plotted as shown in Figure (8.98), which shows the reduction in ultimate strength with increase in X/D ratio. This confirms the earlier findings of Kong et al and other researchers that the deeper the beam, the higher is the ultimate strength.

(c) The effect of skew reinforcement on the ultimate strength.

To study the effect of skew reinforcement on the ultimate strength four more continuous girders were designed by the direct design technique with different skew angles from those covered in the experimental programme. The details of these girders are given in Figures (8.99) to (8.102).

Nonlinear finite element analysis was carried out to predict the ultimate strengths.

The results are given in Table 8.5, which indicates that skew reinforcement takes higher ultimate strengths. A graph of ultimate strengths versus skew angle is given in Figure (8.103) which includes both the experimental and theoretical predictions. It clearly shows that strength increases steadily up to skew angle of 10°, after which it increases more rapidly. It was found that an angle between 15° and 20° was the best for the girders in this study.

(d) The effect of different reinforcement distribution on the ultimate strength.

Two different reinforcement distribution have been studied experimentally in this investigation. But because of the variation in the material properties, it was not possible to make conclusions about the effectiveness of these distributions on the ultimate strength. Therefore, in this section the material properties were kept constant in order to study different reinforcement distributions:

(i) Girder TRGRAS3 was identical to girder TRGRAS6 except for the reinforcement distribution and material properties. Therefore, girder T41 (i.e TRGRAS6) was numerically studied by using the same material properties as girder TRGRAS3. Girder T41 produced 30% less strength than girder TRGRAS3.

(ii) Girder TRGRAS4 was identical to girder TRGRAS5 except for the reinforcement distribution and material properties. Therefore, girder T42 (i.e TRGRAS5) was numerically studied by using the same material properties as girder TRGRAS4. Girder T42 produced 8% less strength than girder TRGRAS5 produced numerically.

However, the results have indicated that CIRIA Guide 2 distribution is not so effective as that of the direct design technique.

8.5 Discussion of finite element analysis

The aim of this study was to assess the general predictions which may be made from the nonlinear finite element model. The predictions have confirmed that large scale continuous and single span girders with web openings can be satisfactorily analysed by nonlinear finite element analysis. The load–deflection behaviour,

cracking, failure mechanism, yielding of steel were found to be in reasonable agreement with experimental behaviour. This suggests that the model can be used confidently for further numerical parametric studies.

Its versatility in predicting most aspects of behaviour allows additional information to be obtained which cannot be observed experimentally. For example, the maximum shear strains and deformed shapes have provided extra information about the failure mechanism rather than relying on crack patterns alone.

The use of a constant shear retention factor of 0.25 for girders designed by direct design technique in conjunction with the averaging procedure gave a reasonable prediction when compared with observed ultimate strengths.

Although the use of tension stiffening for girder TRGRAS5 demonstrated that it would improve the ultimate load and load deformations, it also provided much stiffer response for steel behaviour. However an increase in the ultimate strength would give worse predictions for other girders of this study. Thus, tension stiffening was omitted.

8.6 Comparison of the direct design technique with various proposed formulae

As mentioned in chapter two, a considerable amount of work has been reported on the simple supported deep beams, and a lot less on continuous deep beams. Various empirical formulae and truss models have been proposed from time to time for both design and analysis purposes. This study has verified experimentally and by nonlinear analysis that the direct design technique is satisfactory in both serviceability and ultimate behaviour, showing that it is a natural design–oriented method. This section will compare the use of some of these other formulae on the girders tested in this study in order to highlight the suitability of the direct design method as a design tool for producing economic reinforcement.

8.6.1 Design of tested transfer girders

Six formulae, already described in detail in Chapter Two, have been used to design the reinforcement for the girders tested in this study. All, except Kotsovos's formula, have been used widely either in U.S.A or British practice, or appear in the European work. These formulae are as follows: Portland Cement Association (PCA) method[6], CEB–FIP Model Code[7], ACI Code[8], CIRIA Guide 2[9], Kong et al[10] and Kotsovos's[11] formulae.

Most of these formulae were developed from single span deep beam studies, but include design rules for continuous deep beams as well. They give procedures for obtaining main and shear reinforcement, although some disregard shear reinforcement altogether, while some of the other formulae provide shear reinforcement on an ad hoc basis. Table 8.6 to 8.11 summarizes the reinforcement designs given by these formulae and compare them with the direct design method. These tables clearly shows that the direct design technique is generally economical in the use of both main and shear reinforcement. Because all the code–prescribed formulae have provided higher reinforcement than the direct design technique, however, some formulae were supplied with partial factor of safety for steel ($\gamma m = 1.15$). The provision of the shear reinforcement is on ad hoc basis, also there is no idea how design will behave in serviceability and ultimate behaviour whereas direct design is proved to be satisfactory in both serviceability and ultimate behaviours.

The development of the plastic truss model by MacGregor et al[12,13] has been applied to continuous deep beams and its use has been advocated for designing deep beams. The author tried to apply the plastic truss model to the girders tested in this study, but it was found that MacGregor et al had used an iterative process of rebuilding the geometry of tested beams and using a different concrete effectiveness factor for their two different series of beams. For example, in reference 12 they used effectiveness factor $\nu' = 1.0$, but they could not get good predictions for some beams, and so they varied the effectiveness from 1.0 to 0.5 to get a closer prediction without any specific criteria. In reference 13, the effectiveness factor used

was $\nu' = 1.0$. Therefore, rather than analysing the girders of this study, the direct design technique was applied to a series of five beams tested by MacGregor et al[13]. The details of this series of five beams is given in Figures (8.104) to (8.108) and the material properties are given in Tables 8.12 and 8.13. The design ultimate load of these beams was not given, but it was assumed to be the actual failure load of the beams which is on the conservative side.

Beams designed by the direct design technique are illustrated in Figure (8.109) to (8.113) and a comparison with the plastic truss model is given in Table 8.14. The results indicate that the direct design technique gives a considerable saving in main reinforcement, whereas shear reinforcement is higher than that required by the plastic truss model.

However, it is clear that the overall direct design technique compares favourably with the plastic truss model. This study has shown that the measured ultimate loads were always 30% to 60% higher than the design ultimate loads. Therefore since MacGregor's failure load was taken as the design load, the direct design method is even more economical than the table would at first suggest. The difference in the shear reinforcement between these techniques might be due to the fact that in the plastic truss model shear reinforcement is provided on an ad hoc basis, whilst the direct design method has a sound theoretical framework for its calculation.

8.6.2 Analysis of ultimate strength by empirical formulae

There are various formulae for predicting the ultimate strengths of simply supported and continuous deep beams and these were discussed in Chapter Two. A sample of some prominent formulae are examined in this section. These are, Ramakrishnan and Ananthanayrana[14], de Paiva and Siess[15], ACI Code[8], Kong et al[10] and CIRIA Guide 2[9]. These formulae were calibrated on the test data for simply supported deep beams which were loaded either at the centre or at the third point. Therefore, the estimation of shear strength of a shear span can be multiplied by 2 to get the overall shear capacity, because at the ultimate stage both shear spans are assumed to

be failed even if a failure only occurred in one shear span. In a continuous deep girder, failure is always in the interior shear span, therefore, the estimation of the shear strength based on the same criteria as simply supported may not be correct. It is difficult to know the shear strength of the exterior shear span, because it did not fail in any continuous girder reported in this thesis. In order to accommodate this, an elastic distribution of shear force was utilized to estimate the shear strength. According to the elastic distribution of reaction, 31% shear is taken by the exterior shear span and 69% by the interior shear span, if a load is acting at the centre of the span.

In addition to that, experimental results have revealed that at the ultimate load stage 57% of the load was carried by the intermediate supports for girders whose span to depth (L/D) ratio was 1.07 and 63% was carried for girders whose span to depth (L/D) ratio was 1.61.

The various formulae were modified to take these (i.e elastic and ultimate reaction) distribution into account and the summary of the results is presented in Tables 8.15 to 8.19. These formulae have been applied with and without the modifications to demonstrate its effect.

Only the ultimate shear strength of solid girders has been estimated, because there is no formulae to predict the ultimate shear strength of perforated deep girders when the openings are not placed symmetrically in both shear spans.

The estimated results from the empirical formulae are far from the experimental measured strengths. However, the modified version of the Ramakrishnan and Ananthanayrana[14] formula is fairly close to the experimental results.

8.7 Conclusion

The following conclusions can be drawn from the analytical studies made in this chapter:

1: (a) Theoretical results indicate the applicability of the nonlinear finite element model for analysing the complicated general behaviour of large scale continuous and solid span girders. The basic characteristics of the behaviour, namely the pre–cracking and post–cracking behaviour, ultimate strengths and crack patterns, overall deformations and failure mechanism are predicted with reasonable accuracy for the majority of girders examined. The finite element analysis provided additional information, such as deformational behaviour and maximum shear strains, which is difficult if not impossible to obtain in experiments.

(b) All the girders were analysed using the same material and solution parameters. The results demonstrate that for the type of transfer girders tested in this study, satisfactory behaviour is obtained if tension stiffening is not used ($\alpha 2 = 0.0$) and a constant shear retention factor of 0.25 is selected.

(c) Steel response was found to be stiffer, however, the comparison was generally satisfactory. This could have been due to the assumption of full bond between concrete and steel in the finite element analysis.

(d) An increase in shear reinforcement increased the ultimate strength.

(e) For the decreasing shear span to depth (X/D) ratios the ultimate strength increased.

(f) The use of skew reinforcement produced higher ultimate strengths; however, an angle of 15° to 20° were the most efficient.

(g) CIRIA Guide 2 reinforcement distribution produced less satisfactory behaviour and lower ultimate strengths than the direct design method.

2. Various other design methods required a higher amount of reinforcement than the direct design technique, suggesting that the direct design method is the more economical technique.

3. The predicted ultimate strengths by empirical derived formulae by other researchers greatly overestimated the actual measured strengths. This suggests that these empirical formulae cannot be reliably applied to continuous deep beams. Nevertheless, the modification to Ramakrishnan and Ananthanayrana's[14] formulae produced reasonable predictions.

TABLE 8.1

Comparison of the experimental and predicted ultimate strength of the test girders

Series No.	Girder No.	Experimental Failure load kN	Theoretical Failure load kN	Tu/Pu	Mean	S.D
1	TRGRAS1	1333	1312	0.98		
	TRGRAS2	1216	1237	1.02		
	TRGRAS3	1500	1462	0.97		
	TRGRAS6	1486	1425	0.96	0.98	0.026
2	TRGRAS4	1143	1144	1.0		
	TRGRAS5	1243	975	0.78	0.89	0.155
3	TRGRAS7	1420	1425	1.02		
	TRGRAS8	1312	1350	1.03	1.02	0.019
4	TRGRAS9	1046	1110	1.06		
	TRGRAS10	891	840	0.94	1.0	0.084
5	TRGRAS11	1750	1800	1.03	1.03	

TABLE 8.2

The effect of shear retention factor on the ultimate shear strength for girder TRGRAS1

Girder	Shear retention factor	Actual strength Pu	Predicted strength Tu
TRGRAS1	0.01	1333.0	1125kN
	0.25	1333.0	1312kN
	0.50	1333.0	1388kN
	0.75	1333.0	1462kN

TABLE 8.3

The effect of tension stiffening factor on the ultimate shear strength for girder TRGRAS5

Girder	Tension stiffening factor	Ultimate strength Pu	Predicted strength Tu
TRGRAS5	NTS	1243kN	975kN
	$\alpha 1=0.4$ $\alpha 2=10.0$	1243kN	1125kN
	$\alpha 1=0.5$ $\alpha 2=10.0$	1243kN	1200kN
	$\alpha 1=0.6$ $\alpha 2=10.0$	1243kN	1350kN

TABLE 8.4

The details of girders analysed in parametric study.

Girder No.	Depth D	Length L	L/D Ratio	X/D Ratio	Type of Reinforcement
TRGRAS2	900	960	1.07	0.38	Orthogonal
T11	900	960	1.07	0.38	Orthogonal
T12	900	960	1.07	0.38	Orthogonal
T21	900	960	1.07	0.30	Orthogonal
TRGRAS2	900	960	1.07	0.38	Orthogonal
T22	900	1300	1.44	0.50	Orthogonal
TRGRAS4	900	1450	1.61	0.64	Orthogonal
TRGRAS2	900	960	1.07	0.38	Orthogonal
T31	900	960	1.07	0.38	Skew θ=5°
T32	900	960	1.07	0.38	Skew θ=9°
TRGRAS8	900	960	1.07	0.38	Skew θ=10°
TRGRAS7	900	960	1.07	0.38	Skew θ=15°
T33	900	960	1.07	0.38	Skew θ=20°
T34	900	960	1.07	0.38	Skew θ=25°
TRGRAS3	900	960	1.07	0.38	Orthogonal
T41	900	960	1.07	0.38	Orthogonal
TRGRAS4	900	1450	1.61	0.64	Orthogonal
T42	900	1450	1.61	0.64	Orthogonal

TABLE 8.5

The summary of ultimate strengths obtaind in parametric study

Girder No.	L/D Ratio	X/D Ratio	Type of reinforcement	Ultimate strength kN
TRGRAS2	1.07	0.38	Orthogonal	1216
T11	1.07	0.38	Orthogonal	1237
T12	1.07	0.38	Orthogonal	1312
T21	1.07	0.30	Orthogonal	1320
TRGRAS2	1.07	0.38	Orthogonal	1237
T22	1.44	0.50	Orthogonal	1162
TRGRAS4	1.61	0.64	Orthogonal	1144
TRGRAS2	1.07	0.38	Orthogonal	1237
T31	1.07	0.38	Skew θ=5°	1312
T32	1.07	0.38	Skew θ=9°	1387
TRGRAS8	1.07	0.38	Skew θ=10°	1350
TRGRAS7	1.07	0.38	Skew θ=15°	1425
T33	1.07	0.38	Skew θ=20°	1662
T34	1.07	0.38	Skew θ=25°	1462
TRGRAS3	1.07	0.38	Orthogonal	1500
T41	1.07	0.38	Orthogonal	1125
TRGRAS4	1.61	0.64	Orthogonal	1143
T42	1.61	0.64	Orthogonal	900

TABLE 8.6

Comparison of Reinforcement design for transfer girders tested in this study with PCA Method.

Girder No.	Direct Design Method			PCA Method			Ratio of
	Main	Shear	Total	Main	Shear	Total	PCA/DDM
TRGRAS1	329	171	500	935	—	935	1.87
TRGRAS2	329	114	443	935	—	935	2.11
TRGRAS3	373	114	487	1082	—	1082	2.22
TRGRAS4	430	285	715	952	—	952	1.33
TRGRAS5	417	285	702	952	—	952	1.36
TRGRAS6	417	114	531	1209	—	1209	2.28
TRGRAS7	329	114	443	935	—	935	2.11
TRGRAS8	329	114	443	935	—	935	2.11

TABLE 8.7

Comparison of Reinforcement design for transfer girders tested in this study with CEB– FIP Method.

Girder No.	Direct Design Method			CEB–FIP Method			Ratio of
	Main	Shear	Total	Main	Shear	Total	CEB-FIP/DDM
TRGRAS1	329	171	500	583	370	953	2.15
TRGRAS2	329	114	443	583	370	953	2.15
TRGRAS3	373	114	487	675	370	1045	2.15
TRGRAS4	430	285	715	789	470	1259	1.76
TRGRAS5	417	285	702	789	470	1259	1.79
TRGRAS6	417	114	531	754	370	1124	2.12
TRGRAS7	329	114	443	583	370	953	2.15
TRGRAS8	329	114	443	583	370	953	2.15

TABLE 8.8

Comparison of Reinforcement design for transfer girders tested in this study with ACI Code Method.

Girder No.	Direct Design Method			ACI Code Method			Ratio of
	Main	Shear	Total	Main	Shear	Total	ACI/DDM
TRGRAS1	329	171	500	935	485	1420	2.84
TRGRAS2	329	114	443	935	485	1420	2.84
TRGRAS3	373	114	487	1082	485	1567	3.22
TRGRAS4	430	285	715	952	571	1523	2.13
TRGRAS5	417	285	702	952	571	1523	2.13
TRGRAS6	417	114	531	1209	485	1694	3.19
TRGRAS7	329	114	443	935	485	1420	2.84
TRGRAS8	329	114	443	935	485	1420	2.84

TABLE 8.9

Comparison of Reinforcement design for transfer girders tested in this study with CIRIA Guide 2 Method.

Girder No.	Direct Design Method			CIRIA Guide 2			Ratio of
	Main	Shear	Total	Main	Shear	Total	CIRIA/DDM
TRGRAS1	329	171	500	610	475	1085	2.17
TRGRAS2	329	114	443	610	475	1085	2.45
TRGRAS3	373	114	487	706	475	1181	2.42
TRGRAS4	430	285	715	761	588	1349	1.89
TRGRAS5	417	285	702	761	588	1349	1.92
TRGRAS6	417	114	531	789	475	1264	2.38
TRGRAS7	329	114	443	610	475	1085	2.45
TRGRAS8	329	114	443	610	475	1085	2.45

TABLE 8.10

Comparison of Reinforcement design for transfer girders tested in this study with Kong et al's proposed Method.

Girder No.	Direct Design Method			Kong's Method			Ratio of
	Main	Shear	Total	Main	Shear	Total	KONG/DDM
TRGRAS1	329	171	500	522	—	522	1.04
TRGRAS2	329	114	443	522	—	522	1.18
TRGRAS3	373	114	487	604	—	604	1.24
TRGRAS4	430	285	715	789	—	789	1.10
TRGRAS5	417	285	702	789	—	789	1.12
TRGRAS6	417	114	531	675	—	675	1.27
TRGRAS7	329	114	443	522	—	522	1.18
TRGRAS8	329	114	443	522	—	522	1.18

TABLE 8.11

Comparison of Reinforcement design for transfer girders tested in this study with Kotsovos's proposed Method.

Girder No.	Direct Design Method			Kotsovos Method			Ratio of
	Main	Shear	Total	Main	Shear	Total	KOTSOV/DDM
TRGRAS1	329	171	500	934	—	934	1.89
TRGRAS2	329	114	443	934	—	934	2.10
TRGRAS3	373	114	487	1091	—	1091	2.24
TRGRAS4	430	285	715	1448	—	1448	2.03
TRGRAS5	417	285	702	1448	—	1448	2.06
TRGRAS6	417	114	531	1220	—	1220	2.30
TRGRAS7	329	114	443	934	—	934	2.10
TRGRAS8	329	114	443	934	—	934	2.10

TABLE 8.12

Concrete properties of Ricketts and MacGregor's Beams

Beam No.	fc' N/mm^2	ft' N/mm^2	Ec N/mm^2	Age days
1	35.4	—	25600	52
2	31.3	2.7	21700	42
3	3160	—	21000	56
4	3160	3.0	25300	50
5	3160	3.0	23900	48

TABLE 8.13

Reinforcing properties of Ricketts and MacGregor Beams

Bar size mm	fy N/mm^2	Es N/mm^2
20	410	219000
20*	440	206000
10	435	203000
6	451	190000

Note:- 20*mm bar is only used for beam 1

TABLE 8.14

Comparison of reinforcement calculated by direct design technique and Ricketts and Macgregor's

Beam No.	Ricketts & MacGregor's			Direct design technique			Difference %
	Main mm^2	Shear mm^2	Total mm^2	Main mm^2	Shear mm^2	Total mm^2	
1	2199	342	2541	1533	1006	2539	—
2	2514	2670	5184	2273	1414	3673	29
3	2199	969	3168	1759	1188	2947	7
4	2199	969	3168	2110	1414	3524	-10
5	2199	969	3168	1758	1188	2946	7

TABLE 8.15

Comparison of ultimate strengths predicted by Ramakrishnan and Anathanayrana's formula

Girder No	Exp. Load Pu	Predicted P1′	P1′/Pu	Elastic formula P1	P1'/Pu	Ultimate P1''	P1''/Pu
TRGRAS1	1333	1809	1.35	1327	0.99	1621	1.22
TRGRAS2	1216	2078	1.70	1327	1.09	1621	1.22
TRGRAS3	1500	1920	1.28	1295	0.86	1584	1.06
TRGRAS4	1143	1694	1.48	1211	1.06	1326	1.16
TRGRAS5	1243	2293	1.85	1311	1.06	1436	1.16
TRGRAS6	1486	2395	1.61	1295	0.87	1568	1.06
TRGRAS7	1440	1474	1.02	1262	0.88	1526	1.06
TRGRAS8	1312	1920	1.46	1343	1.02	1626	1.24
TRGRAS11	1750	2097	1.20	1815	1.04	——	——

TABLE 8.16

Comparison of ultimate strengths predicted by de Paiva and Siess's formula

Girder No	Exp. Load Pu	Predicted P2′	P2′/Pu	Elastic formula P2	P1'/Pu	Ultimate P2''	P2''/Pu
TRGRAS1	1333	2084	1.56	1510	1.13	1828	1.37
TRGRAS2	1216	2128	1.75	1540	1.26	1863	1.53
TRGRAS3	1500	2012	1.34	1588	1.04	1922	1.28
TRGRAS4	1143	1460	1.28	1180	1.03	1292	1.13
TRGRAS5	1243	1628	1.31	1466	1.18	1606	1.29
TRGRAS6	1486	2024	1.36	1558	1.05	1821	1.22
TRGRAS7	1440	1256	0.87	910	0.63	1101	0.76
TRGRAS8	1312	2140	1.63	1550	1.18	1877	1.43
TRGRAS11	1750	988	0.56	——	——	——	——

TABLE 8.17

Comparion of ultimate strengths predicted by ACI Code's formula

Girder No	Exp. Load Pu	Predicted P3′	P3′/Pu	Elastic formula P3′	P3′/Pu	Ultimate P3′′	P3′′/Pu
TRGRAS1	1333	1212	0.91	878	0.66	1061	0.84
TRGRAS2	1216	1176	0.97	852	0.70	1029	0.80
TRGRAS3	1500	1132	0.75	820	0.55	992	0.66
TRGRAS4	1143	1124	0.98	814	0.71	891	0.78
TRGRAS5	1243	1196	0.96	867	0.70	949	0.76
TRGRAS6	1486	1132	0.76	820	0.55	992	0.66
TRGRAS7	1440	1116	0.78	809	0.56	978	0.68
TRGRAS8	1312	1180	0.90	855	0.65	1035	0.79
TRGRAS11	1750	1222	0.70	——	——	——	

TABLE 8.18

Comparion of ultimate strengths predicted by Kong et al formula

Girder No	Exp. Load Pu	Predicted P4′	P4′/Pu	Elastic formula P4′	P4′/Pu	Ultimate P4′′	P4′′/Pu
TRGRAS1	1333	1626	1.22	1177	0.88	1425	1.07
TRGRAS2	1216	1824	1.57	1322	1.09	1660	1.31
TRGRAS3	1500	1740	1.16	1260	0.84	1524	1.01
TRGRAS4	1143	1436	1.26	1041	0.91	1140	1.0
TRGRAS5	1243	1868	1.50	1353	1.09	1728	1.39
TRGRAS6	1486	2184	1.47	1582	1.06	1914	1.29
TRGRAS7	1440	1380	0.96	1000	0.72	1210	0.84
TRGRAS8	1312	1716	1.30	1273	0.97	1540	1.17
TRGRAS11	1750	2220	1.27	——	——	——	——

TABLE 8.19

Comparion of ultimate strengths predicted by CIRIA Guide 2's formula

Girder No	Exp. Load Pu	Predicted P5	P5/Pu	Elastic formula P5'	P5'/Pu	Ultimate P5''	P5''/Pu
TRGRAS1	1333	1032	0.77	748	0.56	905	0.68
TRGRAS2	1216	1040	0.86	754	0.62	912	0.75
TRGRAS3	1500	1032	0.69	748	0.50	905	0.74
TRGRAS4	1143	884	0.77	640	0.56	680	0.60
TRGRAS5	1243	980	0.86	710	0.57	760	0.61
TRGRAS6	1486	1076	0.86	780	0.52	944	0.63
TRGRAS7	1440	1000	0.69	725	0.50	877	0.60
TRGRAS8	1312	1048	0.80	759	0.58	917	0.69
TRGRAS11	1750	1268	0.72	——	——	——	——

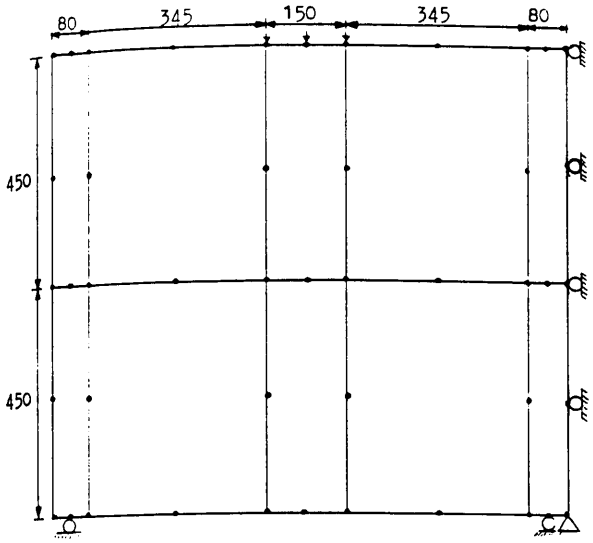

CASE I

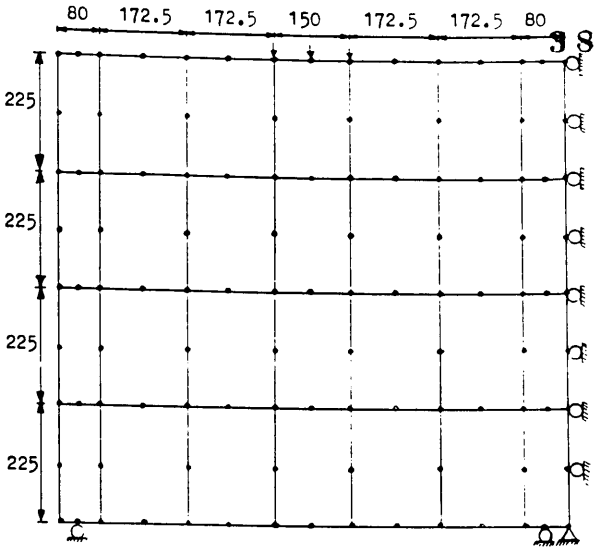

CASE III

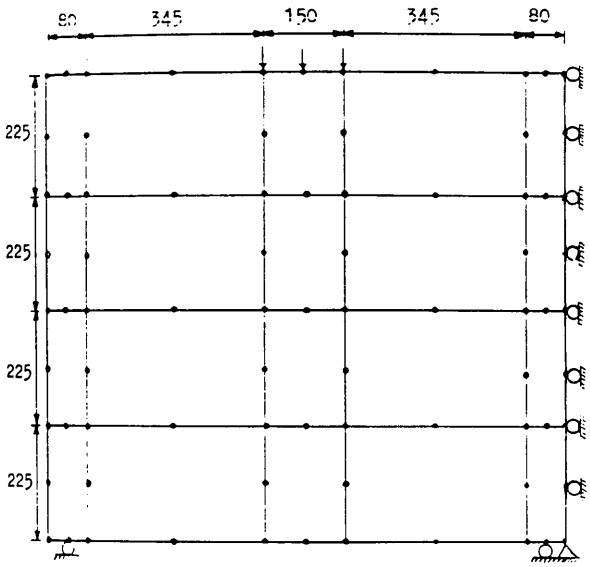

CASE II

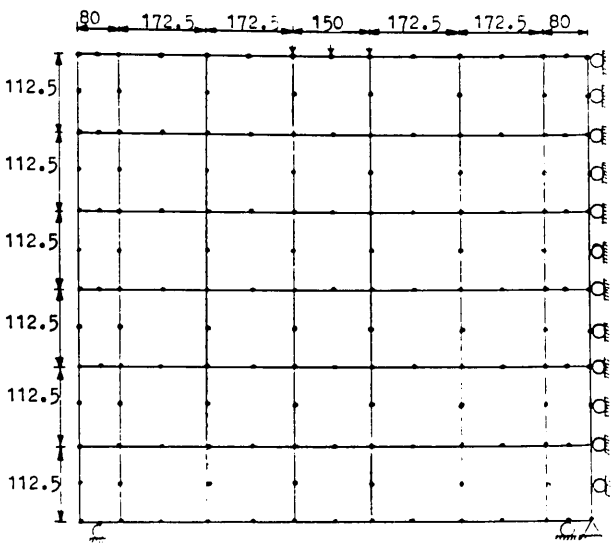

CASE IV

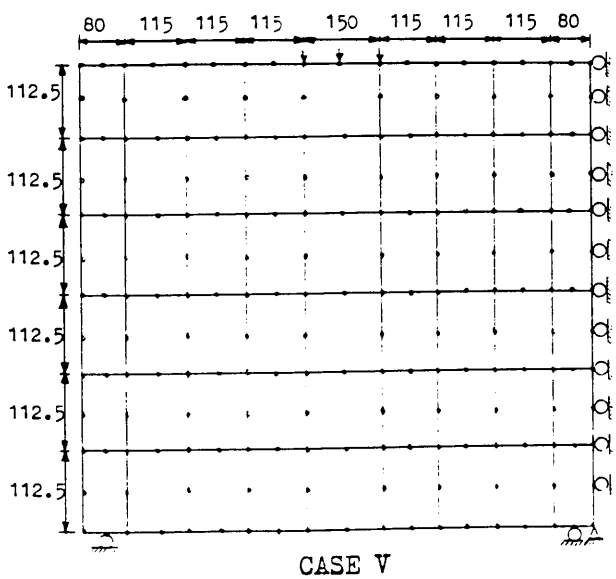

CASE V

Figure(8.1) Different finite element meshes examined for mesh convergence study

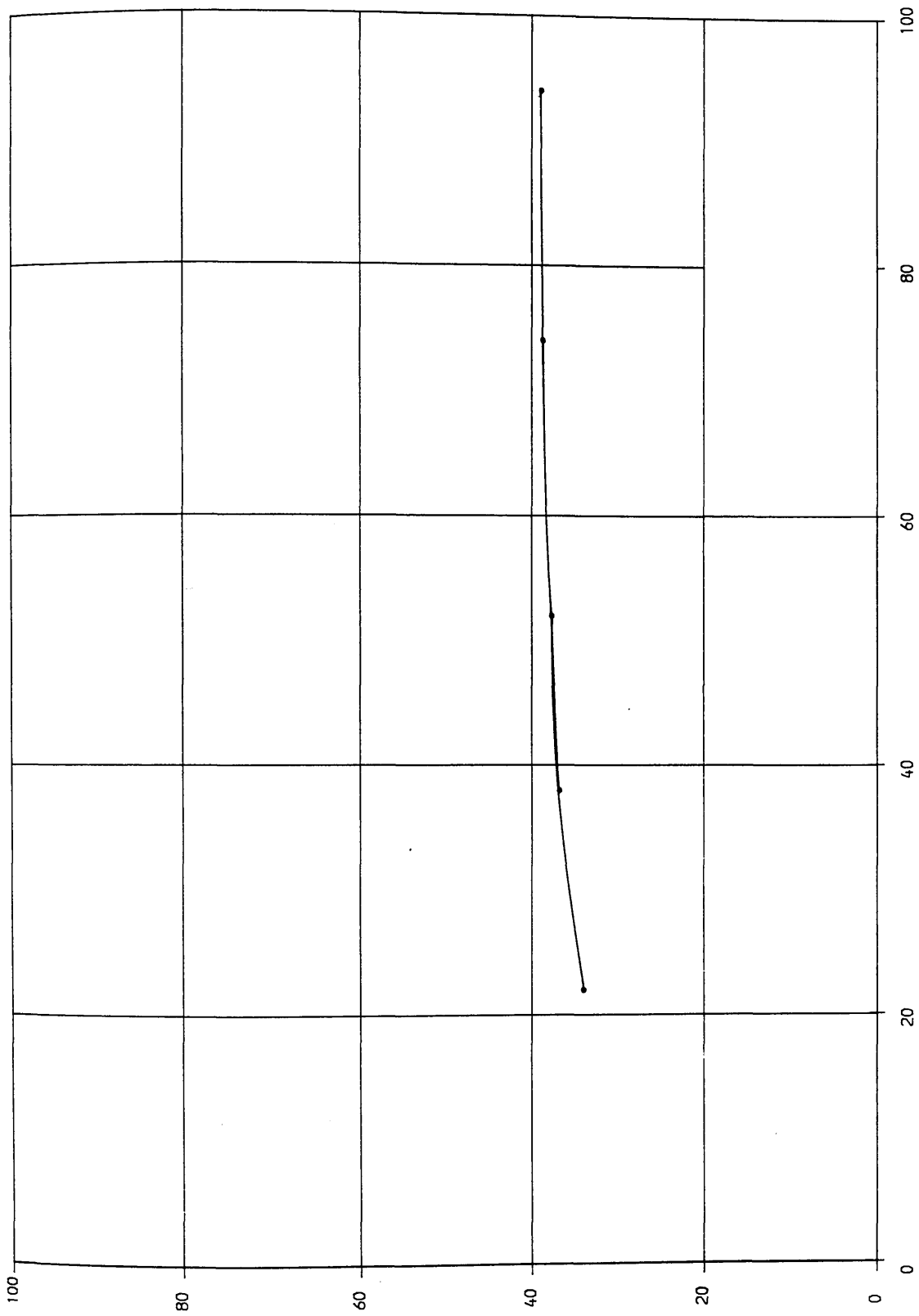

FIG (8.2) Mesh convergence study for specimen TRGRAS1

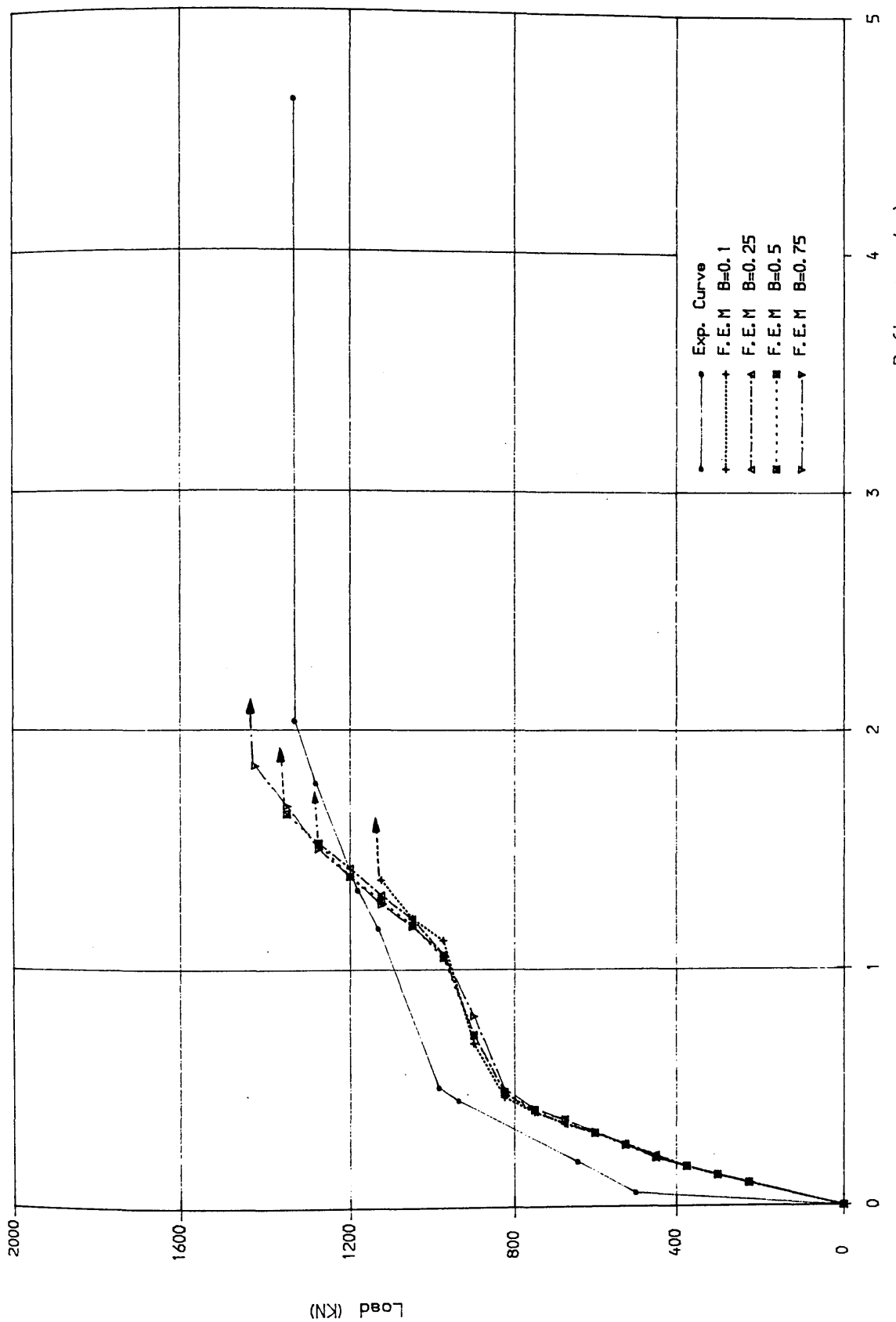

FIG(8.3) Load deflection curve for girder TRGRAS1 using different shear retention factor models

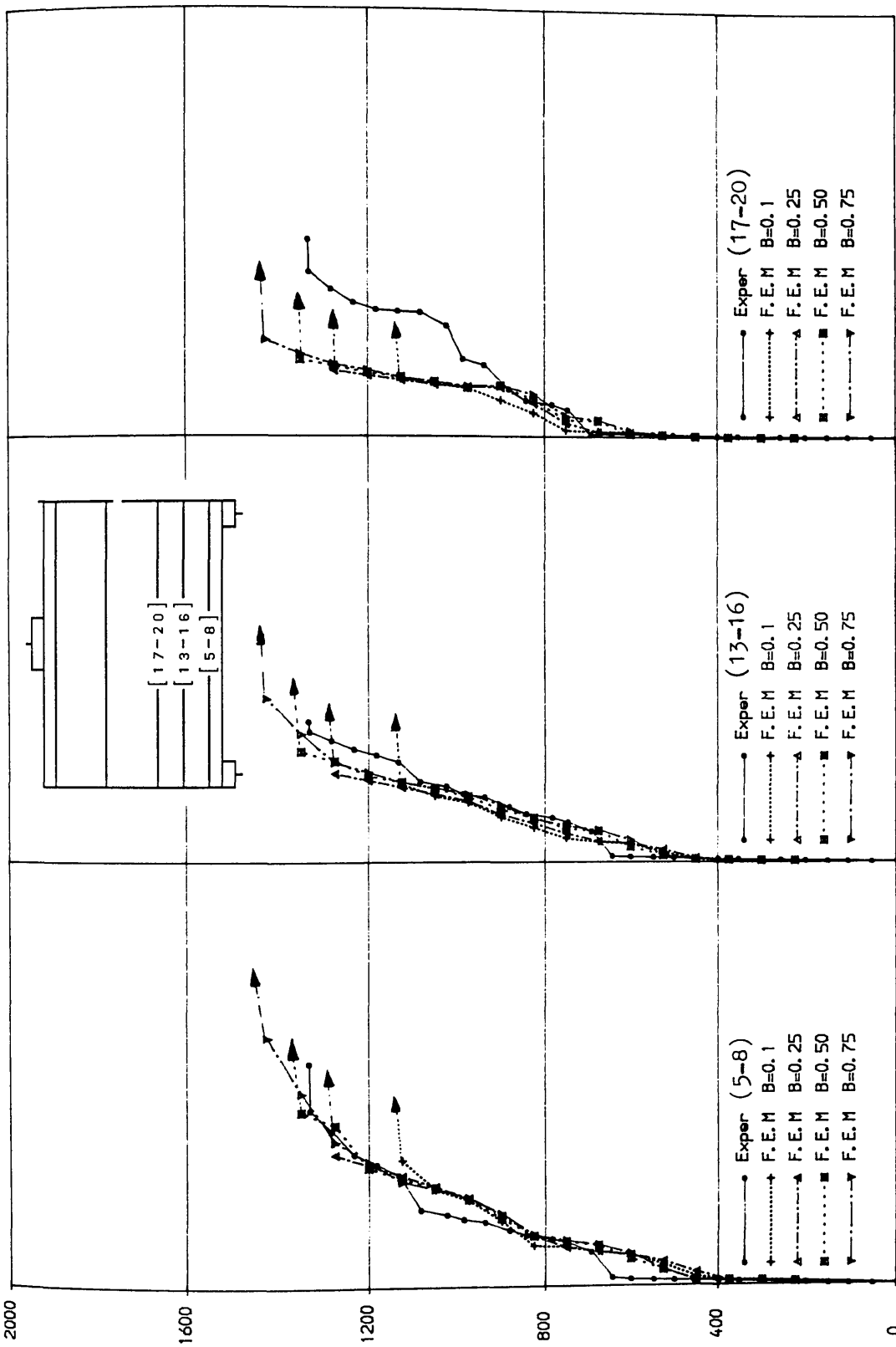

FIG (8.4) Comparison of longitudinal steel strains using different shear retention factor for girder TRGRAS1

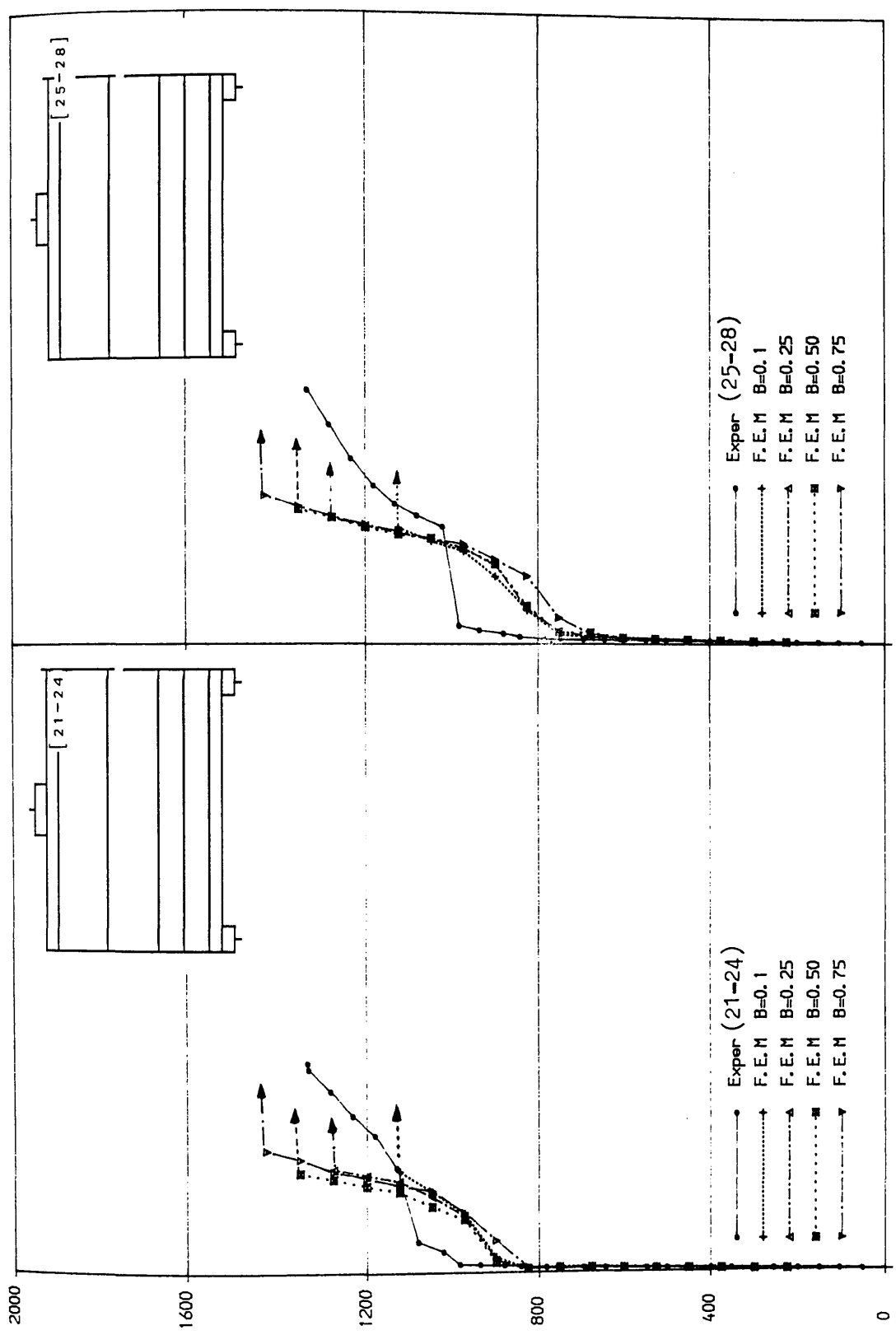

FIG (8.4) Continued

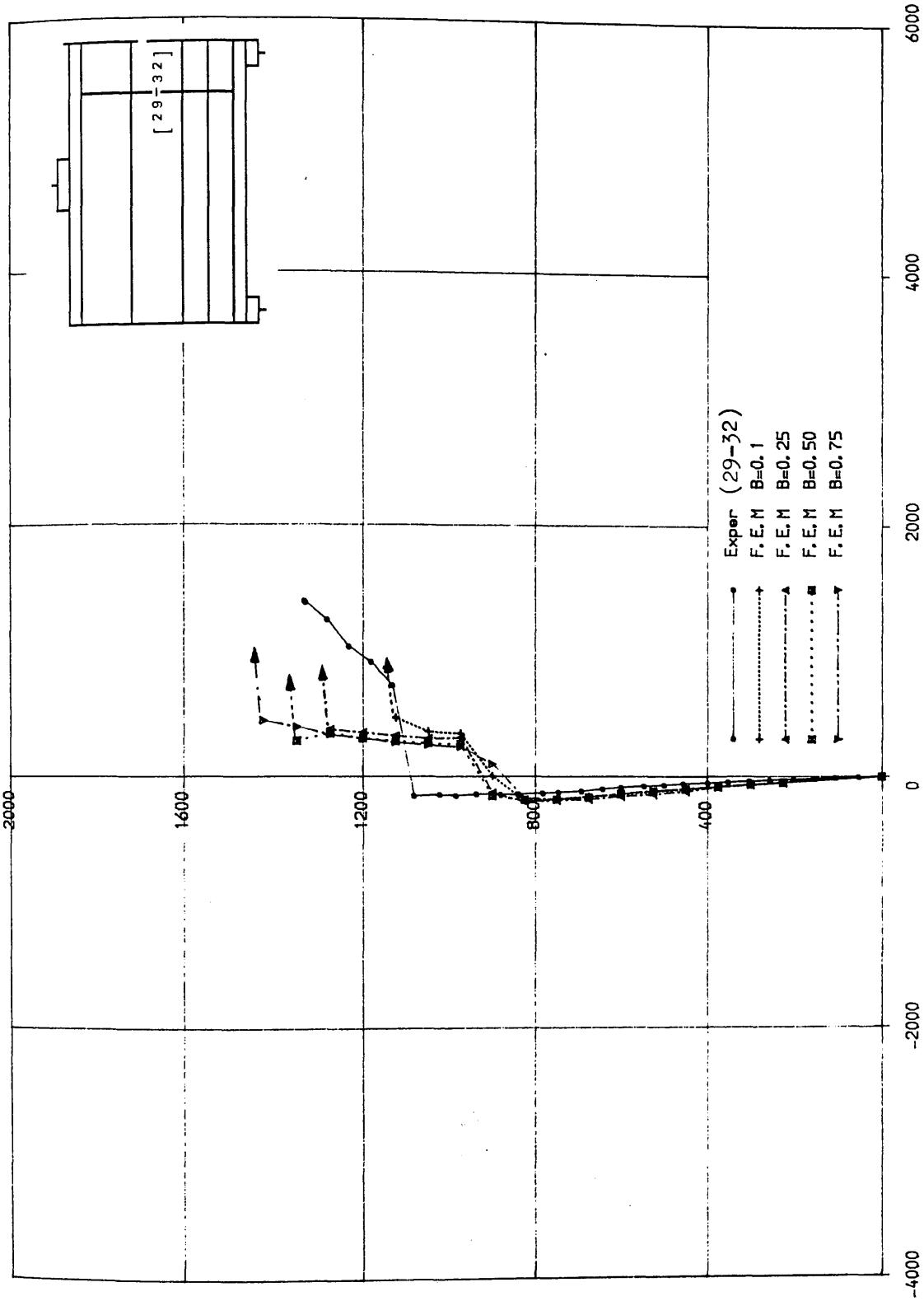

FIG(8.5) Comparison of stirrup strain in interior shear span using different shear retention factor models for girder TRGRAS1

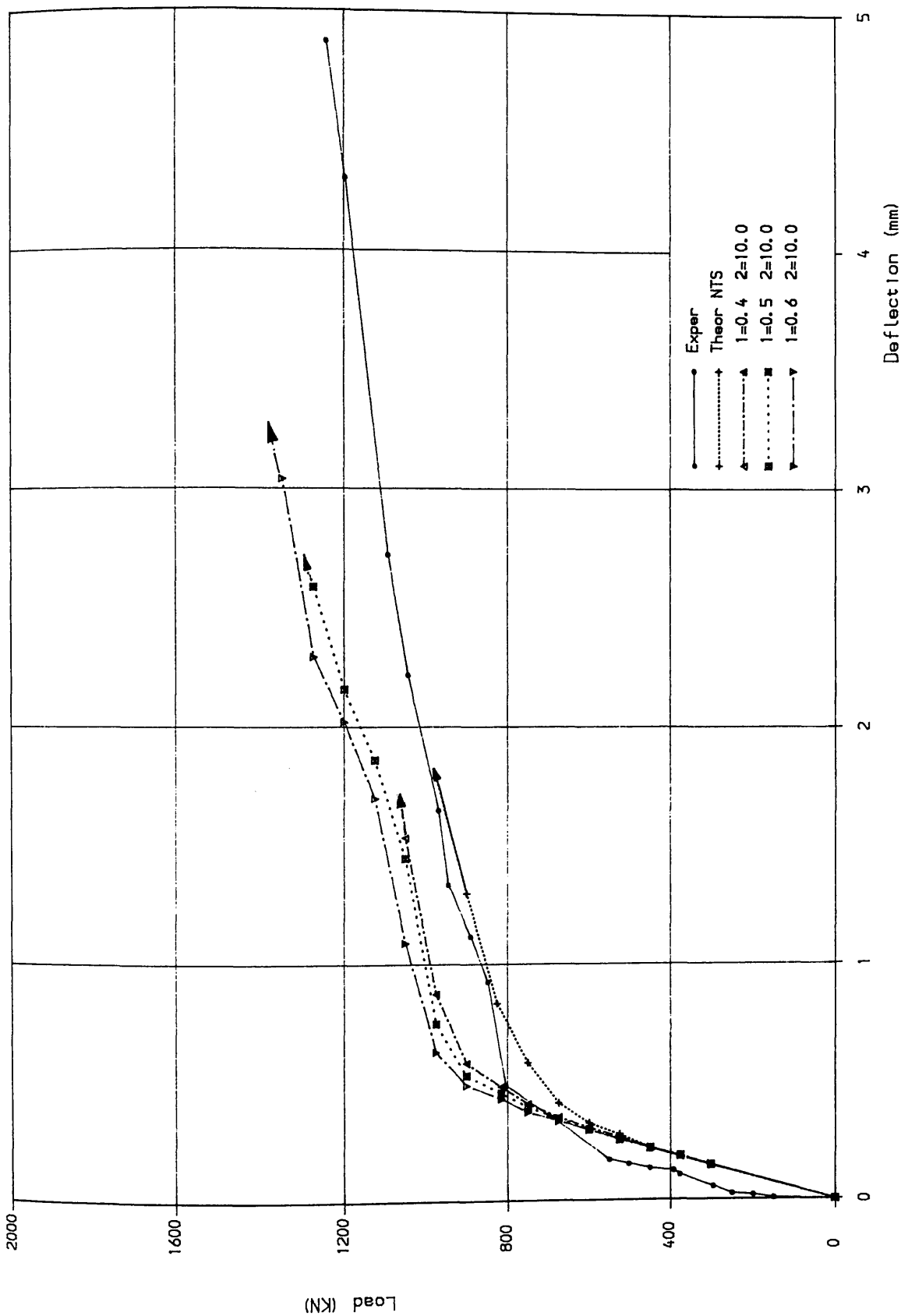

FIG(8.6) Load deflection curve for girder TRGRA55 using different tension stiffening models

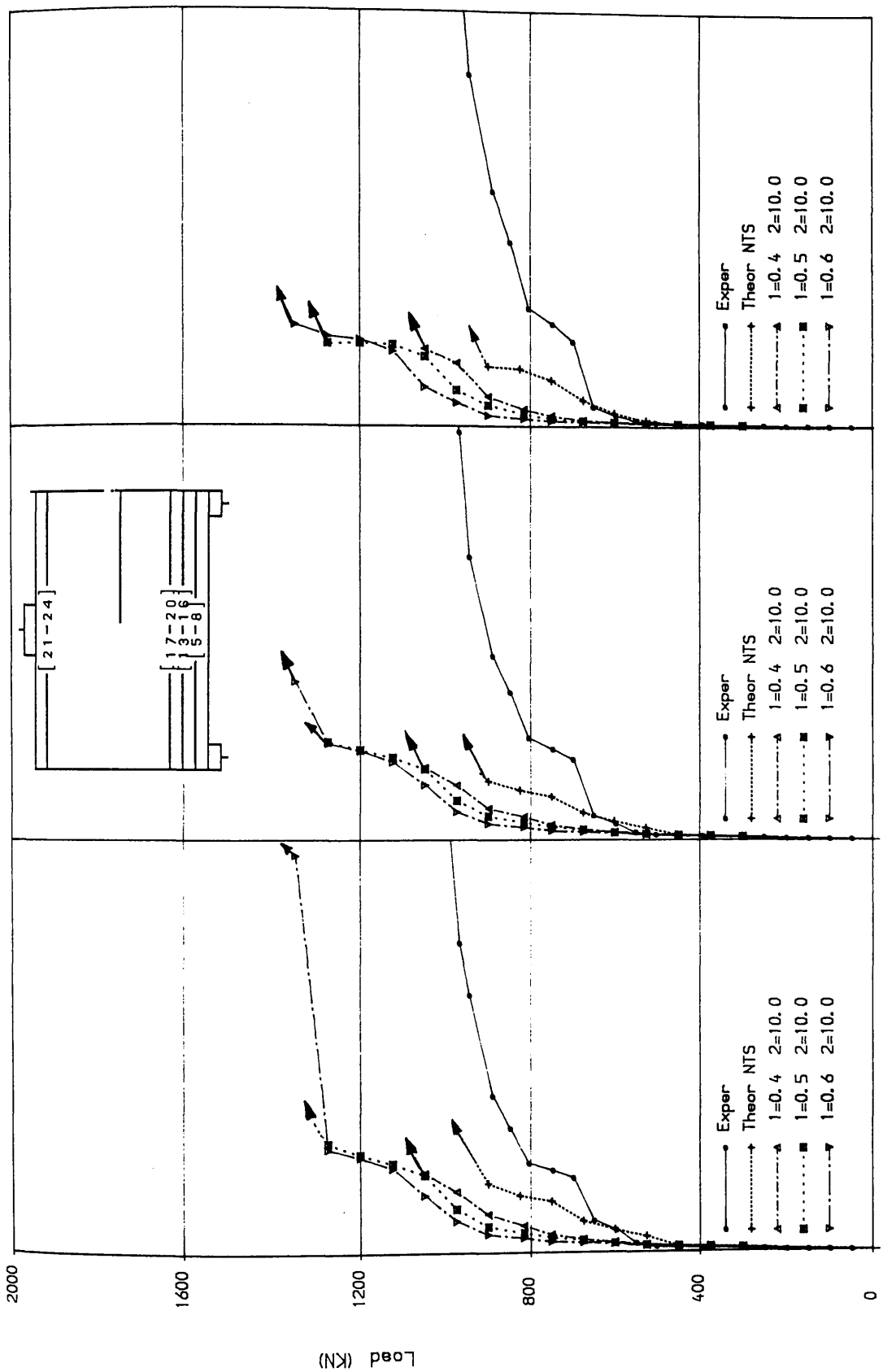

FIG(8.7) Comparison of longitudinal steel strains using different tension stiffening models for girder TRGRA55

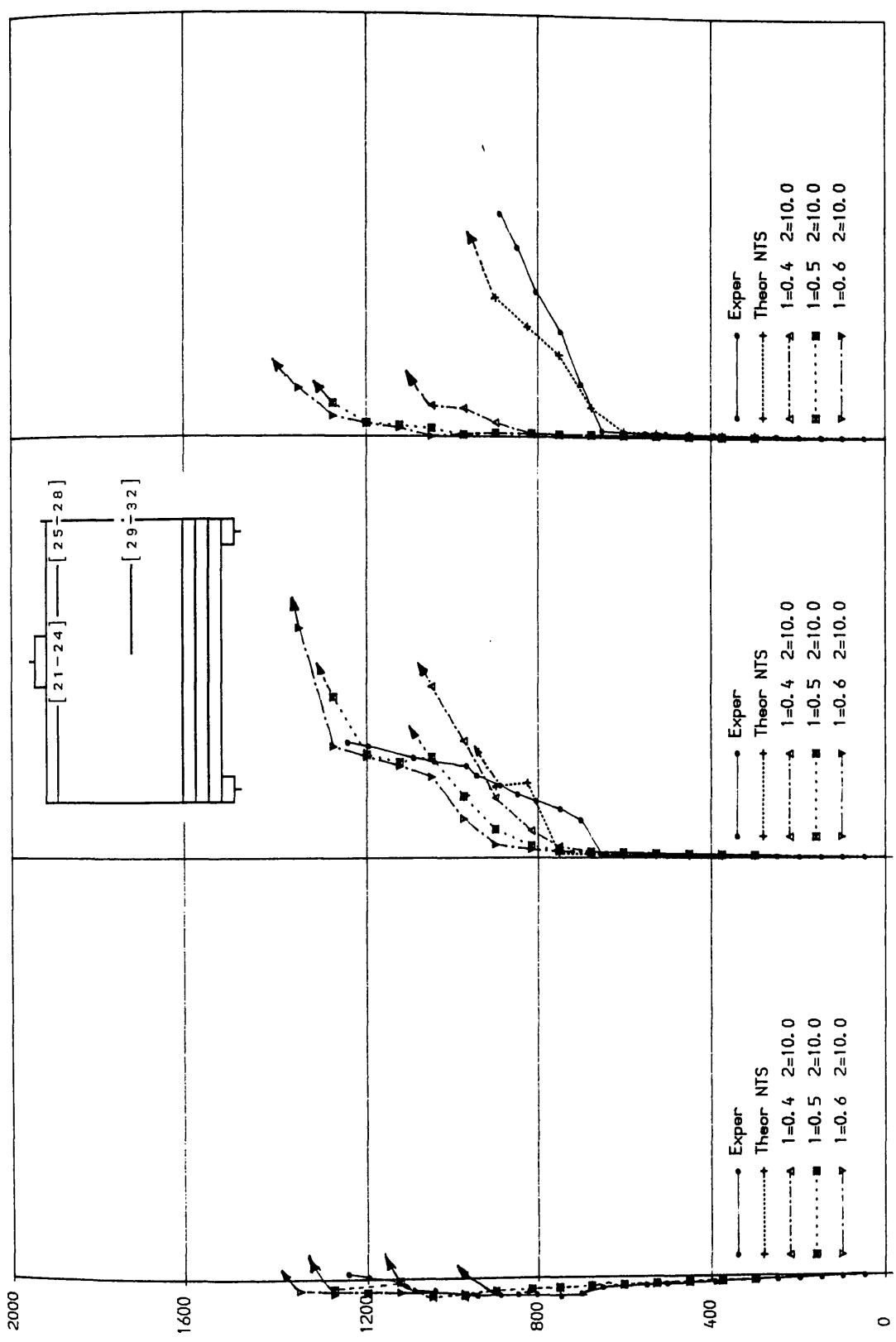

FIG (8.7) Continued

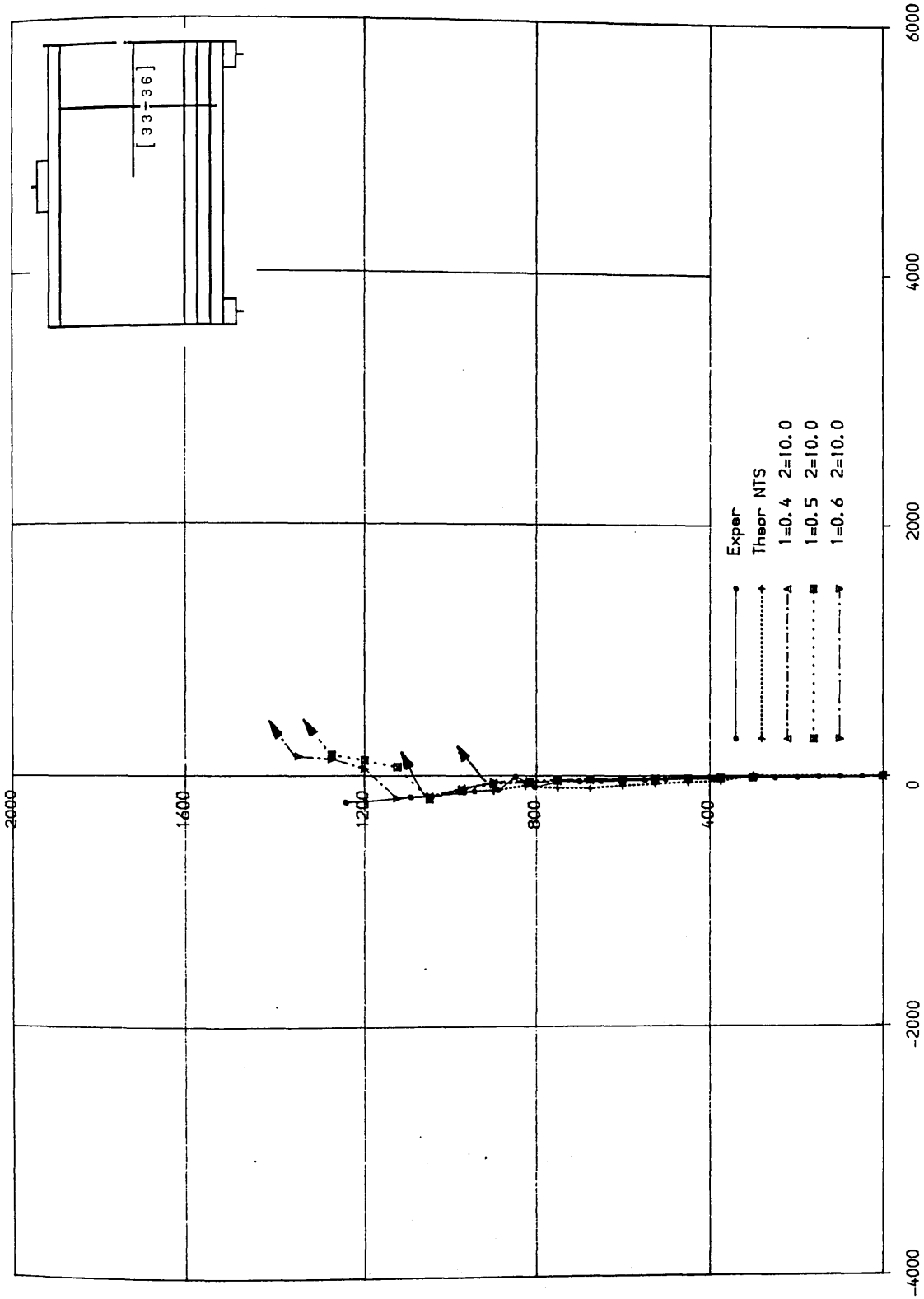

FIG (8.8) Comparison of stirrup strain in interior shear span using different tension stiffening models for girder TRGRASS

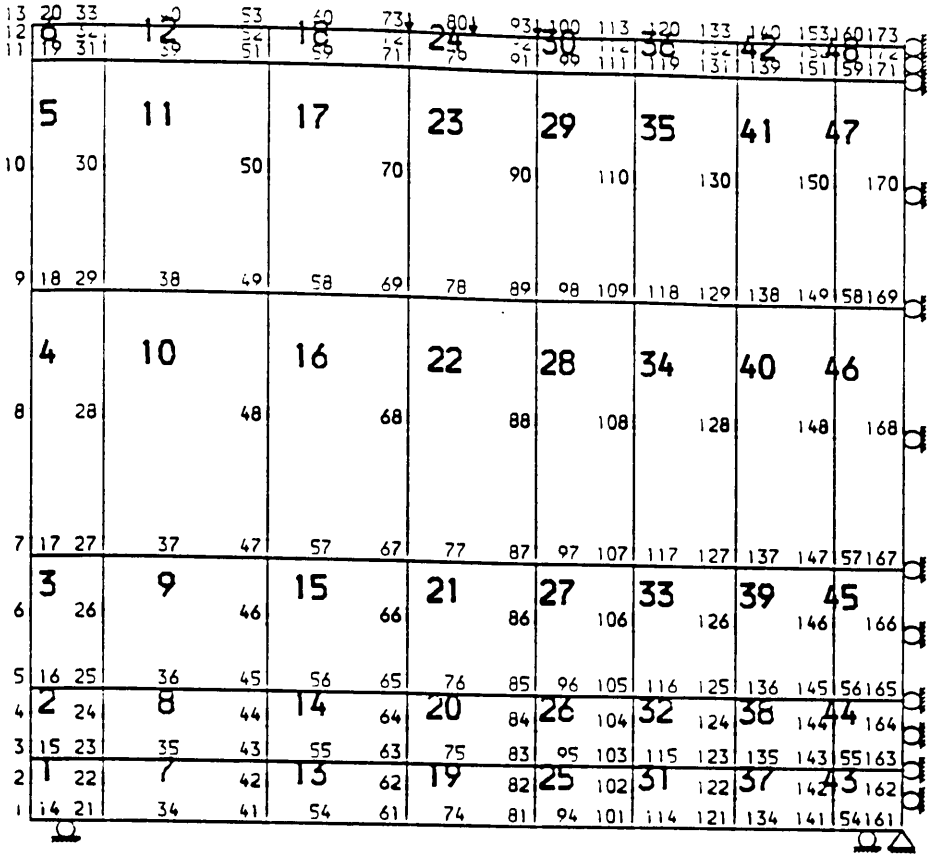

Figure(8.9) Finite element analysis mesh for girder TRGRAS1

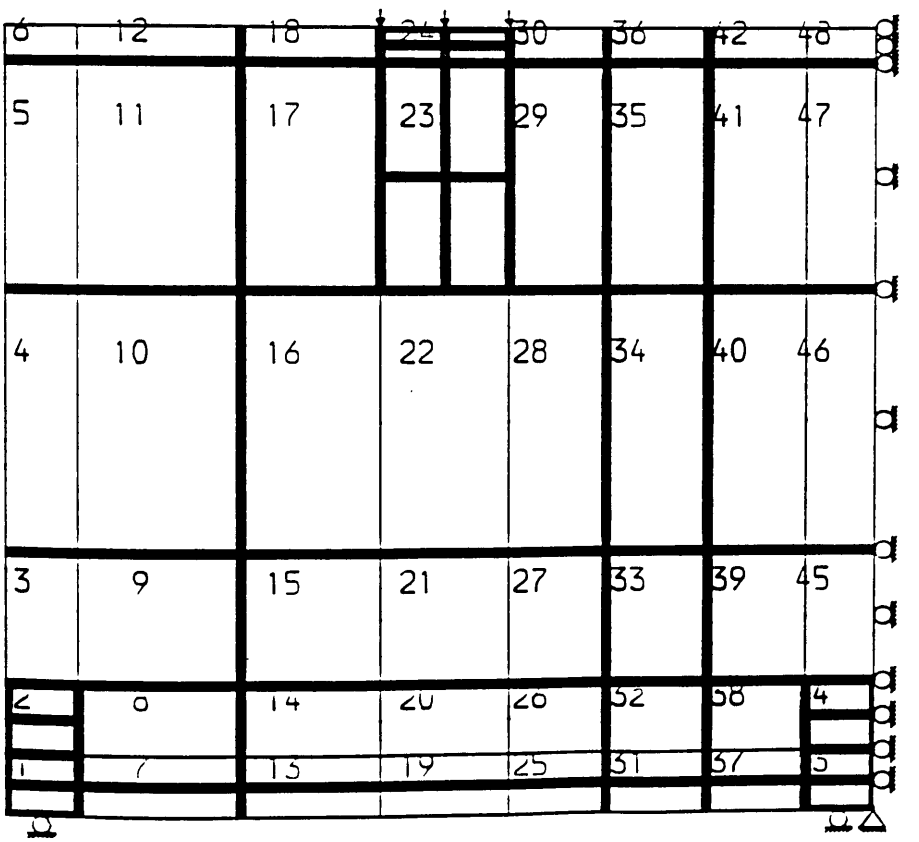

Figure(8.10) Reinforcement detail in finite element analysis for girder TRGRAS1

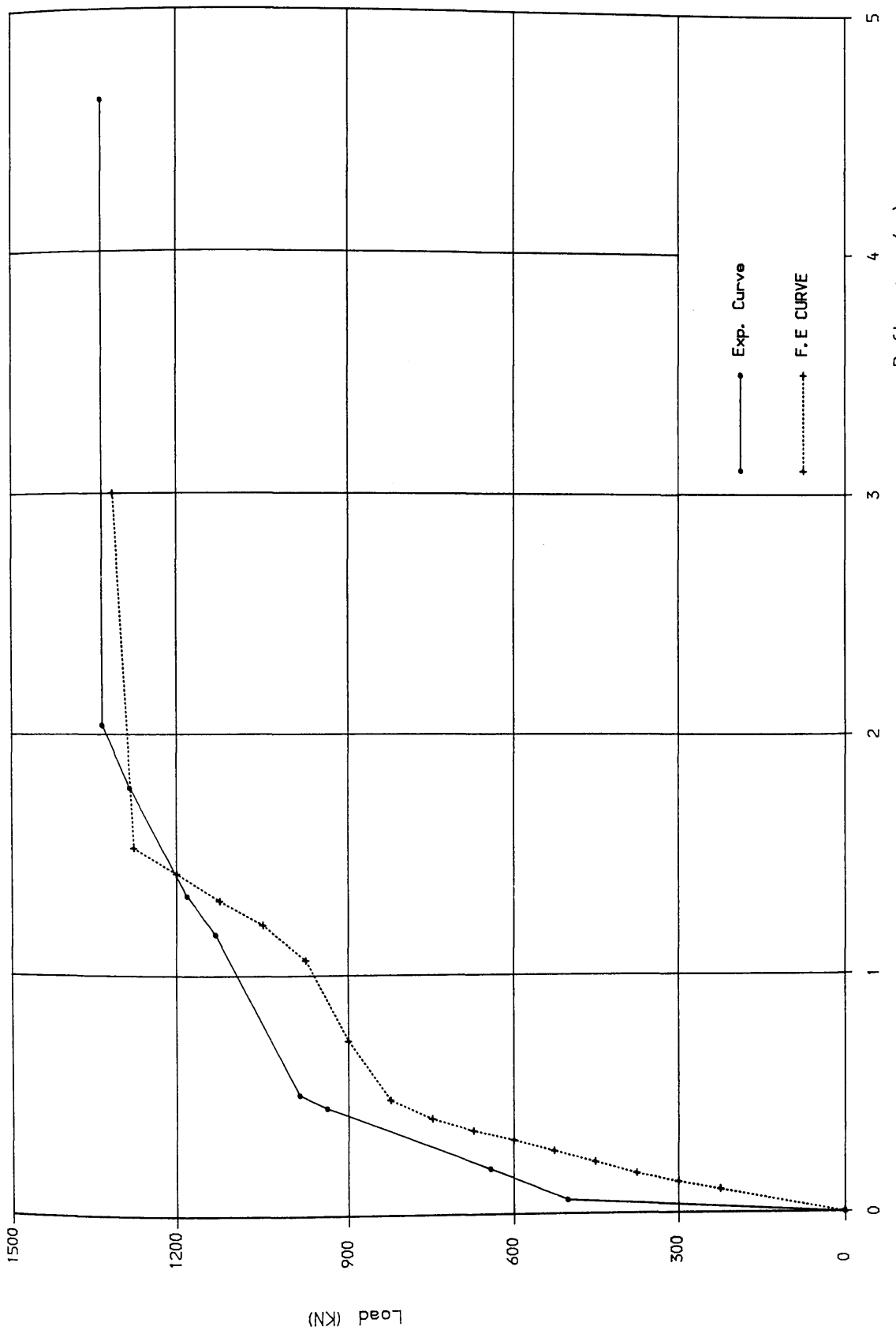

FIG(8.11) Load deflection curve for girder TRGRAS1

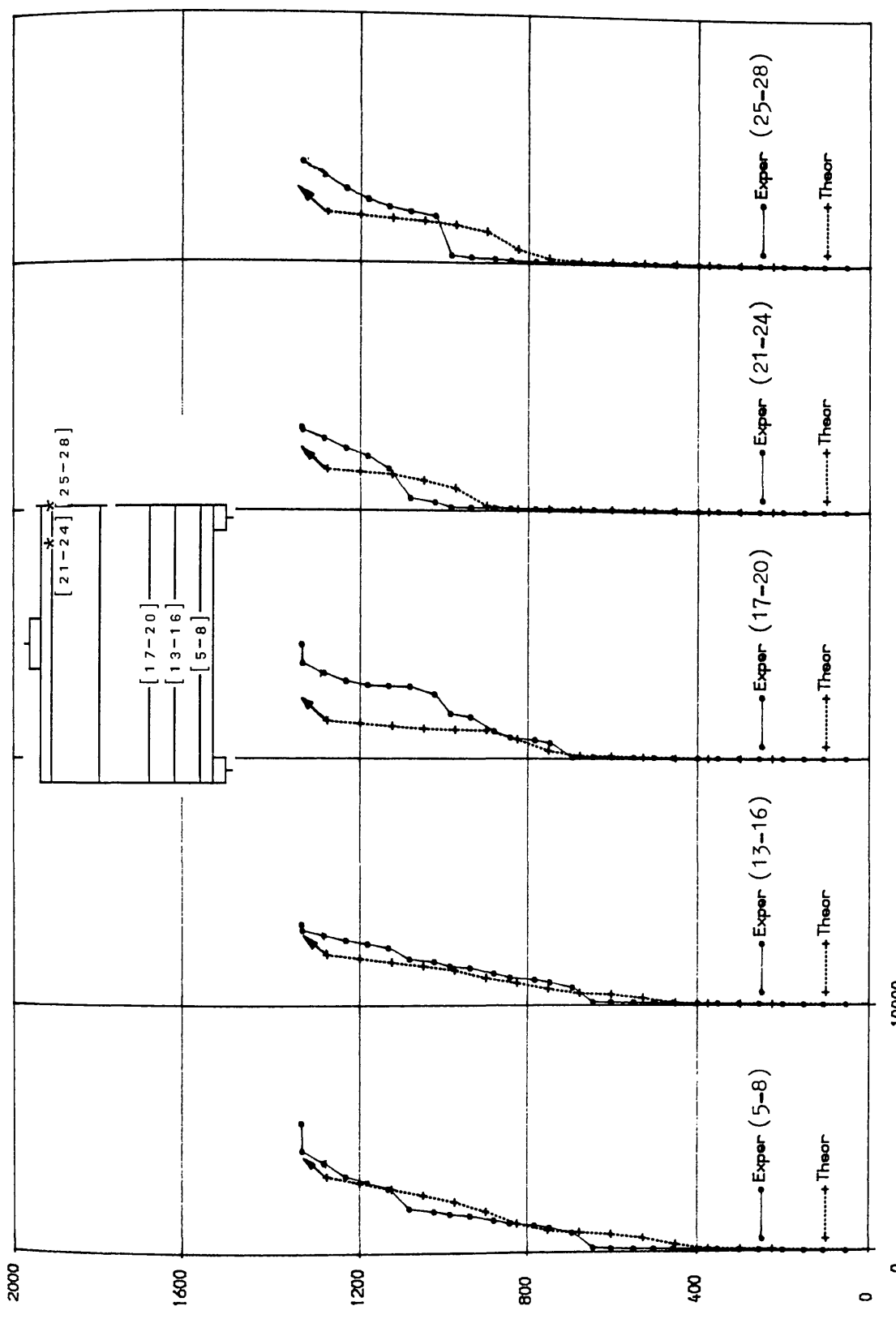

FIG(8.12) Comparison of longitudinal steel strains at centre of girder span for girder TRGRAS1

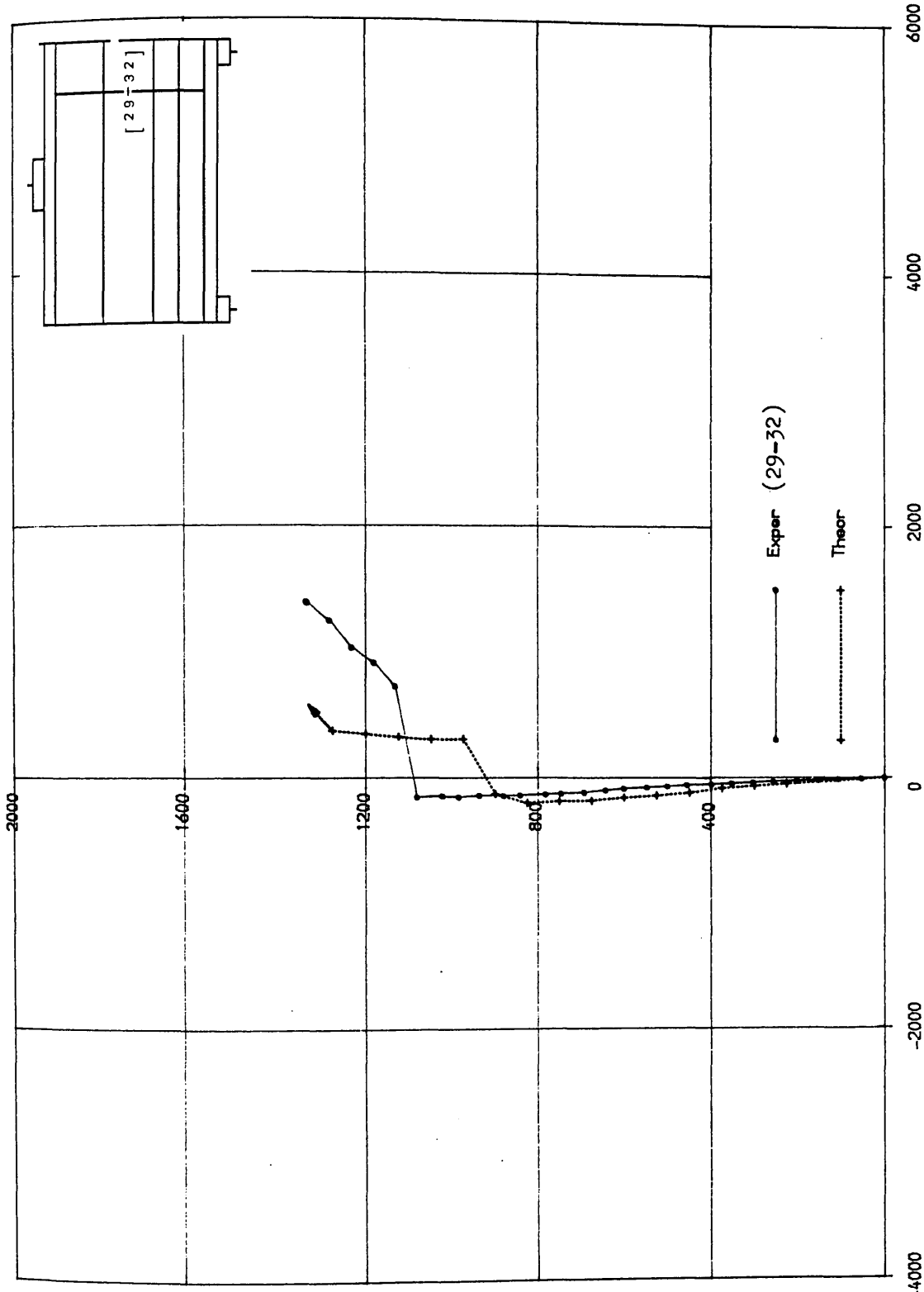

FIG (8.13) Comparison of stirrup strain in interior shear span for girder TRGRAS1

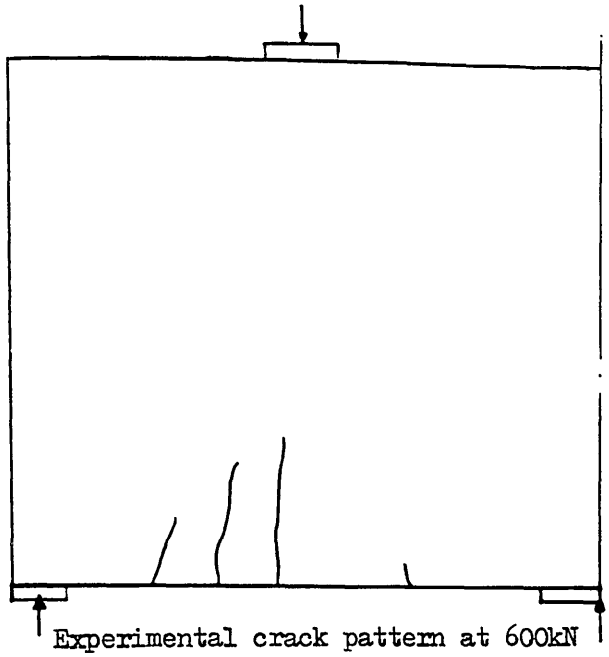

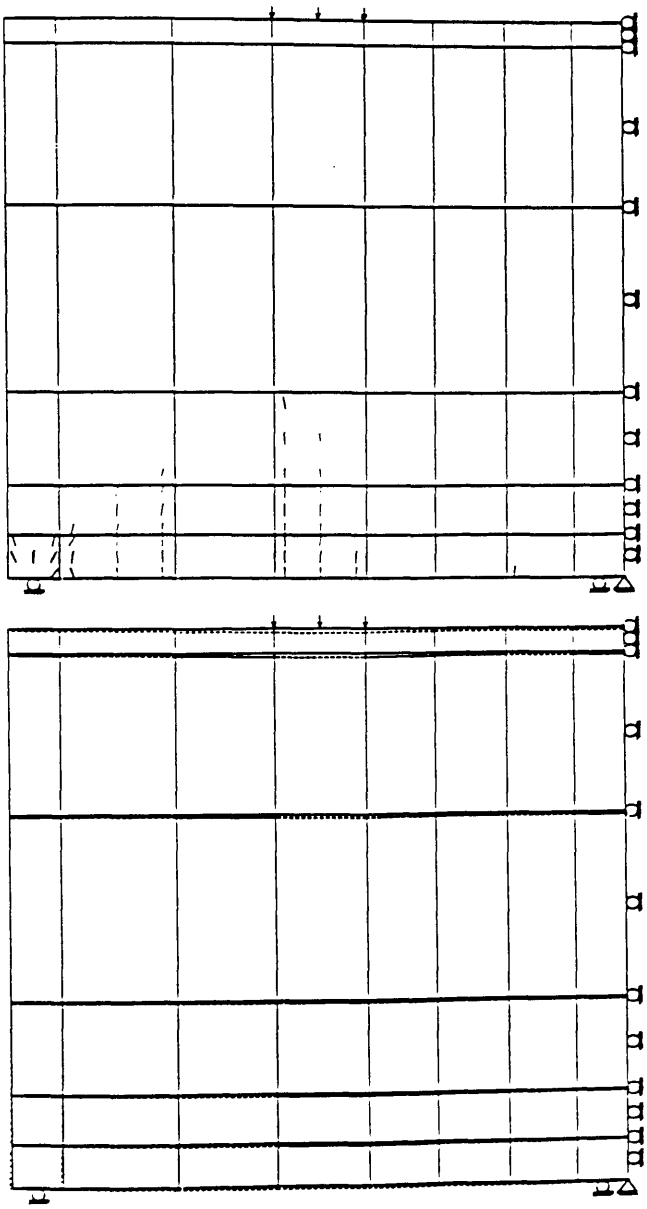

Figure(8.14) Predicted crack pattern and deformed shape at 600kN (TRGRAS1)

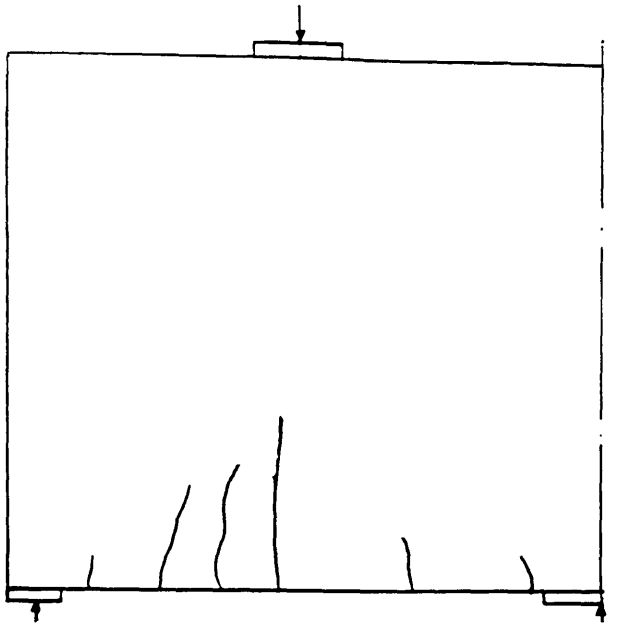

Experimental crack pattern at 750kN

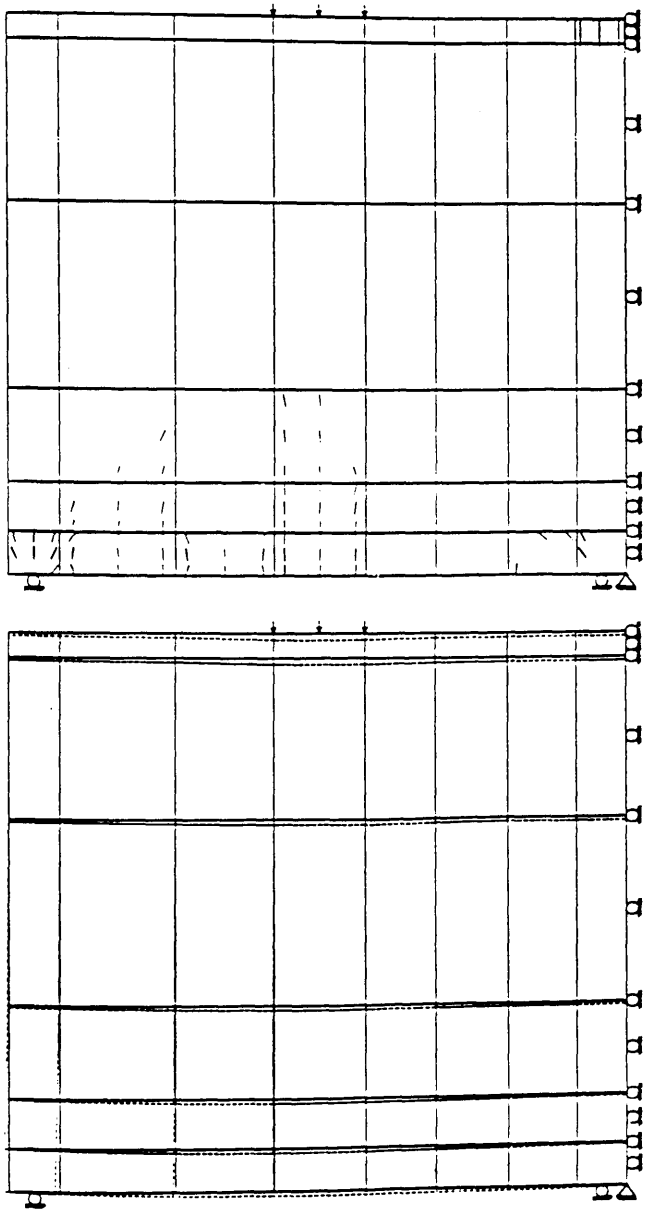

Figure(8.15) Predicted crack pattern and deformed mesh at load 750kN (TRGRAS1)

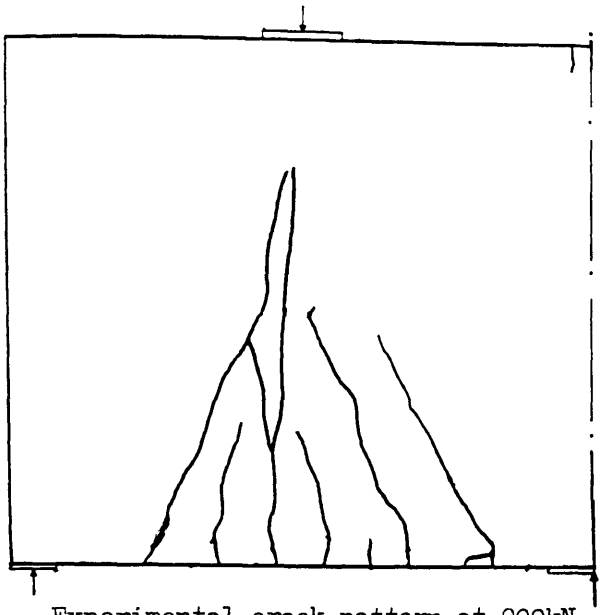

Experimental crack pattern at 900kN

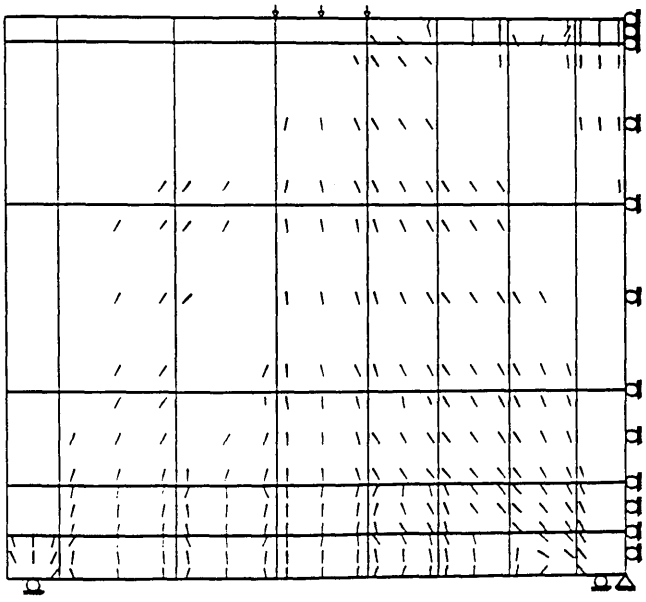

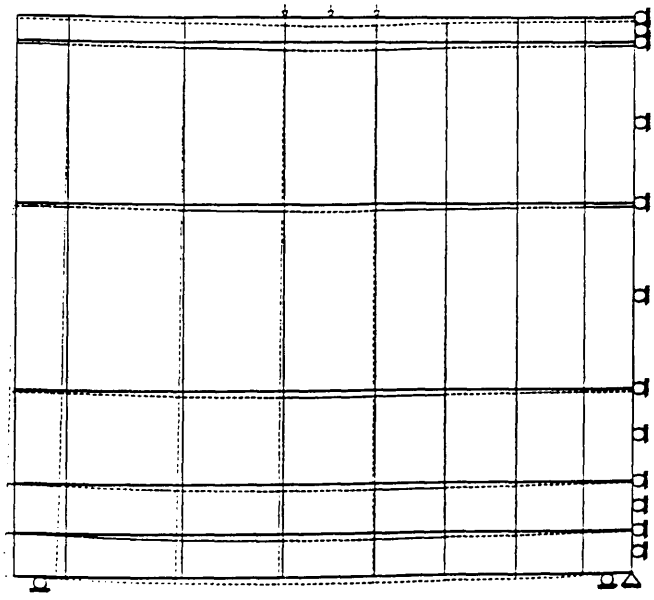

Figure(8.16) Predicted crack pattern and deformed mesh at load 900kN (TRGRAS1)

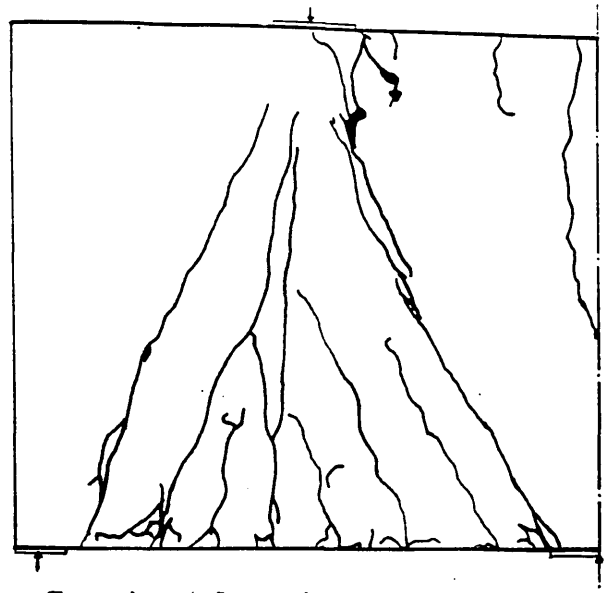

Experimental crack pattern at 1333kN

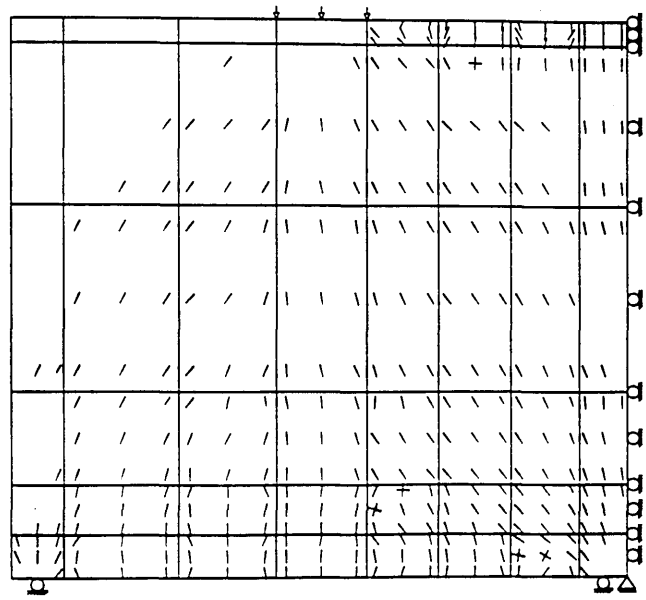

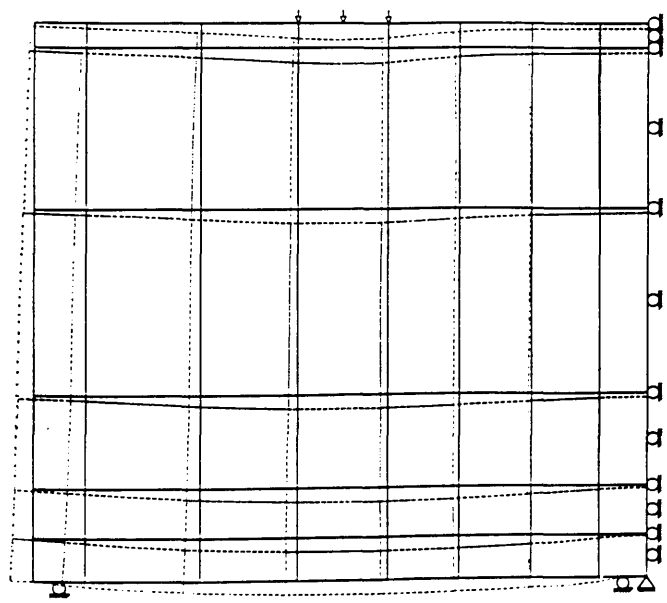

Figure(8.17) Predicted crack pattern and deformed mesh at load 1275kN (TRGRAS1)

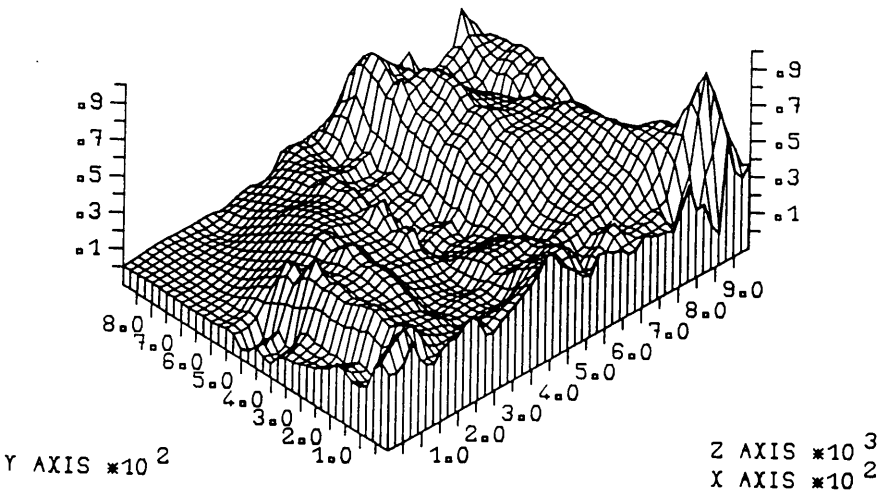

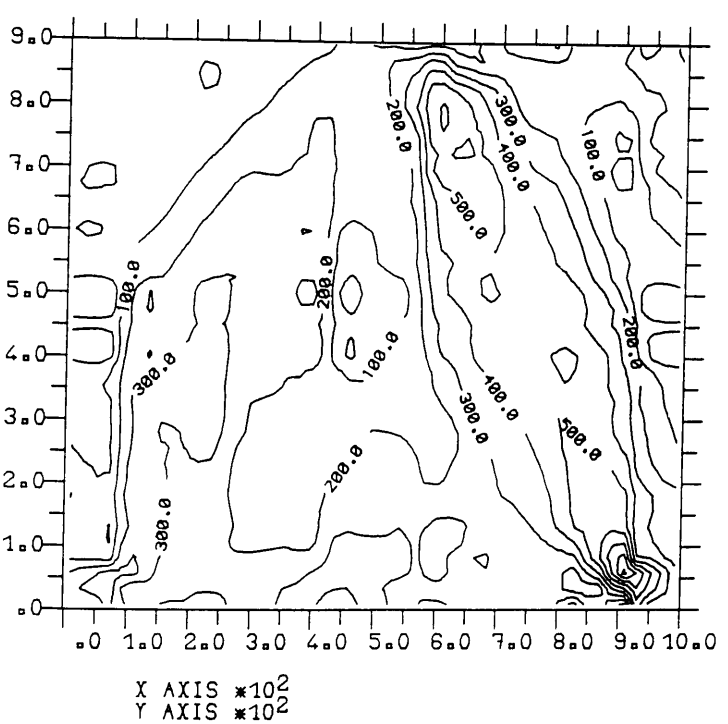

Figure(8.19) Predicted maximum shear strain*10^{-5} at ٣٥٢ kN (TRGRAS1)

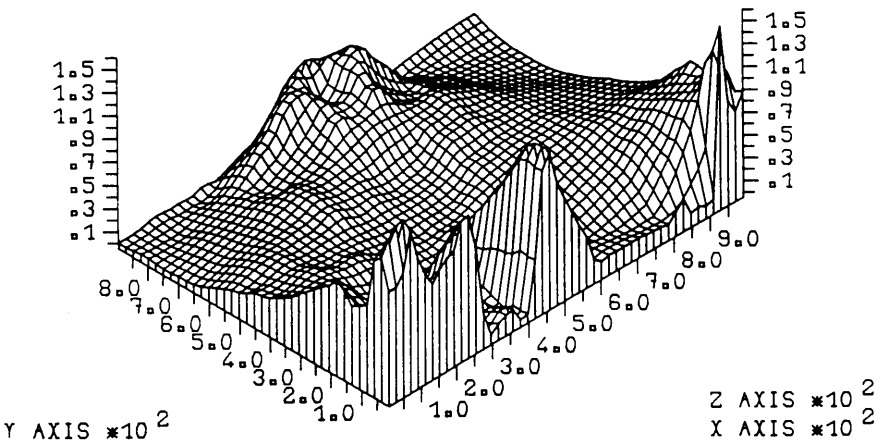

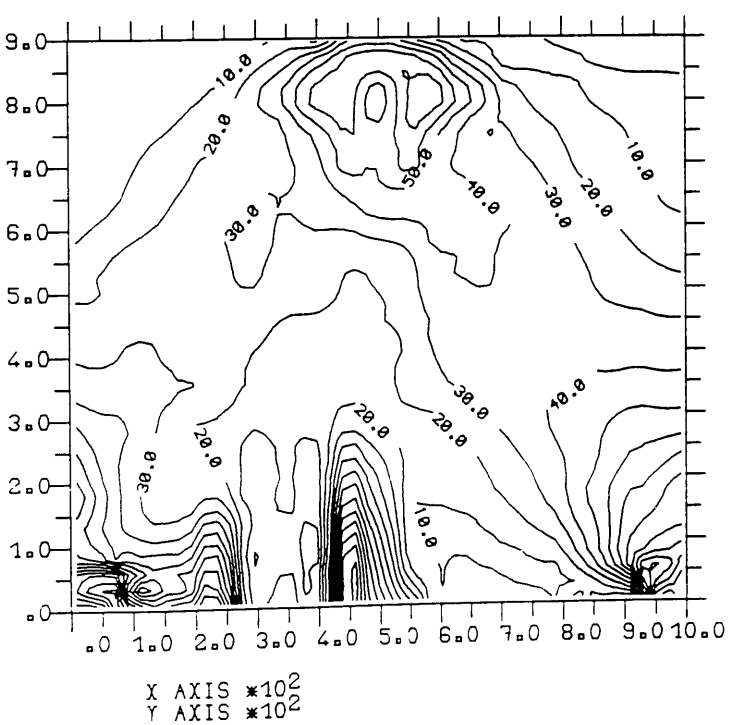

Figure(8.18) Predicted maximum shear strain*10^{-5} at 600kN (TRGRAS1)

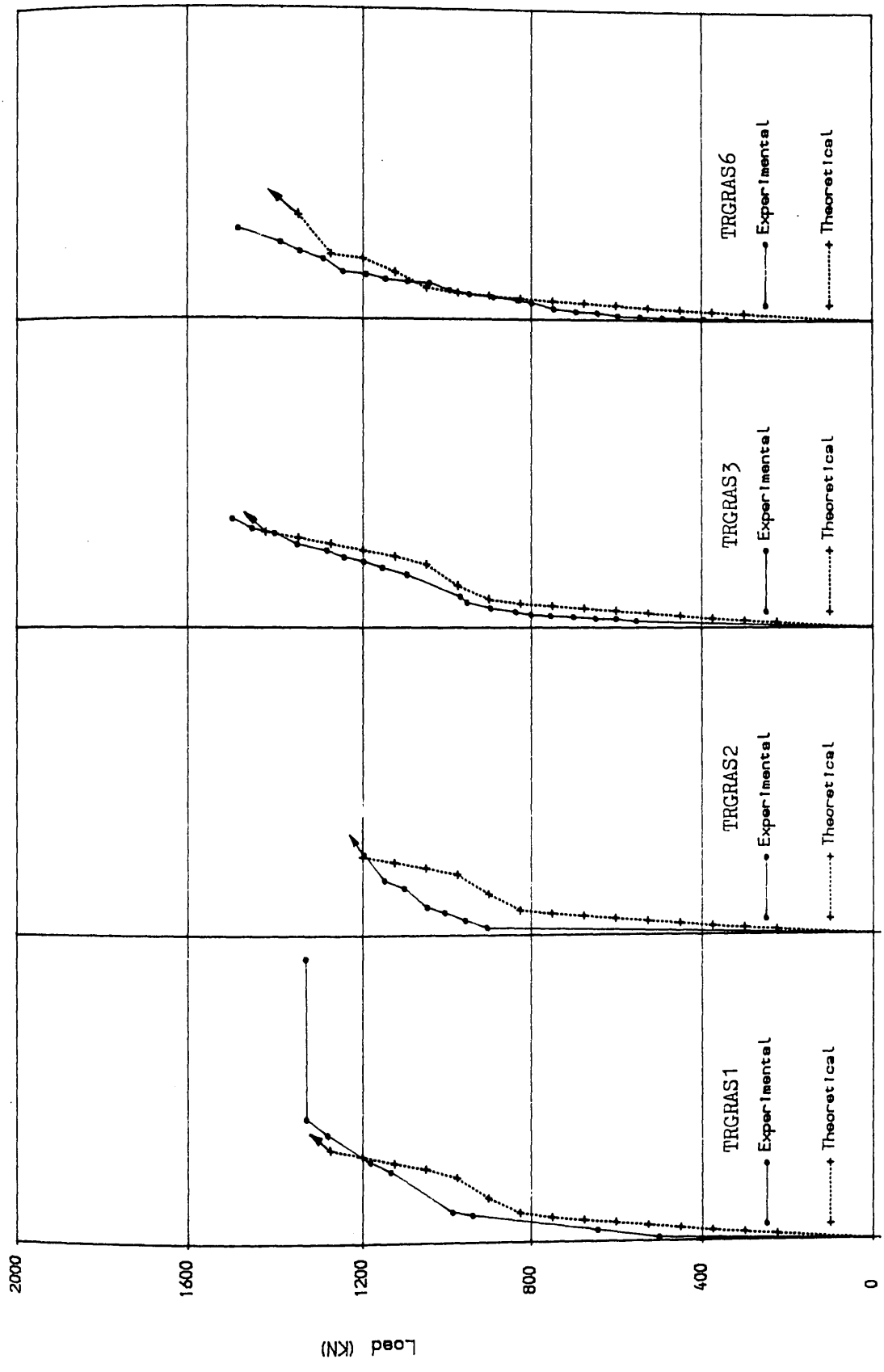

FIG (8.20) Load deflection curves for girders TRGRAS1 TRGRAS2, TRGRAS3 and TRGRAS6

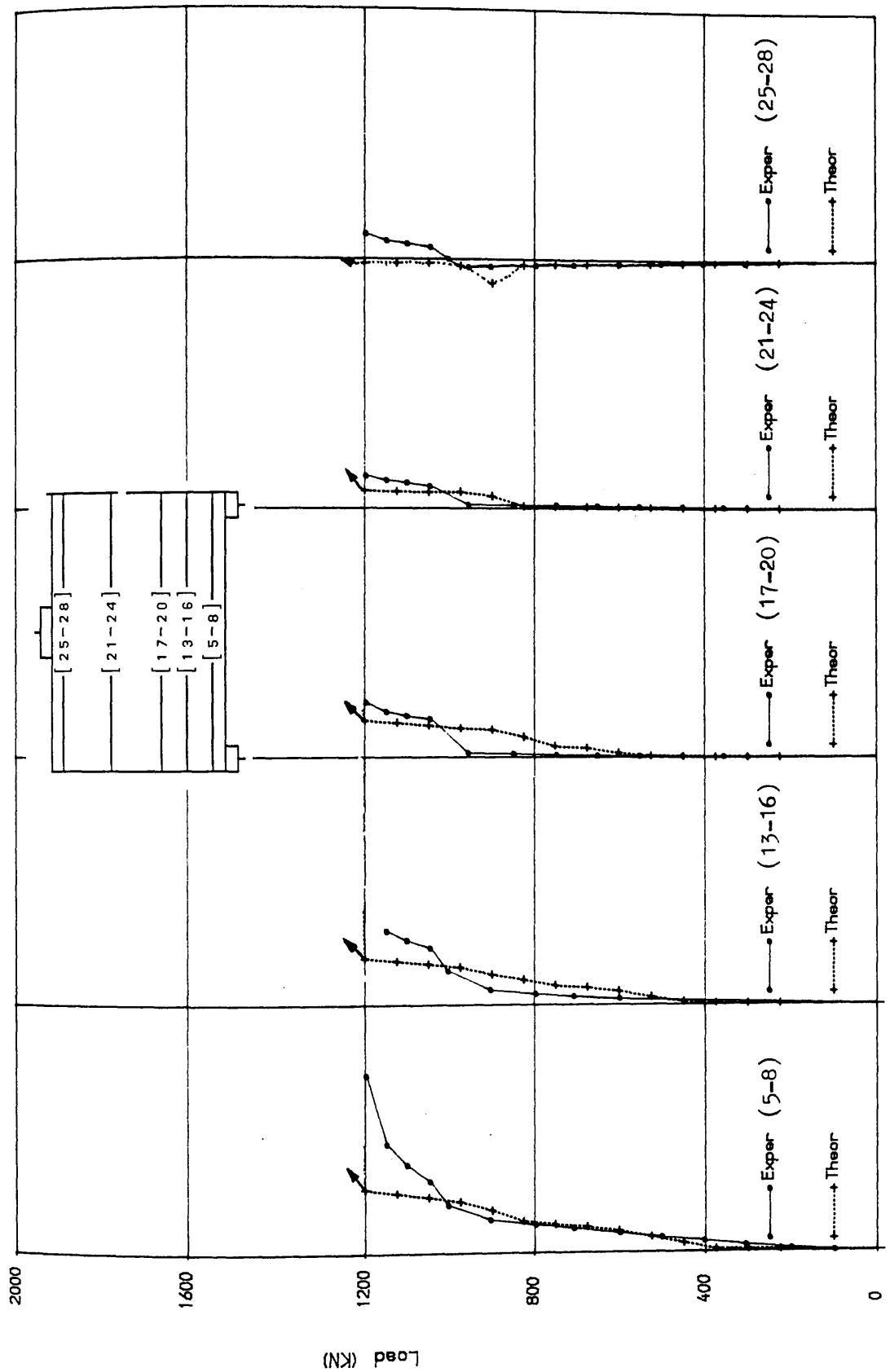

FIG (8.21) Comparison of longitudinal steel strains at centre of girder span for girder TRGRAS2

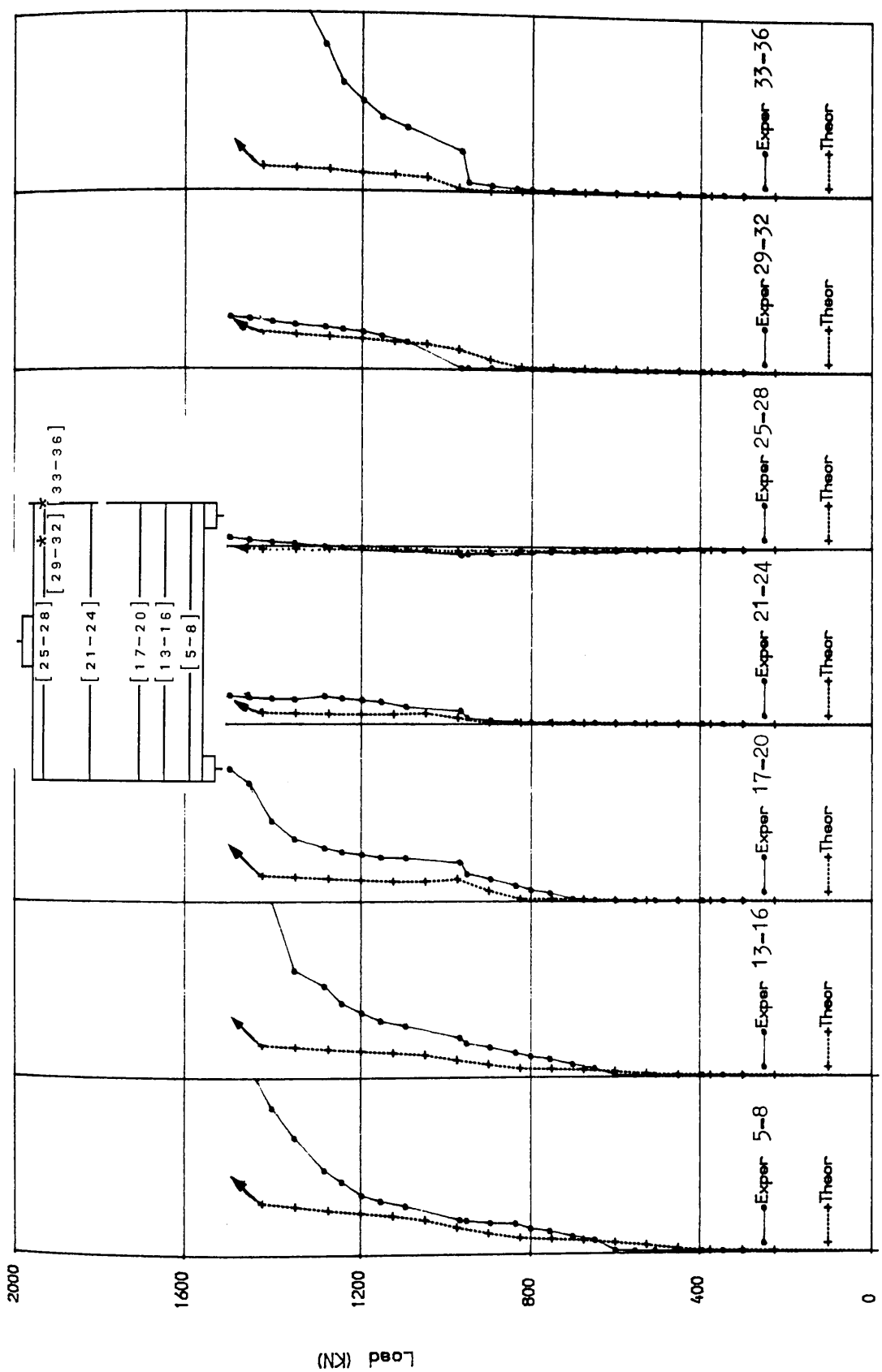

FIG (8.22) Comparison of longitudinal steel strains at centre of girder span for girder TRGRAS3

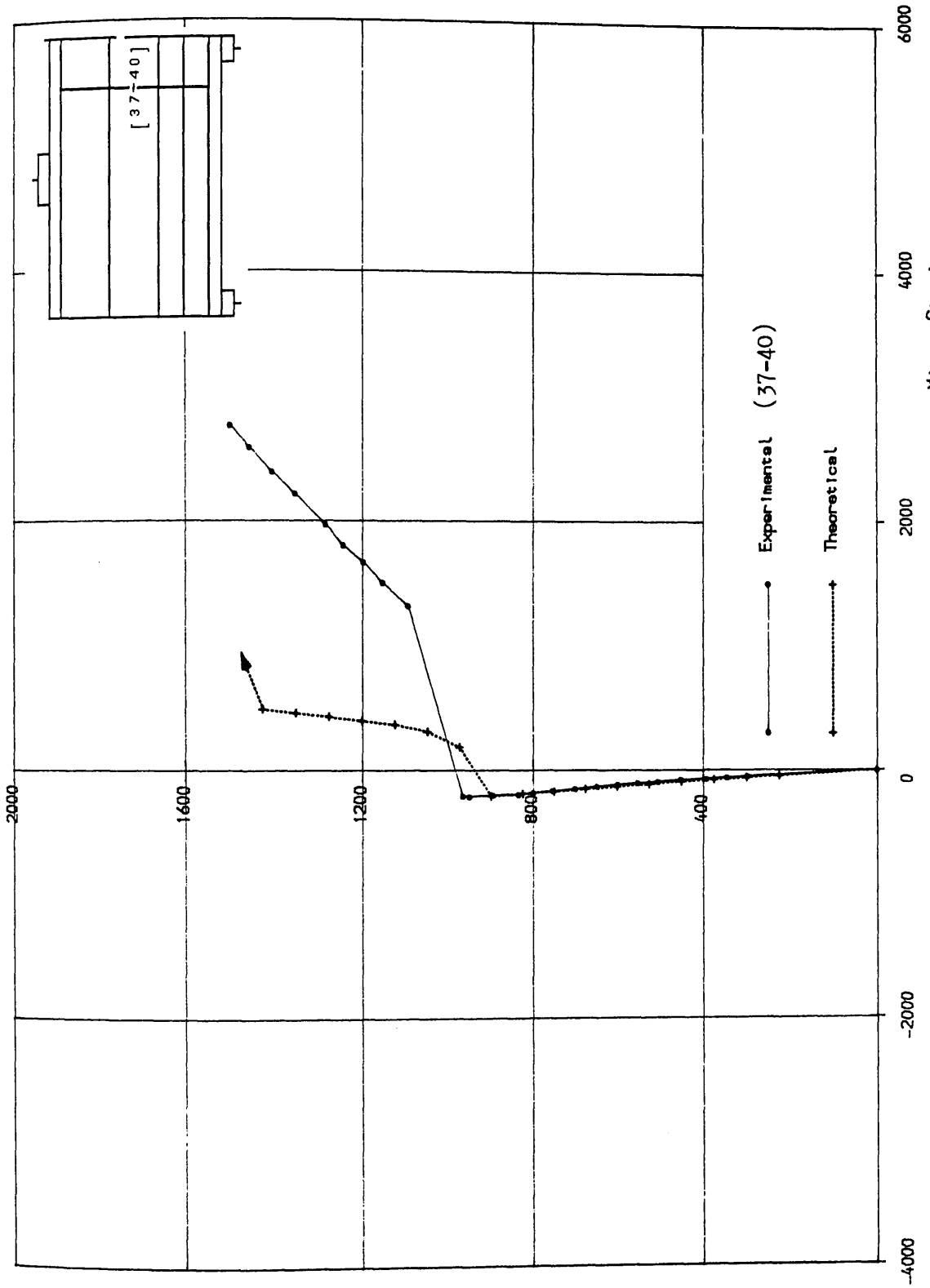

FIG (8.23) Comparison of stirrup strain in interior shear span for girder TRGRAS3

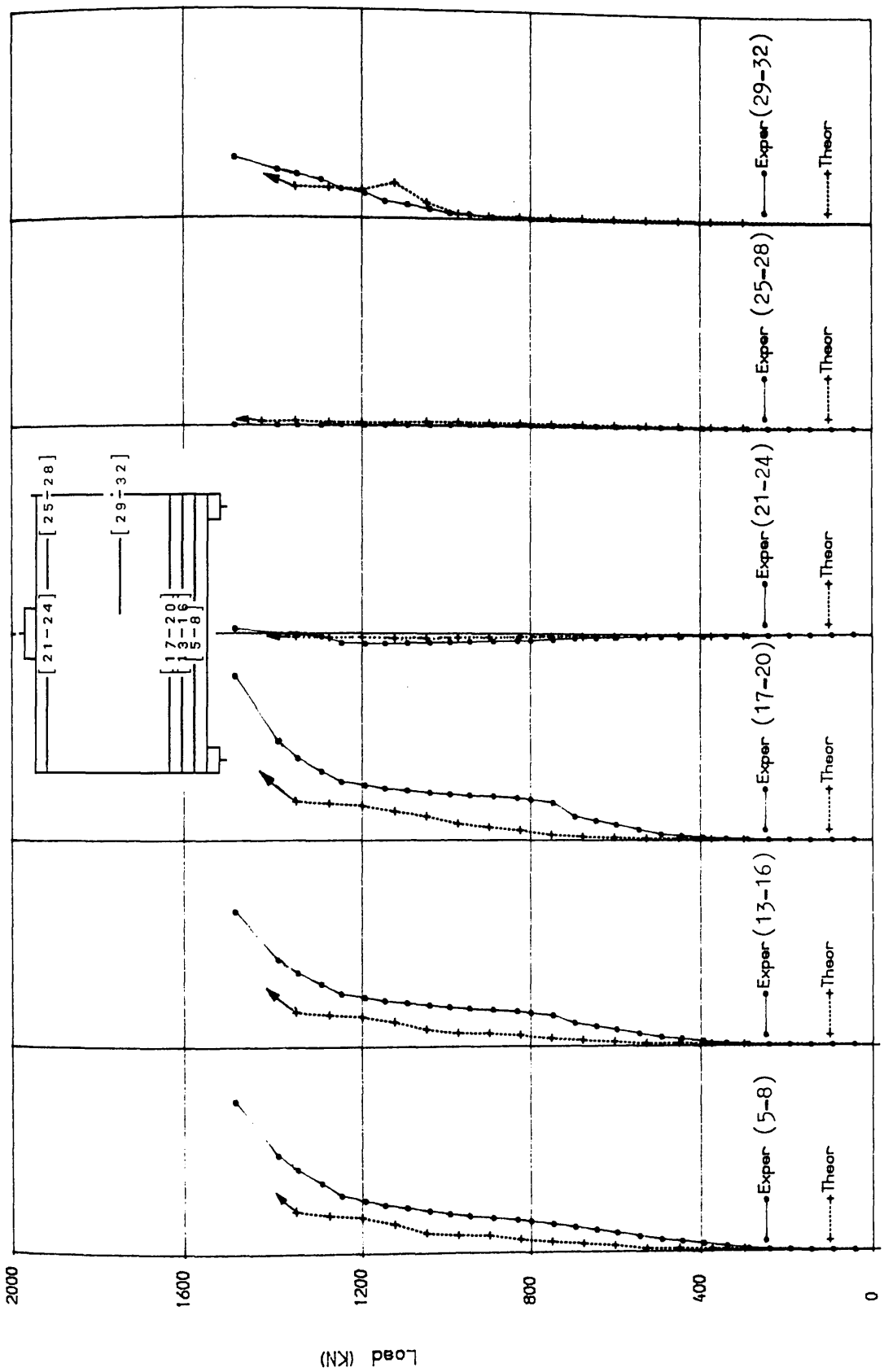

FIG (8.24) Comparison of longitudinal steel strains at centre of girder span for girder TRGRAS6

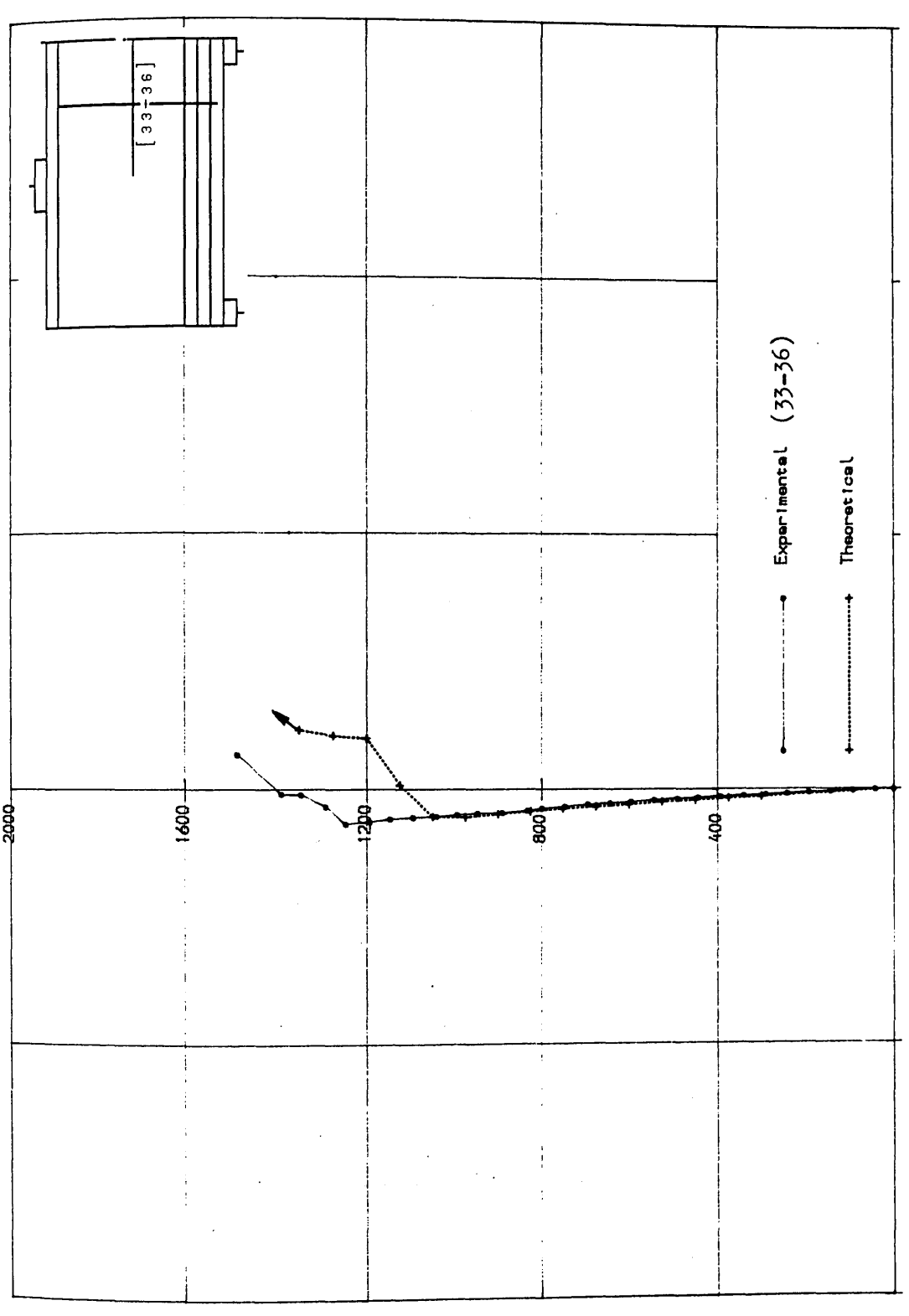

FIG(8.25) Comparison of stirrup strain in interior shear span for girder TRGRAS6

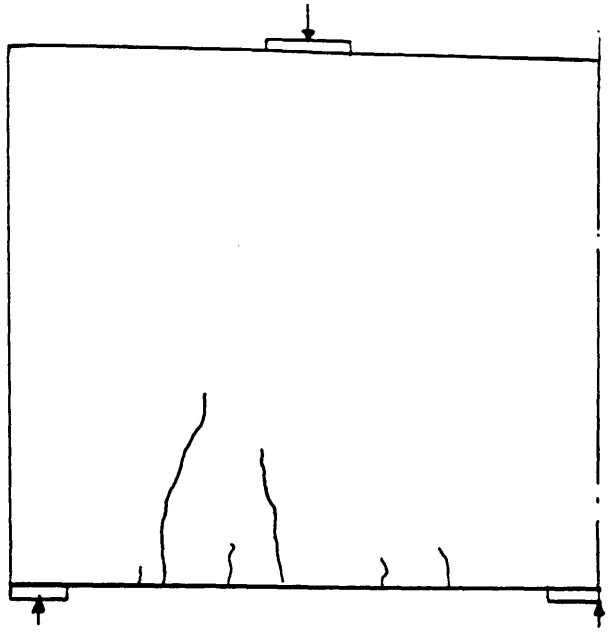

Experimental crack pattern at 600kN

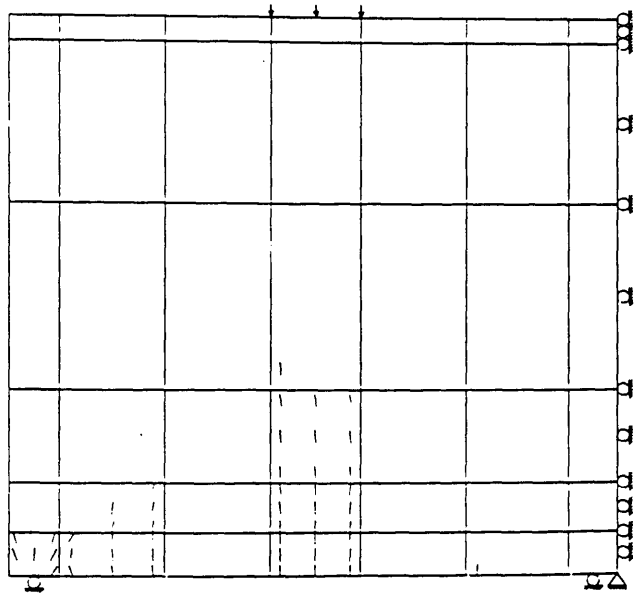

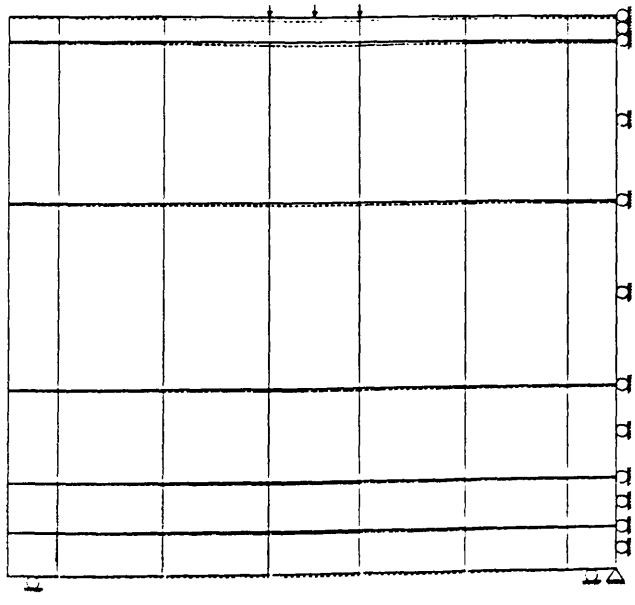

Figure(8.26) Predicted crack pattern and deformed shape at 600kN (TRGRAS2)

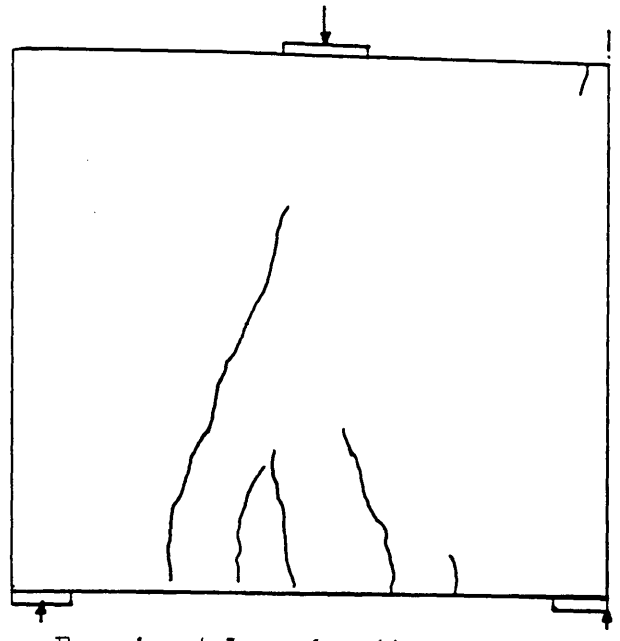

Experimental crack pattern at 950kN

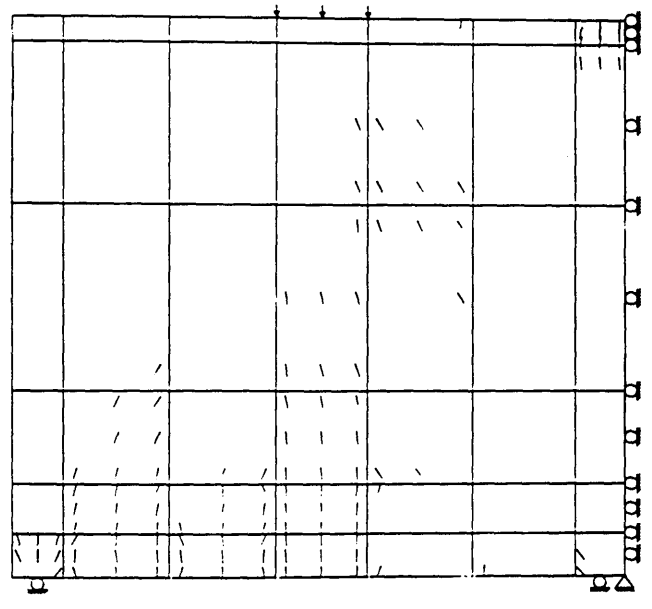

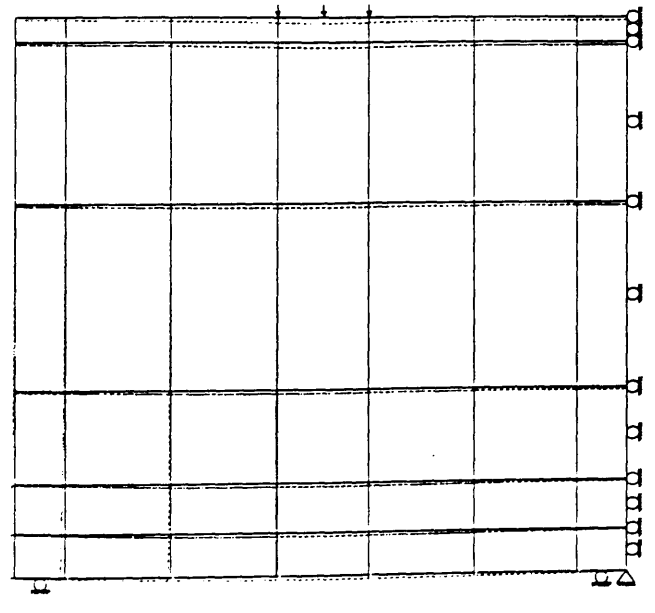

Figure(8.27) Predicted crack pattern and deformed shape at 950kN (TRGRAS2)

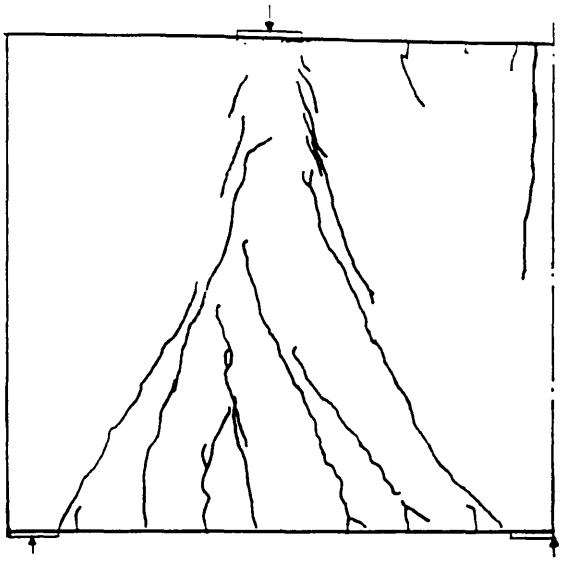

Experimental crack pattern at 1200kN

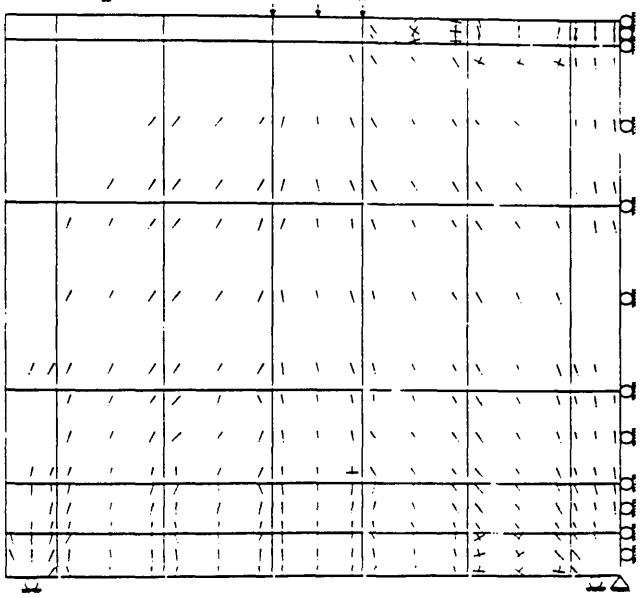

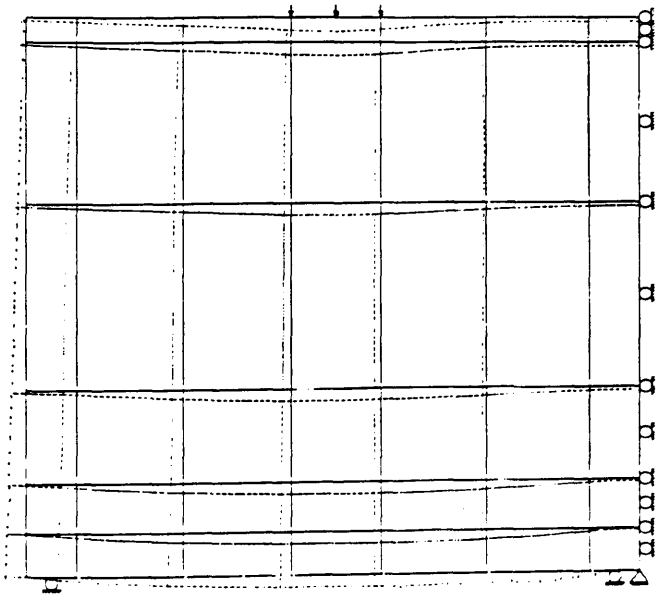

Figure(8.28) Predicted crack pattern and deformed shape at 1200kN (TRGRAS2)

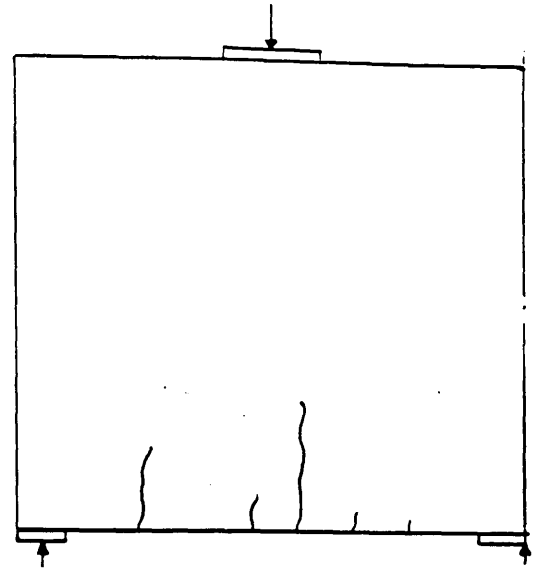

Experimental crack pattern at 600kN

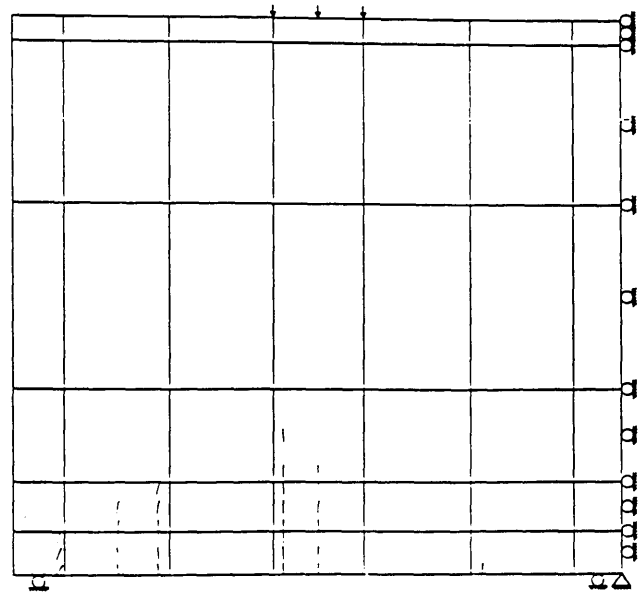

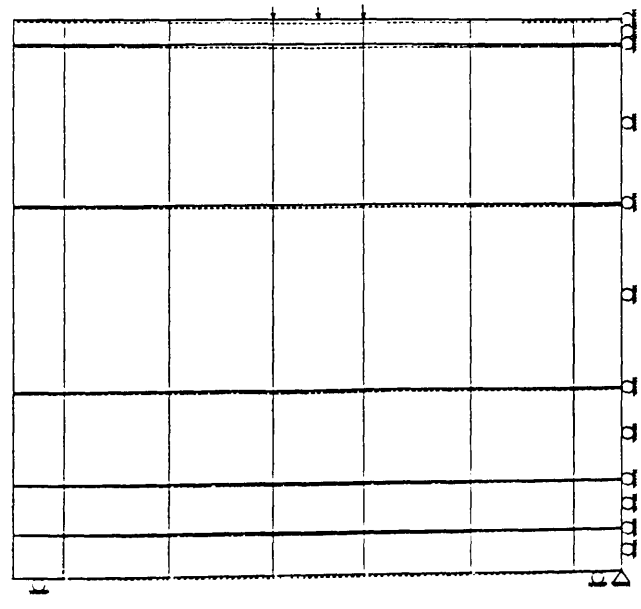

Figure(8.29) Predicted crack pattern and deformed shape at 600kN (TRGRAS3)

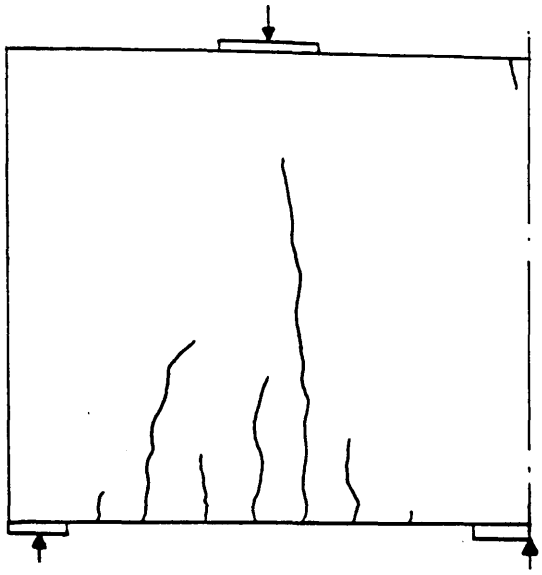

Experimental crack pattern at 900kN

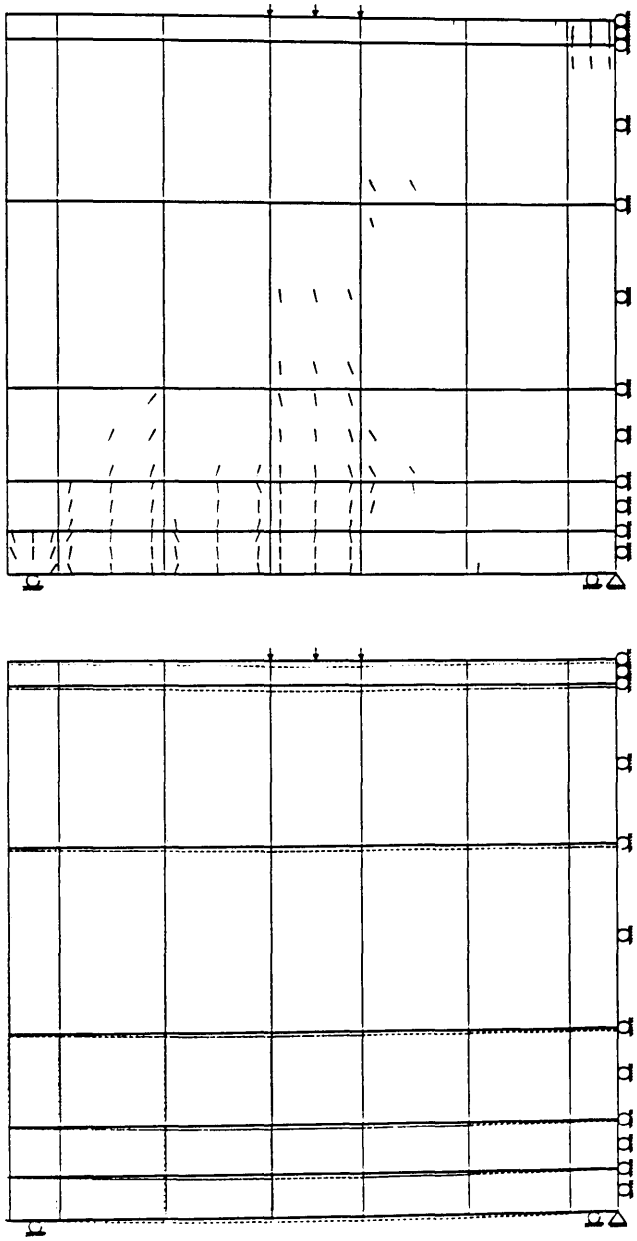

Figure(8.30) Predicted crack pattern and deformed shape at 900kN (TRGRAS3)

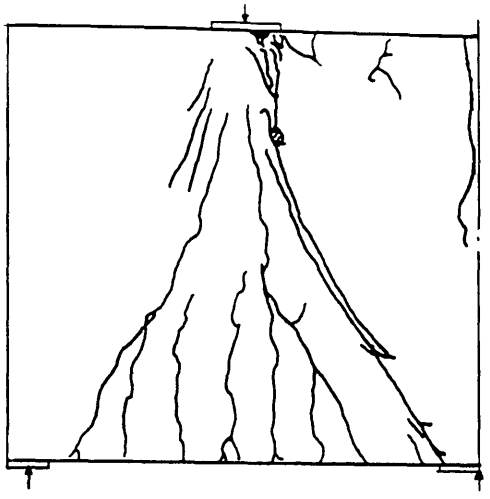

Experimental crack pattern at 1500kN

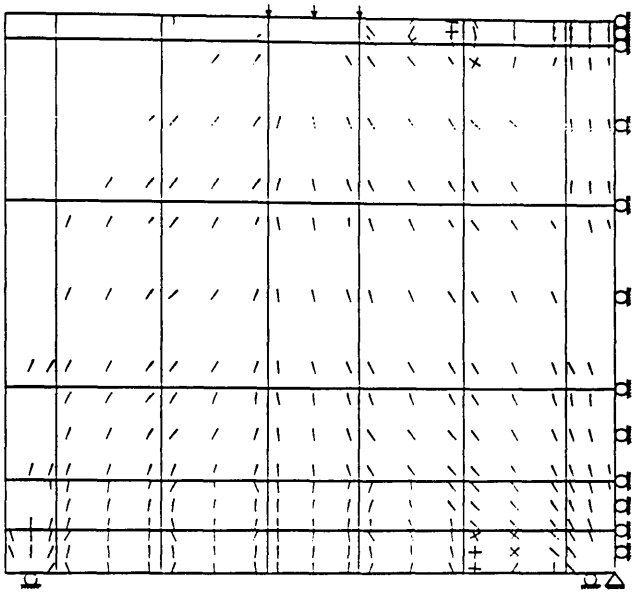

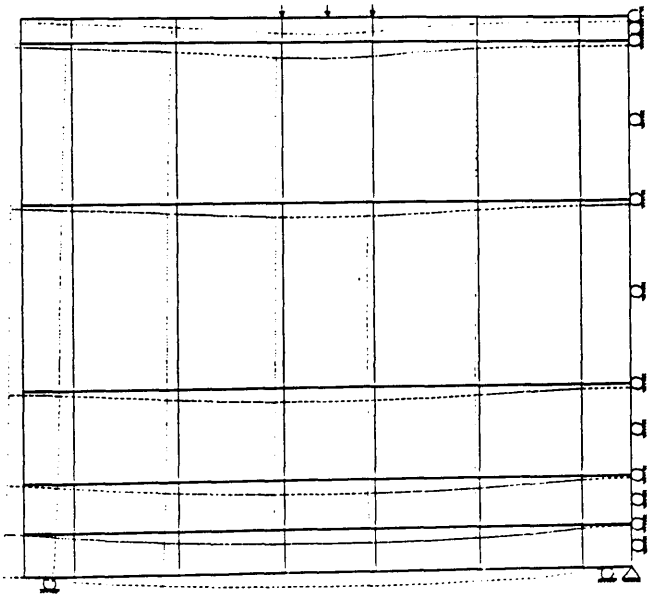

Figure(8.31) Predicted crack pattern and deformed shape at 1425kN (TRGRAS3)

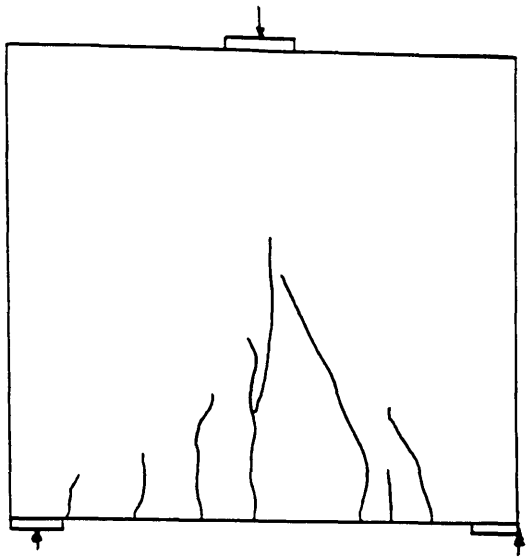

Experimental crack pattern at 950kN

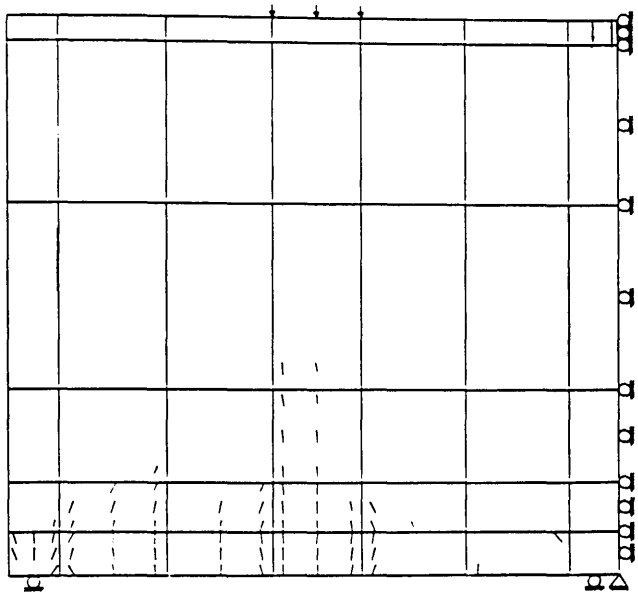

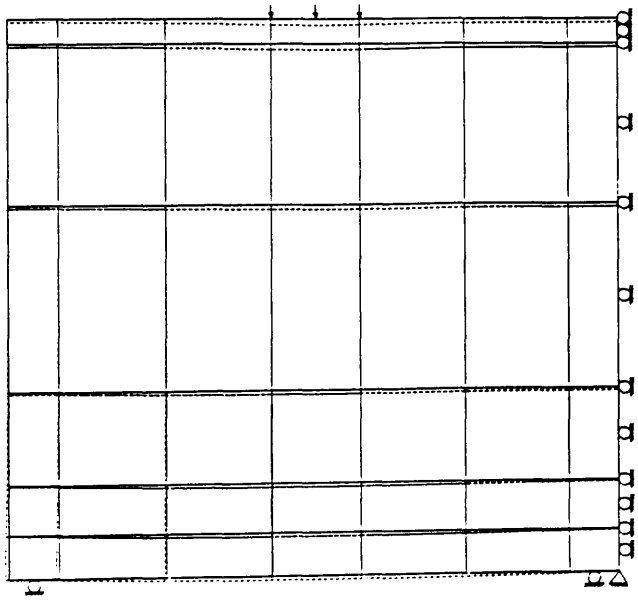

Figure(8.32) Predicted crack pattern and deformed shape at 950kN (TRGRAS6)

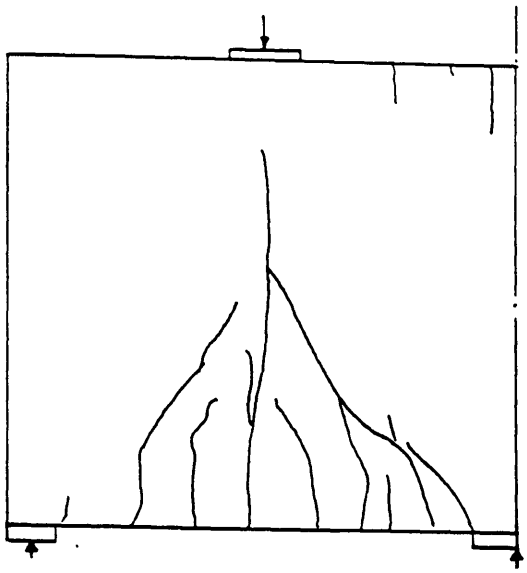

Experimental crack pattern at 1050kN

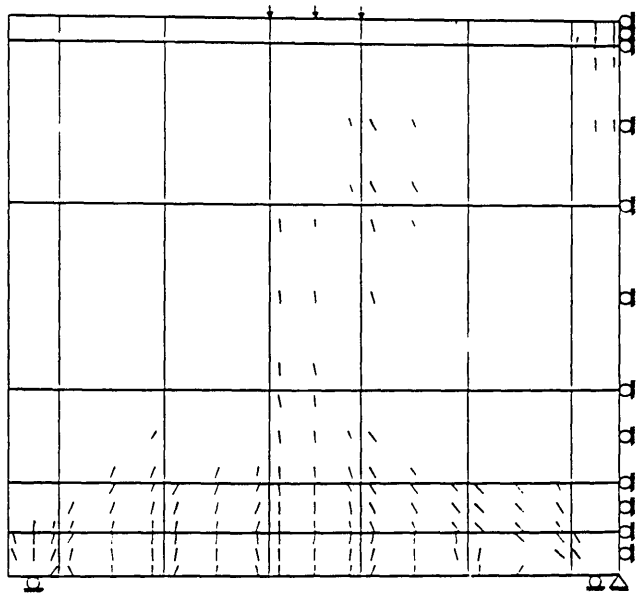

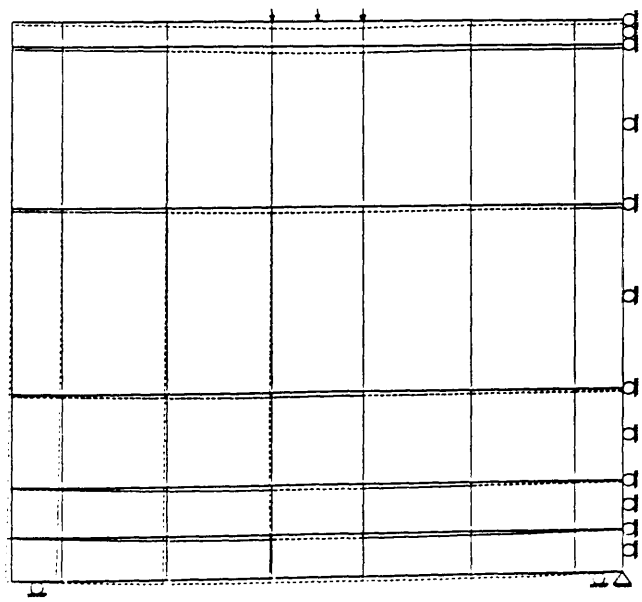

Figure(8.33) Predicted crack pattern and deformed shape at 1050kN (TRGRAS6)

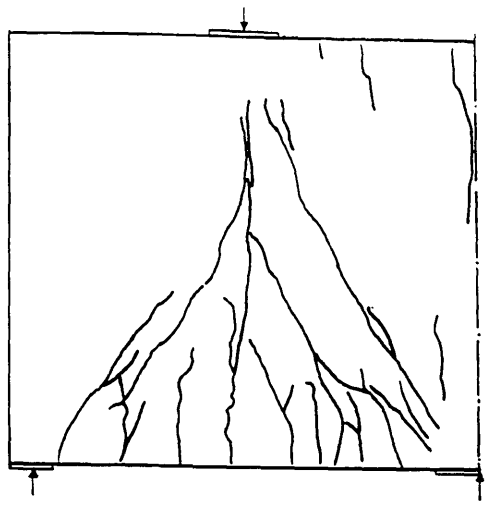

Experimental crack pattern at 1350kN

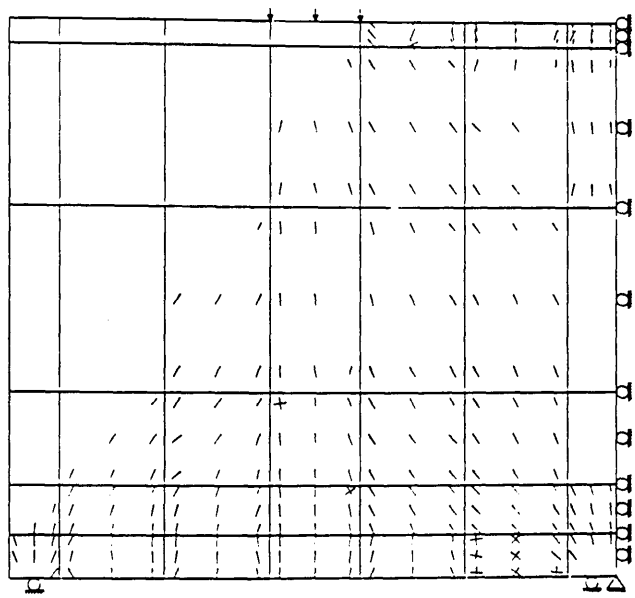

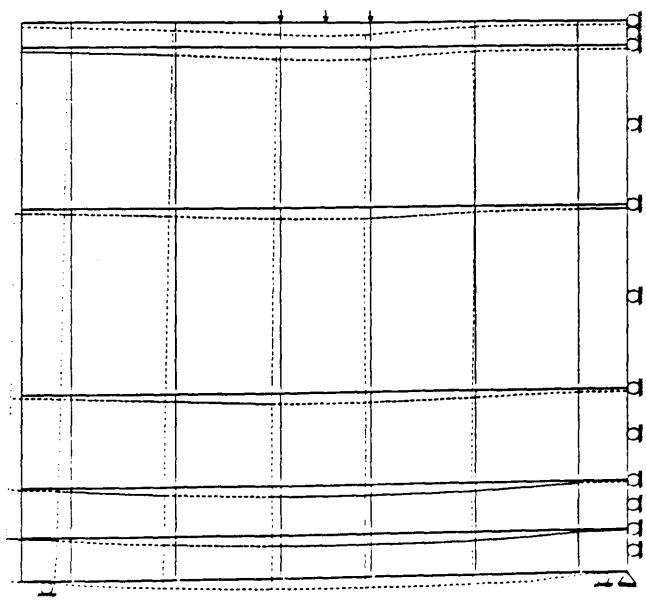

Figure(8.34) Predicted crack pattern and deformed shape at 1350kN (TRGRAS6)

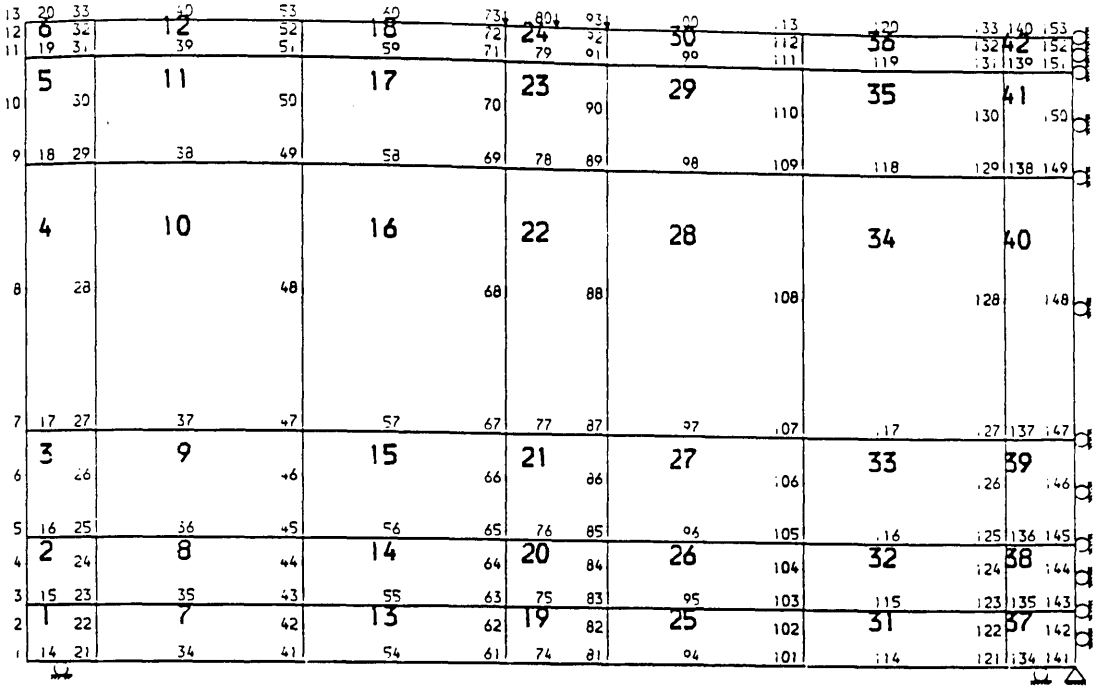

Figure(8.35) Finite element analysis mesh for girder TRGRAS4

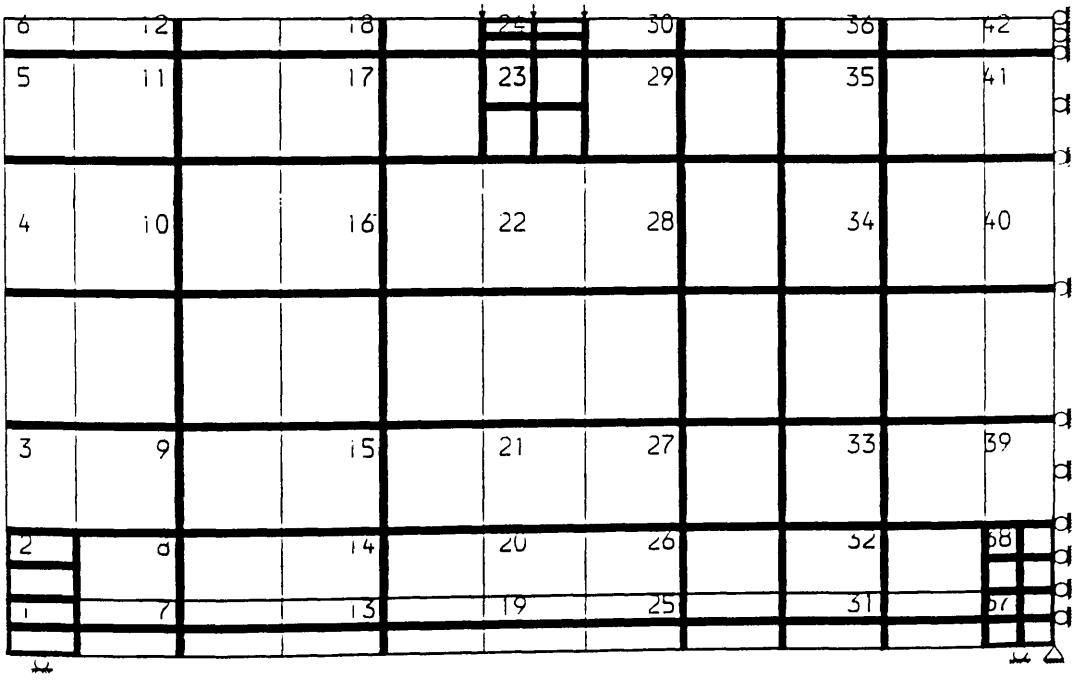

Figure(8.36) Reinforcement detail in finite element analysis for girder TRGRAS4

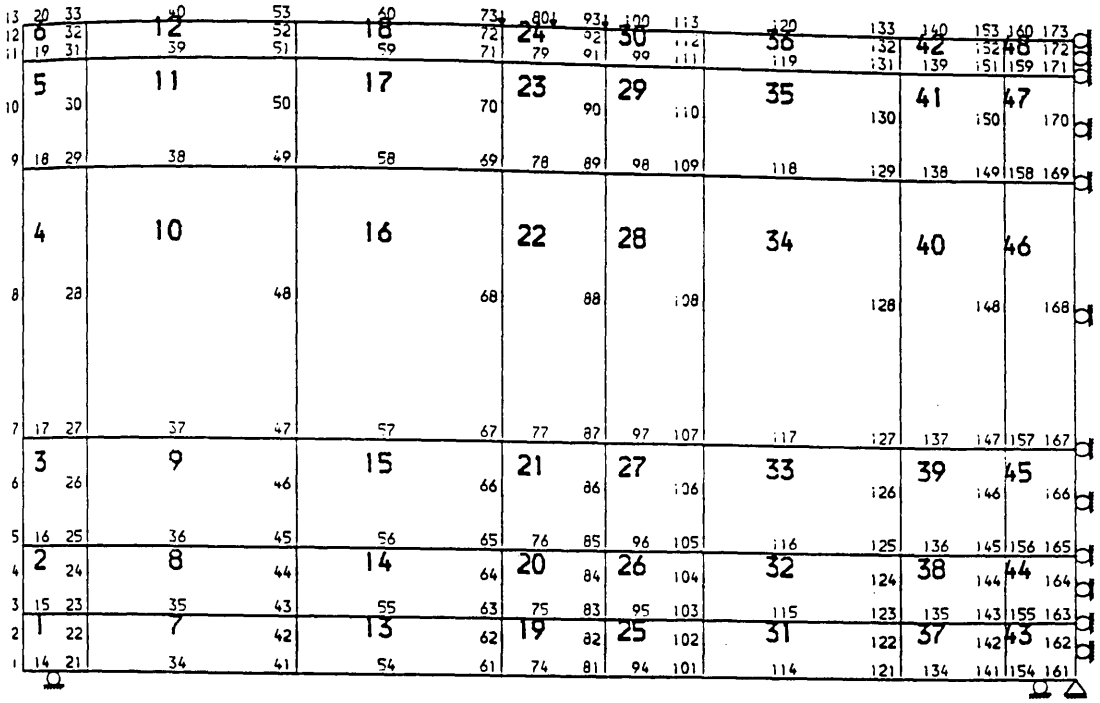

Figure(8.37) Finite element analysis mesh for girder TRGRAS5

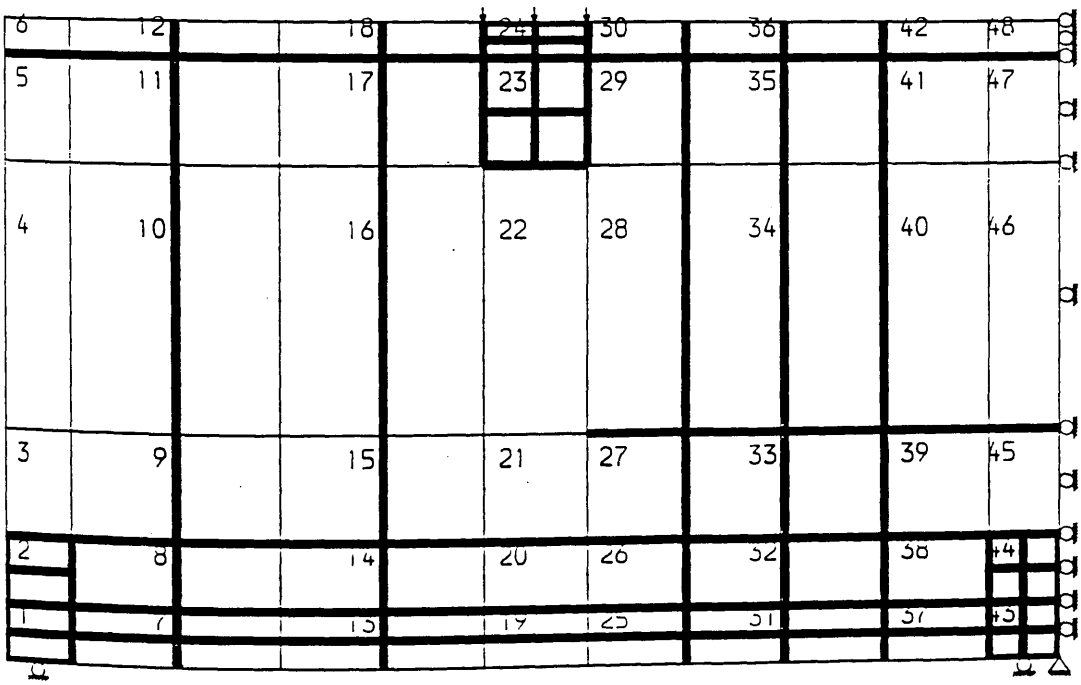

Figure(8.38) Reinforcement detail in finite element analysis for girder TRGRAS5

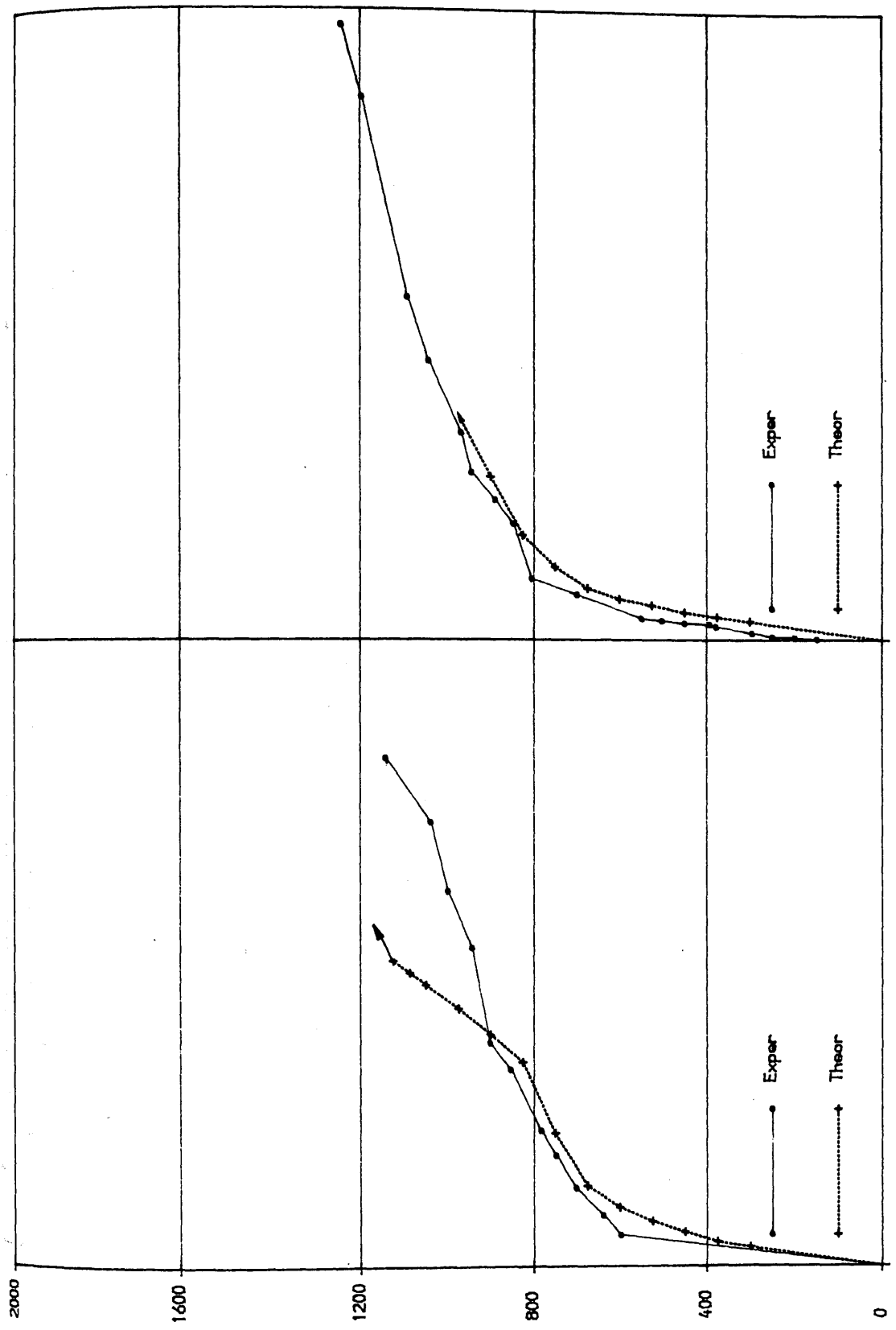

FIG (8.39) Load deflection curves for girders TRGRAS4 and TRGRAS5

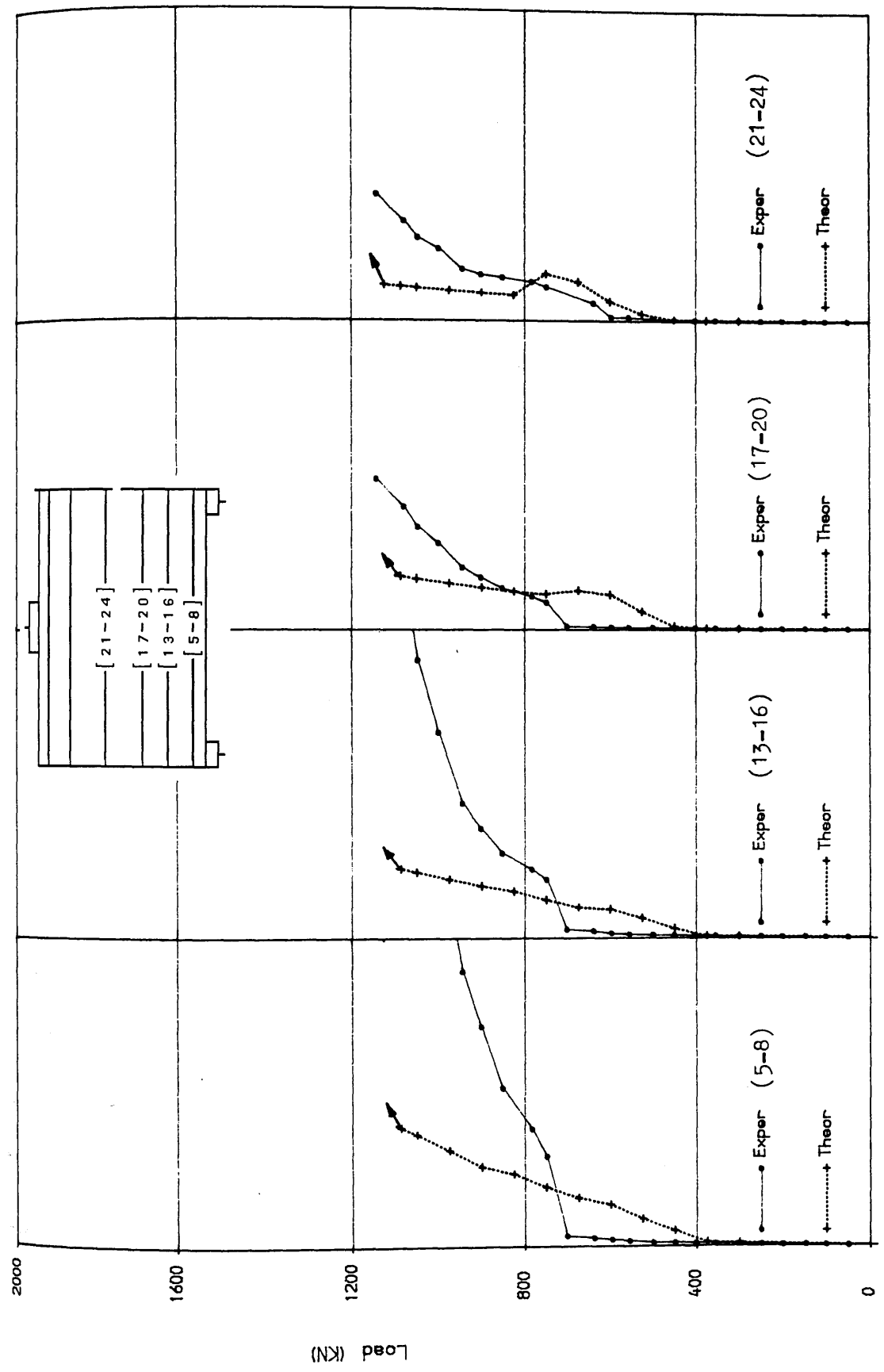

FIG (8.40) Comparison of longitudinal steel strains at centre of girder span for girder TRGRAS4

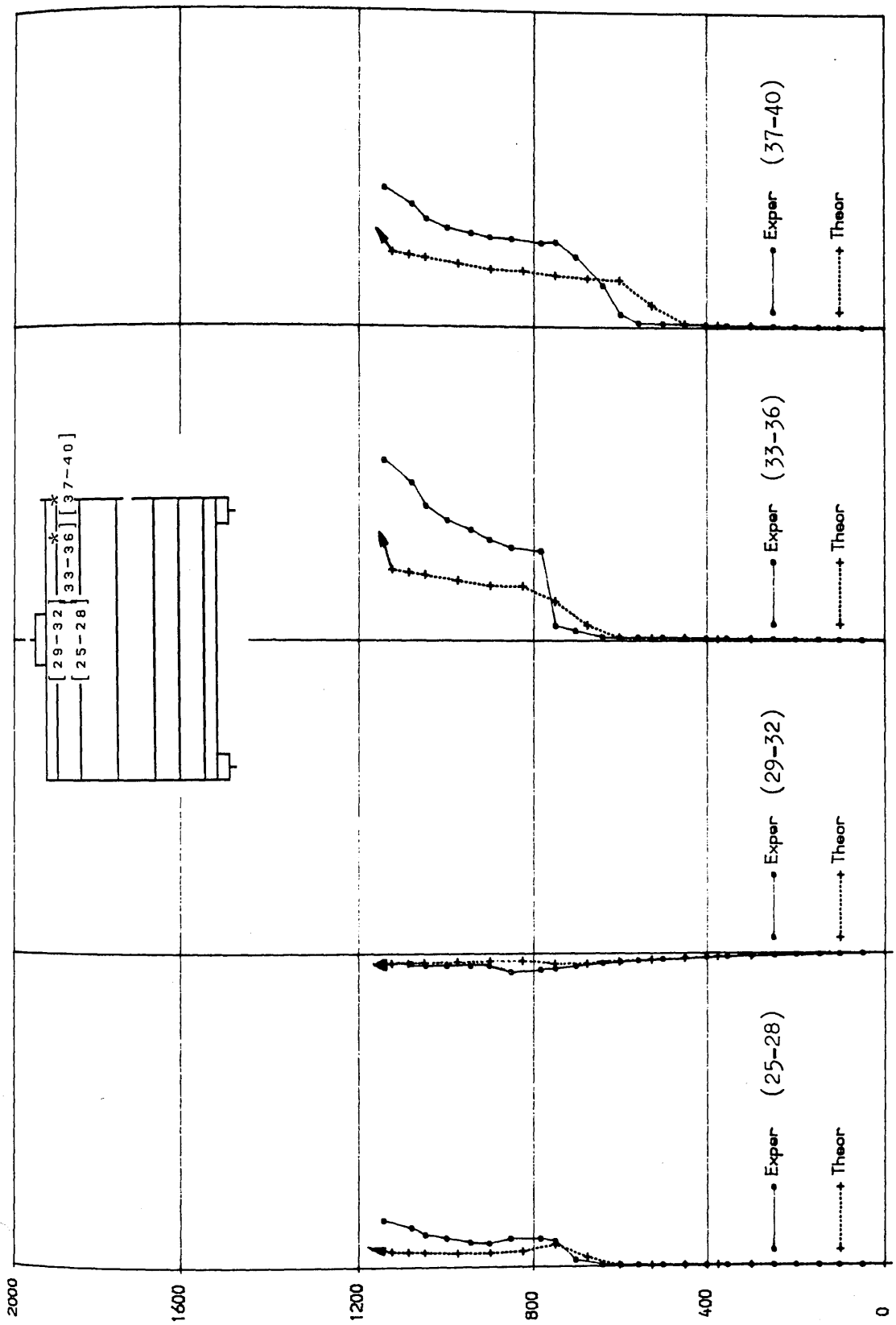

FIG (8.40) Continued

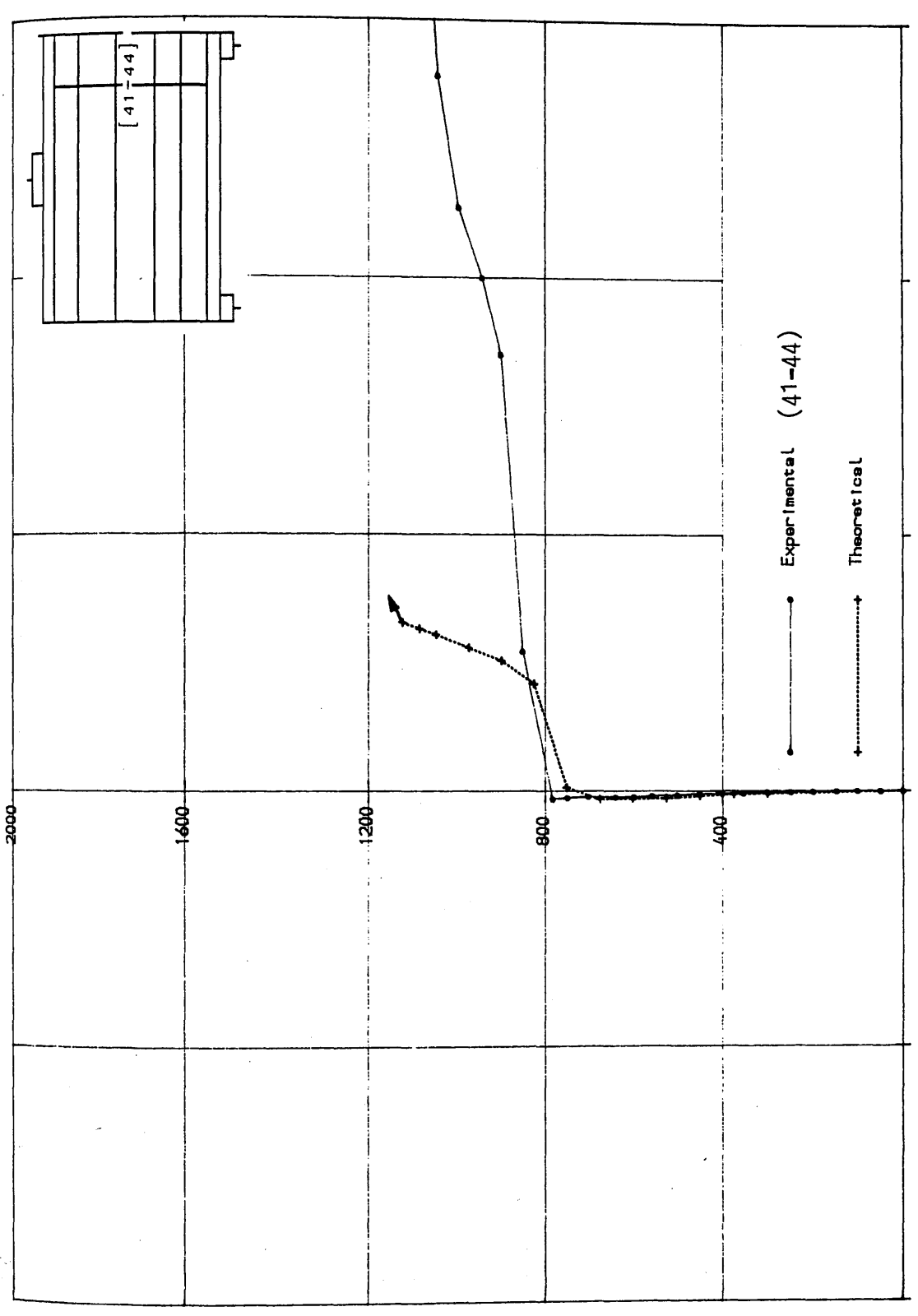

FIG(8.41) Comparison of stirrup strain in interior shear span for girder TRGRAS4

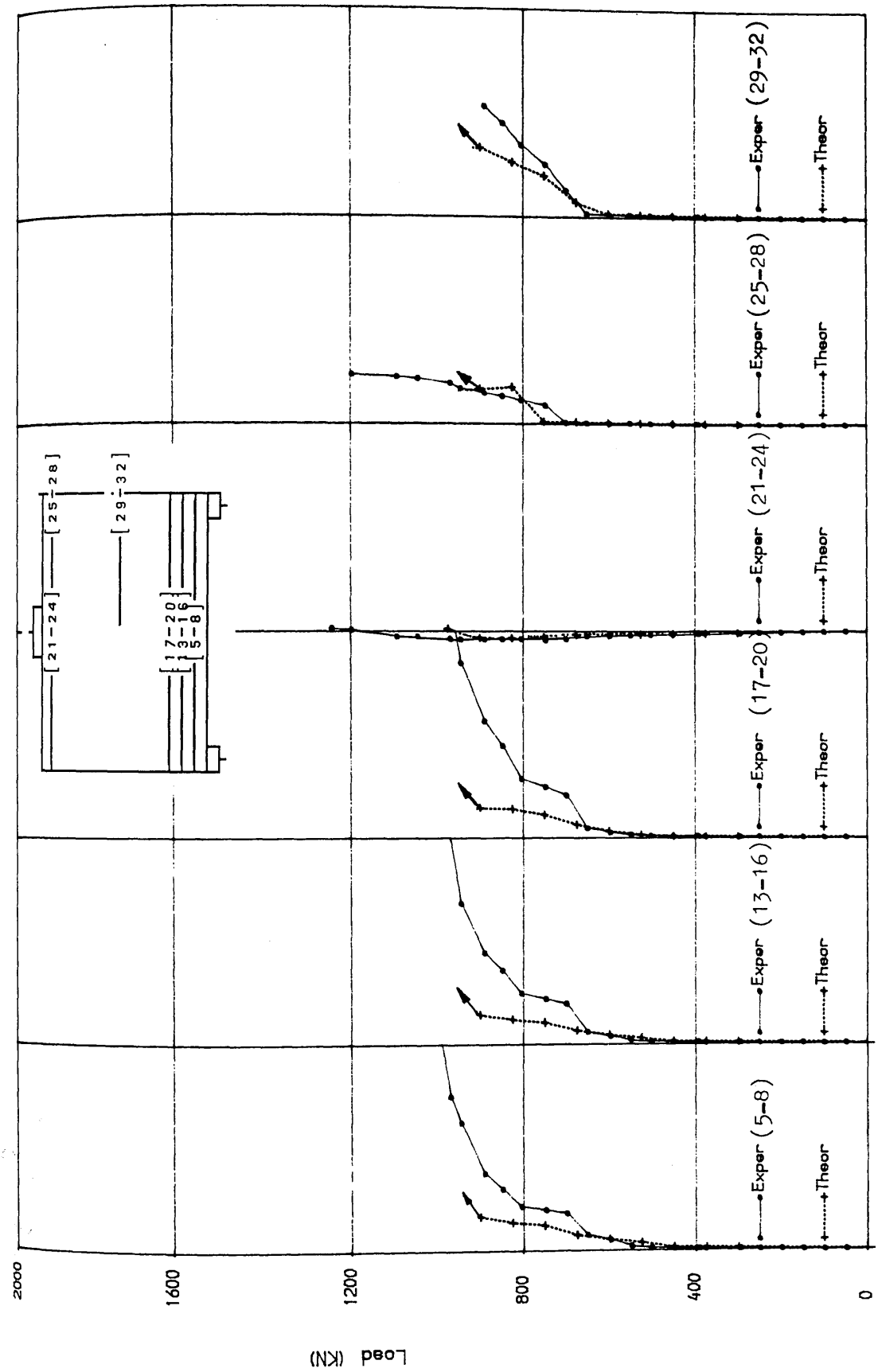

FIG (8.42) Comparison of longitudinal steel strains at centre of girder span for girder TRGRASS

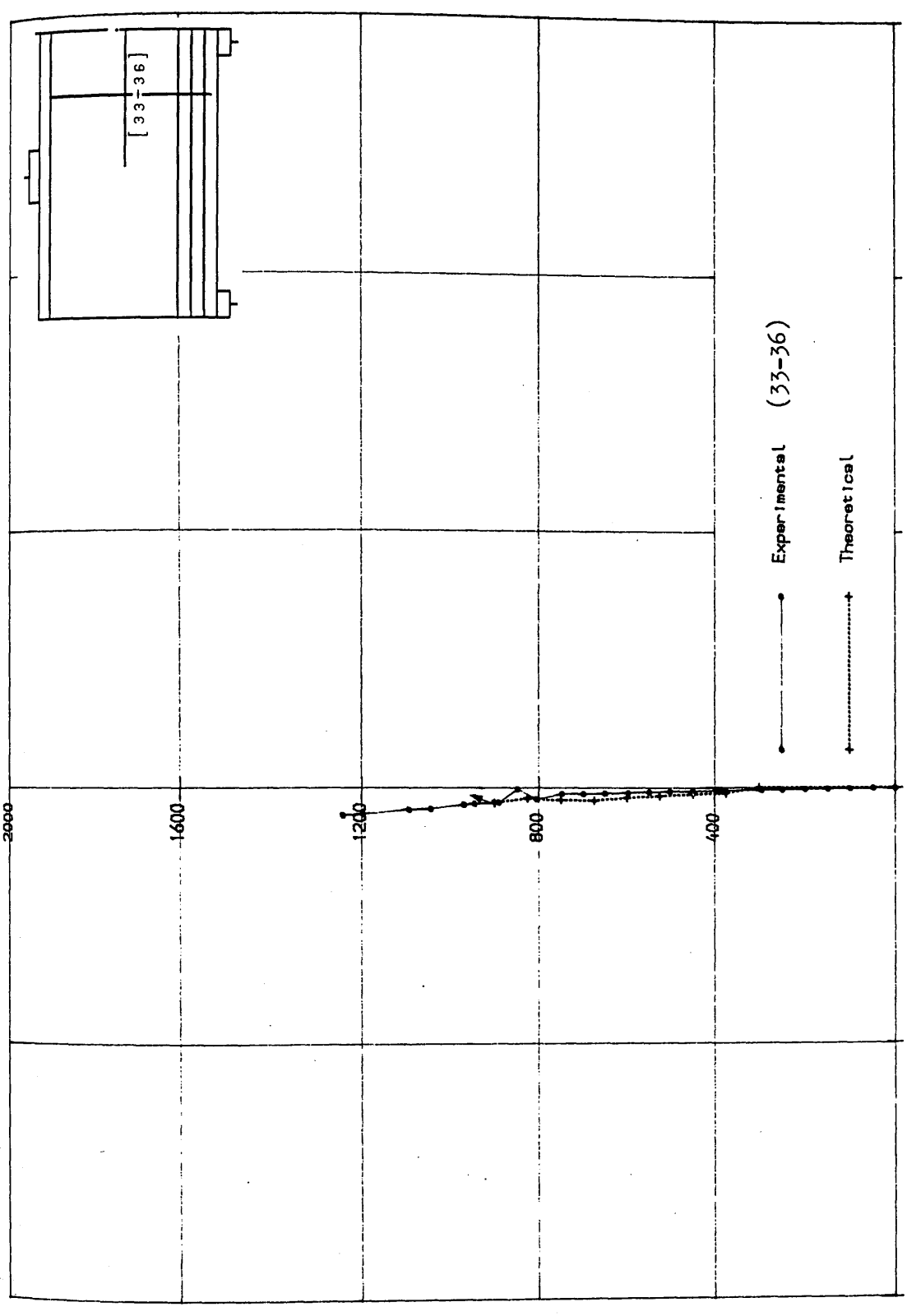

FIG (8.43) Comparison of stirrup strain in interior shear span for girder TRGRASS

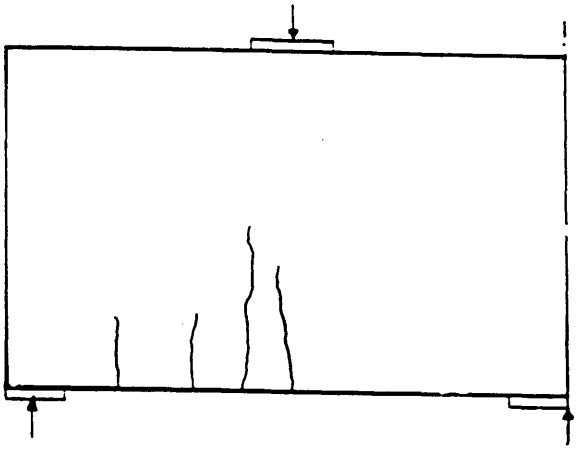

Experimental crack pattern at 450kN

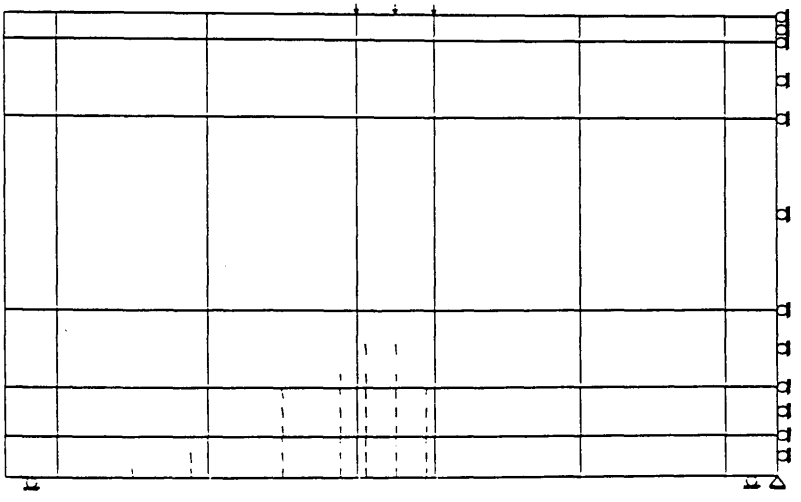

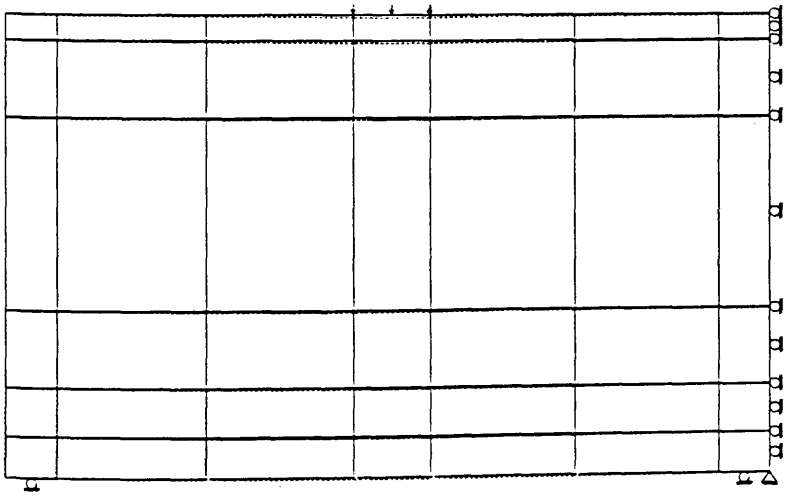

Figure(8.44) Predicted crack pattern and deformed shape at 450kN (TRGRAS4)

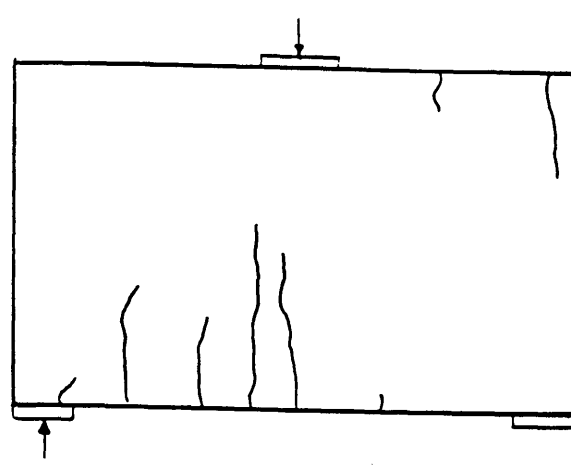

Experimental crack pattern at 600kN

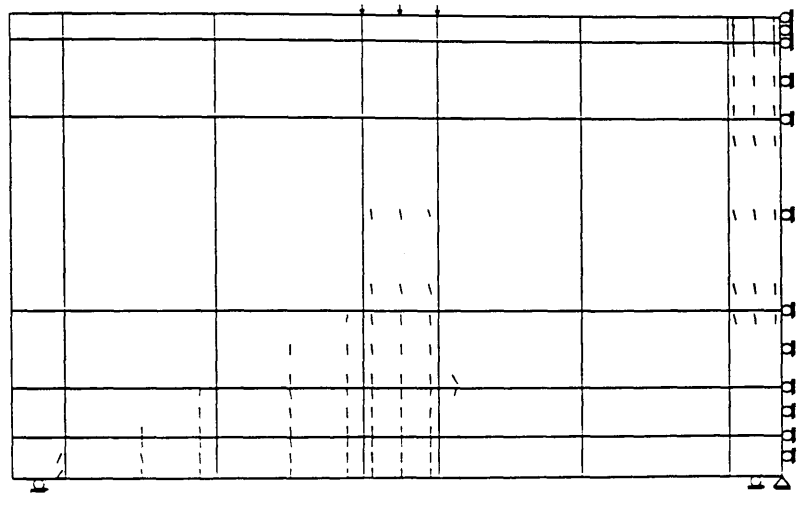

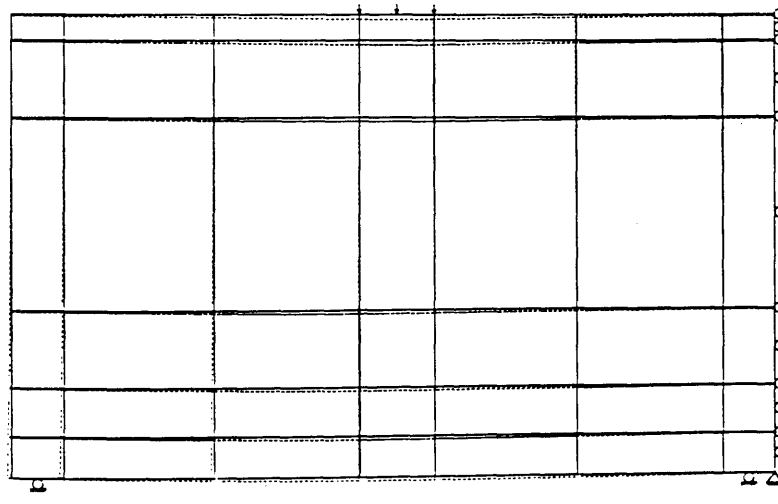

Figure(8.45) Predicted crack pattern and deformed shape at 600kN (TRGRAS4)

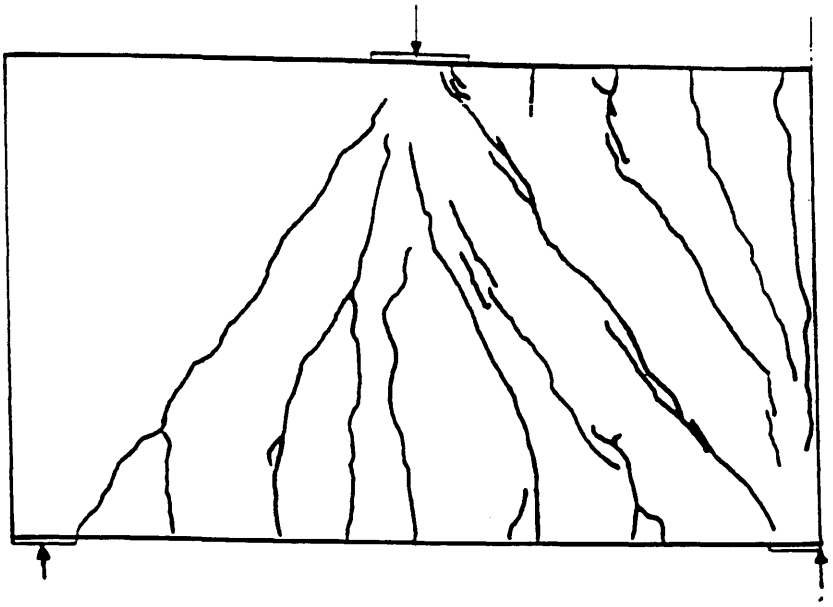

Experimental crack pattern at 1143kN

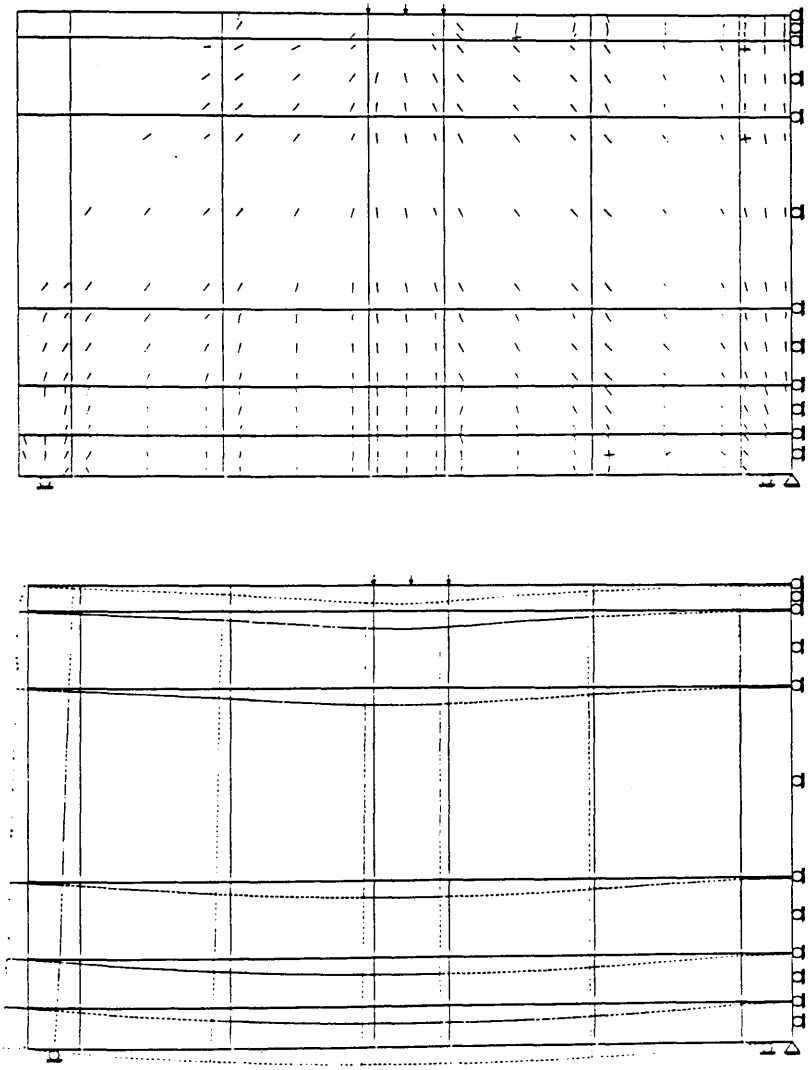

Figure(8.46) Predicted crack pattern and deformed shape at 1125kN (TRGRAS4)

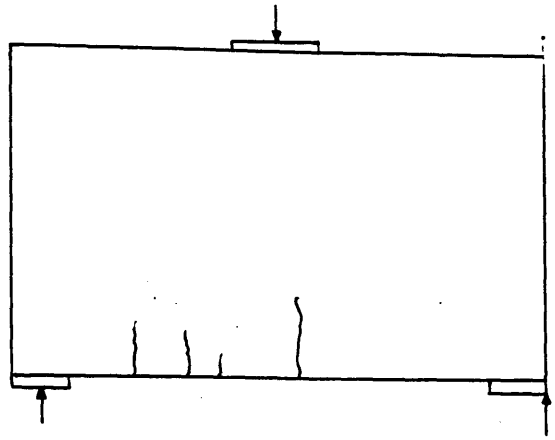

Experimental crack pattern at 600kN

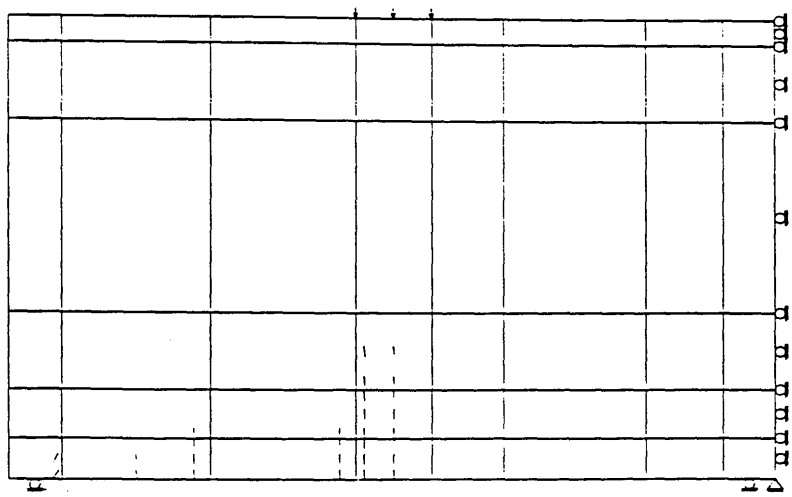

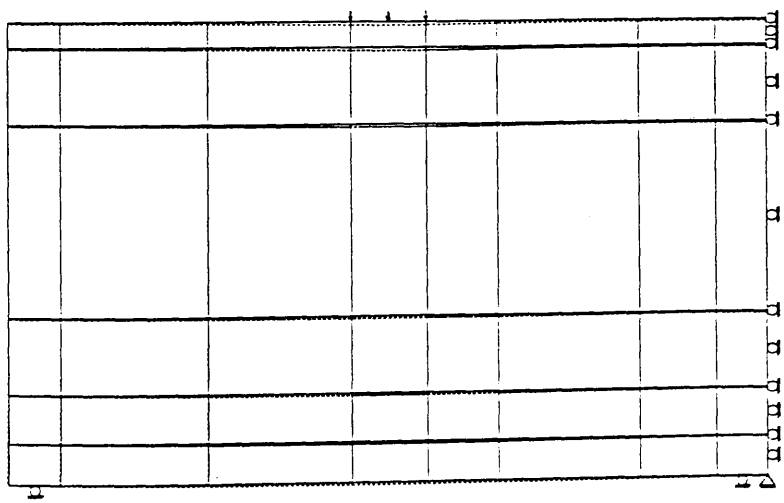

Figure(8.47) Predicted crack pattern and deformed shape at 600kN (TRGRAS5)

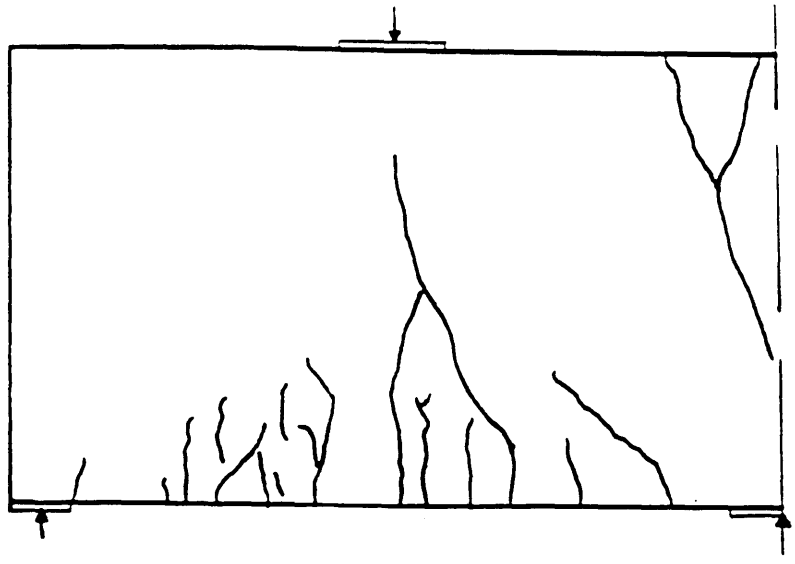

Experimental crack pattern at 750kN

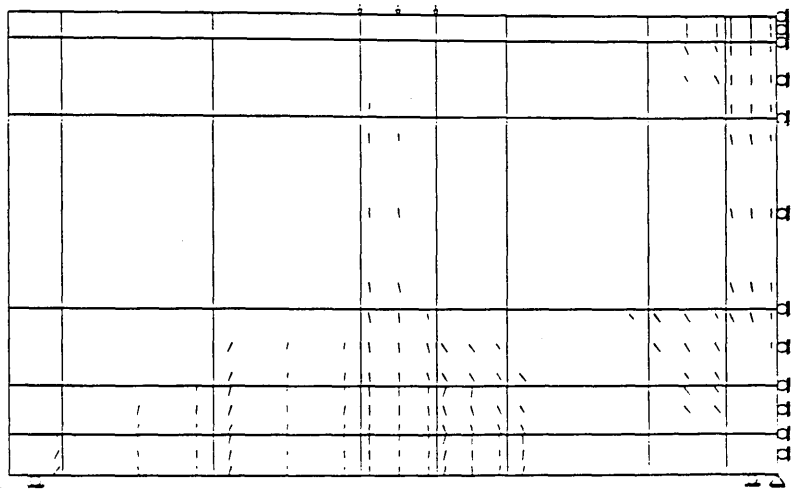

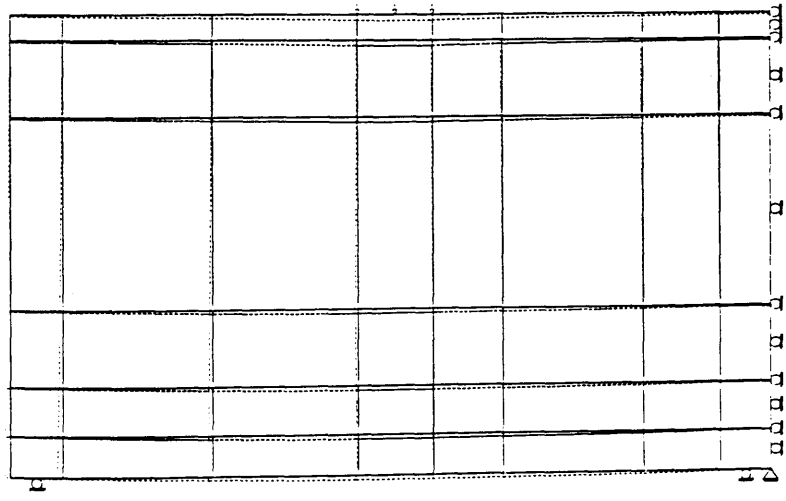

Figure(8.48) Predicted crack pattern and deformed shape at 750kN (TRGRAS5)

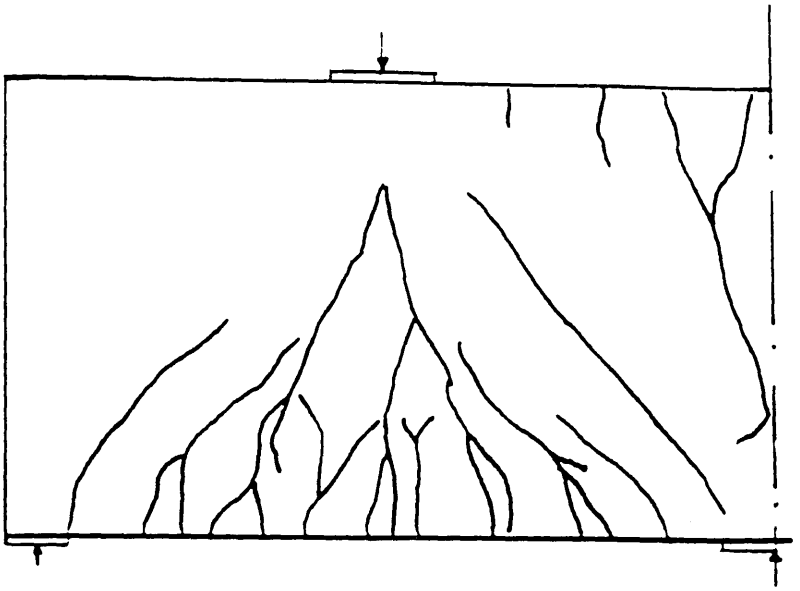

Experimental crack pattern at 975kN

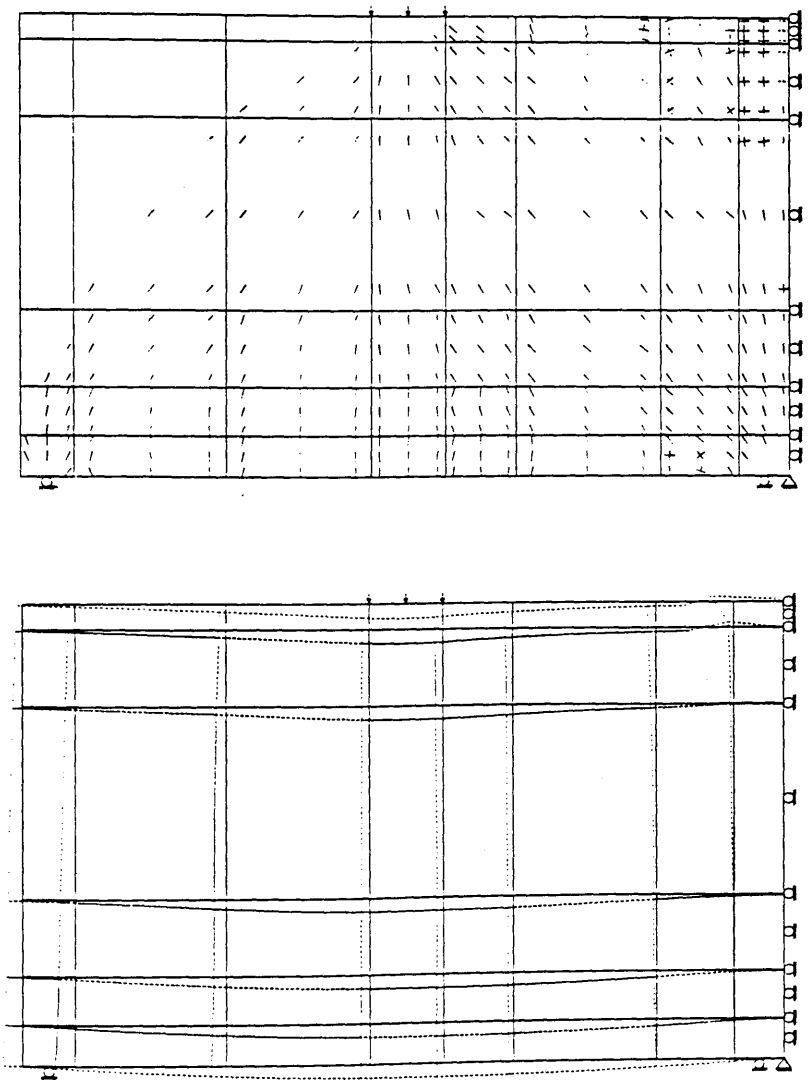

Figure(8.49) Predicted crack pattern and deformed shape at 975kN (TRGRAS5)

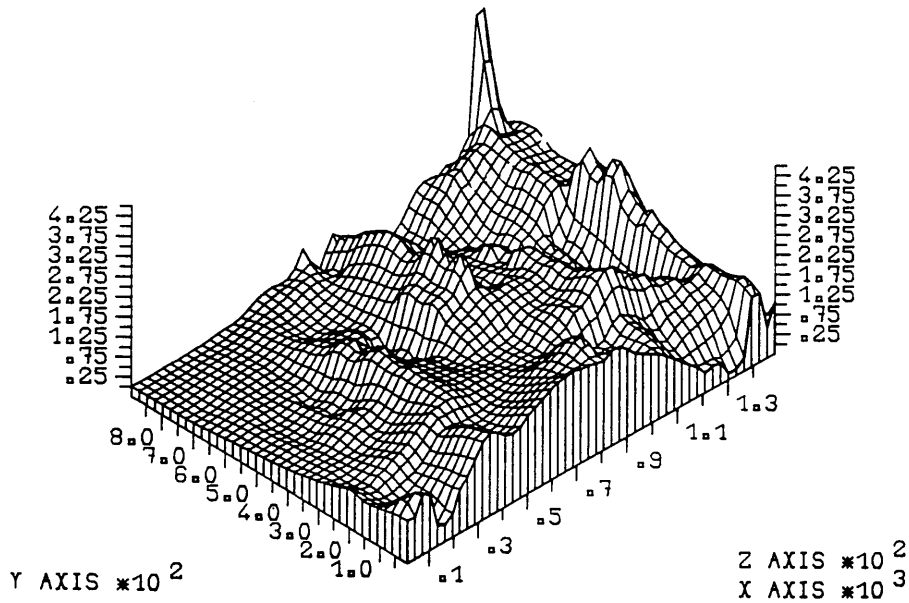

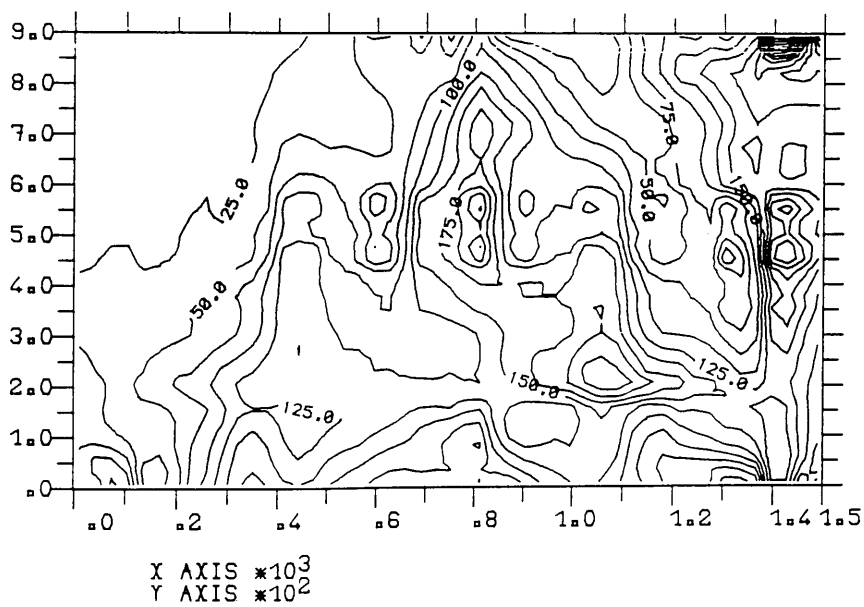

Figure(8.50) Predicted maximum shear strain*10^{-5} at 750kN (TRGRAS4)

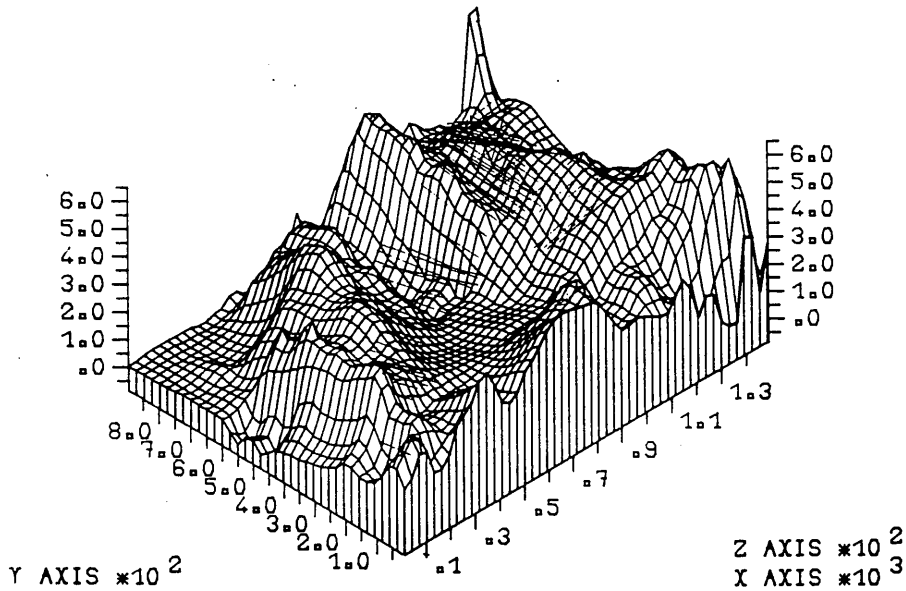

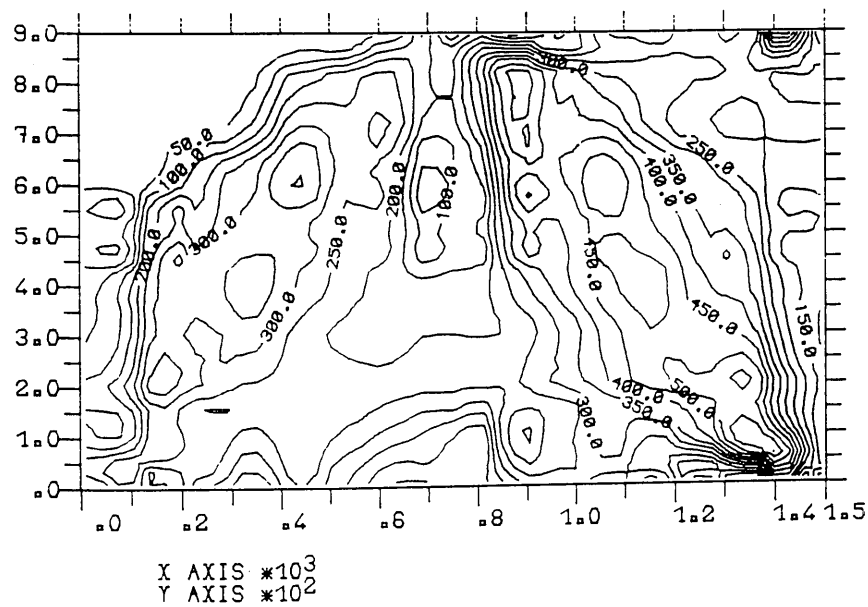

Figure(8.51) Predicted maximum shear strain*10^{-5} at 1125kN (TRGRAS4)

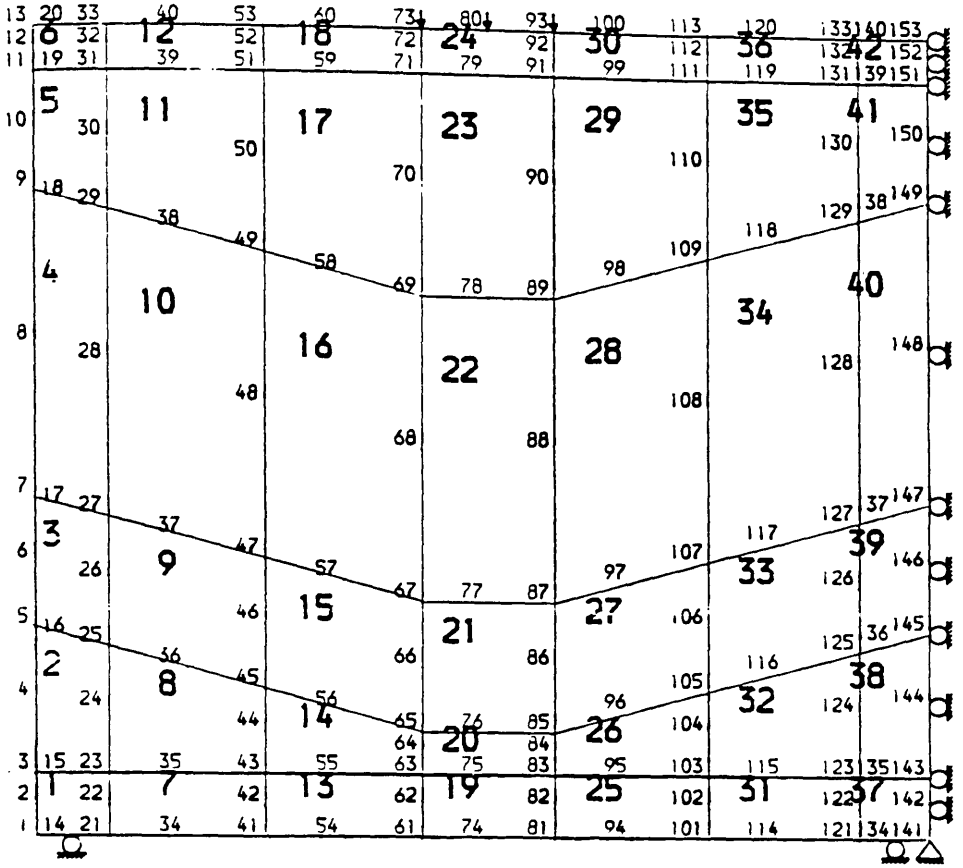

Figure(8.52) Finite element analysis mesh for girder TRGRAS7

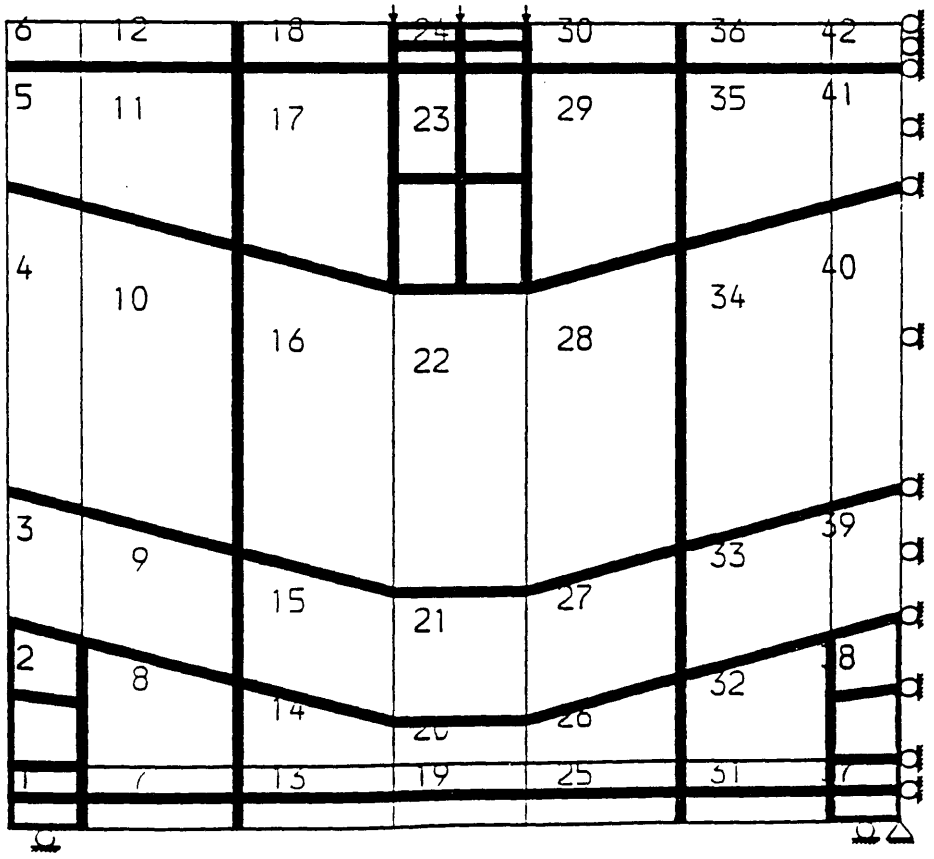

Figure(8.53) Reinforcement detail in finite element analysis for girder TRGRAS

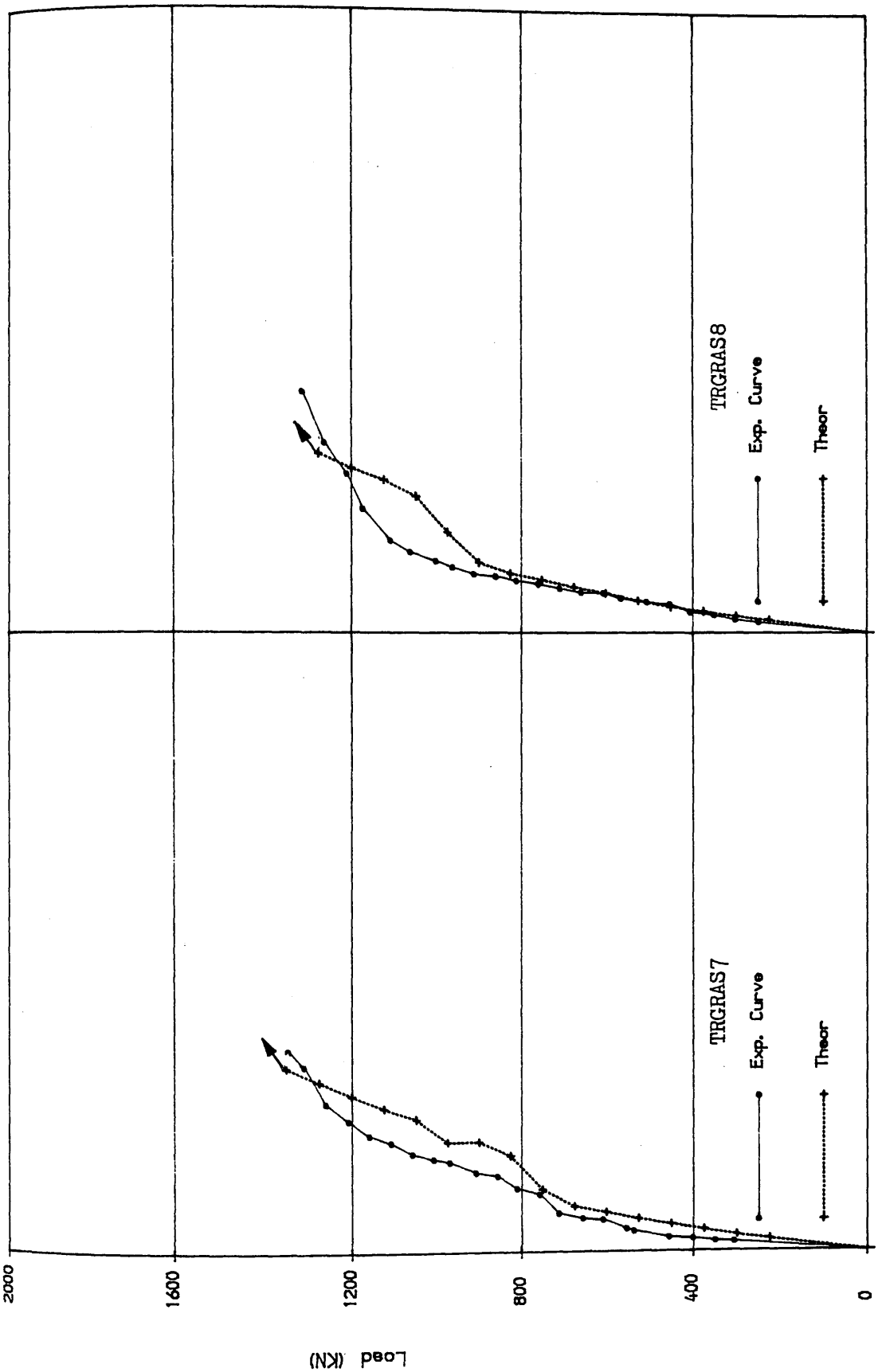

FIG (8.54) Load deflection curves for girders TRGRAS7 and TRGRAS8

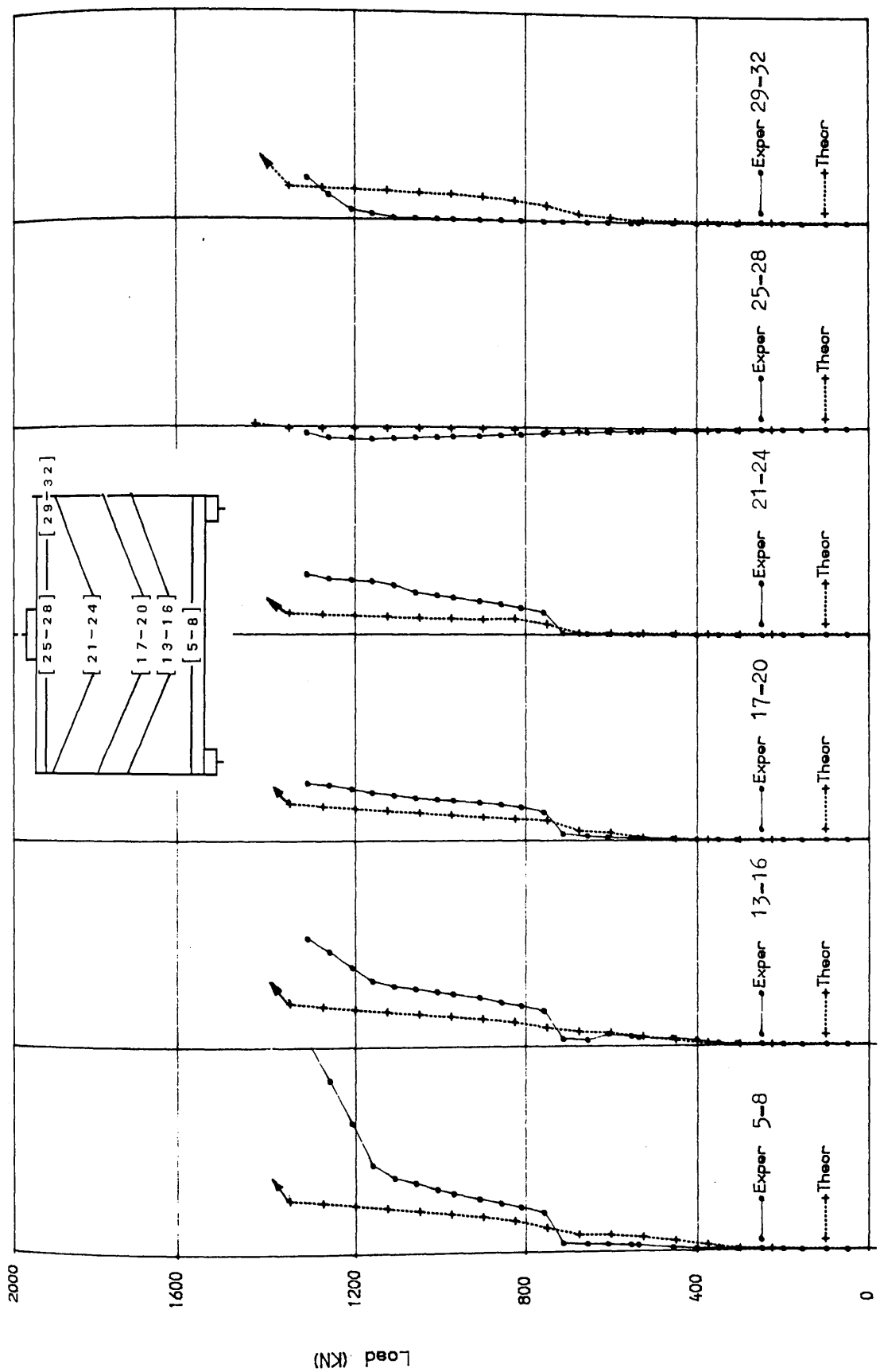

FIG (8.55) Comparison of longitudinal steel strains at centre of girder span for girder TRGRAS7

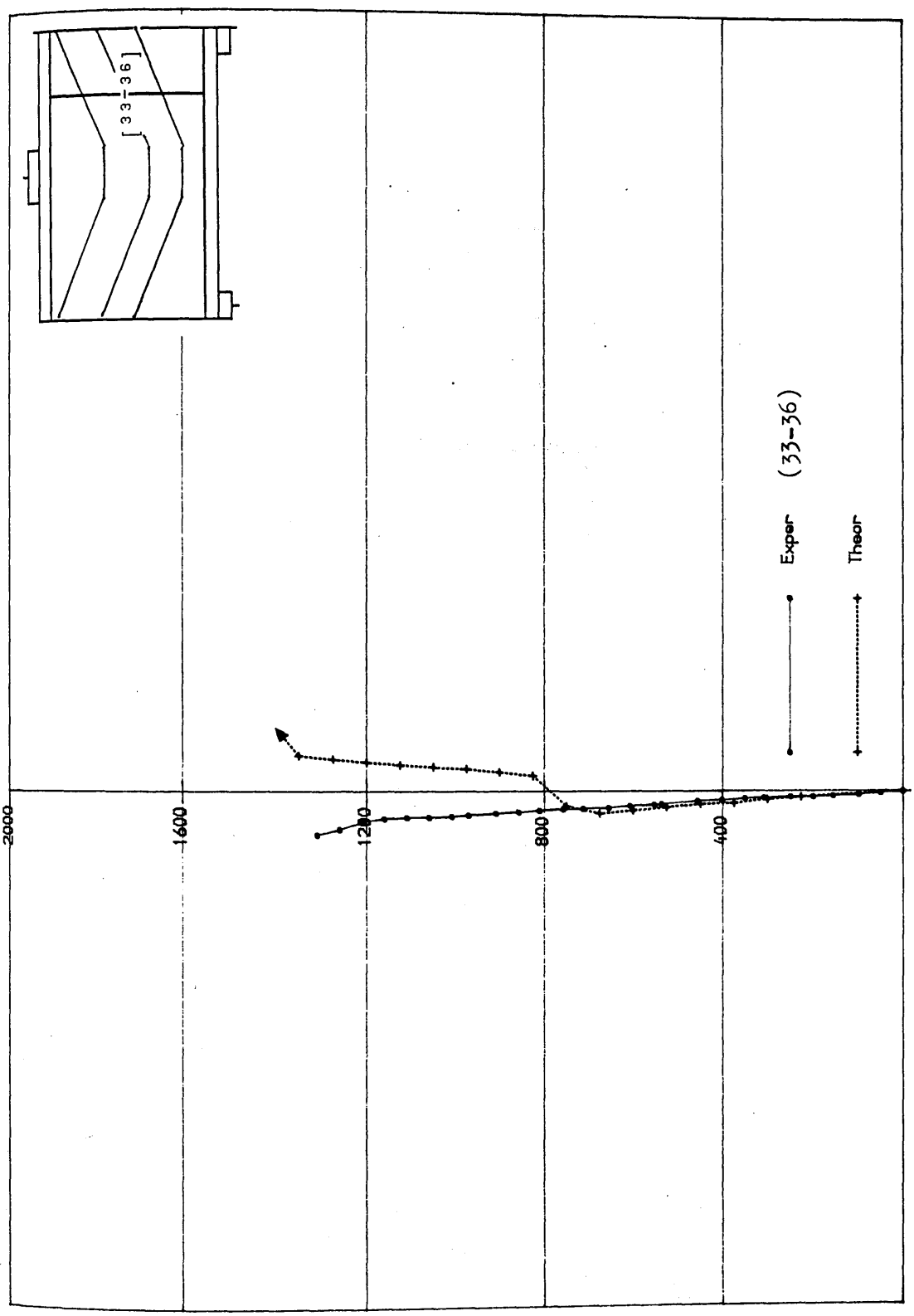

FIG (8.56) Comparison of stirrup strain in interior shear span for girder TRGRA57

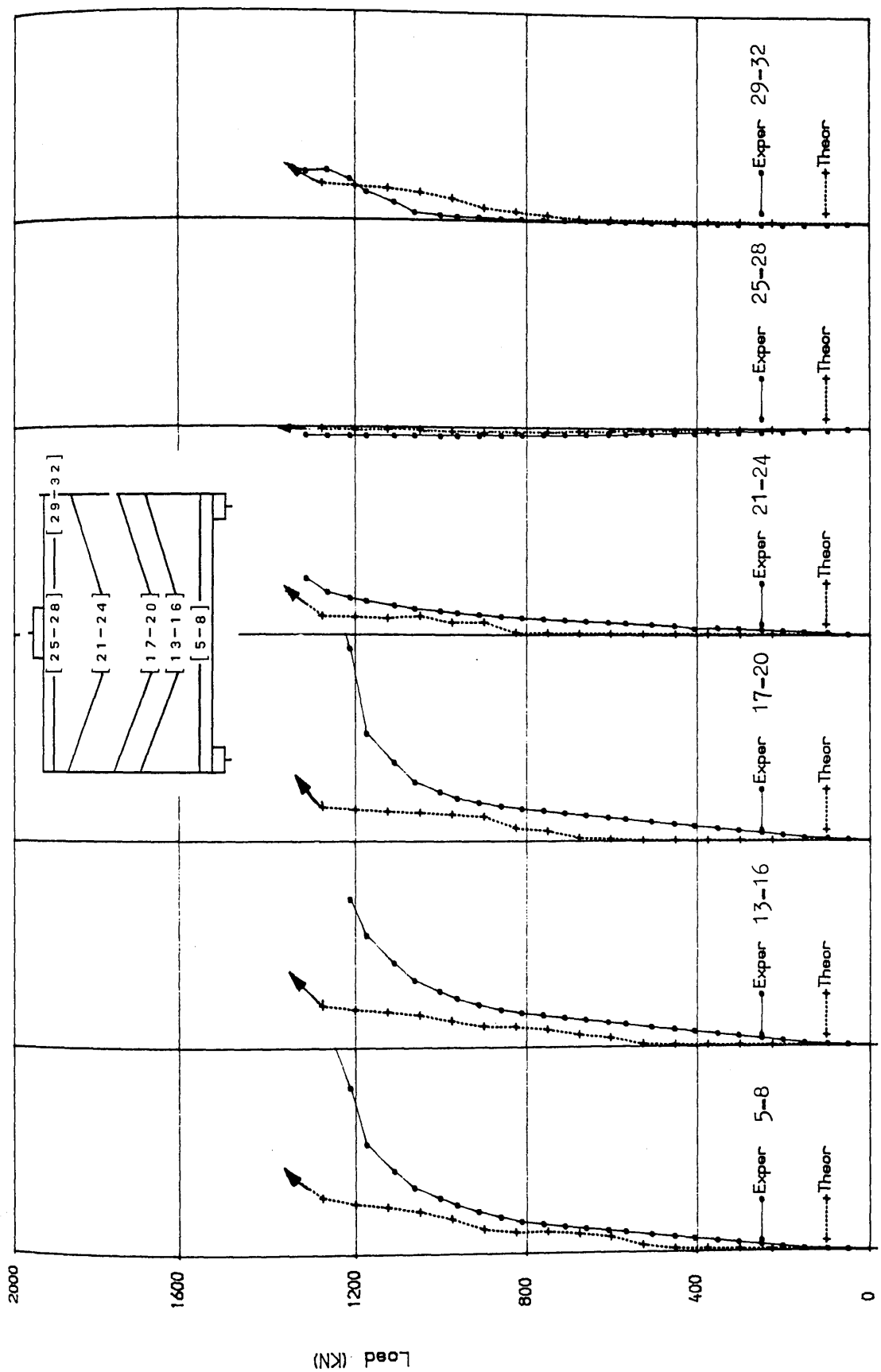

FIG (8.57) Comparison of longitudinal steel strains at centre of girder span for girder TRGRA38

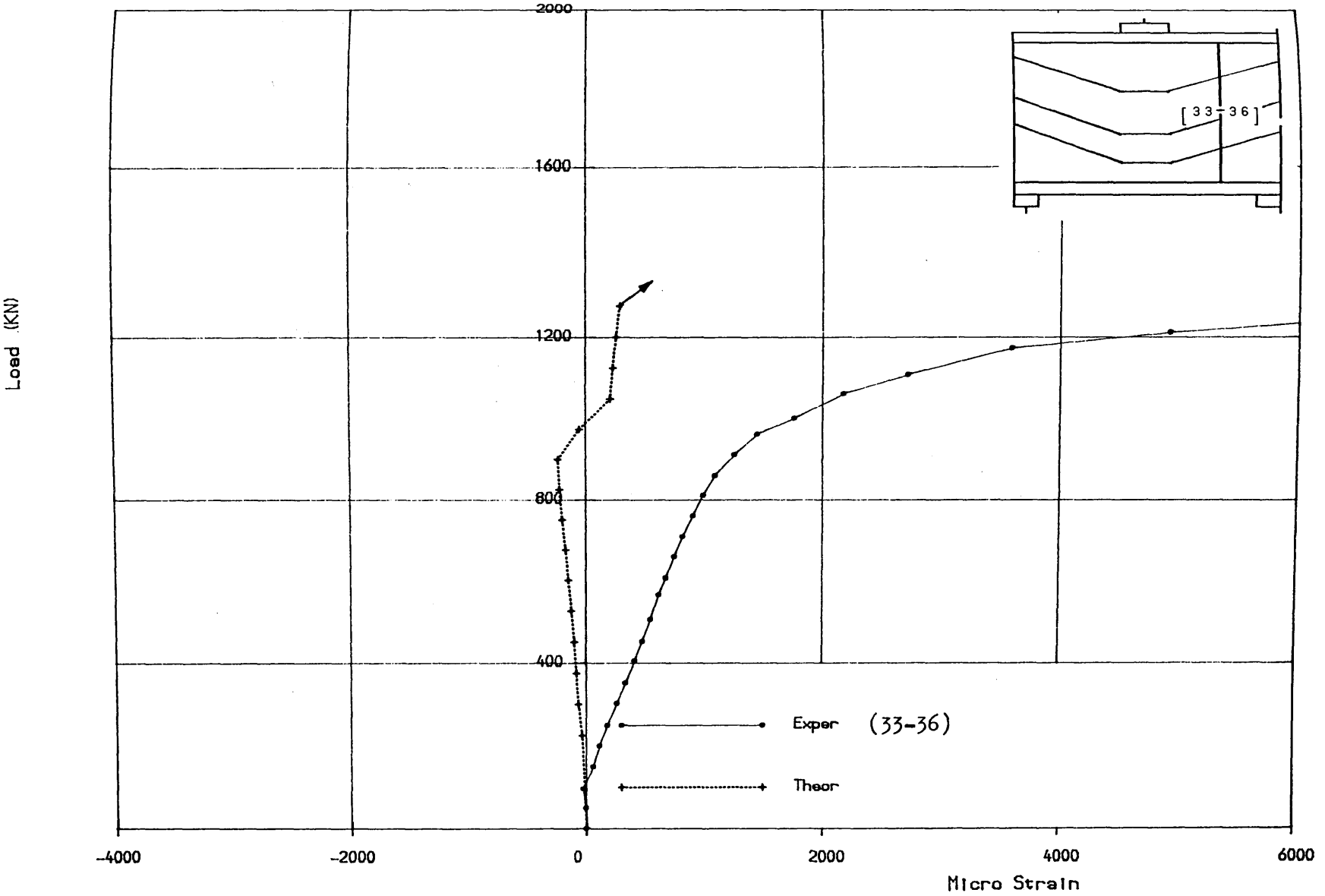

FIG (8.58) Comparison of stirrup strain in interior shear span for girder TRGRAS8

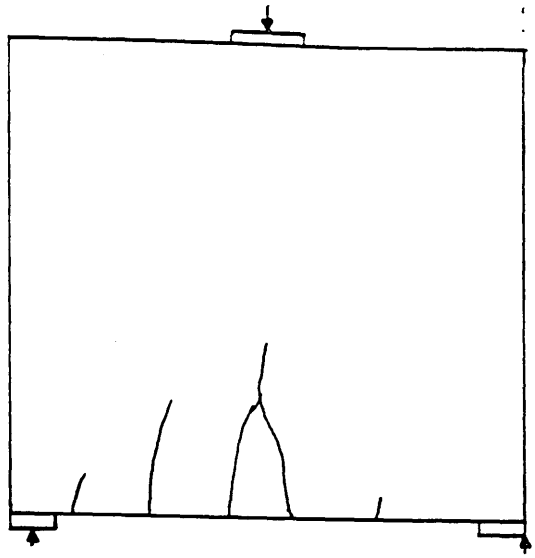

Experimental crack pattern at 600kN

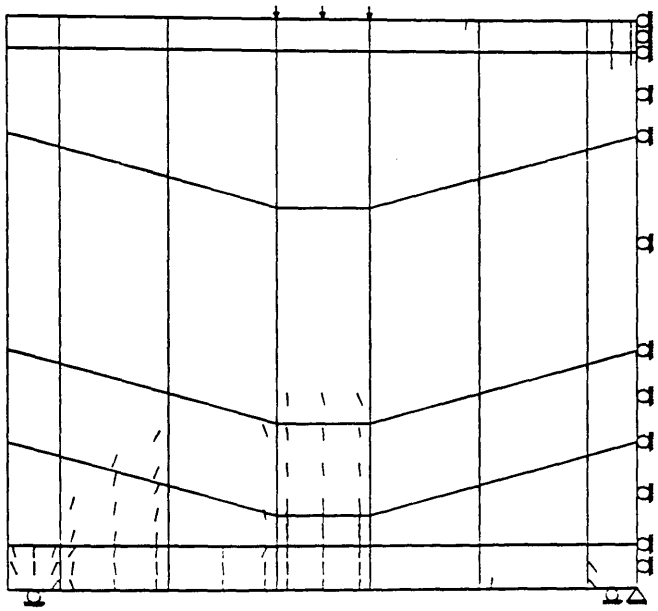

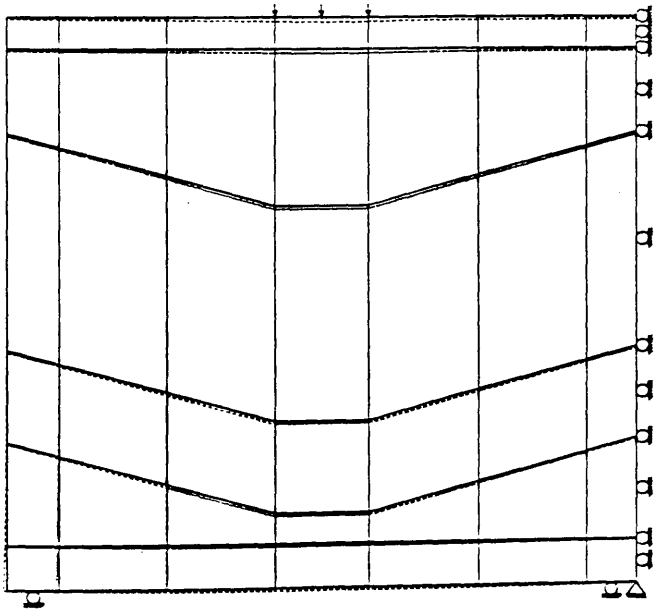

Figure(8.59) Predicted crack pattern and deformed shape at 600kN (TRGRAS7)

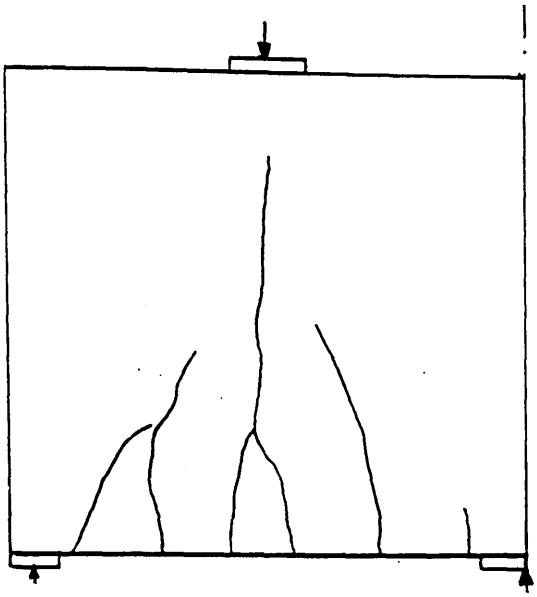

Experimental crack pattern at 800kN

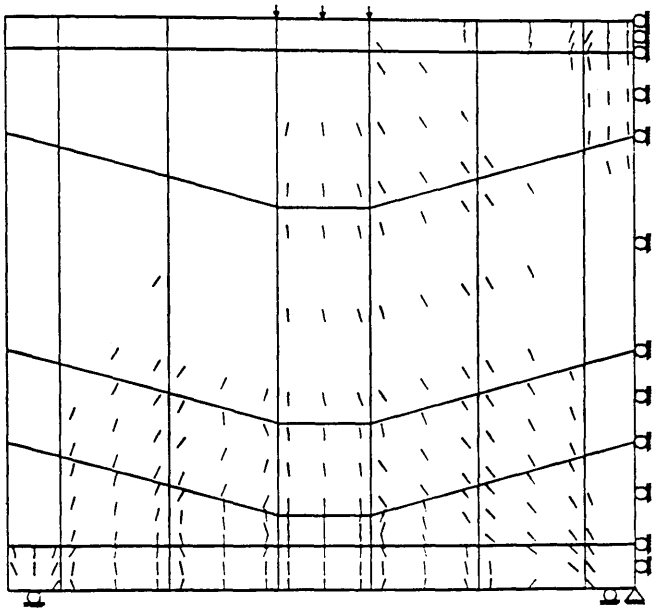

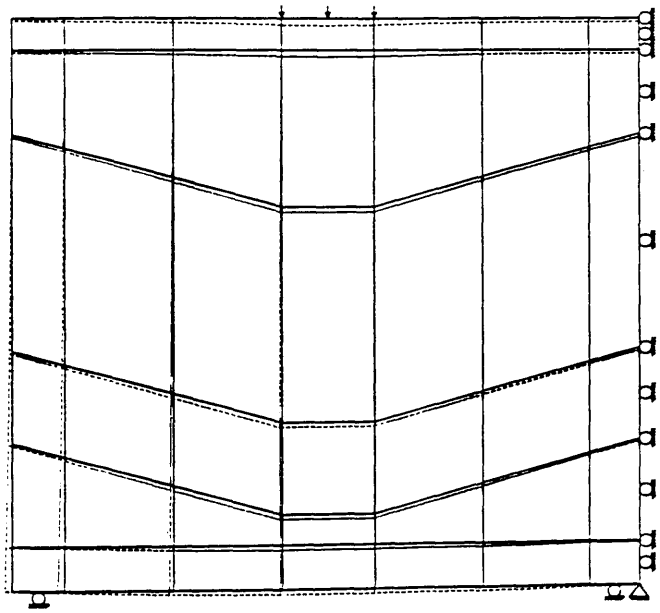

Figure(8.60) Predicted crack pattern and deformed shape at 825kN (TRGRAS7)

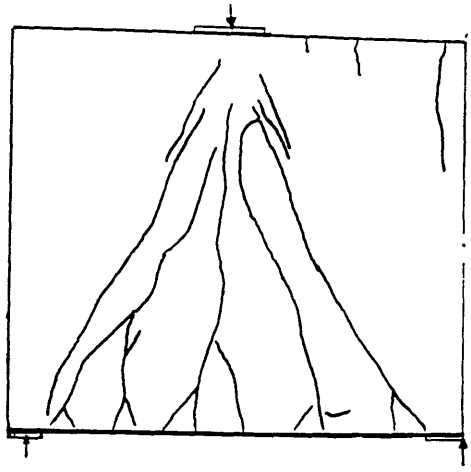

Experimental crack pattern at 1350kN

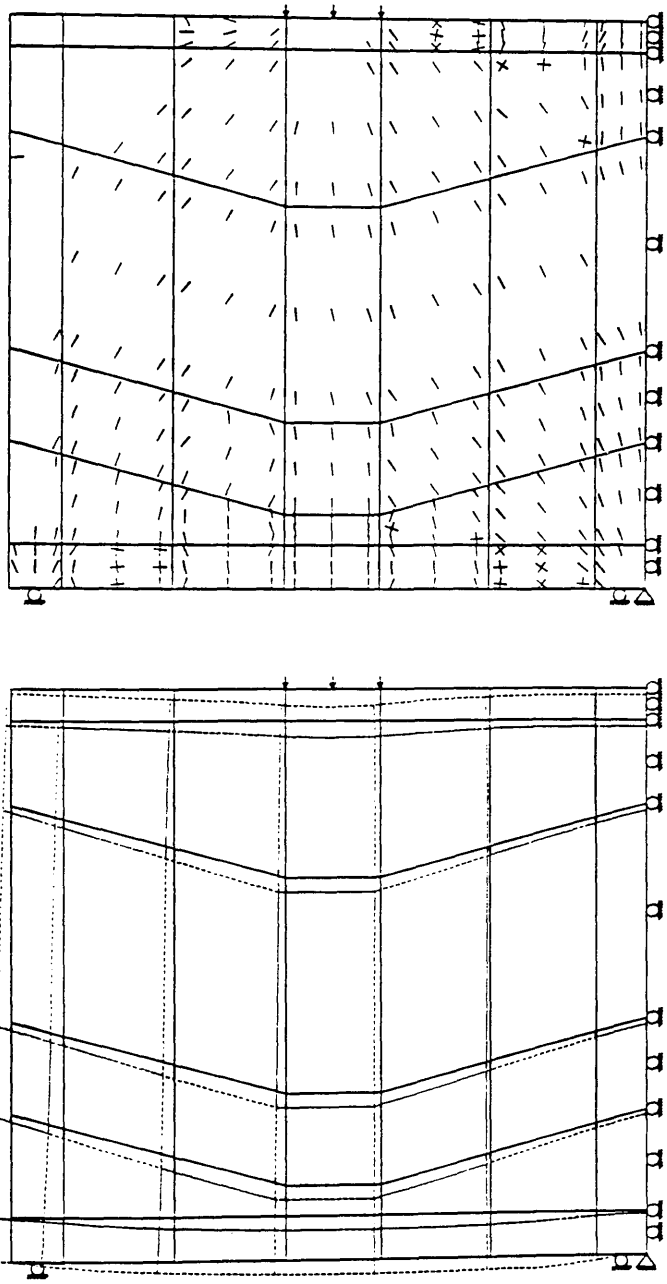

Figure(8.61) Predicted crack pattern and deformed shape at 1350kN (TRGRAS7)

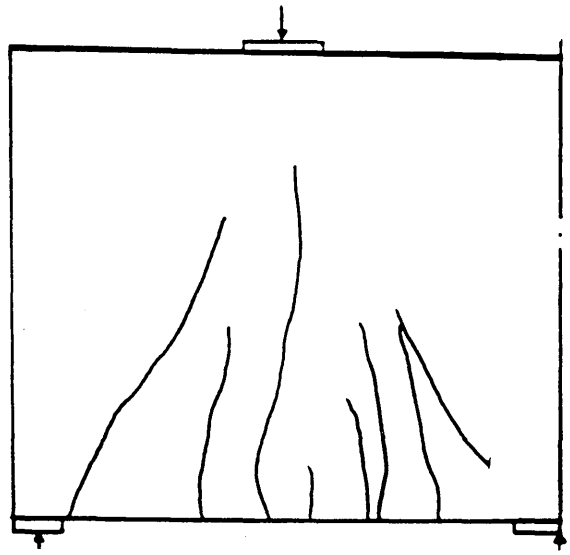

Experimental crack pattern at 500kN

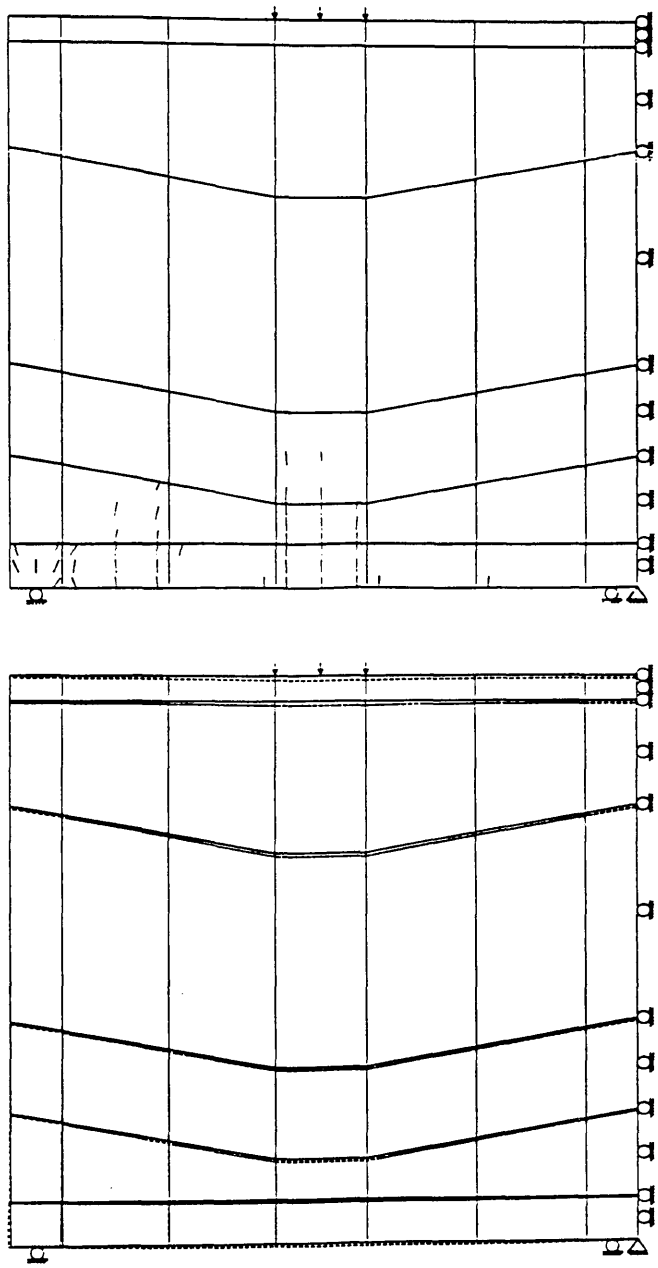

Figure(8.62) Predicted crack pattern and deformed shape at 525kN (TRGRAS8)

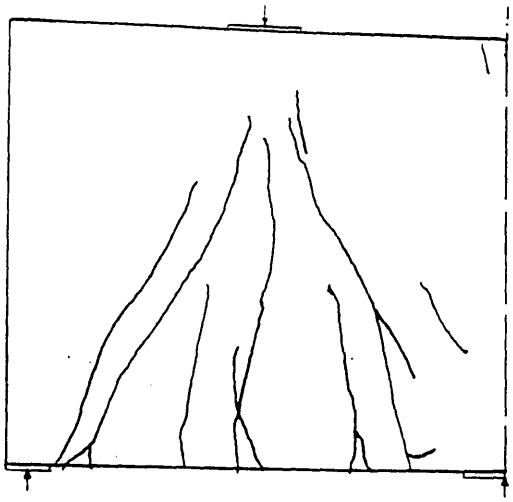

Experimental crack pattern at 800kN

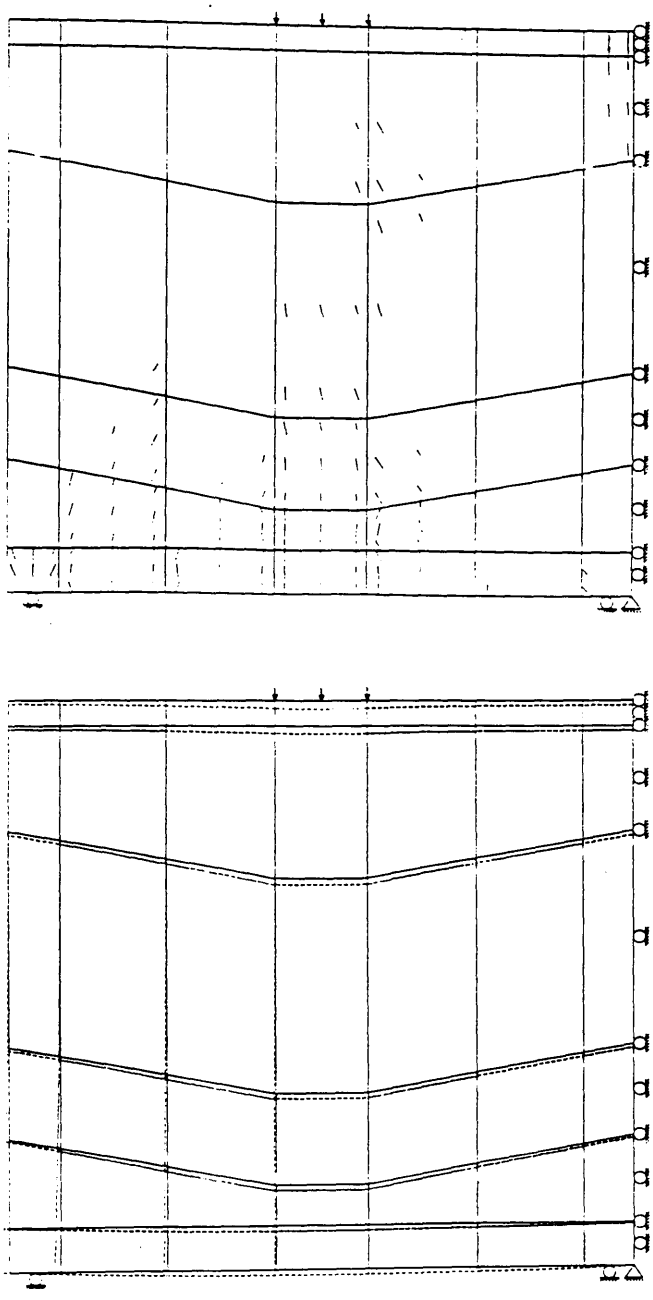

Figure(8.63) Predicted crack pattern and deformed shape at 825kN (TRGRAS8)

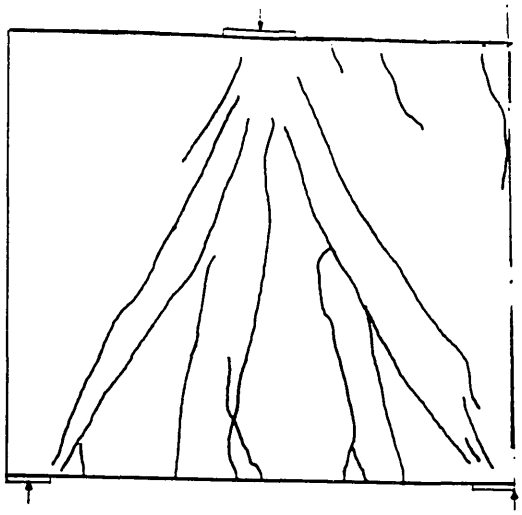

Experimental crack pattern at 1250kN

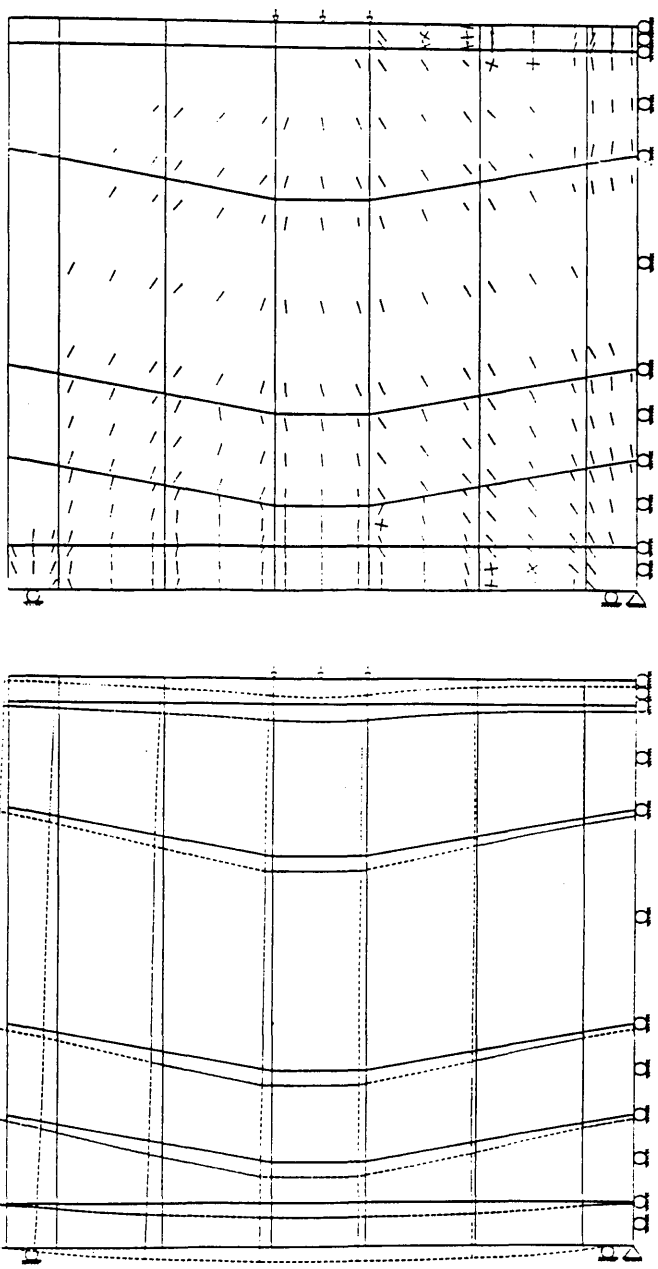

Figure(8.64) Predicted crack pattern and deformed shape at 1275kN (TRGRAS8)

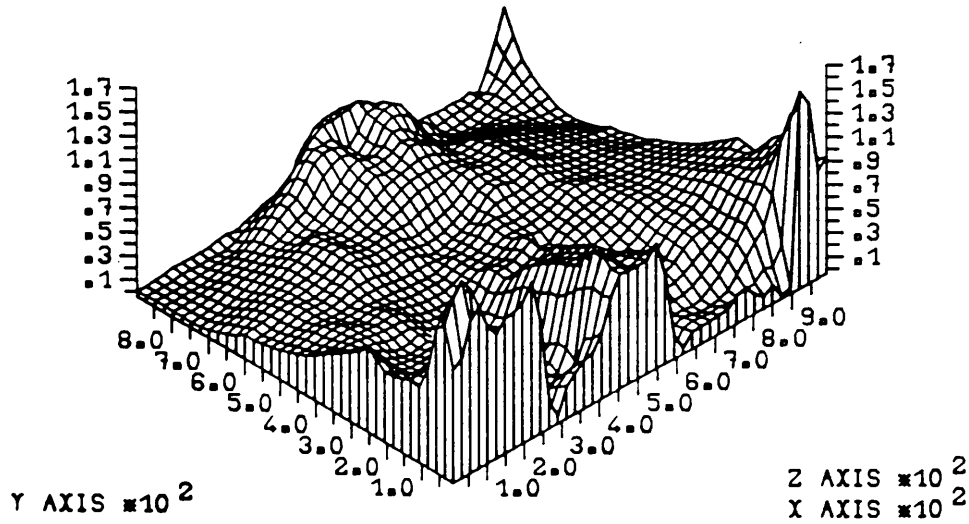

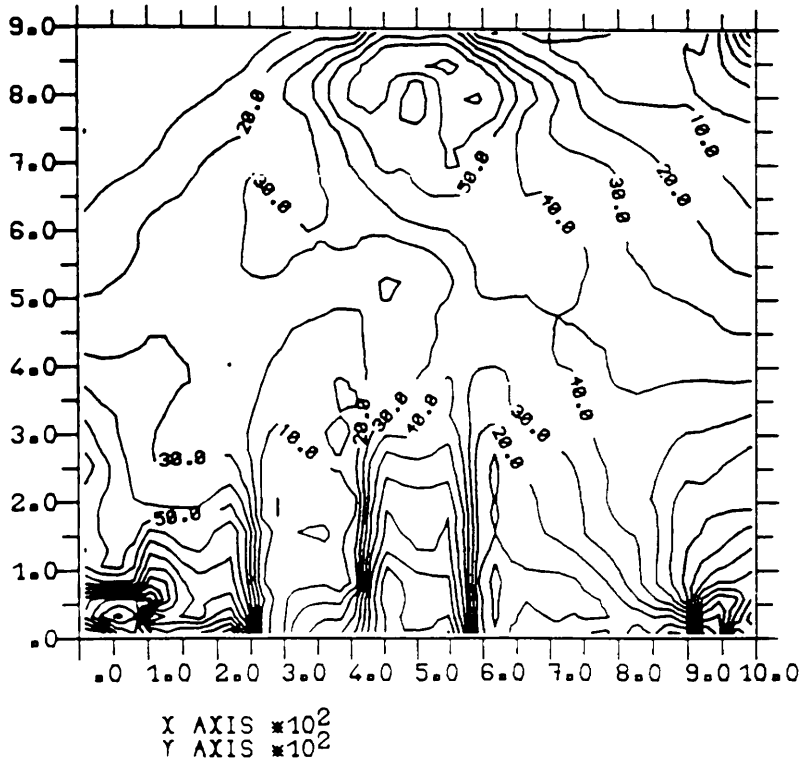

Figure(8.65) Predicted maximum shear strain*10^{-5} at 600kN (TRGRAS7)

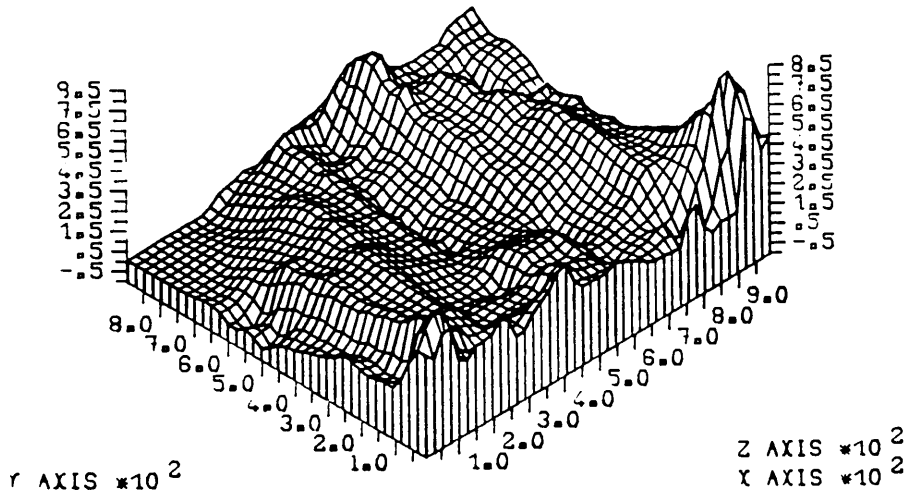

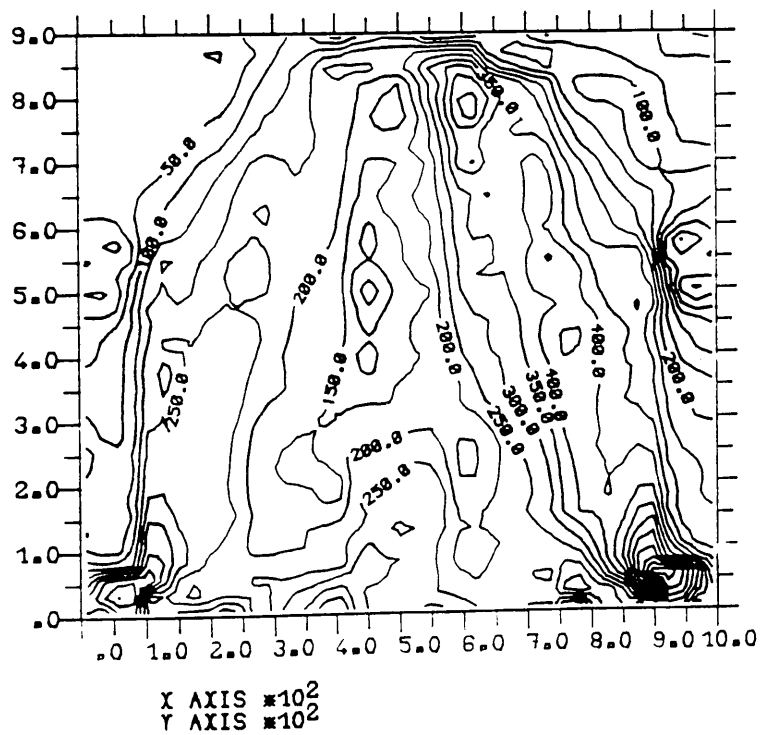

Figure(8.66) Predicted maximum shear strain*10^{-5} at 1350kN (TRGRAS7)

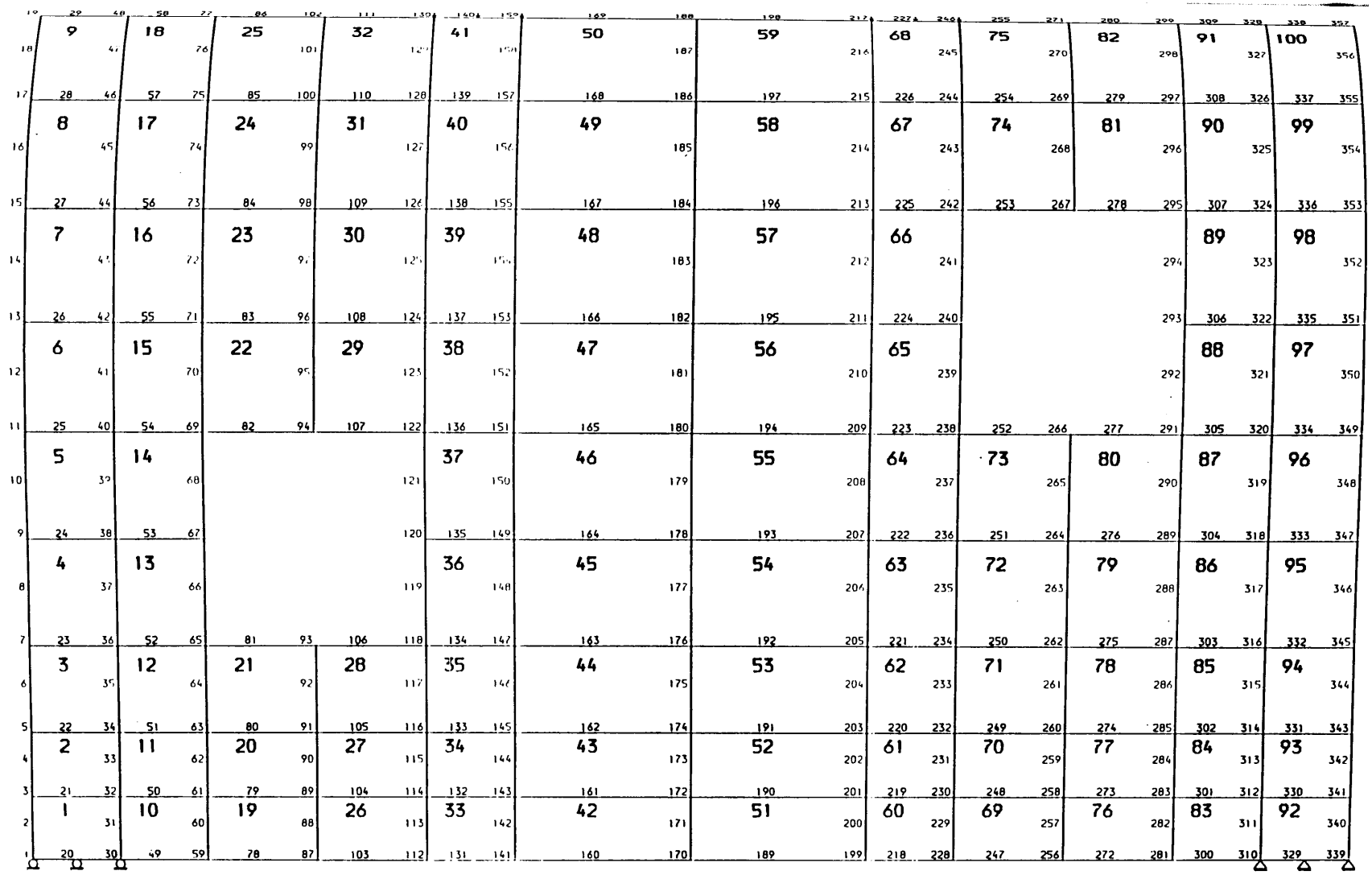

Figure(8.67) Finite element analysis mesh for girder TRGRAS9

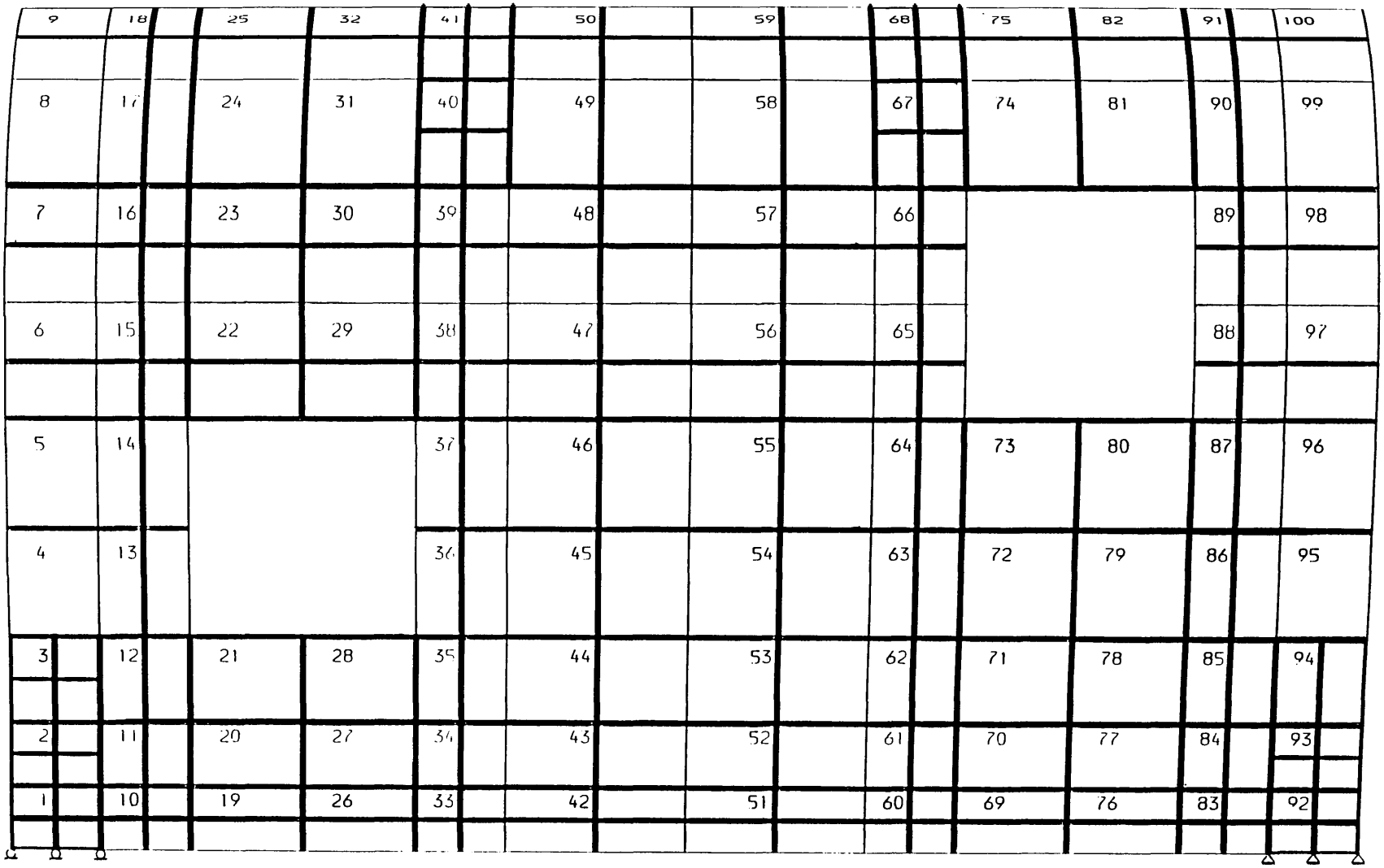

Figure(8.68) Reinforcement detail in finite element analysis for girder TRGRAS9

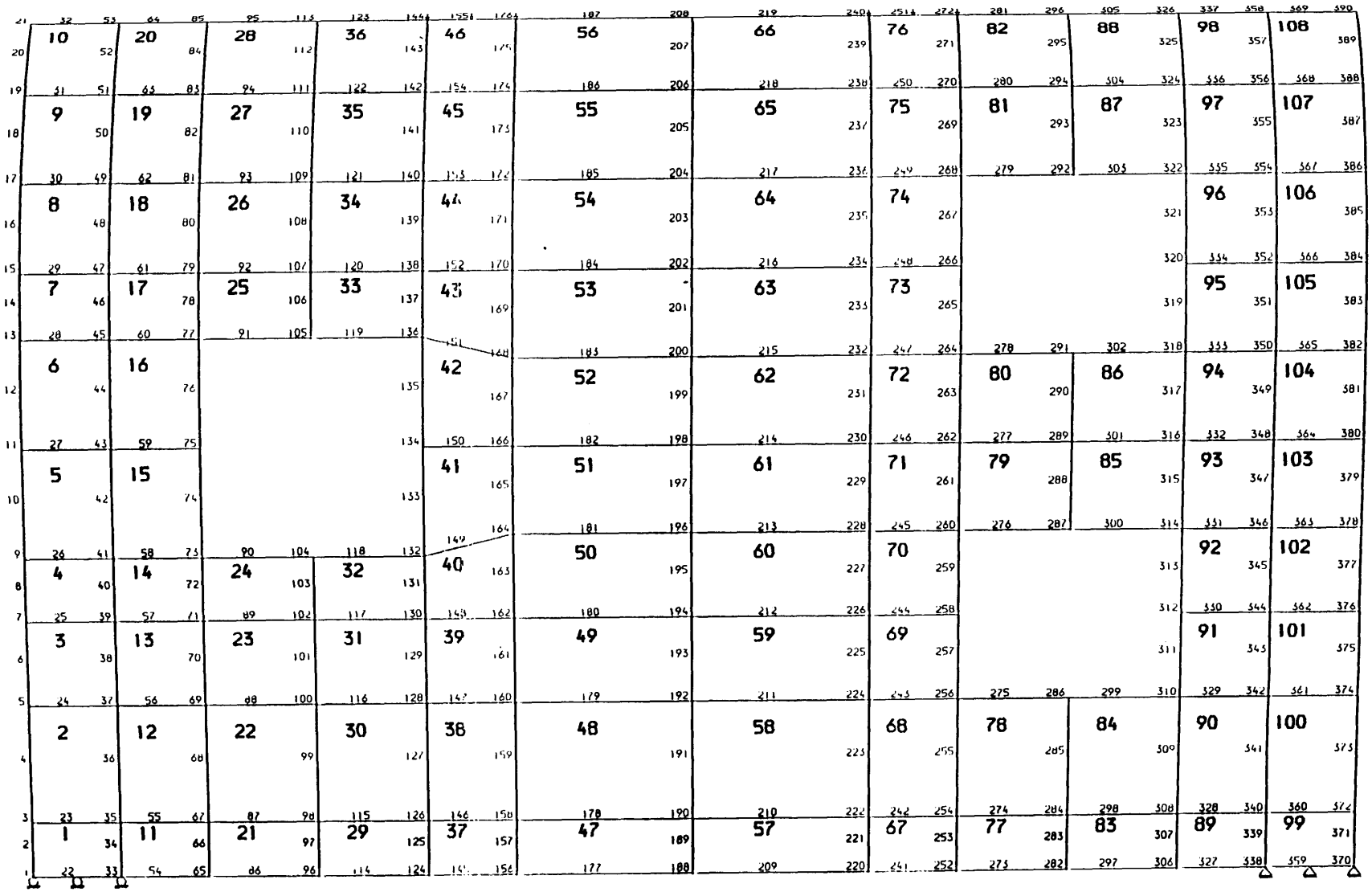

Figure(8.69) Finite element analysis mesh for girder TRGRAS10

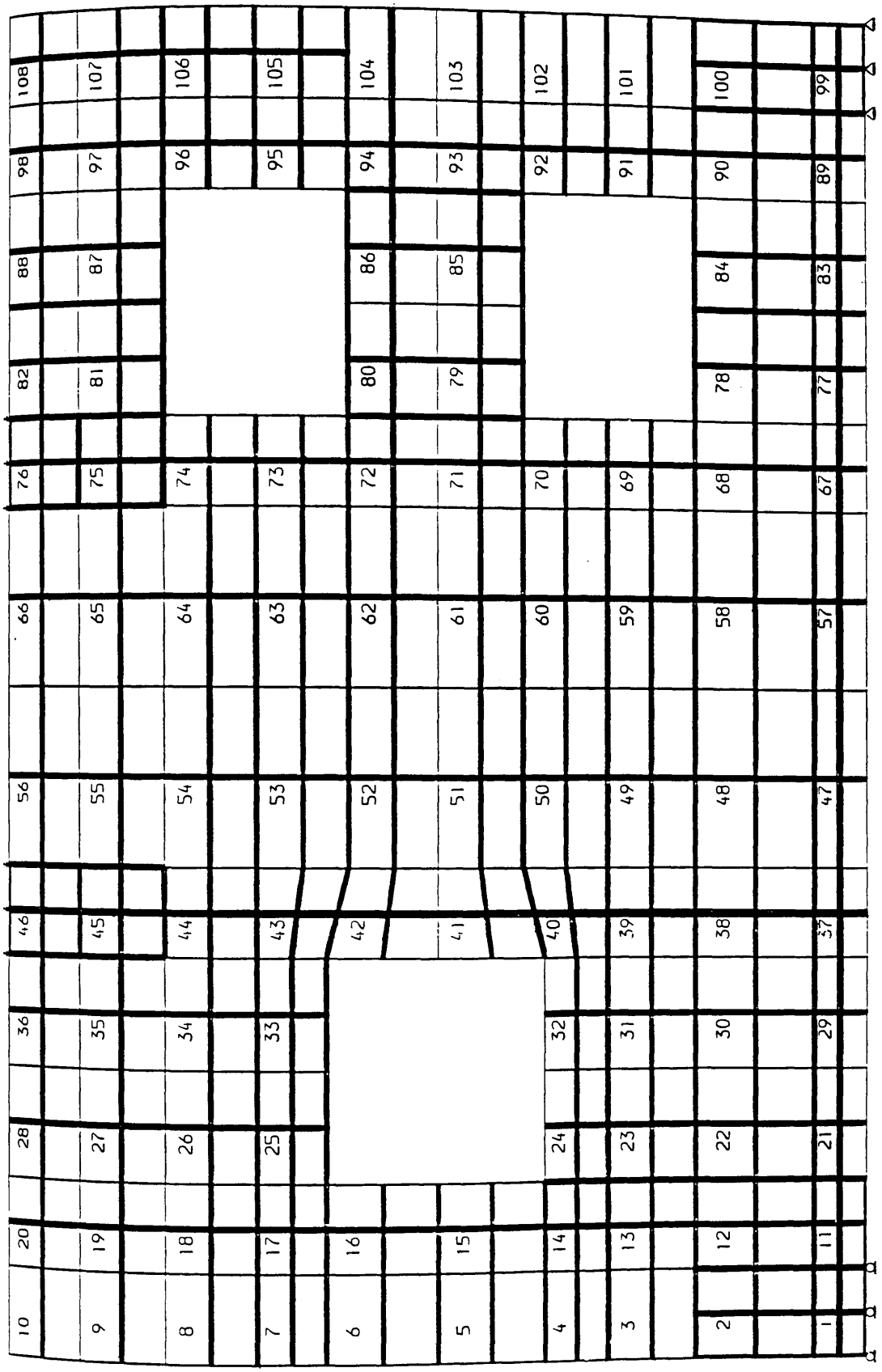

Figure(8.70) Reinforcement detail in finite element analysis for girder TRGRAS10

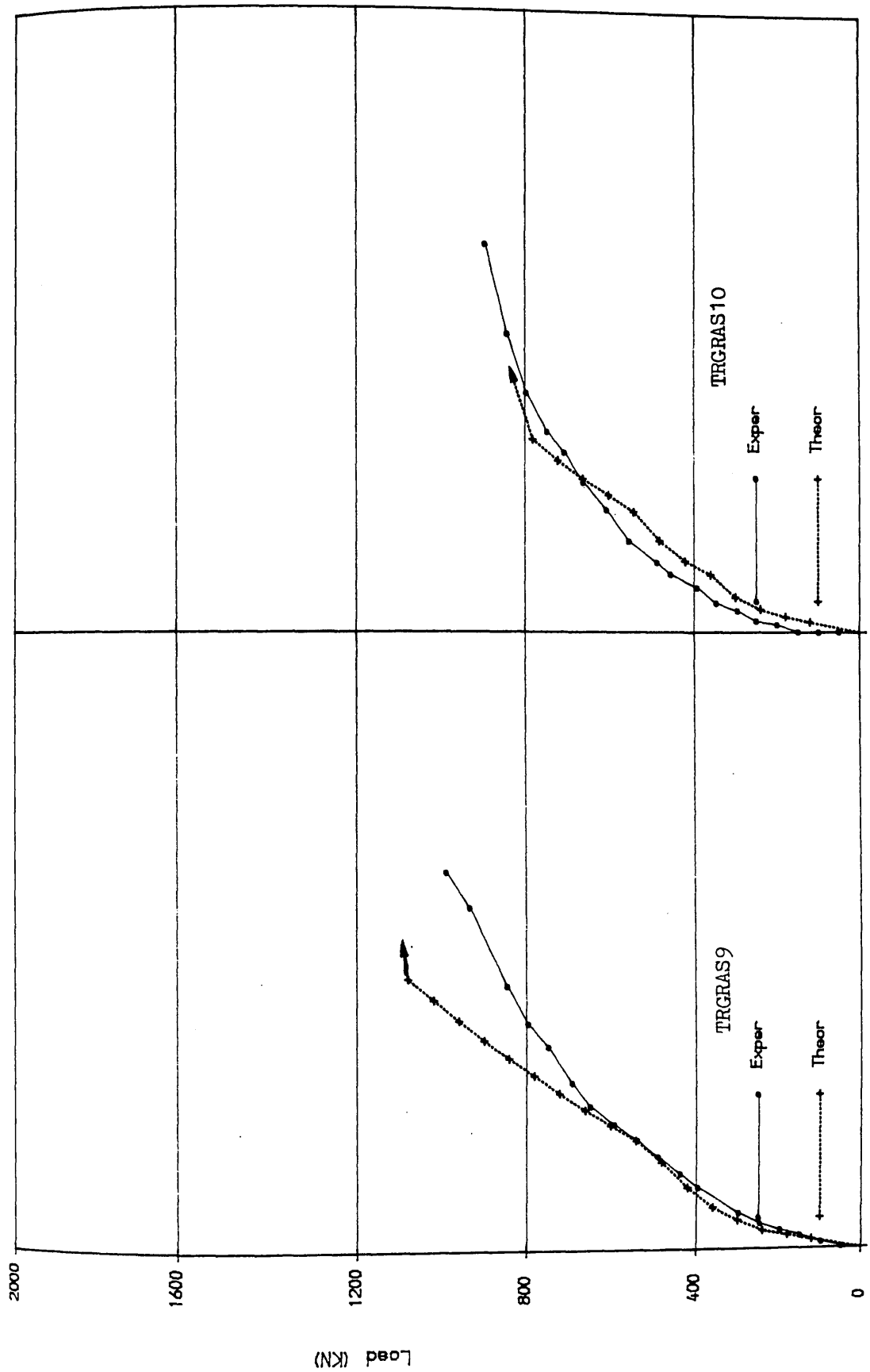

FIG (8.71) Load deflection curves for girders TRGRAS9 and TRGRAS10

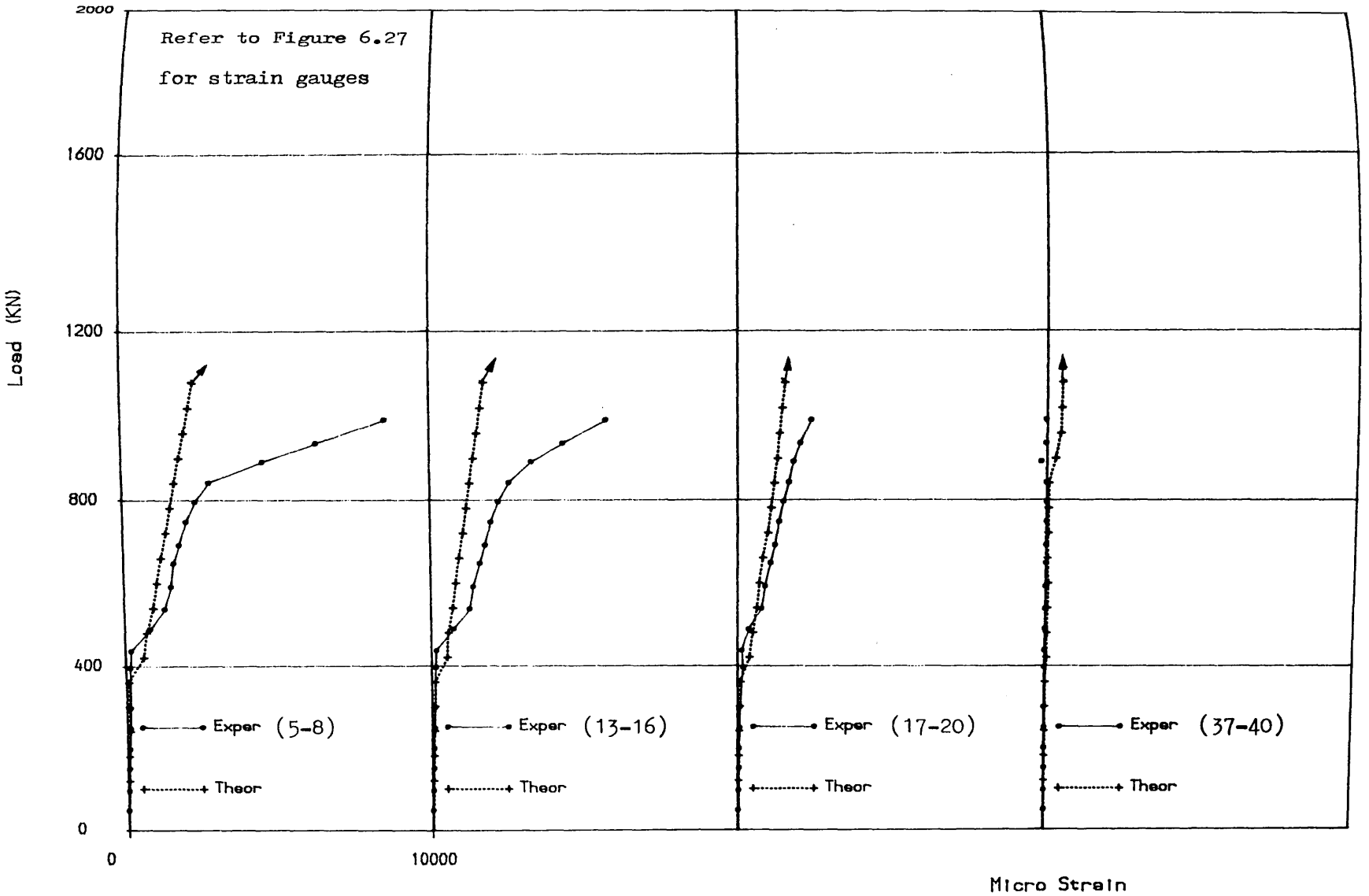

FIG (8.72) Comparison of longitudinal steel strains for girder TRGRAS9

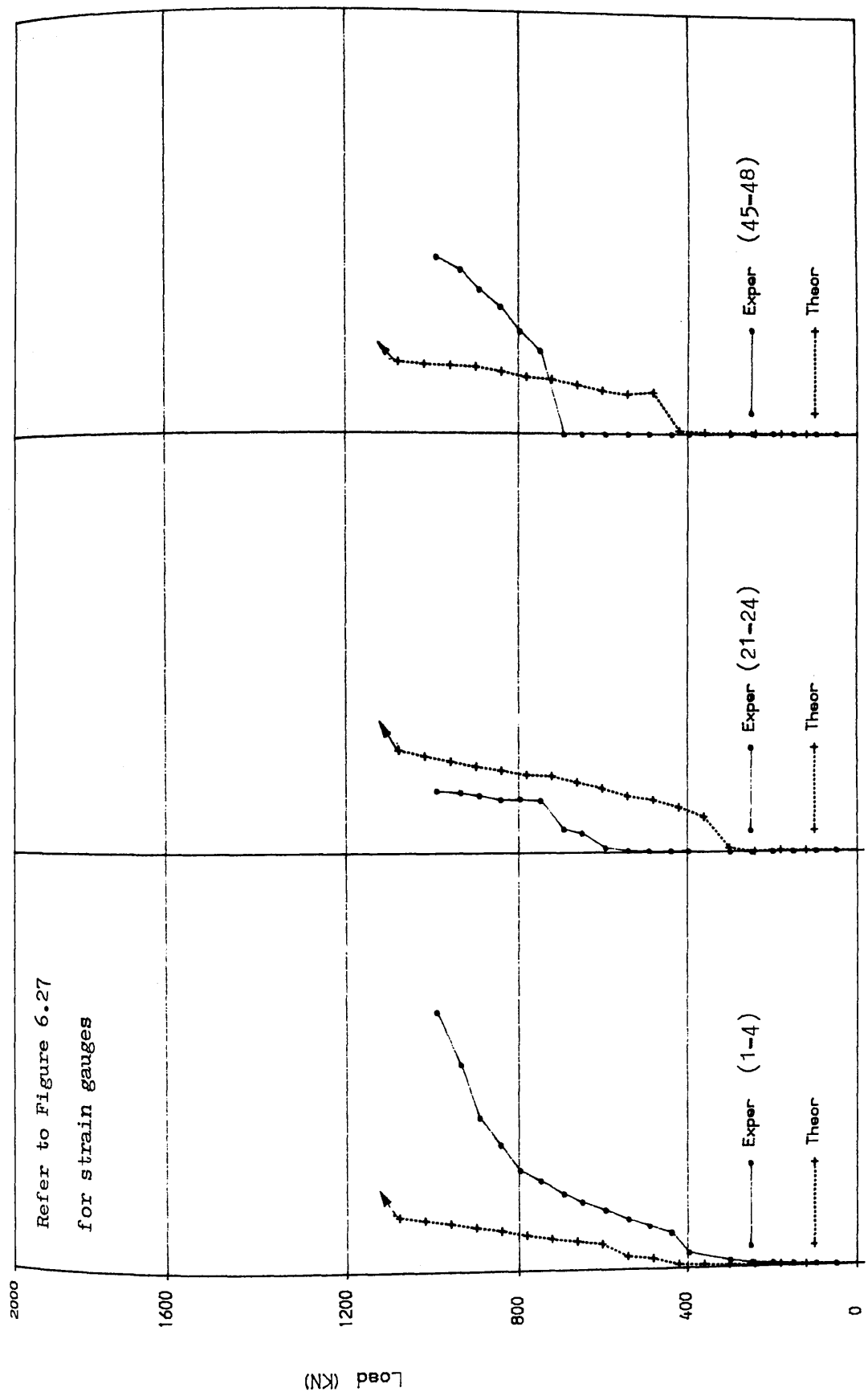

FIG (8.72) Continued

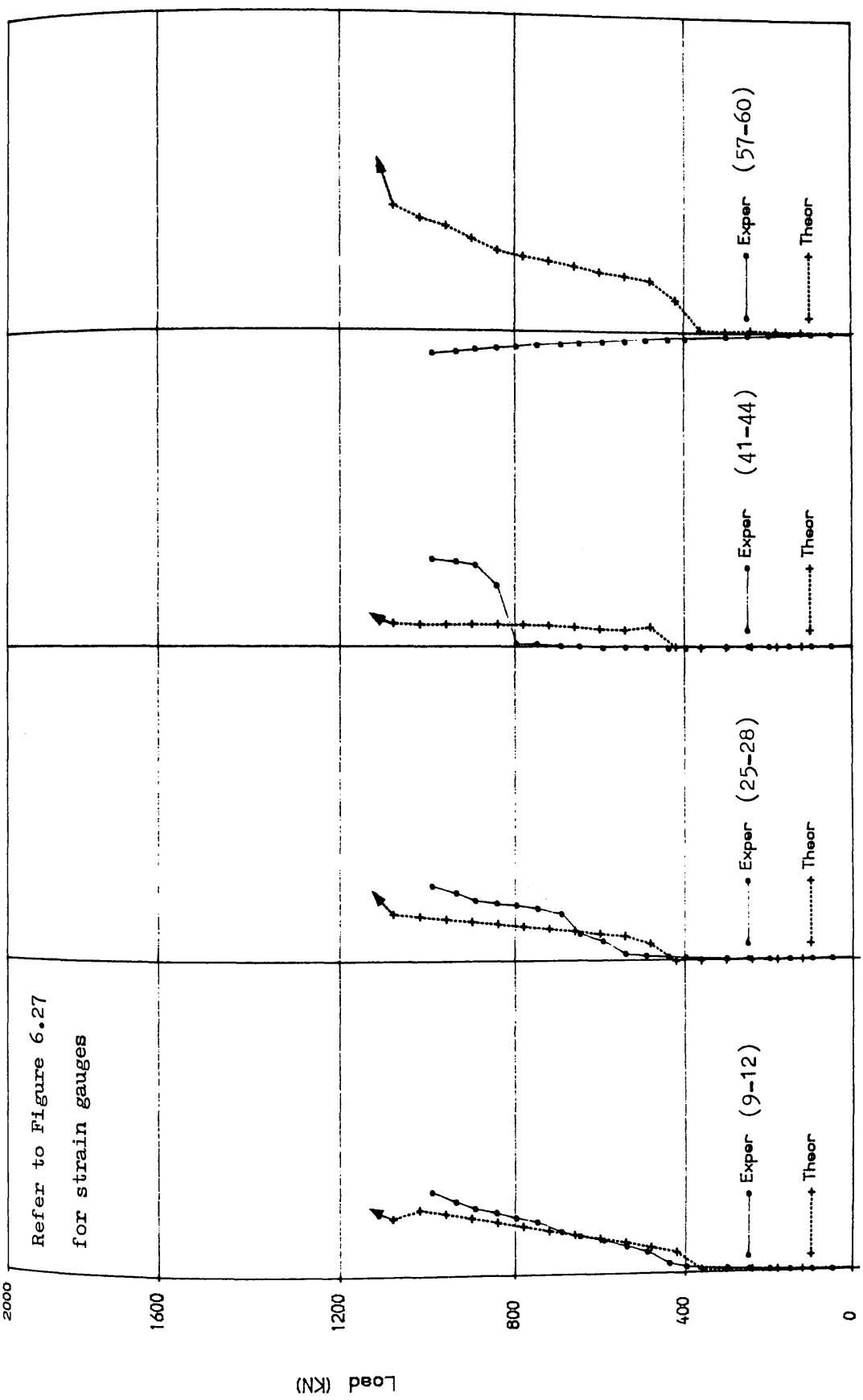

FIG (8.72) Continued

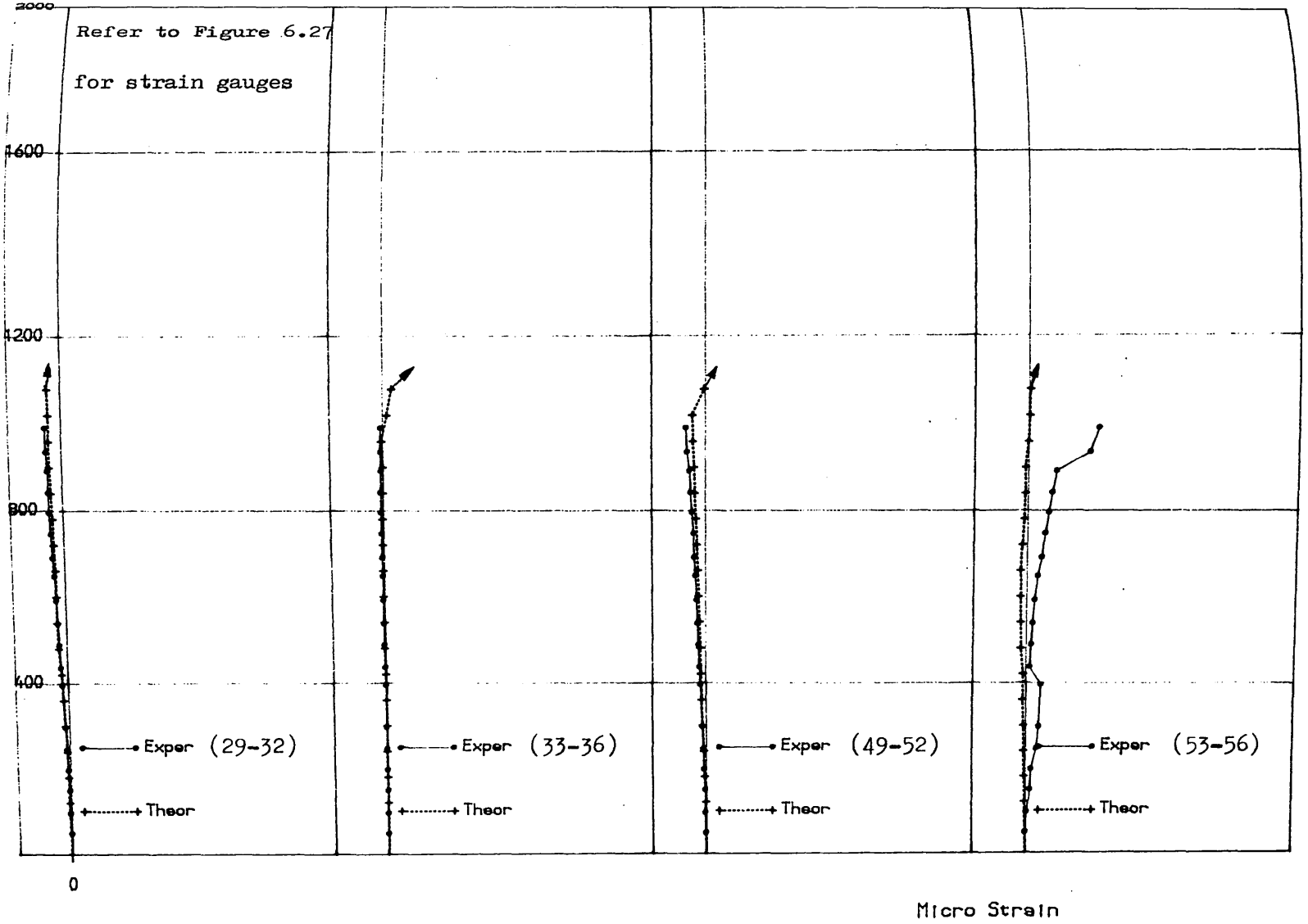

FIG (8.73) Comparison of stirrup strain in shear span for girder TRGRAS9

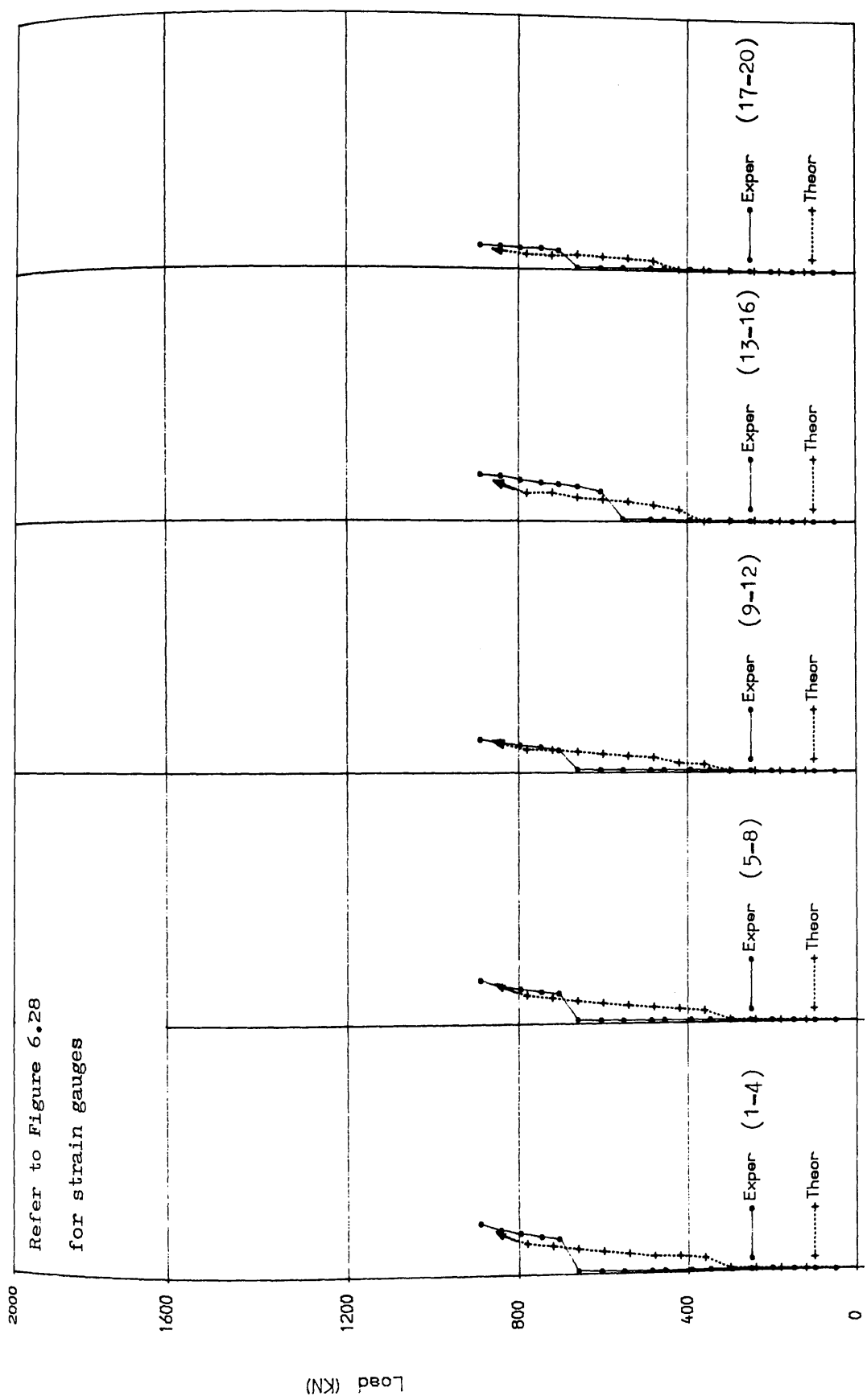

FIG(8.74) Comparison of longitudinal steel strains for girder TRGRAS10

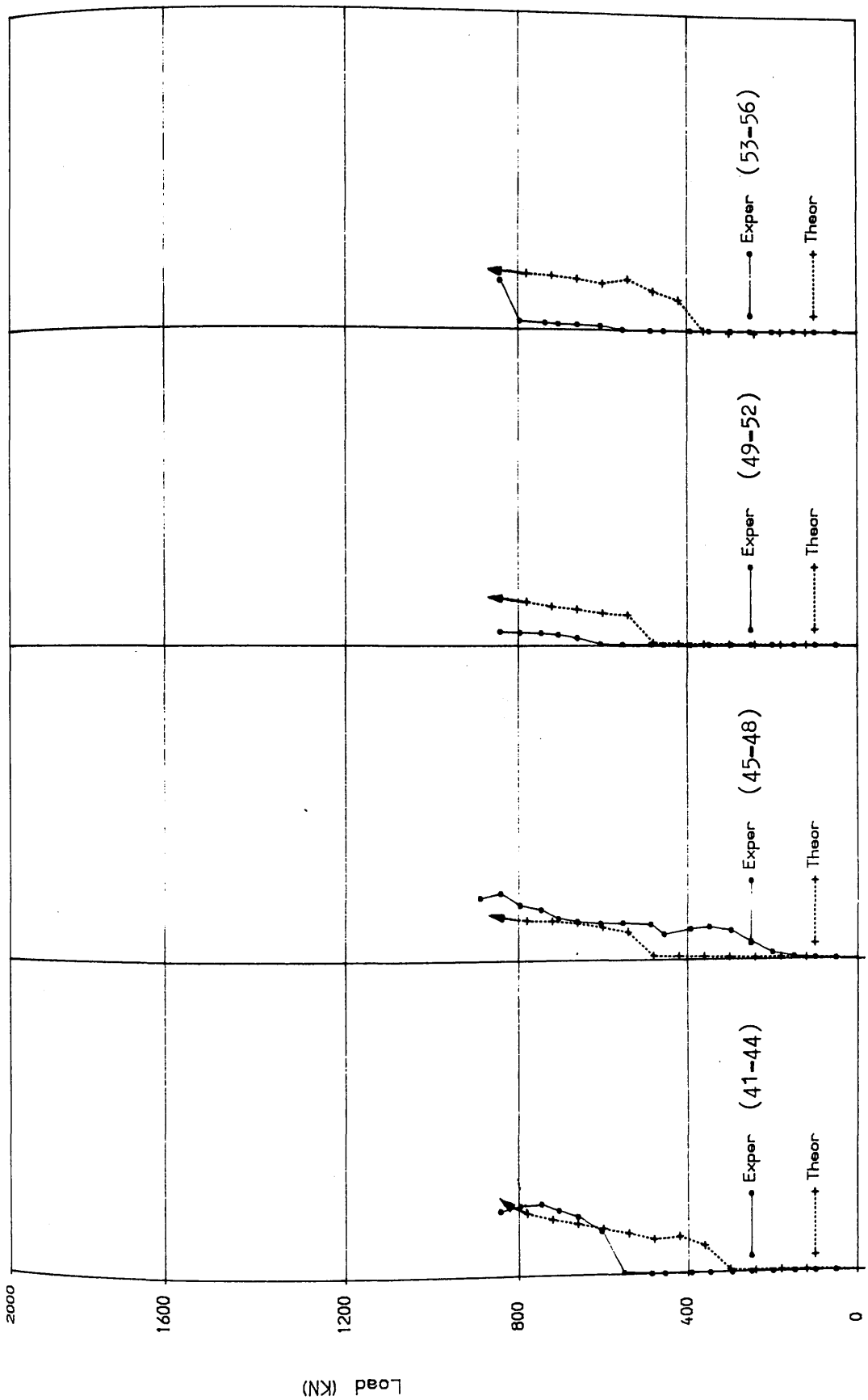

FIG (8.74) Continued

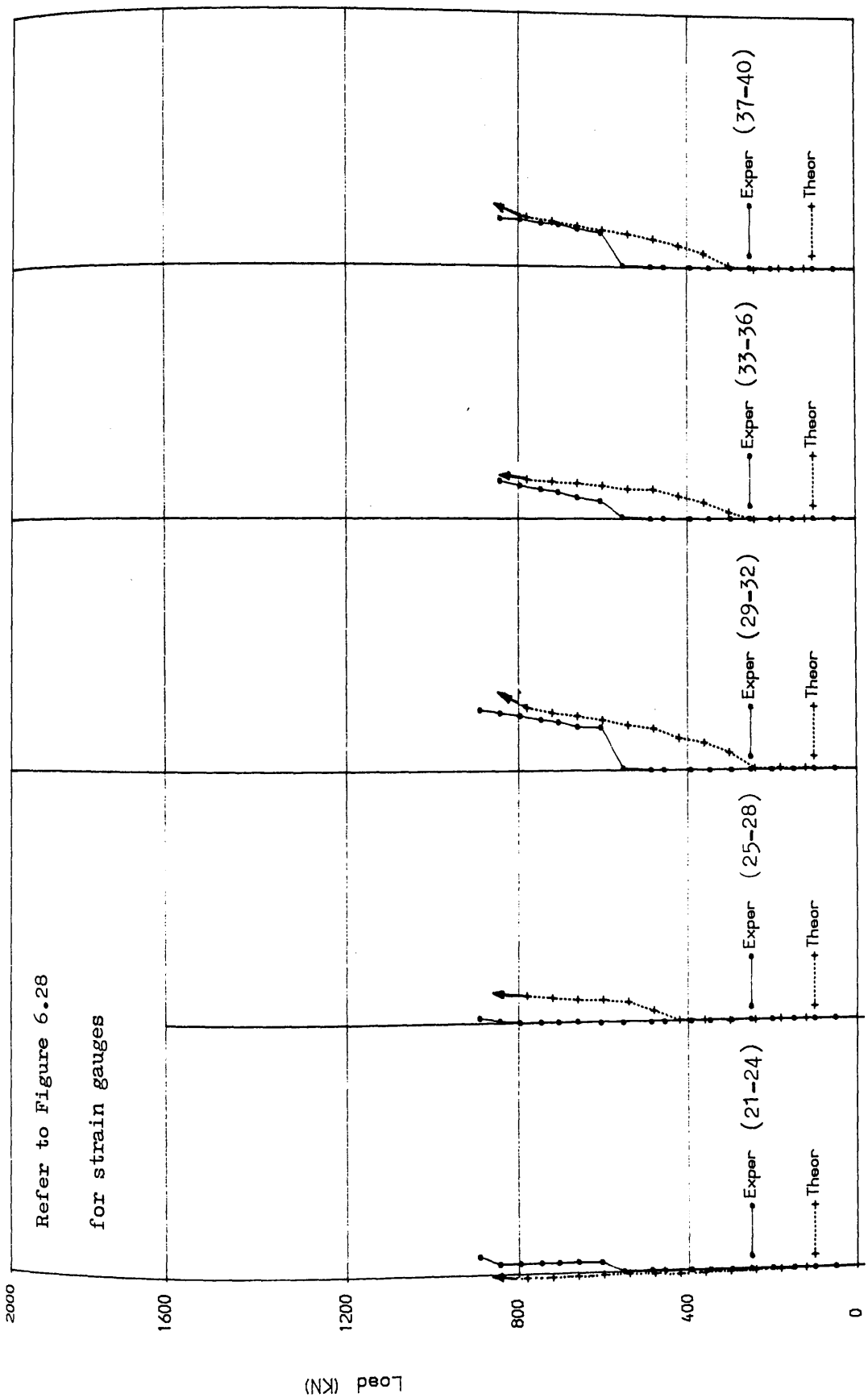

FIG (8.74) Continued

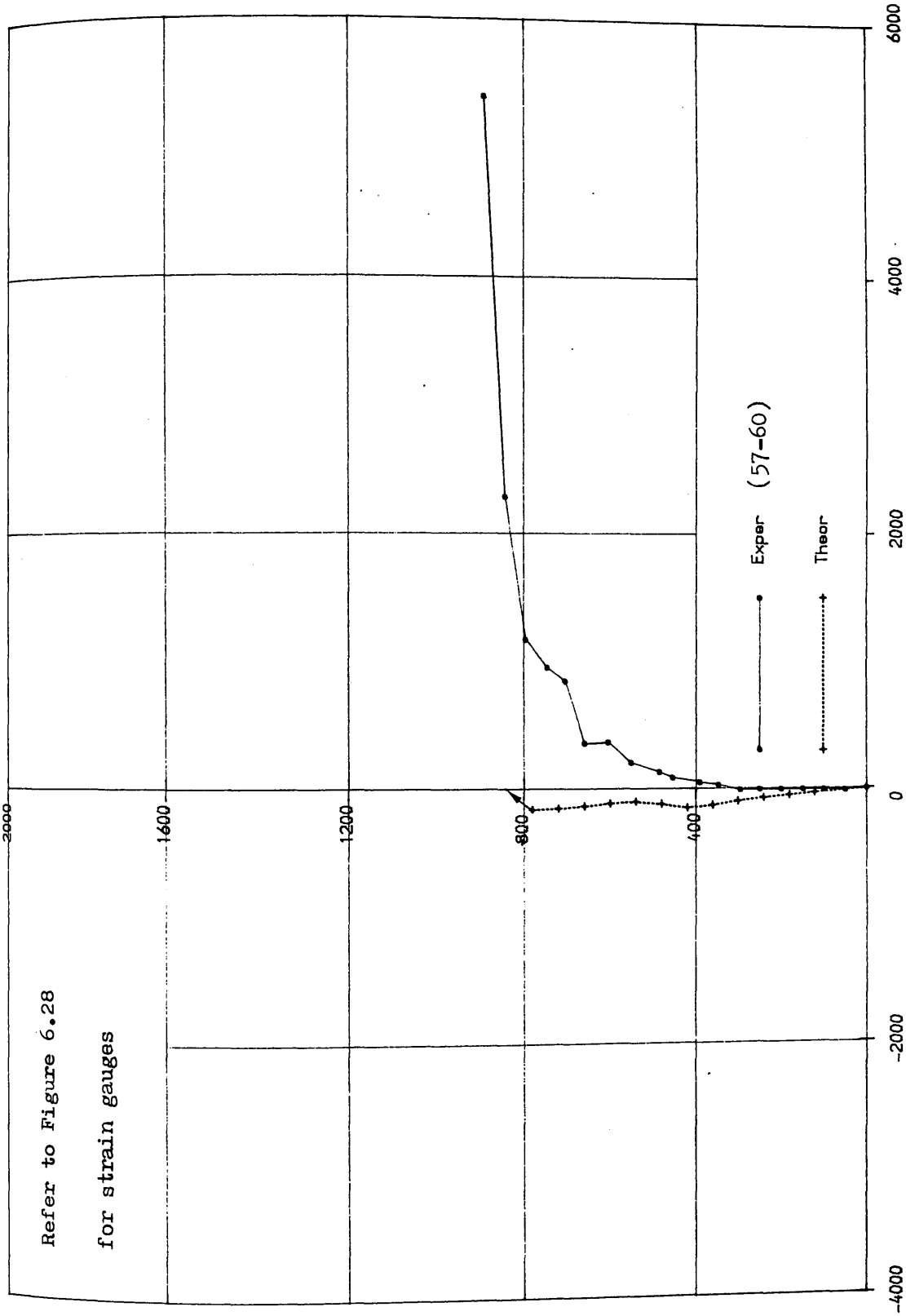

FIG(8.75) Comparison of stirrup strain in shear span for girder TRGRAS10

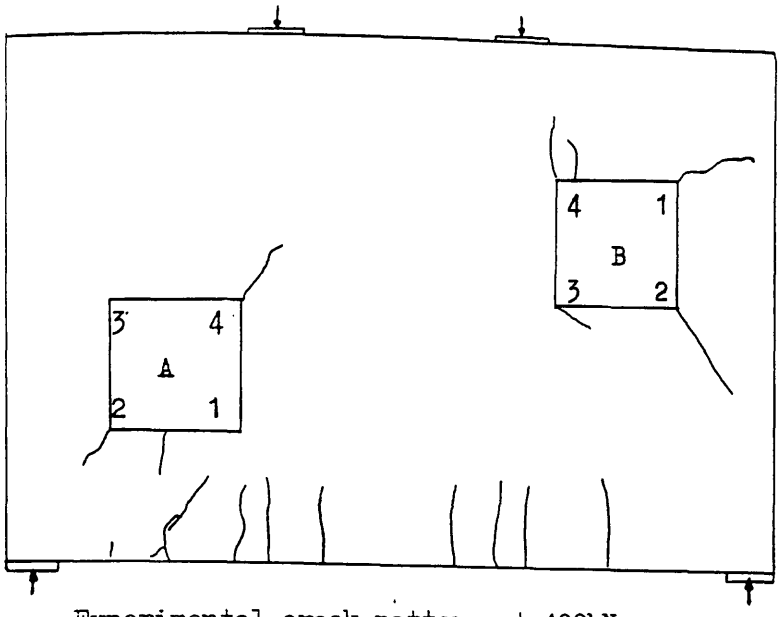

Experimental crack pattern at 400kN

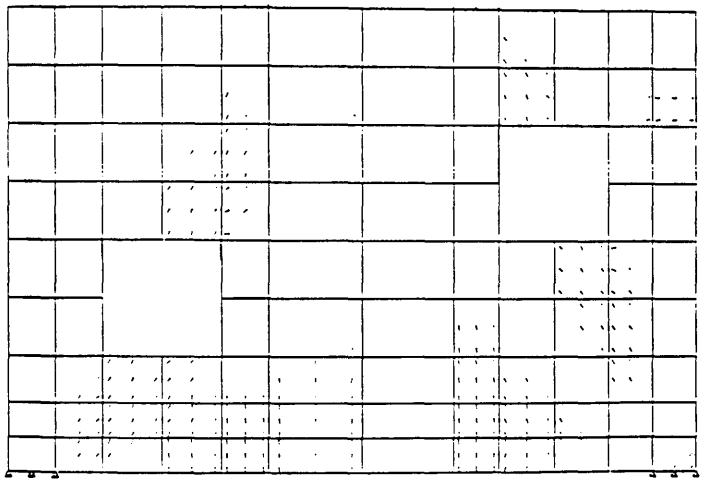

Predicted crack pattern at 420kN

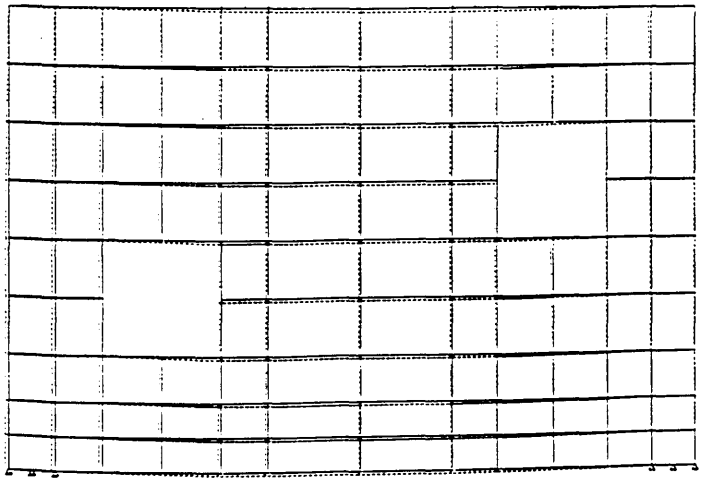

Predicted deformed shape at 420kN

Figure(8.76) Predicted crack pattern and deformed shape at 420kN (TRGRAS9)

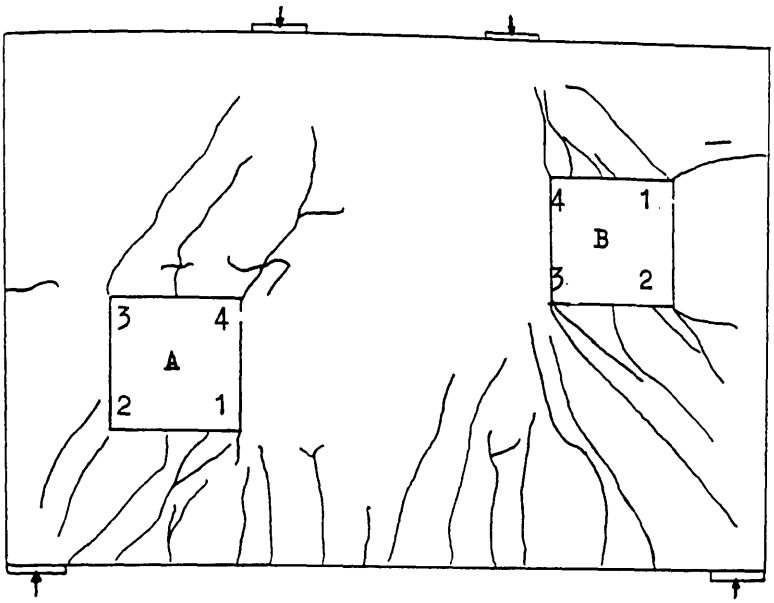

Experimental crack pattern at 700kN

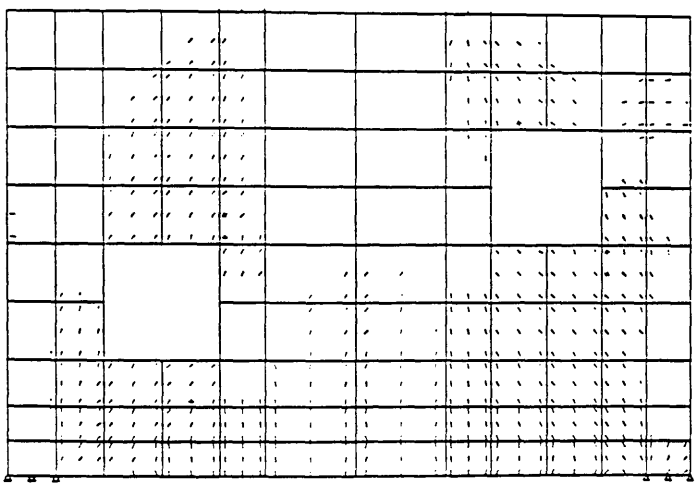

Predicted crack pattern at 720kN

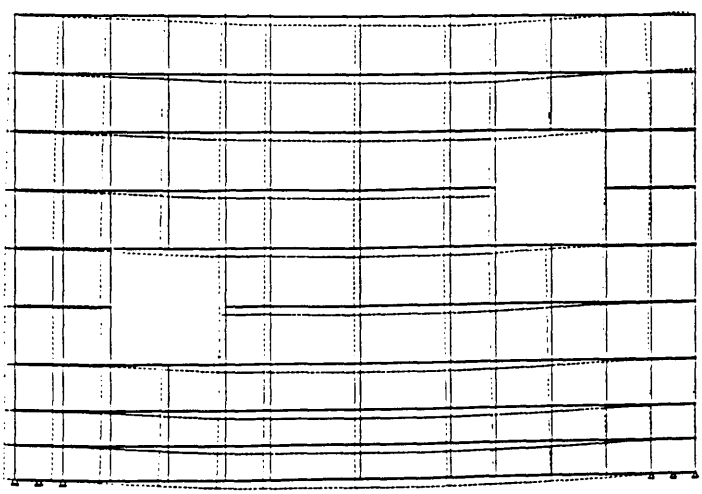

Predicted deformed shape at 720kN

Figure(8.77) Predicted crack pattern and deformed shape at 720kN (TRGRAS9)

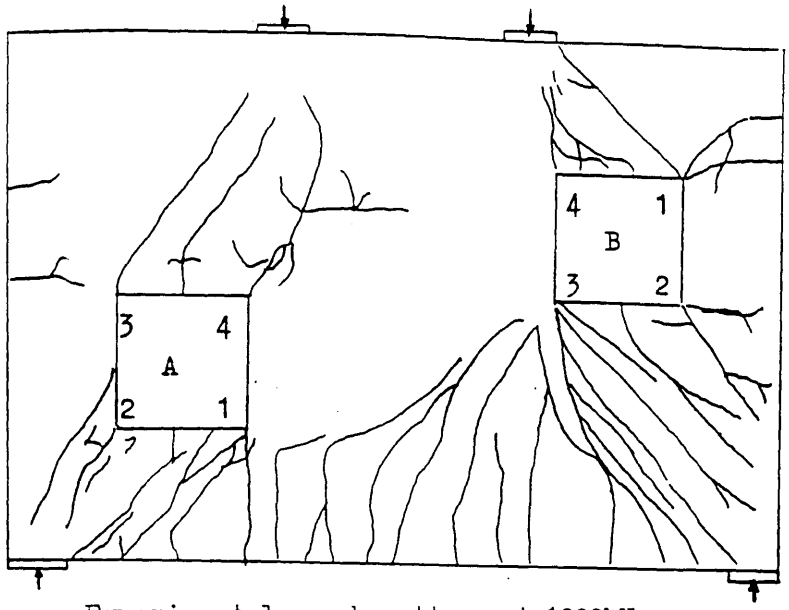

Experimental crack pattern at 1000kN

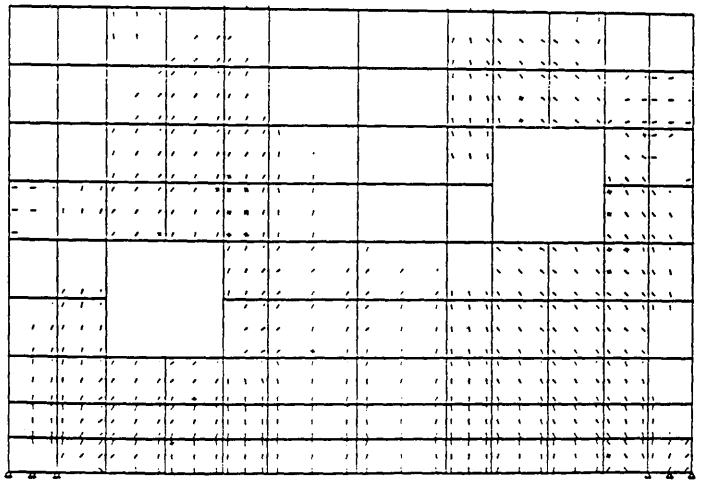

Predicted crack pattern at 1020kN

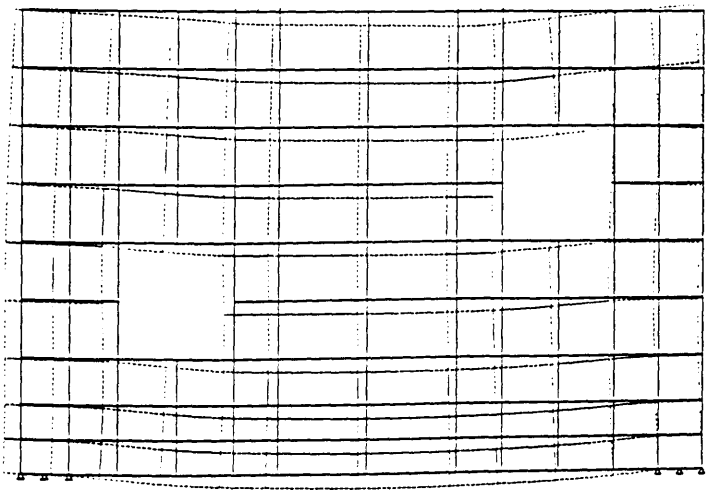

Predicted deformed shape at 1020kN

Figure(8.78) Predicted crack pattern and deformed shape at 1020kN (TRGRAS9)

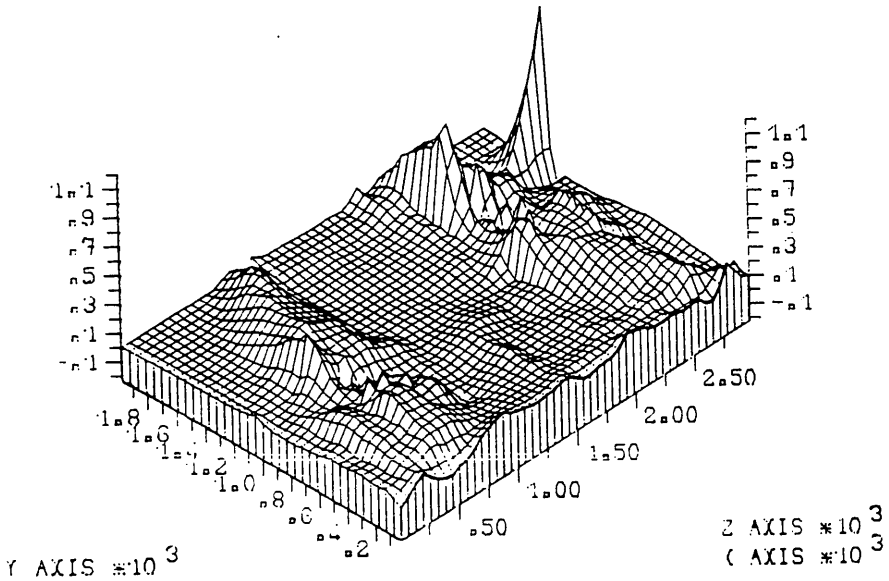

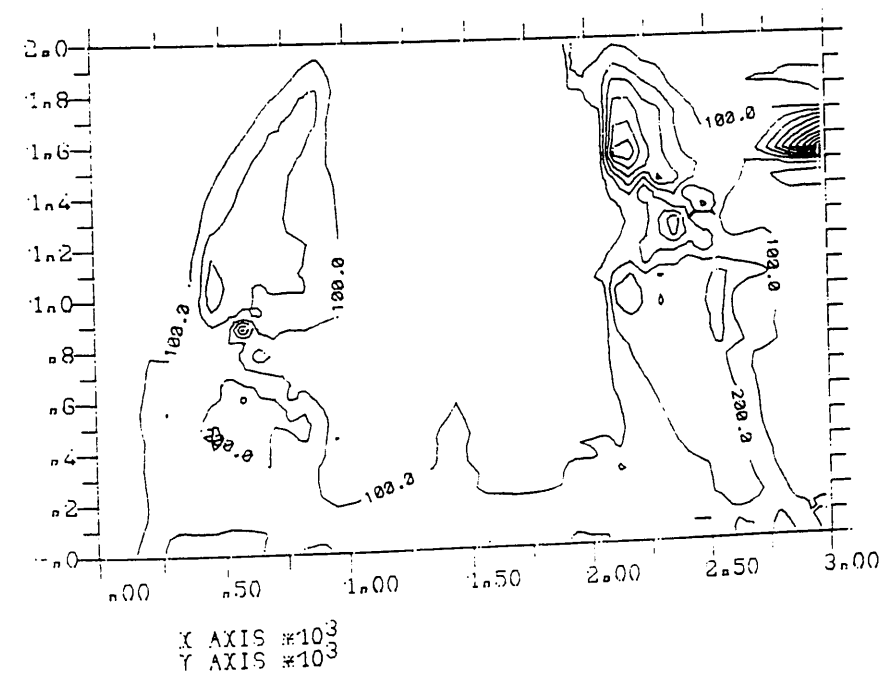

Figure (8.79) Predicted maximum shear strain*10^{-5} at 1760kN (TRGRAS9).

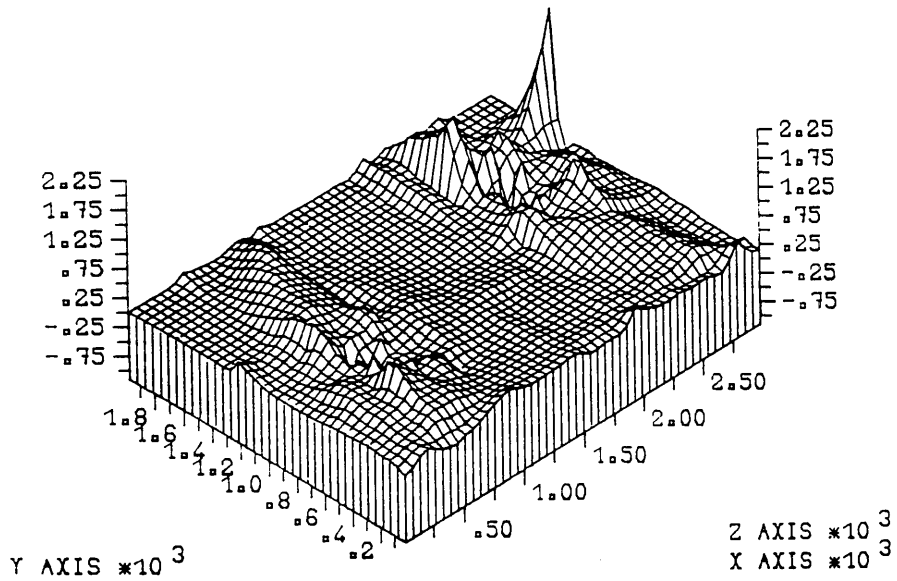

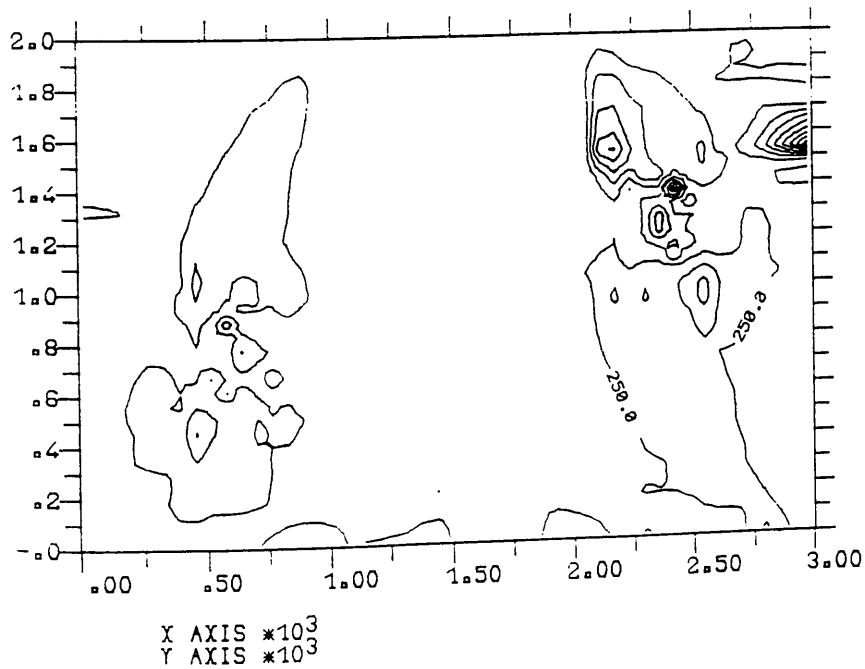

Figure (8.80) Predicted maximum shear strain*10^{-5} at 1080kN (TRGRAS9).

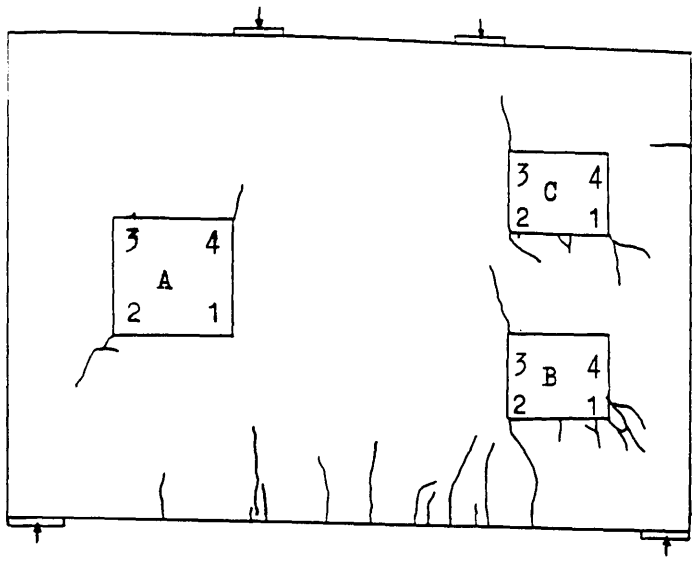

Experimental crack pattern at 400kN

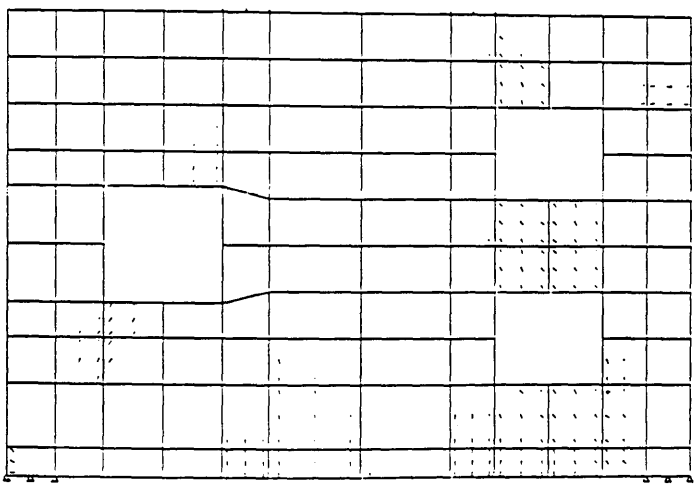

Predicted crack pattern at 420kN

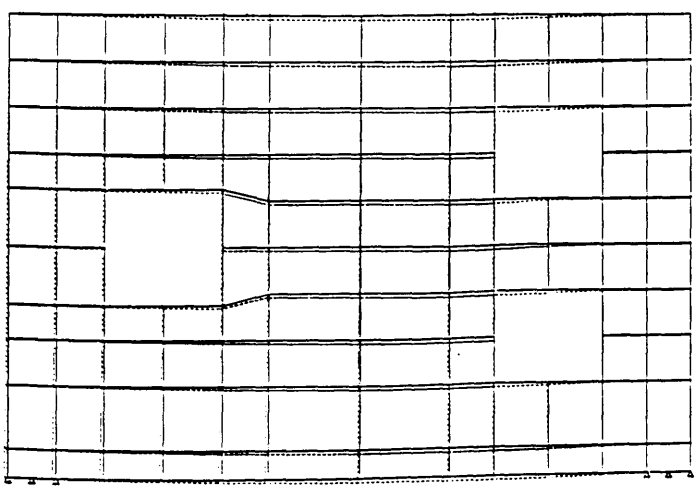

Predicted deformed shape at 420kN

Figure(8.81) Predicted crack pattern and deformed shape at 420kN (TRGRAS10)

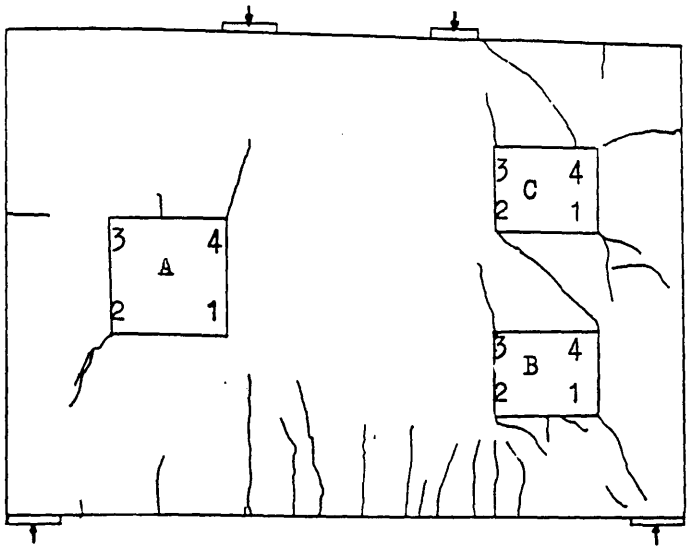

Experimental crack pattern at 700kN

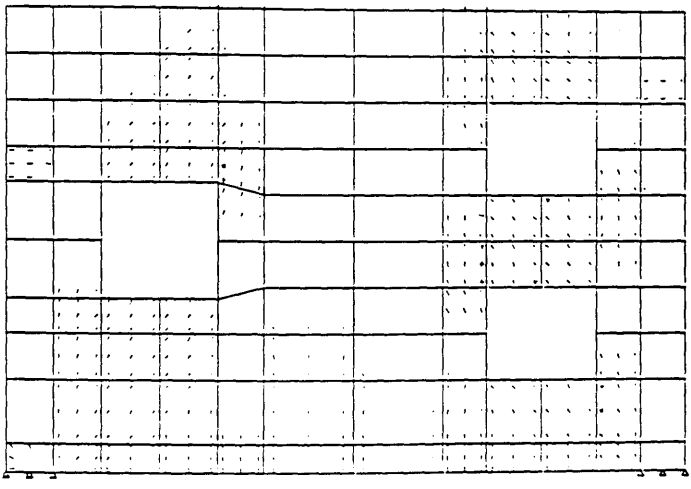

Predicted crack pattern at 720kN

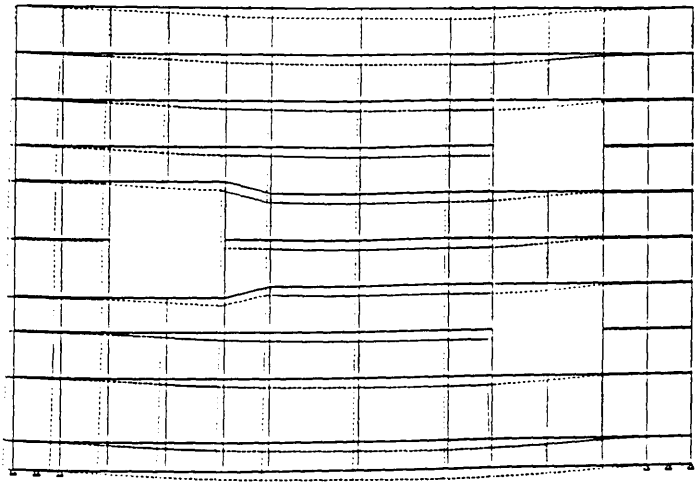

Predicted deformed shape at 720kN

Figure(8.82) Predicted crack pattern and deformed shape at 720kN (TRGRAS10)

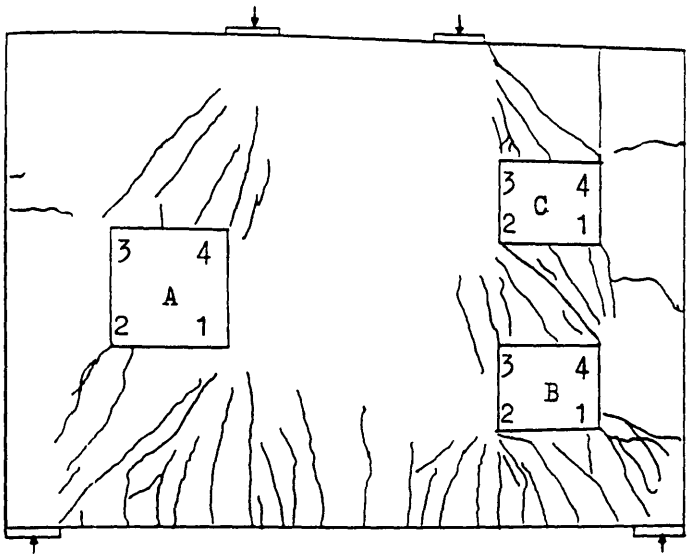

Experimental crack pattern at 800kN

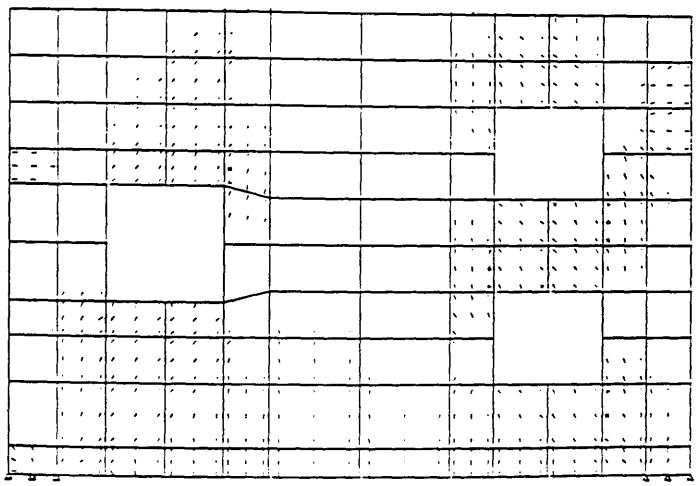

Predicted crack pattern at 780kN

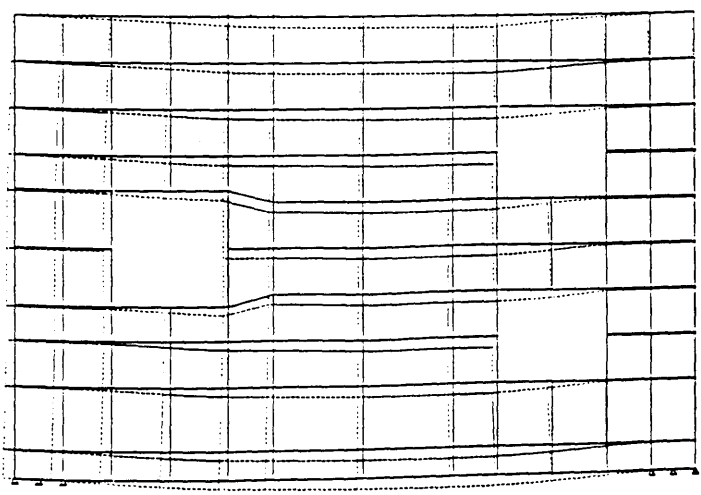

Predicted deformed shape at 760kN

Figure(8.83) Predicted crack pattern and deformed shape at 780kN (TRGRAS10)

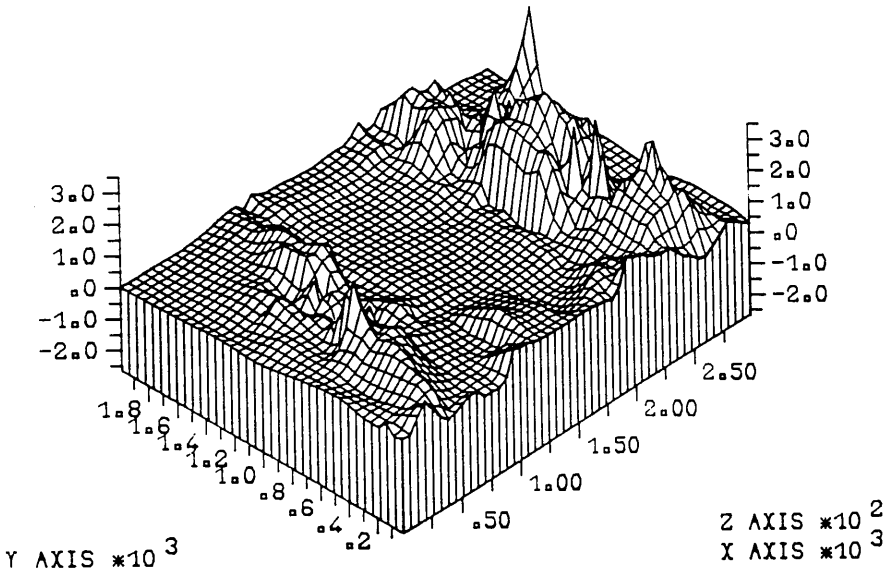

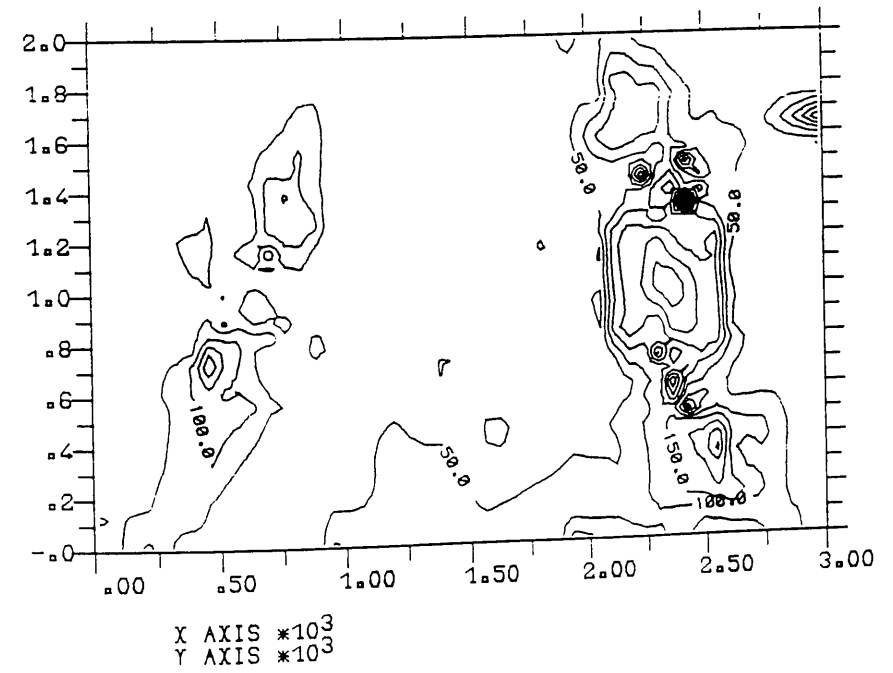

Figure (8.84) Predicted maximum shear strain*10^{-5} at 480kN (TRGRAS10).

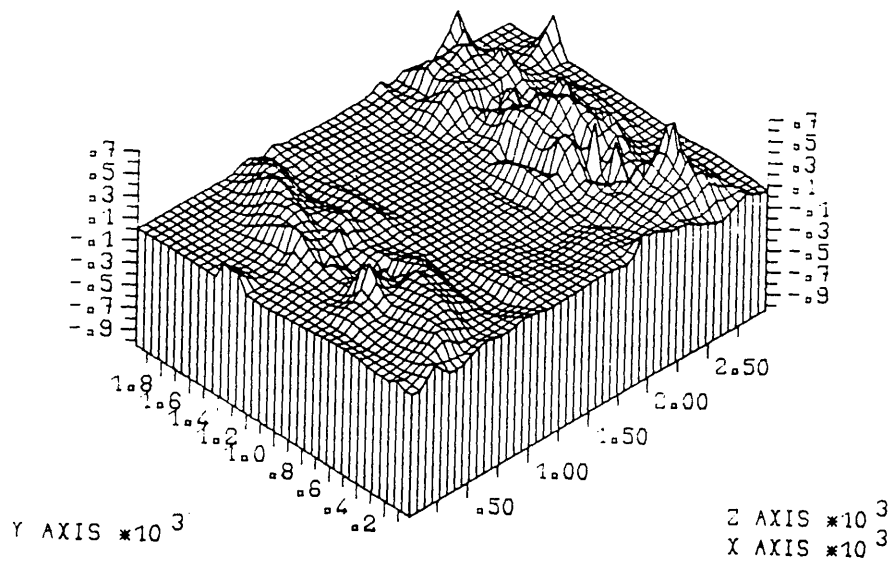

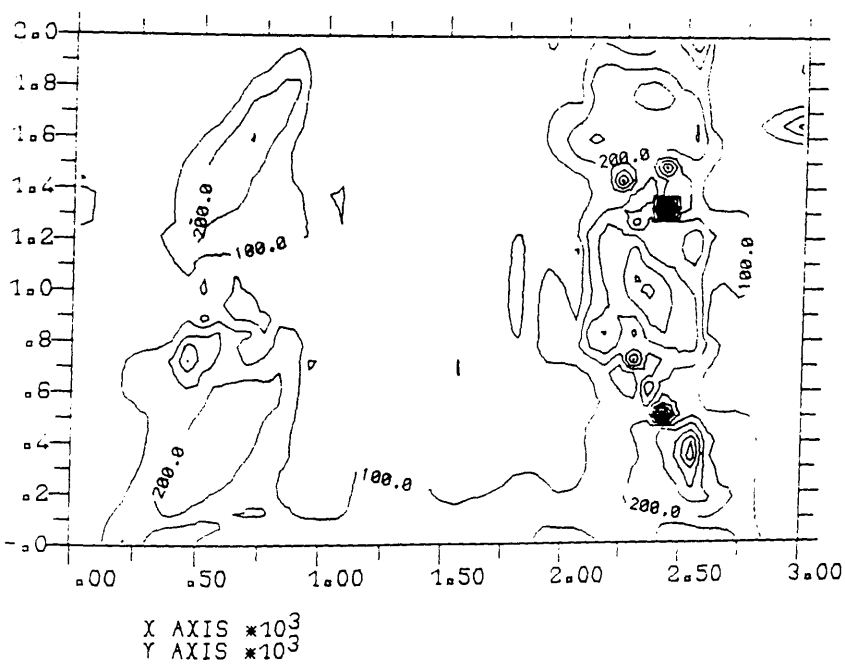

Figure (8.85) Predicted maximum shear strain*10^{-5} at 720kN (TRGRAS10).

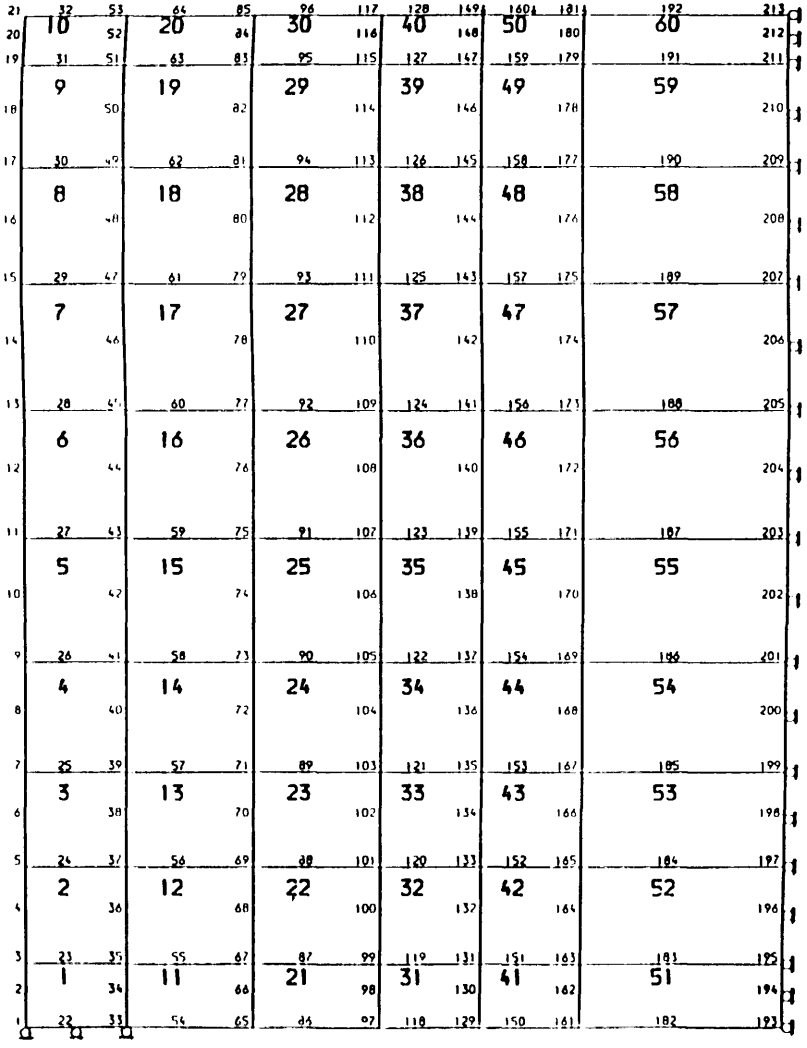

Figure(8.86) Finite element analysis mesh for for girder TRGRAS11

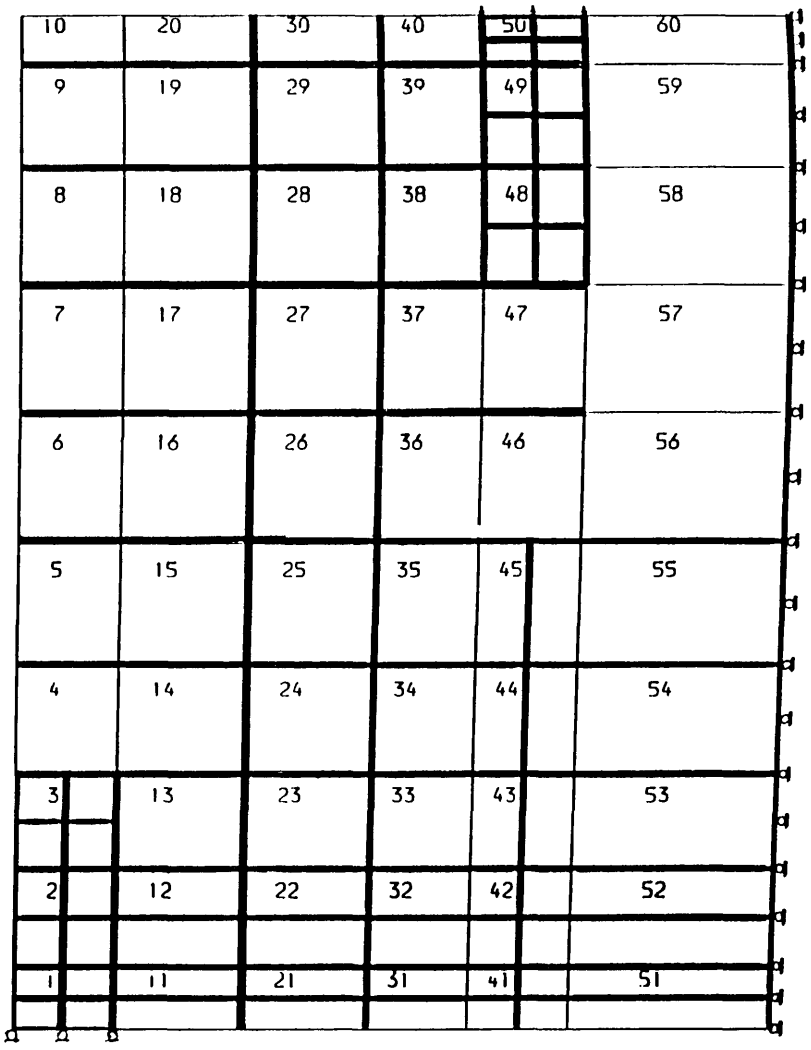

Figure(8.87) Reinforcement detail in finite element analysis for girder TRGRAS11

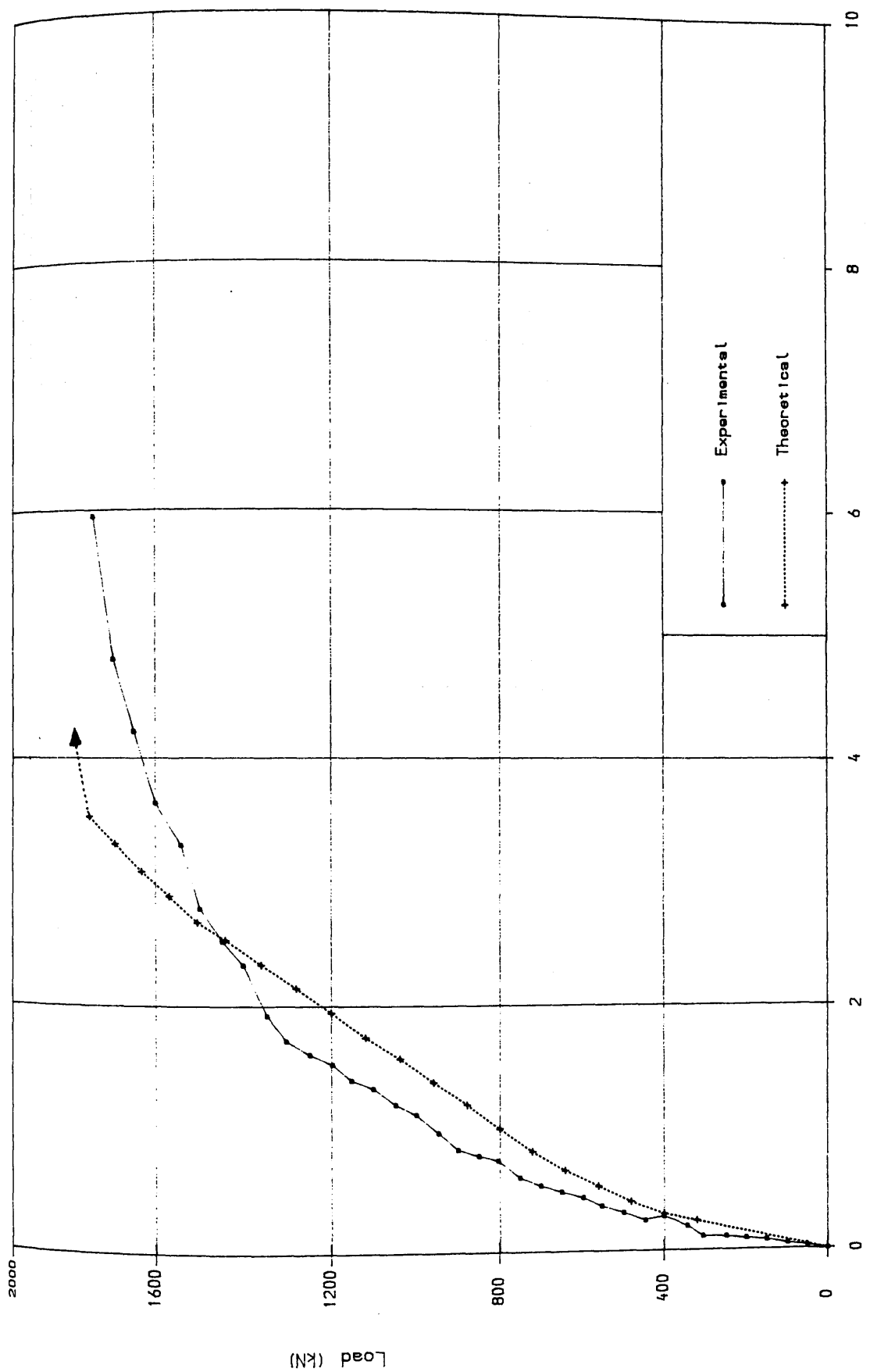

FIG (8.88) Load deflection curve for girder TRGRAS11

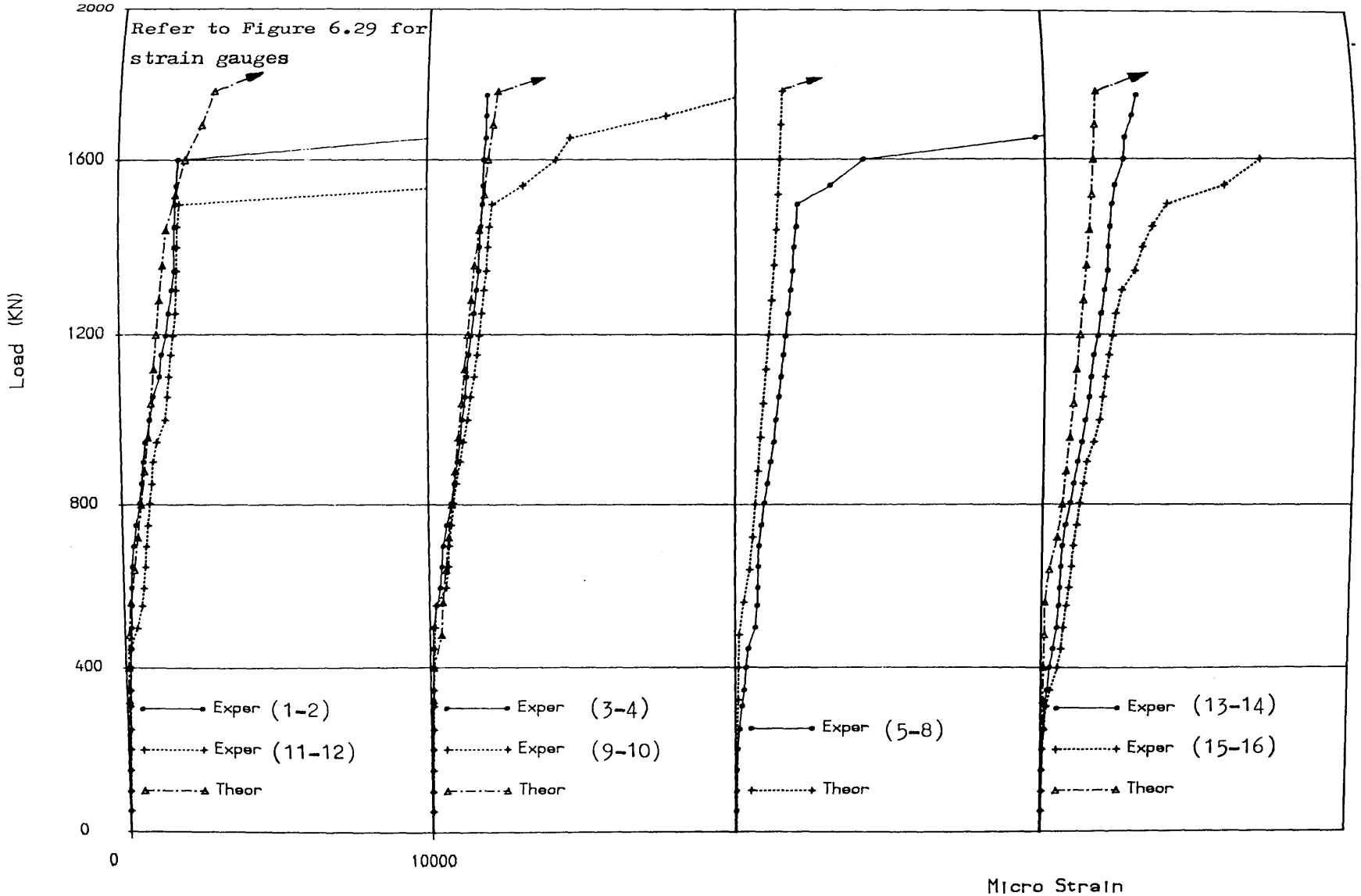

FIG (8.89) Comparison of longitudinal steel strains for girder TRGRAS11

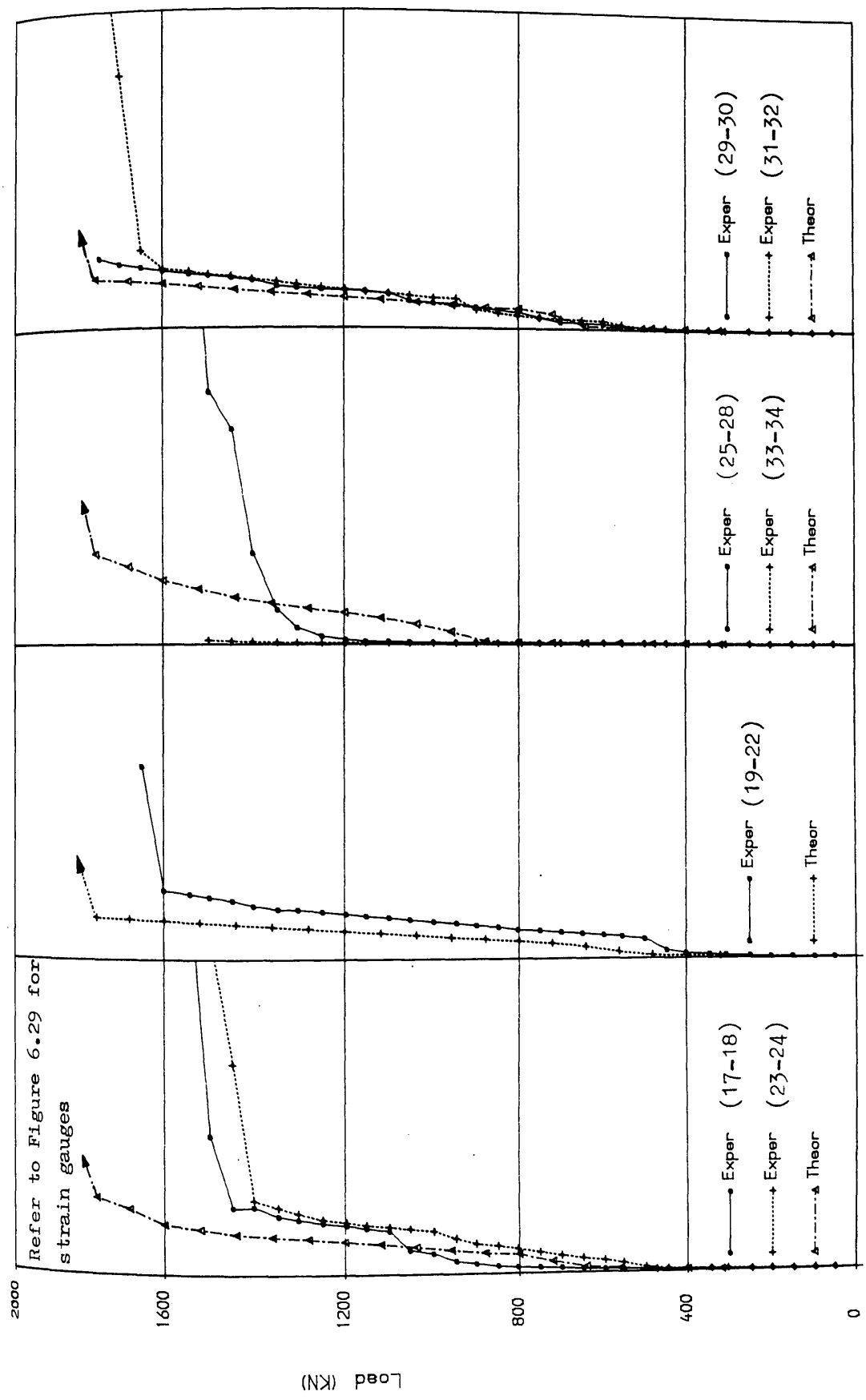

FIG (8.89) Continued

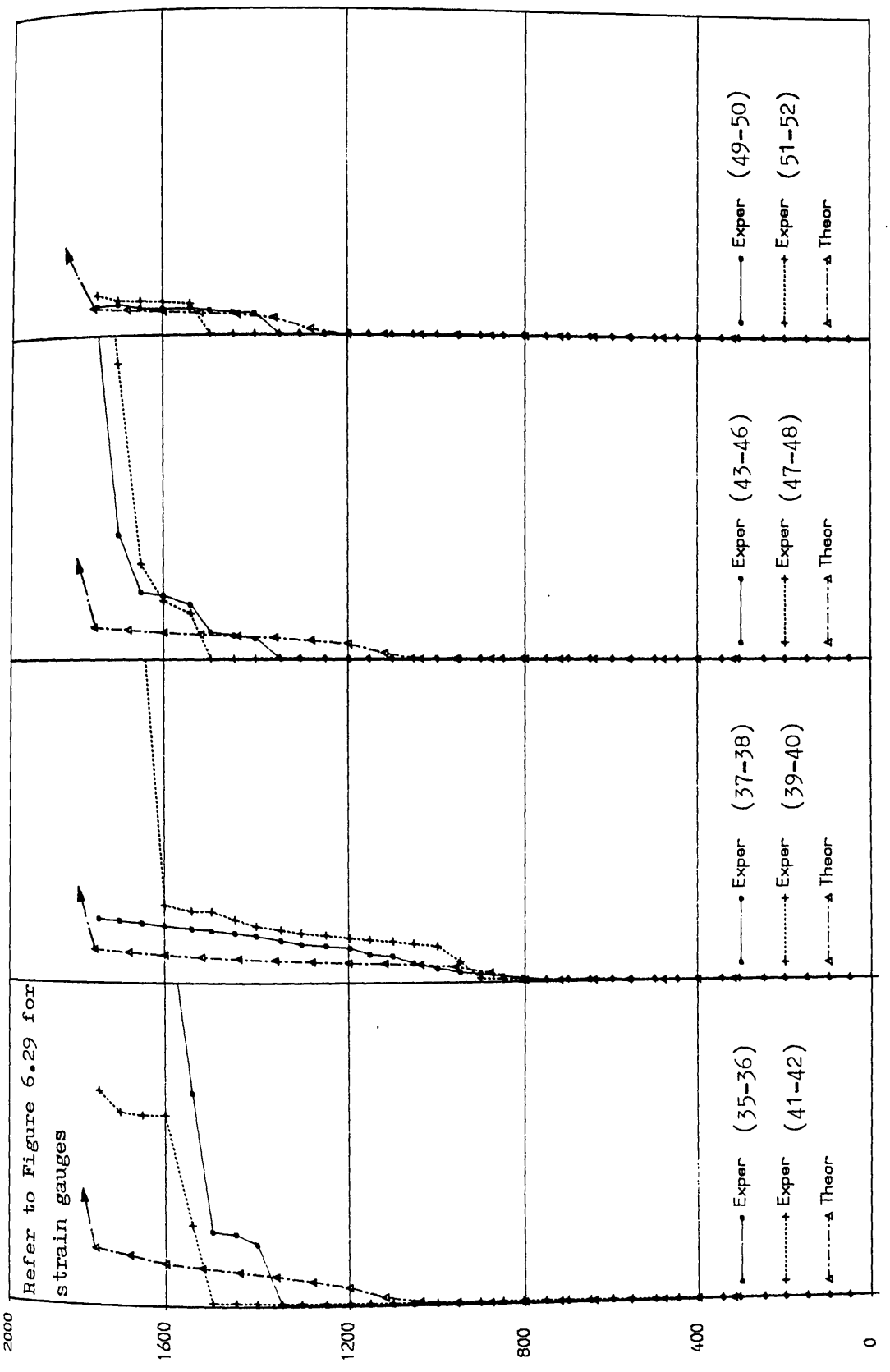

FIG (8.89) Continued

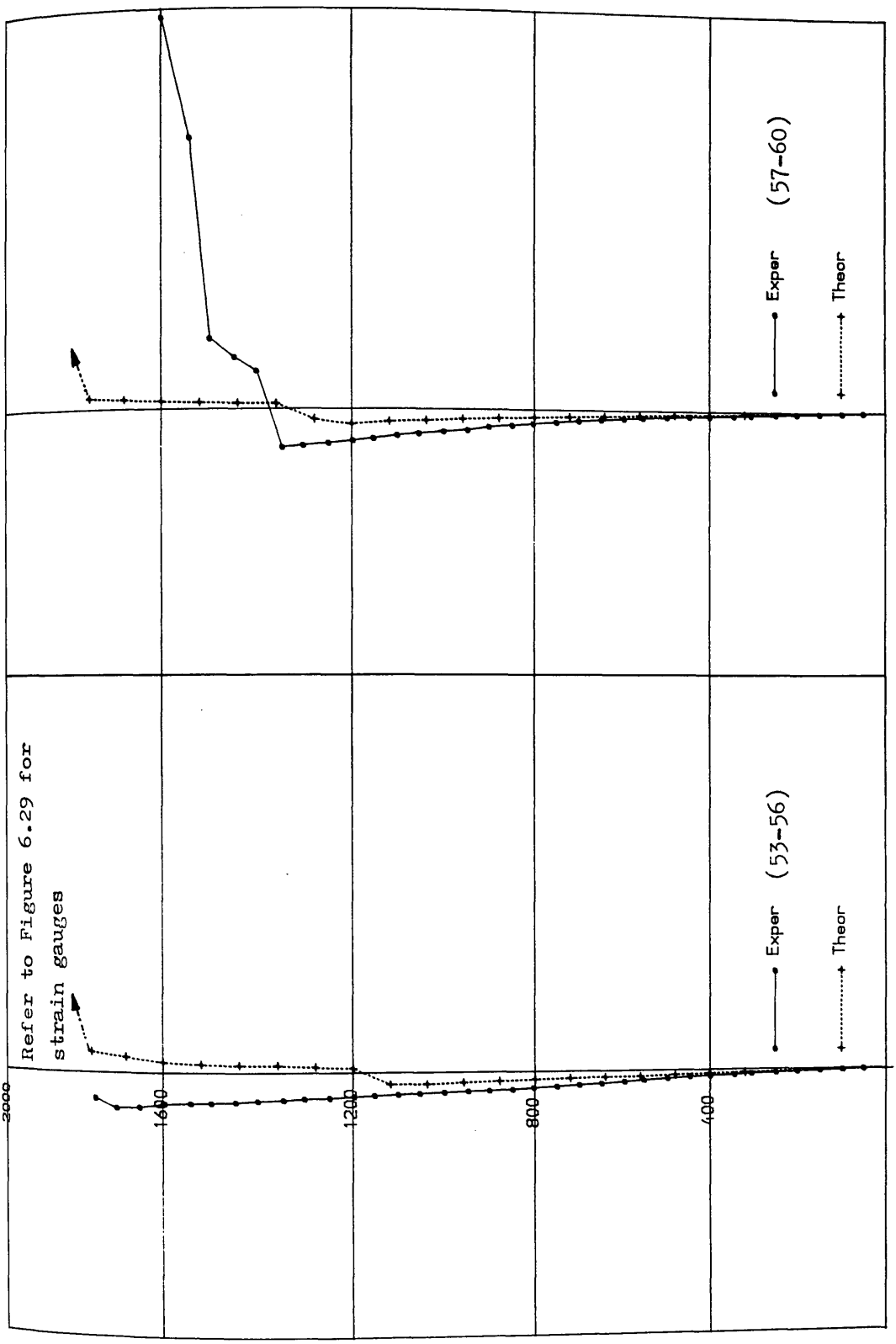

FIG(8.90) comparison of stirrup strain in shear span for girder TRGRAS11

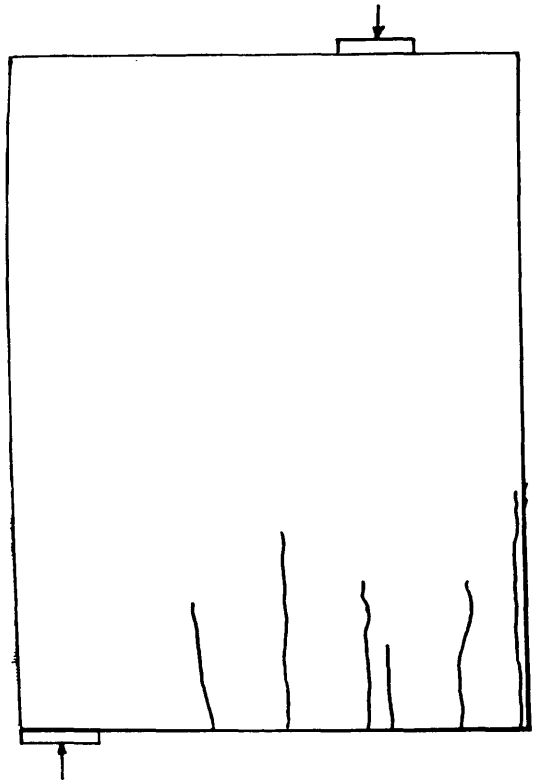

Experimental crack pattern
at 600kN

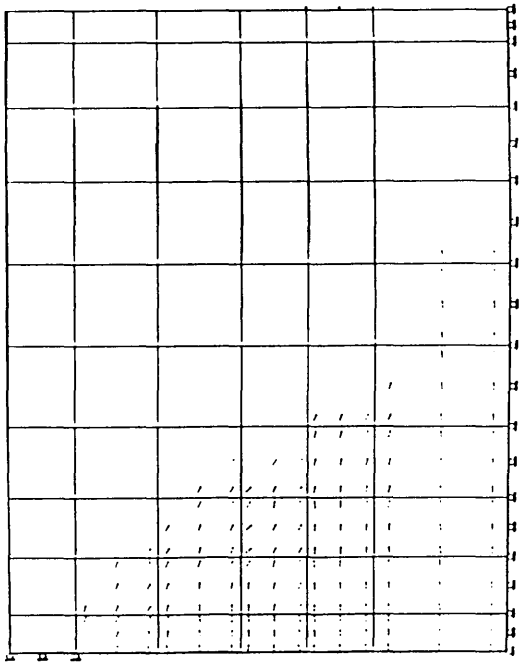

Predicted crack pattern
at 640kN

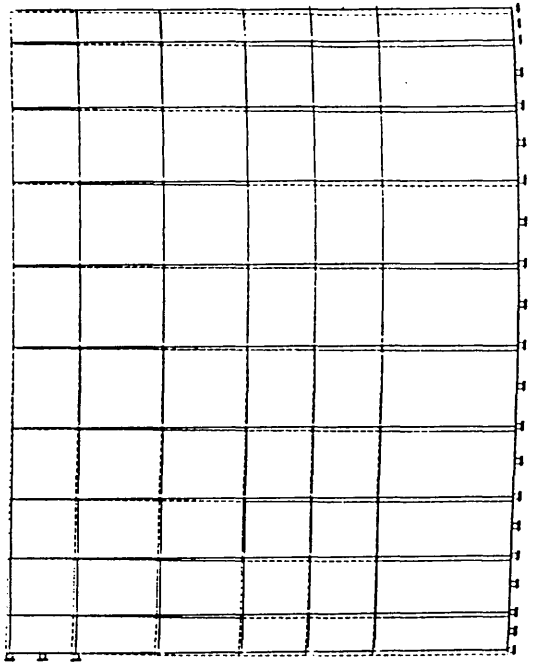

Predicted deformed shape
at 640kN

Figure(8.91) Predicted crack pattern and deformed shape at 640kN (TRGRAS11)

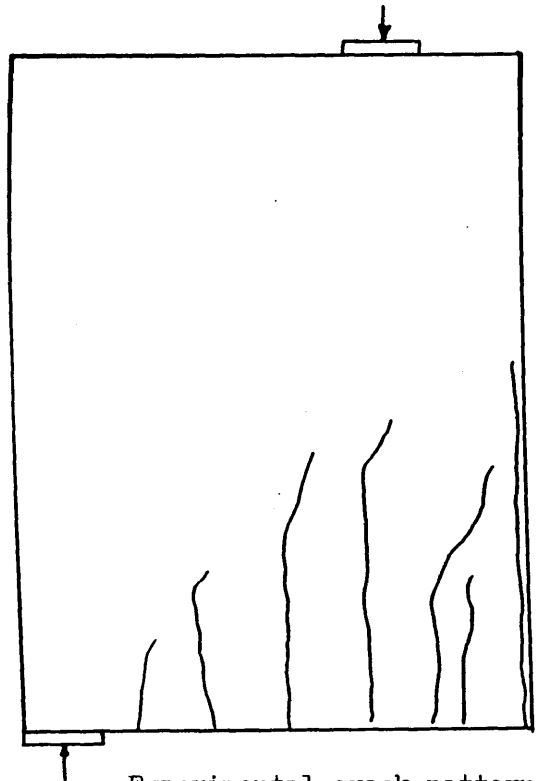

Experimental crack pattern
at 800kN

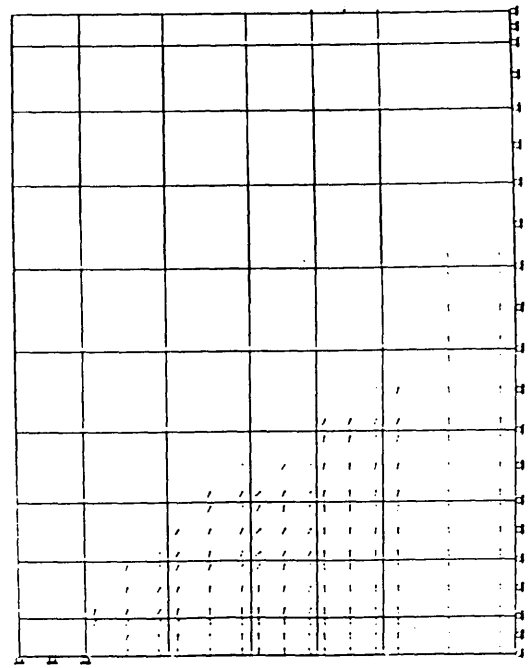

Predicted crack pattern
at 800kN

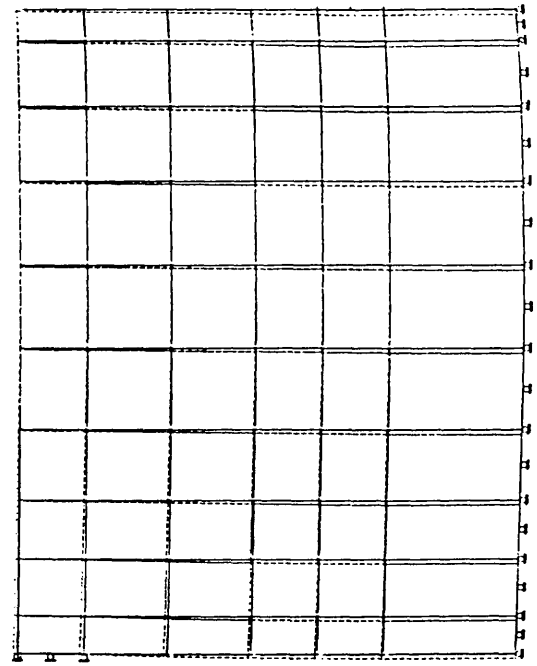

Predicted deformed shape
at 800kN

Figure(8.92) Predicted crack pattern and deformed shape at 800kN (TRGRAS11)

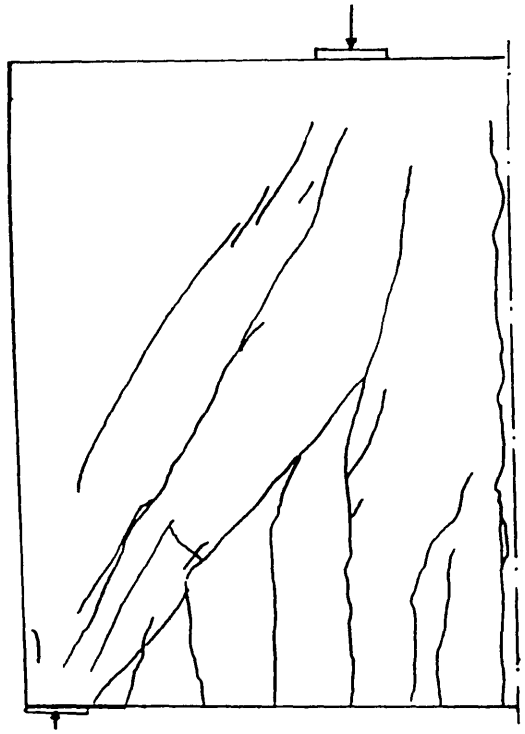

Experimental crack pattern
at 1750kN

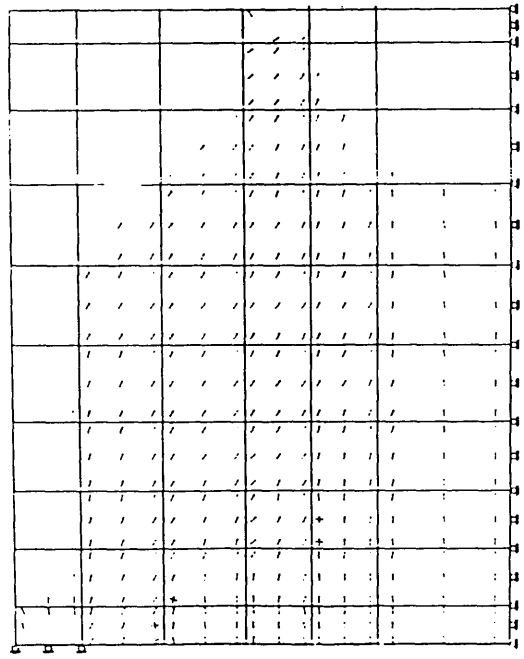

Predicted crack pattern
at 1760kN

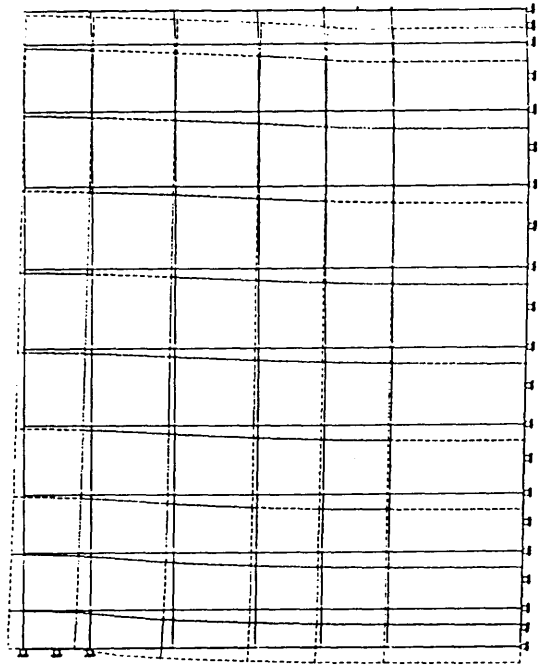

Predicted deformed shape
at 1760kN

Figure(8.93) Predicted crack pattern and deformed shape at 1760kN (TRGRAS11)

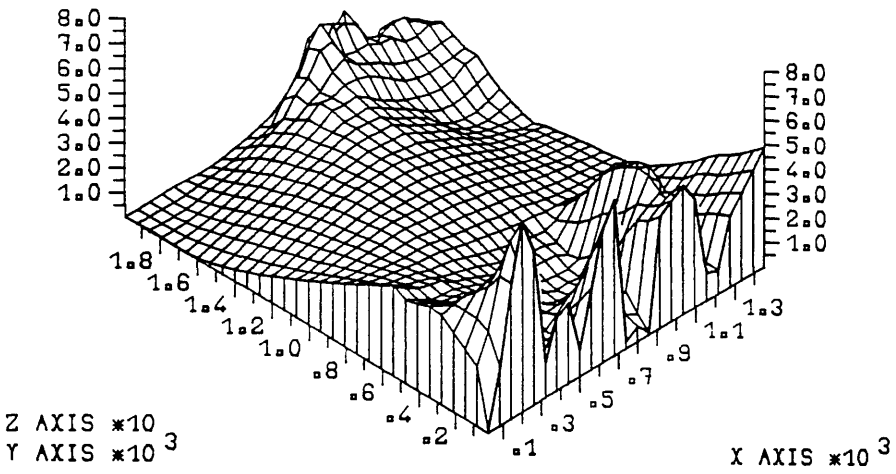

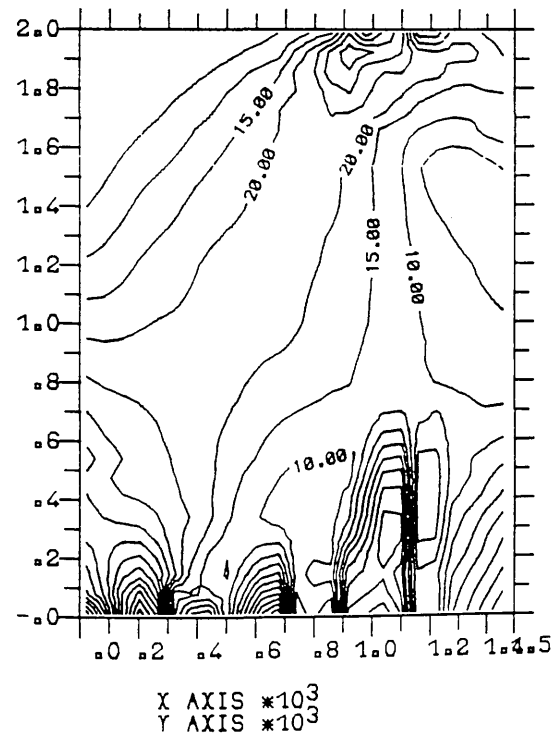

Figure (8.94) Predicted maximum shear strain*10^{-5} at 560kN (TRGRAS11).

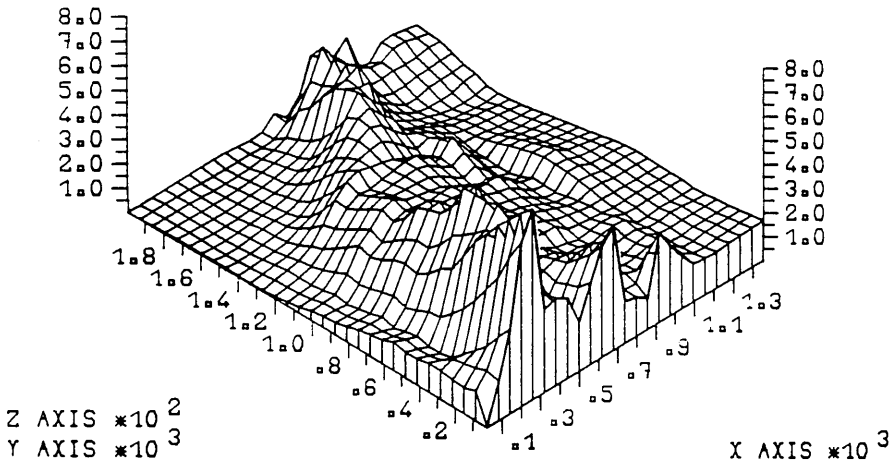

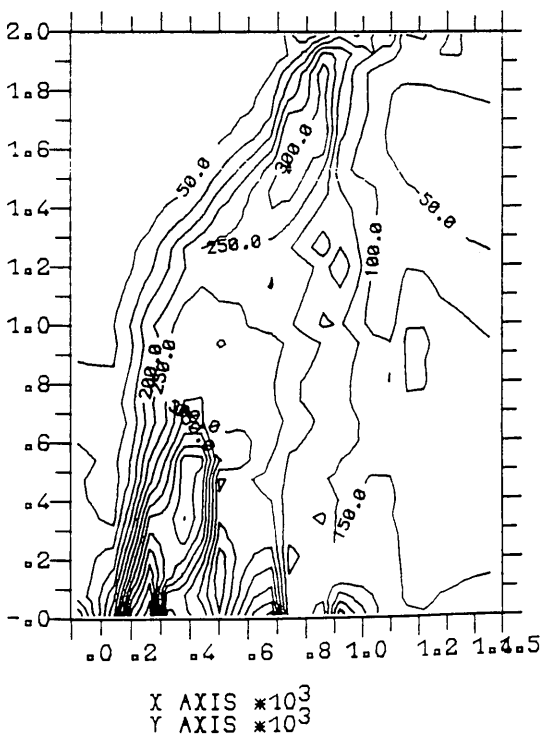

Figure (8.95) Predicted maximum shear strain*10^{-5} at 1760kN (TRGRAS11).

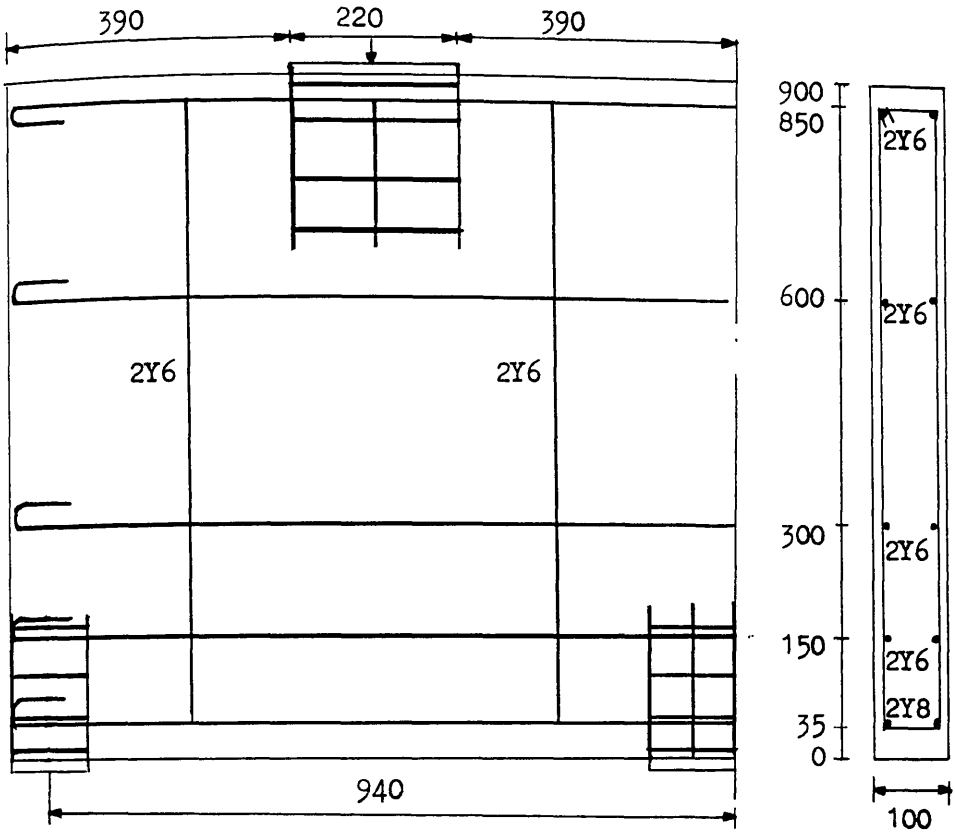

Figure(8.96) Dimensions and details for girder T21

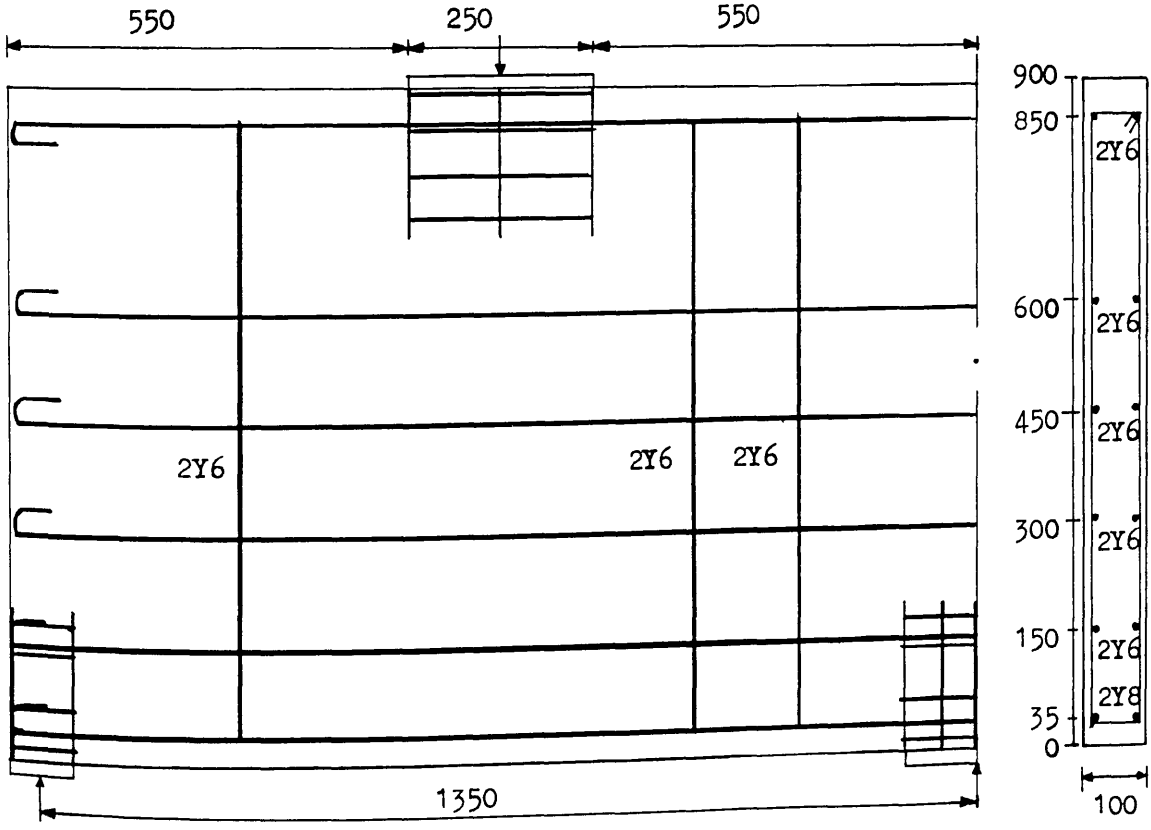

Figure(8.97) Dimensions and details for girder T22

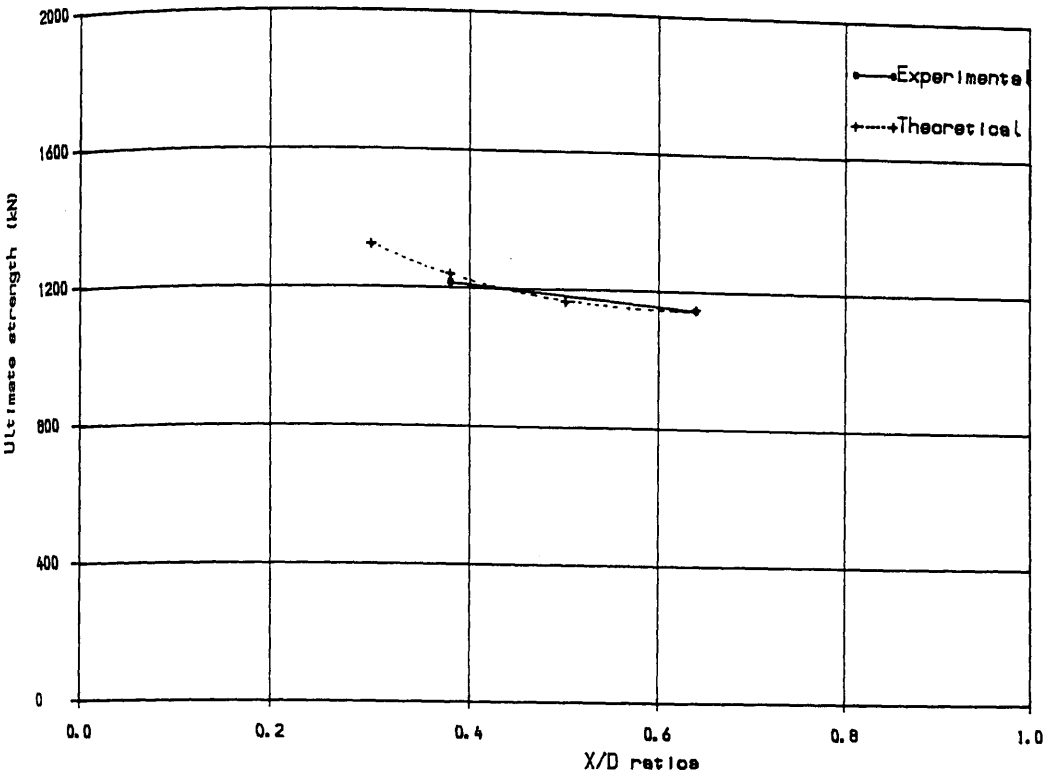

FIG(8.98) Ultimate strength versus X/D ratios

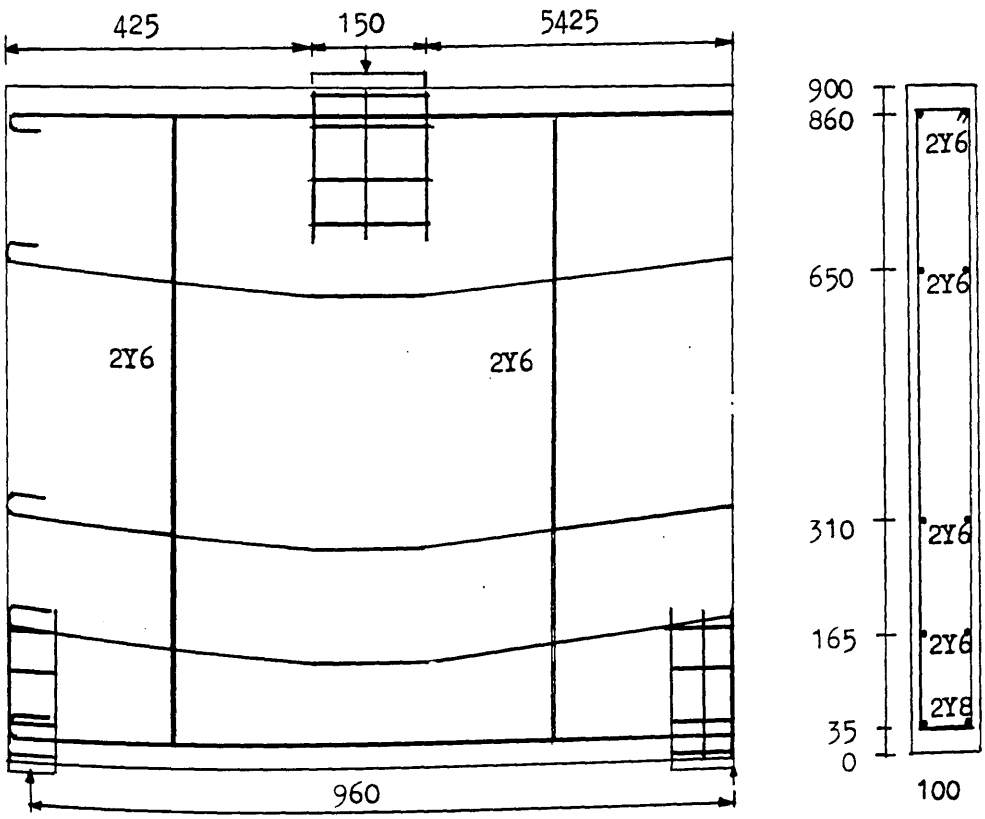

Figure(8.99) Dimensions and details for girder T31 ($\theta=5^{o}$)

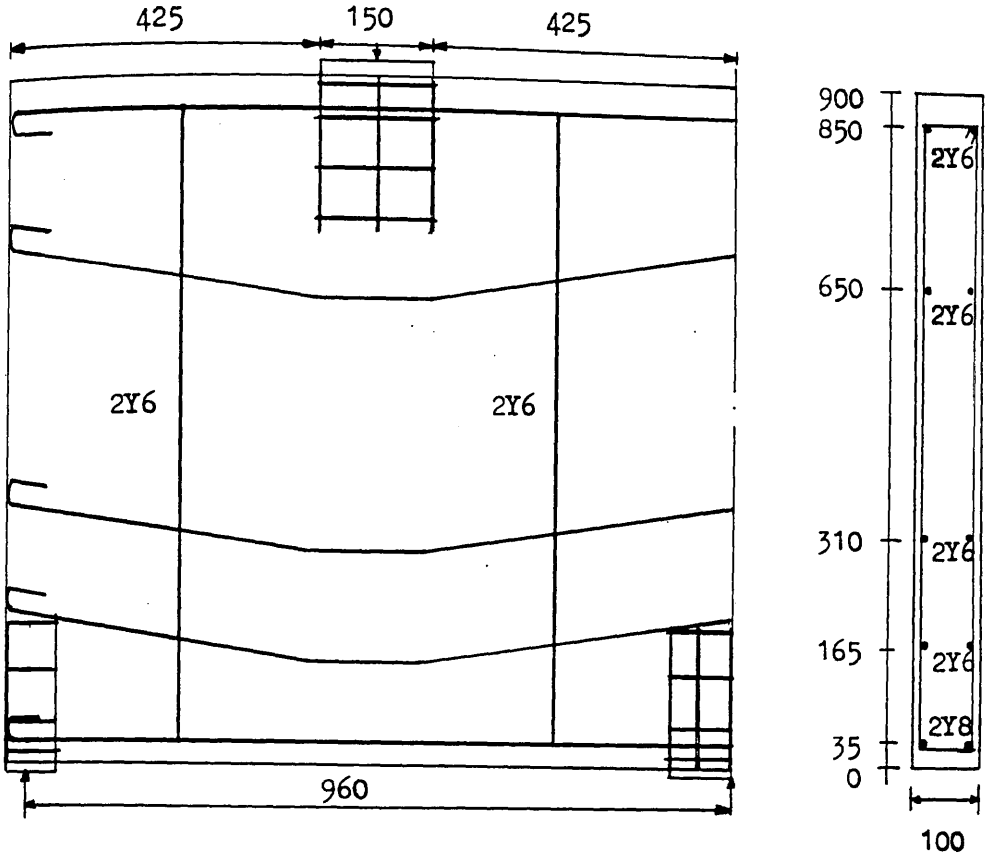

Figure(8.100) Dimensions and details for girder T32 ($\theta=9^{o}$)

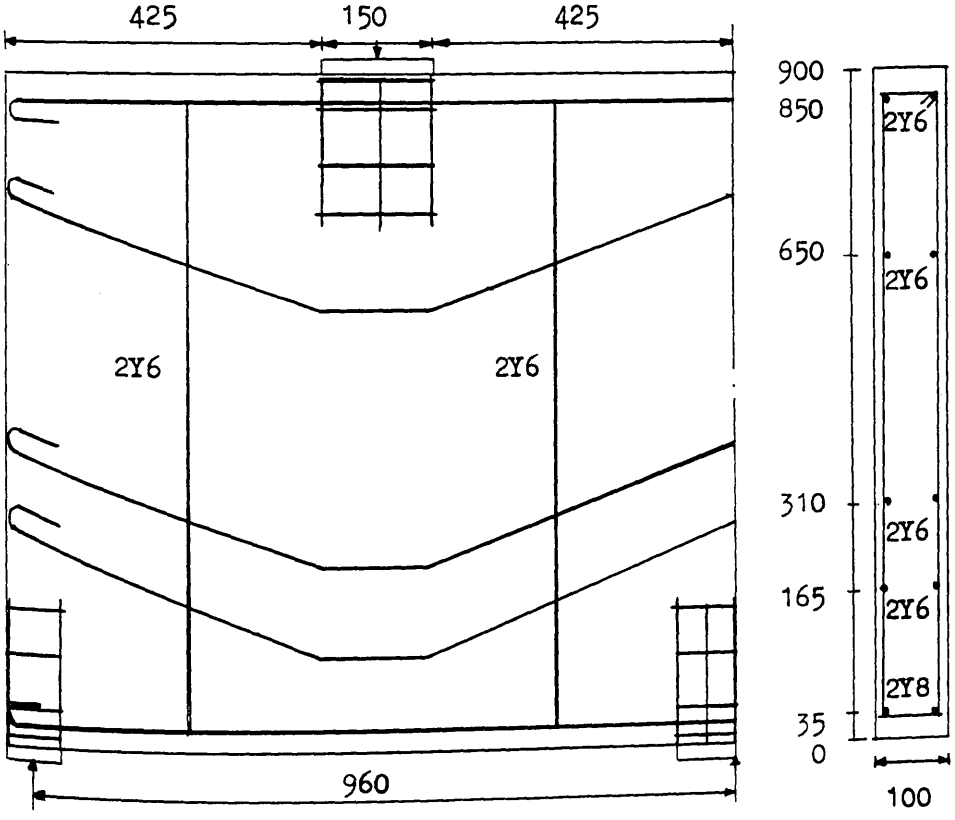

Figure(8.101) Dimensions and details for girder T33 ($\theta=20^{o}$)

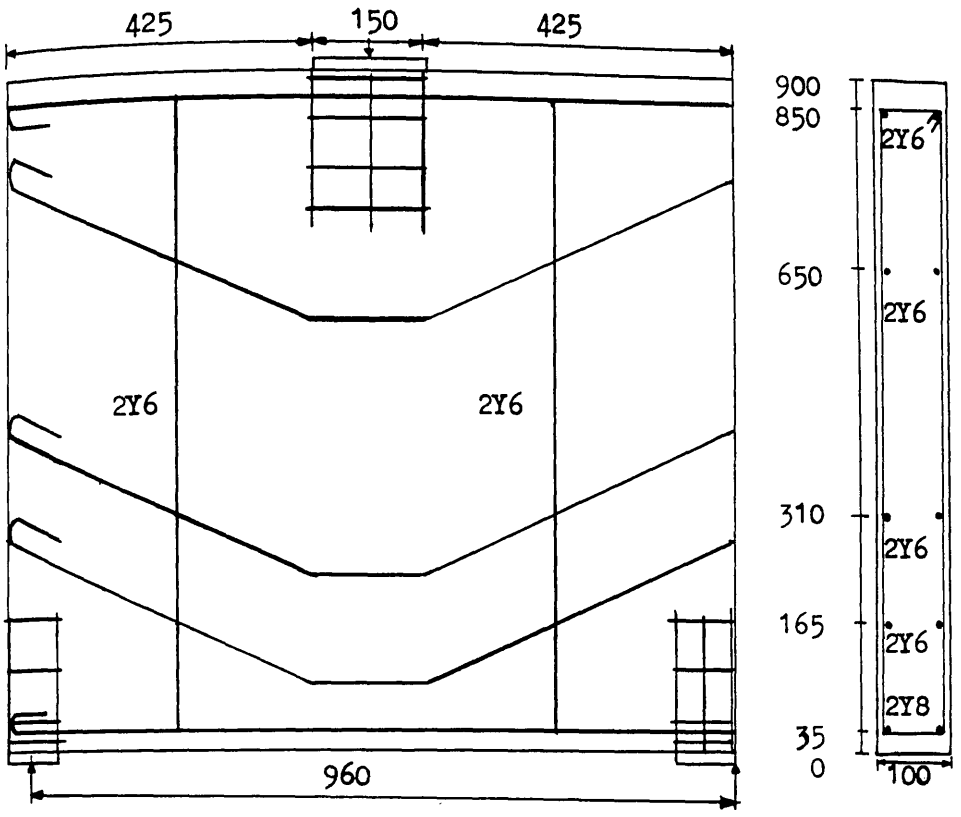

Figure(8.102) Dimensions and details for girder T34 (θ=25°)

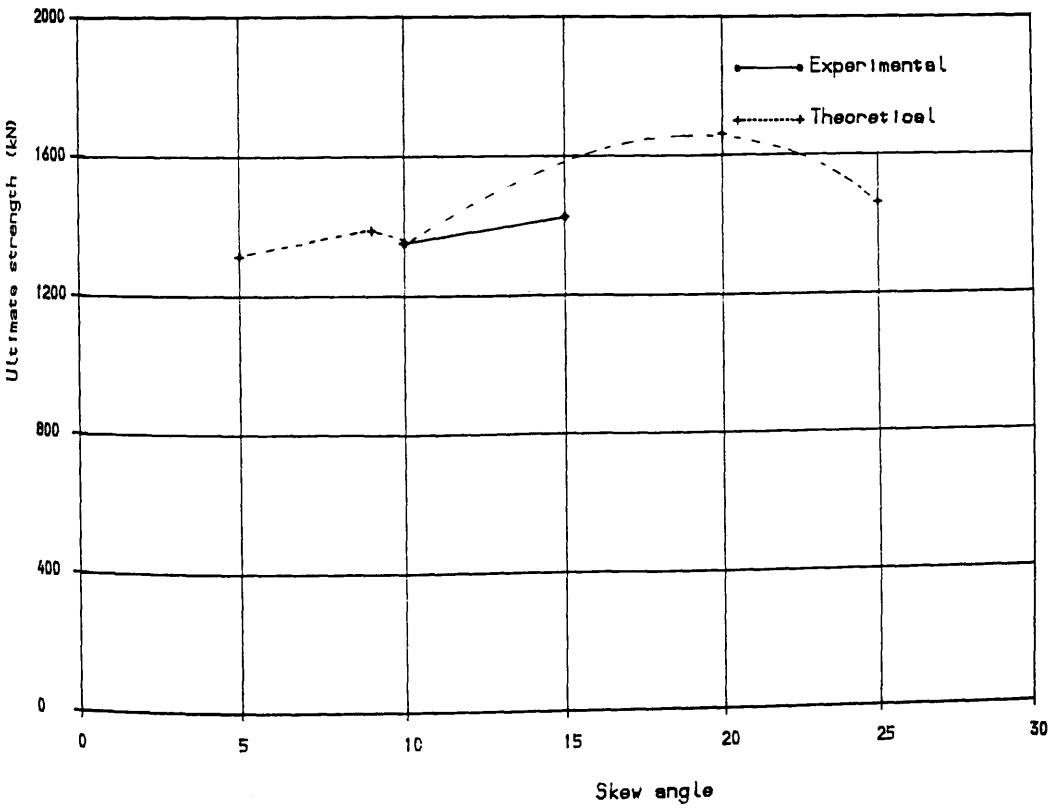

FIG(8.103) Ultimate strength versus skew angle

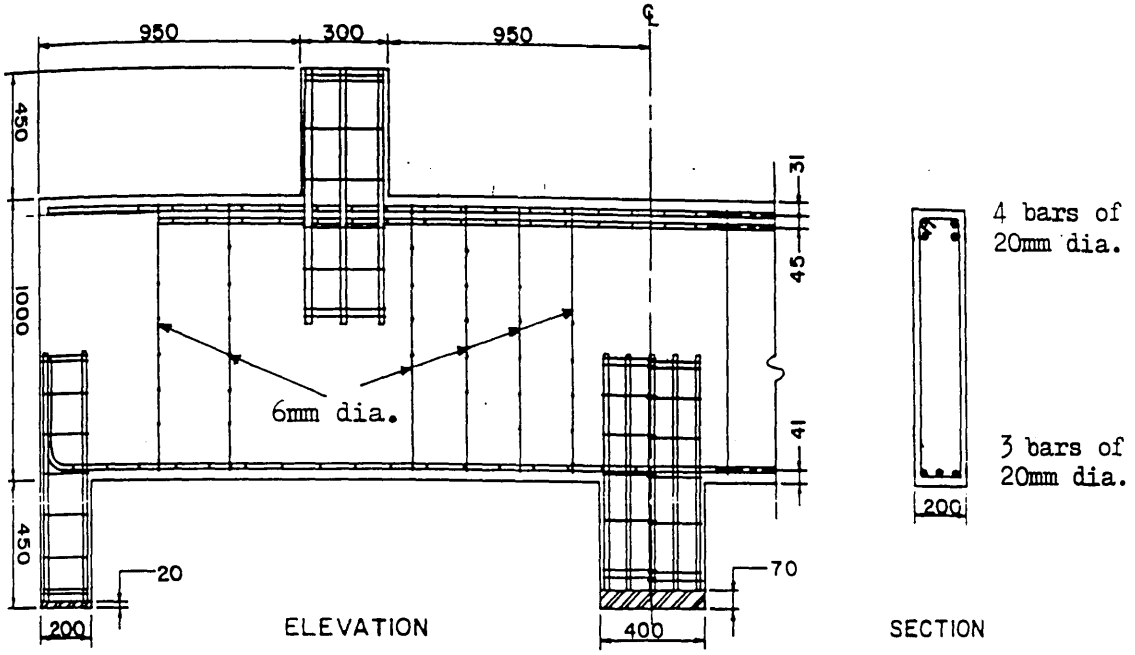

Figure (8.104) Dimensions and details of Beam 1 (MacGregor et al)

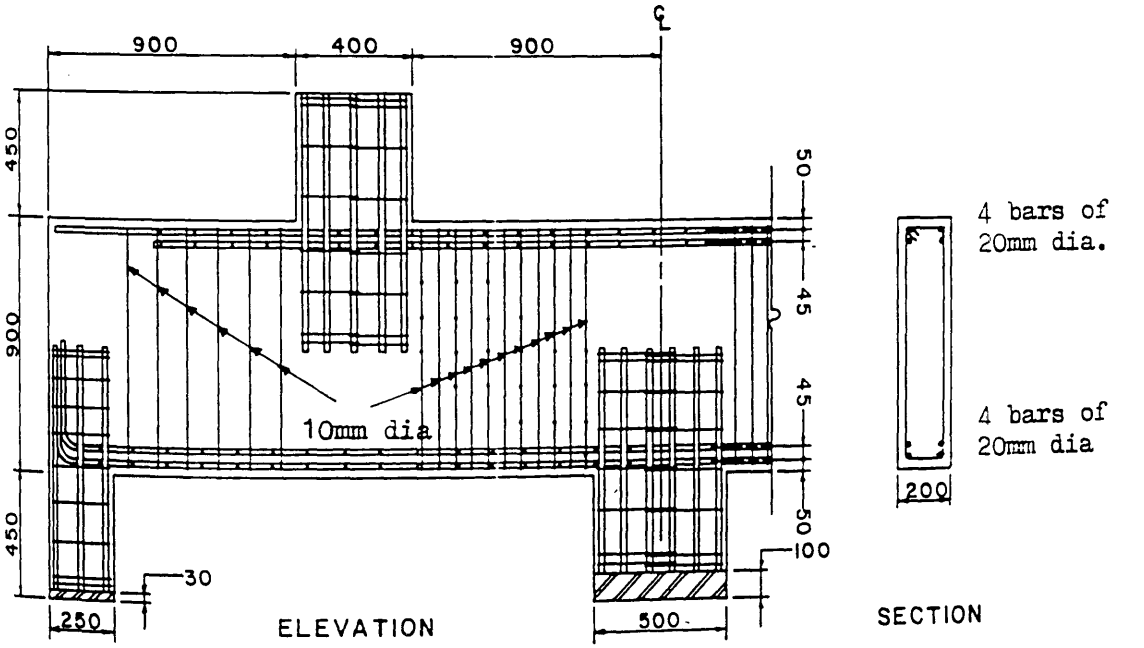

Figure (8.105) Dimensions and details of Beam 2 (MacGregor et al)

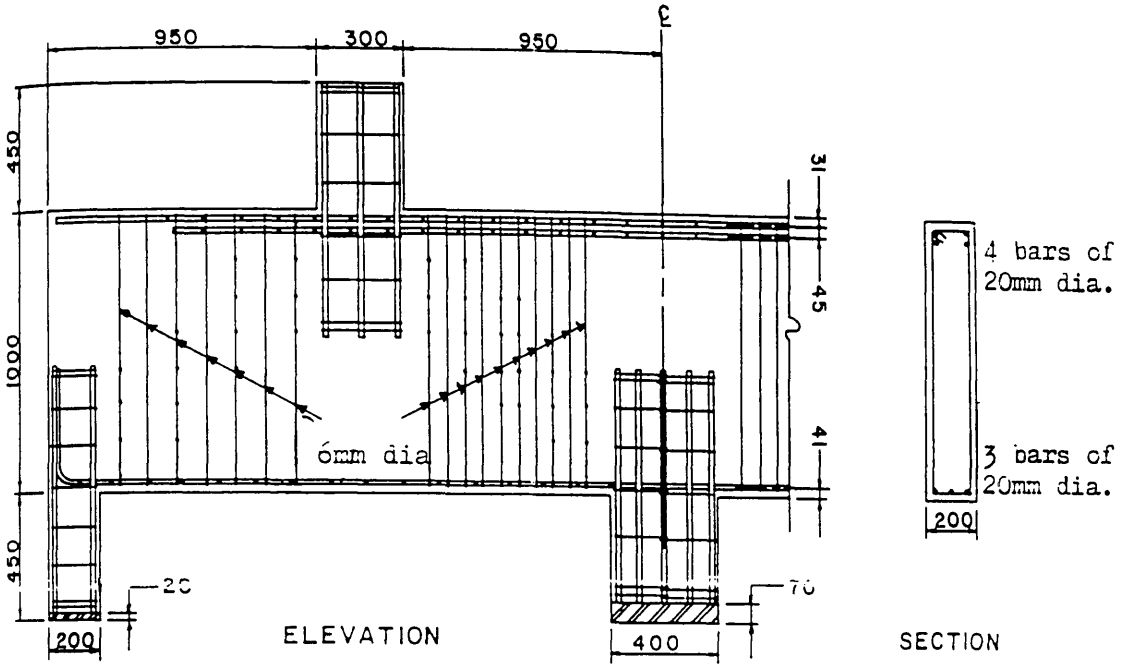

Figure (8.106) Dimensions and details of Beam 3 (MacGregor et al)

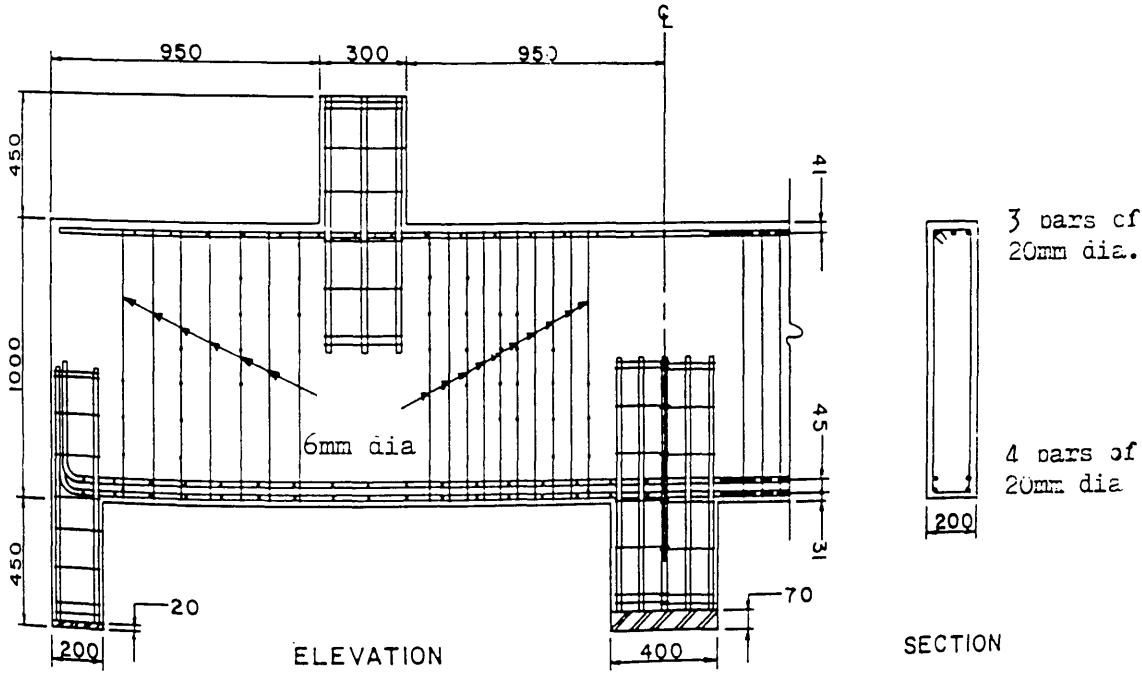

Figure (8.107) Dimensions and details of Beam 4 (MacGregor et al)

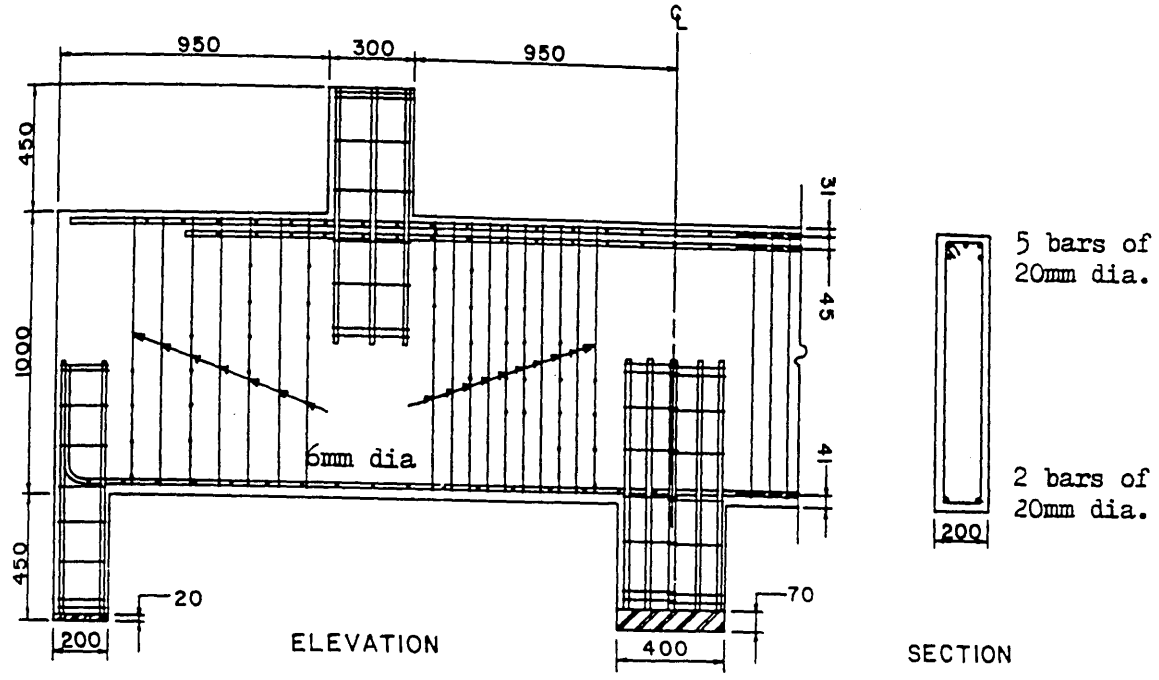

Figure (8.108) Dimensions and details of Beam (MacGregor et al)

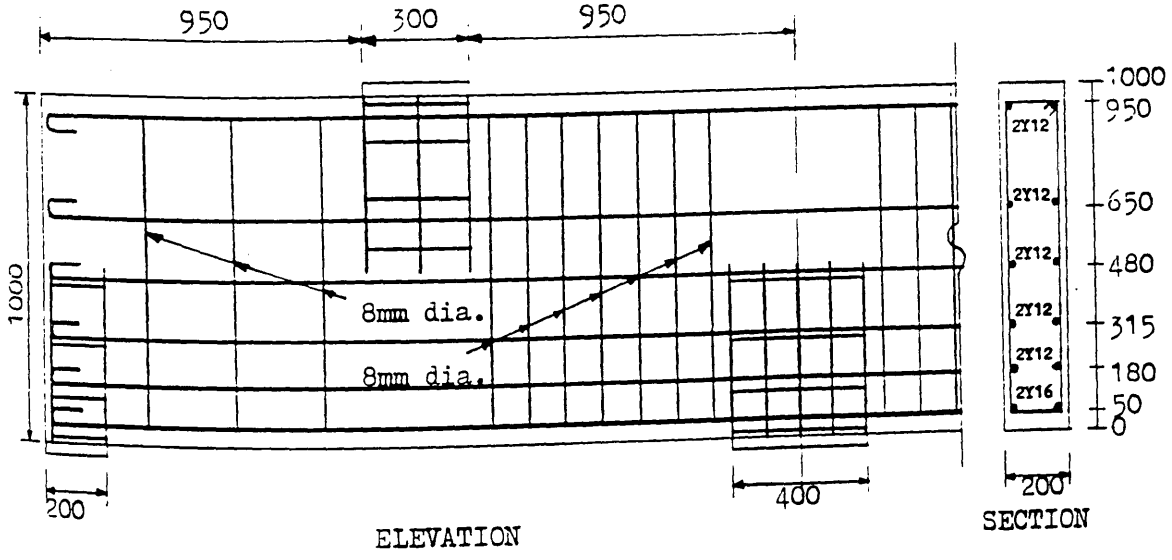

Figure (8.109) Dimensions and details of Beam 1 designed by direct design method

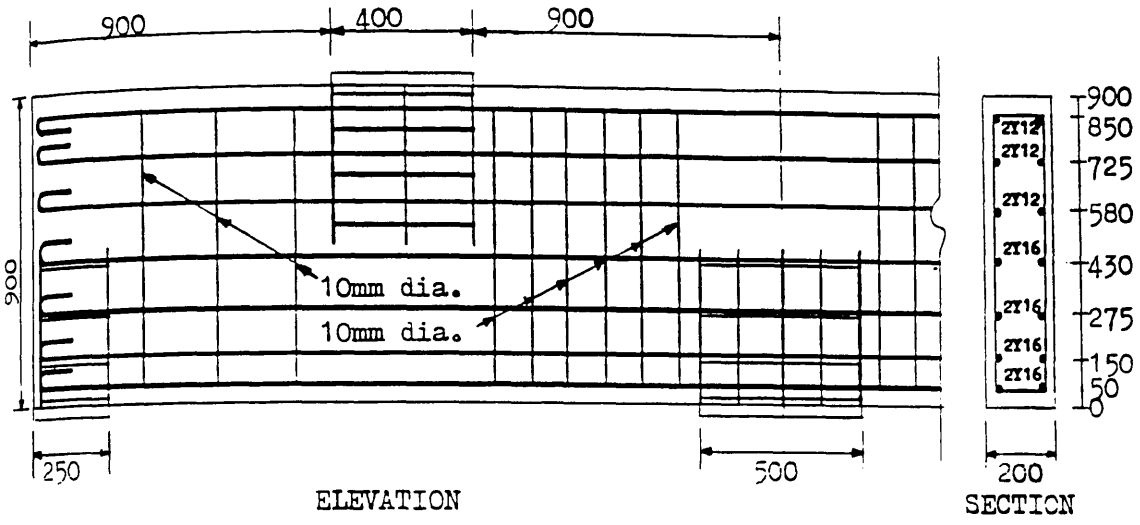

Figure (8.110) Dimensions and details of Beam 2 designed by direct design method

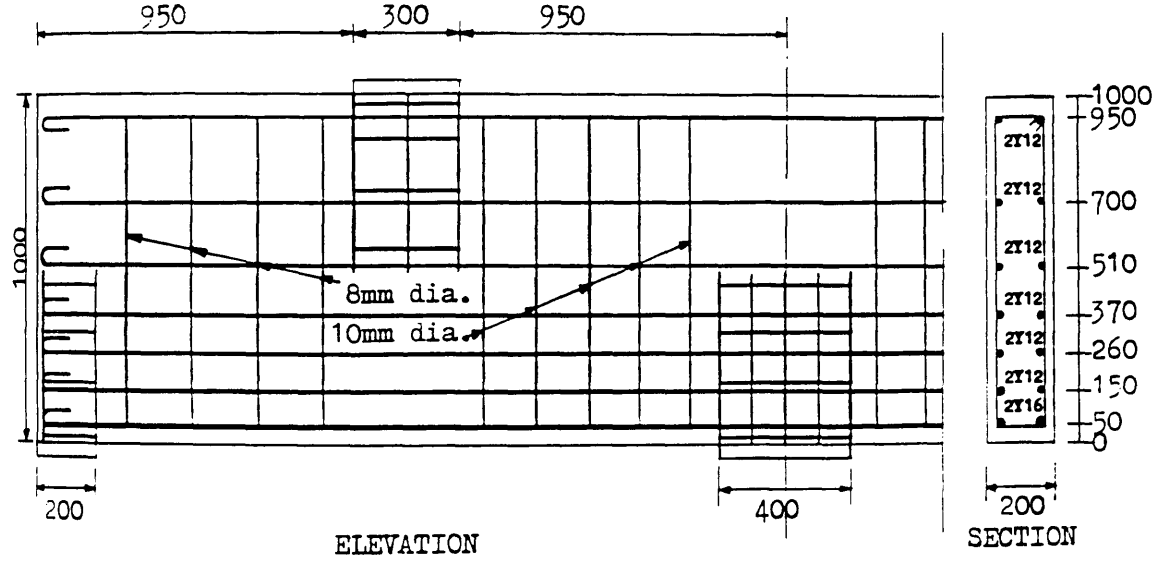

Figure (8.111) Dimensions and details of Beam 3 designed by direct design method

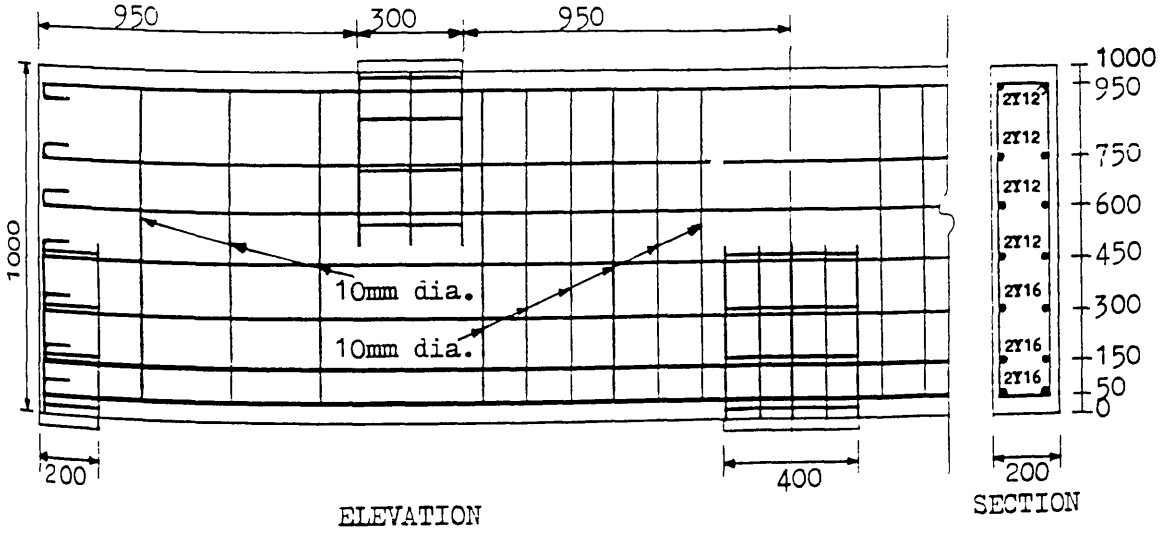

Figure (8.112) Dimensions and details of Beam 4 designed by direct design method

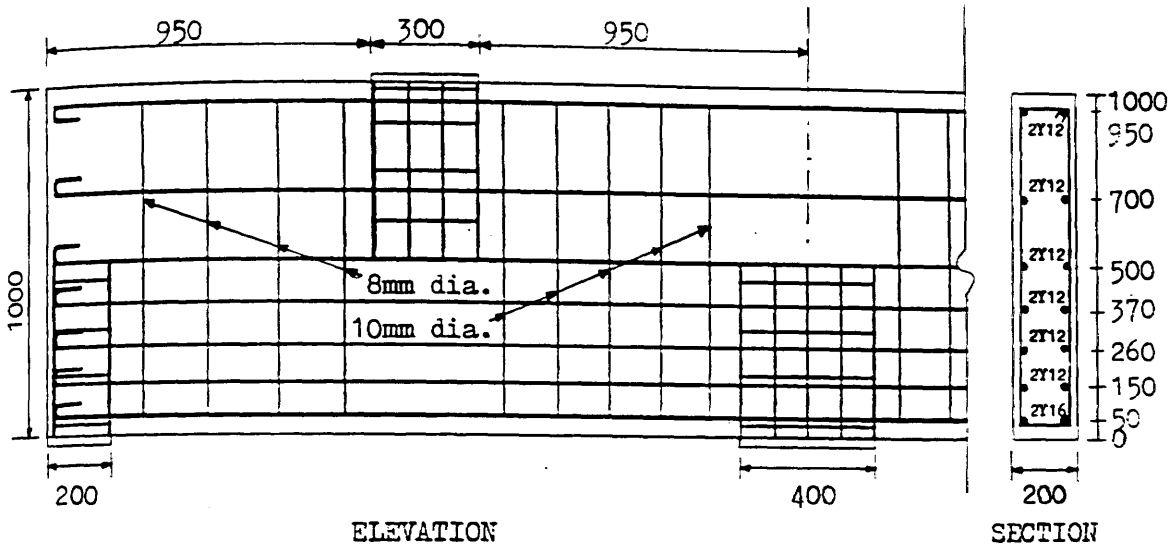

Figure (8.113) Dimensions and details of Beam 5 designed by direct design method

References

1. Al-MANSEER A.A. and PHILLIPS, D.V. "Numerical study of some post-cracking material parameters affecting nonlinear solutions in RC deep beams", Canadian Journal of civil engineering, Volume 14, Nov. 1987.

2. PHILLIPS, D.V., "Nonlinear analysis of structural concrete by finite element methods", Ph.D Thesis, University of Wales, Swansea 1972

3. AGRAWAL, A.B., JAEGER, L.G. and MUFTI, A.A., "Crack propagation and plasticity of reinforced concrete shear-Wall under monotonic and cyclic loading", in conference on cinite element methods in engineering 1976, University of Adelaide, Adelaide, Australia Dec.1976.

4. AL-MAHADI, R.S.H, "Nonlinear finite element analysis of reinforced concrete deep members", Report No. 79-1, Dept. of structural and enviroment engineering, -Cornell University, Jan. 1979.

5. ABDEL-HAFEZ, L.M. "Direct design of reinforced concrete skew slabs", Ph.D. Thesis, University of Glasgow, 1986.

6. PORTLAND CEMENT ASSOCIATION, "Design of deep girders", Concrete information, No. ST66, 1946, (10PP).

7. CEB-FIP Committee, "International recommendation for the design and construction of concrete structures", Principles and recommendations", Prague, FIP sixth congress, Jun. 1970.

8. ACI STANDARD 318-77, "Building code requirements for reinforced concrete (ACI 318-77)", Detroit, Michigan 48219, American concrete institute, 1971.

9. CIRIA Guide 2, "The design of deep beams in reinforced concrete", London, CIRIA publication, 1977.

10. KONG, F.K., ROBINS, P.J. and SHARP, G.R. "The design of reinforced concrete deep beams in current practice", The structural engineer, Volume 53, No. 4, April 1975 (PP. 173-180).

11. KOTSOVOS, M.D., "Design of reinforced concrete deep beams", The structural engineer, Vol. 66, No. 2, Jan. 1988 (PP. 28-32).

12. ROGOWSKY, D.M. and MACGREGOR, J.G. "Shear strength of deep reinforced

concrete continuous beams", Structural engineering report No. 110, Department of civil engineering, University of Alberta, Canada 1983.

13. RICKETTS, D.R. and MACGREGOR, J.G. "Ultimate behaviour of continous reinforced concrete deep beams", Structural engineering report No. 126, Department of Civil engineering, University of Alberta, Canada 1985.

14. RAMAKRISHNAN, V. and ANANTHANARAYANA, Y., "Ultimate strength of deep beams in shear", Proceedings of the american concrete institute (ACI), Vol. 65, 1968, (PP. 87– 98).

15. DE PAIVA, H.A.R. and SIESS, C.P., "Strength and behaviour of deep beams in shear", Journal of the structural division, ASCE, Vol. 91, No. ST5, Oct., 1965, (PP. 19– 41).

CHAPTER NINE

CONCLUSIONS

9.1 From the theoretical and experimental investigations reported in this thesis, the following conclusions can be drawn.

9.1.1 Direct Design Method

The large scale experimental tests and nonlinear finite element modelling have verified that the direct design method, in conjunction with the averaging procedure used in this study, produces practical designs for a range of in-plane structures, and for continuous girders in particular. The direct design technique is a natural design-oriented method for continuum concrete structures because of the way it combines analysis and design into one continuous automatic operation. Some of its advantages are as follows:

(i) Once the direct design equations are codified in conjunction with any numerical technique, such as the finite element technique, into a computer program, the design of reinforcement can be easily and conveniently obtained. Once initiated, this does not in general require any intervention by the designer. This method provides all the relevent information regarding the intended design in a graphical and tabular form. This technique can become a core for the development of computer aided designs (CAD), which is the demand of current practice.

(ii) It is based on the principles of plasticity, and is a lower bound approach. It has an intrinsic safeguard against unsatisfactory serviceability and collapse behaviour by aiming for simultaneous yielding throughout the structure.

(iii) It uses steel economically, because the design equations are based on

minimising steel requirements. It can handle any geometrical shape and different material properties.

Two span continuous girders

(i) Service loads were near to the design ultimate load. Additionally, the average ultimate loads were found to be 45% and 50% higher than the designed and service loads respectively and hence there is an intrinsic safety factor against collapse. No girder failed before attaining the design ultimate load.

(ii) All the Codes of Practice underestimate the ultimate shear capacity of the reinforced concrete deep girders and are uneconomical in reinforcement design.

(iii) An increase in shear reinforcement influenced the ultimate strength, however, it was not possible, with the limited data in this investigation, to offer a relationship.

(iv) Less skew reinforcement than the orthogonal reinforcement was required from 0.2 to 0.8 of the depth from the bottom of the beam whereas more skew reinforcement was required in the other zones than orthogonal reinforcement.

a) Skew reinforcement produced a saving of 17% at an angle of 15 degree and 12% at an angle of 10 degree to the x− axis.

b) Skew reinforcement produced better cracking control by reducing crack widths and consequently producing higher service and ultimate loads.

(v) The strength of concrete influences the ultimate load and serviceability behaviour.

(vi) No girder failed prematurely by bearing failure.

Perforated girders

(i) The applicability of the results, from the direct design technique in

conjunction with the averaging procedure on perforated deep girders, showed that the ultimate strength of a girder depends primarily on the extent to which it intercepts the "load path" i.e the path joining the load bearing blocks at the loading point and the support reaction points, and on the location at which this interception occurs. The position of the openings are significant only in so far as these affect the extent and location of such interception.

(a) When a girder had two perforations the load path was intercepted to a lesser extent so that the measured ultimate load was slightly higher than the design load, however, serviceable behaviour based on the crack width limit was not satisfactory.

(b) When a girder had three perforations the load path was intercepted to a larger extent, because of the interception of the load path by two openings, the measured ultimate load was smaller than the design load. Also the serviceable behaviour was not satisfactory based on the crack width limit.

(c) The position of the opening in the lower mid-depth zone intercepted the load path to a lesser extent than the opening in the upper mid-depth zone of the girder. This indicated that if the opening is placed in the lower mid-depth zone, the ultimate strength could be improved.

(ii) The experimental results has indicated the use of extra diagonal steel bars at the corners of the openings (i.e the local zones) as the local zones at support and load points are reinforced with steel cages. This is because in the high concentration zones direct design procedure might have difficulty in coping with.

Special girder

The behaviour of the single span deep girder, which was reinforced as

close as possible to that required by the direct design equations behaved satisfactorily in ultimate and serviceable behaviour. But it carried an ultimate load 75% and 66% higher than the designed and service loads respectively. This is because (i) the provided steel areas were higher at some points due to practical constraints (ii) the contribution of the dowel action and aggregate interlocking in shear transfer. This demonstrates the intrinsic safety factor against collapse. An interesting behaviour was observed in this model that progressive yielding of steel was very close to the simultaneous yielding of the steel throughout the structure, which confirms the ideal situation of simultaneous yielding of steel which is one of the basic assumptions of the direct design technique.

9.1.2 Finite element study:

(i) The nonlinear finite element analysis proved to be satisfactory in predicting general behaviour. The predicted ultimate load and steel strains were in reasonable agreement with the measured values, whilst the crack pattern predicted by the fixed smeared crack model demonstrates that it is an adequate approximation to real behaviour.

(ii) A constant shear retention factor of 0.25 was found suitable for the girders designed by the direct design method.

(iii) Tension stiffening model was found not to be useful and hence was ignored in this study.

(iv) Girders with smaller span to depth (L/D) ratios gave higher ultimate strength than girders with larger span to depth (L/D) ratios.

(iv) The finite element analysis provided useful additional information, such as deformational and maximum shear strain behaviour, this was used in order to ascertain the failure mechanism.

9.2 Suggestion for future work

The following are some suggestions for further research in this area:

(i) The two span continuous girders in this study were tested with top point loads at the centre of the span, and the single span girders at the third points. There is a need to test the behaviour of transfer girders subjected to multiple load cases which frequently occur in practice.

(ii) Since deep beams are frequently used as panels, it would be worthwhile to test some beams with supporting frames.

(iii) The use of the deep beams in a shearwall supporting system involves slab and floor connections, hence it will be useful to test I–section deep girders to simulate this situation.

(iv) In this study the girders were designed using an elastic stress field. An elasto–plastic model was also developed for the design of transfer girders, but was not adequately assessed. It would be worthwhile to design some girders using an elasto–plastic stress field to ascertain if a more economical distribution of reinforcement resulted.

(v) The design program is currently semi–automatic. It should be extended to select reinforcing bars and spacing automatically according to the averaging procedure in conjunction with the rules and regulations prescribed by various codes, so that the final drawings may be directly obtained from the computer.

(vi) In this study skew reinforcement was handled by the skew elements in the nonlinear program which can cause some numerical difficulties. Modification of the program is essential to simplify the handling of skew reinforcement, so that the orientation of the bar is independent of the main mesh.

(vii) The nonlinear program is currently not incorporated into the design process. It would be more useful for the design and nonlinear analysis program to be joined together, so that the complex structure can then be designed and analysed within the same process to check the ultimate load

and other important behaviour, such as failure mechanism, cracking of concrete, yielding history of steel and deformational behaviour.

APPENDIX A

MODES OF FAILUE INVESTIGATED IN DIFFERENT STUDIES

Shear failure is generally classified as "diagonal tension failure" or "diagonal compression failure". The mechanism of this failure was first described by Laupa et al at University of Illinois. Ramakrishnan and Ananathanayarana later extended it under the title of "Ultimate strength of deep beams". They described these various modes of failure, which occured throughout their experimental investigation, on the deep beam behaviour as:

1 Diagonal tension failure : For a concentrated load, a clear and sudden fracture along a line joining the inside face of the support (in continuous deep beams inside face of the interior support) with the loading point, which is nearest to the support. It is shown in Figure (A1a) that for a concentrated load and for a uniformly distributed load, a clear fracture occurs along the line joining the support to the nearst third span (Figure 1Ab).

2 Diagonal compression failure : In this type of failure, an inclined crack develops first along the line joining the loading point with the support, then after a small increase in the load, a second parallel inclined crack appears near to the first one. The final failure is due to the destruction of a portion of the concrete between these two parallel inclined cracks (Figure 2Aa).

3 Shear compression failure : If the inclined crack continues to grow as the beam carries additional loads, the crack extends into the compression zone and concrete starts crushing, this failure is to be called the shear compression failure (Figure 2Ab).

4 Flexure failure : This failure of the deep beam is due to either failure of the "arch rib", where concrete in the arch crushes in the maximum tension region at mid-span or "tie" failure where the tie ruptures at flexural failure (Figure 3Aa).

5 Flexure-shear failure : In this type of failure, first the flexural cracks develope and then a diagonal crack suddenly develop and causes the failure of the beam. This type of failure is due to the combination of either diagonal tension failure and flexure failure or diagonal compression failure and flexure failure (Figure 3Ab).

6 Splitting failure : In this type of failure, failure occurs by clear vertical fracture of the compression zone at the top of an inclined crack at one edge of the loading block under the concentrated load (Figure 4Aa).

7 Splitting spalling failure : It is similar to splitting failure, except that the start of the destruction of the beam occurs over the support and extends vertically upward (Figure 4Ab).

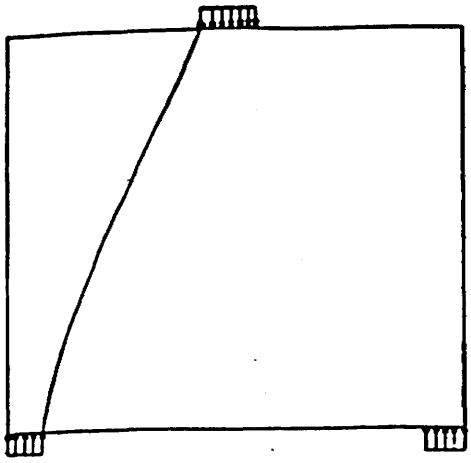

Figure(1Aa) Diagonal Tension failure

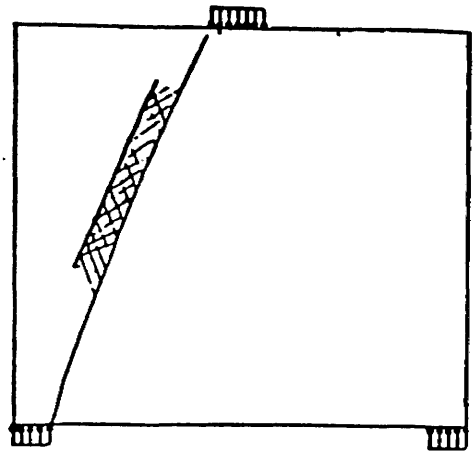

Figure(2Aa) Diagonal compression failure

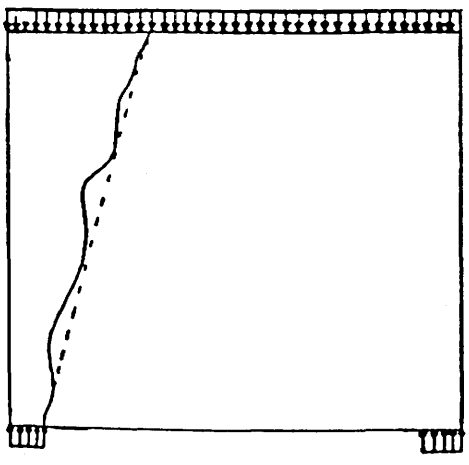

Figure(1Ab) Diagonal tension failure

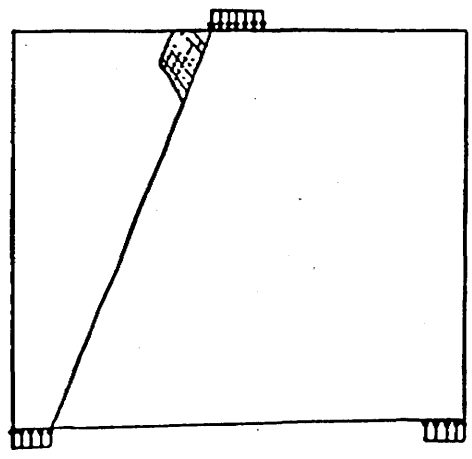

Figure(2Ab) Shear-compression failure

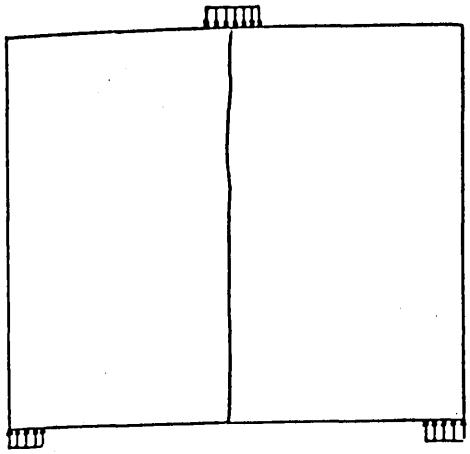

Figure(3Aa) Flexure failure

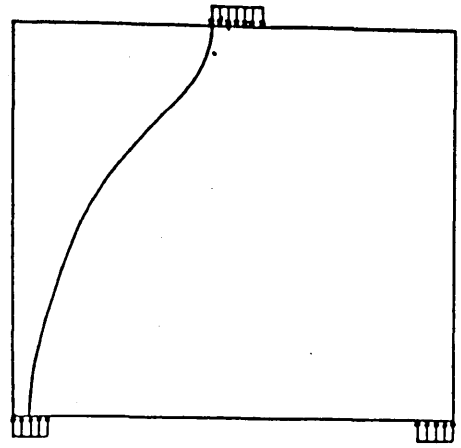

Figure(4Aa) Splitting-shear failure

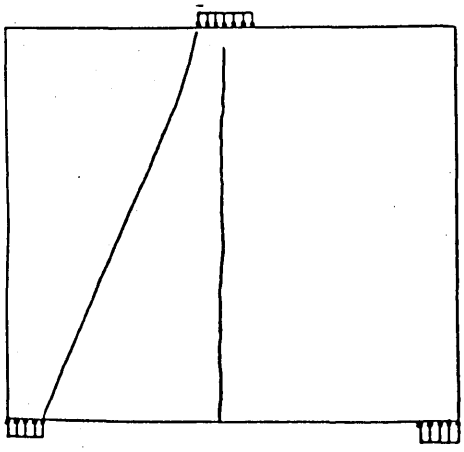

Figure(3Ab) Flexure-shear failure

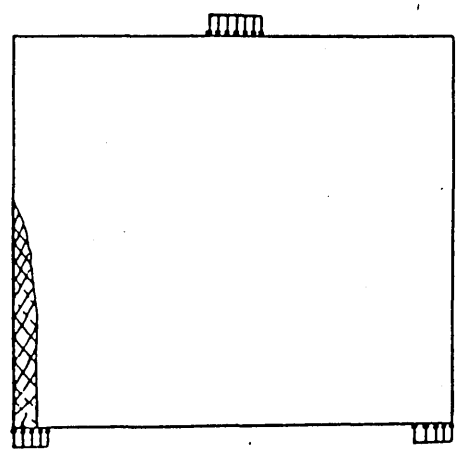

Figure(4Ab) Splitting-spalling failure